Neogene to Quaternary Foraminifera from the Western Margin of Southern Africa

Eugene W. Bergh

Thesis Presented for the Degree of

PHILOSOPHIAE DOCTOR

in

GEOLOGICAL SCIENCES

in the

FACULTY OF SCIENCE

of the

UNIVERSITY OF CAPE TOWN

Supervisor: Associate Professor John S. Compton

Co-supervisor: Professor Gerhard Schmiedl (University of Hamburg)

Co-supervisor: PD Dr Peter Frenzel (University of Jena)

October 2018

Declaration

I know the meaning of plagiarism and declare that all of the work in this thesis, apart from that which is properly acknowledged, is my own. This thesis is submitted for the degree of Doctor of Philosophy in the Department of Geological Sciences, Faculty of Science at the University of Cape Town. I declare that no part of this research has been submitted elsewhere for this degree at any other university.

Signed by candidate

Date: 25 October 2018

Eugene Bergh

BRGEUG002

Inclusion of Publications

I confirm that I have been granted permission by the University of Cape Town's Doctoral Degrees Board to include the following publications in my PhD thesis, and where co-authorships are involved my co-authors have agreed that I may include the publications.

1. Compton, J.S., Bergh, E.W., 2016. Phosphorite deposits on the Namibian shelf. Marine Geology 380, 290-314.
2. Bergh, E.W., Compton, J.S., Frenzel, P., 2018. Late Neogene foraminifera from the northern Namibian continental shelf and the transition to the Benguela Upwelling System. Journal of African Earth Sciences 141, 33-48.

Contributions of authors

In publication 1 Compton, J.S. (JSC) was the main investigator of the overarching phosphorite project and is listed as the main author for this publication. JSC selected some of the material for strontium isotope stratigraphy (SIS) analysis, provided certain images, synthesised data from published and unpublished work, developed a depositional model on the formation of phosphorites. Bergh, E.W. (EWB) logged 18 cores, provided a biostratigraphic model based on foraminifera, identified foraminifera, mollusc species and associated components, provided species lists on foraminifera and molluscs from 20 cores from the Namibian margin, provided some of the images, wrote sections with particular reference to the foraminifera and molluscs and identified and selected material for SIS from some of the cores.

In publication 2 EWB was the main investigator and logged two of the cores, identified foraminifera and associated components, processed samples, created images, developed graphs and wrote all sections. JSC and Frenzel, P (PF) proof read, provided discussion on the development of the article, discussed statistical aspects of the data and assisted with editing of the manuscript.

Signed by candidate

Date: 25 October 2018

Eugene Bergh

BRGEUG002

Table of Contents

List of Figures

List of Plates

Plate 6. 1a. *Gyroidinoides soldanii* (apertural view); 1b. *Gyroidinoides soldanii* (spiral view) (core 2670, 158 cm); 2. *Gyroidina broeckhiana* (spiral view) (core 2670, 108 cm); 3a. *Gyroidina broeckhiana* (umbilical view); 3b. *Gyroidina broeckhiana* (apertural view); 3c. *Gyroidina broeckhiana* (spiral view) (core 2670, 88 cm); 4a. *Globorotalia praescitula* (umbilical view); 4b. *Globorotalia praescitula* (apertural view); 4c. *Globorotalia praescitula* (spiral view) (core 2670, 98 cm); 5. *Globigerina bulloides* (apertural view) (core 2670, 168 cm); 6. *Globigerina bulloides* (spiral view) (core 2670, 148 cm); 7. *Globigerinella siphonifera* (core 2670, 148 cm)*;* 8. *Globigerinella siphonifera* (core 2670, 148 cm)*;* 9. *Globigerinoides bisphericus* (core 2670, 168 cm); 10. *Globigerinoides bisphericus* (oblique spiral view showing secondary apertures) (core 2670, 168 cm); 11. *Globigerinoides bisphericus* (lower spiral view) (core 2670, 118 cm). 118

Plate 7. 1. *Globigerinoides ruber* white (primary apertural view) (core 2670, 168 cm); 2. *Globigerinoides ruber* white (spiral view showing secondary apertures) (core 2670, 168 cm); 3. *Trilobatus immaturus* (spiral view showing secondary apertures) (core 2670, 148 cm); 4. *Trilobatus immaturus* (lower spiral view showing secondary apertures) (core 2670, 148 cm);5. *Trilobatus immaturus* (primary apertural view) (core 2670, 148 cm); 6. *Trilobatus sacculifer* (primary apertural view) (core 2670, 89 cm); 7. *Trilobatus sacculifer* (spiral view showing secondary apertures) (core 2670, 118 cm); 8. *Globoquadrina dehiscens* (apertural view) (core 2670, 168 cm); 9. *Globoquadrina dehiscens* (apertural view) (core 2670, 168 cm); 10a. *Globoquadrina dehiscens* (apertural view); 10b. *Globoquadrina dehiscens* (oblique spiral view) (core 2670, 138 cm); 11. *Orbulina universa* (core 2670, 77 cm). 119

Plate 8. 1a. *Eggerella bradyi;* 1b. *Eggerella bradyi* (apertural view) (GeoB 8336, 199 cm); 2a. *Eggerella bradyi;* 2b. three upper chambers of *Eggerella bradyi* with aperture visible (GeoB 8336, 189 cm); 3. *Karreriella bradyi* (GeoB 8336, 189 cm); 4a. *Karreriella bradyi* with aperture visible; 4b. *Karreriella bradyi* (apertural view) (GeoB 8336, 229 cm); 5a. *Martinottiella communis;* 5b. aperture of *Martinottiella communis* (GeoB 8336, 254 cm); 6. *Bigenerina nodosaria* (GeoB 8336, 254 cm)*;* 7. *Siphotextularia concava* (GeoB 8336, 399 cm); 8-9. *Cylindroclavulina bradyi* (GeoB 8336, 254 cm); 10a. *Spiroloculina communis*; 10b. aperture on neck of *Spiroloculina communis* (GeoB 8336, 210 cm)*;* 11a. *Siphonaperta* sp.; 11b. side view of *Siphonaperta* sp.; 11c. *Siphonaperta* sp (apertural view) (GeoB 8336, 254 cm); 12. *Quinqueloculina laevigata* (GeoB 8336, 210 cm). 258

Plate 9. 1a. *Pyrgo lucernula;* 1b. *Pyrgo lucernula* (side view) (GeoB 8336, 289 cm); 2. internal chambers of *P. lucernula* (GeoB 8336, 404 cm); 3. Aperture of *P. lucernula* (GeoB 8336, 289 cm); 4a. *Pyrgo murrhina;* 4b. *Pyrgo murrhina* (apertural view) (GeoB 8336, 204 cm); 5-6. *Pyrgo serrata* (GeoB 8336, 204 cm)*;* 6b. *Pyrgo serrata* (apertural view) (GeoB 8336, 204 cm); 7. *Dentalina* sp. (GeoB 8336, 199 cm); 8-9. *Nodosaria laevigata* (GeoB 8336, 339 cm); 9b. *Nodosaria (Glandulina) laevigata* (apertural view) (GeoB 8336, 339 cm); 10-11. *Lenticulina gibba* (GeoB 8336, 254 cm; 264 cm); 11b. *Lenticulina gibba* (marginal view) (GeoB 8336, 264 cm); 12. *Oolina globosa* (GeoB 8336, 299 cm). 259

Plate 10. 1a. *Oolina seminuda;* 1b. *Oolina seminuda* with aperture visible (GeoB 8336, 299 cm); 2. Lower portion of *Vaginulina spinigera* with basal spines (GeoB 8336, 289 cm); 3-4. *Lagena demorpha* (GeoB 8336, 279 cm; 254 cm)*;* 4b. *Lagena demorpha* (apertural view) (GeoB 8336, 254 cm); 5. hirsute *Lagena* sp. with borings (GeoB 8336, 259 cm); 6a. *Lagena sulcata;* 6b. aperture on neck of *L. sulcata* (GeoB 8336, 279 cm); 7. broken *Procerolagena gracilis* (GeoB 8336, 199 cm); 8. *Favulina hexagona;* 8b. *Favulina hexagona* (apertural view) (GeoB 20601, 73 cm); 9-10. *Fissurina* spp. (GeoB 8336, 299 cm; 274 cm). 260

Plate 11. 1-2. *Bolivina* spp. (GeoB 20601, 249 cm) ; 3. *Brizalina alata* (GeoB 20601, 73 cm); 4. *Cassidulina laevigata* (spiral view) (GeoB 20601, 73 cm); 5a. *Cassidulina laevigata* (oblique marginal view); 5b. *Cassidulina laevigata* (apertural view) (GeoB 20601, 73 cm); 6. *Cassidulina laevigata* (umbilical view) (GeoB 20601, 73 cm); 7a. *Globocassidulina crassa*; 7b. aperture of *Globocassidulina crassa* (GeoB 20601, 69 cm); 8. *Globocassidulina subglobosa* (GeoB 20601, 233 cm); 9. *Ehrenbergina trigona* (GeoB 8336, 329 cm)*;* 10. *Bulimina aculeata* (GeoB 20601, 73 cm). 261

List of Tables

Abstract

The western margin of southern Africa underwent major palaeoceanographic changes since the initiation of the Benguela Upwelling System during the Neogene. Microfossils in marine sediments provide key proxies in our understanding of how the margin evolved. Fossil shells (tests) of foraminifera (single-celled protists) from twenty cores from the Namibian shelf (199 to 309 m water depth) and three cores from the western slope (874 to 3631 m water depth) of South Africa were studied to determine the middle Miocene to Quaternary stratigraphy, palaeoenvironment and palaeoceanography of the western margin of southern Africa. Cores from the Namibian shelf recovered middle Miocene calcareous mud in erosional contact with overlying Pliocene to Pleistocene phosphatic sediments. Strontium isotope stratigraphy and planktic foraminifera biostratigraphy provide age control of the Namibian shelf sediments. The planktic indicator species *Globoquadrina dehsicens* and *Globigerinoides bisphericus* support strontium isotope stratigraphy results for the olive-green mud unit of the northern Namibian shelf indicating an age of 16 to 14 Ma, and the overlying Plio-Pleistocene age of the phosphorite-rich unit supported by planktic indicator species *Globorotalia truncatulinoides* and *Globorotalia (Globoconella) inflata.* Middle Miocene foraminifera reflect a warmer, oligotrophic, subtropical, deeper environmental setting in contrast to the shallower depositional environment, cooler conditions and a eutrophic bottom water setting indicated by Pleistocene foraminifera in the phosphatic units. The palaeoenvironment on the Namibian shelf was progressively shoaling during the Pleistocene as sea level amplitudes increased. An *Uvigerina* spp.-dominated association occurs in deeper shelf deposits dated to the early Pleistocene and the *Ammonia beccarii* association occurs in shallower shelf deposits of the late Pleistocene to Holocene. The planktic and benthic foraminiferal stable oxygen isotope records, colour reflectance (L*) and non-carbonate mineral counts provide age control on cores from the western slope of South Africa, whose records extend to just beyond Glacial Termination (GT) II. Sediment and benthic foraminiferal accumulation rates were higher during interglacial periods and lower during glacial periods. The major planktic species in the slope cores include *Globorotalia (Globoconella) inflata, Globigerina bulloides* and *Neogloboquadrina incompta.* Principal component analysis (PCA) reveals that the major factors influencing planktic foraminiferal abundances are upwelling intensity, the penetration of colder waters during glacial periods and the inflow of subtropical waters from the South Indian Ocean during interglacial periods. The major benthic species in the slope cores include *Uvigerina peregrina, Uvigerina hispidocostata* and *Cibicidoides wuellerstorfi* indicating the delivery of organic matter and oxygen availability to have the largest influence on the benthic foraminiferal faunal composition. *Uvigerina* spp. on the slope show increased relative abundances during periods of lower oxygen conditions. Bottom water masses identified by εNd (neodymium isotopic compositions) values recorded by foraminifera, along with the stable carbon isotope composition and abundance of the benthic foraminifer *C. wuellerstorfi* indicate shifts from Southern Component Water to North Atlantic Deep Water during GT II and I. Variation in εNd values in an upper slope core (874 m water depth) indicate Antarctic Intermediate Water (AAIW) influence was stronger during glacial periods compared to interglacial periods.

Chapter 1

Introduction

1. Introduction

The biostratigraphy of marine sediments has played an important role in geologic exploration and palaeoceanographic studies along the southwestern margin of Africa (Compton et al., 2002, 2004; Wigley and Compton, 2006; Compton and Bergh, 2016). A reliable microfossil group is required to determine the biostratigraphy and depositional environments of marine sediments. Foraminifera have proven to be the most reliable microfossil group in marine carbonate sediments (e.g. Kucera, 2007; Srinivasan, 2007). This is no different along the southwestern margin of Africa. Although foraminifera have been used in biostratigraphic and palaeoenvironmental studies along the margin, the foraminiferal record remains fragmented. For example, the Ocean Drilling Program (ODP) Leg 175 record (Wefer et al., 1998) did not recover middle Miocene foraminifera and the biostratigraphic record for this period has not been established in the area. Quaternary foraminifera from the South African shelf have been identified (Compton et al., 2002, 2004; Wigley and Compton, 2006), but the Namibian sediments and microfossils have not received attention until now when phosphorite exploration was undertaken. Studies on foraminifera from the Namibian shelf have been restricted to surface grab samples (Lowry, 1987; Schmidt-Sinns, 2008; Leiter and Altenbach, 2010) and the lack of core material studies from this shelf has restricted biostratigraphic and palaeoenvironmental analyses of the shelf sediments. Rau (2002) and Rau et al. (2002) studied planktic foraminifera from the western continental slope of South Africa, but did not incorporate benthic foraminifera into their study. Benthic foraminifera are important in deciphering deep water mass and ocean floor conditions during the time of deposition. In addition to the importance of foraminifera in the stratigraphy, palaeoceanographic and biogeochemical history of marine sediments, a thorough and in-depth understanding of these processes is important in contributing to modern and future ocean-climate analyses (e.g. Robinson et al., 2008; McInerney and Wing, 2011; Langer et al., 2013; Weinmann et al., 2013). This study is therefore an important contribution to a complete understanding of the stratigraphy and palaeoceanographic history of the southwestern margin of Africa and creating a reference towards working on future ocean-climate and sea level change modelling.

1.1 The usefulness of foraminifera in geologic and palaeoceanographic studies

Foraminifera are widely distributed within marine sediments (Fenton et al., 2016) and the preserved shells (tests) of these protists in marine sediments have proven to be extremely useful in investigating these changes (Kucera, 2007). Approximately 50% of the global ocean floor (Kennish, 2000) and most of the Atlantic seafloor are covered with biogenic siliceous and calcareous oozes of which fossil foraminifera form a major component (Berger, 1970; Kennish, 2000). When alive, these unicellular marine protists are found in shallow to deep waters and are environment-specific. Foraminifera occur as benthic and planktic forms. Planktic foraminifera live floating in the photic zone (Bé and Tolderlund, 1971) and benthic foraminifera live on and within the bottom sediment (Rathburn et al., 2018; and references therein). The shells of calcareous

foraminifera are composed of calcium carbonate ($CaCO_3$), incorporating seawater elements into their shells as they grow, making them extremely useful in climate and palaeoenvironmental studies. Agglutinated foraminifera live on the ocean floor and construct their tests from the surrounding sand grains and particles (Gooday, 2003).

Apart from the physical properties of foraminifera, e.g. shell size, calcification intensity and preservation state (Kucera, 2007), foraminifera can act as proxies in mainly two ways, namely through (1) biological and (2) chemical methods (Murray, 2001). Methods relying on the biological and taxonomic attributes of foraminifera are important for the interpretation of data and in the determination of further biological and chemical methods to be explored (Gooday, 2003). Current species identification is primarily based on the test morphology, enabling modern and fossil data to be comparable (Fenton et al., 2016). The morphology of foraminifera is generally assessed based on the features of the test. For example, wall structure, internal chamber arrangement, the number, shape and location of apertures and surface ornamentation, such as spines, carinae, pustules, costae and sutures are determined in identifying species (Ellis and Messina 1940; Reiss, 1958; Boltovskoy and Wright, 1976; Haynes, 1981; Loeblich and Tappan, 1988; Srinivasan, 2007). Miscroscopy has largely aided in taxonomy, but the advancement of technology over the past few decades has contributed immensely to the identification of foraminifera. Image analyses through scanning electron microscopy (SEM) and more recent computer tomography (CT) scanning techniques lend themselves well to test surface feature identification and morphometric analyses (Srinivasan, 2007). The challenge to this species concept in which foraminifera are classified according to morphological features is that evolutionary relationships and ancestral groups are not considered. It could be argued that the morphological similarities in foraminifera are in themselves as a result of the evolution of species based on ancestral groups, but this has to be tested with more certainty (Holzmann, 2000). Recent advances in the classification of foraminifera employ a molecular approach in understanding the taxonomy and phylogeny of foraminifera (e.g. Darling et al., 1996; de Vargas et al., 1997, 1999; Pawlowski, 2000; Pawlowski et al., 2007; Pawlowski and Holzmann, 2007; Darling and Wade, 2008; Ujiie et al., 2010; Quillevere et al., 2013; Spezzaferri et al., 2015; Darling et al., 2016). Molecular techniques, particularly DNA sequence analysis, provide information independent of morphological characters. This is especially relevant for taxa with polymorphic species and convergent evolution of features (Holzmann, 2000). Taxa which are morphologically similar, but belong to different species are called cryptic species (Darling and Wade, 2008). Some of the morphospecies and cryptic species contain different genetic types and also exhibit contrasting ecologies and distributions. For example, the right-coiling variant of *Neogloboquadrina pachyderma* has been reclassified as *Neogloboquadrina incompta* (Darling et al., 2006). The left-coiling variant of *Ng. pachyderma* has a colder-water distribution and is classified as a polar species, whereas *Ng. incompta* is classified as a subpolar species (Kucera, 2007). A more recent study by Spezzaferri et al. (2015) used morphometrics and DNA sequencing to conclude that the genus

Globigerinoides can be divided into two separate groups. Species such as *Gs. immaturus*, *Gs. sacculifer* and *Gs. trilobus* were reassigned to a new genus *Trilobatus.* DNA sequencing in foraminifera therefore allows for the verification or revision of certain taxa, and can resolve the question around certain cryptic species. There are, however, some challenges to these studies. For example, the influence of taphonomic processes on the preservation of molecules and contamination of material may complicate DNA sequencing in certain samples (Srinivasan, 2007).

Sea surface conditions play an important role in the distribution of planktic foraminifera (Kucera, 2007). Their reliance and adaptation to sea surface temperatures led to five bioprovinces being recognised for planktic foraminifera (Bé and Tolderlund, 1971; Bé, 1977; Vincent and Berger, 1981; Kucera, 2007; Fig. 1.1). The distribution of benthic foraminifera, on the other hand, depends on various factors which include water depth, latitude, food sources, substrate, salinity levels, availability of nutrients, organic matter flux rates, temperature, oxygen levels and bottom water currents (Jorissen et al., 1995; Gooday, 2003; Armstrong and Brasier, 2005; Murray, 2006; Fenton et al., 2016).

Chemical methods are hinged upon the ability of the tests of foraminifera to incorporate elements and isotopic signatures into their structure. Chemical analyses on foraminifera include stable isotopes (e.g. Emiliani, 1955; Lisiecki and Raymo, 2005; Kucera, 2007, etc.) and element ratios (e.g. Lear et al., 2002; Barker et al., 2005; Lynch-Styglietz, 2006; van Raden et al., 2011, etc.). The isotopic and elemental ratios in foraminifera can be influenced by changes in productivity, ice volume, temperature and salinity of the oceans (Gooday, 2003; Kucera, 2007). These methods have been applied on fossil foraminifera in sedimentary deposits along the southwestern margin of Africa to investigate the stratigraphy, palaeoenvironments and palaeoceanographic changes in the oceans dating to as far back as the Cretaceous period (Table 1.1).

1.1.1. Foraminifera in sedimentary and palaeoenvironmental studies along the southwestern continental shelf of Africa

The abundance of fossil foraminifera in rock and sedimentary strata, where macrofossils are largely absent, as well as the rapid evolution of certain species make foraminifera good biostratigraphic indicators (Kucera, 2007). The first appearance datum (FAD) and last appearance datum (LAD) of index species combined with isotopic compositions can constrain the ages of sedimentary units (Depaolo and Finger, 1991). Along the continental shelf of Namibia and western South Africa, Compton et al. (2002, 2004), Wigley and Compton (2006) and Compton and Bergh (2016) have dated components in sedimentary units which include phosphorites and biogenic material through strontium isotope stratigraphy (SIS) and planktic foraminifera indicator species. The $^{87}Sr/^{86}Sr$ ratio in authigenic and biogenic minerals reflects the $^{87}Sr/^{86}Sr$ ratio in sea water. Strontium is taken up in these minerals and is derived from the erosion of continental crust and upper mantle sources. As a result of the long residence time of strontium in the oceans, the isotopic composition of seawater is globally homogenous, but changes through time. The changing Sr isotopic ratios over time reflect the shifting balance between volcanic and terrestrial

sources (Elderfield, 1986; McArthur and Howarth, 2005; McArthur et al., 2012). Calcareous foraminifera are one of these components in which the $^{87}Sr/^{86}Sr$ ratio can be measured (Depaolo and Finger, 1991). In foraminifera from the western margin of southern Africa the $^{87}Sr/^{86}Sr$ ratio analysis was performed on tests at intervals where these microfossils are abundant. Results from studies along the western shelf of South Africa have dated sediments to the upper Oligocene to Holocene (Compton et al. 2002, 2004; Wigley and Compton, 2006) and along the Namibian shelf from the middle Miocene to Holocene (Compton and Bergh, 2016).

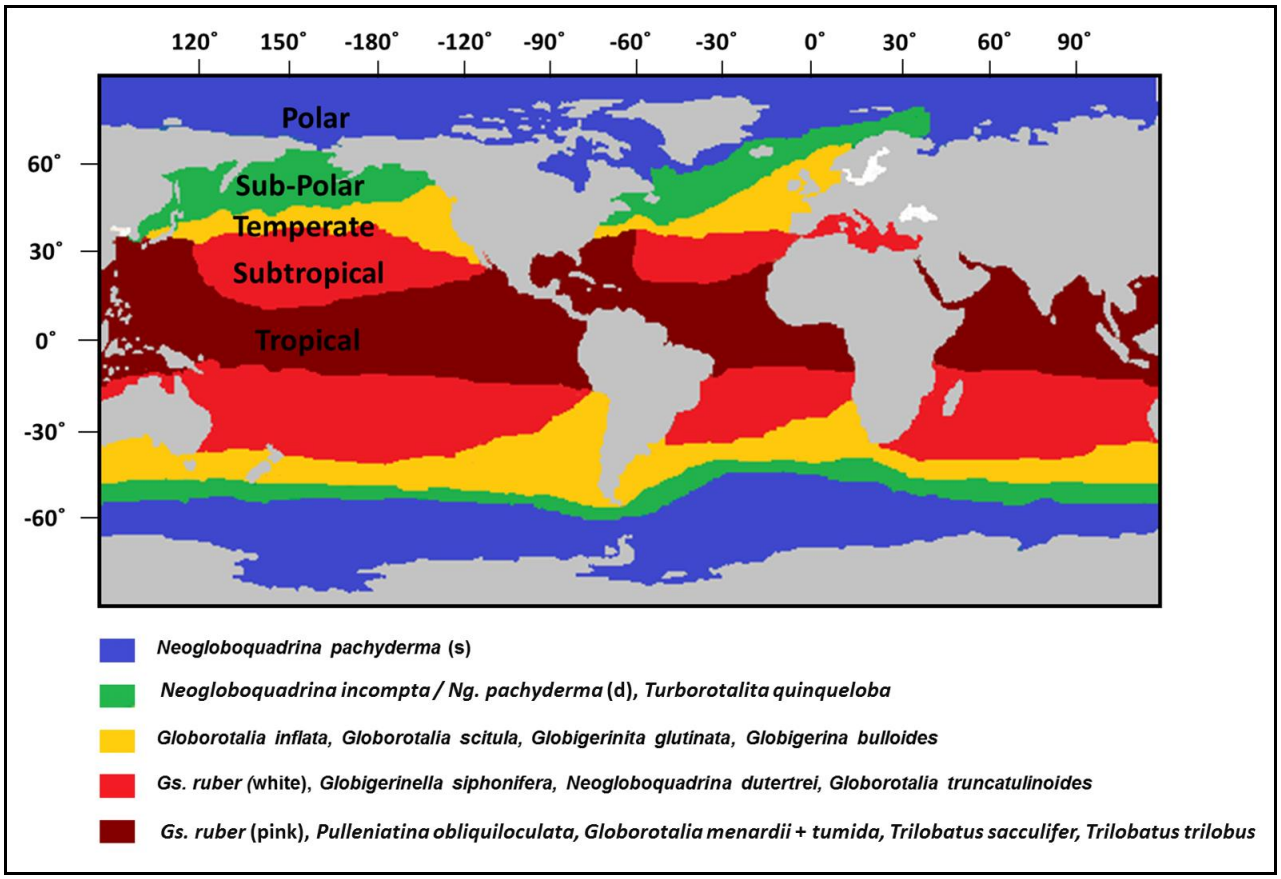

Fig. 1.1. The five planktic foraminiferal provinces (Bé, 1977; Vincent and Berger, 1981; Kucera, 2007) and some of the major taxa occurring in each province (Kucera et al., 2005; Kucera, 2007).

Further work along the shelf has included palaeoenvironmental and modern environmental studies. Late Quaternary foraminifera from the inner to middle shelf north of the Orange River mouth were assessed by McMillan (1987a). Pleistocene-aged foraminifera from South Africa were studied by McMillan (1990), Dale and McMillan (1999), Franceschini and Compton (2004) Franceschini et al. (2005) and Franceschini and Compton (2007). These studies found similar influences on the depositional environments of inner shelf, estuarine and littoral deposits. Studies that document Holocene-aged foraminifera or foraminifera in surface grab samples along the southwestern margin of South Africa include Ehrenberg (1845, 1863), Brady (1884), Pearcey (1908), Chapman

(1924), Martin (1974, 1981), McMillan (1987b), Dale and McMillan (1998), Compton et al. (2002) and Schmidt-Sinns (2008). Giraudeau (1993) provided a study into planktic foraminifera in surface sediments along the shelf and slope of Namibia and western South Africa. The major planktic foraminifera preserved in the sediments were found to be *Globigerina bulloides*, *Globorotalia (Globoconella) inflata* and *Neogloboquadrina pachyderma.* Lowry (1987) documented an extensive list of foraminiferal species occurring in surface samples along the entire coastline of Namibia and South Africa. Schmidt-Sinns (2008) also documented benthic foraminifera in shelf sediments along the margin and determined bottom water oxygen content to have an important influence on the distribution of benthic foraminifera in surface shelf sediments. Leiter and Altenbach (2010) determined the assemblage composition of species in Namibian inner shelf surface sediments to be under the influence of anoxic bottom water conditions.

Table 1.1. Studies from the western margin of southern Africa in which foraminifera have been used relevant to this study.

Study	Location of study area	Age of sediments or foraminifera	Use of foraminifera in study
Ehrenberg, 1845	Global	Recent (surface grab samples)	Taxonomic
Ehrenberg, 1863	South Africa	Recent	Taxonomic
Martin, 1974	Southern Namibian continental shelf	Recent (surface grab samples)	Palaeoenvironmental
Bolli, 1978	Western continental slope of Africa	Cretaceous to Quaternary (discontinuous sediments)	Stratigraphic indicators
Martin, 1981	Southern Namibian continental shelf	Recent (surface grab samples)	Palaeoenvironmental
Lowry, 1987	Continental margin from northern Namibia, South Africa and southern Mozambique	Recent (surface grab samples)	Taxonomic
McMillan, 1987a	Inner southernmost continental shelf of Namibia	Late Quaternary	Taxonomic
McMillan, 1987b	Southern African coast	Quaternary	Potential as stratigraphic indicators
McMillan, 1990	Onshore sediments Cape Town, South Africa	Pleistocene	Stratigraphic indicators and palaeoenvironmental
Giraudeau, 1993	Continental margin of Namibia and western South Africa	Recent (surface grab samples)	Palaeoceanographic (planktic foraminifera)
Schmiedl, 1995	Continental margin from Angola to western South Africa	Late Quaternary	Palaeoceanographic
Little et al., 1997	Continental slope of Namibia; one core central Namibian slope, one core northern Namibian slope	Late Quaternary	Palaeoceanographic

Table 1.1 *(continued)*

Study	Location of study area	Age of sediments or foraminifera	Use of foraminifera in study
Schmiedl and Mackensen, 1997	Continental slope of Namibia	Late Quaternary	Palaeoceanographic
Schmiedl et al., 1997	Continental margin of Namibia	Late Quaternary	Palaeoceanographic
Dale and McMillan, 1998	Inner to middle continental shelf of northwestern South Africa and Sierra Leone (West Africa)	Holocene	Environmental
Wefer et al., 1998	Continental slope of Namibia and western South Africa	Neogene to Quaternary	Stratigraphic indicators
Bickert and Wefer, 1999	South Atlantic; continental margin of southern Africa to Argentine Basin	Late Quaternary	Palaeoceanographic
Dale and McMillan, 1999	Onshore west coast of South Africa (Saldanha region)	Quaternary	Stratigraphic indicators and palaeoenvironmental classification
Rutberg et al., 2000	South Atlantic	Late Quaternary	Palaeoceanographic
Compton et al., 2002	Northwestern continental shelf South Africa	Holocene	Stratigraphic indicators
Diester-Haass et al., 2002	Northern continental slope of Namibia and western South Africa	Late Miocene	Palaeoceanographic (Palaeoproductivity)
Rau, 2002	Western continental slope of South Africa	Late Pleistocene	Palaeoceanographic (planktic foraminifera)
Rau et al., 2002	Western continental slope of South Africa	Late Pleistocene	Palaeoceanographic (planktic foraminifera)
Compton et al., 2004	Outer continental shelf of South Africa north of the Cape Canyon	Quaternary	Stratigraphic indicators
Diester-Haass et al., 2004	Western continental slope of South Africa	Late Miocene	Palaeoceanographic (Palaeoproductivity)
Diester-Haass et al., 2005	Northern continental slope of Namibia and western South Africa	Late Miocene	Palaeoceanographic (Palaeoproductivity)
Franceschini et al., 2005	Southwest coast of South Africa	Late Quaternary	Palaeoenvironmental
Toefy et al., 2005	Coast around Cape Town, Victoria Bay and Port Elizabeth, South Africa	Modern	Taxonomic
Wigley and Compton, 2006	Outer continental shelf of South Africa north of the Cape Canyon	Neogene to Quaternary	Stratigraphic indicators
Franceschini and Compton, 2007	Southwest coast of South Africa	Holocene	Taphonomic and palaeoenvironmental
Klevenz et al., 2008	Walvis Ridge	Late Miocene	Palaeoceanographic
Schmidt-Sinns, 2008	Continental shelf of Namibia and western South Africa	Recent (surface grab samples)	Palaeoenvironmental
Leiter and Altenbach, 2010	Central Namibian inner to middle continental shelf	Recent (surface grab samples)	Environmental

Table 1.1 *(continued)*

Study	Location of study area	Age of sediments or foraminifera	Use of foraminifera in study
Toefy, 2010	Southwestern South African coast	Modern	Environmental (pollution indicators)
Compton and Bergh 2016 (as part of this study)	Outer continental shelf of Namibia	Neogene to Quaternary	Stratigraphic indicators
Hu et al., 2016	Western continental slope of South Africa and South Atlantic	Late Quaternary	Palaeoceanographic
Von Koslowski, 2017	Lower slope of western South Africa	MIS 3 to MIS 1	Palaeoceanographic
Bergh et al., 2018 (as part of this study)	Outer continental shelf of Namibia	Neogene to Quaternary	Palaeoenvironmental

Foraminifera have also increasingly been used as pollution indicators. Toefy (2010) used trace metal contents in modern benthic foraminifera tests to determine levels of pollution in the southwestern Cape region. Studies on foraminifera in shallow water environments included Franceschini et al. (2005) in which the foraminifera of the Langebaan Lagoon salt marsh (110 km north of Cape Town) was investigated and revealed that different foraminifera inhabit different faunal zones within the lagoon. On the southwestern coast of South Africa, Toefy et al. (2005) gave an overview of intertidal foraminifera in rocky environments.

1.1.2. Foraminifera in stratigraphy, palaeoenvironmental and palaeoceanographic studies along the southwestern continental slope of Africa

The ages of slope sediments from the southwestern margin of Africa derived from foraminifera have relied upon planktic foraminiferal index species (Wefer et al., 1998) and the oxygen isotope composition ($\delta^{18}O$) of the tests (Rau et al., 2002). Along the western slope of southern Africa, foraminifera have been used as biostratigrahic indicators in slope sediments in cores of the Deep Sea Drilling Program (DSDP) Leg 40 (Bolli, 1978; Jenkins, 1978; Toumarkine, 1978) and the Ocean Drilling Programme (ODP) Leg 175 (Wefer et al., 1998). The DSDP leg retrieved discontinuous sediments dating back to the Cretaceous while ODP core sediments dated back to the late Miocene (ODP sites 1081, 1082, 1085, 1086 and 1087), Pliocene (1083, 1084) and the Pleistocene (1080). Planktic foraminifera species lists and benthic species abundances were provided in the ODP report with preliminary findings into the environmental influences along the core sites (Wefer et al., 1998).

Oxygen isotope ratios, expressed as $\delta^{18}O$ in foraminifera depend on the temperature and salinity of the seawater during calcification of the test and are linked to global ice volume change (Pearson, 2012; Rohling, 2013). During glacial periods ^{16}O is preferentially concentrated in ice sheets resulting in enrichment of ^{18}O in the ocean and in the tests of foraminifera. Conversely, during interglacial periods the ocean and the tests of foraminifera are less enriched in ^{18}O. These fluctuations in oxygen isotopes relate to cold and warm periods that are

mainly influenced by Earth's orbital eccentricity (~100 kyr) and obliquity (~41 kyr) (Berger, 1978) and are defined by marine isotope stages (MIS). Studies on multiple samples of foraminifera have resulted in stacked $\delta^{18}O$ curves (Shackleton, 1967; Imbrie et al., 1984; Lisiecki and Raymo, 2005) to which data can be correlated and ages derived. Ages derived by correlation to stacked $\delta^{18}O$ curves are, however, time averaged over millennial scales and somewhat depend on the degree of continuous sedimentation on the slope. Rau et al. (2002) used the $\delta^{18}O$ composition in the tests of the planktic *Globorotalia (Globoconella) inflata* and in the benthic *Cibicidoides wuellerstorfi* as stratigraphic age control in cores from the western margin of South Africa.

The Benguela Upwelling System (BUS) is a highly productive system (Weeks and Shillington, 1994; Heymans and Baird, 2000; Diester-Haass et al., 2002; Inthorn et al., 2006). The carbon isotope ratio of foraminifera expressed as $\delta^{13}C$, is a useful proxy to determine palaeoproductivity and past upwelling conditions (Wefer et al., 1999; Giraudeau et al., 2002; Fontanier et al., 2006, and references therein). The difference in the $\delta^{13}C$ between surface dwelling planktic and bottom dwelling benthic foraminifera ($\Delta\delta^{13}C$) can indicate changes in productivity. Surface waters will be enriched in ^{13}C compared to subsurface waters as a result of photosynthetic processes whereby ^{12}C is preferentially taken up. The use of carbon isotopes as indicators of palaeoproductivity is however complicated by factors such as the aging of water masses, variations in sedimentation rates, sediment burial rates, and bacterial break down of organic carbon (Wefer et al., 1999).

Another method to estimate the palaeoproductivity of the oceans is the calculation of benthic foraminiferal accumulation rates (BFARs). This method was used by Schmiedl and Mackensen (1997) and Diester-Haass et al. (2002, 2004, 2009) to estimate productivity levels in different regions of the Benguela Upwelling System during the Quaternary and Miocene, respectively. Foraminiferal biomass has been positively correlated to the organic carbon flux rate to the sea floor (Altenbach and Sarnthein, 1989; Herguera and Berger, 1991; Herguera, 1992, 1994) and has led to the formulation of an equation by Herguera and Berger (1991). The equation in calculating BFARs is the product of the number of benthic foraminiferal tests, the sedimentation rate and the dry bulk density of the sample. The accuracy of BFARs is, however, complicated when samples are from oxygen depleted environments and when there has been dissolution of calcareous tests (Gooday, 2003).

Along the western margin of southern Africa palaeoproductivity was found to have increased at 12 Ma coinciding with the timing of an increase in upwelling and increased terrigenous input. Diester-Haass et al. (2005) found a decrease in carbonate material between 12 and 9 Ma and attributed it to increased input of clastic material from the Orange River. Palaeoproductivity then increased by ~7 Ma during a time when the sea-level was lower and glauconitic and shell material was transported to the continental shelf. The increase in palaeoproductivity was suggested to be global rather than locally confined (Diester-Haass et al., 2005). Rau (2002) determined that productivity levels were higher in the Northern Benguela Region (NBR) followed by the Southern

Benguela Region (SBR) and lowest in the Agulhas region further to the south with productivity levels lower during glacial than during interglacial periods.

Factors related to the productivity of the region play a role in the distribution of foraminifera. Schmiedl et al. (1997) found that the distribution patterns of Recent benthic foraminifera from the eastern South Atlantic depends on the seasonality of the food supply, organic carbon flux rates, dissolved oxygen content in bottom waters, lateral advection of deep water masses, bottom water corrosion, energy of bottom water currents and the grain size composition of the substrate. It was also suggested by Schmiedl et al. (1997) that the southwest African shelf foraminifera are adapted to high food supply and low oxygen content in bottom waters.

Foraminifera have also provided valuable contributions to understanding oceanographic changes during the late Quaternary along the western margin of southern Africa. The polar species *Ng. pachyderma* dominates the modern-day coastal upwelling centre assemblage along the slope of Namibia with *G. bulloides* and *Ng. incompta* being more abundant along the fringes of upwelling cells. *Gr. (Gc.) inflata* occurs abundantly in waters between newly upwelled waters and transitional waters where nutrient levels are reduced (Little et al., 1997). These faunas do not remain constant over time and the changes in their abundances and occurrences can reveal the palaeoceanographic history of the region. For example, Rau et al. (2002) studied planktic foraminifera in an attempt to understand how the surface waters are influenced by the Agulhas Retroflection on the southwestern slope of South Africa. It was determined that the influx of warmer waters from the Agulhas Current was continuous during the Quaternary with more pronounced intervals during glacial terminations. This was determined through the warm water indicator species *Globorotalia menardii.* The continuous inflow of warm saline waters from the South Indian Ocean was attributed to the equatorward migration of the Subtropical Convergence (STC) not reaching as far north to shut off Agulhas leakage during glacial periods (Peeters et al., 2004).

Bottom water mass variations on the slope of the eastern South Atlantic on glacial-interglacial timescales have been investigated through $\delta^{13}C$ and εNd in foraminifera. In the Southern Ocean the North Atlantic Deep Water (NADW) flows southward from its northern origins. Southern Component Water (SCW) which is composed of Antarctic Bottom Water (AABW) and Lower Circumpolar Deep Water (LCDW) flows northwards from its origins in the Weddell Sea (Reid, 1989). These two major water masses (NADW and SCW) have different oxygen and nutrient contents which have been documented in studies on $\delta^{13}C$ in foraminifera (Bickert and Mackensen, 2003). Previous studies have also explored the use of neodymium isotopic compositions in foraminifera as a tracer of bottom water masses (e.g. Klevenz et al., 2008; Hu et al., 2016; von Koslowski, 2017). Neodymium isotopic compositions in seawater components are influenced by continental weathering and the age of continental sediment input into the ocean basins on submillenial scale resolutions (Vance and Burton, 1999; Rutberg et al., 2000; Goldstein and Hemming, 2003; Pahnke et al., 2008; Piotrowski et al., 2012).

The different source areas of the water masses would reflect varying Nd isotopic compositions which are preserved in the tests of foraminifera (Piepgrass and Wasserburg, 1987; Pahnke et al., 2008). Southern sourced waters will have higher εNd and lower $\delta^{13}C$ compared to the oxygen-rich NADW which has lower εNd and higher $\delta^{13}C$ (e.g. Bickert and Mackensen, 2003; Lynch-Stieglitz, 2006; Ravelo and Hillaire-Marcel, 2007). Schmiedl and Mackensen (1997), Rutberg et al., (2000) and Hu et al., (2016) found NADW to strengthen during interglacial periods and SCW strengthens during glacial periods along the western margin of southern Africa and in the Southern Atlantic Ocean. Recently, von Koslowski (2017) found the influence of the SCW to have weakened and the NADW to have strengthened during the MIS 2/1 transition along the western slope of South Africa.

1.2 Aims and Objectives

The rationales behind the objectives of this thesis are:

i. Studies on foraminifera along the southwestern margin of Africa are not well documented spatially and temporally. Species lists have been provided from DSDP and ODP reports and shelf studies off South Africa, but data are largely lacking from further studies along the Namibian shelf and the western South African slope. Martin (1981), Lowry (1987) and Schmidt-Sinns (2008) documented foraminifera along the margins (mostly the continental shelf) of Namibia and South Africa, but these studies were on foraminifera in surface grab samples. Apart from the research articles presented as part of this thesis, previously published literature has not documented foraminifera from the Namibian outer shelf. Rau et al. (2002) documented planktic foraminifera from the western South Africa slope, but benthic foraminifera were not included. The analyses of benthic foraminifera can inform on how the bottom water conditions, sedimentation and productivity can affect foraminiferal distributions along the margin. These studies can inform on how the climates and oceans have changed over time in the region and how it feeds into the global climate-ocean system.
ii. Shelf sediments along Namibia have not been dated prior to this study and therefore this study aims to provide ages based on index species and oxygen and strontium isotope stratigraphy. The oxygen isotopes derived from *Globorotalia (Globoconella) inflata* and *Cibicidoides wuellerstorfi* will also add to existing oxygen profiles for the southeast Atlantic. These ages are crucial for stratigraphic age control and for further palaeoceanographic, palaeoclimate and palaeoenvironmental analyses to be conducted.
iii. There have been large inputs from previous studies to decipher the palaeoproductivity history of the Benguela Upwelling System, but little attention has been paid to palaeoenvironmental shifts based on foraminiferal assemblages along the Namibian shelf and the western South African slope. This thesis aims to provide palaeoenvironmental information derived from the foraminifera in shelf and slope sediments prior to the initiation of the BUS as well as during the intensification thereof. These studies are important to understand how the intensification of the BUS has

changed the foraminiferal faunas, distributions, productivity, depositional environments and sedimentation over time.

iv. Studies along the margin have largely focussed on the productivity record of the region. Schmidt-Sinns (2008) and Leiter and Altenbach (2010) studied foraminifera from the continental shelf, but these studies were also based on surface grab samples. The Namibian outer shelf cores from this study provide a record spanning the middle Miocene to Holocene. These outer shelf records provide an opportunity to determine how the depositional environments changed since the initiation of the BUS. Schmiedl and Mackensen (1997) studied foraminifera from predominantly slope depths along the Namibian margin. Rau (2002) and Rau et al. (2002) studied two cores (1408 to 2488 m water depth) from the southwestern margin of South Africa. The cores at slope depths from this study are from the western margin of South Africa and are from shallower (874 m) and deeper (~3 500 m) water depths compared to the cores from Rau et al. (2002). Therefore, this study contributes to understanding depositional environments over a larger area on the margin over time as applied to foraminifera.

v. Schmiedl and Mackensen (1997) studied the water mass history in late Quaternary foraminifera using $\delta^{13}C$ and species occurrences. Rutberg et al. (2000), Hu et al. (2016) and von Koslowski (2017) studied the εNd in foraminifera in slope cores from the southeast Atlantic Ocean. This study aims to investigate deep and intermediate water mass variations using all three methods and determine if the methods provide consistent results. The cores from this study also allow for comparisons to be drawn between these studies. The record from von Koslowski (2017) is extended in this study and the location of one of the cores at 874 m is investigated to determine any variation in Antarctic Intermediate Waters (AAIW). The AAIW has not been studied as extensively as other water masses in terms of its glacial-interglacial behaviour (Pahnke et al., 2008).

Drawing from the rationales of this research the following questions are aimed to be answered through this study:

i. How did the initiation of the BUS influence the depositional sediments and microfossil assemblages along the western margin of southern Africa?

ii. How did the increasing sea level amplitudes affect the sediments and microfossil assemblages along the western margin of southern Africa?

iii. What are the potential controlling factors affecting the microfossil assemblages along the margin during the late Cenozoic?

iv. How did glacial terminations affect the oceanographic configuration during the late Quaternary along the margin and are these palaeoceanographic changes reflected in foraminiferal distributions and stable carbon isotopes?

From these questions the overarching aim of this project is formulated. The overarching aim of this research is to determine how the initiation of the BUS and late Cenozoic oceanographic changes influenced the sedimentation, stratigraphy, palaeo-environmental and palaeoceanographic changes during the Neogene and Quaternary along the

southwestern margin of Africa based on faunal occurrences, abundances and isotopic compositions of planktic and benthic foraminifera.

The objectives within this aim include:

i. To contribute to existing knowledge on shelf and slope foraminifera along the southwestern margin of Africa.
ii. To determine the stratigraphy of shelf and slope sediments through indicator species (biostratigraphy) and stable isotopes.
iii. To provide a palaeoenvironmental history of the continental shelf during the initiation and intensification of the Benguela Upwelling System.
iv. To determine which depositional, environmental and oceanographic influences affect the faunal compositions of Neogene to Quaternary foraminifera along the margin.
v. To investigate the Quaternary deep and intermediate water mass history of the margin using Nd isotopes and its relation to $\delta^{13}C$ and benthic faunal abundances.

1.3 Background to Chapters

This thesis is divided into 9 chapters. The first chapter provides a background to the study of foraminifera along the western margin of southern Africa and its applications to previous work in the BUS. It also provides the aims and objectives of the study as well as the layout of the thesis.

Chapter 2 provides the regional setting of the cores studied in this project, giving the context of the cores in terms of bathymetry, sedimentary record and oceanographic features of the western margin of southern Africa.

Chapter 3 is a published research article by Compton and Bergh (2016). The publication primarily focuses on the phosphorite-rich sediments on the Namibian shelf. The origin, depositional history, stratigraphy and geochemistry of the phosphorites are discussed in the publication. Foraminifera and molluscs were correlated to SIS as stratigraphic age control for the cores studied.

Chapter 4 presents a summary of the middle Miocene foraminifera recovered from the northern Namibian shelf. Species that could be identified to at least the genus level are described with brief comparisons drawn between this study and previous global studies. Ecological examples, bathymetric preferences and stratigraphic ranges (where available) are also provided. The regional distribution of each species is also presented based on previous studies. This chapter highlights many species that are reported for the first time along the southwestern shelf of Africa.

Chapter 5 is a published research article by Bergh et al. (2018). The palaeoenvironments of middle Miocene to Pleistocene foraminifera are investigated and the biostratigraphy is presented and indicator species identified. Comparisons between the assemblages and the sedimentary units are also determined. The change in bathymetry, palaeo sea-surface conditions and microhabitat between the middle-Miocene and the Pleistocene are explored based on the assemblages found in the sedimentary units.

Chapter 6 expands the study area from Chapter 5 to include the mollusc and foraminiferal datasets from 16 cores of the Walvis Bay-Luderitz shelf. Comparisons between the two study areas are made and the Quaternary regional distribution discussed to include previous studies from the western shelf of South Africa. A discussion on the palaeoenvironments of the southwestern shelf of Africa is given based on the influence of the BUS on the assemblages found in Pleistocene to Recent sediments.

The western slope of South Africa is investigated in chapters 7 to 8 using stable isotopes and foraminiferal assemblages. The oxygen isotope record of three cores (874 to 3613 m water depth) along the western slope of South Africa is obtained from $\delta^{18}O$ measurements in *Globorotalia (Globoconella) inflata* and *Cibicidoides wuellerstorfi* and compared to previously published benthic oxygen isotope stacked records (Lisiecki and Raymo, 2005). The relative abundances of benthic and planktic foraminifera are discussed in Chapter 7 and indicator species were used to determine palaeoceanographic changes in the late Quaternary record from MIS 8 to MIS 1. The major influences on the planktic and benthic faunal record are also determined by principal component analysis.

Chapter 8 focusses on determining variations in deep (SCW/NADW) and intermediate (AAIW) water mass influences from MIS 8 to MIS 1 in the three western South African slope cores based on foraminiferal εNd, $\delta^{13}C$ and *C. wuellerstorfi* faunal abundances. This chapter also primarily assesses if the last two glacial terminations had a pronounced influence on the reconfiguration of ocean masses over time.

Chapter 9 synthesises results from this thesis to give an overview on the Neogene to Quaternary foraminiferal, depositional, palaeo-environmental and palaeoceanographic history of the southwestern margin of Africa.

1.4 Acknowledgements

My supervisors are thanked for their contribution to this project and thesis. Associate Professor John Compton is thanked for his guidance throughout my project, for valuable discussions and his suggestions on how to improve my manuscripts and chapters in this thesis. PD Dr Peter Frenzel (University of Jena) is thanked for the valuable discussions on statistical aspects of my research, on how to improve my manuscripts and his suggested edits to chapters of my thesis. Professor Dr Gerhard Schmiedl (Hamburg University) is thanked for his comments to my manuscripts and reviewing identifications of the foraminifera.

Dr Ian McMillan has been a catalyst in embarking on this research. He has also provided his thoughts and comments to the manuscripts of this thesis.

The Namibian outer shelf cores were provided by MineMakers Australia Pty Ltd. and permission granted to continue further research on the core material.

The support from researchers at the University of Bremen has also been valuable to this project. PD Dr Matthias Zabel, as project leader of the Regional Archives for Integrated Investigations (RAiN) initiative, is thanked for his support and

encouragement of this research. The RAiN initiative was funded by the Bundesministerium für Bildung und Forschung. Dr Annette Hahn provided colour reflectance data and assisted with materials for sampling at the University of Bremen. Lukas Gander assisted in sampling core GeoB 20601-4 on-board the RV Meteor. Dr Henning Kuhnert performed $\delta^{18}O$ and $\delta^{13}C$ analyses on the samples. The Zentrum für Marine Umweltwissenschaften (MARUM), University of Bremen granted permission to sample and study the GeoB cores relevant to this thesis.

Fayrooza Rawoot assisted in the sample preparation for Neodymium isotope analysis and Dr Petrus le Roux from UCT provided the results of the analysis.

Miranda Waldron, Albe Bosman, Jody Oliver, Phathutshedzo Mutheiwana and Dwayne Cloete assisted in coating of specimens and initial SEM imaging

Assistance in laboratory work, processing of some of the cores and checking of certain information were also made possible by fourth year students and interns. Melissa Oosthuizen logged, sampled, sieved and weighed dried fractions of two of the northern Namibian cores, as well as SEM imaged and microphotographed some of the grain types from the two cores. Teboho Mosito processed pre-sampled material, sieved and weighed dried fractions of core GeoB 20601-4. Louis Jonk is thanked for his assistance in checking taxonomic information of the Quaternary slope foraminifera.

The National Research Foundation (NRF) through the Thuthuka PhD fund track provided funding for research equipment, supplies and laboratory analyses.

Dr Hamish Robertson, former Director of Natural History/Research and Exhibitions at Iziko Museums is thanked for his support and motivation in this project. The staff and management of Iziko are also thanked for their support and funding.

Personal thanks and appreciation are extended to my family for their unwavering support and encouragement in my journey throughout my studies.

References

Altenbach, A.V., Sarnthein, M., 1989. Productivity Record in Benthic. Productivity of the ocean: present and past 8, 255-269.

Armstrong, H.A., Brasier, M.D., 2005. Microfossils, 2nd edition. Blackwell, Oxford, 296 pp.

Barker, S., Cacho, I., Benway, H., Tachikawa, K., 2005. Planktonic foraminiferal Mg/Ca as a proxy for past oceanic temperatures: a methodological overview and data compilation for the Last Glacial Maximum. Quaternary Science Reviews 24, 821-834.

Bè, A.W.H., 1977. An ecological, zoogeographic and taxonomic review of Recent planktonic foraminifera. In: Ramsey, A.T.S. (Ed.), Oceanic micropaleontology. Academic Press, London, pp. 1-110.

Bè, A.W.H., Tolderlund, D.S., 1971. Distribution and ecology of planktonic foraminifera. In: Funnell, B.M., Riedel, W.R. (Eds), The micropaleontology of oceans. Cambridge University Press, London, pp. 105-149.

Berger, A.L., 1978. Long-term variations of daily insolation and Quaternary climatic changes. Journal of the Atmospheric Sciences 35, 2362-2367.

Berger, W.H., 1970. Biogenous deep-sea sediments: fractionation by deep-sea circulation. Geological Society of America Bulletin 81, 1385-1402.

Bergh, E.W., Compton, J.S., Frenzel, P., 2018. Late Neogene foraminifera from the northern Namibian continental shelf and the transition to the Benguela Upwelling System. Journal of African Earth Sciences 141, 33-48.

Bickert, T., Mackensen, A., 2003. Last Glacial to Holocene changes in South Atlantic deep water circulation. In: The South Atlantic in the Late Quaternary. Springer, Berlin, Heidelberg, pp. 671-693.

Bickert, T., Wefer, G., 1999. South Atlantic and benthic foraminifer $\delta^{13}C$ deviations: implications for reconstructing the Late Quaternary deep-water circulation. Deep Sea Research Part II: Topical Studies in Oceanography 46(1-2), 437-452.

Bolli, H., 1978. Synthesis of the Leg 40 biostratigraphy and paleontology. In: Bolli, H.M., Ryan, W.B.F., McKnight, B.K., Kagami, H., Melguen, M., Siesser, W.G., Longoria, J.F., Decima, F.P., Foresman, J.B., Hottman, W.E., Natland, H. (Eds.). Leg 40; Cape Town, South Africa to Abidjan, Ivory Coast. Initial Reports of the Deep Sea Drilling Program 40: Washington D.C., U.S. Government Printing Office, 1063-1067.

Boltovskoy, E., Wright, R., 1976. Recent Foraminifera. The Hague: Junk Publishers, 515 pp.

Brady, H.B., 1884. Report of the foraminifera dredged by H.M.S. Challenger during the years 1873-1876. In Brady, H.B. (Ed.) Report on the Scientific Results of the Voyage of the H.M.S. Challenger during the years 1873-1876. Zoology 9, 1-814.

Chapman, F., 1924. A first report of foraminifera collected by the S. African Government Fisheries and Marine Biological Survey. Union of South Africa Fisheries and Marine Biological Survey Report 3, Special Report XI, 1-19.

Compton, J.S., Bergh, E.W., 2016. Phosphorite deposits on the Namibian shelf. Marine Geology 380, 290-314.

Compton, J.S., Mulabisana, J., McMillan, I.K., 2002. Origin and age of phosphorite from the Last Glacial Maximum to Holocene transgressive succession off the Orange River, South Africa. Marine Geology 186 (3-4), 243-261.

Compton, J.S., Wigley, R., McMillan, I.K., 2004. Late Cenozoic phosphogenesis on the western shelf of South Africa in the vicinity of the Cape Canyon. Marine Geology 206, 19-40.

Dale, D.C., McMillan, I.K., 1998. Mud belt and middle shelf benthonic and planktonic foraminiferal assemblages and sedimentation processes compared through the Holocene successions at two tropical African (Sierre Leone) and two temperate African (western offshore South Africa) sites. South African Journal of Science 94, 319– 340.

Dale, D.C., McMillan, I.K., 1999. On the beach: A field guide to the Late Cainozoic micropalaeontological history, Saldanha region, South Africa. Earthyear Environmental Communications, 127 pp.

Darling, K.F., Kroon, D., Wade, C.M., Leigh Brown, A.J., 1996. Molecular phylogeny of the planktonic foraminifera. Journal of Foraminiferal Research 26, 324-330.

Darling, K.F., Kucera, M., Kroon, D., Wade, C.M., 2006. A resolution for the coiling direction paradox in *Neogloboquadrina pachyderma*. Paleoceanography 21, PA2011. https://doi.org/10.1029/2005PA001189.

Darling, K.F., Schweizer, M., Knudsen, K.L., Evans, K.M., Bird, C., Roberts, A., Filipsson, H.L., Kim, J.H., Gudmundsson, G., Wade, C.M. and Sayer, M.D., 2016. The genetic diversity, phylogeography and morphology of Elphidiidae (Foraminifera) in the Northeast Atlantic. Marine Micropaleontology 129, 1-23.

Darling, K.F., Wade, C.M., 2008. The genetic diversity of planktic foraminifera and the global distribution of ribosomal RNA genotypes. Marine Micropaleontology 67, 216– 238.

de Vargas, C., Zaninetti, L., Hilbrecht, H., Pawlowski, J., 1997. Phylogeny and rates of molecular evolution of planktonic foraminifera: SSU rDNA sequences compared to the fossil record. Journal of Molecular Evolution 45, 285-294.

de Vargas, C., Norris, R., Zaninetti, L., Gibb, S.W., Pawlowski, J., 1999. Molecular evidence of cryptic speciation in planktonic foraminifers and their relation to oceanic provinces. Proceedings of the National Academy of Science USA 96, 2864-286

Depaolo, D.J., Finger, K.L., 1991. High-resolution strontium-isotope stratigraphy and biostratigraphy of the Miocene Monterey Formation, central California. Geological Society of America Bulletin 103(1), 112-124.

Diester-Haass, L., Billups, K., Emeis, K.C., 2005. In search of the late Miocene-early Pliocene “biogenic bloom” in the Atlantic Ocean (Ocean Drilling Program Sites 982, 925 and 1088). Paleoceanography 20, 1-13.

Diester-Haass, L., Billups, K., Gröcke, D.R., François, L., Lefebvre, V., Emeis, K.C., 2009. Mid-Miocene paleoproductivity in the Atlantic Ocean and implications for the global carbon cycle. Paleoceanography and Paleoclimatology, 24(1), PA1209, doi:10.1029/2008PA001605

Diester-Haass, L., Meyers, P.A., Bickert, T., 2004. Carbonate crash and biogenic bloom in the late Miocene: evidence from ODP sites 1085, 1086 and 1087 in the Cape Basin, southeast Atlantic Ocean. Paleoceanography 19, 1-19.

Diester-Haass, L., Meyers, P.A., Vidal, L., 2002. The late Miocene onset of high productivity in the Benguela Current upwelling system as part of a global pattern. Marine Geology 180(1-4), 87-103.

Ehrenberg, C.G., 1845. Uber das kleinste organische leben en mehren bischer nicht untersuchten erdpunkten, mikroskopische lebensformen von Portugal, und Spanien, Süd Afrika, hinter-Indien, Japan und Kurdistan. Monatsbericht der Königliche Preussische Akademie der Wissenschaften zu Berlin, Bericht, 357-381.

Ehrenberg, C.G., 1863. Beitrag zur kenntnis der unterseeischen Agulhas-Bank an der Südspitze Afrikas al seines sich kundgebengen grünsandigen polythalamien-kalkfelsens. Monatsbericht der Königliche Preussische Akademie der Wissenschaften zu Berlin, Bericht, 357-381.

Elderfield, H., 1986. Strontium isotope stratigraphy. Palaeogeography, palaeoclimatology, palaeoecology 57(1), 71-90.

Ellis, B.F.S., Messina, A.R., 1940. Catalogue of Foraminifera. New York: American Museum of Natural History, Micropaleontology Press.

Emiliani, C., 1955. Pleistocene temperatures. The Journal of Geology 63(6), 538-578.

Fenton, I.S., Pearson, P.N., Jones, T.D., Purvis, A., 2016. Environmental Predictors of Diversity in Recent Planktonic Foraminifera as Recorded in Marine Sediments. PloS one 11, e0165522.

Fontanier, C., Mackensen, A., Jorissen, F.J., Anschutz, P., Licari, L., Griveaud, C., 2006. Stable oxygen and carbon isotopes of live benthic foraminifera from the Bay of Biscay: Microhabitat impact and seasonal variability. Marine Micropaleontology 58(3), 159-183.

Franceschini, G., Compton, J.S., 2004. Aeolian and marine deposits of the Tabakbaai Quarry area, Western Cape, South Africa. South African Journal of Geology 107.4, 619-632.

Franceschini, G., Compton, J.S., 2007. Abrasion of foraminifera tests along an active dune cordon, Western Cape, South Africa. Palaios 22, 686-690.

Franceschini, G., McMillan, I.K., Compton, J.S., 2005. Foraminifera of Langebaan Lagoon salt marsh and their application to the interpretation of late Pleistocene depositional environments at Monwabisi, False Bay coast, South Africa. South African Journal of Geology 108, 285-296.

Giraudeau, J., 1993. Planktonic foraminiferal assemblages in surface sediments from the southwest African continental margin. Marine Geology 110, 47-62.

Giraudeau, J., Meyers, P.A., Christensen, B.A., 2002. Accumulation of organic and inorganic carbon in Pliocene-Pleistocene sediments along the SW African margin. Marine Geology 180, 49-69.

Goldstein, S.L., Hemming, S.R., 2003. Long-lived isotopic tracers in oceanography, paleoceanography, and ice-sheet dynamics. Treatise on Geochemistry 6, 625.

Gooday, A.J., 2003. Benthic foraminifera (Protista) as tools in deep-water palaeoceanography: environmental influences on faunal characteristics. Advances in Marine Biology 46, 1-90.

Haynes, J.R., 1981. Foraminifera. London: MacMillan Publishers Ltd., 443 pp.

Herguera, J.C., 1992. Deep-sea benthic foraminifera and biogenic opal: glacial to postglacial productivity changes in the western equatorial Pacific. Mar. Micropaleontoly 19, 79-98.

Herguera, J.C., 1994. Nutrient, mixing and export indices: A 250 kyr paleoproductivity record from the western equatorial pacific. In: Zahn, R., Pedersen, T.F., Kaminski, M.A., Labeyrie, L (Ed.), Carbon Cycling in the Glacial Ocean: Constraints on the Ocean's Role in Global Change. NATO ASI Series I 17, 481-519.

Herguera, J.C., Berger, W., 1991. Paleoproductivity from benthic foraminifera abundance: Glacial to postglacial change in the west-equatorial Pacific. Geology 19(12), 1173-1176.

Heymans, J.J., Baird, D., 2000. A carbon flow model and network analysis of the northern Benguela upwelling system,

Namibia.Ecological Modelling 126 (1), 9-32.

Holzmann, M., 2000. Species concept in foraminifera: Ammonia as a case study. Micropaleontology 46, 21-37.

Hu, R., Noble, T.L., Piotrowski, A.M., McCave, I.N., Bostock, H.C., Neil, H.L., 2016. Neodymium isotopic evidence for linked changes in Southeast Atlantic and Southwest Pacific circulation over the last 200 kyr. Earth and Planetary Science Letters 455, 106-114.

Imbrie, J., Hays, J.D., Martinson, D.G., McIntyre, A., Mix, A.C., Morely, J.J., Pisias, N.G., Prell, W.L., Shackleton, N.J., 1984. The orbital theory of Pleistocene climate: support for a revised chronology of the marine $\delta^{18}O$ record: In: Berger, A., Imbrie, J, Hays, J.D., Kukla, G and Saltzman, B (Eds.). Milankovitch and Climate, Part 1. Reidel, Dordecht, pp. 269-305.

Inthorn, M., Wagner, T., Scheeder, G., Zabel, M. 2006. Lateral transport controls distribution, quality, and burial of organic matter along continental slopes in high-productivity areas. Geology 34(3), 205-208.

Jenkins, D.G., 1978. Neogene planktonic foraminifers from DSDP Leg 40 Sites 360 and 362 in the southeastern Atlantic. In: Bolli, H.M., Ryan, W.B.F., McKnight, B.K., Kagami, H., Melguen, M., Siesser, W.G., Longoria, J.F., Decima, F.P., Foresman, J.B., Hottman, W.E, Natland, .H. (Eds.). Leg 40; Cape Town, South Africa to Abidjan, Ivory Coast. Initial Reports of the Deep Sea Drilling Program 40, Washington D.C., U.S. Government Printing Office, 723-732.

Jorissen, F.J., de Stigter, H.C., Widmark, J.G., 1995. A conceptual model explaining benthic foraminiferal microhabitats. Marine Micropaleontology 26, 3-15.

Kennish, M.J., 2000. Practical Handbook of Marine Science. Crc press, 896 pp.

Klevenz, V., Vance, D., Schmidt, D.N., Mezger, K., 2008. Neodymium isotopes in benthic foraminifera: core-top systematics and a down-core record from the Neogene south Atlantic. Earth and Planetary Science Letters 265, 571-587.

Kucera, M., 2007. Planktonic foraminifera as tracers of past oceanic conditions. In: Hillaire-Marccel, C., de Vernal, A. (Eds.). Proxies in Late Cenozoic Paleoceanography. Elsevier, Amsterdam, pp. 213-262.

Kucera, M., Weinelt, M., Kiefer, T., Pflaumann, U., Hayes, A., Weinelt, M., Chen, M-T., Mix, A.C., Barrows, T.T., Cortijo, E., Duprat, J., Juggins, S., Waelbroeck, C., 2005. Reconstruction of sea-surface temperatures from assemblages of planktonic foraminifera: Multi-technique approach based on geographically constrained calibration datasets and its application to glacial Atlantic and Pacific Oceans. Quaternary Science Reviews 24, 951–998.

Langer, M.R., Weinmann, A.E., Lötters, S., Bernhard, J.M., Rödder, D., 2013. Climate-driven range extension of Amphistegina (Protista, Foraminiferida): models of current and predicted future ranges. PLoS One 8(2), e54443.

Lear, C.H., Rosenthal, Y., Slowey, N., 2002. Benthic foraminiferal Mg/Ca paleothermometry: A revised core-top calibration. Geochimica et Cosmochimica Acta 66, 3375-3387.

Leiter, C., Altenbach, A.V., 2010. Benthic foraminifera from the diatomaceous mud belt off Namibia: characteristic species for severe anoxia. Palaeontologica Africana 13(2), 11A, 19p.

Lisiecki, L.E., Raymo, M.E., 2005. A Pliocene-Pleistocene stack of 57 globally distributed benthic $\delta^{18}O$ records. Paleoceanography 20, PA1003, doi:10.1029/2004PA001071.

Little, M.G., Schneider, R.R., Kroon, D., Price, B., Bickert, T., Wefer, G., 1997. Rapid palaeoceanographic changes in the Benguela Upwelling System for the last 160,000 years as indicated by abundances of planktonic foraminifera. Palaeogeography, Palaeoclimatology, Palaeoecology 130(1-4), 135-161.

Loeblich, A.J., Tappan, H., 1988. Foraminiferal genera and their classification. New York: Van Nostrand Reinhold Company 1-2, 1-970.

Lowry, F.M.D., 1987. Foraminiferal thanatocoenoses from the continental shelf of southern Africa. Unpublished PhD. thesis, University College, London, 443 pp.

Lynch-Stieglitz, J., 2006. Tracers of past ocean circulation. Treatise on Geochemistry 6, 433-451.

Martin, R.A., 1974. Benthonic foraminifera from the western coast of southern Africa. Bulletin Joint Geological Survey of South Africa/ University of Cape Town Marine Geology Programme Technical Report 6, 83-87.

Martin, R.A., 1981. Benthic foraminifera from the Orange-Lüderitz shelf southern African continental margin. Bulletin Joint Geological Survey of South Africa/ University of Cape Town Marine Geoscience Unit 11, 75 pp.

McArthur, J., Howarth, R.J., 2005. Strontium isotope stratigraphy. In: A Geologic Time Scale, pp. 96-105.

McArthur, J.M., Howarth, R.J., Shields, G.A., 2012. Strontium isotope stratigraphy. In: The geologic time scale, pp. 127-144.

McInerney, F.A., Wing, S.L., 2011. The Paleocene-Eocene Thermal Maximum: A perturbation of carbon cycle, climate, and biosphere with implications for the future. Annual Review of Earth and Planetary Sciences 39, 489-516.

McMillan, I.K. 1987a. Late Quaternary foraminifera from the southern part of offshore South West Africa/Namibia. Unpublished Ph.D. thesis, University of Wales, Aberystwyth.

McMillan, I.K. 1987b. The genus *Ammonia* Brünnich, 1772 (Foraminiferida) and its potential for elucidating the latest Cainozoic stratigraphy of South Africa. South African Journal of Science 83, 32-42.

McMillan, I.K., 1990. Foraminifera from the Late Pleistocene (latest Eemian to earliest Weichselian) shelly sands of Cape Town city centre, South Africa. Annals of the South African Museum 99, 121-186.

Murray, J.W., 2001. The niche of benthic foraminifera, critical thresholds and proxies. Marine Micropaleontology 41, 1-7.

Murray, J.W., 2006. Ecology and applications of benthic foraminifera. Cambridge University Press, 426pp.

Pahnke, K., Goldstein, S.L., Hemming, S.R., 2008. Abrupt changes in Antarctic Intermediate Water circulation over the past 25,000 years. Nature Geoscience 1, 870.

Pawlowski, J., 2000. Introduction to the molecular systematics of foraminifera. Micropaleontology 46, 1-12.

Pawlowski, J., Bowser, S.S., Gooday, A.J., 2007. A note on the genetic similarity between shallow-and deep-water Epistominella vitrea (Foraminifera) in the Antarctic. Deep Sea Research Part II: Topical Studies in Oceanography 54(16-17), 1720-1726.

Pawlowski, J., Holzmann, M., 2007. Diversity and geographic distribution of benthic foraminifera: a molecular perspective. In: Protist Diversity and Geographical Distribution, Springer: Dordrecht, pp. 83-94.

Pearcey, F.G., 1908. On the genus *Botellina* (Carpenter), with a description of a new species. Transactions of the South African Philosophical Society 17, 185-194.

Pearson, P.N., 2012. Oxygen isotopes in foraminifera: Overview and historical review. The Paleontological Society Papers 18, 1-38.

Peeters, F.J.C., Acheson, R., Brummer, G.J.A., de Ruijter, W.P.M., Schneider, R.R., Ganssen, G.M., Ufkes, E., Kroon, D., 2004. Vigorous exchange between the Indian and Atlantic oceans at the end of the past five glacial periods. Nature 430, 661–665.

Piepgras, D.J., Wasserburg, G.J., 1987. Rare earth element transport in the western North Atlantic inferred from Nd isotopic observations. Geochimica et Cosmochimica Acta 51, 1257-1271.

Piotrowski, A.M., Galy, A., Nicholl, J.A. L., Roberts, N., Wilson, D.J., Clegg, J.A., Yu, J., 2012. Reconstructing deglacial North and South Atlantic deep water sourcing using foraminiferal Nd isotopes. Earth and Planetary Science Letters 357, 289-297.

Quillevere, F., Morard, R., Escarguel, G., Douady, C.J., Ujiié, Y., De Garidel-Thoron, T., de Vargas, C., 2013. Global scale same-specimen morpho-genetic analysis of *Truncorotalia truncatulinoides*: A perspective on the morphological species concept in planktonic foraminifera. Palaeogeography, Palaeoclimatology, Palaeoecology 391, 2-12.

Rathburn, A.E., Willingham, J., Ziebis, W., Burkett, A.M., Corliss, B.H., 2018. A New biological proxy for deep-sea paleo-oxygen: Pores of epifaunal benthic foraminifera. Scientific Reports 8(1), 9456.

Rau, A.J., 2002. A late Quaternary history of Agulhas-Benguela interactions from two sediment cores on the western continental slope of South Africa. Unpublished PhD. University of Cape Town, 315 pp.

Rau, A.J., Rogers, J., Lutjeharms, J.R.E., Giraudeau, J., Lee-Thorp, J.A., Chen, M-T., Waelbroeck, C., 2002. A 450-kyr record of hydrological conditions on the western Agulhas Bank Slope, south of Africa. Marine Geology 180, 183-201.

Ravelo, A.C., Hillaire-Marcel, C., 2007. Chapter Eighteen the use of oxygen and carbon isotopes of foraminifera in Paleoceanography. Developments in Marine Geology p1, 735-764.

Reid, J.L., 1989. On the total geostrophic circulation of the South Atlantic Ocean: Flow patterns, tracers, and transports. Progress in Oceanography 23, 149-244.

Reiss, Z., 1958. Classification of lamellar foraminifera. Micropaleontology 4, 51-70.

Robinson, M.M., Dowsett, H.J., Chandler, M.A., 2008. Pliocene role in assessing future climate impacts. Eos, Transactions American Geophysical Union 89(49), 501-502.

Rohling, E.J., 2013. Oxygen isotope composition of seawater. The Encyclopedia of Quaternary Science. Elsevier, Amsterdam 2, 915-922.

Rutberg, R.L., Hemming, S.R., Goldstein, S.L., 2000. Reduced North Atlantic Deep Water flux to the glacial Southern Ocean inferred from neodymium isotope ratios. Nature 405, 935.

Schmidt-Sinns, J., 2008. Rezente benthische Foraminiferen im Bereich des Benguelastroms, Südwestafrika– Verbreitungsmuster und ihre steuernden Faktoren. PhD thesis, Universitätsund Landesbibliothek, Bonn, 1-261.

Schmiedl, G., 1995. Rekonstruktion der spätquartären Tiefenwasserzirkulation und Produktivität im östlichen Südatlantik anhand von benthischen Foraminiferenvergesellschaftungen / Late Quaternary benthic foraminiferal assemblages from the eastern South Atlantic Ocean: reconstruction of deep water circulation and productivity changes. Berichte zur Polarforschung (Reports on Polar Research) 160, 207 pp.

Schmiedl, G., Mackensen, A., 1997. Late Quaternary paleoproductivity and deep water circulation in the eastern South Atlantic Ocean: Evidence from benthic foraminifera. Palaeogeography, Palaeoclimatology, Palaeoecology 130, 43-80.

Schmiedl, G., Mackensen, A., Müller, P.J., 1997. Recent benthic foraminifera from the eastern South Atlantic Ocean: dependence on food supply and water masses. Marine Micropaleontology 32, 249-287.

Shackleton, N., 1967. Oxygen isotope analyses and Pleistocene temperatures re-assessed. Nature 215, 15-17.

Spezzaferri, S., Kucera, M., Pearson, P.N., Wade, B.S., Rappo, S., Poole, C.R., Morard, R., Stalder, C., 2015. Fossil and genetic evidence for the polyphyletic nature of the planktonic foraminifera" Globigerinoides", and description of the new genus Trilobatus. PLoS One 10(5), p.e0128108.

Srinivasan, M.S., 2007. A journey through morphological micropaleontology to molecular micropaleontology. Indian Journal of Marine Sciences 36(4), 251-271.

Toefy, R., 2010. Extant benthic Foraminifera from two bays along the SW coast of South Africa, with a comment about their use as indicators of pollution. Unpublished PhD. University of the Western Cape

Toefy, R., Gibbons, M.J., McMillan, I.K., 2005. The foraminifera associated with the alga *Gelidium pristoides*, South Africa. African Invertebrates 46, 1-26.

Toumarkine, M., 1978. Planktonic foraminiferal biostratigraphy of the Paleogene of sites 360 to 364 and the Neogene of sites 362A, 363 and 364 Leg 40. In: Bolli, H.M., Ryan, W.B.F., McKnight, B.K., Kagami, H., Melguen, M., Siesser, W.G., Longoria, J.F., Decima, F.P., Foresman, J.B., Hottman, W.E, Natland, H. (Eds.). Leg 40; Cape Town, South Africa to Abidjan, Ivory Coast. Initial Reports of the Deep Sea Drilling Program 40, Washington D.C., U.S. Government Printing Office, 679-721.

Ujiié, Y., de Garidel-Thoron, T., Watanabe, S., Wiebe, P., de Vargas, C., 2010. Coiling dimorphism within a genetic type of the planktonic foraminifer Globorotalia

truncatulinoides. Marine Micropaleontology 77(3-4), 145-153.

Van Raden, U.J., Groeneveld, J., Raitzsch, M., Kucera, M., 2011. Mg/Ca in the planktonic foraminifera *Globorotalia inflata* and *Globigerinoides bulloides* from Western Mediterranean plankton tow and core top samples. Marine Micropalaeontology 78, 101-112.

Vance, D., Burton, K., 1999. Neodymium isotopes in planktonic foraminifera: a record of the response of continental weathering and ocean circulation rates to climate change. Earth and Planetary Science Letters 173, 365-379.

Vincent, E., Berger W.H., 1981. Planktonic foraminifera and their use in Paleoceanography. In: Emiliani, C. (Ed.), The oceanic lithosphere. The sea. Wiley-Interscience Hoboken, pp. 1025-1119.

Von Koslowski, R., 2017. Glacial-interglacial variations of the water masses in the southeast Atlantic Ocean derived from foraminiferal neodymium isotope ratios. Unpublished Master's thesis, University of Cape Town, 75 pp.

Weeks, S.J., Shillington, F.A., 1994. Interannual scales of variation of pigment concentrations from coastal zone color scanner data in the Benguela Upwelling system and the Subtropical Convergence zone south of Africa. Journal of Geophysical Research: Oceans 99(C4), 7385-7399.

Wefer, G., Berger, W.H., Bijma, J., Fischer, G. 1999. Clues to ocean history: a brief overview of proxies. In: Fischer, G and Wefer, G., (Eds.) Use of Proxies in Palaeoceanography: Examples from the South Atlantic. Springer-Verlag, Berlin, pp 1-68.

Wefer, G., Berger, W.H., Richter, C., Adams, D.D., Anderon, L.D., Andreasen, D.J., Brüchert, V., Cambray, H., Christensen, B.A., Frost, G.M., Giraudeau., Gorgas, T.J., Hermelin, O., Lange, C.B., Laser, B., Lin, H-L., Maslin, M., Meyers, P.A., Motoyama, I., Murray, R.W., Pato, D., Perez, M.E., Pufahl, P.K., Spiess, V., Vidal. L., Wigley, R., Yamazaki, T., 1998. Proceedings of the Ocean Drilling Program volume 175, 385-428.

Weinmann, A.E., Rödder, D., Lötters, S., Langer, M.R., 2013. Traveling through time: The past, present and future biogeographic range of the invasive foraminifera Amphistegina spp. in the Mediterranean Sea. Marine Micropaleontology 105, 30-39.

Wigley, R., Compton, J.S., 2006. Late Cenozoic evolution of the outer continental shelf at the head of the Cape Canyon, South Africa. Marine Geology 226, 1-23.

Wright, J.D., Miller, K.G., Fairbanks, R.G. 1992. Early and middle Miocene stable isotopes: implications for deepwater circulation and climate. Paleoceanography 7(3), 357-389.

Chapter 2

Regional Setting

2. Regional Setting

2.1 Location and core selection

Cores from the Namibian shelf and the western South African slope were investigated for the aim and objectives of this thesis. Four vibracores from the northern Namibian shelf south of the Kunene River mouth and sixteen vibracores from the central Namibian shelf between Walvis Bay and Lüderitz were analysed (Table 2.1; Fig. 2.1). These cores were studied as part of a phosphorite exploration project made possible by Minemakers Pty. Ltd. Outer shelf cores from the Namibian margin were not available prior to phosphate exploration along the Namibian margin. Western South African outer shelf cores were studied previously (Compton et al 2002, 2004; Wigley and Compton, 2006, 2007; Herbert and Compton, 2007), but Namibian outer shelf records received less attention in the past. The selection of such a large number of shelf cores makes the sample size larger as the sediments along the southwestern shelf of southern Africa are discontinuous, condensed and the stratigraphy is not entirely preserved in some areas (Wigley and Compton, 2006). From the multiple shelf cores four were selected from the northern Namibian shelf for further analyses and five from the central Namibian shelf. These cores were selected based on the completeness of their stratigraphy (chapters 4, 5 and 6). Photographs of the northern Namibian cores were first studied to assess the stratigraphy of the cores before the four were selected. Thereafter, the cores were logged and processed for sampling and analyses.

In contrast to the larger number of cores selected from the shelf, only three gravity cores at different water depths were chosen from the western slope of South Africa in the eastern South Atlantic (eastern slope of the Cape Basin). The gravity cores preserve a longer record and are more continuous compared to the shelf cores (Compton and Bergh, 2016). Therefore only three cores were selected from the western continental slope of South Africa.The two deeper water cores also provide an opportunity for any differences to be observed in the record or to confirm faunal occurrences and deep water conditions.

Foraminifera from the Namibian slope have been studied by Schmiedl and Mackensen (1997), Schmiedl et al. (1997) and Bickert and Mackensen (2003) to a larger degree compared to the South African western slope. Apart from the reports from ODP records (Wefer et al., 1998), only planktic foraminifera from three slope cores from the western margin of South Africa were studied by Rau (2002) and Rau et al. (2002). For these reasons, and for the reason that the Namibian margin and the Western margin of South Africa are influenced by the Benguela Upwelling System (BUS), shelf cores were selected from the Namibian margin and slope cores were selected from the western margin of South Africa.

Table 2.1. Water depth and location coordinates of cores studied and analysed in this project. Locations are illustrated on the locality map (Fig. 2.1). VC = vibracore; GC = gravity core

Core number	Core type	Location	Water depth (mbsl)	Latitude (S)	Longitude (E)
MMC 2634	VC	Namibian shelf	142	19°36'23"	12°21'24"
MMC 2658	VC	Namibian shelf	211	19°25'22"	12°11'44"
MMC 2670	VC	Namibian shelf	219	19°21'00"	12°09'04"
MMC 2682	VC	Namibian shelf	229	19°12'14"	12°03'45"
BON 1307	VC	Namibian shelf	199	24°09'46"	14°01'28"
BON 1364	VC	Namibian shelf	199	24°10'52"	14°01'27"
BON 1657	VC	Namibian shelf	200	24°10'31"	14°01'13"
BON 1397	VC	Namibian shelf	200	24°11'20"	14°00'14"
BON 1313	VC	Namibian shelf	205	24°09'46"	14°00'46"
BON 1384	VC	Namibian shelf	206	24°11'07"	14°00'31"
BON 1441	VC	Namibian shelf	223	24°10'33"	13°58'24"
BON 1442	VC	Namibian shelf	231	24°10'33"	13°57'27"
BON 1478	VC	Namibian shelf	241	24°10'34"	13°56'31"
BON 1401	VC	Namibian shelf	244	24°32'14"	13°53'28"
BON 1479	VC	Namibian shelf	245	24°10'33"	13°55'34"
BON 1404	VC	Namibian shelf	285	24°32'12"	13°50'38"
BON 1407	VC	Namibian shelf	291	24°34'21"	13°49'39"
BON 1405	VC	Namibian shelf	297	24°32'11"	13°49'41"
BON 1408	VC	Namibian shelf	303	24°34'21"	13°48'44"
GeoB 20601-4	GC	Western SA slope	874	31° 59'47"	15°58'11"
GeoB 8342-6	GC	Western SA slope	3522	31°18'00"	13°00'01"
GeoB 8336-6	GC	Western SA slope	3631	29°12'35"	12°20'38"

2.2. Geology and Bathymetry of Study Area

The southwestern margin of Africa is divided into the Equatorial West African and Southwest African margins by the Walvis Ridge (Sérame and Anka, 2005). The divergent continental margin off southwestern Africa is situated between two major crustal lineaments namely the modern Walvis Ridge and the Agulhas Fracture Zone (Dingle, 1992; Fig. 2.1).

The inner shelf is characterised by Late Proterozoic to Palaeozoic aged graywackes, granites and sandstones. Cretaceous to Tertiary aged strata onlap onto the seaward edge of the inner shelf (Stevenson and McMillan, 2004). The Cretaceous break-up of Africa from South America resulted in the infilling of rift valleys by lava and continental detritus followed by anoxic marine sedimentation. Large marine delta fans accumulated along the Orange River and in the bight of the Walvis Ridge during the Cretaceous to Oligocene (Dingle, 1992).

Palaeogene outcrops on the seafloor consist of bluish-green clays and overlying littoral, yellow sands, green clays and pebble beds (Dale and McMillan, 1999). Authigenic and biogenic sedimentation dominates over terrigenous sedimentation during the late Cenozoic. Large-scale erosion took place during the late Cenozoic as sediment starvation led to lower accumulation rates on the continental shelf (Dingle, 1992). Neogene beds that outcrop across the outer shelf

are dominated by early to middle Miocene carbonate-rich biogenic mud and limestone. The Quaternary is largely characterised by phosphorite and biogenic sediments on the shelf (Compton et al., 2002; Compton and Bergh, 2016) and foraminiferal-nannofossil rich sediments on the slope (Wefer et al., 1998).

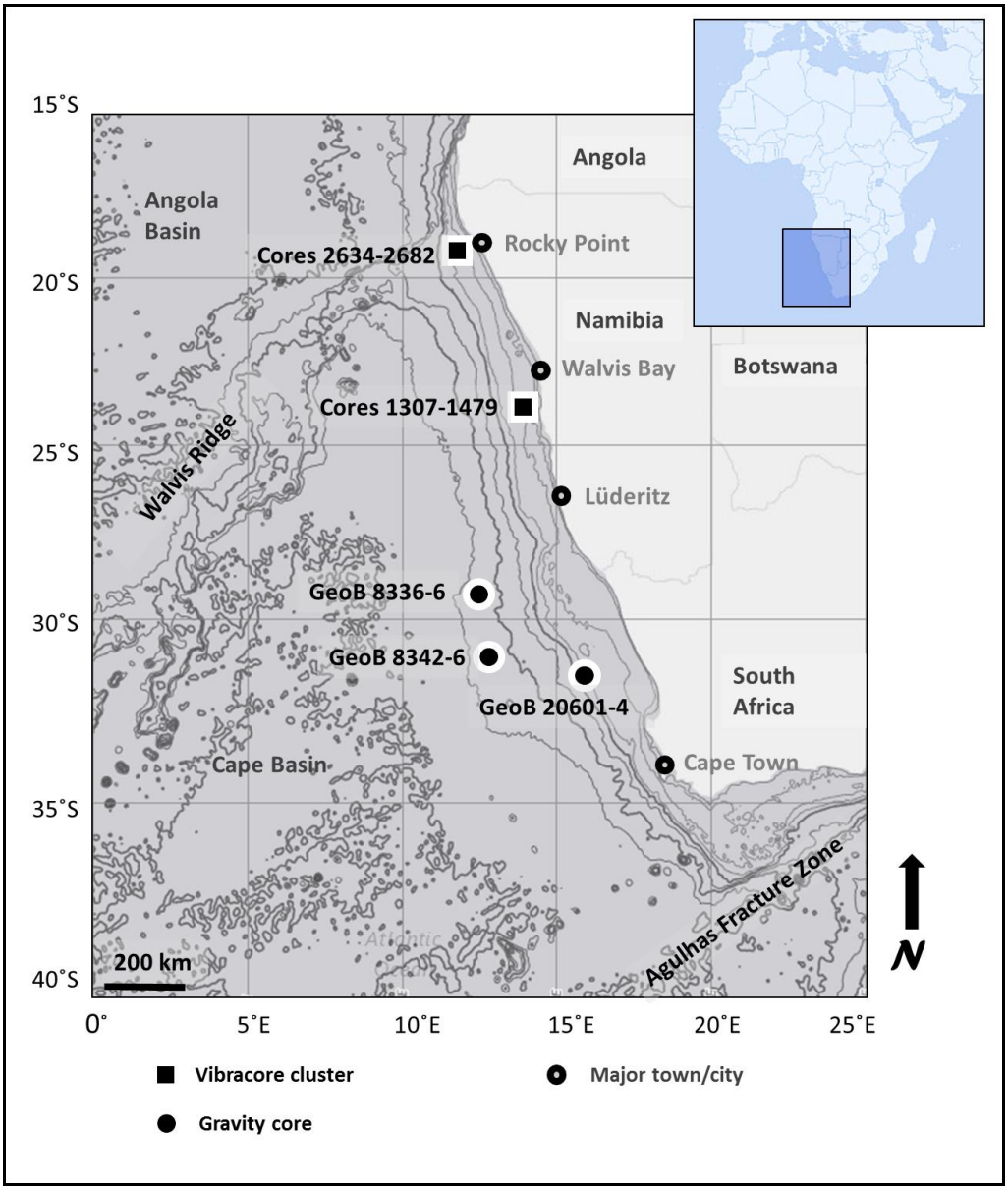

Fig. 2.1. Bathymetric map of the western margin of southern Africa showing the location of the cores studied in this project. The basemap is from the National Oceanic and Atmospheric Administration (NOAA) Bathymetric Data Viewer. Contours are spaced at 100 m intervals up to 500 m on the shelf. Thereafter contour lines are spaced at 1000 m.

The shelf along the southwestern margin of Africa is relatively broad and deep, and can be divided into the inner shelf which is 0 to 130 m in water depth, the middle shelf between 130 to 200 m and the outer shelf between 200 and 400 to 500 m water depth (Rogers, 1977). The inner shelf is distinguished from the outer shelf by a wave-cut terrace formed during sea-level lowstands. The

middle shelf has a lower gradient than the inner shelf and the outer shelf steepens to 400 m where it is marked by the shelf break where the gradient increases into the upper slope (Compton and Bergh, 2016). The abyssal depths feature the Cape Basin in the southeast Atlantic south of the Walvis Ridge extending to the west of southwestern South Africa and the Angola Basin to the north of the Walvis Ridge (Bornhold, 1973; Noël and Melguen, 1978; Sérame and Anka, 2005).

The upper layers of the slope (below 500 m) are dominated by Pliocene to Holocene sediments and are composed primarily of olive-gray to greenish gray foraminifer-nannofossil ooze (Pufahl et al., 1998; Rau et al., 2002) that are moderately bioturbated and intercalated (Pufahl et al., 1998). Detrital components from slope sediments include quartz grains (Pufahl et al., 1998; Compton and Wiltshire, 2009), glauconite (Compton and Wiltshire, 2009) and trace amounts of silt-sized pyrite aggregates or framboids, apatite, rutile and titanite (Pufahl et al., 1998).

Pelagic settling of biogenic material to the seafloor dominates the sedimentation of the Cape Basin. Deposition has been continuous since the middle Miocene with very few breaks in sedimentation (Pufahl et al., 1998). Sedimentation along the continental slope is variable and has been recorded as being as high as >10 cm/kyr (Giraudeau et al., 1998). Sedimentation rates during the Plio-Pleistocene were determined to be 16.7±0.2 to 22.5±3.5 cm/kyr on the continental slope between Walvis Bay and Lüderitz (Brüchert et al., 2000) and 15-20 cm/kyr south of the Agulhas Retroflection Area (Kuhn and Diekmann, 2002; and references therein). Vidal et al., (1999) measured sedimentation rates of 8 cm/kyr for the late Pleistocene at the Walvis Ridge and for the Holocene mudbelt off the Orange River mouth Leduc et al. (2010) determined sedimentation rates to be between 4.7 to 4.8 cm/kyr. Compton and Wiltshire (2009) determined sedimentation rates to be between 1.0 and 4.4 cm/kyr along the southwestern slope of South Africa.

2.3. Surficial Sediments

The thickness of sedimentary successions along the margin is unevenly distributed with the Orange and Kunene rivers supplying a terrigenous influx of sediment onto the margin (Sérame and Anka, 2005). The shelf and upper slope from the Kunene River to the eastern Agulhas Bank are characterised by terrigenous, authigenic and biogenic surficial sediments. Terrigenous sediments on the shelf and upper slope are sourced from windblown dust and river outflow into the ocean, mainly from Africa, but minor contributions are from distant sources such as South America and Antarctica. Sediments from distant sources reach the area through suspension by Antarctic Intermediate Water (AAIW), North Atlantic Deep Water (NADW) and surface currents. Clay mineral compositions along the margin typically include smectite, illite, kaolinite and chlorite (Kuhn and Diekmann, 2002).

Authigenic sediments result from the remineralisation of components on the seafloor. The biogenic sediments result from the flux of the remains of organisms from the surface waters to the seafloor with foraminifera being a dominant component (Rogers and Bremner, 1991; Compton and Wiltshire, 2009).

The middle to outer shelf is characterised by Pleistocene to Holocene phosphorite and biogenic-rich sediments of approximately 1 m thickness. The biogenic components include foraminifera,

ostracods, mollusc shells, bryozoan fragments, cetacean bone, fish scales and fish bone fragments (Compton and Bergh, 2016). Compton et al. (2002) suggest an initial phosphogenesis episode to have started in the latest Oligocene/earliest Miocene. Phosphorite formation started in the late Miocene along the Namibian shelf with more major phosphogenic episodes in the Plio-Pleistocene. The phosphorite deposits of the Namibian continental shelf have also been found to be larger than the South African deposits covering an area of more than 24 000 km^2. The large nature of phosphorite formation is mainly due to the high productivity levels of the BUS. Phosphorous delivered to the surface through coastal upwelling is taken up by primary producers and delivered to the ocean floor as organic P. The organic P is released by microbial degradation and further concentrated by bacteria. This created the conditions for francolite formation. These supersaturation conditions over large areas concentrated phosphorite formation over such an extensive area (Compton and Bergh, 2016).

The inner shelf is characterised by an approximately 15 m thick Holocene mud belt off the Namibian coast between 50 m and 140 m (Bremner, 1977) and is similar to the Holocene mud belt along the western inner shelf of South Africa (Herbert and Compton, 2007). These mud belts are fed by the Kunene (Bremner, 1977) and Orange rivers (Herbert and Compton, 2007), respectively. In contrast to the thin phosphorite-rich sediments of the outer shelf and the Holocene mud belt on the inner shelf, the upper slope sediments are 400 to 600 m in thickness and rich in foraminifera, nannofossils and diatoms (Wefer et al., 1998).

2.4. Deep water masses

The bottom water masses of the South Atlantic are sourced from the North Atlantic, the Weddell Sea and the Antarctic Circumpolar Current (Piepgras and Wasserburg, 1982; Reid, 1989; Rahmstorf, 2002). These water masses are characterised by different densities, temperature, salinities, oxygen and nutrient contents (Reid et al., 1977; Reid, 1989; Fig. 2.2) which have been attributed to the different source regions and mixing of water masses along their flowpaths (Reid et al., 1977). The Antarctic Bottom Water (AABW), which is sourced from the Weddell Sea, flows northwards and is the densest, coldest (<0˚C) and deepest water mass in the Cape Basin. The production of AABW is closely tied to changes around the Antarctic shelf ice. The surface waters forming around the Antarctic shelf are sufficiently dense to sink. The shelf waters descend over the continental shelf and the resulting AABW flows northward (Stramma and England, 1999) below 4 500 m water depth. Above the AABW the Lower Circumpolar Deep Water (LCDW) flows up to a depth of 4000 m. The LCDW is composed of a mixture of waters from the Weddell Sea, North Atlantic, Pacific and Indian oceans. The temperatures of LCDW range between 0.1˚C and 2.0˚C. Together with the AABW, the LCDW is also referred to as Southern Component Water (SCW). The northwards flow of these currents transport heat from the Southern Ocean to the North Atlantic (Kuhlbrodt et al., 2007). The SCW is largely restricted by the Mid-Atlantic Ridge to the west of the Cape Basin and the Walvis Ridge to the north with only small quantities of the LCDW passing through sills and the Walvis Passage (Bickert and Mackensen, 2003; and references therein).

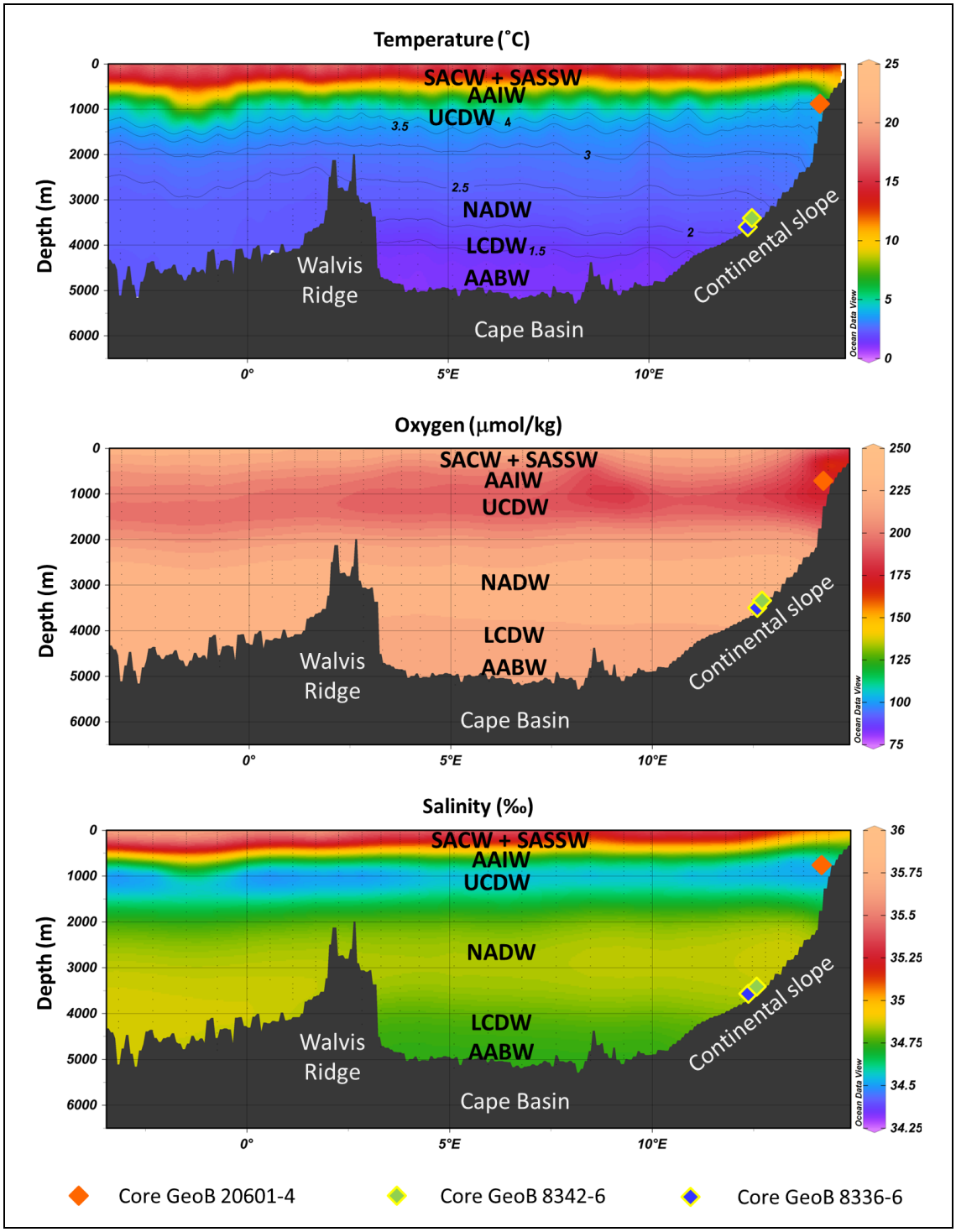

Fig. 2.2 Temperature, oxygen and salinity profile of water masses in the southeast Atlantic at 30˚S latitude. AABW = Antarctic Bottom Waters; LCDW = Lower Circumpolar Deep Waters; NADW = North Atlantic Deep Waters; AAIW = Antarctic Intermediate Waters; SACW = South Atlantic Central Water; SASSW = South Atlantic Subtropical Surface Water. Data used for the sections were based on references cited in the text and from the CARINA (CARbon IN the Atlantic) project (Key et al., 2009). Sections were created in Ocean Data View (Schlitzer, 2018).

Although the SCW is relatively high in oxygen, the overlying NADW is more enriched in oxygen (Fig. 2.2). The oxygen content of the AABW decreases along its flowpath away from the source region (Gordon, 1966).

In contrast to the Cape Basin, the lower depths of the Angola Basin are predominantly filled with North Atlantic Deep Water (NADW) (Reid, 1989) which forms around the Greenland and Norwegian Seas in the North Atlantic (Gordon, 2009). Compared to the SCW, the NADW is also more saline (Fig. 2.2), but lower in nutrients and silicate concentrations. The NADW mixes with additional water masses from the North Atlantic to produce a slightly warmer (>1˚C) water mass (Gordon, 2009). The NADW flows southwards at depths below 1 500 m (Rutberg et al., 2000) and overlies the denser SCW south of 40˚N (Gordon, 2009). Cores GeoB 8342-6 (3532 m) and 8336-6 (3631 m) are located at water depths at which the modern-day NADW flows. At ~45˚S, the relatively warm and saline North Atlantic Deep Water (NADW) divides the northward flowing Circumpolar Deep Water (CPW) into the LCDW and the Upper Circumpolar Deep Water (UCDW) (Reid et al., 1977).

Above the NADW the UCDW mass flows between 1000 and 1500 m. The CDW is within the density range of the NADW, but has lower salinity and oxygen ranges (Reid et al., 1977; Fig. 2.2). Upwelled CDW advects northwards where it sinks at the Subantarctic Front (SAF) forming Antarctic Intermediate Water (AAIW) which also flows northwards (Stramma and England, 1999). The AAIW flows between 500 and 1000 m water depth (Reid, 1989) and currently occupies the main thermocline across the Southern Hemisphere and part of the Northern Hemisphere (Lynch-Stieglitz et al., 1994). The AAIW is also oxygen-poor in relation to NADW and AABW. Core 20601-4 is located within an oxygen-poor region at a depth at which the AAIW flows (Fig. 2.2). Intermediate waters are fed into the southeast Atlantic through Agulhas Current leakage (Stramma and England, 1999). The AAIW is lower in salinity compared to the water masses below it (Reid et al., 1977). As the AAIW flows northwards it contributes to the production of NADW in the Northern Hemisphere (Broecker and Takahashi, 1981), but on its flow path it is prone to modification from the NADW (Hu et al., 2016). Core GeoB 20601-4 is located at a water depth (874 m) at which the AAIW flows.

Above the AAIW the South Atlantic Central Water (SACW) flows at 200 to 500 m water depth and is warmer and more oxygenated compared to the underlying AAIW (Stramma and England, 1999; Fig. 2.2). Together with the South Atlantic Subtropical Surface Water (SASSW) at <200 m, the SACW form the uppermost water masses of the Cape Basin (Emery and Meincke, 1986; Reid, 1989; Stramma and Peterson, 1990).

2.5. Benguela Current and the Benguela Upwelling System (BUS)

The Benguela Current forms the eastern limb of the South Atlantic subtropical gyre (Lutjeharms and Meeuwis, 1987; Shannon et al., 1990; Stramma and Peterson, 1990; Peterson and Stramma, 1991). This northward flowing current influences the oceanography of the margin along Namibia and western South Africa, and is divided into the inner Benguela Coastal Current (BCC) and the outer Benguela Oceanic Current (BOC) at around 28°S (Gorgas and Wilkens, 2002). The prevailing southerly winds drive the major coastal upwelling of cold, nutrient-rich waters along the

margin of Namibia and South Africa (Shannon, 1985).

The BCC is separated from the South Atlantic Gyre where South Atlantic Central Water (SACW), which is sourced from the Subtropical Convergence Zone, is upwelled into the BUS. Through the action of prevailing winds, waters from a depth of approximately 200 m (Hart and Currie, 1960; Shannon, 1985) are welled up to the surface (Shannon, 1985) to form cold nutrient-rich waters (Shannon, 1985; Lutjeharms and Stockton, 1987). Anticyclonic eddies feature at the Agulhas retroflection to the south of the Agulhas Current (Shannon, 1985).

The expansion of Antarctic ice sheets during the middle to late Miocene promoted the supply of cool intermediate waters to mid-latitude surface waters which decreased moisture levels in the atmosphere (Flower and Kennett, 1994). This middle to late Miocene ocean-atmosphere reconfiguration contributed to the initiation of the Benguela Upwelling System (BUS) during the late Miocene (Siesser, 1980). The strengthening of upwelling along the margin at ~10.5 Ma has been associated with a northward shift of the Benguela Current (Diester-Haass et al., 1990, 1992) and the Angola-Benguela Front (ABF) since the middle to late Miocene (Hoetzel et al., 2017).

Today, the BUS is one of four major upwelling systems in the world and stretches from Cape Agulhas (35°S) in the south to Cape Frio at 18°S in the north (Nelson and Hutchings, 1983). The system is driven by south-east trade winds with upwelling occurring along the shelf at 16 to 34°S. The BUS is bounded to the north and south by warm tropical to subtropical currents namely the Angola and Agulhas currents, respectively (Lett et al., 2007). The Northern Benguela Region (NBR) receives perennial upwelling stretching from the ABF to the Lüderitz cell and Orange River mouth off the Namibia-South Africa border (Lett et al., 2007; and references therein). The Southern Benguela Region (SBR) which stretches along the western coast of South Africa receives seasonal upwelling during spring and summer (Lutjeharms and Meeuwis, 1987).

References

Bickert, T., Mackensen, A., 2003. Last Glacial to Holocene changes in South Atlantic deep water circulation. In: The South Atlantic in the Late Quaternary. Springer, Berlin, Heidelberg, pp. 671-693.

Bornhold, B.D., 1973. Late Quaternary sedimentation in the eastern Angola Basin, PhD dissertation, Woods Hole Oceanographic Institution.

Bremner, J.M., 1977. Sediments on the continental margin off Southwest Africa between Sylvia Hill and the Kunene River. Unpublished PhD thesis, University of Cape Town.

Broecker, W.S., Takahashi, T., 1981. Hydrography of the central Atlantic—IV. Intermediate waters of Antarctic origin. Deep Sea Research Part A. Oceanographic Research Papers 28(3), 177-193.

Brüchert, V., Perez, M.E., Lange, C.B., 2000. Coupled primary production, benthic foraminiferal assemblage, and sulfur diagenesis in organic-rich sediments of the Benguela upwelling system. Marine Geology 163, 27-40.

Compton, J.S., Bergh, E.W., 2016. Phosphorite deposits on the Namibian shelf. Marine Geology 380, 290-314.

Compton, J.S., Malubisana, J., McMillan, I.K., 2002. Origin and age of phosphorite from the Last Glacial Maximum to Holocene transgressive succession off the Orange River, South Africa. Marine Geology 186, 243-261.

Compton, J.S., Wigley, R., McMillan, I.K., 2004. Late Cenozoic phosphogenesis on the western shelf of South Africa in the vicinity of the Cape Canyon. Marine Geology 206, 19-40.

Compton, J.S., Wiltshire, J.G., 2009. Terrigenous sediment export from the western margin of South Africa on glacial to interglacial cycles. Marine Geology 266, 212-222.

Dale, D.C., McMillan, I.K., 1999. How do microscopic fossils help diamond exploration? Earthyear: The Essential Environmental Guide 20, 114-115.

Diester-Haass, L., Meyers, P.A., Rothe, P., 1990. Miocene history of the Benguela Current and Antarctic ice volumes: Evidence from rhythmic sedimentation and current growth across the Walvis Ridge (Deep Sea Drilling Project Sites 362 and 532). Paleoceanography and Paleoclimatology 5(5), 685-707.

Diester-Haass, L., Meyers, P.A., Rothe, P., 1992. The Benguela Current and associated upwelling on the southwest African Margin: a synthesis of the Neogene-Quaternary sedimentary record at DSDP sites 362 and 532. Geological Society, London, Special Publications 64, 331-342.

Dingle, R.V., 1992. Structural and sedimentary development of the continental margin off southwestern Africa. Communications of the Geological Survey of Namibia 8, 35-43.

Emery, W.J., Meincke, J., 1986. Global water masses-summary and review. Oceanologica Acta 9, 383-391.

Flower, B.P., Kennett, J.P., 1994. The middle Miocene climatic transition: East Antarctic ice sheet development, deep ocean circulation and global carbon cycling. Palaeogeography, Palaeoclimatology, Palaeoecology 108, 537-555.

Giraudeau, J., Christensen, B.A., Hermelin, O., Lange, C.B., Motoyama, I., Shipboard Scientific Party., 1998. 19. biostratigraphic age models and sedimentation rates along the southwest african margin. In: Proceedings Ocean Drilling Program, Initial Reports 175, pp. 543-546.

Gordon, A.L., 1966. Potential temperature, oxygen and circulation of bottom water in the Southern Ocean. In: Deep Sea Research and Oceanographic Abstracts, vol. 13, no. 6, pp. 1125-1138.

Gordon, A.L., 2009. Bottom water formation. Ocean Currents, 263-269.

Gorgas, T.J., Wilkens, R.H., 2002. Sedimentation rates of SW Africa since the late Miocene deciphered from spectral analyses of borehole and GRA bulk density profiles: ODP Sites 1081-1084. Marine Geology 180, 29-47.

Hart, T.J., Currie, R.I. 1960. The Benguela Current. Discovery Reports 31, 123-297.

Herbert, C.T., Compton, J.S., 2007. Geochronology of Holocene sediments on the western margin of South Africa. South African Journal of Geology 110, 327-338.

Hoetzel, S., Dupont, L.M., Marret, F., Jung, G., Wefer, G., 2017. Steps in the intensification of Benguela upwelling over the Walvis Ridge during Miocene and Pliocene. International Journal of Earth Sciences 106, 171-183.

Hu, R., Noble, T.L., Piotrowski, A.M., McCave, I.N., Bostock, H.C., Neil, H.L., 2016. Neodymium isotopic evidence for linked changes in Southeast Atlantic and Southwest Pacific circulation over the last 200 kyr. Earth and Planetary Science Letters 455, 106-114.

Key, R.M., Tanhua, T., Olsen, A., Hoppema, M., Jutterström, S., Schirnick, C., Van Heuven, S., Lin, X., Wallace, D.W., Mintrop, L., 2009. The CARINA data synthesis project: introduction and overview. Earth System Science Data 2, 105-121.

Kuhlbrodt, T., Griesel, A., Montoya, M., Levermann, A., Hofmann, M., Rahmstorf, S., 2007. On the driving processes of the Atlantic meridional overturning circulation. Reviews of Geophysics, 45(2), doi:10.1029/2004RG000166.

Kuhn, G., Diekmann, B., 2002. Late Quaternary variability of ocean circulation in the southeastern South Atlantic inferred from the terrigenous sediment record of a drift deposit in the southern Cape Basin (ODP Site 1089). Palaeogeography, Palaeoclimatology, Palaeoecology 182, 287-303.

Leduc, G., Herbert, C.T., Blanz, T., Martinez, P., Schneider, R., 2010. Contrasting evolution of sea surface temperature in the Benguela upwelling system under natural and anthropogenic climate forcings. Geophysical Research Letters, 37(20), doi:10.1029/2010GL044353.

Lett, C., Veitch, J., van der Lingen, C.D., Hutchings, L., 2007. Assessment of an environmental barrier to transport of ichthyoplankton from the southern to the northern Benguela ecosystems. Marine Ecology Progress Series 347, 247-260.

Lutjeharms, J.R.E., Meeuwis, J.M., 1987. Extent and variability of SE Atlantic upwelling. In: Payne, A.I.L., Gulland, J.A., Brink, K.H. (Eds.), The Benguela and Comparable Ecosystems. South African Journal of Marine Sciences 5, 51 – 62.

Lutjeharms, J.R.E., Stockton, P.L., 1987. Kinematics of the upwelling front off Southern Africa. In: Payne, A.I.L., Gulland, J.A and Brink, K.H. (Eds.), The Benguela and Comparable Ecosystems. South African Journal of Marine Science 5, 35-49.

Lynch-Stieglitz, J., Fairbanks, R.G., Charles, C.D., 1994. Glacial-interglacial history of Antarctic Intermediate Water: relative strengths of Antarctic versus Indian Ocean sources. Paleoceanography and Paleoclimatology 9(1), 7-29.

Nelson, G., Hutchings, L., 1983. The Benguela upwelling area. Progress in Oceanography 12, 333-356.

Noël, D., Melguen, M., 1978. Nannofacies of cape basin nd walvis ridge sediments, lower Cretaceous to Pliocene (leg 40). Initial Reports of the Deep Sea Drilling Project 60, 473-510.

Peterson, R., Stramma, L., 1991. Upper-level circulation in the South Atlantic. Progress in Oceanography 26, 1-73.

Piepgras, D.J., Wasserburg, G.J., 1982. Isotopic composition of neodymium in waters from the Drake Passage. Science 217, 207–217.

Pufahl, P.K., Maslin, M.A., Anderson, L., Brüchert, V., Jansen, F., Lin, H., Vidal, L., 1998. Lithostratigraphic summary for Leg 175: Angola-Benguela upwelling system. In: Wefer, G., Berger, W.H., Richter, C. (Eds.) Proceedings of the Ocean Drilling Program 175, pp. 532-544.

Rahmstorf, S., 2002. Ocean circulation and climate during the past 120,000 years. Nature 419, 207.

Rau, A.J., 2002. A late Quaternary history of Agulhas-Benguela interactions from two sediment cores on the western continental slope of South Africa. Unpublished PhD. University of Cape Town, 315 pp.

Rau, A. J., Rogers, J., Lutjeharms, J. R. E., Giraudeau, J., Lee-Thorp, J. A., Chen, M. T., Waelbroeck, C., 2002. A 450-kyr record of hydrological conditions on the western Agulhas Bank Slope, south of Africa. Marine Geology 180, 183-201.

Reid, J.L., 1989. On the total geostrophic circulation of the South Atlantic Ocean: Flow patterns, tracers, and transports. Progress in Oceanography 23, 149-244.

Reid, J.L., Nowlin, W.D., Patzert, W.C., 1977. On the characteristics and circulation of the southwestern Atlantic Ocean. Journal of Physical Oceanography 7(1), 62-91.

Rogers, J., 1977. Sedimentation on the continental margin off the Orange River and the Namib Desert.Unpublished PhD. thesis, University of Cape Town.

Rogers, J., Bremner, J.M., 1991. The Benguela Ecosystem. Part VII. Marine-geological aspects. In: Barnes, M (ed.). Oceanography and Marine Biology: Annual Review 29, 1-85.

Rutberg, R.L., Hemming, S.R., Goldstein, S.L., 2000. Reduced North Atlantic Deep Water flux to the glacial Southern Ocean inferred from neodymium isotope ratios. Nature 405, 935.

Schlitzer, R., 2018. Ocean Data View, odv.awi.de

Schmiedl, G., Mackensen, A., 1997. Late Quaternary paleoproductivity and deep water circulation in the eastern South Atlantic Ocean: Evidence from benthic foraminifera. Palaeogeography, Palaeoclimatology, Palaeoecology 130, 43-80.

Schmiedl, G., Mackensen, A., Müller, P.J., 1997. Recent benthic foraminifera from the eastern South Atlantic Ocean: dependence on food supply and water masses. Marine Micropaleontology 32, 249-287.

Sérame, M., Anka, Z., 2005. South Atlantic continental margins of Africa: a comparison of the tectonic vs. climate interplay on the evolution of equatorial west Africa and SW Africa margins. Journal of African Earth Sciences 43, 283-300.

Shannon, L.V., 1985. The Benguela ecosystem. I: Evolution of the Benguela physical features and processes. Oceanography and Marine Biology 23, 105-182.

Shannon, L.V., Agenbag, J.J., Walker, N.D., Lutjeharms, J.R.E., 1990. A major perturbation in the Agulhas retroflection area in 1986. Deep-Sea Research 37, 493–512.

Siesser, W.G., 1980. Late Miocene origin of the Benguela Upwelling System off Northern Namibia. Science 208 (4441), 283-285.

Stevenson, I.R., McMillan, I.K., 2004. Incised valley fill stratigraphy of the Upper Cretaceous succession, proximal Orange Basin, Atlantic margin of southern Africa. Journal of the Geological Society 161, 185-208.

Stramma, L., England, M., 1999. On the water masses and mean circulation of the South Atlantic Ocean. Journal of Geophysical Research: Oceans 104(C9), 20863-20883.

Stramma, L and Peterson, R.G. 1990. The South Atlantic Current. Journal of Physical Oceanography 20, 846-859.

Vidal, L., Schneider, R.R., Marchal, O., Bickert, T., Stocker, T.F., Wefer, G., 1999. Link between the North and South Atlantic during the Heinrich events of the last glacial period. Climate Dynamics 15, 12, 909-919.

Wefer, G., Berger, W.H., Richter, C., Adams, D.D., Anderon, L.D., Andreasen, D.J., Brüchert, V., Cambray, H., Christensen, B.A., Frost, G.M., Giraudeau., Gorgas, T.J., Hermelin, O., Lange, C.B., Laser, B., Lin, H-

L., Maslin, M., Meyers, P.A., Motoyama, I., Murray, R.W., Pato, D., Perez, M.E., Pufahl, P.K., Spiess, V., Vidal. L., Wigley, R., Yamazaki, T., 1998. Proceedings of the Ocean Drilling Program 175, 385-428.

Wigley, R., Compton, J.S., 2006. Late Cenozoic evolution of the outer continental shelf at the head of the Cape Canyon, South Africa. Marine Geology 226, 1-23.

Wigley, R., Compton, J.S., 2007. Oligocene to Holocene glauconite-phosphorite grains from the Head of the Cape Canyon on the western margin of South Africa. Deep-Sea Research Part II (54), 1375-1395.

Chapter 3

Phosphorite Deposits on the Namibian Shelf

Published article: Compton, J. S., Bergh, E.W. 2016. Phosphorite deposits on the Namibian shelf. Marine Geology 380, 290-314.

3. Phosphorite deposits on the Namibian shelf

John S. Compton[a], Eugene W. Bergh[a,b]

[a] Department of Geological Sciences and the Marine Research Institute, University of Cape Town, Rondebosch 7700, South Africa

[b] Natural History Department, Iziko Museums of South Africa, P.O. Box 61, Cape Town 8000, South Africa

Abstract

Phosphorite deposits provide a source of fertilizer to feed an increasingly populated world and they provide a record of paleoceanographic changes in upwelling systems linked to climate. The Benguela Upwelling System (BUS) is among the most productive today and is associated with major phosphorite deposits exposed over an area of 24,700 km^2 on the Namibian shelf. Analyses of cores associated with recent offshore mineral exploration provide new insights into the age and origin of these phosphorite deposits. The deposit consists of coarsening upward muddy to gravelly pelletal phosphorite sand, up to several meters thick, on the middle to outer shelf (190 and 350 m water depth) offshore of Lüderitz and Walvis Bay. Less extensive and less continuous deposits occur offshore of Walvis Bay as far north as the Kunene River mouth on the inner to middle shelf (50 and 250 m water depth). Pelletal phosphorite sand (some concentrically banded) and concretionary phosphorite pebbles are the dominant grain types consisting of up to 90 wt.% carbonate fluorapatite (francolite) cement and inclusions of organic matter, pyrite and terrigenous mud. Strontium isotope stratigraphy and foraminiferal biostratigraphy indicate that phosphogenesis was initiated in the latest Miocene but that most phosphorite formed in the Plio/Pleistocene during early burial diagenesis of organic-rich mud as it does today in the Holocene diatomaceous mud belt. The highly-condensed, coarsening-upward succession reflects increasingly high amplitude Pleistocene sea-level fluctuations. Phosphorite formation correlates to terrestrial aridification as well as to marine proxies of intensified coastal upwelling in the 600 m thick equivalent successions on the upper slope. Repeated phosphorite formation and reworking over Pleistocene glacial to interglacial cycles resulted in the economic concentration of phosphorite, with an estimated total resource of 7800 million tons of phosphate rock at an average grade of 19 wt.% P_2O_5 on the Namibian shelf.

3.1 Introduction

Phosphorite is a rock type rich in phosphorus (>18 wt.% P_2O_5). Phosphorus (P) in most marine phosphorite deposits occurs as phosphate (PO_4^{3-}) in the carbonate fluorapatite mineral francolite, which commonly contains >1 wt.% fluorine and 3–6 wt.% carbonate substituting for phosphate (Jarvis et al., 1994). Francolite typically occurs as cryptocrystalline, pore-filling or carbonate replacing cement in phosphorite sand to pebble sized grains, as well as bioskeletal bone and teeth.

Phosphorite represents a major long term sink of biologically active P from the oceans and is important to our understanding of how marine biological productivity has varied in the past and relates to changes in the global carbon and phosphorus cycles, as well as to changes in climate (Föllmi, 1996; Compton et al., 2000; Ruttenberg, 2003). In addition, P is a non-renewable resource in the production of fertilizer. Use of fertilizer to increase agricultural yield has been an important component of the 'Green Revolution' and has contributed to the doubling of human population since 1970 (Amundson et al., 2015). To date most P has been mined from large marine phosphorite deposits exposed on land through tectonic uplift and lowering of sea level (Notholt et al., 1989). Greater demand and higher prices, combined with advances in offshore mining technology, have increased exploration of potentially minable offshore phosphorite deposits.

The western margin of southern Africa is renowned for its phosphorite deposits, first described from dredged samples during the HMS Challenger Expedition (Murray and Renard, 1891). The full extent and richness of phosphorite on the margin was only confirmed much later by systematic seafloor sampling. Seafloor mapping was initially carried out by Russian oceanographers during expeditions in the early 1960s (Senin, 1970) and later by the marine geology group at the University of Cape Town and the geological survey (Summerhayes et al., 1973). Samples from these and later surveys formed the basis for early mapping of the sediment distribution of the continental margin of South Africa and Namibia (Birch, 1975; Bremner, 1977; Rogers, 1977; Baturin, 1982). These surveys revealed that the unconsolidated surface sediment included regions of unusually high P content (Fig. 3.1), particularly on the middle to outer shelf of Namibia where surface sediments contain >25 wt.% phosphorite and have bulk sediment grades of 17 to 24 wt.% P_2O_5 (Summerhayes et al., 1973).

There have been a number of studies on the petrography, mineralogy, chemistry and microbiology of phosphorite-rich deposits on the shelf (Baturin, 1969, 1982, 2000; Birch, 1975, 1979a,b,c, 1980, 1990; Bremner, 1977; Bremner and Rogers, 1990; Rogers, 1977; Compton et al., 2002, 2004;Wigley and Compton, 2006, 2007; Schulz and Schulz, 2005) (for a comprehensive review of the literature prior to 1990 refer to Rogers and Bremner (1991)). The phosphorite deposits offshore of South Africa are late Oligocene to Pleistocene in age based on biostratigraphy and strontium isotope stratigraphy (Compton et al., 2002, 2004). Holocene phosphorite from the diatomaceous mud belt is well established on the Namibian inner shelf (Bremner, 1977; Baturin, 1982, 2000), but the age and origin of the far more extensive phosphorite deposits on the Namibian middle to outer shelf are poorly known (Dingle et al., 1996).

Phosphorite and glauconite (potassium-rich, 'green sands') have been recent targets of offshore mineral exploration on the shelf (Coles et al., 2002). Cores recovered from these exploration programs have greatly increased our understanding of the subsurface extent and nature of the shelf phosphorite and glauconite deposits off South Africa (Wigley and Compton, 2006, 2007). This paper integrates unpublished and published studies on the phosphorite

deposits on the Namibian shelf to derive a more complete understanding of the extent, age and origin of these deposits. A model is proposed on how these economic phosphorite deposits formed and how their formation is possibly linked to paleoceanographic as well as climatic changes in southern Africa during the Quaternary.

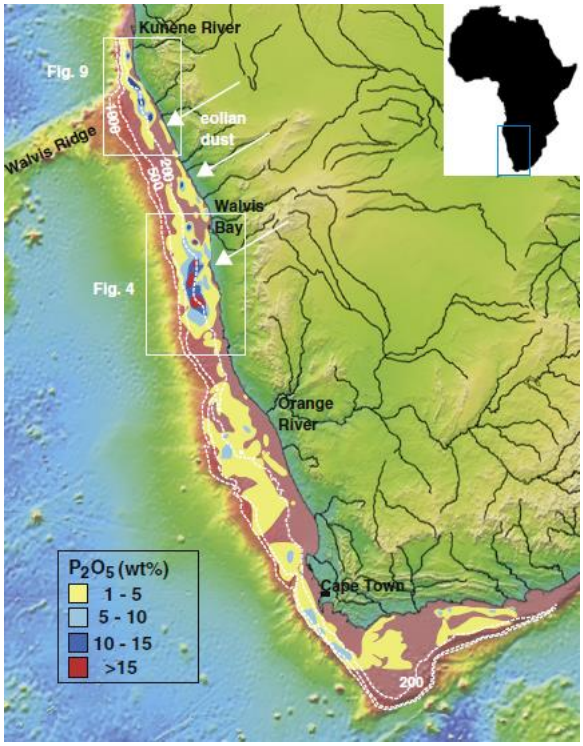

Fig. 3.1. The continental shelf of southern Africa (pink) and distribution of phosphorite deposits as indicated by bulk sediment P_2O_5 content (Birch, 1975; Bremner, 1977; Rogers, 1977). The richest deposits (>15 wt.% P_2O_5) occur on the Namibian shelf south of Walvis Bay.

3.2. Geological and oceanographic setting

The Namibian continental passive margin formed during the Cretaceous breakup of Gondwana. The margin has an unusually broad and deep shelf that extends to 400 m water depth (Fig. 3.1). The shelf can be divided into an inner, middle and outer shelf (Rogers, 1977). The inner shelf extends to approximately 130 m water depth where it is commonly marked by a wave cut terrace or notch formed when the inner shelf area of the margin was exposed during sea-level lowstands of glacial periods. The middle shelf is a relatively low gradient area that extends to approximately 200 m water depth. The outer shelf extends from 200 to 400 m water depth and has a steeper gradient than the middle shelf. The shelf break occurs between 400 and 500 m and is marked by the increased gradient of the upper slope.

Precambrian basement rocks are exposed on the rocky shoreline and extend onto the inner shelf, with seaward dipping reflectors further offshore on the shelf interpreted to be Cretaceous to Cenozoic deposits (Rogers, 1977). The Cenozoic succession on the shelf is relatively thin and poorly documented from several dredged samples of Neogene limestone and stiff clay (Bremner, 1977). The seaward dipping beds form an erosional surface which is variably overlain by Pleistocene to Recent (Holocene) sediment. The suspended mud fraction delivered by the Kunene River is transported by bottom water currents (the poleward undercurrent) along the margin to form the Holocene diatomaceous mud belt, a wedge of sediment up to 15 m thick that stretches along the Namibian inner shelf between water depths of 50 m and 140 m (Bremner, 1977). The Namibian mud belt is similar to the Holocene Orange River (Namaqualand) mud belt off South Africa (Herbert and Compton, 2007), but grades into an organic-rich, diatomaceous ooze south of the Kunene River. Surface currents along the western margin are complex and consist of seasonal equatorward drift, coastal filaments and Ekman drift (Shannon and Nelson, 1996).

All other rivers draining into the Atlantic Ocean between the Orange and Kunene rivers are

ephemeral and only episodically deliver sediment to the coast during floods. Although mostly dry, these ephemeral river beds and surrounding areas are sources of windblown sediment, particularly in regions north of the Namib Desert. A significant amount of terrigenous sediment is delivered to the shelf by wind, primarily during Berg wind conditions when air descends from the Great Escarpment and transports sediment offshore (Eckardt and Kuring, 2005). Inboard of the mud belt are coastal sands and gravels subject to periodic storms throughout the year having wave heights exceeding 5 m (Rossouw, 1984). The predominant swell direction is from the southwest and net longshore drift of coastal quartz-rich sand is to the north (Rogers, 1977; Bremner, 1977). Rather than accumulating on the shelf, most quartz sand ends up windblown onto land, feeding the Namib Sand Sea and most is ultimately sourced from the Orange River (Vermeesch et al., 2010).

Besides terrigenous sediment offshore of the Kunene River mouth, the middle to outer shelf is dominated by carbonate-rich sediments. Bottom currents and internal waves suspend and transport mud from the middle and outer shelf onto the upper slope (Monteiro et al., 2005; Inthorn et al., 2006; Compton and Wiltshire, 2009). The result is a mix of relict shelly gravel and foraminiferal sand on the middle to outer shelf that transitions into increasingly muddy nannofossil foraminiferal ooze on the upper slope. Highly condensed, relict phosphorite deposits are exposed on the middle shelf region between 130 and 400 m water depth and correspond to Plio/Pleistocene organic-rich, nannofossil and diatomaceous mud successions 400 to 600 m thick on the upper slope (Wefer et al., 1998a).

The Namibian margin occupies a classic eastern boundary setting with significant coastal upwelling associated with the Benguela Upwelling System (BUS) (Shannon and Nelson, 1996). The BUS extends along the western margin of southern Africa from Cape Town to the Kunene River mouth (Fig. 3.2). The Benguela Coastal and Benguela currents are distinct from the BUS, forming the eastern limb of the South Atlantic gyre and flow equatorward further offshore of the BUS. Seasonally strong, predominantly southerly winds drive the BUS through Ekman transport of surface waters away from the coast as they are replaced by deeper, nutrient-rich waters from below. The upwelling of nutrient-rich waters results in high productivity, with the BUS measured as one of the world's most productive eastern boundary upwelling systems (Carr, 2002; Carr and Kearns, 2003) that supports a large commercial sea fisheries industry. The intensity of the modern BUS varies along the margin and is greater off Namibia than South Africa (Carr, 2002).

3.3. Methods

Samples for this study include surface grab and dredge samples taken during early surveys (Bremner, 1977; Rogers, 1977), but most are from recent vibracores and gravity cores from offshore exploration companies. A total of 19 cores were described and analyzed in detail from the southern area offshore Lüderitz and Walvis Bay and compared to core logs of several hundred cores from the area. A total of 4 cores were described and analyzed in detail from the northern area off Rocky Point and compared to core logs and photos of an additional 38 cores

from the area. Cores were split, described and sampled for grain size analysis, petrography, biostratigraphy and strontium isotope stratigraphy. Bulk sediment samples were suspended in water, placed in an ultrasonic bath to disperse and wet sieved to separate the gravel (>2 mm), sand (0.063–2 mm) and coarse silt (38–63 μm) fractions. The fine silt (2–38 μm) and clay (<2 μm) fractions were separated by settling. The mineralogy and texture of silt to gravel sized grains were determined using a binocular microscope as well as from petrographic thin sections. The mineralogy of the clay-sized fraction was determined by X-ray diffraction (XRD). Bulk sediment and individual grains were observed using scanning electron microscopy.

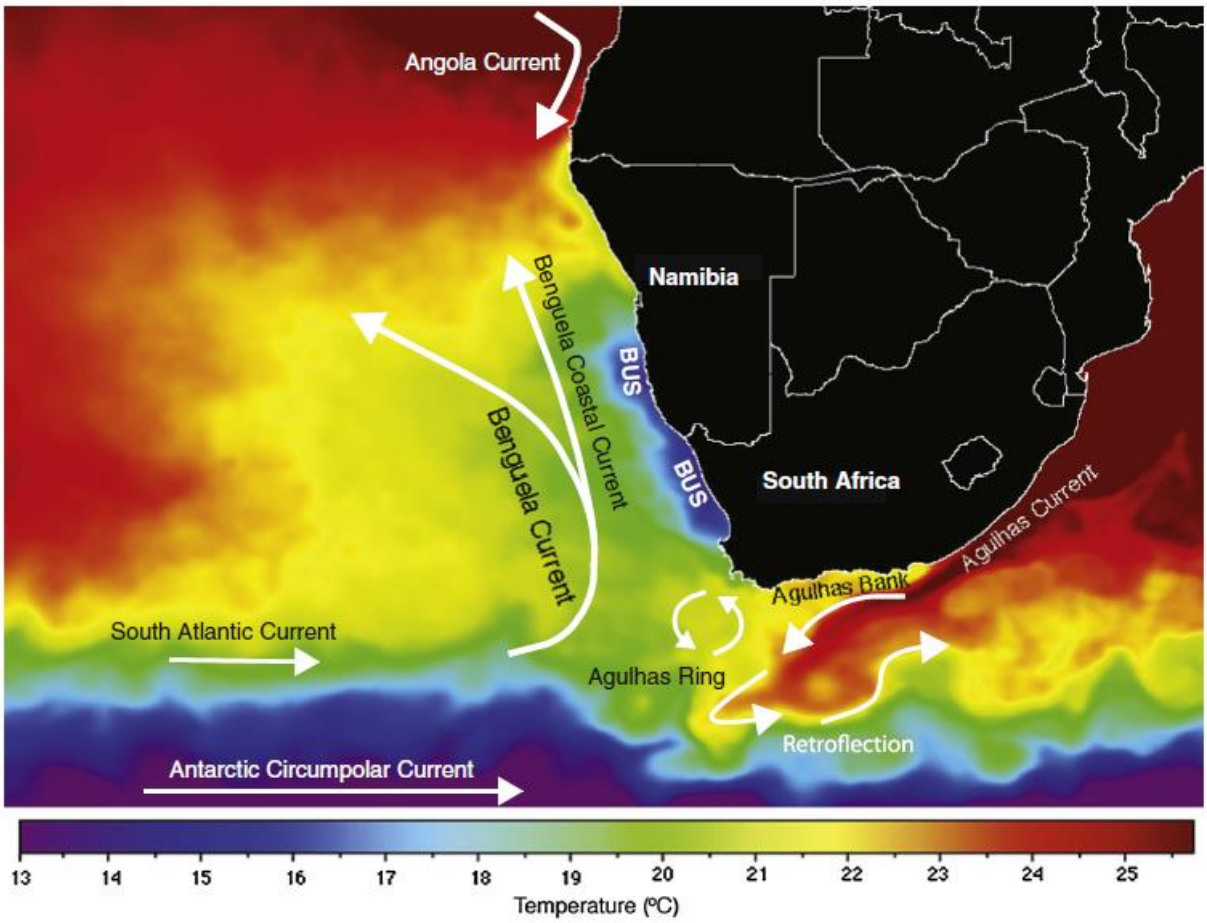

Fig. 3.2. Sea surface temperatures (3 February 2008; data from noc.ac.uk) reflect cold upwelled waters of the Benguela Upwelling System (BUS; dark blue); the Benguela Coastal and Benguela currents are part of the South Atlantic gyre, while the warm water Agulhas Current retroflects back into the Indian Ocean and sheds warm water rings into the South Atlantic.

Biostratigraphic ages are based on the foraminiferal assemblages described for the Miocene (Christison, 1985; Gawlinski, 1987), Pliocene (Dale and McMillan, 2000) and Pleistocene (McMillan, 1987, 1993; Dale and McMillan, 1998). Different grain types that included pelletal phosphorite grains, concretionary phosphorite pebbles, skeletal phosphorite (bone, teeth or scales), foraminifera and mollusc shell were handpicked from bulk

gravel and sand size material for strontium isotope stratigraphy (SIS). Grains were cleaned of all surface and interior sediment in an ultrasonic bath before dissolving in twice-distilled 5M acetic acid. Acetic acid was used for SIS analyses in order to minimize dissolution of other minerals by stronger (HCl) acid digestion (McArthur, 1994).

Strontium isotope ratios were measured at the University of Cape Town on a Nu Instrument multi collector mass spectrometer with mass fractionation normalized to an $^{86}Sr/^{88}Sr$ ratio of 0.1194 and to Standard Reference Material 987 $^{87}Sr/^{86}Sr$ ratio of 0.710255 using an in-house carbonate standard. Within-run precision on single measurements ranges from ±0.000009 to ±0.000017 (2σ error), whereas the long-term sample reproducibility averaged ±0.000023 (n=54) over the time frame of the measurements. The age of the samples was obtained from the Sr lookup table (V4B: 08/04) after subtracting 0.000007 to adjust for the SRM value of 0.710248 used in the Sr lookup table (Howarth and McArthur, 1997; McArthur et al., 2001). The range in ages given in Table 3.1 corresponds to the uncertainty in the measured Sr isotope values based on reproducibility of the standard (±0.000023) and the steepness of the marine Sr isotope curve (Fig. 3.3). The use of the Sr isotope composition to determine the age of phosphorite formation assumes that the Sr ratio reflects that of ambient seawater and that the Sr ratio has not altered since it was acquired during the diagenetic precipitation of francolite. Phosphorite grains, particularly concentrically banded pelletal phosphorite or large and texturally complex phosphorite pebbles, can have multiple generations of francolite cement. Therefore, the age ranges reported for multiple grain samples represent the average age of the sample.

3.4. Results

3.4.1. Stratigraphy of the southern phosphorite deposits

The area of the Namibian shelf having the highest phosphorite content (between 5 and 50 wt.% phosphorite) is located on the middle to outer shelf between 180 and 500 m water depth extending from 25.5°S offshore of Hottentot Bay (60 km north of Lüderitz) to 23°S offshore of Walvis Bay (Fig. 3.4). The 70–90 km wide deposit was independently determined by Russian (Senin, 1970) and South African (Summerhayes et al., 1973; Bremner, 1977; Rogers, 1977) surveys. The phosphorite-rich sediment trends north-south and the central, phosphorite-rich core of the deposit is defined by surface sediment having greater than 50 wt.% phosphorite (>15 wt.% P_2O_5). The deposit runs parallel to shore and partially overlaps with the modern Lüderitz upwelling cell of the BUS.

All cores from the southern area between Lüderitz and Walvis Bay exhibit a coarsening upward succession from basal mud to sandy mud to muddy sand to gravelly sand (Figs. 3.5 and 3.6). The basal mud (unit 5) is a dark olive gray (Munsell chart 5Y 3/2) clayey mud with only minor (0.1 to 9 wt.%) phosphorite sand, fecal pellets and skeletal material such as fish vertebra. The maximum recovery of the basal mud unit is 0.5 m. The basal mud unit varies from massive, mottled or laminated in structure. In places, the basal mud contains reworked biogenic grains (calcareous shells and foraminifera tests) of middle to late Miocene age (Fig. 3.5).

Table 3.1. Strontium isotope analyses and minimum and maximum ages.

Core	Sample (cm)	Sample description	87/86 Sr	2σ	Age min	Age max
1460	88–94	1 concretionary pebble	0.709141	13	0.5	1.4
1460	182–186	1 concretionary pebble	0.709167	11	0.0	1.1
1460	182–186	Skeletal grains (4 mm max)	0.709130	12	0.8	1.7
1460	182–186	Pelletal phosphorite (>250) etched	0.709122	14	1.0	1.9
1463	42–48	1 large skeletal bone	0.709166	15	0.0	1.1
1463	42–48	1 concretionary pebble	0.709125	15	0.9	1.8
1463	164–168	1 large vertebrate bone	0.709183	11	0.0	0.7
1463	164–168	Skeletal (bone, 6 mm max)	0.709120	15	1.1	1.9
1463	164–168	Pelletal phosphorite (<125)	0.709046	10	2.8	5.7
1463	164–168	Pelletal phosphorite (>500)	0.709042	15	3.1	5.7
1469	115–119	1 resinous phosphorite pebble	0.709161	13	0.0	1.2
1469	168–172	1 amber vertebra bone	0.709208	15	0.0	0.0
1469	168–172	1 tan concretionary pebble	0.709166	12	0.0	1.1
1469	171–175	Skeletal (amber vertebra, 5 mm max)	0.709168	10	0.0	1.1
1469	171–175	Pelletal phosphorite (>250)	0.709134	12	0.7	1.6
1469	185–189	1 concretionary pebble	0.709143	14	0.5	1.4
1408	0–4	Shell fragments (fresh)	0.709220	14	0.0	0.0
1408	0–4	1 concretionary pebble	0.709143	12	0.5	1.4
1408	0–4	Pelletal phosphorite (>250)	0.709136	14	0.7	1.5
1408	0–4	Pelletal phosphorite	0.709118	14	1.0	2.0
1408	26–30	Shell fragments	0.709163	12	0.0	1.1
1408	26–30	Pelletal phosphorite (>250)	0.709136	10	0.7	1.5
1408	26–30	4 phoshorite grains (3mm max)	0.709113	15	1.1	2.2
1408	26–30	Phosphorite pebble	0.709011	13	5.2	6.3
1408	30–32	Pelletal phosphorite	0.709121	11	1.1	1.9
1408	30–32	1 phosphorite pebble	0.709069	13	1.9	5.0
1408	37–39	1 concretionary pebble	0.709122	13	1.1	1.9
1408	37–39	8 phoshorite grains (3.5 mm max)	0.709115	12	1.2	1.9
1408	37–39	Shell fragments	0.709115	10	1.2	1.9
1408	37–39	Pelletal phosphorite (>250)	0.709084	13	1.5	4.2
1408	53–55	Pelletal phosphorite	0.709133	15	0.7	1.6
1408	55–57	Shell fragments	0.709177	11	0.0	0.9
1408	55–57	Skeletal phosphorite (amber)	0.709113	9	1.1	2.2
1408	55–57	Pelletal phosphorite (>250)	0.709101	13	1.3	2.6
1408	77–79	Pelletal phosphorite	0.709130	11	0.8	1.5
1408	99–101	Pelletal phosphorite	0.709152	10	0.2	1.3
1408	99–101	2 concretionary pebbles	0.709096	14	1.3	2.8
1408	119–121	Pelletal phosphorite (>250)	0.709079	13	1.6	4.6
1408	121–123	Pelletal phosphorite (>250)	0.709102	15	1.3	2.5
1408	132–136	Pelletal phosphorite (>250)	0.709106	8	1.2	2.4
1408	132–136	Skeletal (amber vertebra)	0.709069	15	1.9	5.0
1408	132–136	Shell fragments (weathered)	0.708902	15	8.6	10.6
1408	132–136	Forams (benthic/planktic mix)	0.708850	13	10.4	13.0
2145	42–44	Bivalve shell	0.709182	13	0.0	0.7
2145	42–44	Pelletal phosphorite (125–250)	0.709144	13	0.5	1.4
2145	83–86	1 concretionary pebble	0.709191	15	0.0	0.6
2145	83–86	1 concretionary pebble	0.709188	12	0.0	0.6
2145	83–86	1 amber skeletal bone	0.709182	13	0.0	0.7
2145	83–86	Pelletal phosphorite (>0.5 mm)	0.709181	15	0.0	0.8
2145	83–86	1 clear vertebra	0.709174	13	0.0	0.9
2145	83–86	1 concretionary pebble	0.709152	16	0.3	1.3
2145	162–165	1 bone vertebra	0.709262	14	0.0	0.0
2145	162–165	1 bone vertebra	0.709199	14	0.0	0.3
2145	170–177	1 glassy bone fragment	0.709252	15	0.0	0.0
2145	170–177	Pelletal phosphorite (>500)	0.709199	14	0.0	0.3
2145	203–206	1 amber fish bone	0.709225	14	0.0	0.0
2145	203–206	Pelletal phosphorite (1–2 mm)	0.709230	14	0.0	0.0
2145	203–206	Pelletal phosphorite(<0.5 mm)	0.709202	13	0.0	0.2
2145	203–206	1 concretionary pebble	0.709190	13	0.0	0.6
2145	203–206	Fish scales (0.5–1 mm)	0.709187	13	0.0	0.6
2145	203–206	Fish scales (>2 mm)	0.709174	12	0.0	0.9
2145	223–233	Pelletal phosphorite (fine sand size)	0.709235	13	0.0	0.0
2145	223–233	Skeletal phosphorite grains	0.709163	17	0.0	1.1
1313	0–4	Phosphorite pebble	0.709149	13	0.3	1.3
1313	0–4	1 concretionary pebble	0.709132	14	0.7	1.6
1313	7–10	Shell fragments	0.709180	11	0.0	0.8
1313	7–10	Pelletal phosphorite (>250)	0.709114	14	1.1	2.2
1313	40–42	1 concretionary pebble	0.709149	17	0.3	1.3
1313	43–45	Skeletal phosphorite (7 mm max)	0.709122	13	1.0	1.9
1313	43–45	Pelletal phosphorite (>250)	0.709121	13	1.0	1.9
1313	43–45	6 phoshorite grains (2.5 mm max)	0.709118	11	1.0	2.0
1313	50–52	1 concretionary pebble	0.709152	13	0.2	1.3
1313	50–52	Phosphorite pebble	0.709137	16	0.6	1.5
1313	52–54	Pelletal phosphorite (>125)	0.709155	16	0.2	1.2
1313	52–54	Skeletal phosphorite (3.5 mm max)	0.709155	12	0.2	1.2

Table 3.1 *(continued)*

Core	Sample (cm)	Sample description	87/86 Sr	2σ	Age min	Age max
1313	52–54	Pelletal phosphorite (>250)	0.709091	10	1.4	3.4
1313	52–54	6 phoshorite grains (2 mm max)	0.709079	15	1.6	4.6
1313	74–76	Pelletal phosphorite (>500)	0.709163	12	0.0	1.1
1313	96–98	Pelletal phosphorite (>125)	0.709174	14	0.0	0.9
1313	96–98	1 skeletal translucent bone	0.709171	13	0.0	1.0
1313	96–98	1 concretionary pebble (matrix)	0.709153	17	0.2	1.3
1313	96–98	Pelletal phosphorite (>250)	0.709125	12	0.9	1.8
1313	96–98	Skeletal phosphorite (4 mm max)	0.709121	13	1.0	1.9
1313	96–98	Pelletal phosphorite from cP pebble	0.709101	15	1.3	2.6
1313	96–98	Phosphorite pebble	0.709097	14	1.3	2.7
1313	96–98	Fish scales (3.5 mm max)	0.709081	12	1.6	4.5
1313	140–145	Pelletal phosphorite (fine to med)	0.709067	16	2.0	5.1
2325	26–28	1 concretionary pebble	0.709152	12	0.2	1.3
2325	69–73	Pelletal phosphorite (250–500 um)	0.709169	16	0.0	1.0
2325	69–73	1 shark's tooth	0.709153	12	0.2	1.3
2325	69–73	1 concretionary pebble	0.709144	13	0.5	1.4
2325	69–73	1 concretionary pebble	0.709143	14	0.5	1.4
2325	69–73	1 concretionary pebble	0.709111	11	1.1	2.2
2325	106–108	1 skeletal grain (bone)	0.709156	14	0.1	1.2
2325	197–200	1 concretionary pebble (matrix)	0.709195	13	0.0	0.4
2325	197–200	Pelletal phosphorite from cP pebble	0.709185	15	0.0	0.7
2325	197–200	Pelletal phosphorite (>500)	0.709175	13	0.0	0.9
2325	197–200	1 concretionary pebble	0.709162	12	0.0	1.1
2325	267–275	Subsample 1 of large bone	0.709236	15	0.0	0.0
2325	267–275	Subsample 2 of large bone	0.709237	14	0.0	0.0
2325	267–275	Subsample 3 of large bone	0.709249	14	0.0	0.0
2325	267–275	1 concretionary pebble	0.709169	12	0.0	1.0
2325	267–275	Pelletal phosphorite (63–125)	0.709169	14	0.0	1.0
2325	267–275	Fish scales (>1 mm)	0.709113	14	1.1	2.2
Rocky Point						
2634	15–20	Pelletal phosphorite (250–500)	0.709105	13	1.2	2.4
2634	35–40	Skeletal phosphorite (bone)	0.709119	12	1.0	2.0
2634	95–97	Shell, bivalve, gastropod	0.709177	16	0.0	0.9
2634	95–97	Phosphorite pebble	0.709132	11	0.7	1.6
2634	95–97	Shark's tooth	0.709087	13	1.5	3.8
2634	95–97	1 skeletal phosphorite	0.709038	11	3.6	5.8
2634	95–97	Phosphorite pebble	0.709034	10	4.0	5.9
2634	95–97	Pelletal phosphorite (>500)	0.708997	11	5.6	6.7
2634	100–105	Phosphorite pebble (1/2)	0.709033	11	4.1	5.9
2634	100–105	Phosphorite pebble (2/2)	0.709028	13	4.6	6.0
2634	112–116	Phosphorite pebble	0.709132	14	0.7	1.6
2634	112–116	1 fish vertebra	0.709017	11	5.0	6.1
2634	112–116	Pelletal phosphorite (>250)	0.709057	15	2.3	5.3
2634	112–116	Skeletal phos (>500)	0.709053	15	2.4	5.4
2670	0–5	Phosphorite pebble	0.709218	9	0.0	0.0
2670	0–5	Phosphorite pebble (shell)	0.709206	11	0.0	0.0
2670	0–5	Pelletal phosphorite (>500)	0.709161	13	0.0	1.2
2670	0–5	Bivalve shells (2)	0.709158	16	0.0	1.2
2670	74–79	Phosphorite pebble (shell)	0.709194	11	0.0	0.4
2670	74–79	1 concretionary pebble	0.709191	15	0.0	0.6
2670	74–79	1 fish vertebra	0.709171	13	0.0	1.0
2670	74–79	Phosphorite pebble	0.709168	13	0.0	1.1
2670	74–79	Pelletal phosphorite (>500)	0.709102	13	1.3	2.5
2670	82–87	Phosphorite pebble (shell)	0.709164	13	0.0	1.1
2670	82–87	Bone fragment	0.709134	15	0.7	1.6
2670	82–87	Pelletal phosphorite (500–1000)	0.709096	13	1.3	2.8
2670	82–87	Shell fragments	0.709013	11	5.1	6.2
2670	125–130	Phosphorite pebble (mould)	0.709148	13	0.3	1.3
2670	125–130	Pelletal phosphorite (>500)	0.709123	13	0.9	1.8
2670	125–130	Forams	0.708765	11	14.8	15.9
2670	135–140	Forams (>500)	0.708751	13	15.2	16.1
2670	175–180	Forams (>500)	0.708756	13	15.1	16.0
2670	185–190	Forams (>500)	0.708776	13	14.4	15.7

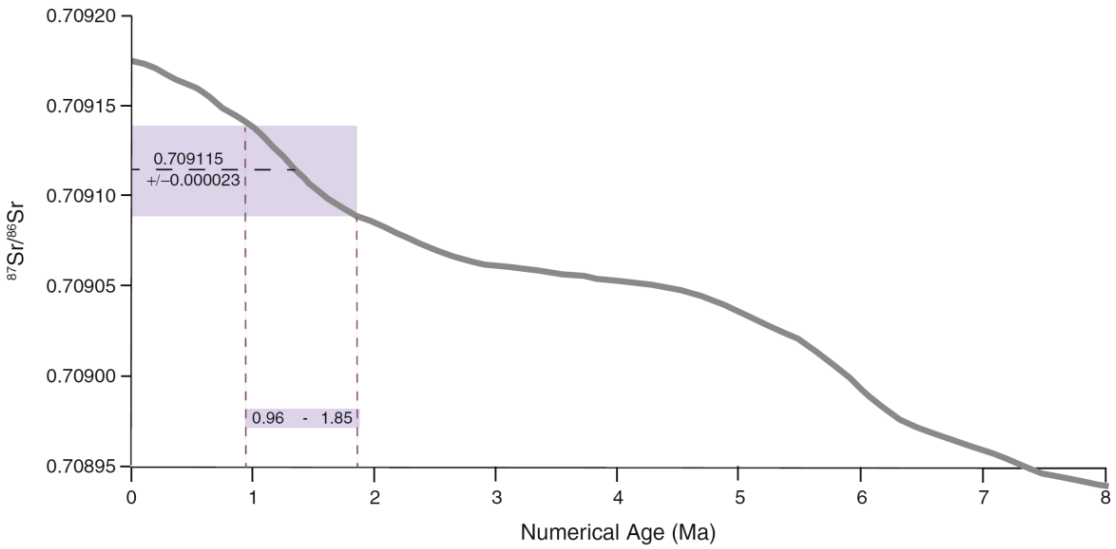

Fig. 3.3. Marine $^{87}Sr/^{86}Sr$ ratio since 8 Ma from the Sr lookup table V4B: 08/04 (McArthur et al., 2001) showing the range in ages corresponding to a sample with a ratio of 0.709115 (0.709122 before subtraction of 0.000007) and ±0.000023 uncertainty (long-term reproducibility).

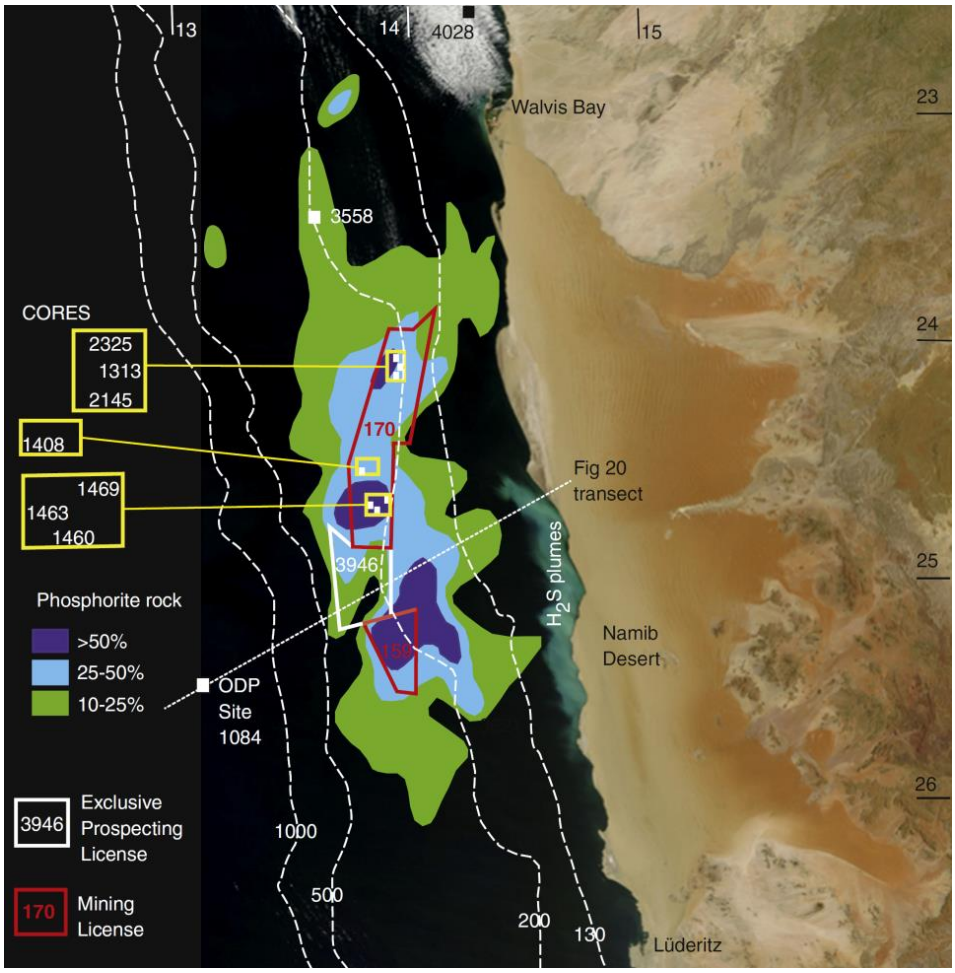

Fig. 3.4. Extent of phosphorite-rich sediment outcropping on the Namibian shelf between Hottentots Bay (60 km north of Lüderitz) and Walvis Bay (Bremner, 1977; Rogers, 1977). The milky area inshore of the deposit is an H_2S plume (image from NASA). Line represents cross section of shelf in Fig. 3.20.

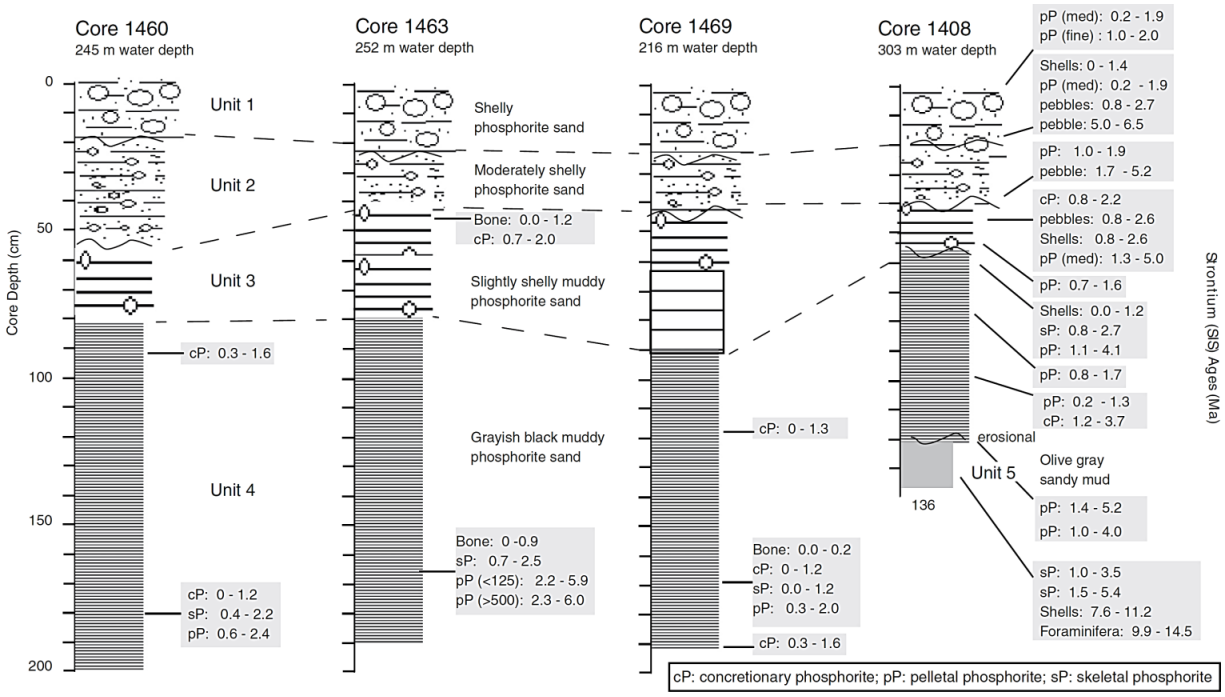

Fig. 3.5. Lithostratigraphy of cores from the central area of the Lüderitz–Walvis deposit (core locations in Fig. 3.4; SIS ages from Table 3.1).

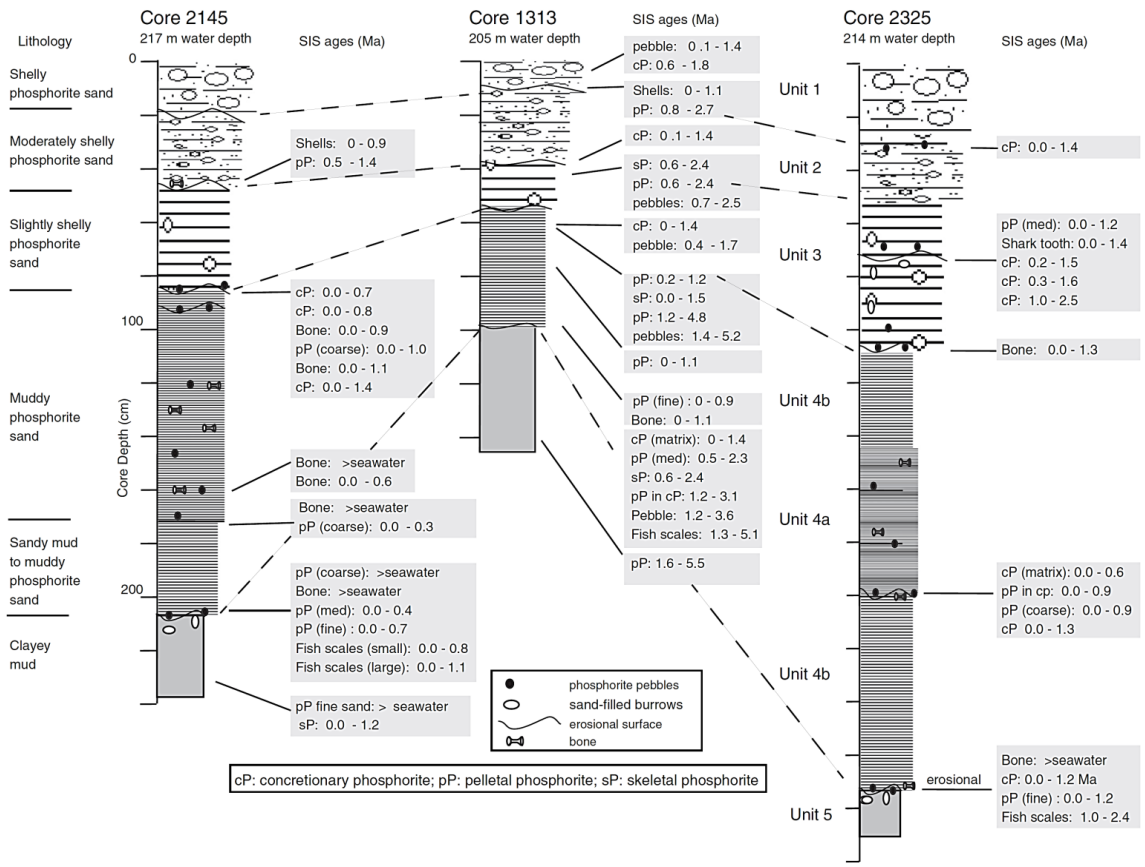

Fig. 3.6. Lithostratigraphy of cores from the northern area of the Lüderitz–Walvis Bay deposit (core locations in Fig. 3.4; SIS ages from Table 3.1).

The lower mud unit has an abrupt, erosional contact with the overlying phosphorite sand unit marked by an increase to between 36 and 74 wt.% sand and often associated with gravel-size bone. The phosphorite sandy mud to muddy phosphorite sand (unit 4) is dark olive gray (Munsell chart 5Y 3/1) and has a maximum thickness of approximately 1 m. The thickness and phosphorite sand content are highly variable, but the lower half of the unit (4b) generally has less sand than the upper half of the unit (4a).

The transition from the muddy phosphorite sand to overlying shelly phosphorite sand varies from gradational to sharp. The contact is marked by an increase in calcareous shell fragments. The basal slightly gravelly phosphorite sand (unit 3) has a dark gray color (Munsell chart 5Y 2.5/1) and contains less than 12% shell gravel. It grades into an overlying moderately gravelly phosphorite sand containing 10–25% shell gravel (unit 2), which is overlain by gravel-rich phosphorite sand containing 30–60% shell gravel (unit 1). The sand size fraction of units 1–3 is predominantly composed of black to brown pelletal phosphorite grains and includes variable amounts of shell fragments, whole juvenile bivalves and gastropod shells, planktonic and benthic foraminifera (some in-filled by glauconite), echinoid spines, sponge spicules, biogenic fish debris (bone, teeth, scales, otoliths), fecal pellets, few ostracod valves, and minor detrital quartz grains. The gravel size fraction is made up mostly of mollusc shells (a mixture of whole and fragmented gastropod and bivalve shells), but also includes bryozoan fragments, fish and mammal bone fragments, phosphorite pebbles, phosphatized shell fragments and minor angular quartz. There is evidence of multiple erosional surfaces within the shelly phosphorite sand (units 1–3) which has a mean total thickness of between 0.3 and 0.9 m.

Most cores show an increase in shell gravel content at the expense of sand while the mud content remains more or less constant at 4–6 wt.% in units 3 to 1. Phosphorite pebbles and bone generally make up a minor portion of the gravel sized material, which is dominated by mollusc shells. The degree of shell fragmentation decreases upcore with unaltered, articulated bivalves confined to the uppermost 10 to 20 cm of sediment. The gravelly muddy sand of units 2 and 3 is dominated by *Lucinoma capensis* (assemblage Mb) and the gastropod *Turritella declivis* (Fig. 3.7). The uppermost shelly sand of unit 1 is dominated by the bivalve *Dosinia lupinus* and the gastropod *Nassarius vinctus* (assemblage Mc3). Foraminifera taxa in the basal muddy unit 5 could not be established due to the fragmented nature of the tests (assemblage Fb; Fig. 3.8). The overlying pelletal phosphorite sand (unit 4) contains sparse foraminifera, with ribbed *Uvigerina* sp. being the only taxa found in this unit. Species richness increased in the uppermost unit (assemblage Fd) with *Ammonia japonica/A. beccarii* being the dominant benthic and *Globigerina bulloides* the dominant planktonic foraminifera.

3.4.2. Stratigraphy of the northern phosphorite deposits

Surface sediments on the northern Namibian shelf off Rocky Point contain between 5 and 50 wt.% pelletal phosphorite. The phosphorite-rich sediment trends north-south just inboard of the 200 m isobaths from 18 to 20°S, with the highest phosphorite content occurring directly

offshore of Rocky Point (Fig. 3.9). A total of 38 vibracores recovered up to 2.3 m of sediment from offshore of Rocky Point in water depths of 140 to 230 m. The cores show a similar overall stratigraphy consisting of a basal foraminiferal sandy mud capped by shelly, gravelly phosphorite sand (Fig. 3.10). The basal foraminiferal nannofossil mud has a mottled, bioturbated texture with burrow structures defined by variations in pale gray–green color.

The basal foraminiferal mud unit includes minor gravel as shell fragments in some cores, identified as *Pecten* sp. (Fig. 3.10). Predatory drill holes in the shell are common, some infilled by pyrite. The basal mud unit has a variable mixture of the clay minerals illite, smectite and kaolinite as well as diagenetic pyrite and dolomite.

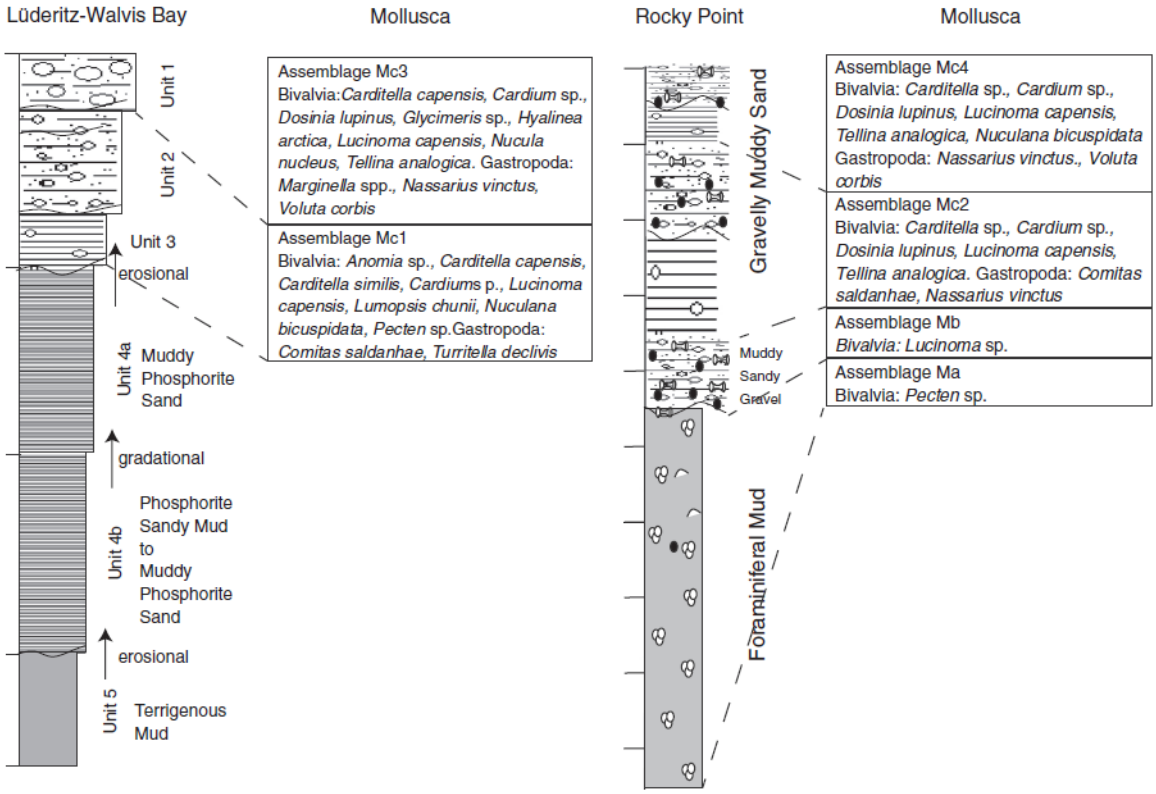

Fig. 3.7. Mollusc assemblages of cores from the southern and northern study areas.

The basal mud unit is in sharp erosional contact with the overlying muddy sandy gravel unit. The contact is heavily bioturbated in places with dark phosphorite sand burrows extending several tens of centimeters below the contact. The overlying gravelly muddy sand unit is a complex mixture of grain sizes and grain types. The gravel fraction consists of shell and shell fragments along with phosphorite pebbles and bone. The sand consists of pelletal phosphorite grains with minor glauconite and quartz. The mud consists of clay minerals illite, smectite and kaolinite. Together the muddy sandy gravel and gravelly muddy sand units rarely exceed one meter in thickness. The stratigraphy is fairly consistent across the study area, although in many cores the succession is incomplete.

Mollusc shell becomes far more abundant above the basal muddy contact. The muddy sandy gravel unit is dominated by *L. capensis* (assemblage Mb, Fig. 3.7), with the dominant gastropod being *N. vinctus*. The gravelly muddy sand unit has a rich diversity of mollusc shells (assemblages Mc3 and Mc4, Fig. 3.7) and includes articulated bivalves in the uppermost 10–20 cm. The mollusc assemblages in the Rocky point cores are distinct from those in the southern cores, although some bivalves occur in both areas (*L. capensis*, *D. lupinus*, *Carditella* spp., *Cardium* sp. and *Tellina analogica*) as well as some gastropods (*N. vinctus* and *V. lutosa*).

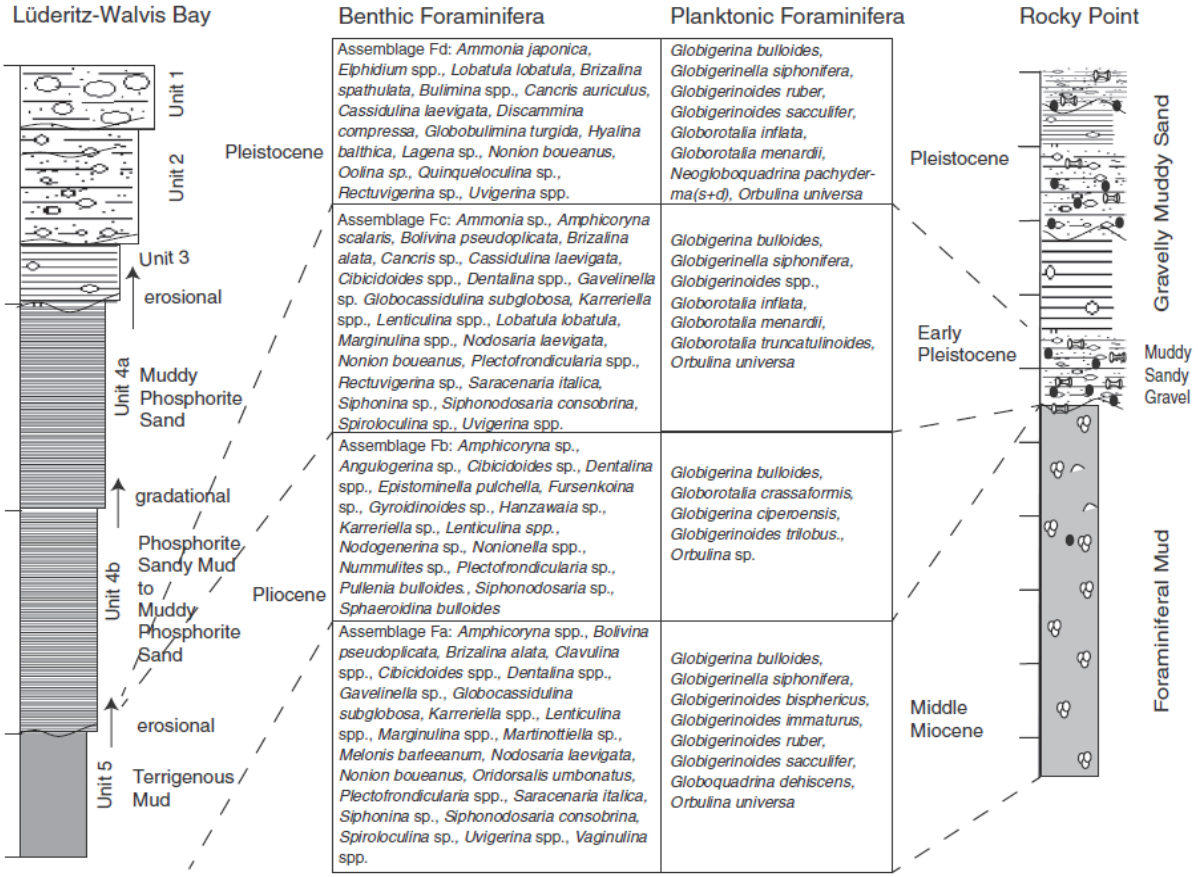

Fig. 3.8. Foraminifera associated with the lithological units of cores from the southern (Lüderitz–Walvis Bay) and northern (Rocky Point) areas.

Abundant foraminifera occur throughout the Rocky Point cores and define three assemblages (Fig. 8). Although the foraminiferal assemblages are similar, the basal unit in the Rocky Point area contains several distinct taxa (Fa). The Rocky Point cores also contain a distinct transitional assemblage (Fc) within the muddy sandy gravel unit. The taxa from the uppermost gravelly muddy sand (assemblage Fd) largely overlap between the Rocky Point and Lüderitz Walvis Bay areas. Pyrite commonly occurs within some foraminifera chambers.

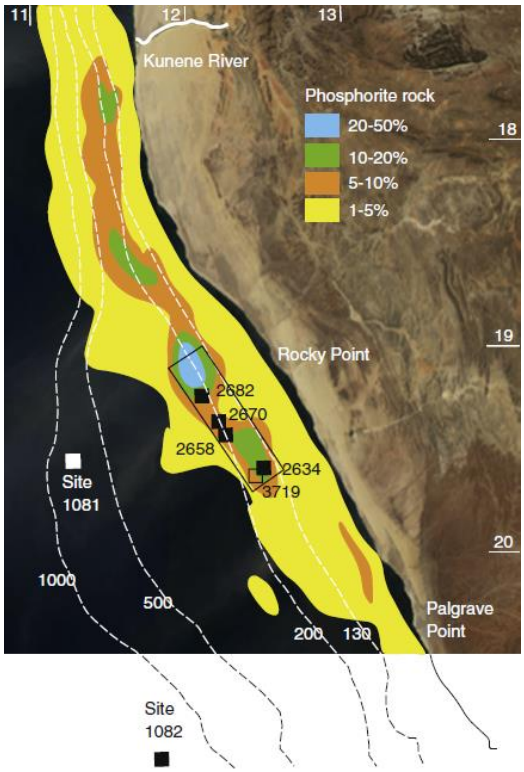

Fig. 3.9. Extent of phosphorite-rich deposits outcropping on the northern Namibian shelf between Palgrave Point and the Kunene River (Bremner, 1977). Location of cores from this study is shown as well as those from ODP sites 1081 and 1082 (Wefer et al., 1998a)

3.4.3. Phosphorite petrography

The texture and petrography of phosphorite grains are similar for surface grab and core samples from the Namibian shelf. Phosphorite is mostly present as very fine to coarse sand-size pelletal phosphorite grains. Pelletal phosphorite grains are well rounded to subrounded and range from nearly spherical to ellipsoidal in shape. Most pelletal phosphorite has polished dark brown to black surfaces, but in some samples the surfaces are pitted and bleached. The pelletal phosphorite sand grains show a variety of internal structures. Many have a nucleus of bone, foraminiferal test, echinoid spine or shell fragment (Fig. 3.11) and concentric banding showing multiple generations of phosphorite growth is common (Bremner, 1977). Intraclasts of quartz and glauconite sand occur and intraclasts of organic matter and sulfide minerals (mostly pyrite) are common (Fig. 3.11).

Although less abundant than pelletal phosphorite sand, concretionary phosphorite (cP) and skeletal phosphorite (sP) grains (bone, teeth, scales) are common, particularly in the gravel size fraction (Fig. 3.12). Skeletal phosphorite grains typically show original structures of the bone, teeth and scales, and are translucent or amber to dark brown. Concretionary phosphorite grains are tan to light brown in color and variably friable and porous, some contain intraclasts of pelletal phosphorite sand grains. Rock phosphorite formed by the replacement of limestone rock is rare on the Namibian shelf, but phosphorite pebbles of mollusc molds and phosphatized mollusc shell fragments are observed. Pelletal phosphorite sand can also occur as composite, cemented sandstone pebbles (Fig. 3.12).

Carbonate fluorapatite (francolite) occurs as extremely fine crystalline cement, too fine to resolve individual crystals in thin section. Under the SEM, the francolite cement occurs as massive or radial clusters of elongate crystals except where francolite grows into voids where it can form several different structures (Fig. 3.13). The smallest are submicron sized pods having smooth, elliptical surfaces. Bigger pods can show terminal crystal faces suggesting that they formed as a cluster of elongate crystals showing poorly-formed hexagonal crystal habit. In other cases, the elongate francolite crystals grow together forming crosses, stars or fan-like structures. How individual francolite crystals growing into voids relate to adjacent massive

francolite cement is unclear, but in some cases the cement appears to be the product of many intergrown radial francolite crystal clusters.

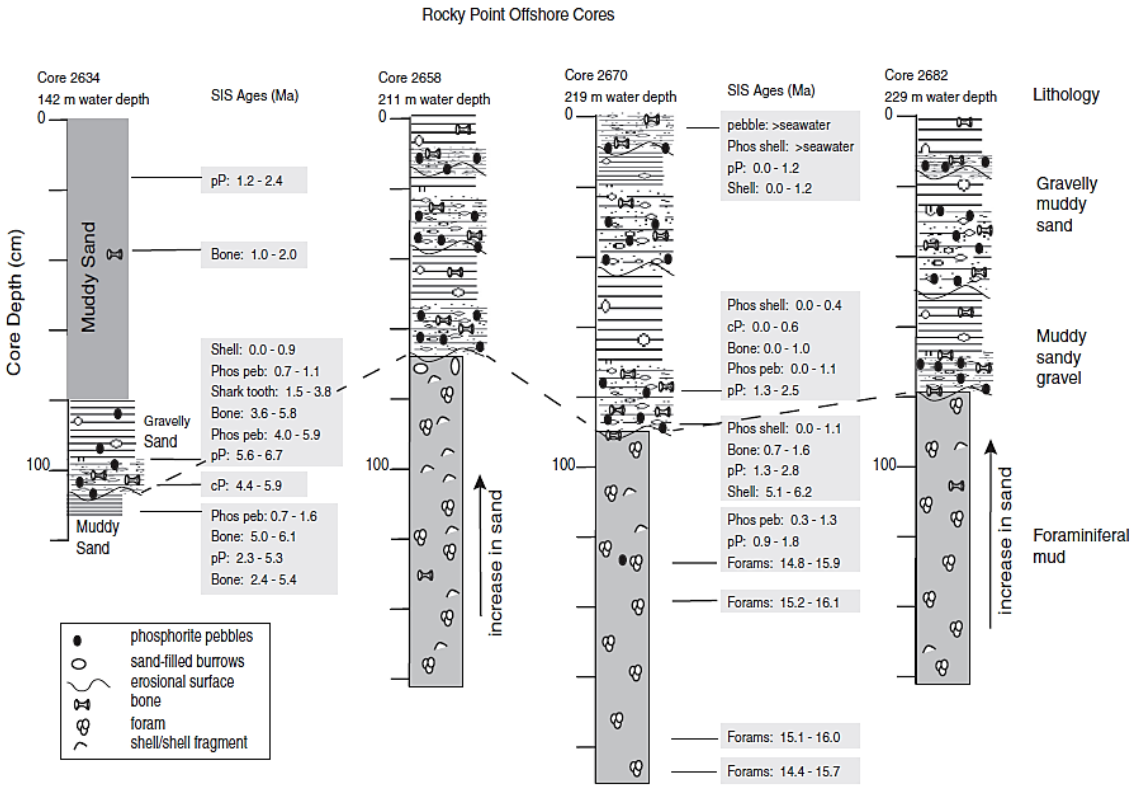

Fig. 3.10. Lithostratigraphy of cores from offshore Rocky Point (refer to Fig. 3.9 for location; SIS ages from Table 3.1).

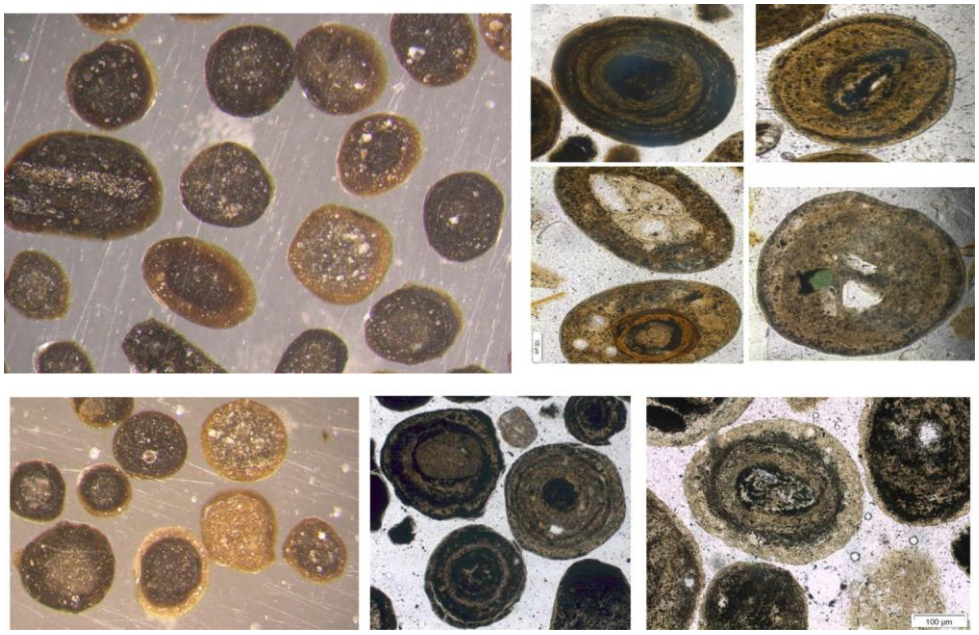

Fig. 3.11. Pelletal phosphorite grains viewed under transmitted light showing internal nuclei and concentric banding (scale bar is 0.1 mm).

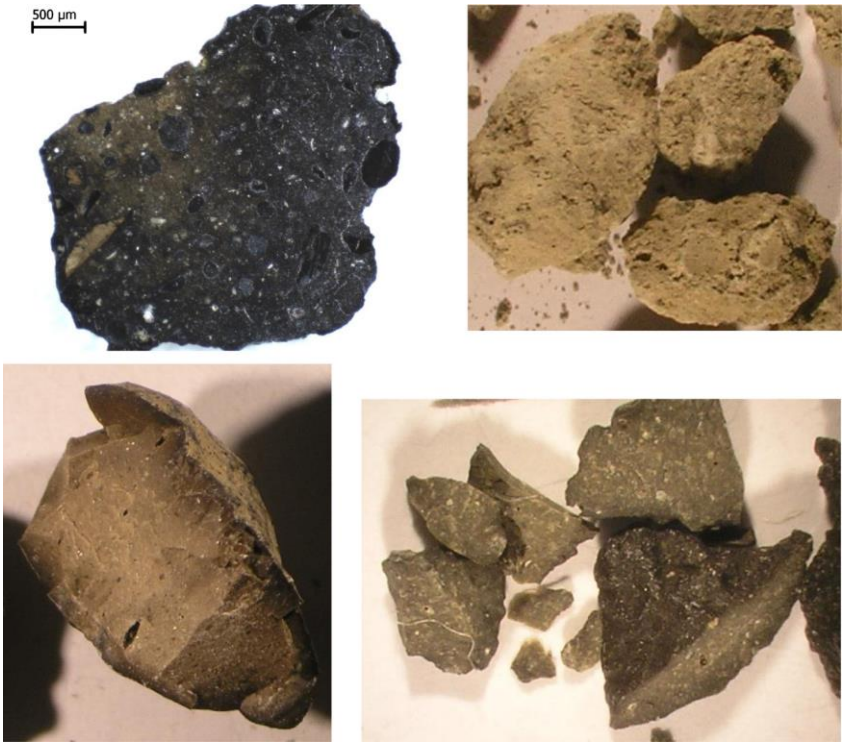

Fig. 3.12. Various phosphorite pebble types: composite phosphorite pebble (pelletal sandstone) (A), concretionary phosphorite (porous and friable) (B), phosphorite interior molds of molluscs (fragmented) (C and D) (scale bar is 0.5 mm).

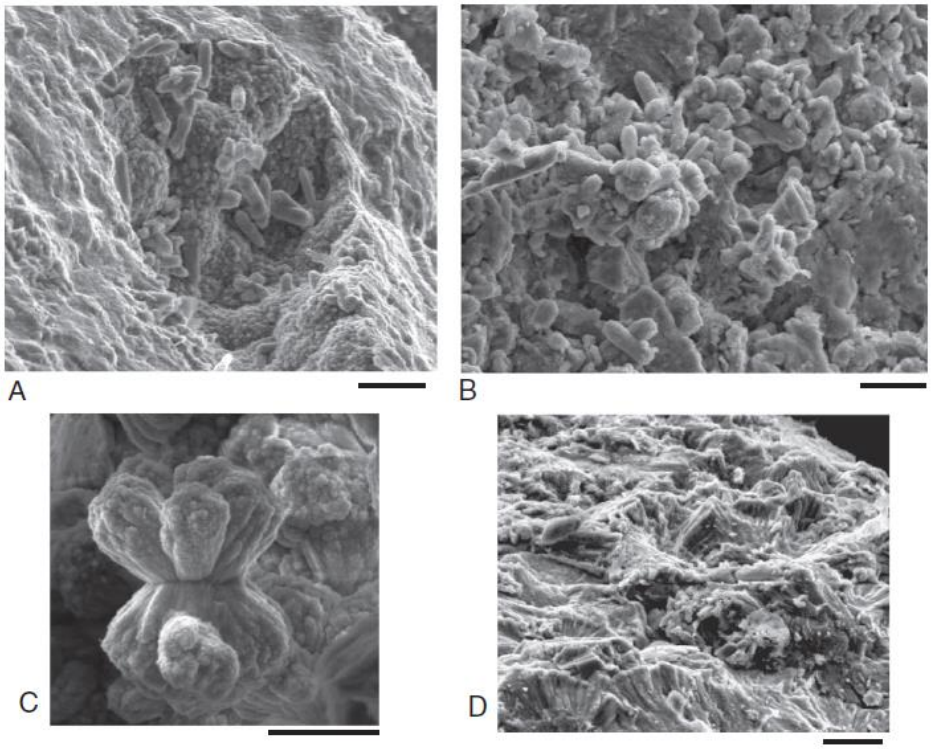

Fig. 3.13. SEM images of phosphorite grains showing various structures of francolite crystals and crystal clusters: individual crystals within a void space (A), closeup of francolite crystals (B), intergrown francolite crystals (C) and radial structure of francolite crystals (D) (scale bar is 2 µm).

3.4.4. Geochemistry of phosphorite grains

As is typical for most marine phosphorite, XRD analyses reveal that the principal P-bearing mineral in phosphorite from the Namibian shelf is francolite. Francolite is a carbonate fluorapatite mineral with 3–6 mol% carbonate ion substitution for phosphate ion and significant amounts of fluoride (>1 wt.% F) in place of hydroxide (OH). Phosphorite from the Namibian shelf contains between 3.2 and 6.5 wt.% CO_2 present in the francolite as carbonate ion substituting for the phosphate ion (Table 3.2). A typical chemical formula for francolite is $Ca_{4.7}Na_{0.2}Mg_{0.1}(PO_4)_{2.6}(CO_3)_{0.4}F_{1.28}$ (Jarvis et al., 1994). Sr substitutes for Ca in the francolite structure and samples contain between 0.1 and 0.3 wt.% Sr. The chemical composition of different phosphorite rock types including concretionary and pelletal phosphorite from the Namibian shelf has been determined by a number of workers (Price and Calvert, 1978; Bremner, 1977; Thomson et al., 1984; Baturin, 2002). The major element data reveal that the chemical composition of the phosphorite grains is largely similar, having between 27 and 33 wt.% P_2O_5 whereas the bulk sediment or sand fraction has 18 to 27 wt.% P_2O_5 (Table 3.2). Besides phosphatized shell and bone material (skeletal phosphorite grains), most marine phosphorite grains are not composed of pure francolite, but have inclusions of pyrite, calcite, organic matter, glauconite, clay minerals, biogenic silica and quartz. All of these other components occur in highly variable amounts and typically constitute between 5 and 40 wt.% of phosphorite grains.

The sulfur and iron content of the phosphorite samples reflect the presence of pyrite (FeS_2) evident in thin section (Fig. 3.14). The SiO_2 content reflects the presence of quartz grains, amorphous biogenic silica (mostly present as diatoms and sponge spicules), and silica associated with clay and mica minerals. The mineral composition of the phosphorite samples can be estimated by allocating the elements from the elemental oxide analyses with the minerals detected by XRD. Combining these two analyses indicates that concretionary phosphorite from the diatomaceous mud belt consists of 90% francolite (CFA), <1% quartz and biogenic silica, up to several percent calcite, 0.5–2% clay minerals and 1.4 to 2.8% pyrite, whereas the pelletal phosphorite sands contain less francolite (78%) and more quartz/biogenic silica, calcite, clay minerals and pyrite (Table 3.3). The bulk sand-size fractions of phosphorite-rich sediment from the mid to outer shelf have a mean composition of 65% francolite, 5.7% quartz/biogenic silica, 12% calcite, 10.7% clay minerals and 5.1% pyrite, with the balance of 2% probably largely present as organic matter (not analyzed for) within the phosphorite grains.

3.5. Discussion

3.5.1. Age model

An age model for phosphorite formation and final sediment deposition is derived from the integration of biostratigraphy and strontium isotope stratigraphy (SIS). The strontium isotope ratios range from 0.708751 to 0709262, corresponding to SIS ages of middle Miocene to values greater than modern seawater (Table 3.1). The age resolution possible using SIS depends on the steepness of the marine strontium isotope curve, which is relatively flat and of low resolution throughout the Pliocene between 2.6

and 5.3 Ma, but somewhat steeper and of higher resolution on either side of the Pliocene during the late Miocene and Pleistocene (Fig. 3.3). The SIS ages of phosphorite from this study are consistent with previously reported SIS ages of Pliocene (4.1–5.8 Ma) phosphorite offshore of Walvis Bay and of Pleistocene (0.4–1.3 Ma) phosphorite from offshore Rocky Point (samples 3558 and 3719, respectively in Figs. 3.4 and 3.9) (McArthur et al., 1990; SIS ages updated to the look-up table V4: 08/04).

In general, the SIS ages young up section as expected, but the different grain types within a sample can show a wide range of ages (Table 3.1; Figs. 3.5, 3.6 and 3.10). For example in Core 1313 at a depth of 96–98 cm, pelletal phosphorite grains are older than the matrix of the concretionary phosphorite pebble surrounding them as expected. Bone from the same sample is similar in age to the concretionary phosphorite whereas pelletal phosphorite sand and fish scales have mean SIS ages that overlap with the included pelletal phosphorite grains (Fig. 3.15). The differences in age found for different grains from the same sample in this study are consistent with sedimentological and petrographic evidence for complex reworking and multiple episodes of phosphorite formation (Fig. 3.11). Therefore, it is not unusual or unexpected that different phosphorite grains and fossils have significantly different ages in the same sample (Compton et al., 2002, 2004). In a sample from Core 2325, a concretionary phosphorite pebble is of similar age to fine pelletal phosphorite sand and both are younger than associated fish scales, while a large bone has Sr isotope values greater than modern seawater (Fig. 3.16).

Strontium isotope ratios greater than modern seawater were reported for concretionary phosphorite from the Holocene diatomaceous mud belt off Walvis Bay (sample 4028 in Fig. 3.4; mislabeled 4208 in McArthur et al. (1990)). McArthur et al. (1990) attributed the higher than seawater Sr value to the dissolution of radiogenic Sr (^{87}Sr) from terrigenous (wind-blown) mica. Radiogenic Sr may have been leached from included minerals by the acetic acid used to digest the phosphorite grains. Although acetic acid is a less aggressive acid than HCl, it may still result in the release of sufficient radiogenic Sr to impact the measured ratios of the phosphorite samples (McArthur, 1994). Alternatively, the phosphorite may have incorporated radiogenic Sr that was released from terrigenous minerals into pore waters during the time of its formation. Therefore, radiogenic Sr contamination from detrital minerals is a concern in the application of SIS to phosphorite samples from the Namibian shelf, with actual ages potentially older than the ages in Table 3.1. Just how much older the phosphorite samples may be is unknown and depends to what extent radiogenic Sr was acquired during phosphorite formation or released during acid digestion. A total of 8 of the 120 phosphorite grains analysed in this study had Sr isotope values that averaged 0.00006 and ranged from 0.000031 to 0.000087 greater than seawater. These relatively modest offsets, along with the general agreement of biostratigraphic and SIS ages discussed below, suggest that alteration of the Sr isotope ratios was limited and unlikely to significantly impact the SIS ages, particularly when considering the relatively low age resolution (low gradient) of the Pliocene marine Sr isotope curve (Fig. 3.3). Contamination by radiogenic Sr is predicted to

shift the SIS ages older, with a shift from the predominantly Pleistocene SIS ages to include a broader spread of Pliocene to late Miocene ages. However, shifts to ages older than the latest Miocene are considered unlikely because of the steepness of the late Miocene marine Sr curve. Contamination by radiogenic Sr is not an issue for biogenic calcite samples (unrecrystallized foraminifera and mollusc shell).

Table 3.2. Elemental analyses of phosphorite samples.

Diatomaceous mudbelt		SiO_2	Al_2O_3	TiO_2	Fe_2O_3	MgO	CaO	Na_2O	K_2O	P_2O_5	CO_2	F	Sr	CO_3^{2-}
Price and Calvert (1978)	cP	1.80	0.47	0.07	0.95	0.60	50.90	nd	0.17	31.60	4.30	2.23	0.21	5.37
	cP	1.00	0.27	0.05	0.81	0.60	51.60	nd	0.09	32.60	4.10	2.54	0.19	5.13
	pP	4.60	1.25	0.10	2.52	0.90	45.40	nd	0.39	29.40	3.50	2.03	0.21	4.38
	pP	5.00	1.17	0.11	3.32	0.90	42.90	nd	0.39	27.20	3.90	2.80	0.18	4.88
	Skeletal	1.10	0.15	0.06	1.56	0.40	50.00	nd	0.09	31.70	5.30	2.02	0.16	6.63

Baturin (2002)		SiO_2	Al_2O_3	TiO_2	Fe_2O_3	MgO	CaO	Na_2O	K_2O	P_2O_5	CO_2	F	S	Corg	H_2O
	cP	1.44	0.61	nd	1.50	1.12	48.40	0.92	nd	30.75	5.03	3.44	1.50	1.28	10.10
	cP	0.40	0.05	nd	0.43	1.45	49.50	1.52	nd	32.45	6.03	nd	nd	0.88	nd
	cP	0.29	0.16	nd	1.06	1.52	nd	1.66	nd	30.98	6.47	nd	nd	0.93	nd
	cP	2.65	0.69	nd	2.85	1.39	nd	1.58	nd	32.82	3.40	nd	nd	0.57	nd
	mold	9.21	1.71	nd	2.63	1.29	43.20	1.47	nd	26.22	4.35	nd	nd	1.01	nd
	mold	2.17	0.09	nd	nd	nd	47.50	nd	nd	31.05	nd	nd	nd	nd	nd
	caprolite	0.49	0.08	nd	0.17	1.39	nd	1.35	nd	33.10	5.92	nd	nd	1.08	nd
	caprolite	0.30	0.03	nd	0.46	1.39	50.90	1.47	nd	32.28	6.22	nd	nd	0.97	nd
Bremner (1977)		SiO_2	Al_2O_3	TiO_2	Fe_2O_3	MgO	CaO	Na_2O	K_2O	P_2O_5	CO2	F	S	Corg	LOI
	pP (4)	4.97	1.12	0.46	2.54	0.83	46.93	0.50	0.38	28.04	3.60	3.20	2.31	2.70	12.03

Thomson et al. (1984)		SiO_2	Al_2O_3	TiO_2	Fe_2O_3	MgO	CaO	Na_2O	K_2O	P_2O_5	CO_2	F	Sr	CO_2tot
	friable cP	4.50	0.26	0.07	0.16	3.97	19.35	nd	0.16	27.90	2.30	1.77	0.02	13.24
	pP	8.40	1.69	0.11	3.56	0.50	41.78	nd	0.63	28.00	4.10	1.76	0.11	6.27
	glauc pP	7.40	1.73	0.12	7.98	0.43	37.57	nd	1.03	27.70	3.70	1.76	0.10	2.90
	friable cP	6.70	1.06	0.07	0.48	0.74	44.56	nd	0.21	30.20	2.70	1.91	0.16	5.83
	lithified cP	2.40	0.69	0.05	0.46	0.63	45.26	nd	0.18	30.50	nd	2.42	0.15	5.57
	lithified cP	4.80	0.81	0.06	0.33	0.51	40.01	nd	0.24	27.50	2.30	1.73	0.28	5.35
	lithified cP	0.50	0.16	0.04	0.03	0.61	46.53	nd	0.12	31.40	2.60	2.78	0.18	6.67
	lithified cP	0.40	0.03	0.02	0.02	0.71	46.21	nd	0.09	30.70	1.10	2.74	0.17	6.71
	lithified cP	13.50	4.54	0.21	1.50	0.72	36.02	nd	0.71	24.90	1.50	2.06	0.17	6.60
	lithified cP	0.70	0.32	0.04	0.09	0.35	47.70	nd	0.13	30.80	2.30	2.99	0.12	6.53

Mid to outer shelf		SiO_2	Al_2O_3	TiO_2	Fe_2O_3	MgO	CaO	Na_2O	K_2O	P_2O_5	S	LOI
ML 170	bulk sand	7.24	2.56	0.11	3.16	0.65	42.75	2.54	0.16	19.52	nd	15.38
ML 170	bulk sand	6.89	2.19	0.08	2.30	1.80	43.76	2.77	<0.02	18.00	nd	19.05
ML 170	bulk sand	10.13	2.14	0.15	4.16	2.07	41.11	2.90	0.46	23.77	nd	6.98
ML 170	bulk sand	11.68	2.19	0.14	3.82	1.15	39.96	<0.02	0.15	17.72	nd	12.31
ML 170	bulk sand	14.37	5.87	0.27	4.20	2.04	33.59	2.76	1.43	20.54	nd	9.76
ML 170	bulk sand	14.85	4.85	0.30	3.73	1.64	31.73	3.62	0.98	20.26	nd	12.11
ML 170	bulk sand	15.73	5.26	0.27	4.17	2.28	35.51	2.01	1.07	23.15	nd	5.88
ML 170	bulk sand	19.37	6.73	0.32	4.86	3.13	31.34	2.93	1.48	20.24	nd	5.70
Rogers (2007)												
ML170	bulk sand	11.53	1.47	0.14	3.86	0.88	41.14	0.69	0.53	21.51	2.86	10.56
ML170	bulk sand	8.34	1.42	0.13	4.09	0.89	43.16	0.71	0.55	22.75	2.93	10.42
ML170	bulk sand	6.65	1.33	0.12	3.84	0.79	43.71	0.52	0.43	20.29	2.77	14.57
ML170	bulk sand	9.80	1.45	0.14	4.08	0.86	41.18	0.70	0.59	24.61	2.95	9.44
ML159	bulk sand	6.88	1.37	0.12	3.03	0.96	44.50	0.80	0.38	24.47	2.30	10.78
ML159	bulk sand	7.18	1.44	0.13	3.32	0.98	44.33	0.66	0.51	23.81	2.26	11.59
ML159	bulk sand	7.24	1.39	0.13	3.47	1.02	44.02	0.73	0.64	25.09	2.37	9.69
ML159	bulk sand	8.20	1.42	0.13	3.80	0.99	42.07	0.71	0.75	27.11	2.44	9.53

Frenay (2004)

ML159		SiO_2	Al_2O_3	TiO_2	Fe_2O_3	MgO	CaO	Na_2O	K_2O	P_2O_5	S	F	CO_2	Corg	Sr
	bulk sand	12.74	1.27	0.12	3.94	1.05	44.90	1.34	0.53	27.10	3.30	3.10	4.90	1.06	0.28

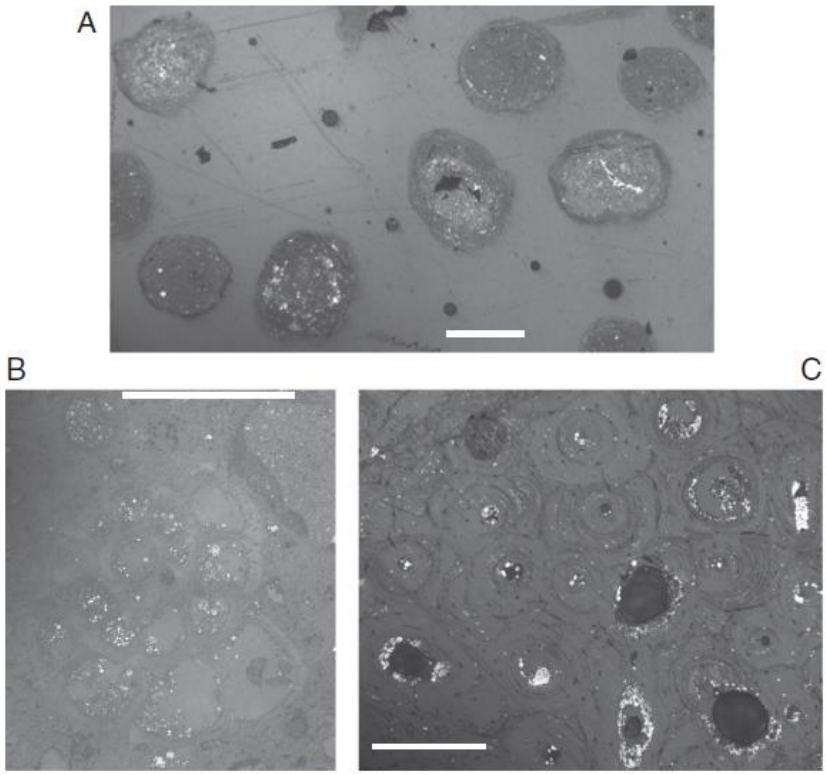

Fig. 3.14. Pyrite makes up 1.4 to 6.9 wt.% of phosphorite grains (Table 3.3) shown here as bright areas under reflected light. Samples are from core 2682: pelletal phosphorite grains (A), foraminiferal test (B) and bone (C) (scale bar is 0.2 mm).

Table 3.3. Phosphorite composition

Diatomaceous mud belt phosphorite grains								
grain type	CFA	Quartz/ diatoms	Biogenic carbonate	Clay minerals illite/smectite	pyrite	Sr + TiO_2	Corg	Total
cP	90.9	0.9	0.7	1.7	1.6	0.3	nd	96.1
cP	91.0	0.5	2.6	1.0	1.4	0.2	nd	96.7
cP	89.4	0.3	0.0	2.0	2.6	0.2	1.3	95.8
sP	88.6	0.8	3.1	0.5	2.8	0.2	nd	96.0
pP	80.8	2.3	1.9	4.2	4.4	0.3	nd	93.9
pP	77.3	2.8	1.9	4.0	5.8	0.3	nd	92.0
pP	78.4	2.9	8.2	3.7	4.6	0.5	2.7	100.9
mean	85.2	1.5	2.6	2.4	3.3	0.3	0.6	95.9
Mid to outer shelf phosphorite bulk sands								
	CFA	Quartz/ diatoms	Biogenic carbonate	Clay I/S	minerals kaolinite	pyrite	Sr + TiO_2	Total
	58.1	3.8	23.8	2.1	5.0	5.5	0.5	98.8
	54.5	4.0	30.2	4.7	3.3	1.5	0.2	98.4
	71.9	6.2	6.9	8.1	0.0	5.4	0.5	99.0
	50.6	8.6	22.2	3.6	3.4	5.8	0.5	94.7
	62.0	3.5	4.6	21.1	0.3	4.5	0.4	96.4
	62.8	6.6	2.0	13.0	2.9	5.6	0.3	93.2
	69.2	6.4	0.0	20.4	0.3	2.6	0.7	99.6
	62.5	7.2	0.0	25.7	0.1	3.4	0.7	99.6
	60.6	8.7	15.5	5.2		6.5	0.2	96.8
	66.9	5.7	14.5	5.0		6.9	0.2	99.1
	58.9	4.1	23.4	5.1		5.9	0.2	97.6
	71.5	7.0	7.2	5.2		6.9	0.2	98.0
	71.2	4.3	13.5	4.9		5.0	0.2	99.0
	69.2	4.5	15.0	5.1		5.5	0.2	99.5
	73.8	4.6	9.7	5.2		5.5	0.2	98.9
	74.6	5.5	9.4	5.6		5.7	0.2	101.0
Mean	64.9	5.7	12.4	8.8	1.9	5.1	0.3	98.1

Fig. 3.15. Different grain types from Core 1313 (96–98 cm) and their SIS ages (scale bar is 0.5 mm).

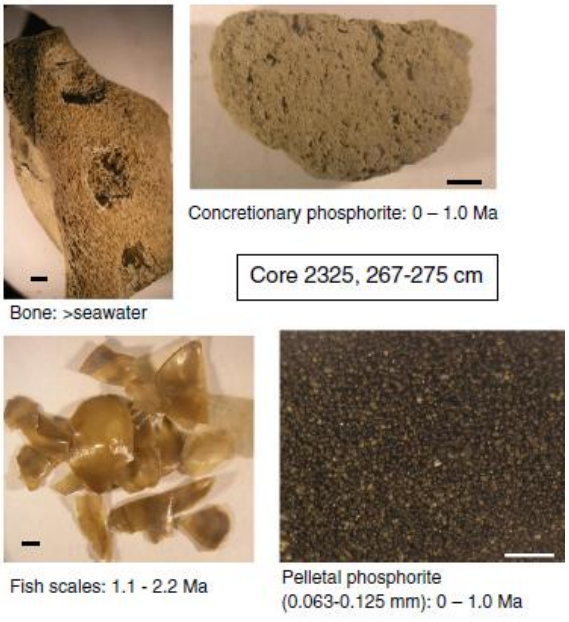

Fig. 3.16. Different grain types from Core 2325 (267–275 cm) and their SIS ages. The bone was sampled in three places (scale bar is 0.5 mm).

SIS allows for the separate dating of different grains from the same bulk sediment sample and, when combined with biostratigraphy, can provide a far more detailed understanding of the complex history of phosphorite deposits (McArthur et al., 1990; McArthur, 1994; Compton et al., 2002, 2004; Wigley and Compton, 2012). The basal mud (unit 5) is considered to be the latest Miocene to Pliocene in age (2.6–6 Ma) based on the biostratigraphy (foraminiferal assemblage Fb, Fig. 3.8, which includes *Epistominella pulchella* and benthic foraminifera associated with the '*Stilostomella* extinction event,' such as *Plectofrondicularia* and *Siphonodosaria*). The SIS ages of phosphorite grains from unit 5 range from 0 to 5.1 Ma, while reworked shell fragments and foraminifera have middle to late Miocene SIS ages (8.6–13.0 Ma; Table 3.1). The overlying phosphorite sandy mud to muddy phosphorite sand (unit 4) and gravelly (shelly) phosphorite sand (units 1–3) are considered to be Pleistocene in age based on the foraminifera *Globorotalia inflata* and *Globorotalia truncatulinoides* (foraminiferal assemblage Fd, Fig. 3.8). These Pleistocene depositional units contain phosphorite grains that have mostly Pleistocene SIS ages, but include some reworked phosphorite grains that are as old as

latest Miocene. Biostratigraphy and SIS are unable to further resolve the age of the Pleistocene deposits. However, unit 4 is considered early Pleistocene in age (0.78–2.6 Ma) and units 2 and 3 are considered to be Middle Pleistocene in age (0.78 Ma), whereas the highly shelly phosphorite sand (unit 1) is considered to be Late Pleistocene (0.126 Ma) to Holocene (less than 11 5 ka) in age. These Pleistocene depositional ages are based on the coarsening upward succession and increasingly high-energy environments on the shelf associated with high amplitude Pleistocene sea-level fluctuations.

The basal foraminiferal mud in cores from offshore Rocky Point is mid-Miocene in age (14–16 Ma) based on the occurrence of the planktonic foraminifera *Globoquadrina dehiscens* and *Globigerinoides bisphericus* (foraminiferal assemblages Fa, Fig. 3.8) and SIS ages of foraminifera of between 14.4 and 16.1 Ma (Core 2670, 125–190 cm; Table 3.1). A major erosional hiatus separates the overlying shelly phosphorite sand units, which are considered to have a Pleistocene depositional age based on the occurrence of the planktonic foraminifera *G. inflata* and *G. truncatulinoides* (foraminiferal assemblages Fc and Fd, Fig. 3.8). The SIS ages of phosphorite grains in Core 2670 are all Pleistocene in age, whereas phosphorite grains range in age from latest Miocene to Pleistocene in Core 2634 (Fig. 3.10; Table 3.1).

3.5.2. Origin of the phosphorite

Large phosphorite deposits, such as those on the Namibian shelf, represent a long-term sink of bioavailable P from the ocean reservoir. The extraction of P from seawater to sedimentary phosphorite deposits involves two major enrichment steps. The first is in the extraction of minor to trace amounts of dissolved or particulate P from surface seawater by primary producers (algae). In the case of skeletal phosphorite grains, P enrichment occurs in the water column as primary producers are consumed up the food chain by larger organisms and P becomes concentrated in skeletal biological forms, such as the bone, teeth and scales of fish. Skeletal phosphorite grains can then transform (recrystallize) from their original biological forms of apatite into carbonate fluorapatite (francolite) during early burial diagenesis with no further P enrichment required. Although generally ubiquitous, skeletal phosphorite grains typically constitute no more than 10–20% of the total phosphorite in samples from the Namibian shelf.

For the formation of most (nonskeletal) phosphorite grains, the second enrichment step occurs during the early burial diagenetic transfer of organic P to the carbonate fluorapatite mineral francolite, rich in inorganic P (37 wt.% P_2O_5). The majority of phosphorite grains are pelletal sand followed by concretionary phosphorite, mollusc molds and phosphatized calcareous fossils. The petrography of these nonskeletal grains indicates that they formed by the precipitation of pore-filling authigenic francolite or by francolite replacing calcite. Pelletal and concretionary phosphorite grains on the Namibian shelf are between 50% and 91% pore-filling francolite cement, with the balance a mix of biogenic calcite (shell, nannofossils and foraminifera), pyrite, clay minerals, mica, glauconite, quartz, diatom frustules and organic matter (Table 3.3).

An early diagenetic origin of phosphorite in organic-rich marine sediment is supported by geochemical studies of, for example, carbon and sulfur isotopes of carbonate and sulfate ion substituted in francolite (McArthur et al., 1986; Mallinson and Compton, 1998). The carbon isotope composition of carbonate substituting in the francolite structure ranges from −3‰ to −9‰ and the sulfur isotope values are slightly depleted relative to seawater (McArthur et al., 1986). This combination of depleted carbon and sulfur isotope values indicates that the francolite formed near the suboxic to anoxic boundary where intense microbial processes rapidly remove oxygen from the sediment and oxidize hydrogen sulfide diffusing up from below. Bacteria, and in particular sulfur bacteria such as *Thiomargarita* and *Beggiatoa*, may play an important role in phosphorite formation on the Namibian shelf through the concentration of P stored as intracellular polyphosphates that are episodically released to form pore water phosphate concentration maxima (Schulz and Schulz, 2005; Brock and Schulz-Vogt, 2011; Bailey et al., 2013).

Other authigenic marine minerals commonly associated with phosphorite are pyrite, glauconite and dolomite. Pyrite is nearly ubiquitous in phosphorite grains from the Namibian margin, with pelletal phosphorite containing an average of 5.1 (1.5–6.9) wt.% pyrite and phosphorite from the diatomaceous mud belt containing an average of 3.3 (1.4–5.8) wt.% pyrite (Table 3.3). The pyrite commonly occurs as microcrystalline spherical clusters (framboids) (Fig. 3.17) either randomly distributed or focused in specific concentric bands within pelletal grains (Fig. 3.14). These textures suggest that the mineral francolite commonly co-precipitates with pyrite, and reflects sulfidic conditions in pore waters that host complex and variable geochemical and microbial processes. Most iron is removed as pyrite precursors and, in some sediments, the amount of available iron appears to limit pyrite formation.

Glauconite is an iron-rich authigenic clay mineral whose formation is associated with mixed-redox environments. Glauconite and phosphorite often occur together and appear to form synchronously. For example, glauconite is commonly observed to form in microenvironments, such as the interior chambers of fossil foraminifera tests where the original calcareous test wall has been replaced by francolite (Birch, 1975, 1979c; Wigley and Compton, 2007). Glauconite occurs as individual sand-sized grains included within phosphorite grains on the Namibian shelf and is most abundant in deposits offshore of Rocky Point. Glauconite grains occur sporadically in upper slope sediments offshore of Rocky Point (ODP Sites 1081/2), but are largely absent from shelf and upper slope sediment offshore of Lüderitz (ODP Site 1084) (Wefer et al., 1998b). The abundance of glauconite on the shelf and upper slope offshore of Rocky Point may reflect the relatively large amounts of iron-rich terrigenous sediment delivered by the Kunene River to the margin.

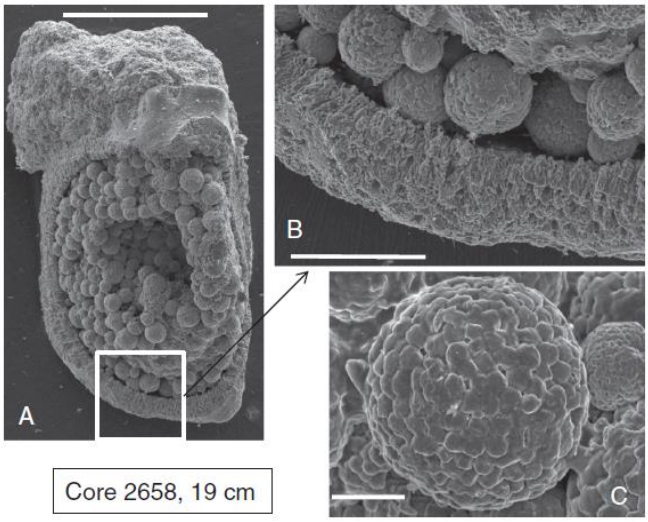

Fig. 3.17. Pyrite framboids within phosphatized shell (scale bar is 100 µm in A, 20 µm in B and 5 µm in C).

Dolomite, like glauconite, is only observed in relatively minor to trace amounts in the phosphorite deposits on the Namibian shelf. Dolomite occurs on the inner shelf of Namibia, but its origin is associated with sea-level lowstands and the mixing of meteoric and marine waters rather than upwelling (Compton et al., 2001). The origin of finely disseminated, concretionary and layered dolomite indicated to occur on the upper slope is most probably related to the high organic matter content and burial diagenesis leading to the precipitation of organogenic dolomite (Wefer et al., 1998b; Compton, 1988). It is not clear why organogenic dolomite is not more common on the shelf, but it may relate to the generally deeper and slower precipitation of dolomite in comparison to francolite during burial diagenesis, with the peak concentration of phosphate ion at shallower burial depths than peaks in carbonate alkalinity (e.g., Wefer et al., 1998a).

Although the diatomaceous mud belt underlying the BUS makes for an obvious modern analog, it is not entirely clear how modern phosphorite formation on the inner shelf mud belt relates to the larger, older and texturally more diverse phosphorite deposits on the middle to outer shelf. It appears to be a complex process that perhaps starts with partial cementation by francolite as concretionary phosphorite grains, some as large as bivalve molds while others may be as small as the interior of individual cells of giant sulfur-oxidizing bacteria or silt to sand-sized fecal pellets. Once these grains are cemented sufficiently by francolite to hold together during the transition to higher-energy lowstand conditions, they may be too big to transport beyond the shelf. Retained on the shelf, they remain prone to reburial, even if only temporarily or episodically, by organic-rich sediment. The presence of already-nucleated francolite may promote further growth until grains become highly cemented, indurated pelletal or pebble phosphorite grains observed today. In this scenario, porous and friable concretionary phosphorite grains could be viewed as initial precipitates, whereas hard cemented grains may have experienced multiple

cementation events, similar to what is observed on the Peru margin today (Garrison and Kastner, 1990). Some phosphorite grains have well defined origins (interior mollusk and foraminiferal chamber molds, phosphatized carbonate shell fragments) whereas the origin of others is vague and may include individual large bacteria (Bailey et al., 2013), fecal pellets and possibly coprolites in the case of concretionary pebbles.

3.5.3. Pleistocene sea-level fluctuations

Phosphorite is commonly observed in organic-rich sedimentary rocks where it forms in place; however, such occurrences of phosphorite are nearly always sub-economic because the phosphorite grains are too diluted by other sediment components. Economic phosphorite deposits require the physical reworking and preferential removal of non-phosphorite grains to concentrate the phosphorite, most typically into sand or gravel erosional lag deposits (Föllmi, 1996; Notholt et al., 1989; Compton et al., 2000). On continental shelves, one of the principal mechanisms for alternating between phosphorite formation in organic rich mud deposits and reworking into an erosional phosphorite sand lag deposit is changes in sea level as argued for the South African shelf (Birch, 1979a, b, c; Baturin, 1982; Compton et al., 2002, 2004; Wigley and Compton, 2006). If sea level repeatedly rises and falls over a long enough period of time, then an economic phosphorite deposit may form. The depositional and diagenetic history of the Namibian shelf succession is argued here to largely reflect changes in sea level, both the relative height of sea level and the amplitude and frequency of sea-level fluctuations.

Sediment deposits in the Lüderitz–Walvis Bay area dating back to the latest Miocene represent the highly condensed equivalent of the 600 m of sediment on the upper slope at ODP Site 1084 (Fig. 3.18), while the deposits off Rocky Point correspond to 400 to 600 m of sediment on the upper slope at ODP Sites 1081 and 1082, respectively (Fig. 3.19). The middle Miocene basal foraminiferal mud offshore Rocky Point and the Pliocene basal mud (unit 5) offshore the Lüderitz–Walvis Bay area are interpreted to have been deposited during the relatively high and steady sea levels at these times (Miller et al., 2005). Lowering of sea level and increased amplitude in sea-level fluctuations resulted in major erosional hiatuses during the deposition of the overlying Pleistocene phosphorite shelly sands. At the shallower water depths offshore Rocky Point, the Pliocene is missing and only represented by reworked Pliocene phosphorite grains in the overlying Pleistocene shelly sands.

The Pliocene to Pleistocene boundary at 2.59 Ma is associated with initial Northern Hemisphere glaciation (NHG) and the onset of significant sea-level fluctuations. Sea-level fluctuations between 2.6 and 0.9 Ma included lowstands on the order of 60 to 80 m below present day (Bintanja et al., 2005). The phosphorite sandy mud to muddy phosphorite sand in the Lüderitz–Walvis Bay area (unit 4) is interpreted to have been deposited during the early Pleistocene between 2.6 and approximately 0.9 Ma. During this period, the amplitude of sea-level fluctuations was sufficient to periodically suspend and rework mud off the shelf and to concentrate a residual lag deposit of sandy mud to muddy sand in which the sand fraction is predominantly pelletal phosphorite grains.

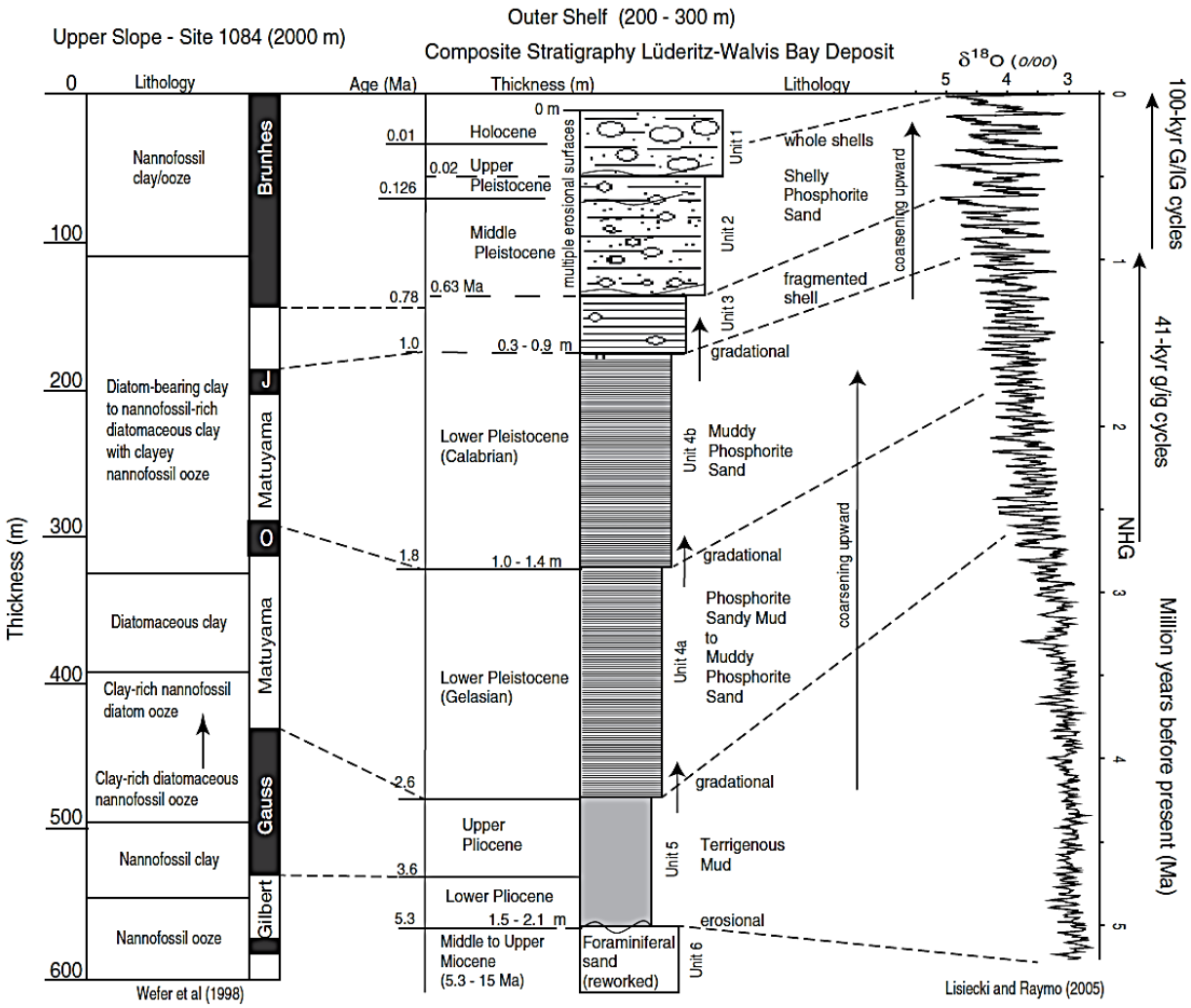

Fig. 3.18. The correlation of Plio/Pleistocene sediments on the upper slope (ODP Site 1084; Wefer et al., 1998a) to the highly condensed phosphorite deposits on the shelf and the proposed relation of shelf depositional units to global climate change reflected in the marine oxygen isotope record (Lisiecki and Raymo, 2005).

The transition from only minor amounts of gravel to sediment having up to 10% shell gravel in the Lüderitz–Walvis Bay area (unit 3) and the abrupt erosional transition to muddy sandy gravel in the offshore Rocky Point area are interpreted to correspond to the increased amplitude of sea-level fluctuations at 0.9 Ma (Elderfield et al., 2012). Upper Miocene deposits in the offshore Rocky Point area have been reworked into Pleistocene deposits. The multiple erosional surfaces and coarsening upward succession in both areas are interpreted to correspond to the high-frequency (100 kyr) and high-amplitude (130 m) fluctuations associated with major glacial/interglacial sea-level cycles established by 0.9Ma. Although the age resolution of SIS is unable to test this interpretation, the biostratigraphy suggests that the bulk of the reworked succession is middle to late Pleistocene in age (Fig. 3.8). The presence of whole and some articulated molluscs in the uppermost sediment suggests that the sediment was last reworked during the Last Glacial Maximum (MIS2) from 28 to 18 ka, with deposition since 18 ka associated with the marine transgression to the Holocene interglacial highstand, established since 11.5 ka.

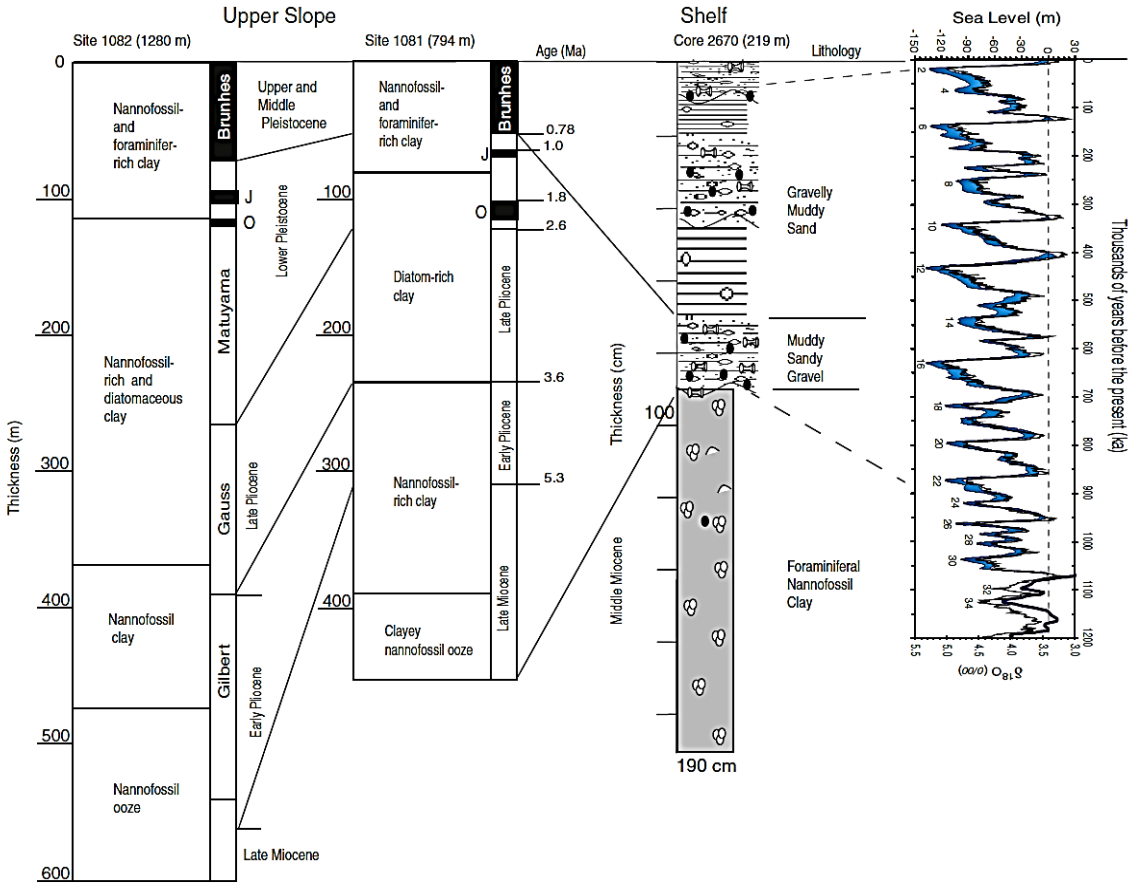

Fig. 3.19. Correlation of Plio/Pleistocene sediments on the upper slope (ODP sites 1081/2; Wefer et al., 1998a) to highly condensed phosphorite deposits offshore of Rocky Point (Fig. 3.10). The deposition of shelly phosphorite sands having multiple erosional contacts is related to major Pleistocene sea-level fluctuations (Lisiecki and Raymo, 2005; Bintanja et al., 2005).

Reworked phosphorite grains exposed on the seafloor to the low phosphate concentrations of bottom waters may have undergone partial dissolution of francolite cement and oxidation of included pyrite. For example, some pelletal phosphorite grains have irregular pitted and bleached surfaces, while others have irregular interior layers, some of which are iron-oxide stained and overgrown with younger phosphorite layers (Compton et al., 2002). However, the low solubility of francolite in seawater appears to have limited the return of P to the ocean, with a large net accumulation of phosphorite on the Namibian shelf through Pleistocene glacial/interglacial cycles. Upwelling, deposition of organic-rich mud and phosphorite formation continued during glacial periods, but was focused over the present-day middle and outer shelf regions. Unlike the present-day Holocene highstand mud belt, glacial period mud belts were probably less stable and shorter lived, as less accommodation space made them more prone to episodic reworking (Fig. 3.20). Repeated cycles of organic-rich mud deposition and phosphogenesis followed by reworking would explain the concentric layered pelletal phosphorite grains, older pelletal grains cemented in concretionary phosphorite pebbles, as well as complex, multi-generational composite phosphorite pebbles.

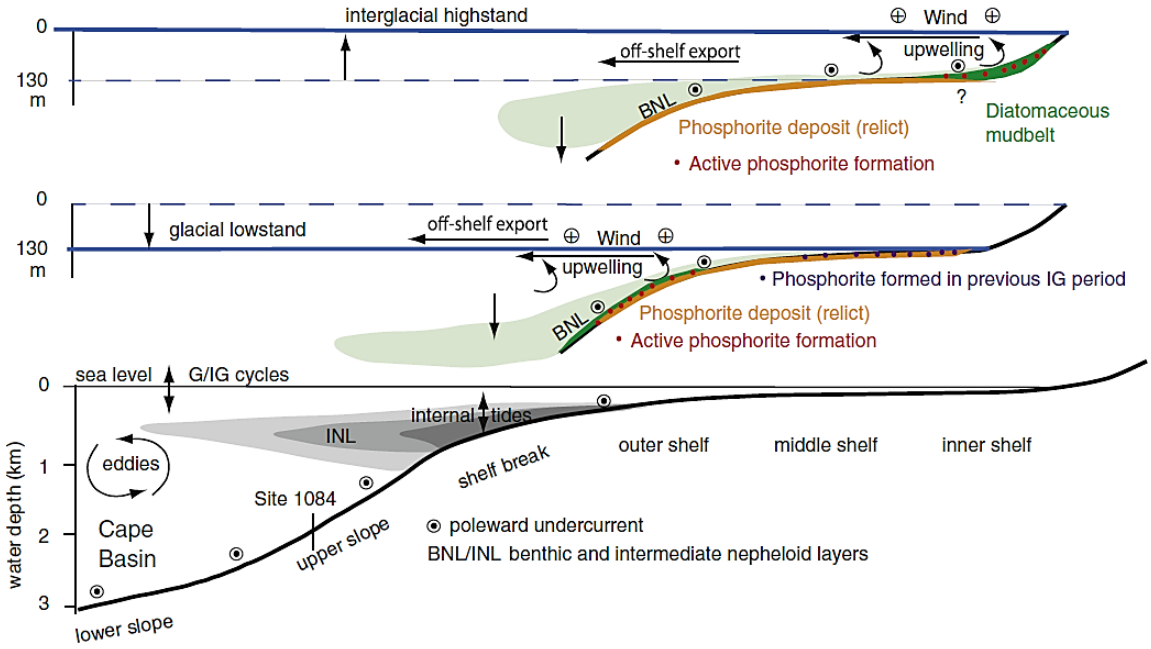

Fig. 3.20. Depositional model of phosphorite deposits on the Namibian shelf based on a margin transect (lower profile; Fig. 3.4) and expanded profiles (above) to show the shift in phosphogenesis on the shelf over glacial/interglacial cycles (refer to text for discussion).

Some older phosphorite deposits on the present-day inner shelf may be covered by dune sands deposited during glacial lowstands. For example, the Holocene diatomaceous mud belt is interpreted to rest upon relict lowstand dune sands directly offshore of Walvis Bay (Bremner, 1977). The extent to which relict phosphorite deposits may occur below the Holocene mud belt and lowstand dune deposits on the inner shelf is unknown. However, it is possible that much of the phosphorite formed in highstand inner shelf mud belt deposits was reworked during marine regressions and transported to the middle and outer shelf regions where it has accumulated from repeated sediment reworking by dissipation of wave base energy, shelf break internal waves and bottom currents (Monteiro et al., 2005; Inthorn et al., 2006; Compton and Wiltshire, 2009). At glacial terminations when sea level rose rapidly, the reworked pelletal phosphorite sands on the outer and middle shelf were bypassed and generally starved of sediment as today, while those on the middle to inner shelf were partially overlain by the next highstand organic-rich mud deposits. Phosphorite formation was renewed within the highstand mud belt either as new phosphorite grains or as additional layers on reworked grains forming, for example, concentrically banded pelletal phosphorite grains (Figs. 3.11 and 3.14). Therefore, phosphorite formation likely continued throughout Pleistocene glacial to interglacial cycles, but it was sea-level fluctuations that reworked the phosphorite into highly condensed, economic deposits (Fig. 3.20).

3.5.4. Phosphorite, upwelling intensity and aridification

Phosphorite formation on the Namibian shelf is ultimately driven by the highly productive Benguela Upwelling System. High productivity over a shallow shelf enhances the delivery of relatively fresh organic matter to the seafloor where it is rapidly degraded by bacteria.

Bacterial release of organic-bound P, especially the episodic release from large sulfur bacteria, to pore water promotes the precipitation of francolite pore-filling cement. Additional P may be sourced from the release of iron-bound P associated with terrigenous iron oxide particles under reducing conditions. Francolite variably cements the host organic-rich mud into silt- to pebble-sized phosphorite grains sufficiently hard and durable to be retained on the shelf. In this way, phosphorite retained on the shelf as sand and gravel lag deposits is a proxy for intense upwelling conditions over the shelf, even if most of the original organic-rich mud deposits in which it formed are later removed by reworking and dispersal beyond the shelf.

In general, the phosphorite SIS ages correspond to other proxies of upwelling intensity on the Namibian margin, such as sea surface temperature (SST), organic carbon mass accumulation rate (Corg MAR) and diatom abundance index (DAI) recorded in higher-resolution and better-dated upper slope deposits (Figs. 3.21 and 3.22). The SIS ages of phosphorite grains indicate that phosphogenesis extended from the latest Miocene to the present, with most phosphorite formed during the Plio/Pleistocene. Relating specific episodes of phosphorite formation to SST, Corg MAR and DAI records are limited by the age resolution of the phosphorite samples. SIS ages in most cases represent the average age of multiple grains and have uncertainties associated with the steepness of the marine Sr isotope curve and possible uptake of radiogenic Sr discussed above. Despite these limitations, the diagenetic and depositional histories of phosphorite deposits on the Namibian shelf provide new perspectives into the evolution of the BUS.

The onset of phosphorite formation in the latest Miocene (7–5 Ma) is consistent with other evidence for the initiation of Benguela upwelling as recorded by SST, Corg MAR and diatom abundance centered on the Walvis Ridge at Site 362 (Siesser, 1980) and Site 1081 (Wefer et al., 1998a; Hoetzel et al., 2013). The relatively small amount of phosphorite of latest Miocene age is also consistent with the relatively modest indicators of upwelling intensity on the margin at this time (Fig. 3.22). The possibility of phosphorite older than samples recovered and dated in this study seems unlikely because reworked middle Miocene foraminifera, but not phosphorite, were recovered from both offshore Rocky Point (14–16 Ma) and Lüderitz–Walvis Bay (10–13 Ma) areas. Therefore, the oldest phosphorite dated from the Namibian shelf is in agreement with other indicators that the northern BUS was initiated in the latest Miocene.

The phosphorite from this study is largely Plio/Pleistocene in age and centered on the period between 3 and 0.5 Ma (Figs. 3.21 and 3.22). These ages broadly overlap with upper slope margin records of major increases in upwelling intensity for the BUS north of the Orange River. Variations among the individual records suggest asynchronies in upwelling indicators along the margin; however, most proxies of increased upwelling intensity are centered on the period from 3 to 0.5 Ma. These records include colder SST, increased Corg MAR and higher diatom abundance (DAI) for sites near the Walvis Ridge (1081 and 1082) and Site 1084 offshore of Lüderitz (Wefer et al., 1998a; Lange et al., 1999; Marlow et al., 2000; Etourneau et al., 2009). These records, as well as other regional records of upwelling

productivity changes (Ravelo et al., 2004), suggest two major cooling shifts in global climate associated with upwelling intensity. The first cooling step corresponds to the gradual establishment of Northern Hemisphere glaciation (NHG) between roughly 3 and 2.6 Ma, followed by a second cooling step from roughly 2 to 1.5 Ma (Ravelo et al., 2004). The SST records from Namibia show marked cooling events approximately 3 to 2 Ma, but a pause in cooling from roughly 2 to 1.4 Ma, followed by increased variability since 1.4 Ma and a major cooling step from 1.4 to 0.6 Ma (Marlow et al., 2000; Etourneau et al., 2009). Overall, SST has dropped 10°C since 3.2 Ma at Site 1084 (Marlow et al., 2000). The cooling of SST is associated with increased organic carbon and diatom deposition on the upper slope, most of which was likely sourced from the reworking of organic-rich mud deposits off the shelf (Fig. 3.20). Therefore, although the deposition of organic rich mud associated with upwelling over the shelf is ephemeral, much of it ends up buried longterm on the slope, although at relatively low organic carbon burial efficiencies (Compton et al., 2008).

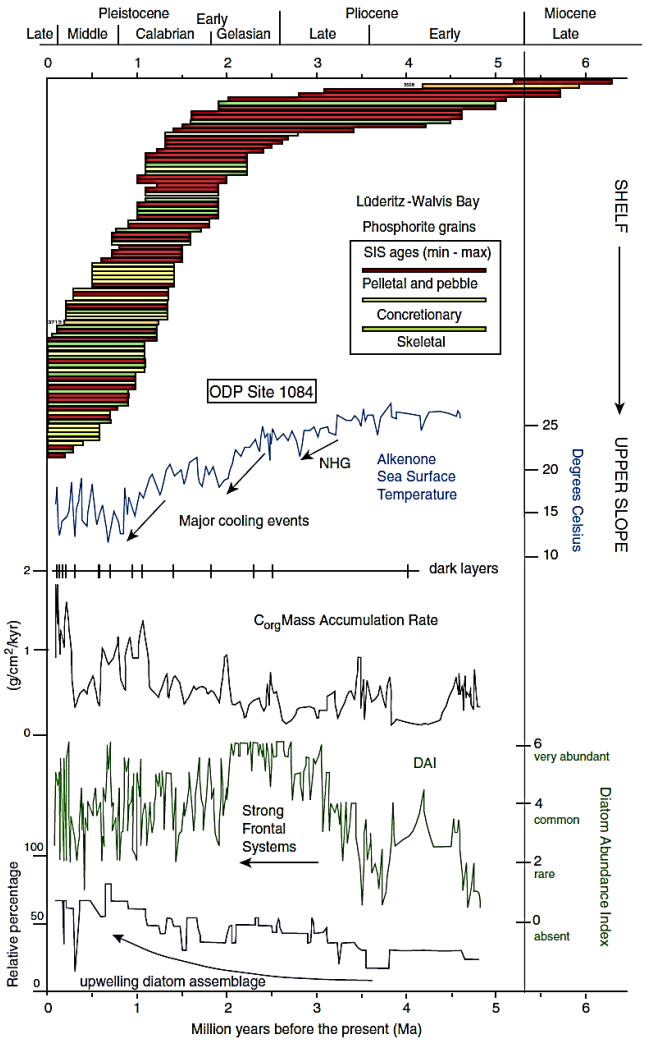

Fig. 3.21. Comparison of phosphorite SIS age ranges (min–max ages in Table 3.1) from the Lüderitz–Walvis Bay shelf area to the SST, CorgMAR, DAI and upwelling species from ODP Site 1084 (Wefer et al., 1998a; Marlow et al., 2000).

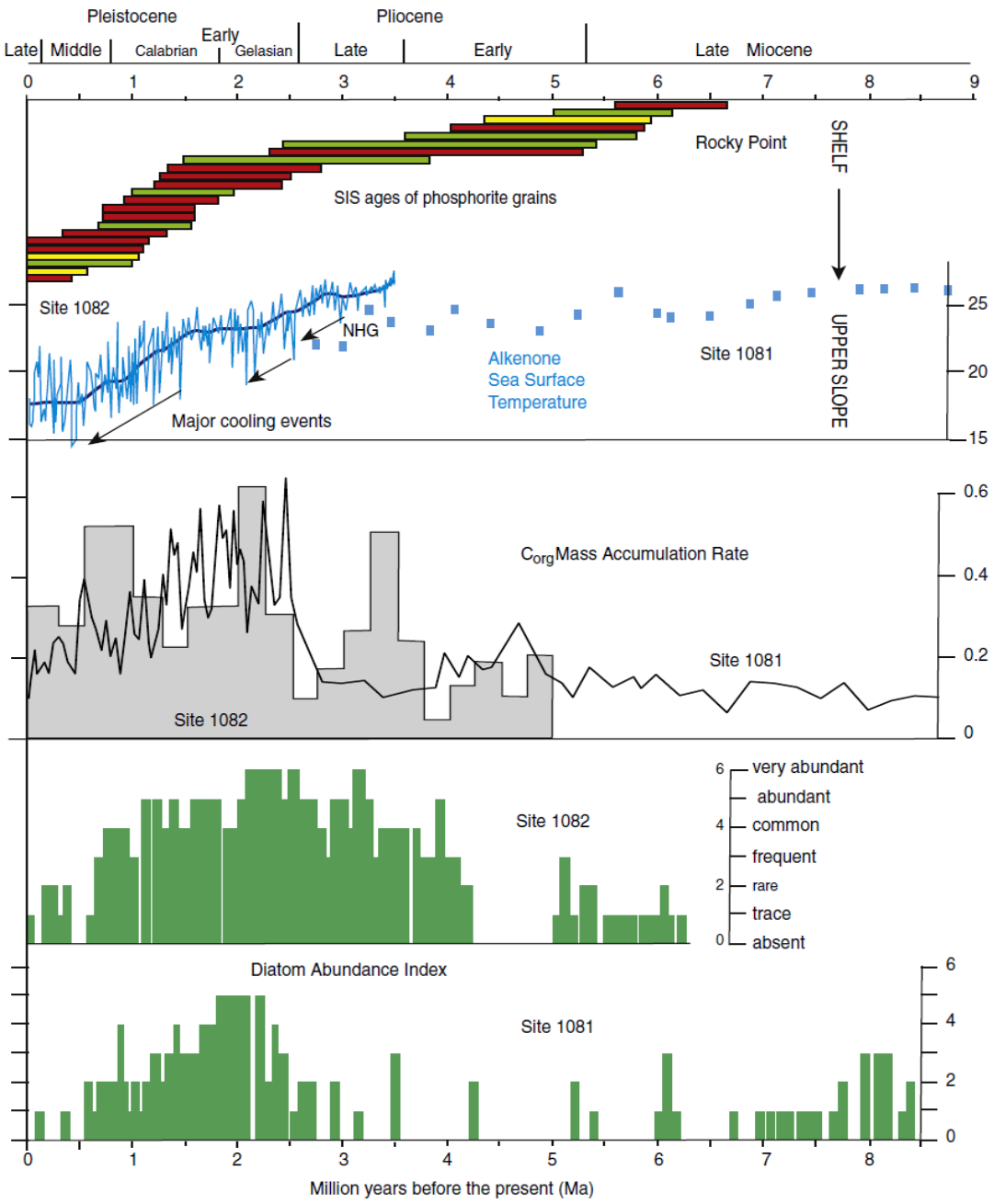

Fig. 3.22. Comparison of phosphorite SIS age ranges (min–max ages in Table 3.1) from offshore Rocky Point to the SST record from site 1081 (Hoetzel et al., 2013) and 1082 (Etourneau et al., 2009), and Corg MAR and DAI from 1081 and 1082 (Wefer et al., 1998a).

The large Lüderitz–Walvis Bay phosphorite deposits are comparable in extent and occur on the shelf immediately offshore of the Namib Desert (Fig. 3.5), but to what extent are the Namib Desert aridification and the BUS linked? The record of the Namib Desert consists of the Tsondab Sandstone Formation eolianites with an aerial extent exceeding that of the overlying unconsolidated dunes of the Namib Sand Sea (Ward, 1987; Ward and Corbett, 1990). The Tsondab Sandstone Formation is estimated to be early to middle Miocene in age based on fossils (Pickford and Senut, 1999; Senut, 2000). However, no indicators of upwelling or high productivity are known from the Namibian margin older than late Miocene. Either older

phosphorite deposits are yet to be recovered from the Namibian margin or the earliest Namib Desert was not associated with phosphorite formation and coastal upwelling. The Namib Desert Tsondab Sandstone Formation does, however, overlap with major episodes of phosphorite formation on the South African shelf (southern BUS), associated with possibly warm rather than cold water coastal upwelling since the latest Oligocene (Compton et al., 2002, 2004; Wigley and Compton, 2006).

Arid desert conditions are considered to have persisted since deposition of the Tsondab Sandstone, although less arid climates may have occurred before hyperaridity associated with the Namib Sand Sea was established (Ward, 1987; Ward and Corbett, 1990). The unconsolidated dunes of the Namib Sand Sea are considered to be at least one million years old based on cosmogenic nuclides (Vermeesch et al., 2010) and are estimated to be 2.4 to 2.7 Ma based on molecular dating of the appearance of Namibian dung beetles adapted to hyperaridity (Sole et al., 2005). The Pliocene to Pleistocene pollen record from Site 1082 off the Kunene River indicates increased seasonality from 2.7 Ma and a general increase in semi-arid plants in the broader, interior regions from 2.7 to 1.8 Ma (Dupont et al., 2005). Together, these records are consistent with the age of phosphorite formation and the SST records indicating upwelling of colder waters since roughly 3 Ma (Figs. 3.21 and 3.22). Therefore, support for linking coastal hyperaridity to the BUS appears fairly robust in the case of unconsolidated dunes of the Namib Sand Sea, but is less obvious for the underlying older eolianites of the Tsondab Sandstone Formation.

The modern BUS can be divided into a southern BUS (Cape Point to Orange River) and northern BUS (Orange River to Kunene River) based, in part, on differences in total annual productivity, with the present-day northern BUS significantly more productive than the southern BUS (Carr, 2002). The distribution, abundance, texture and age of phosphorite on the margin provide evidence for the long-term geological evolution of the BUS. Phosphorite occurs along the entire stretch of the BUS including the Agulhas Bank, but there are marked differences in the phosphorite deposits from the southern and northern regions of the BUS. Phosphorite from the northern BUS is latest Miocene to Holocene in age, with most of the phosphorite Plio/Pleistocene in age. In contrast, phosphorite from the southern BUS is latest Oligocene to Holocene in age, with most of the phosphorite latest Oligocene to early Miocene in age (26 to 16 Ma) (Compton et al., 2002, 2004). The age of phosphorite from the Agulhas Bank is poorly known, but from fossil evidence most phosphorite is thought to range from late Eocene to Pliocene in age (Dingle, 1974). These ages suggest that the BUS initiated in the southern region, perhaps in relation to the final opening of Drake's Passage (Compton et al., 2004). Upwelling in the southern BUS was most intense from the latest Oligocene to middle Miocene and then generally tapered off but continued to the present-day. Upwelling appears to have shifted focus to the northern BUS starting in the latest Miocene and then intensified through the Pliocene and Pleistocene. Like today, upwelling continued throughout the BUS, but was far more intense in the northern than southern BUS (Carr, 2002).

Far more intense upwelling in the northern than the southern BUS is supported by differences in the abundance, composition and texture of the phosphorite. The amount of phosphorite (wt.% P_2O_5) in the northern BUS deposits is far greater overall and by unit area than in deposits of the southern BUS (Fig. 3.1). Glauconite is generally the dominant authigenic mineral in the southern BUS, whereas glauconite is a relatively minor to trace mineral in the phosphorite deposits in the northern BUS. Pyrite is common to both areas, but pyrite is particularly abundant in phosphorite grains from the northern BUS. Pelletal sand grains dominate Namibian phosphorite, whereas phosphatized limestone and biogenic carbonate tend to be the dominant phosphorite grains in the southern BUS.

More intense upwelling in the northern BUS resulted in a greater abundance of siliceous (diatoms) than calcareous algae, and greater organic carbon accumulation rates, more intense microbial activity, greater phosphate ion release and more phosphorite formation. Both the northern and southern BUS receive abundant terrigenous clay and iron associated with mud delivered by the Kunene River and Orange River and deposited in similar inner to middle shelf mud belts. The large production of H_2S in highly reducing, organic-rich muds may lead to efficient sequestration of available iron by pyrite formation, thereby limiting the amount of glauconite that can form. Sediment on the Namibian margin has significantly higher organic carbon content (Mollenhauer et al., 2002; Inthorn et al., 2006) and H_2S gas eruptions are observed on the Namibian shelf (Fig. 3.4). These factors may contribute to the large difference observed in the regional glauconite content of the BUS.

3.5.5. Economic significance

The exclusive prospecting license (EPL) areas between Lüderitz and Walvis Bay cover an area of 7642 km^2. Based on the total thickness and grade (wt.% P_2O_5) of the phosphorite deposit from recovered cores, these areas are estimated to have a total of 551 Mt P_2O_5, equivalent to 2900 Mt phosphorite ('phosphate rock') at an average grade of 19 wt.% P_2O_5. Extrapolating beyond the heavily cored EPL areas to the entire 18,350 km^2 area between Lüderitz and Walvis Bay having phosphorite-rich seabed sediment yields an estimated total of 1312 Mt P_2O_5 (equivalent to 6900 Mt phosphate rock at an average grade of 19 wt.% P_2O_5). Taking the average thickness (0.6 m), density (1.2 g/cm^3) and mean phosphorite content (20 wt.%) of cores recovered from offshore of Rocky Point yields an estimated total of 246 Mt phosphate rock over an area of 1716 km^2. Extrapolating beyond the cored area to the entire 6340 km^2 between Palgrave Point and the Kunene River having phosphorite-rich seabed sediment (>5 wt.% phosphorite; Fig. 3.9), yields an estimated total of 900 Mt phosphate rock in the northern area.

Although crude, these estimates suggest that the Namibian shelf is host to a world-class phosphorite deposit, containing a phosphate rock resource on the order of 7800 Mt at an average grade of 19 wt.% P_2O_5 exposed over a seabed area of 24,700 km^2. The Namibian shelf deposit represents approximately 2–5% of the estimated global phosphate rock resource (USGS, 2015; Edixhoven et al., 2014). The largest producers of onshore phosphate rock are currently China, Morocco and the USA (USGS, 2015), but there has yet to be any significant mining of offshore phosphorite deposits.

Although several mining licenses have been issued, there is a moratorium on mining phosphorite on the Namibian shelf pending an assessment of the potential impacts, particularly to the sea fisheries industry.

3.6. Conclusions

Although extensive surface deposits were known since the 1970's, recent mineral exploration has recovered a large number of cores that provide new insights into the stratigraphy, age, origin and size of phosphorite deposits on the Namibian shelf. The largest deposit outcrops over an area of 18,350 km^2 offshore between Lüderitz and Walvis Bay while a secondary deposit outcrops over an area of 6340 km^2 offshore between Palgrave Point and the Kunene River mouth. The overall stratigraphy of the deposits is similar and consists of a sharp erosional contact overlain by a coarsening-upward succession of phosphorite sandy muds, muddy sands and gravelly (shelly) sands. Integration of biostratigraphy and strontium isotope stratigraphy indicates that the phosphorite is as old as latest Miocene (7–5 Ma), but that the majority of the phosphorite formed in the Pliocene to Pleistocene. The highly condensed, coarsening-upward succession is interpreted to reflect changes in the frequency and amplitude of sea-level fluctuations, with the lower muddy sands reworked by modest glacial to interglacial cycles during the early Pleistocene and the overlying shelly sands reworked by major glacial to interglacial cycles during the middle to late Pleistocene.

Pelletal sand is the dominant phosphorite grain type, with variable amounts of concretionary and skeletal grains. Pelletal and concretionary grains formed by the early diagenetic precipitation of francolite (carbonate fluorapatite) pore-filling cement in organic-rich, pyritic mud, similar to modern phosphorite formation in the Holocene diatomaceous mud belt. The major Namibian phosphogenic Plio/Pleistocene episode corresponds to other proxies of intensified upwelling from the Namibian margin, such as organic carbon accumulation rates, diatom abundance and sea surface temperature, as well as to global cooling events. Increased coastal upwelling delivered P to the surface where it was taken up by primary producers and transported to the seafloor as organic P. Microbial degradation released the organic P, some of which was further concentrated by other P-accumulating bacteria, creating supersaturated conditions that led to the precipitation of francolite cement. Cemented phosphorite grains became concentrated in lag deposits during periods of lowered sea level when energy dispersion preferentially suspended and removed organic-rich mud deposits off the shelf. Repeated cycling of phosphorite formation and reworking resulted in the natural beneficiation of the phosphorite into a world-class economic deposit having an estimated 7800 Mt of phosphate rock with an average grade of 19 wt.% P_2O_5. The phosphorite deposits on the Namibian shelf are younger, larger and less glauconitic than those studied on the South African shelf and indicate that the Benguela Upwelling System intensified and shifted its focus north over the Namibian shelf since the Plio/Pleistocene.

Acknowledgments

This study was supported by the National Research Foundation and the University of Cape Town Research Council. The cores and some of the data in this study were provided by

Minemakers and LL Namibia Phosphates. This study incorporates the results from the UCT Honours (4th year) projects of Melissa Oosthuizen, Mary P. Hikumuah, Leilah Gharbaharan and Bright V. Duze, as well as the report of Gettie Mulokoshi from the University of Namibia. Ian McMillan assisted with the initial identification of the foraminifera and John Pether with the initial identification of molluscs from the Lüderitz–Walvis Bay area. Petrus le Roux, Fayrooza Rawoot and Kerryn Gray assisted with the Sr isotope analyses. We thank K. Föllmi and J. Bailey for their reviews.

References

Amundson, R., Berhe, A.A., Hopmans, J.W., Olson, C., Sztein, A.E., Sparks, D.L., 2015. Soil and human security in the 21st century. Science 348, 647.

Bailey, J.V., Corsetti, F.A., Greene, S.E., Crosby, C.H., Liu, P., Orphan, V.J., 2013. Filamentous sulphur bacteria preserved in modern and ancient phosphatic sediments: implications for the role of oxygen and bacteria in phosphogenesis. Geobiology 11, 397-405.

Baturin, G.N., 1969. Authigenic phosphate concentrations in Recent sediments of the SouthWest African shelf. Doklady Earth Sciences. Section English Translation 189, 227-230.

Baturin, G.N., 1982. Phosphorites on the sea floor. Developments in Sedimentology 33. Elsevier, Amsterdam, 343 pp.

Baturin, G.N., 2000. Formation and evolution of phosphorite grains and nodules on the Namibian shelf, from Recent to Pleistocene. Marine Authigenesis: From Global to Microbial, SEPM Special Publication 66, 185-199.

Baturin, G.N., 2002. Nodular Fraction of Phosphatic Sand from the Namibia Shelf. Lithology and Mineral Resources 37, 1–17.

Bintanja, R., van de Wal, R.S.W., Oerlemans, J., 2005. Modelled atmospheric temperatures and global sea levels over the past million years. Nature 437, 125-128.

Birch, G.F., 1975. Sediments on the continental margin off the West Coast of South Africa. Unpublished PhD. thesis, University of Cape Town.

Birch, G.F., 1979a. Phosphorite pellets and rock from the western continental margin and adjacent coastal terrace of South Africa. Marine Geology 33, 91-116.

Birch, G.F., 1979b. Phosphatic rocks on the western margin of South Africa. Journal of Sedimentary Petrology 49, 93-110.

Birch, G.F., 1979c. The nature and origin of mixed apatite/glauconite pellets from the continental shelf off South Africa. Marine Geology 29, 313-334.

Birch, G.F., 1980. A model of penecontemporaneous phosphatization by diagenetic and authigenic mechanisms from the western margin of Southern Africa. In: Bentor, Y.K. (Ed.), Marine phosphorites – geochemistry, occurrence, genesis. SEPM Special Publication 29, 79-100.

Birch, G. F., 1990. Phosphate deposits on the South African continental margin and coastalterrace. In: Burnett, W.C. and Riggs, S.R, (Eds.), Phosphate Deposits of the World, vol. 3: Neogene to Recent

Phosphorites. Cambridge University Press, Cambridge, pp. 153-158.

Bremner, J. M., 1977. Sediments on the continental margin off South West Africa between Sylvia Hill and the Kunene River.Unpublished PhD. thesis, University of Cape Town.

Bremner, J.M., Rogers, J., 1990. Phosphorite Deposits on the Namibian Continental Shelf. In: Burnett, W.C., Riggs, S.R. (Eds.), Phosphate Deposits of the World, vol. 3: Neogene to Recent Phosphorites. Cambridge University Press, Cambridge, pp. 143–152.

Brock, J., Schulz-Vogt, H.N., 2011. Sulfide induces phosphate release from polyphosphate in cultures of a marine *Beggiatoa* strain. The International Society for Microbial Ecology Journal 5, 497-506.

Carr, M-E., 2002. Estimation of potential productivity in Eastern Boundary Currents using remote sensing. Deep-Sea Research Part II 49, 59-80.

Carr, M-E., Kearns, E.J., 2003. Production regimes in four Eastern Boundary Current systems. Deep-Sea Research Part II 50, 3199-3221.

Christison, I.D., 1985. Foraminifera from the continental shelf of southwest Africa. Unpublished MSc thesis. University College of Wales, Aberystwyth, 174 pp.

Coles, S.K.P., Wright, C.I., Sinclair, D.A., Van den Bossche, P., 2002. The potential for environmentally sound development of marine deposits of potassic and phosphatic minerals offshore, southern Africa. Marine Georesources and Geotechnology 20 (2), 87-110.

Compton, J. S., 1988. Degree of supersaturation and precipitation of organogenic dolomite. Geology 16, 318-321.

Compton, J.S., Harris, C., Thompson, S., 2001. Pleistocene dolomite from the Namibian shelf: High $^{87}Sr/^{86}Sr$ and $\delta^{18}O$ values indicate an evaporative, mixed-water origin. Journal of Sedimentary Research 71, 800-808.

Compton, J.S., Herbert, C., Schneider, R., 2008. Holocene organic-rich terrigenous mud on the western margin of South Africa: Nutrient source to the Southern Ocean? Global Biogeochemical Cycles 23, GB4030; doi:10.1029/2008GB003427

Compton, J.S., Mallinson, D., Glenn, C.R., Filippelli, G., Föllmi, K., Shields, G., Zanin, Y., 2000. Variations in the global phosphorus cycle. Marine Authigenesis: From Global to Microbial, SEPM Special Publication 66, pp. 1-11.

Compton, J.S., Mulabisana, J., McMillan, I.K.., 2002. Origin and age of phosphorite from the Last Glacial Maximum to Holocene trangressive succession off the Orange River, South Africa. Marine Geology 186, 243-261.

Compton, J.S., Wigley, R., McMillan, I., 2004. Late Cenozoic phosphogenesis on the western shelf of South Africa in the vicinity of the Cape Canyon. Marine Geology 206, 19-40.

Compton, J.S.., Wiltshire, J.G., 2009. Terrigenous sediment export from the western margin of South Africa on glacial/interglacial cycles. Marine Geology 266, 212-222.

Dale, D.C., McMillan, I.K., 1998. Mud belt and middle shelf benthonic and planktonic

foraminiferal assemblages and sedimentation processes compared through the Holocene successions at two tropical African (Sierre Leone) and two temperate African (western offshore South Africa) sites. South African Journal of Science 94, 319– 340.

Dale, D.C., McMillan, I.K., 2000. Pliocene foraminifera and biostratigraphic correlations of the Atlantic continental margin of South Africa and southern Namibia. 14th African Colloquium on Micropalaeontology, Luanda, Angola, 21 – 24 May 2000 (Abstract).

Dingle, R.V., 1974. Agulhas Bank phosphorites: a review of 100 years of investigation. Transactions of the Geological Society of South Africa 77, 261-264.

Dingle, R.V., Bremner, J.M., Giraudeau, J., Buhmann, D., 1996. Modern and Paleo-Oceanographic Environment under Benguela Upwelling Cells Off Southern Namibia, Palaeogeography, Palaeoclimatology, Palaeoecology 123, 85–105.

Dupont, L.M., Donner, B., Vidal, L., Pérez, E.M., Wefer, G., 2005. Linking desert evolution and coastal upwelling: Pliocene climate change in Namibia. Geology 33, 461-464.

Eckardt F.D., Kuring, N., 2005. SeaWiFS identifies dust sources in the Namib Desert. International Journal of Remote Sensing 26, 4159–4167.

Edixhoven, J.D., Gupta, J., Savenije, H.H.G., 2014. Recent revisions of phosphate rock reserves and resources: a critique. Earth System Dynamics 5, 491–507.

Elderfield, H., Ferretti, P., Greaves, M., Crowhurst, S., McCave, I.N., Hodell, D., Piotrowski, A.M., 2012. Evolution of ocean temperature and ice volume through the Mid-Pleistocene climate transition. Science 337, 704-709.

Etourneau, J., Martinez, P., Blanz, T., Schneider, R., 2009. Pliocene–Pleistocene variability of upwelling activity, productivity, and nutrient cycling in the Benguela region. Geology 37, 871-874.

Föllmi, K.B., 1996. The phosphorus cycle, phosphogenesis and marine phosphate-rich deposits. Earth Science Reviews 40, 55–124.

Frenay, J., 2004. Mineralogical characterization of sample Namphos phosphate concentrate. Laboratorie de Genie Mineral et Recyclage, University de Liege.

Garrison, R.E., Kastner, M., 1990. Phosphatic sediments and rocks recovered from the Peru margin during ODP Leg 112. Proceedings of the Ocean Drilling Program. Scientific Results 112, pp. 111-134 (College Station, TX).

Gawlinski, S., 1987. Benthonic foraminifera from the continental shelf of southwest Africa. Unpublished MSc thesis. University College of Wales, Aberystwyth. 127 pp.

Herbert, C., Compton, J.S., 2007. Geochronology of Holocene sediments on the western margin of South Africa. South African Journal of Geology 110, 327-338.

Hoetzel, S., Dupont, L., Schefuß, E., Rommerskirchen, F., Wefer, G., 2013. The role of fire in Miocene to Pliocene C4 grassland and ecosystem evolution. Nature Geoscience 6, 1027-1030.

Howarth R.J., McArthur J.M., 1997. Statistics for strontium isotope stratigraphy. A robust LOWESS fit to the marine Sr-isotope curve for 0 - 206 Ma, with look-up table for the derivation of numerical age. Journal of Geology 105, 441-456.

Inthorn, M., Wagner, T., Scheeder, G., Zabel, M., 2006. Lateral transport controls distribution, quality, and burial of organic matter along continental slopes in high-productivity areas. Geology 34, 205-208.

Jarvis, I., Burnett, W.C., Nathan, Y., et al., 1994. Phosphorite Geochemistry: State of the Art and Environmental Concerns, Eclogae Geologicae Helvetiae, 87, 643–700.

Lange, C.B., Berger, W.H., Lin, H.-L., Wefer, G., and Shipboard Scientific PartyLeg 175, 1999. The early Matuyama Diatom Maximum off SW Africa, Benguela. Marine Geology 161, 93–114.

Lisiecki, L.E., Raymo, M.E., 2005. A Pliocene-Pleistocene stack of 57 globally distributedbenthic $\delta^{18}O$ records. Paleoceanography 20, PA1003, doi:10.1029/2004PA001071.

Mallinson D., Compton, JS., 1998. The influence of iron sulfide oxidation on the sulfur isotope analysis of Miocene phosphorites from Florida, USA. Geochimica et Cosmochimica Acta 62, 3689-3694.

Marlow, J.R., Lange, C.B., Wefer,G., Rosell-Mele, A., 2000. Upwelling intensification as part of the Pliocene-Pleistocene climate transition. Science 290, 2288-2291.

McArthur, J.M., 1994. Recent trends in strontium isotope stratigraphy. Terra Nova 6, 331-358.

McArthur, J.M., Benmore, R.A., Coleman, M.L., Soldi, C., Yeh, H.W., O'Brien, B.W., 1986. Stable isotopic characterisation of francolite formation. Earth and Planetary Science Letters 77, 20-34.

McArthur J.M., Sahami, A.R., Thirlwall, M., Hamilton, P.J., Osborn, A.O., 1990. Dating phosphogenesis with strontium isotopes. Geochimica et Cosmochimica Acta 54, 1343-1351

McArthur J.M., Howarth, R.J., Bailey, T.R., 2001. Strontium Isotope Stratigraphy: LOWESS Version 3: Best Fit to the Marine Sr-Isotope Curve for 0–509 Ma and Accompanying Look-up Table for Deriving Numerical Age. The Journal of Geology 109, 155–170.

McMillan, I.K., 1987. Late Quaternary foraminifera from the southern part of offshore southwest Africa/Namibia. Unpublished PhD thesis. University College of Wales, Aberystwyth.565 pp.

McMillan, I.K., 1993. Foraminiferal biostratigraphy, sequence stratigraphy and interpreted chronostratigraphy of marine Quaternary sedimentation on the South African continental shelf. South African Journal of Science 89, 83– 89.

Miller, K.G., Kominz, M.A., Browning, J.V., Wright, J.D., Mountain, G.S., Katz, M.E., Sugarman,P.J., Cramer, B.S., Christie-Blick, N., Pekar, S.F., 2005. The Phanerozoic Record of Global Sea-Level Change. Science 310, 1293-1298.

Mollenhauer, G., Schneider, R.R., Müller, P.J., Spieß, V., Wefer, G., 2002. Glacial/interglacial variability in the Benguela upwelling system: Spatial distribution and budgets of organic carbon

accumulation, Global Biogeochemical Cycles, 16(4), 1134, doi:10.1029/2001GB001488.

Monteiro, P.M.S., Nelson, G., van der Plas, A., Mabille, E., Bailey, G.W., Klingelhoeffer, E., 2005. Internal tide – shelf topography interactions as a forcing factor governing the large-scale distribution and burial fluxes of particulate organic matter (POM) in the Benguela upwelling system. Continental Shelf Research 25, 1864-1876.

Murray, J., Renard, A.F., 1891. Report on the deep sea deposits based on specimens collected during the voyage of the HMS Challenger: Report on the scientific results of the exploring voyage of HMS Challenger 1873-1876, pp. 391-400 London: Her Majesty's Stationary Office. (http://www.19thcenturyscience.org/HMSC/HMSC-Reports/1891-DeepSeaDeposits/htm/doc.html)

Notholt, A.J.G., Sheldon, R.P., Davidson, D.F., 1989. Phosphate Deposits of the World, vol. 2: Phosphate rock resources. Cambridge University Press, Cambridge.

Pickford, M., Senut, B., 1999. Geology and palaeobiology of the central and southern Namib Desert, southwestern Africa.In: Memoir of the Geological Survey of Namibia 18, 1–155.

Price, N.B., Calvert, S.E., 1978. The geochemistry of phosphorites from the Namibian shelf. Chemical Geology 23, 151–170.

Ravelo, A.C., Andreasen, D.H., Lyle, M., Lyle, A.O., Wara, M.W., 2004. Regional climate shifts caused by gradual global cooling in the Pliocene epoch. Nature 429, 263-267.

Rogers, J., 1977. Sedimentation on the continental margin off the Orange River and the Namib Desert.Unpublished PhD. thesis, University of Cape Town.

Rogers, J., 2007. Geological report on pelletal phosphorite from the outer shelf off Namibia. SAMICOR Consultancy Report.

Rogers, J., Bremner, J.M., 1991. The Benguela Ecosystem. Part VII. Marine-geological aspects. In: Barnes, M. (Ed.) Oceanography and Marine Biology Annual Reviews 29, 1-85.

Rossouw, J., 1984. Review of existing wave data, wave climate and design waves for South African snd South West African (Namibian) coastal waters. Report CSIR Stellenbosch, T/SEA 8401, 1-66.

Ruttenberg, K.C., 2003. The Global Phosphorus Cycle. In: Schlesinger,W.H. (Ed.), Treatise on Geochemistry. vol. 8, pp. 585–643.

Schulz, H.N., Schulz, H.D., 2005. Large sulphur bacteria and the formation of phosphorite. Science 307, 416-418.

Senin, Y.M., 1970. Phosphorus in Bottom Sediments on the Shelf of Southwestern Africa, Litologiyai Poleznye Iskopaemye 1, 11–27.

Senut, B. 2000. Fossil ratite eggshells: A useful tool for Cainozoic biostratigraphy in Namibia. Communications of the Geological Survey of Namibia 12, 421-428.

Shannon, L.V., Nelson, G., 1996. The Benguela: Large scale features and processes and system variability. In: Wefer, G., Berger, W.H., Siedler, G., Webb, D.J. (Eds.), The South Atlantic: Present and Past Circulation.Springer-Verlag, Berlin Heidelberg, pp. 163-210.

Siesser, W.G., 1980. Late Miocene origin of the Benguela Upwelling System off northern Namibia. Science 208, 283-285.

Sole, C.L., Scholtz, C.H., Bastos, A.D.S., 2005. Phylogeography of the Namib Desert dung beetles Scarabaeus (Pachysoma) MacLeay (Coleoptera: Scarabaeidae). Journal of Biogeography 32, 75-84.

Summerhayes, C.P., Birch, G.F., Rogers, J., Dingle, R.V., 1973. Phosphate in sediments off South-western Africa. Nature 243, 509-511.

Thomson, J., Calvert, S.E., Mukherjee, S., Burnett, W.C., Bremner, J.M., 1984. Further studies of the nature, composition and ages of contemporary phosphorite from the Namibian Shelf. Earth and Planetary Science Letters 69, 341-353.

USGS, 2014. Mineral Commodity Summaries, Phosphate Rock, United States Geological Survey, Washington, DC.

Vermeesch, P., Fenton, C.R., Kober, F., Wiggs, G.F.S., Bristow, C.S., Xu, S., 2010. Sand residence times of one million years in the Namib Sand Sea form cosmogenic nuclides. Nature Geoscience 3, 862-864.

Ward, J.D., 1987. The Cenozoic succession in the Kuiseb Valley central Namib Desert. Geological Survey of South West Africa/Namibia Memoirs 9.

Ward, J.D., Corbett, I., 1990. Towards an age for the Namib. In: Seely, M.K. (Ed.), Namib Ecology: 25 Years of Namib Research. Transvaal Museum, Pretoria, Transvaal Museum Monographs 7, pp. 17-26.

Wefer, G., Berger, W.H., Richter, C., et al., 1998a. Proceedings of the Ocean Drilling Programme, Initial Reports. Ocean Drilling Program. College Station, TX, pp. 175.

Wefer, G., Berger, W.H., Richter, C., et al., 1998b. Facies patterns and authigenic minerals of upwelling depostis off southwest Africa. Proceedings of the Ocean Drilling Programme, Initial Reports. Ocean Drilling Program. College Station, TX, pp. 467-504.

Wigley, R.A., Compton, J.S., 2006. Late Cenozoic evolution of the outer continental shelf at the Head of the Cape Canyon, South Africa. Marine Geology 226, 1-23.

Wigley, R., Compton, J.S., 2007. Oligocene to Holocene glauconite-phosphorite grains from the Head of the Cape Canyon on the western margin of South Africa. Deep-Sea Research Part II (54), 1375-1395.

Wigley, R. and Compton, J.S., 2012. Microstratigraphy of a Miocene layered phosphatic pebble from the western margin of South Africa. Sedimentology 60, 666-678.

Chapter 4

Distribution and Taxonomic Overview of Middle Miocene Foraminifera from the Northern Namibian Continental Shelf

4. Distribution and taxonomic overview of Middle Miocene foraminifera from the northern Namibian continental shelf

Abstract

Middle Miocene foraminifera from the northern Namibian shelf are indicators of a period prior to the initiation of the Benguela Upwelling System (BUS) that includes the Middle Miocene Climatic Optimum (MMCO). The distribution, taxonomic descriptions and ecological preferences of 53 benthic and 9 planktic foraminiferal species from the northern Namibian shelf are summarised here. Most species are reported for the first time from the middle Miocene on the southwestern shelf of Africa off Namibia. Eleven taxa reported here have previously only been reported on the genus level on the southwestern shelf of South Africa. All planktic taxa, except *Globigerinoides ruber*, occurred along the southwestern margin from the Congo Basin to South Africa during the middle Miocene. Certain benthic species from the study area, such as *Glandulina laevigata, Brizalina alata, Sphaeroidina bulloides* and *Gyroidinoides soldanii* continued to occur in Plio-Pleistocene to Recent sediments along the southwestern continental shelf of Africa. Many of the species reported in this study from the shelf have also been documented in continental slope studies. At least 15 benthic taxa are reported from Northern Hemisphere middle Miocene deposits and indicate their widespread distribution during this time period.

4.1. Introduction

Fossil foraminifera are valuable proxies in biostratigraphy, palaeoecology, palaeoclimate and palaeoceanography studies, and in the petroleum exploration industry. The long evolutionary record of foraminifera and their high abundance in the fossil record aid in geologic and exploration studies (Armstrong and Brasier, 2005). The taxonomy and correct identification of the taxa are the first steps to unlocking and understanding the palaeo-environment and determining the age of strata. The distribution of foraminifera allows for a better understanding of the palaeoenvironment and oceanographic changes over time.

Along the margin of southern Africa, foraminifera have been utilised in the interpretation of geologic outcrops (Dale and McMillan, 1999), palaeoceanographic studies (Schmiedl and Mackensen, 1997; Marlow et al., 2000; Rau et al., 2002; Jahn et al., 2003; Baumann and Freitag, 2004; Diester-Haass et al., 2004; Lazarus et al., 2008; Leiter and Altenbach, 2010) and biostratigraphy (Compton et al., 2004; Compton and Bergh, 2016). Although foraminifera have been studied for ~150 years along the southern African coast, taxonomic work has been restricted to South African studies (Ovechkina et al., 2010). Taxonomic information on Miocene-aged foraminiferal faunas from southern Africa is not well documented despite the Miocene representing an important time interval in which tropical to subtropical foraminifera disappeared at southern latitudes in the southern oceans off Namibia

(Bergh et al., 2018) and the Benguela Upwelling System (BUS) initiated along the northern Namibian margin (Siesser, 1980). Information for southern African taxa found in the Miocene can only be referred to in global studies with the exception of Kender et al. (2008) in which Miocene-aged foraminifera from the Congo Basin were described.

Considering the few Miocene foraminiferal studies along the western margin of southern Africa, this chapter aims to contribute to existing knowledge from studies in the Congo Basin and along the western margin of South Africa. This chapter also provides a taxonomic and palaeoecological summary of middle Miocene foraminifera. This time interval represents a global period of warmer temperatures prior to the initiation of the BUS. These assemblages from the middle Miocene can therefore be used as reference to a warmer period in Earth's history.

4.2. Materials and Methods

Thirty samples from the basal olive-green mud unit of three cores from the northern Namibian shelf (core 2658 from a water depth of 211 mbsl; core 2670 from a water depth of 219 mbsl and core 2682 from a water depth of 229 mbsl) (Fig. 4.1) studied by Bergh et al. (2018) were processed. Samples were taken at a mean spacing of 5 cm which allowed for multiple samples to be analysed for the time period investigated. Each sample was washed, sieved and split into <63 µm (mud), 63 µm to 2 mm (sand) and >2 mm (gravel) fractions. The units were dated using biostratigraphic indicators according to Bolli et al. (1985) and Kennett and Srinivasan (1983), and Sr-isotope stratigraphy as described in Compton and Bergh (2016).

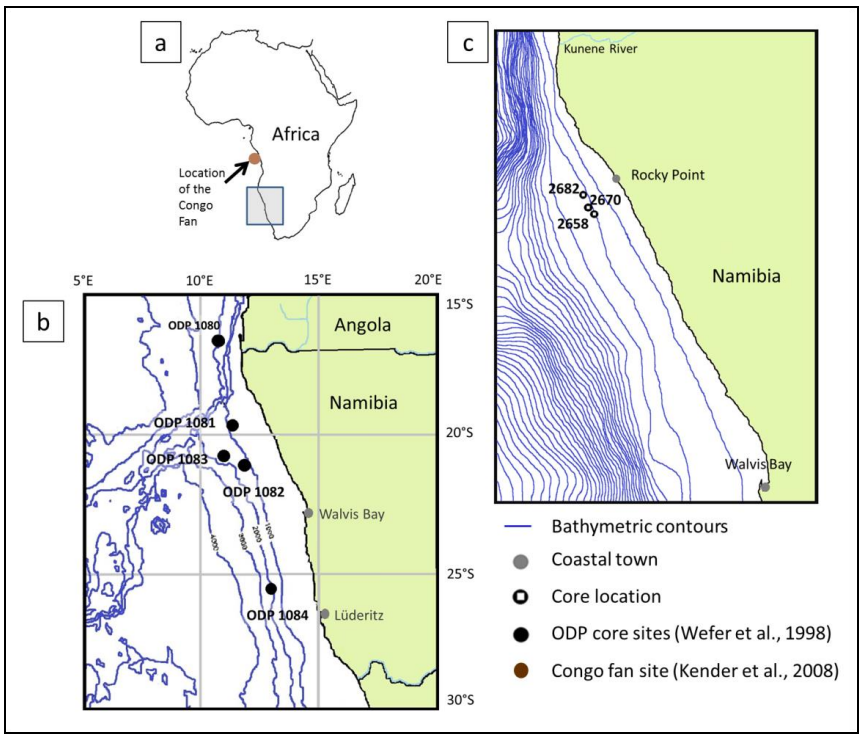

Fig. 4.1. a) Location of the study area (blue shaded box) in the context of Africa; b) and relative to ODP sites (black circles) and c) the location of cores discussed in this study. The contour intervals for the bathymetric lines in b are 1000 m and in c 100 m. Adapted from maps provided by Minemakers Australia Pty Ltd.

The bulk sediment and foraminifera from the sand fractions were put in an ultrasonic bath for up to 1 minute to disaggregate and suspend the sediment particles. The separated sand-sized fraction was oven dried at 70°C and foraminifera were picked and identified under a binocular microscope. Picked specimens were mounted onto black adhesive carbon tabs and coated with Gold-Palladium using a BIO-RAD SEM coating system before images were taken with a JEOL JSM-5200 scanning electron microscope (SEM) at Iziko Museums of South Africa in Cape Town and a Nova NanoSEM scanning microscope at the Electron Microscope Unit of the University of Cape Town. Photomicrographs were also taken with a Leica EZ4D stereo microscope.

The ages of the samples were based on Compton and Bergh (2016) and results on the identification and distributions from this study were compared to previous studies (Martin, 1981; Hay et al., 1984; Lowry, 1987; Wefer et al., 1998; Compton et al., 2004; Kender, 2007; Kender et al., 2008) in which lists of taxa were given to determine the occurrence and distribution of foraminifera along the southwestern margin of Africa since the Miocene.

4.3. Stratigraphy

The core lithostratigraphy is composed of a basal olive-green mud overlain by gravelly pelletal phosphorite sands that coarsen upwards (Fig. 4.2). Components in core 2670 were dated using strontium isotope stratigraphy (SIS) (Howarth and McArthur, 1997). Picked foraminifera in the basal mud unit had a SIS middle Miocene age (14.4 to 16.1 Ma) and the overlying pelletal phosphorite units had SIS ages indicating a Plio-Pleistocene depositional age (Compton and Bergh, 2016). Shell fragments at the contact between the phosphorite units and the basal muddy unit had SIS ages of Mio-Pliocene (5.1 to 6.2 Ma). In the overlying units above the contact phosphorite pebbles had SIS ages of 0.0 to 1.3 Ma and fish bone 0.0 to 1.6 Ma. Bivalve shells in the upper sections of the core had SIS ages of 0.0 to 1.2 Ma (Compton and Bergh, 2016).

Indicator species *Globigerinoides bisphericus* (early to middle Miocene; Bolli et al., 1985) and *Globoquadrina dehiscens* (early to late Miocene; Kennett and Srinivasan, 1983) in the basal olive-green mud agree with the bulk foraminiferal sand SIS ages of middle Miocene for the basal unit. The occurrence of the indicator species in cores 2658 and 2682 is cross-correlated with the SIS ages and indicator species in core 2670. The biostratigraphic ages of the indicator species in the overlying gravelly pelletal phosphorite sands, *Globorotalia (Globoconella) inflata* and *Globorotalia truncatulinoides*, are consistent with the Plio-Pleistocene ages obtained by SIS.

4.4. Taxonomic overview

Taxonomic descriptions of all the benthic and planktic foraminiferal species that could be identified to at least the genus level are given. The generic classification of foraminifera is based on the morphology of the tests by Loeblich and Tappan (1988). Planktic species are discussed following the benthic forms according to taxonomic classification. Species identified as genus sp. could not be identified with certainty beyond the genus level.

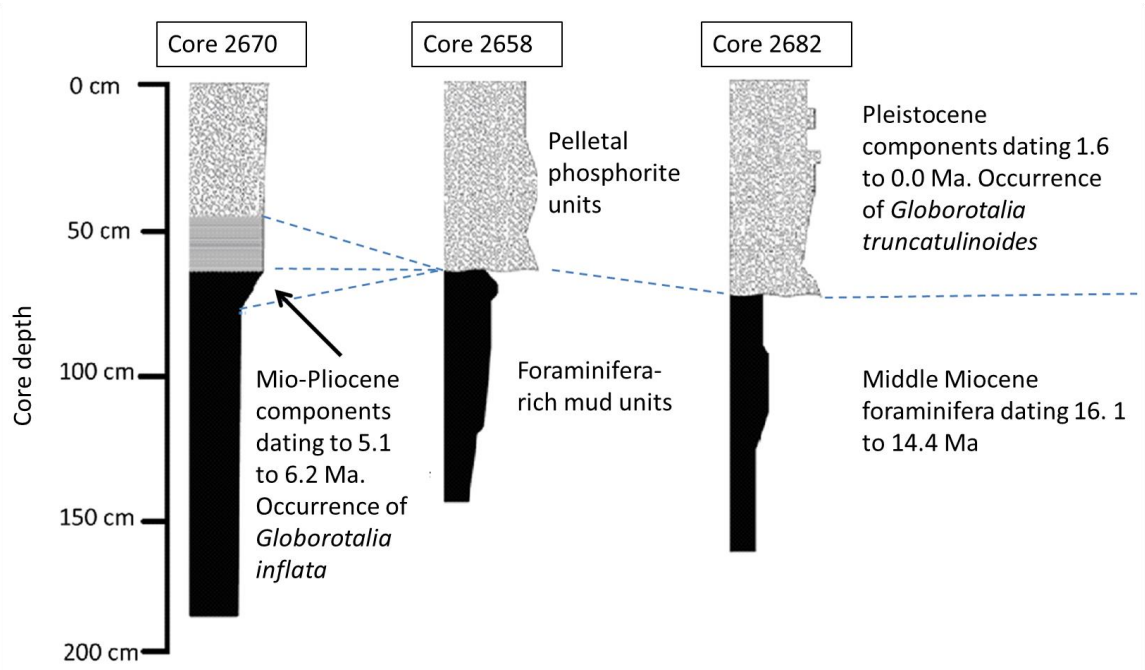

Fig. 4.2. Statigraphy for the three cores of this study (core 2670 at a depth of 219 mbsl; core 2658 at 211 mbsl and 2682 at 229 mbsl) based on planktic indicators and SIS of different components within and above the Miocene section of core 2670 (Compton and Bergh, 2016).

Synonymies and associated references for each identified species are given followed by a short description and justification to the identification of the specific taxa. Remarks on the abundance of the taxa within the cores and dimensions of the tests are given together with a global or regional stratigraphic range for some of the foraminifera. The stratigraphic ranges are based on relevant publications (e.g. Jones, 1994; Holbourn et al., 2013). The occurrences of the taxa are given in a regional context incorporating results from previous studies such as Martin (1981), Lowry (1987), the Ocean Drilling Program Leg 175 (Wefer et al., 1998), Compton et al. (2004), Kender (2007) and Kender et al. (2008). Many of the taxa have been recorded in a variety of environments and their ecological preferences are given as examples.

4.4.1. Benthic Foraminifera

Order: LITUOLIDA Lankester, 1885

Family: SPIROPLECTAMMINIDAE Cushman, 1927a

Genus: SPIROPLECTAMMINA Cushman, 1927a

***Spiroplectammina* sp.**

Pl. 1 figs. 1a-b

Description: The chamber walls are agglutinated and well cemented. The test is flattened and broad with the margins rounded. In cross section the test is trapezoid in shape. Chambers are biserially arranged with flush sutures. The arched aperture is situated along the margin of the terminal chamber.

Remarks: Only a few tests were identified (not exceeding 5% in samples) in core 2670

measuring up to 0.4x0.6 mm. Tests are commonly broken or have predatory holes.
Ecological examples: Species of the genus *Spiroplectammina* are infaunal in low oxygen environments (Hallam and Wignall, 1997) of increased food availability (Alegret and Thomas, 2007)
Regional occurrence: Middle Miocene on the continental shelf south of the Kunene River mouth.

Family: EGGERELLIDAE Cushman, 1937
Genus: KARRERIELLA Cushman, 1933

Karreriella siphonella (Reuss, 1851)
Pl. 1 figs. 2-3
Gaudryina siphonella Reuss, 1851, p.78, pl.5, figs. 40a, b; 42a, b
Karreriella siphonella King, 1989, p. 456, pl. 9.2, fig. 3; Hemleben et al., 1990, p. 194, pl. 12, fig. 17-18; pl. 25, fig. 8.
Description: The chamber walls are agglutinated. The test is elongate, rounded in cross-section and trochospiral in the early stage reducing to triserial and biserial in the adult stage. The chambers enlarge toward the terminal end. Sutures are depressed. The aperture is terminal and slit-like.
Remarks: Large test size of up to 0.2x1.5 mm. Major component of the agglutinate foraminifera in this study in all three cores, but minor component (<5%) of total benthic foraminiferal assemblage.
Ecological examples: The genus *Karreriella* is epifaunal, unattached and prefers muddy sediments on the outer shelf to slope (Murray, 2006).
Global stratigraphic range: Genus occurs from the Eocene to Recent (Loeblich and Tappan, 1988)
Regional occurrence: Middle Miocene on the continental shelf south of the Kunene River mouth.

Genus: MARTINOTIELLA Cushman, 1933

Martinottiella communis (d'Orbigny, 1846)
Pl. 1 fig. 4
Clavulina communis d'Orbigny, 1846, p. 196, pl. 12, fig. 1-2
Martinottiella communis Kohl, 1985, p. 33, pl. 4, fig. 2; Cicha et al., 1998, p. 111, pl. 9, fig. 6-7; Kender et al., 2008, p. 507, pl. 12, fig. 8-10
Description: The chamber walls are agglutinated and well cemented. The test is elongate and mostly uniserial. The sutures are depressed. The aperture is terminal and rounded in the centre of the final chamber. The test is trochospiral in the early stage reducing to triserial and biserial in the adult stage. The aperture is rounded on a short neck above the terminal chamber.
Remarks: Large test size of up to 0.2x1.5 mm. Few specimens have been found in cores 2670 and 2682 forming trace components (<1%) of the total benthic foraminifera assemblage.
Ecological examples: The genus *Martinottiella* is epifaunal, unattached and prefers muddy sediments on the outer shelf to slope (Murray, 2006). The species *M. communis* has been reported from variable environmental conditions. It has been associated with low-oxygen water from the outer shelf to upper abyssal depths (Kaiho and Hasegawa, 1986), but it has also been reported in low numbers in comparatively well oxygenated lower continental slope environments in late Quaternary sediments (Schmiedl and Mackensen, 1997).
Global stratigraphic range: Oligocene to Recent (Jones, 1994)

Regional occurrence: Middle Miocene on the northern Namibian continental shelf (this study) and in the Congo Basin (Kender et al., 2008). Specimens of *Martinottiella communis* have been recovered in Miocene to Pleistocene-aged sediments in minor relative abundances (<10%) from the western continental slope of Namibia (Hay et al., 1984; Wefer et al., 1998) and South Africa (Wefer et al., 1998). The highest abundances were recorded at the deepest ODP site (1084) during the Pleistocene.

Family: VALVULINIDAE Berthelin, 1880

Genus: CLAVULINA d'Orbigny, 1826

Clavulina angularis (d'Orbigny, 1826)

Pl. 1 figs. 5-6

Clavulina angularis Brady, 1884, p. 396, pl.48, figs. 22-24; Said, 1949, p. 8, pl. 1, fig. 19; Le Calvez, 1977, p.10, figs. 1-3; Banner and Pereira, 1981, pl. 9, figs. 5-6, pl. 10, figs. 4, 6, 10; Weidich, 1988, p. 340, pl, 2, figs. 1-24; Hottinger et al., 1993, p. 41-42, pl. 21, figs. 1-13

Clavulina pacifica, Cushman, 1924, p. 22; Coleman, 1980, figs. 1-3, pl. 1, figs. 1-8.

Description: The test wall is agglutinated and well cemented, semi-triangular in section and tricarinate in form. The early stage is triserial becoming uniserial and angular as chambers are added. Sutures are depressed. The aperture is rounded, dentate and terminal.

Remarks: Large test size of up to 0.5x2 mm. Few specimens of *Clavulina angularis* have been found in core 2670 forming trace components (<1%) of the total benthic foraminifera population.

Ecological examples: The species *C. angularis* has been reported to be infaunal and occurring in muddy sands (Abu-Zied et al., 2011).

Regional occurrence: Middle Miocene on the Namibian continental shelf south of the Kunene River mouth.

Clavulina trilatera (Cushman, 1926)

Pl. 1 figs. 7a-b

Clavulina trilatera Cushman, 1926, p. 588, pl. 17, fig. 2

Clavulina trilatera var. *aspera* Cushman, 1926, p. 589, pl. 17, fig. 3; Cushman, 1946, p. 38, pl. 9, figs. 10-16

Clavulinoides trilatera Mello, 1969, p. 50, pl. 1, fig. 3a-b.

Description: The test wall is agglutinated and well cemented. The test is triangular in section tapering towards the initial end and broadening towards the apertural end. The early stage is triserial becoming uniserial and angular as chambers are added. The chambers enlarge as added with flush sutures. The aperture is rounded, dentate and terminal.

Ecological examples: Infaunal (Ali, 2015) at slope to abyssal depths (Alegret et al., 2002; Holbourn et al., 2013).

Remarks: Large test size of up to 0.5x2 mm. Few specimens have been found in core 2670 forming a minor component (<5%) of the total foraminifera composition.

Regional occurrence: Middle Miocene on the Namibian continental shelf south of the Kunene River mouth.

Order: LAGENIDA Delage and Herouard, 1896

Family: NODOSARIIDAE Ehrenberg, 1838

Genus: DENTALINA Risso, 1826

Dentalina acuta (d'Orbigny, 1846)

Pl. 1, fig. 8

Dentalina acuta d'Orbigny, 1846, p.56, pl. 2, fig. 40-43; Beissel, 1891, p. 37, pl. VII, fig. 28-52; Papp and Schmid, 1985, pl. 18, fig. 1-6.

Description: The wall is calcareous, hyaline. The test is elongate, slightly arcuate and uniserial with the initial chamber possessing a spine. Longitudinal costae cover the test surface. The chambers enlarge gradually toward the terminal end. The aperture is terminal and radiate.

Remarks: Few tests were found comprising <1% of the total benthic foraminifera assemblage in core 2670.The tests are up to 3 mm long and thin measuring 0.15 mm in cross-section. .

Ecological examples: Infaunal, adapted to suboxic conditions (Kaiho, 1994)

Global stratigraphic range: Triassic to Quaternary (Collinson, 2012)

Regional occurrence: Middle Miocene on the Namibian continental shelf south of the Kunene River mouth.

Dentalina albatrossi (Cushman, 1923a)

Pl. 1, fig. 9

Nodosaria vertebralis var. *albatrossi*, Cushman, 1923a, p. 47, pl. 15, fig. 1.

Dentalina albatrossi, Jones, 1994, p. 76, pl. 64, figs. 11-12, 14; Hanagata and Nobuhara, 2014, p. 25, fig. 9.12-9.13.

Description: The test wall is calcareous, hyaline. The test is elongate and uniserial. Longitudinal costae cover the test surface. The chambers gradually increase in size towards the terminal end. The aperture is terminal.

Remarks: Few tests, commonly broken, comprising <1% of the total foraminiferal assemblage in core 2670.The tests are long and thin (0.2 mm in cross-section and up to 2.5 mm long).

Ecological examples: Infaunal, adapted to suboxic to dysoxic conditions (Kaiho, 1994, 1999)

Global stratigraphic range: Miocene to Recent (Jones, 1994)

Regional occurrence: Middle Miocene on the Namibian continental shelf south of the Kunene River mouth.

Genus: LAEVIDENTALINA Loeblich and Tappan, 1986

Laevidentalina inornata (d'Orbigny, 1846)

Pl. 1, fig. 10

Dentalina inornata d'Orbigny, 1846, p. 44, pl. 1, figs. 50–51; Papp and Schmid, 1985, p. 28, pl. 9, figs. 5–8.

Description: The test surface is smooth, calcareous, hyaline and circular in cross section. The test is elongate, arcuate and uniserial with nine chambers gradually increasing in size towards the terminal end. The proloculus is rounded. The sutures are depressed and horizontal. The aperture is terminal with slits radiating towards the end.

Remarks: The classification was made as *Laevidentalina* on account of the description in Loeblich and Tappan (1988). It is distinguished from *Dentalina* in having a smooth surface rather than having longitudinal costae.
Few tests comprising <1% of the total foraminiferal assemblage in core 2670. The tests are up to 1 mm long and thin measuring 0.1 mm in cross-section.

Ecological examples: The genus *Laevidentalina* is infaunal (Alegret et al., 2003) and occur under a variety of oxic conditions, e.g. under high oxygen conditions in the

Mediterranean Sea (Cimerman and Langer, 1991; Sgarella and Moncharmont Zei, 1993; Milker and Schmiedl, 2012) and under suboxic to dysoxic conditions (Rögl and Spezzaferri, 2002).

Global stratigraphic range: The stratigraphic range for the genus *Laevidentalina* is Cretaceous to Recent (Loeblich and Tappan, 1988).

Regional occurrence: Middle Miocene on the Namibian continental shelf south of the Kunene River mouth.

***Laevidentalina* sp. A**

Pl. 1, fig. 11

Description: The wall is smooth, calcareous and hyaline. The test is elongate, and uniserial with the chambers gradually increasing in size towards the terminal end. The sutures are depressed. The aperture is terminal with slits radiating towards the end.

Remarks: Similar to *L. inornata*, the classification was made as *Laevidentalina* on account of the description in Loeblich and Tappan (1988). It is distinguished from *Dentalina* in having a smooth surface rather than having longitudinal costae.

The test is 0.1 mm in cross-section diameter and 1 mm in length.

Ecological examples: *Laevidentalina* spp. have been documented as being infaunal (Alegret et al., 2003) under varying oxygen conditions (Cimerman and Langer, 1991; Sgarella and Moncharmont Zei, 1993; Rögl and Spezzaferri, 2002; Milker and Schmiedl, 2012).

Global stratigraphic range: The stratigraphic range for the genus *Laevidentalina* is Cretaceous to Recent (Loeblich and Tappan, 1988).

Regional occurrence: Middle Miocene on the Namibian continental shelf south of the Kunene River mouth.

***Laevidentalina* sp. B**

Pl. 1, fig. 12

Description: The wall is calcareous. The test is elongate, slender, uniserial, arcuate and circular in cross-section. The initial end is pointed. The chambers are separated by flush sutures and gradually increase in size toward the apertural end. The surface of the test is smooth. The aperture is terminal and arcuate in shape produced on a short neck.

Remarks: Few tests making up a trace component (<1%) in core 2670. Tests are relatively large measuring 0.1 mm in cross section and up to 1 mm in length.

Ecological examples: The genus *Laevidentalina* has been reported as being infaunal (Alegret et al., 2003) under high (Cimerman and Langer, 1991; Sgarella and Moncharmont Zei, 1993; Milker and Schmiedl, 2012) and suboxic to dysoxic conditions (Rögl and Spezzaferri, 2002).

Global stratigraphic range: The stratigraphic range for the genus *Laevidentalina* is Cretaceous to Recent (Loeblich and Tappan, 1988).

Genus: GRIGELIS Mikhalevich, 1981

Grigelis semirugosa (d'Orbigny, 1846)

Pl. 1, fig. 13

Nodosaria pyrula d'Orbigny, 1826, p. 253, fig. 13

Nodosaria semirugosa d'Orbigny, 1846, p. 34, pl. 1, fig. 20-23; Papp and Schmid, 1985, p. 24, pl. 4, fig. 6-8

Grigelis semirugosa Jones, 1994, p. 75, pl. 63, fig. 23-27.

Description: The wall is calcareous, hyaline. The test is elongate, uniserial and semi-circular in cross section. The chambers are rounded and oval in shape. A tubular neck separates each chamber from the next. Ridges are prominent on the base of each chamber. The rounded aperture is terminal at the end of a long thin neck.

Remarks: Few specimens comprising <1% of the total foraminiferal assemblage in core 2670. Tests are long measuring 0.25 mm in cross-section and up to 3 mm in length.

Ecological examples: Species of the genus *Grigelis* are infaunal under suboxic conditions (Pezelj et al., 2013)

Global stratigraphic range: Miocene to Recent (Jones, 1994)

Regional occurrence: Middle Miocene on the Namibian continental shelf south of the Kunene River mouth.

Genus: NODOSARIA Lamarck, 1812

Nodosaria latejugata (Gümbel, 1868)

Pl. 1, fig. 14

Nodosaria latejugata Gümbel, 1868, p. 619, pl. 1, fig. 32.

Nodosaria affinis Cushman and Renz, 1942, p. 6, pl. 1, figs. 8-10; Cushman and Jarvis, 1930, p. 34, pl. 10, fig. 13

Description: The wall is calcareous, hyaline. The test is thick, elongate and uniserial with a single spine at the base. The sutures are depressed. Longitudinal costae cover the length of the test from the base to the radiate apertural end.

Remarks: Few, mostly broken specimens comprising <1% of the total foraminiferal assemblage in core 2670. Tests are elongated measuring 0.1 mm in cross-section and up to 3 mm in length.

Ecological examples: Elongated cylindrical species of the genus *Nodosaria* are generally shallow infaunal in the upper 5 cm of the sediment (Olóriz et al., 2006)

Regional occurrence: Middle Miocene on the Namibian continental shelf south of the Kunene River mouth.

Genus: PSEUDONODOSARIA Boomgaart, 1949

Pseudonodosaria brevis (d'Orbigny, 1846)

Pl. 1, fig. 15

Dentalina brevis d'Orbigny, 1846, p. 48, pl. 2, figs. 9, 10

Glandulina discreta Reuss, 1850, p. 366, pl. 46, fig. 3; Loeblich and Tappan, 1964, C522, fig. 408: 5-6

Description: The wall is calcareous, hyaline. The test is large, ovate, globular and circular in cross section. Chambers become larger as added. Sutures are depressed with the aperture radiate projecting slightly from the larger last chamber.

Remarks: One test identified as *Pseudonodosaria brevis* was found between 74 and 79 cm in core 2670. The test is of moderate size measuring 0.4 mm in cross-section and up to 0.9 mm in length.

Ecological examples: Infaunal under suboxic conditions (Pezelj et al., 2013 and references therein)

Regional occurrence: First identification of this species in the area for the middle Miocene Namibian continental shelf, south of the Kunene River mouth. Hay et al. (1984) recorded this species on the slope off the Walvis Ridge in late Miocene to Pleistocene sediments.

Genus: LINGULINA d'Orbigny, 1826

***Lingulina seminuda* (**Hantken, 1875)

Pl. 1, fig. 16

Lingulina costata var. *seminuda* Hantken, 1875, p. 41-42, pl. 4, fig. 8a-b.

Lingulina seminuda Cushman and Jarvis, 1930, p. 361, pl. 33, fig. 3a-b; LeRoy and Levinson, 1974, p. 8, pl. 4, fig. 10-11; Cicha et al, 1998, p. 111, pl. 22, fig. 2; Horváth, 2003, p. 13, pl. I, fig, 13, pl. II, fig, 13.

Description: The wall is calcareous, smooth and finely perforate. The test is large, biconvex, ovate in outline, uniserial and rectilinear. The length of the test is slightly greater than the width. Three distinct chambers can be seen rapidly increasing toward the apertural end. The final chamber is inflated and much larger than the initial two chambers comprising approximately three quarters of the test size. Costae stretch along the margin of the test from the apical end towards the apertural end. The aperture is an elongate terminal slit.

Remarks: This *Lingulina* species differs from *Lingulina costata* in that it is more globular in shape, does not have costae throughout the test surface, but only at the margins. The initial chambers are smaller than those in *Lingulina costata*. The *Lingulina seminuda* specimens from this study best resemble *Lingulina* sp. B in Robertson (1998, p.54, pl.18, fig. 1) and are slightly more inflated than the specimen described in LeRoy and Levinson (1974). The sutures are slightly less depressed than *L. seminuda* in Cushman and Jarvis (1930) and Jones (1994). Only a few specimens (<1% of the total foraminifera assemblage in core 2670) of *Lingulina seminuda* were identified in this study. The test size of specimens in this study ranges between ~1 and 2 mm in diameter. Cushman and Jarvis (1930) mention *Lingulina seminuda* tests from Jamaica to be up to 2.5 mm. LeRoy and Levinson (1974) had test sizes of up to 2.1 mm in length and 1.4 mm in breadth while Horváth (2003) had a size range of 1.5 to 2 mm in length and 1.2 to 1.6 mm in breadth.

Ecological examples: Species of the genus *Lingulina* are shallow infaunal and inhabit low energy, deep environments in soft muddy substrates (Reolid et al., 2013).

Global stratigraphic range: Jones (1994) identified the stratigraphic range of *L. seminuda* to be Pleistocene to Recent. Specimens of *L. seminuda* have however also been found in Miocene-aged deposits (Cushman and Jarvis, 1930; Cicha et al., 1998).

Regional occurrence: Middle Miocene on the Namibian continental shelf south of the Kunene River mouth.

Family: PLECTOFRONDICULARIIDAE
Montanaro-Gallitelli, 1957

Genus: PLECTOFRONDICULARIA Liebus, 1902

***Plectofrondicularia* sp. A**

Pl. 1, fig. 17

Description: The wall is calcareous. The test is flat with a keeled periphery and pronounced proloculus with later uniserial chambers extending in an angular arched chevron-shape towards the terminal chamber. The test widens and curves where it narrows towards the apertural end. The sutures are limbate and the aperture terminal, radiate with projecting laminae fusing centrally.

Remarks: The tests are mostly broken and are moderately large in size (up to 0.6 mm in width and 1 mm in length) in trace abundances (<1%).

Ecological examples: Species of the genus *Plectofrondicularia* are infaunal under suboxic conditions (Pezelj et al., 2013 and references therein).

Regional occurrence: Middle Miocene on the northern Namibian continental shelf, south of the Kunene River mouth (this study).

***Plectofrondicularia* sp. B**

Pl. 1, fig. 18; pl. 2, fig. 1

Description: The wall is calcareous. The test is flat with a keeled periphery; biserial in the early stage becoming uniserial as chambers are added. The later chambers are chevron-shaped. The side abruptly widens and curves where it narrows towards the apertural end. The initial stage protrudes more than the later stage chambers. The sutures are limbate and the aperture terminal, radial with projecting laminae fusing centrally.

Remarks: Tests range between narrow (pl. 1, fig. 18) and broad (pl. 2, fig. 1). The tests are mostly broken and resemble *Frondicularia sagittula* in Jones (1994; pl. 65, fig. 23) and *Plectofrondicularia vaughani* in Holbourn et al. (2013, p. 422), but with a peripheral keel and the absence of a basal spine. In this study the specimens have been classified as *Plectofrondicularia* because of its keeled margin (Loeblich and Tappan, 1988). The specimens in this study were not assigned to *P. vaughani* because of its broader peripheral keel and thicker, more pronounced proloculus.
The tests are large in size (up to 1 mm in width and 3 mm in length) in trace abundances (<1%) in all three cores.

Ecological examples: *Plectofrondicularia* spp. have been documented to occur as infaunal and under suboxic conditions (Pezelj et al., 2013 and references therein).

Regional occurrence: Middle Miocene on the northern Namibian continental shelf, south of the Kunene River mouth (this study). Wefer et al. (1998) recorded minor occurrences of *Plectofrondicularia* spp. (*Plectofrondicularia* cf. *inaequalis*, *Plectofrondicularia* cf. *raricosta* and *Plectofrondicularia* cf. *semicosta*) in late Miocene to Pleistocene-aged sediments along the Namibian and southwestern South African slope. The highest abundances (<10%) were recorded along the northern Namibian slope (Wefer et al., 1998).

***Plectofrondicularia* sp. C**

Pl. 2, fig. 2

Description: The wall is calcareous. The test is flat with a thin keeled periphery. The test slightly broadens midway before narrowing again towards the apertural end. The sides of the test slightly widen and curve where it narrows towards the apertural end. The initial stage protrudes more than the later stage chambers. Costae extend from the initial end to midway of the test.

Remarks: The test is more rounded than *Plectofrondicularia* spp. A-C. The tests are large (up to 0.5 mm in width and 3 mm in length) forming trace abundances (<1%) of the total foaminiferal assemblage.

Ecological examples: Species of the genus *Plectofrondicularia* have been reported to be infaunal under suboxic conditions (Pezelj et al., 2013 and references therein)

Regional occurrence: Middle Miocene on the northern Namibian continental shelf, south of the Kunene River mouth (this study). Wefer et al. (1998) recorded minor occurrences of *Plectofrondicularia* spp. in Miocene to

Pleistocene-aged sediments along the western continental slope of southern Africa.

Family: VAGINULINIDAE Reuss, 1860
Subfamily: LENTICULININAE Chapman et al., 1934
Genus: LENTICULINA Lamarck, 1804

Lenticulina calcar (Linnaeus, 1767)
Pl. 2, figs. 3-4

Nautilus calcar Linnaeus, 1758, p. 709, pl. 14, fig. 14; Linnaeus, 1767, p. 1162, 272.
Lenticulina calcar De Blainville, 1825, p. 390; Barker, 1960, p. 146, pl. 70, figs. 9-12; LeRoy and Levinson, 1974, p. 7, pl. 3, fig. 12; Martin, 1981, p. 32, pl. 8, fig. 6; Kohl, 1985, p. 47, pl. 10, figs. 4-5; Papp and Schmid, 1985, pl. 30, figs. 1-3; Lowry, 1987, p. 165, pl. 9, fig. 4; Bolli et al., 1994, p. 294, pl. 294, pl. 77, fig. 5; Kender et al., 2008, p. 510, pl. 14, fig. 14.
Robulina calcar d'Orbigny, 1846, p. 99, pl. 4, figs. 18-20; Renz, 1948, pl. 3, fig. 6.
Cristellaria calcar Parker et al., 1871, p. 241, pl. 10, figs. 91-94; Brady, 1884, p. 551, pl. 7, figs. 9-12; Nuttall, 1928, pl. 5, fig. 8; Macfayden, 1930, pl. 3, fig. 17.
Robulus calcar Cushman, 1923b, p. 115, pl. 30, fig. 7, pl. 31, figs. 4-5; Bandy, 1956, p. 197, pl. 30, fig. 11; Braga, 1960, p. 101, pl. 10, fig. 4.
Description: The wall is smooth and calcareous. The large test is involute, planispiral, biconvex with a keeled periphery. Tests have three to four spines extending from alternating chambers. There are up to seven limbate chambers visible in the final whorl increasing gradually in size toward the apertural end. The sutures are slightly curved. The aperture is terminal and radiate.
Remarks: Generally in low relative abundances (<1%) in this study. LeRoy and Levinson (1974) reported a maximum diameter of 0.85 mm. Tests in this study are slightly larger with diameters of up to 1 mm.
Ecological examples: Unattached, epifaunal under oxic (Pezelj et al., 2013 and references therein) to suboxic conditions (Kaiho, 1994) preferring muddy substrates (Murray, 1991) on the shelf to middle slope (Gallagher et al., 2001)
Global stratigraphic range: Miocene to Recent (Jones, 1994)
Regional occurrence: Miocene in the Congo Basin (Kender et al., 2008) to south of the Kunene River mouth (this study). Wefer et al. (1998) do not distinguish between the different species, but recorded minor relative abundances for *Lenticulina* spp. of less than 5% along the Namibian slope from the late Miocene to Pleistocene. The occurrence of *Lenticulina calcar* has been recorded along the entire coastline of South Africa in surface sediments (Martin, 1981; Lowry, 1987).

Lenticulina cultrata (de Montfort, 1808)
Pl. 2, figs. 5a-b

Robulus cultrata de Montfort, 1808, p. 214, fig. 54e.
Lenticulina cultrata Kohl, 1985, p. 47, pl. 10, fig. 6-7; Weidich, 1990, p. 123.
Description: The wall is calcareous, smooth and finely perforate. The test is planispiral involute and biconvex with a peripheral keel. The chambers gradually increase in size toward the terminal aperture. The sutures are flush and slightly curved. The aperture is radiate and terminal.
Remarks: Specimens are relatively large with a diameter of up to 1 mm. The relative abundance is generally low forming minor components (<5%) in some of the core samples.

Ecological examples: Species of the genus *Lenticulina* are generally epifaunal under oxic (Pezelj et al., 2013 and references therein) to suboxic conditions (Kaiho, 1994).

Global stratigraphic range: If the identification in McMillan (2003) is correct then the stratigraphic range for *L. cultrata* stretches as far back as the Cretaceous.

Regional occurrence: Reported in Early Cretaceous-aged deposits of the Eastern Cape, South Africa (McMillan, 2003). Middle Miocene on the Namibian continental shelf, south of the Kunene River mouth (this study).

Lenticulina gibba (d'Orbigny, 1839)

Pl. 2, fig. 6a-b

Cristellaria gibba d'Orbigny, 1839, p. 40, pl. 7, figs. 20-21; Brady, 1884, p. 546, pl. 69, figs. 8-9.

Robulus oblongus Coryell and Rivero, 1940, p. 332, pl. 43, fig. 12.

Robulus gibbus Bermúdez, 1949, p. 126, pl. 7, figs. 53-54.

Lenticulina gibba Barker, 1960, pl. 69, figs. 8-9; Lowry, 1987, p. 168, pl. 9, fig.2; Jones, 1994, p. 81, pl. 69, figs. 8-9; Robertson, 1998, p. 66, pl. 22, fig. 4.

Description: The wall is calcareous, smooth and finely perforate. The test is planispiral involute and longer than wide; biconvex in side view. A narrow keel surrounds the periphery of the test becoming narrower along later chambers. There are six to nine chambers in the final whorl. The chambers gradually increase in size toward the terminal chamber. The sutures are flush and slightly curved. The aperture is radiate and terminal.

Remarks: Specimens are moderately sized measuring 0.5 mm in diameter and 0.75 mm in length. The relative abundance is generally low forming minor components (<5%) in some of the core samples.

Ecological examples: Species of the genus *Lenticulina* are generally epifaunal under oxic (Pezelj et al., 2013 and references therein) to suboxic conditions (Kaiho, 1994). The bathymetric range of *Lenticulina gibba* is given as shelf to upper slope (Holbourn et al., 2013).

Global stratigraphic range: Early Miocene to Recent (Holbourn et al., 2013).

Regional occurrence: Middle Miocene on the Namibian continental shelf south of the Kunene River mouth (this study). Lowry (1987) recorded this species on the continental shelf off Cape St. Blaize, Mossel Bay on the southern coast of South Africa in surface sediments.

Lenticulina inornata (d'Orbigny, 1846)

Pl. 2, figs. 7a-b

Robulina inornata d'Orbigny, 1846, p. 102, pl. 4, figs. 25-26;

Cristellaria inornata Reuss, 1866, p. 144.

Cristellaria (Robulus) inornata Ten Dam, 1944, p.88.

Lenticulina inornata Papp and Schmid, 1985, p. 43, pl.31, figs. 6-8; Obaje and Okosun, 2013, p. 360, pl. 1, fig. 15.

Description: The wall is calcareous, smooth and finely perforate. The test is planispiral and is as wide as long with a large central boss; biconvex in side view. The sutures are flush and slightly curved radiating from a narrow small region. There are up to eight chambers visible in the final whorl increasing in size toward the apertural end. The aperture is radiate and terminal.

Remarks: Specimens are relatively large measuring up to 1 mm in diameter. The relative abundance is generally low forming minor components (<5%) in some of the core samples.

Ecological examples: Foraminifera from the genus *Lenticulina* have been reported to be epifaunal to shallow infaunal under oxic (Pezelj et al., 2013 and references therein) to suboxic conditions (Kaiho, 1994).
Global stratigraphic range: Miocene to Recent (Jones, 1994).
Regional occurrence: Middle Miocene on the Namibian continental shelf south of the Kunene River mouth (this study).

Lenticulina iota (Cushman, 1923a)
Pl. 2, fig. 8a-b

Cristellaria cultrata Brady, 1884, p. 550, pl. 70, fig. 4-6.
Cristellaria iota Cushman, 1923a, p. 111, pl. 29, fig. 2; pl. 30, fig. 1.
Lenticulina iota Barker, 1960, pl. 70, fig. 4-6; Thomas, 1988, p. 74, pl. 1, fig. 10; Jones, 1994, p. 81, pl. 70, fig. 4-6; Holbourn et al., 2013, p. 336.
Description: The wall is calcareous, smooth and finely perforate. The test is planispiral, involute and biconvex in side view. A keeled periphery surrounds the test margin. The keel is initially broad narrowing towards the terminal end. The chambers gradually increase in size. The sutures are flush and curved. The aperture is radiate and terminal.
Remarks: Specimens are relatively large measuring up to 1 mm in diameter. The relative abundance is generally low forming minor components (<1%) in some of the core samples.
Ecological examples: Species of the genus *Lenticulina* are generally epifaunal under oxic (Pezelj et al., 2013 and references therein) to suboxic conditions (Kaiho, 1994). The bathymetric range of *Lenticulina iota* is given as shelf to upper slope (Holbourn et al., 2013).
Global stratigraphic range: Miocene to Recent (Thomas, 1988).
Regional occurrence: Middle Miocene on the Namibian continental shelf south of the Kunene River mouth (this study). Lowry (1987) recorded this species from the continental shelf in surface sediments off Cape Agulhas, South Africa.

Genus: SARACENARIA Defrance, 1824

Saracenaria italica (Defrance, 1824)
Pl. 2, figs. 9-10

Saracenaria italica Defrance, 1824, p. 344, pl. 13, fig. 6; Sandidge, 1932, p. 355, pl. XXXII, fig. 18; Barker, 1960, pl. 68, figs. 17-18; 20-23; Braga, 1960, p. 122, pl. 11, fig. 16; McMillan, 1974, p. 49, pl. 4, fig. 8; Martin, 1981, p. 34, pl. 10, fig. 3; Lowry, 1987, p. 177, pl. 9, figs. 16a, b.
Cristellaria italica Brady, 1884, p. 544, pl. 68, figs. 17-18; 20-23; Cushman, 1923a, p. 125, pl. 35, figs. 2, 5-7.
Description: The wall is calcareous and finely perforate. The test is planispiral becoming rectilinear and triangular in cross-section. The sutures are curved and the apertural face is triangular and broad. The aperture is radiate at the dorsal angle of the final chamber.
Remarks: Specimens are relatively large ranging between 0.5 and 1 mm in width and between 1 and 2 mm in length. The relative abundance is low forming trace components (<1%) in some of the samples in core 2670.
Ecological examples: Species of the genus *Saracenaria* are generally epifaunal (Barbieri and Panieri, 2004) under suboxic conditions (Gebhardt, 1999). The species *S. italica* has been documented to occur in shelf and slope environments (Renz, 1948).

Global stratigraphic range: Oligocene to Recent (Renz, 1948).

Regional occurrence: Middle Miocene on the Namibian continental shelf south of the Kunene River mouth (this study). In surface sediments on the continental shelf, Lüderitz, Namibia to north of Durban, South Africa (Martin, 1981; Lowry, 1987).

***Saracenaria* sp.**

Pl. 2, fig. 11

Description: The wall is calcareous, smooth and finely perforate. The test is planispiral becoming rectilinear. The test is triangular in section with a rounded outline. The apertural face is triangular and broad. The aperture is radiate at the dorsal angle of the final chamber.

Remarks: The test is more rounded compared to *Saracenaria italica* with a curved initial end. Specimens are relatively large ranging between 0.5 and 1 mm in width and between 1 and 2 mm in length. The relative abundance is low forming trace components (<1%) in some of the samples in core 2670.

Ecological examples: *Saracenaria* spp. have been reported to be epifaunal (Barbieri and Panieri, 2004) under suboxic conditions (Gebhardt, 1999).

Regional occurrence: Middle Miocene on the Namibian continental shelf south of the Kunene River mouth.

Saracenaria spinosa (Eichenberg, 1935)

Pl. 2, figs. 12a-c

Lenticulina (Saracenaria) spinosa Eichenberg, 1935, pl. 4, fig.5

Saracenaria spinosa Bolli et al., 1994, p. 28, fig. 8.44-8.48

Description: The wall is calcareous, smooth and finely perforate. The test is planispiral becoming rectilinear, triangular in section and almost twice as long as wide. Ridges form along the test surface ending in spines along margins pointing away from the apertural end. Chambers enlarge toward the terminal end with the terminal chamber being the largest. The initial end is slightly curved away from the apertural end. The apertural face is triangular and broad. The aperture is radiate at the dorsal angle of the final chamber.

Remarks: Specimens of this species are relatively large measuring up to 0.5 mm in width and 1 mm in length. The relative abundance is low (<1%).

Bolli et al. (1994) remarked that *S. spinosa* is an index to the Albian and Aptian. If indeed *S. spinosa* is restricted to the Cretaceous then the figured specimen found in this study could have been reworked in the upper part of the Mio-Pliocene section of the core.

Ecological examples: Species of the genus *Saracenaria* are generally epifaunal (Barbieri and Panieri, 2004).

Global stratigraphic range: Cretaceous (Bolli et al., 1994).

Regional occurrence: Possibly reworked in middle Miocene sediments, Namibian continental shelf south of the Kunene (this study).

Genus: ASTACOLUS de Montfort, 1808

Astacolus crepidulus (Fichtel and Moll, 1798)

Pl. 3, fig. 1

Nautilus crepidula Fichtel and Moll, 1798, p. 107, pl. 19, fig. g-i

Cristellaria crepidula Cushman, 1923a, p. 117, pl. 35, fig 3-4.

Lenticulina crepidula Sandidge, 1932, p. 346, pl. XXXII, fig. 6

Astacolus crepidulus Barker, 1960, pl. 67, fig. 20, pl. 68, fig. 1-2; Lowry, 1987, p. 149, pl. 8, fig. 3; Loeblich and Tappan, 1994, p. 72, pl. 130, fig. 1-20; Jones, 1994, p. 80, pl. 68, fig. 1-2

Description: The wall is calcareous, smooth and finely perforate. The test is compressed and some specimens are nearly three times longer than broad. Up to seven chambers increase in size toward the apertural end and the slightly depressed sutures are oblique with the angle between the suture and base of the test increasing as chambers are added. The radiate aperture protrudes at the terminal end of the test.

Remarks: Specimens are moderate in size measuring up to 0.5 mm in width and 1 mm in length. The figured specimen in Sandidge (1932) is 1.2 mm in length. The relative abundance is generally low forming trace components (<1%) in some of the samples in core 2670.

Ecological examples: Infaunal adapted under oxic to dysoxic conditions (Kaminski, 2012).

Global stratigraphic range: Jones (1994) reported *Astacolus crepidulus* to occur from the Miocene to Recent, but Cushman (1923a) extends it back to the Cretaceous.

Regional occurrence: Middle Miocene on the Namibian continental shelf south of the Kunene River mouth (this study) and in Recent sediments off Cape Agulhas, South Africa (Lowry, 1987).

Genus: AMPHICORYNA Schlumberger in Milne-Edwards, 1881

Amphicoryna scalaris* var. *hirsuta (d'Orbigny, 1826)

Pl. 3, figs. 2a-b

Nodosaria hirsuta d'Orbigny, 1826, p.252.

Nodosaria hispida d'Orbigny, 1846, p. 35, pl. 1, figs. 24-25; Papp and Schmid 1985, p. 25, pl. 5, figs. 1-8

Amphicoryna scalaris Yassini and Jones, 1995, p. 136, fig. 724

Description: The wall is calcareous and the surface covered with ridges running along most of the length of the chambers. The test is elongate and uniserial, circular in cross-section with several inflated globular chambers separated by deeply incised sutures. A maximum of approximately twenty ridges run along the terminal chamber. The ridges increase in number towards the terminal chamber and do not extend the full length of the chambers as in the case of *Amphicoryna scalaris*. The tests are covered with small pustulose structures. The aperture is terminal at the end of a long neck.

Remarks: Specimens are small to moderate in size with the larger terminal chamber reaching ~0.15 mm and the test 0.6 mm in length. The relative abundance is generally low forming minor components in some of the core samples.

Ecological examples: The bathymetric range of *Amphicoryna* spp. is broad from the shelf to abyssal depths. The preferred substrate is mud under low oxygen (suboxic) (Rögl and Spezzaferri, 2002; Kaminski, 2012) to high oxygen conditions (Milker and Scmiedl, 2012).

Regional occurrence: Middle Miocene on the continental shelf south of the Kunene River mouth.

***Amphicoryna* sp.**

Pl. 3, figs. 3-4

Description: The wall is calcareous and covered with ridges extending towards the base of each chamber. The test is elongate and uniserial, circular in cross-section with several

inflated globular chambers. Each chamber is not entirely rounded and has a flat base. Approximately twenty ridges run along the terminal chamber. The ridges increase in number towards the final chamber and terminate at the base of each chamber. The aperture is terminal at the end of a long spiral neck.

Remarks: The larger terminal chamber is ~0.2 mm and the test 0.6 mm in length. The relative abundance is generally low forming minor components in some of the core samples.

Ecological examples: The bathymetric range of *Amphicoryna* spp. is broad from the shelf to abyssal depths. The preferred substrate is mud under low oxygen (suboxic) (Rögl and Spezzaferri, 2002; Kaminski, 2012) to high oxygen conditions (Milker and Scmiedl, 2012).

Regional occurrence: Middle Miocene on the continental shelf south of the Kunene River mouth.

Amphicoryna sublineata (Brady, 1884)

Pl. 3, figs. 5a-b

Nodosaria hispida var. *sublineata* Brady, 1884, p. 508, pl. 63, fig. 19-22

Amphicoryna? sublineata LeRoy and Levinson, 1974, p. 7, pl. 3, fig. 9.

Amphicoryna sublineata Jones, 1994, p. 75, pl. 63, fig. 19-22.

Description: The wall is calcareous and covered with short spines. The test is elongate, slightly arcuate, uniserial and circular in cross-section. Approximately six rounded conical chambers are connected to the next by a short neck. The base of each chamber is covered with hirsute structures. The aperture is terminal at the end of a short neck.

Remarks: The specimen is long (2 mm) and thin (0.5 mm). The test in LeRoy and Levinson (1974) is 0.33 mm in diameter and 1.3 mm with thicker and more rounded chambers compared to the specimen in this study. The relative abundance is generally low forming trace components (<1%) in some of the samples of core 2670.

Ecological examples: The bathymetric range of *Amphicoryna* spp. is broad from the shelf to abyssal depths. The preferred substrate is mud under low oxygen (suboxic) (Rögl and Spezzaferri, 2002; Kaminski, 2012) to high oxygen conditions (Milker and Scmiedl, 2012).

Global stratigraphic range: The stratigraphic range for the genus *Amphicoryna* is Miocene to Recent (Loeblich and Tappan, 1988).

Regional occurrence: Middle Miocene on the Namibian continental shelf south of the Kunene River mouth (this study).

Genus: MARGINULINA d'Orbigny, 1826

Marginulina costata (Batsch, 1791)

Pl. 3, figs. 6-11

Nautilus (Orthoceras) costatus Batsch, 1791, p. 2, pl. 1, fig. 1a-g.

Marginulina raphanus d'Orbigny 1826, p. 258, pl. X, fig. 7-8.

Marginulina costata Brady, 1884, p. 528, pl. 65, fig. 10-13; Bagg, 1912, p. 62, pl. XVIII, fig. 4; Cushman, 1921, p. 256, pl. 41, fig. 5-8; Heron-Allen and Earland, 1922, p. 176; Cushman, 1923a, p. 132, pl. 37, fig. 2; Jones, 1994, p. 77, pl. 65, fig. 13; Milker and Schmiedl, 2012, p. 74, fig. 18.26; Obaje and Okosun, 2013, p. 360, pl. 1.18.

Description: The wall is calcareous and finely perforate. The test is elongate, uniserial and circular in cross-section. The initial portion is coiled. Up to nine chambers are visible on the exterior. The chambers are rectilinear arranged and separated by depressed sutures and covered

with longitudinal costae. The costae may extend from the initial to the terminal chamber. The final chamber is globular in shape with a terminal and radiate aperture at the dorsal angle of a pronounced neck.

Remarks: The tests show a variable degree of size and ornamentation. The variety identified as *Marginulina* cf. *costata* (pl. 3, figs. 7-9) resembles that of *M. sendaiensis* in Asano (1949; p. 427, fig. 1) posessinging less or no ornamentation on their terminal chamber and are more abundant (up to 5% in some of the samples) than those having tests completely covered in costae. The relative abundance of *M. costata* is generally low forming trace components (<1%) in some of the samples of core 2670. The tests of *Marginulina* cf. *costata* are smaller than those that are ornamented throughout the test, but are still relatively large, measuring up to 0.2 mm in cross section diameter and 1 mm in length while tests with ornamentation throughout are large measuring up to 0.4 mm in cross section and 2 mm in length. A third variety was identified as *Marginulina costata* var. *hirsuta* (Pl. 3, figs. 10-11). This form resembles *M. costata* in having longitudinal costae but is covered with spinose structures extending in all directions on most of the chambers. The initial chambers were covered with spines becoming less in the later chambers where costae become more visible. The relative abundance of *M. costata* var. *hirsuta* is generally low forming trace components (<1%) in some of the samples of core 2670. Tests are large measuring up to 0.3 mm in cross section diameter and 3 mm in length.

Ecological examples: Species of the genus *Marginulina* are generally shallow infaunal in environments with variable conditions of low (Bernhard, 1986) to high oxygen (Milker and Schmiedl, 2012).

Global stratigraphic range: Jurassic to Recent (Bagg, 1912)

Regional occurrence: Middle Miocene on the continental shelf south of the Kunene River mouth.

Marginulina obesa (Cushman, 1923a)

Pl. 3, figs. 12-13

Marginulina glabra Brady, 1884, p. 527, pl. 65, figs. 5-7; Flint, 1899, p. 133, pl. 60, fig. 1

Marginulina glabra var. *obesa* Cushman, 1923a, p. 128, pl. 37, fig. 1

Marginulina obesa Barker, 1960, pl. 65, figs. 5-6; LeRoy and Levinson, 1974, p. 8, pl. 4, fig. 3-4; Lowry, 1987, p. 174, pl. 9, fig. 12; Jones, 1994, p. 77, pl. 65, figs. 5-6.

Description: The wall is calcareous and smooth. The test is elongate, circular in cross-section, initially curved becoming rectilinear in the later stage. Three inflated chambers increase in size towards the terminal end. The chambers are separated by straight and slightly depressed sutures. The aperture is terminal and radiate.

Remarks: The relative abundance is generally low forming trace components (<1%) in some of the samples of core 2670. The length of the tests in LeRoy and Levinson (1974) is reported to be 1 mm and a diameter of 0.62 mm. The tests in this study are slightly smaller measuring up to 0.4 mm in cross section diameter and 0.7 mm in length.

Ecological examples: The bathymetric disctribution of *M. obesa* is given as slope to abyssal (Holbourn et al., 2013). Species of the genus *Marginulina* are generally shallow infaunal in environments with variable conditions of low (Bernhard, 1986) to high oxygen (Milker and Schmiedl, 2012).

Global stratigraphic range: Miocene to Recent (Jones, 1994).

Regional occurrence: Middle Miocene on the continental shelf south of the Kunene River mouth (this study). In surface samples south coast of South Africa (Lowry, 1987).

Genus: VAGINULINA d'Orbigny, 1826

Vaginulina legumen (Linnaeus, 1758)

Pl. 3, fig. 14

Nautilus legumen Linnaeus, 1758, p.711

Vaginulina badenensis d'Orbigny, 1846, p. 65, pl. 3, figs. 6-8; Papp and Schmid, 1985, p. 36, pl. 20, figs. 6-11

Vaginulina legumen Brady, 1884, p. 580, pl. 66, figs. 13-15; Bagg, 1912, p. 63, pl. XVIII, fig. 6-7; Sandidge, 1932, p. 355, pl. XXXI, fig. 15; Loeblich and Tappan, 1988, pl. 454, figs. 15-17

Description: The wall is calcareous and perforate. The test is large, elongate, compressed, uniserial and lenticular in cross-section. The initial end may be with or without a spine. Sutures are slightly thickened. The aperture is pronounced, terminal and radiate.

Remarks: The relative abundance is generally low forming trace components (<1%) in some of the samples of core 2670. The length of the figured specimen in Sandidge (1932) is 0.7 mm. The tests in this study are larger than that of Sandidge (1932) measuring up to 0.4 mm in cross section and 2 mm in length.

Ecological examples: Infaunal under suboxic conditions (Pezelj et al., 2013 and references therein).

Global stratigraphic range: Triassic to Recent (Bagg, 1912; Sandidge, 1932).

Regional occurrence: Middle Miocene on the continental shelf south of the Kunene River mouth (this study).

***Vaginulina* sp.**

Pl. 3, figs. 15-16

Description: The wall is calcareous and perforate. The test is elongate, compressed, uniserial and lenticular in cross-section. The sutures are slightly flush. The initial chambers are broad, narrowing in later chambers with the terminal chamber broadened and more pronounced than the middle chambers. The aperture is pronounced, terminal and radiate.

Remarks: This species has more basal spines (up to five) compared to *V. legumen*. The relative abundance is generally low forming trace components (<1%) in some of the samples of core 2670. The tests of *Vaginulina* sp. measure up to 0.25 mm in cross section and 1 mm in length.

Ecological examples: Species of the genus *Vaginulina* are generally infaunal (Jenkins, 2013).

Regional occurrence: Middle Miocene on the continental shelf south of the Kunene River mouth (this study).

Family: GLANDULINIDAE Reuss, 1860

Subfamily: GLANDULINIDAE Reuss, 1860

Genus: GLANDULINA Lamarck, 1804

Glandulina laevigata (d'Orbigny, 1839)

Pl. 4, figs. 1a-b

Nodosaria (Glandulina) laevigata var. *ovata* d'Orbigny, 1826, p. 252, pl. 10, fig. 1-3; Brady 1884, p. 490, pl. 61, fig. 20-22; Cushman, 1921, p. 185, pl. 33, fig. 1; Cushman and Applin, 1926, p. 169, pl. 7, figs. 12-13.

Glandulina laevigata d'Orbigny, 1846, p. 29, pl. 1, fig. 4-5; Sandidge, 1932, p. 360, pl. XXXII, fig. 15.
Glandulina laevigata var. *ovata* Ellisor, 1933, pl. 2, fig. 6.

Description: The wall is calcareous and smooth. The test shape is ovate, globular, tapering at each end and circular in transverse section with few chambers increasing toward the apertural end. The final chamber is the largest making up almost two thirds of the test volume. The sutures are fine and flush. The aperture is radiate and projects slightly from the larger last chamber.

Remarks: Also referred to as *Nodosaria (Glandulina) laevigata* and *Nodosaria laevigata* (Loeblich and Tappan, 1988). Few tests comprising <1% of the total foraminiferal assemblage in core 2670. Tests are moderate to large in size ranging from 0.5 mm to nearly 1 mm in cross-section and 0.75 to 1.2 mm in length. The figured specimen of *Glandulina laevigata* in Sandidge (1932) is 0.5 mm in length.

Ecological examples: Infaunal and tolerant of low oxygen conditions (Gupta, 1993).

Global stratigraphic range: Cretaceous to Recent (Sandidge, 1932).

Regional occurrence: Middle Miocene on the continental shelf south of the Kunene River mouth.

Order: ROTALIIDA Delage and Herouard, 1896

Family: BOLIVINITIDAE Glaessner, 1937

Genus: BOLIVINA d'Orbigny, 1839

Bolivina reticulata (Hantken, 1875)

Pl. 4, figs. 2a-b

Brizalina reticulata Hantken, 1875, p. 65, pl. 15, fig. 6; Fenero et al., 2012, p. 292, fig. 5.7; Valchev et al., 2013, p. 95, pl. 1, fig. 16
Brizalina subreticulata Jones, 1994, p. 59, fig. 30-31.

Description: The wall is calcareous and microperforate. The test is small, broad, biserial, triangular-ovoid in shape and elliptical in cross-section. The test is less than twice as long as what it is wide. Irregular, reticulate, interwoven costae cover the entire test giving a reticulate appearance to the test. The aperture is slit-like situated at the base of the terminal chamber.

Ecological examples: Infaunal (Drinia et al., 2007), unattached and prefers muddy sediments under dysoxic conditions (Kaiho, 1994) with a bathymetric distribution from the inner shelf to slope (Murray, 2006).

Remarks: The relative abundance is generally low forming trace components (<1%) in the samples of core 2670. The tests are small measuring 0.2 mm in width and 0.35 mm in length.

Global stratigraphic range: Oligocene to Recent (Fenero et al., 2013).

Regional occurrence: Middle Miocene on the continental shelf south of the Kunene River mouth (this study).

Genus: BRIZALINA Costa, 1856

Brizalina alata (Seguenza, 1862)

Pl. 4, fig. 3

Vulvulina alata Seguenza, 1862, p. 115, pl. 2, fig. 5
Bolivina alata Cushman, 1937, p. 106, pl. 13, figs. 3-11; Cushman and Todd, 1945, p. 42, pl. 6, fig. 25; Renz, 1948, p. 116, pl. 6, fig. 26; pl. 12, fig. 12; Lowry, 1987, p. 280, pl. 18, figs. 3a-b; Bolli et al., 1994, p. 339, figs. 78.4-78.5.

Brizalina alata van Marle, 1991, p. 166, pl. 17, figs. 1-2; Jones, 1994, p. 58, pl. 53, figs. 2-4; Yassini and Jones, 1995, p. 131, figs. 516-517; Robertson, 1998, p. 120, pl. 47, figs. 1-2; Holbourn et al., 2013, p. 76.

Description: The wall is calcareous and coarsely perforate. The test is small, elongate, biserial, strongly compressed and elliptical in cross-section. The chambers increase rapidly and become more inflated towards the apertural end, slightly overlapping the previous chambers. Chambers have a downward pointing spine located at the base giving a serrated edge to the test margin. A peripheral keel surrounds the test. The sutures are slightly depressed and curved. The aperture is loop-shaped and extends up the terminal chamber.

Remarks: Moderately abundant (<10%) in all cores discussed in this study. The tests are small measuring 0.2 mm in width and 0.6 mm in length.

Ecological examples: The genus *Brizalina* is infaunal, unattached and prefers muddy sediments in dysoxic conditions (Kaminski et al., 2002). The species *Brizalina alata* has a shelf distribution (Holbourn et al., 2013).

Global stratigraphic range: Miocene to Recent (Jones, 1994).

Regional occurrence: Middle Miocene on the continental shelf south of the Kunene River mouth (this study). In surface samples on the continental shelf north of the Orange River mouth (Lowry, 1987).

Family: CASSIDULINIDAE d'Orbigny, 1839

Genus: GLOBOCASSIDULINA Voloshinova, 1960

Globocassidulina subglobosa (Brady, 1881)

Pl. 4, figs. 4-5

Cassidulina subglobosa Brady, 1881, p. 60; Brady, 1884, p. 430, pl. 54, fig. 17; Barker, 1960, pl. 54, fig. 17.

Globocassidulina subglobosa LeRoy and Levinson, 1974, p. 14, pl. 7, fig. 8; Tjalsma and Lohmann, 1983, p. 31, pl. 16, fig. 9; Lowry, 1987, p. 239, pl. 14, figs. 7a-c; Miller and Katz, 1987, p. 134, pl. 3, fig. 4; Hermelin, 1989, p. 74; Thomas, 1990, p. 590; Jones, 1994, p. 60, pl. 54, fig. 17; Robertson, 1998, p. 136, pl. 53, figs. 1-2; Kuhnt et al., 2002, p. 144, pl. 10, figs. 3-5; pl. 17, figs. 1-2; Kender et al., 2008, p. 512, pl. 17, fig. 1-2; Milker and Schmiedl, 2012, p. 85, figs. 20.13-20.14; Holbourn et al., 2013, p. 264.

Description: The wall is calcareous and smooth. The test is small, subglobular and subcircular in cross-section. The chambers are biserially arranged, inflated and globular in shape, separated by depressed sutures. The aperture is slit-like situated interio-marginal and stretches along the margin of the terminal chamber.

Remarks: Trace component (<1%) in core 2658, minor component (<5%) in core 2682 and major component (<40%) in core 2670. The tests from this study are smaller than that of LeRoy and Levinson (1974) (diameter of up to 0.75 mm) measuring 0.25 mm in diameter.

Ecological examples: Epifaunal-shallow infaunal (Kaiho, 1994; Vilela, 1995), generally unattached and prefers muddy sediments under oxic (Kaiho, 1994) to suboxic (De and Gupta, 2010) conditions. Schmiedl et al. (1997) recorded *G. subglobosa* in oligotrophic areas under vigorous bottom currents and sandy substrates. Panieri and Gupta (2008) recorded this species in relatively high abundances in muddy substrates. The bathymetric range of *G. subglobosa* is broad, from the middle shelf to abyssal depths (Murgese and de Deckker, 2005; Holbourn et al., 2013).

Global stratigraphic range: Palaeocene to Recent (Holbourn et al., 2013)

Regional occurrence: In Miocene-aged sediments from the Congo Basin (Kender et al., 2008) to the Namibian continental outer shelf south of the Kunene River mouth (this study). Hay et al. (1984) and Wefer et al. (1998) reported the occurrence of *Globocassidulina subglobosa* in late Miocene to Pleistocene-aged sediments along the continental slope in relatively minor abundances (<10%) at most sites. Lowry (1987) recorded occurrences of *G. subglobosa* in surface sediments on the continental shelf between Cape Town and Port Elizabeth.

Family: UVIGERINIDAE Haeckel, 1894

Genus: UVIGERINA d'Orbigny, 1826

Uvigerina peregrina (Cushman, 1923a)

Pl. 4, fig. 6

Uvigerina peregrina Cushman, 1923a, p. 166, pl. 42, figs. 7-10; Martin, 1981, p. 44, pl. 10, fig. 12-14; Milker and Schmiedl, 2012, p. 90, fig. 20.29

Euuvigerina peregrina Barker, 1960, pl. 74, fig. 11-12.

Description: The wall is calcareous and finely perforate. The test is broad, elongate, rounded in cross-section, triserial and covered in longitudinal costae. Later chambers become inflated with depressed sutures. The costae are separated by the sutures. The aperture is terminal produced on a neck with a pronounced lip bordering the edge of the aperture.

Remarks: The tests measure ~0.5 mm in cross section diameter and 0.8 mm in length. Major component (<50%) in all three cores.

Ecological examples: Shallow infaunal, most abundant under high organic carbon (Murray, 2006) adapted to suboxic conditions (Kaiho, 1994).

Regional occurrence: Middle Miocene on the continental shelf of northen Namibia, south of the Kunene River mouth (this study). Low to high abundances in Pleistocene upper slope sediments off western South Africa (GeoB 20601-4, 8342-6, 8336-6) and Namibia (Schmiedl and Mackensen, 1997). Abundant in Recent shelf to slope sediments along Namibia (Lowry, 1987; Schmiedl et al., 1997) and South Africa (Lowry, 1987)

Uvigerina pygmaea (d'Orbigny, 1826)

Pl. 4, fig. 7

Uvigerina pygmaea d'Orbigny, 1826, p. 269, pl. 12, figs. 8-9; Bermúdez, 1949, p. 209, pl. 13, fig. 44; Holbourn et al., 2013, p. 600.

Description: The wall is calcareous and the test is strongly ribbed, short elongate, fusiform, rounded in cross-section, triserial and covered in longitudinal costae with short spines at the end of each chamber. The costae are irregular in length and separated by sutures. Later chambers become inflated with distinct depressed sutures. The aperture is terminal produced on a long neck with a pronounced lip.

Remarks: Very few tests making up a trace component (<1%) in core 2670. Tests are moderate in size measuring 0.5 mm in cross section and 0.8 mm in length.

Ecological examples: Upper slope distribution (Holbourn et al., 2013) under suboxic conditions (Kaiho, 1994).

Global stratigraphic range: Holbourn et al. (2013) confine the chronostratigraphy of *U. pygmaea* from the Late Eocene to the Early Pliocene.

Regional occurrence: Middle Miocene on the continental shelf south of the Kunene River mouth (this study).

Uvigerina spinulosa (Hadley, 1934)

Pl. 4, fig. 8

Uvigerina spinulosa Hadley, 1934, pl. 18, fig. 5; Boersma, 1984, p. 163, pl. 1, figs 1-6; Van Morkhoven et al., 1986, p. 218, pl. 74, figs 1-3; Kender et al., 2018, p. 515, pl. 18, fig. 5.

Description: The wall is calcareous and perforate. The test is triserial elongate, rounded in cross-section and covered in longitudinal costae which end in spines at the base of the chambers. Later chambers are inflated with depressed sutures. Fine hispid structures may cover the initial and terminal ends. The aperture is terminal produced on a neck with a pronounced lip.

Remarks: The tests measure ~0.2 mm in cross section diameter and ~0.5 mm in length. Less abundant than *U. peregrina*.

Ecological examples: The species of the genus *Uvigerina* are generally shallow infaunal; most abundant under high organic carbon (Murray, 2006) adapted to suboxic conditions (Kaiho, 1994).

Regional occurrence: Middle Miocene on the continental shelf of northen Namibia, south of the Kunene River mouth (this study) and in the Congo Basin (Kender et al., 2018).

Family: STILOSTOMELLIDAE Finlay, 1947

Genus: ORTHOMORPHINA Stainforth, 1952

Orthomorphina jedlitschkai (Thalmann, 1937)

Pl. 4, fig. 9

Nodogenerina jedlitschkai Thalmann, 1937, p. 341

Orthomorphina jedlitschkai Barker, 1960, pl. 62, fig. 1-2; Jones, 1994, pl. 62, fig. 1-2, suppl. pl. 1, fig. 16, suppl. pl. 2, fig. 6-7; Hayward et al., 2012, p. 136, pl. 8, fig. 24-27.

Description: The wall is calcareous and generally smooth. The test is elongate, uniserial with globular chambers and circular in cross-section. The chambers are of different diameters and separated from each other by deep incised sutures. The penultimate chamber is larger than the terminal chamber. The aperture is surrounded by a round thick rim.

Remarks: Jones (1994) illustrated the similarity in test morphology between *O. jedlitschkai* and *Glandulonodosaria* spp. Based on the shape of the aperture (slightly protruding and rounded) and resemblance to the test morphology displayed in Jones (1994) this specimen has been assigned to *Orthomorphina jedlitschkai.* Few tests making up a trace component (<1%) in core 2670. Tests are moderate in size. The broadest chamber measures 0.3 mm in cross section and the test measures up to 0.8 mm in length.

Ecological examples: Species of the genus *Orthomorphina* were generally infaunal under suboxic conditions (Pezelj et al., 2013 and references therein)

Global stratigraphic range: Cretaceous to Pleistocene (Hayward et al., 2012)

Regional occurrence: Middle Miocene on the continental shelf south of the Kunene River mouth (this study).

Order: STILOSTOMELLIDA Saidova, 1981

Family: SPHAEROIDINIDAE Cushman, 1927a

Genus: SPHAEROIDINA d'Orbigny, 1826

Sphaeroidina bulloides (d'Orbigny, 1826)

Pl. 4, figs. 10a-b

Sphaeroidina bulloides d'Orbigny, 1826, p. 267; LeRoy and Levinson, 1974, p. 8, pl. 5, fig. 2; Martin, 1981, p. 36, pl. 10, fig. 5; Papp and Schmid, 1985, p. 96, pl. 90, figs. 7-12; Lowry, 1987, p. 379, pl. 27, figs. 7a-c; Jones, 1994, p. 91, pl. 84, figs. 1-2; Yassini and Jones, 1995, p. 160, figs. 936-937; Robertson, 1998, p. 196, pl. 74, fig. 4; Kender et al., 2008, p. 516, pl. 20, fig. 3; Holbourn et al., 2013, p. 520

Sphaeroidina austriaca d'Orbigny, 1846, p. 284, pl. 20, figs. 19-21.

Description: The wall is calcareous, imperforate and its surface smooth. The test is subglobular with globular chambers separated by slightly depressed sutures. The last whorl contains three chambers. The aperture is located near the junction between three chambers and is crescentic in shape with a bordering lip (pl. 4, fig. 10b).

Remarks: The relative abundances of *Sphaeroidina bulloides* in this study decrease toward the deeper cores. In core 2658 *S. bulloides* formed one of the major species in some of the samples (<20%), and in cores 2670 and 2682 minor (<5%).

Test sizes of *Sphaeroidina bulloides* in general are variable. Diameters in LeRoy and Levinson (1974) range between 0.23 and 1.15 mm. The diameter measured in this study is ~0.5 mm.

Ecological examples: Infaunal under suboxic (Kaiho, 1994) to dysoxic conditions (Pezelj et al., 2013 and references therein) on the slope and at abyssal depths (Holbourn et al., 2013).

Global stratigraphic range: Oligocene to Recent (Jones, 1994; Holbourn et al., 2013)

Regional occurrence: In Miocene-aged sediments stretching from the Congo Basin (Kender et al., 2008) to the continental shelf of Namibia south of the Kunene River mouth (this study) and the southwestern shelf of South Africa (Compton et al., 2004). Hay et al. (1984) reported the occurrence of *Sphaeroidina bulloides* in late Miocene to Pleistocene sediments on the slope off the Walvis Ridge. Low relative abundances (<1%) along the slope of Namibia during the late Miocene with higher abundances off the Orange River to the south (<15%). Wefer et al. (1998) recorded high relative abundances of this species (<80%) along the slope off the Walvis Ridge during the Pliocene decreasing in abundance towards the south. Low relative abundances (<1%) along the Namibian slope and minor abundances (<10%) along the southwestern slope of South Africa during the Pleistocene (Wefer et al., 1998). Lowry (1987) documented *Sphaeroidina bulloides* in surface sediments on the continental shelf between Lüderitz and Cape Agulhas.

Family: SIPHONINIDAE Cushman, 1927a

Genus: SIPHONINA Cushman, 1927a

Siphonina pulchra **(**Cushman, 1919)

Pl. 4, figs. 11-13

Siphonina pulchra Cushman, 1919, p. 42, pl. 14, fig. 7a-c; Cushman, 1922a, p. 49, pl. 7, fig. 11-12; Cushman, 1927b, p. 8, pl. 2, fig. 5; Cushman, 1931, p. 69, pl. 14, fig. 2-3; Palmer, 1945, p. 61

Description: The wall is calcareous and perforate. The test is circular in outline, rounded, compressed and biconvex in side view. There are five chambers in the last whorl gradually increasing toward the apertural end of the test.

Sutures are coarsely perforate, distinct and oblique radiating from the broad macroperforate centre of the test. The periphery of the test is unevenly carinate around the margin. The chambers are separated by flush oblique sutures. The elliptical-shaped aperture is produced on a broad tubular neck with a thick bordering lip.

Remarks: The relative abundances recorded for *S. pulchra* were trace (<1%) in all three cores. Several specimens were found to be partially broken or with the aperture missing. The diameter of the tests in Cushman (1931) was reported to be 0.65 mm. Tests in this study are slightly smaller measuring 0.5 mm in diameter.

Ecological examples: The genus *Siphonina* is epifaunal and prefers oxic bottom water conditions (Kaiho, 1994) with a bathymetric distribution from shelf to slope depths (Phleger and Parker, 1951).

Regional occurrence: Middle Miocene on the continental shelf south of the Kunene River mouth (this study).

Family: CIBICIDIDAE Cushman, 1927a

Genus: CIBICIDOIDES Saidova, 1975

Cibicidoides crebbsi (Hedberg, 1937)

Pl. 4, figs. 14a-c

Eponides crebbsi Hedberg, 1937, p. 679, pl. 92, fig. 1; Bolli et al. 1994, p. 240, pl. 55, figs 16-17, p.,298, pl. 79, fig. 8.

Truncatulina floridana Nuttall, 1928, p. 98, pl. 7, figs. 14, 16

Cibicidoides crebbsi van Morkhoven et al., 1986, p. 139, pl. 45; Katz and Miller, 1993a, pl. 2, fig. 5; Kender et al., 2008, p. 516, pl. 20, figs. 4-5; Holbourn et al., 2013, p. 168-169

Description: The wall is calcareous and macroperforate. The test is slightly inflated, trochospiral and planoconvex to unequally biconvex in side view and in cross-section. Approximately ten chambers are visible in the final whorl. The chambers gradually increase in size toward the terminal apertural end. The chambers are separated by flush, less perforate sutures. The sutures on the spiral side are oblique whereas sutures on the umbilical side are more radial and irregular. The aperture is an interio-marginal basal slit.

Remarks: The relative abundances for *Cibicidoides crebbsi* decrease toward deeper depths forming minor (<10%) components in the samples of all three cores. Tests are relatively moderate to large in size measuring up to 1 mm in diameter.

Ecological examples: Species of the genus *Cibicidoides* are generally unattached, epifaunal to shallow infaunal under oxic conditions (Pezelj et al., 2013 and references therein) and prefer muddy substrates (Murray, 1991). The species *C. crebbsi* has a slope distribution (Holbourn et al., 2013).

Global stratigraphic range: Early Oligocene to Early Pliocene (Holbourn et al., 2013).

Regional occurrence: Middle Miocene, continental shelf of Namibia south of the Kunene River mouth (this study) and Congo Basin (Kender et al., 2008).

Cibicidoides dutemplei (d'Orbigny, 1846)

Pl. 5, figs. 1a-c

Rotalina dutemplei d'Orbigny, 1846, p. 157, pl. 8, figs. 19-21

Heterolepa dutemplei Papp and Schmid, 1985, p. 61, pl. 52, figs. 1-6; Loeblich and Tappan, 1988, p. 632, pl. 709, figs. 1-8; Holbourn et al., 2013, p. 294-295

Cibicidoides dutemplei van Morkhoven et al., 1986, p. 112, pl. 35

Description: The wall is calcareous and macroperforate. The test is trochospiral and mainly planoconvex in side view with the umbilical side very convex. Earlier chambers form a slightly convex shape on the spiral side. The approximately eight chambers in the final whorl gradually increase in size toward the apertural end. The chambers are separated by flush, less perforate sutures covering almost the entire earlier chambers of the inner whorl. The sutures on the spiral side are oblique. The aperture is an interio-marginal slit extending along the inflated apertural chamber on the umbilical side.

Remarks: *Cibicidoides dutemplei* is a minor (<5%) component in the samples of all three cores. Tests are relatively moderate to large in size measuring up to 1 mm in diameter.

Ecological examples: Species of the genus *Cibicidoides* are generally unattached, epifaunal to shallow infaunal (Pezelj et al., 2013). *Cibicidoides dutemplei* is adapted to oxic conditions (Russo et al., 2007).

Regional occurrence: Middle Miocene, continental shelf of Namibia south of the Kunene River mouth (this study).

Cibicidoides pseudoungerianus (Cushman, 1922b)

Pl. 5, figs. 2-4

Truncatulina pseudoungeriana Cushman, 1922b, p. 96, pl. 10, fig. 9.

Cibicides pseudoungeriana Cushman, 1931, p. 123, pl. 22, fig. 4.

Cibicidoides pseudoungerianus Cimerman and Langer, 1991, p. 69, pl.74, fig. 2-3; Milker and Schmiedl, 2012, p. 103, fig.24.5-24.9.

Cibicides pseudoungerianus Barker, 1960, pl. 94, fig. 9; Lowry, 1987, p. 322, pl. 21, figs. 3a-c; Milker et al., 2009, p. 218, pl. 3, fig.11;

Description: The wall is calcareous and perforate. The test is trochospiral, subcircular in outline and unequally biconvex in side view and in cross-section. The spiral side is coarsely perforate and the umbilical side is smoother. The umbilical side is more convex than the spiral side. The approximately ten chambers in the final whorl gradually increase in size toward the apertural end. The chambers are separated by flush thick sutures. The sutures on the spiral side are oblique whereas sutures on the umbilical side radiate from a thick central umbo. The aperture is interio-marginal bordered by a thin lip.

Remarks: The relative abundances of *C. pseudoungerianus* decrease toward the deeper cores forming major (<20%) to minor (<5%) components in the samples of all three cores. Tests in this study are moderate in size measuring up to 0.6 mm in diameter.

Ecological examples: Epifaunal to shallow infaunal under oxic bottom water conditions (Murgese and de Deckker, 2005; Murray, 2006). Shelf to slope distributions, but more typical of upper slope environments (Murgese and de Deckker, 2005).

Global stratigraphic range: Oligocene to Recent (Jones, 1994)

Regional occurrence: Middle Miocene on the continental shelf south of the Kunene River mouth (this study).

Cibicidoides ungerianus (d'Orbigny, 1846)

Pl. 5, figs. 5a-c

Rotalina ungeriana d'Orbigny, 1846, p. 157, pl. 8, figs. 16-18; Papp and Schmid, 1985, p. 60, pl. 51, figs. 7-11

Description: The test surface is calcareous and perforate. The test is trochospiral, subcircular in outline and thinly biconvex in side view. The spiral and umbilical sides are coarsely perforate. The chambers in the final whorl gradually increase in size toward the apertural end. The test margin has a thick keel and the chambers are separated by thick sutures with the earlier chambers not clearly visible. The aperture is an interio-marginal slit extending onto the umbilical lip.

Remarks: Less abundant than *C. pseudoungerianus* forming minor (<5%) components in the samples. The tests are generally large measuring up to approximately 1 mm in diameter.

Ecological examples: Species of the genus *Cibicidoides* are generally unattached, epifaunal to shallow infaunal under oxic conditions (Pezelj et al., 2013 and references therein) and prefer muddy substrates (Murray, 1991).

Regional occurrence: Middle Miocene on the continental shelf south of the Kunene River mouth (this study).

Family: NONIONIDAE Schultze, 1854

Genus: MELONIS de Montfort, 1808

Melonis barleeanus (Williamson, 1858)

Pl. 5, fig. 6

Noniona barleeana Williamson, 1858, p. 32, pl. 3, figs. 68-69.

Nonionina crassula Parker and Jones, 1857, p. 14, pl. 11, figs. 5-7.

Nonion barleeanum Cushman, 1930, p. 11, pl. 4, fig. 5.

Melonis barleeanus Loeblich and Tappan, 1994, p. 159, pl. 347, figs. 1-5.

Melonis barleeanum Loeblich and Tappan, 1988, pl. 696, figs. 5-6; Hermelin, 1989, p. 88, pl. 17, fig. 12; Milker and Schmiedl, 2012, p. 115, fig. 26.11-26.12; Holbourn et al., 2013, p. 354.

Description: The wall is calcareous and perforate. The test is planispiral and symmetrical in side view. The periphery of the test is rounded. Up to twelve chambers in the final whorl are separated by smooth slightly curved sutures. The chamber walls are coarsely perforate and the sutures very finely perforate. The sutures radiate from the umbilical region becoming thinner toward the test margin. The chambers gradually increase in size toward the apertural end. The aperture is an interio-marginal slit.

Remarks: The relative abundances of *Melonis barleeanus* decrease toward the deeper cores forming minor (<10%) to trace (<1%) components in the samples of all three cores. Tests are moderate in size measuring up to 0.5 mm in diameter.

Ecological examples: Unattached, mostly infaunal in muddy substrates (Murray, 1991); most abundant in oxic conditions, but also tolerant of dysoxic and suboxic conditions (Kaiho, 1994; Murray, 2006), associated with the nitrate reduction zone (Fontanier et al., 2002) on the shelf to slope (Holbourn et al., 2013).

Global stratigraphic range: Oligocene to Recent (Holbourn et al., 2013)

Regional occurrence: Middle Miocene on the continental shelf of Namibia south of the Kunene River mouth (this study) and in moderate abundances during the late Miocene to Pliocene along the slope of northern Namibia to the southwestern slope of South Africa (Wefer et al., 1998). Wefer et al. (1998) recorded the

occurrence of *M. barleeanus* only in low to moderate (<2 to <20%) abundances along the slope off the Walvis Ridge during the Pleistocene.

Family: GAVELINELLIDAE Hofker, 1956

Genus: GAVELINELLA Brotzen, 1942

Anomalinoides helicinus (Costa, 1855)

Pl. 5, figs. 7a-c

Nonionina helicina Costa, 1855, p. 123, pl. 1, figs. 18a-c

Anomalina helicina Christodolou, 1960, p. 89, pl. 8, figs. 5a-c

Description: The wall is calcareous with coarsely perforate chambers and smooth sutures separating the chambers. The test is rounded and trochospiral with a small central boss. The approximately twelve chambers in the final whorl gradually increase in size and become inflated toward the apertural end. The curved radial sutures appear slightly raised between the coarsely perforate chambers on the umbilical side. The sutures are curved away from the apertural end. A flap extends from each suture between chambers slightly extending over the umbilicus. The aperture is an arched interio-marginal slit against the margin of the previous whorl with an upper lip.

Remarks: The relative abundances of *A. helicinus* are minor (<5%) in all three cores. The tests are moderate in size measuring 0.6 mm in diameter.

Ecological examples: Epifaunal-shallow infaunal (Perez-Asensio et al., 2012)

Regional occurrence: Middle Miocene on the continental shelf south of the Kunene River mouth (this study).

Genus: GYROIDINOIDES Brotzen, 1942

Gyroidinoides soldanii (d'Orbigny, 1826)

Pl. 5, fig. 8; pl. 6, figs. 1a-b

Gyroidina soldani d'Orbigny, 1826, p. 278; d'Orbigny, 1846, pl. 8, figs. 10-12; Papp and Schmid, 1985, p. 60, pl. 50, figs. 4-9.

Gyroidinoides soldanii Lowry, 1987, p. 254, pl. 15, figs. 9a-b; Jones, 1994, p. 106, pl. 107, figs. 6-7; Kender et al., 2008, p. 519, pl. 25, figs. 1-5; Holbourn et al., 2013, p. 278.

Description: The wall is calcareous and microperforate. The test is trochospiral and planoconvex in side view. The spiral side is flat and the umbilical side convex. The eight chambers in the final whorl gradually increase in size toward the apertural end and are separated by slightly depressed sutures. The sutures are radial on the spiral side and straight on the umbilical side. The aperture is interio-marginal.

Remarks: Minor to moderate abundances on the cores. The tests measure up to 0.9 mm in diameter.

Ecological examples: Epifaunal-shallow infaunal (Perez-Asensio et al., 2012), suboxic, unattached, preferring muddy substrates (Murray, 1991) on the slope (Holbourn et al., 2013)

Global stratigraphic range: Oligocene to Recent (Jones, 1994)

Regional occurrence: Kender et al. (2008) reported *G. soldanii* from the Miocene in the Congo Basin. Middle Miocene on the continental shelf of Namibia south of the Kunene River mouth (this study). In minor (<1%) to moderate (<50%) abundances along the slope of Namibia and southwestern South Africa from the late Miocene to Pleistocene. The highest abundances were recorded on the

slope between Walvis Bay and Lüderitz, Namibia (Wefer et al., 1998). Lowry (1987) reported *G. soldanii* in surface sediments off the coast of northern Namibia to around the entire coastline of South Africa.

Family: GAVELINELLIDAE Hofker, 1956
Subfamily: GYROIDINOIDINAE Saidova, 1981
Genus: GYROIDINA d'Orbigny, 1826

Gyroidina broeckhiana (Karrer, 1878)
Pl. 6, figs. 2-3

Rotalina broeckhiana Karrer, 1878, p. 98, pl. 5, fig. 26.
Gyroidina broeckhiana Belford, 1966, pp. 167, 168, pl. 29, figs. 1-7, text-figs. 21-10, 21-11; Jones, 1994, p. 106, pl. 107, fig. 4.
Description: The wall is calcareous and microperforate. The test is trochospiral, subcircular in outline and unequally biconvex in side view and in cross-section. Approximately six to eight chambers are visible externally in the final whorl. The chambers gradually increase in size toward the terminal apertural end and are separated by slightly depressed sutures. The sutures on the spiral side are radial and straight on the umbilical side. The aperture is an extraumbilical to interio-marginal slit.
Remarks: The relative abundances of this species are moderate to high (<10%) in the three cores. Tests in this study are relatively large measuring up to 1 mm in diameter.
Ecological examples: The genus *Gyroidina* has been found to be shallow infaunal (Kaiho, 1994; Jorissen and Wittling, 1999) in suboxic conditions (Kaiho, 1994) and well oxygenated environments (Drinia et al., 2003). This genus is also associated with the oxygen minimum zone (Wilson and Hayek, 2015).
Regional occurrence: Midddle Miocene on the continental shelf south of the Kunene River mouth (this study).

4.4.2. Planktic Foraminifera

Family: GLOBOROTALIIDAE Cushman, 1927a
Genus: GLOBOROTALIA Cushman, 1927a

Globorotalia praescitula (Blow, 1959)
Pl. 6, fig. 4a-c

Globorotalia scitula praescitula Blow, 1959, p. 221, pl. 19, fig. 128.
Globorotalia praescitula Kennett and Srinivasan, 1983, p. 108, pl. 25, figs. 4-6.
Description: The wall surface is smooth and macroperforate. The test is compressed, biconvex in side view with up to five crescent-shaped chambers visible on the umbilical side rapidly increasing toward the apertural end. The chambers increase in size toward the terminal end. Earlier chambers are slightly pustulose on the umbilical side opposite the apertural opening. The sutures are depressed, oblique, radial and slightly curved. The aperture is an extra-umbilical slit.
Remarks: Specimens of *Gr. praescitula* are not very abundant and only occur as trace in some of the samples. The tests are moderate in size measuring 0.4 mm in width and 0.65 mm in length.
Low latitude stratigraphic range: Miocene to Recent (references in Kender, 2007)
Environmental preferences: Cold-water (Zachariasse et al., 1997).
Regional occurrence: Middle Miocene on the continental shelf of Namibia south of the Kunene River mouth (this study).

Family: GLOBIGERINIDAE Carpenter et al., 1862

Genus: GLOBIGERINA d'Orbigny, 1826

Globigerina bulloides d'Orbigny, 1826

Pl. 6, figs. 5-6

Globigerina bulloides d'Orbigny, 1826, p. 277; Banner and Blow, 1960, p. 3, pl. 1, figs. 1a-c; Bolli et al., 1985, p. 321, figs. 4.1-2; Lowry, 1987, p. 354, pl. 24, figs. 1a-c.

Description: The wall is calcareous and macroperforate with the test being covered with short bases from which spines of the living form would extend between pores. The chambers are globular in shape and trochospirally arranged. There are four spherical enlarging chambers in the final whorl with the terminal chamber being the largest. Sutures between chambers on all sides are depressed. One large aperture forming an asymmetric arch in the final chamber, umbilically positioned forming an asymmetric arch.

Remarks: A major component (<80% of the planktic population) in samples of all three cores. The tests are up to 0.5 mm in diameter.

Environmental preferences: Upwelling indicator (Giraudeau, 1993); transitional/ temperate (Kucera, 2007)

Global stratigraphic range: Middle Miocene to Recent (Kennett and Srinivasan, 1983; Bolli et al., 1985).

Regional occurrence: Middle Miocene Continental shelf of northern Namibia (this study); abundant in Quaternary to Recent sediments on shelf and in slope sediments (Lowry, 1987; Giraudeau, 1993; Wefer et al., 1998; Rau, 2002; Rau et al., 2002)

Genus: GLOBIGERINELLA Cushman, 1927a

Globigerinella siphonifera (d'Orbigny, 1839)

Pl. 6, figs. 7-8

Globigerinella siphonifera d'Orbigny, 1839, p. 83, pl. 4, figs. 15-18; Parker, 1962, p. 228, pl. 2, fig. 22-28.

Globigerina aequilateralis Brady, 1884, p. 605, pl. 80, fig. 18-21.

Hastigerina siphonifera Banner and Blow, 1960, p. 22, fig. 2-3.

Globigerinella aequilateralis Cifelli, 1965, p. 22, pl. 7, fig. 3-5; Bé and Hamlin, 1967, p. 101, fig. 18; Kennett and Srinivasan, 1983, p. 238, pl. 59, fig. 1; pl. 60, fig. 4-6; Lowry, 1987, p. 377, pl. 24, fig. 7a-c.

Description: The wall surface is perforate and hispid. The test is nearly completely planispirally coiled with up to six chambers globular in shape and rapidly enlarging toward the apertural opening. The earlier stage may be trochospiral. The sutures between chambers are depressed. The aperture is interiomarginal and forms an arch in the final chamber.

Remarks: The relative abundance of *G. siphonifera* in this study is trace (<1%) in samples of all three cores. The tests are relatively moderate in size measuring up to 0.5 mm in diameter.

Environmental preferences: Subtropical species (Kucera, 2007) in relatively warm surface water conditions (Zachariasse et al., 1997).

Global stratigraphic range: Middle Miocene to Recent (Kennett and Srinivasan, 1985).

Regional occurrence: Middle Miocene, northern Namibian continental shelf, south of the Kunene River mouth (this study). Wefer et al. (1998) reported the occurrence of this

species on the slope offshore of the Orange River during the Pleistocene. This species occurs in surface sediments along the entire coastline of South Africa, but with higher abundances on the east coast (Lowry, 1987).

Genus: GLOBIGERINOIDES Cushman, 1927a

Globigerinoides bisphericus (Todd, 1954)

Pl. 6, figs. 9-11

Globigerinoides bisphericus Todd, 1954, p. 681, pl. 1, fig.1; Reed, 1965, p. 83, pl. 15, fig. 1-2; Bolli et al., 1985, p. 199, pl. 24, fig.8; Kender et al., 2008, p. 520, pl. 27, figs. 5, 8.

Globigerinoides sicanus Kennett and Srinivasan, 1983, p. 62, pl. 13, fig. 4-6.

Description: The wall surface is macroperforate and cancellate. The test is rounded and circular in cross section. The three to four chambers in the final whorl are globular in shape. The larger chamber envelops earlier chambers hiding the umbilicus. Sutures are strongly depressed. Secondary apertures form along deep sutures.

Remarks: Bolli et al. (1985) note *Gs. trilobus* (reassigned to *Trilobatus trilobus* by Spezzaferri et al., 2015) to be ancestral to *Gs. bisphericus*. The relative abundances of *G. bisphericus* is trace (<1%) in samples of all three cores. The tests are small measuring 0.3 mm in diameter.

Environmental preferences: Warm waters (Bicchi et al., 2003).

Global stratigraphic range: Indicator species of the Early to Mid-Miocene (Kennett and Srinivasan, 1983; Bolli et al., 1985)

Regional occurrence: Kender et al. (2008) reported *G. bisphericus* from the Miocene of the Congo Basin. Middle Miocene on the continental shelf south of the Kunene River mouth (this study).

Globigerinoides ruber (d'Orbigny, 1839)

Pl. 7, figs. 1-2

Globigerina rubra d'Orbigny, 1839, p. 82, pl. 4, figs. 12-14

Globigerinoides ruber Todd, 1942, p. 65, pl. 25, fig. 6; Banner and Blow, 1960, p. 19, pl. 3, figs. 8a-b; Whittaker and Hodgkinson, 1979, p. 98, pl. 8, fig. 15; Kennett and Srinivasan, 1983, p. 78, pl. 10, fig. 6; pl. 17, fig. 1-3; Bolli et al., 1985, p. 196, figs. 20.1, 2, 6; Lowry, 1987, p. 359, pl. 25, fig. 4; Zapata and Cea, 2002, p. 64, pl. 2, fig. 3-4.

Description: The wall surface is macroperforate and cancellate-spinose. The test is trochospiral, globular and semi-circular in cross section. The chambers are rounded with two basal chambers separated by a deep incised suture overarched by a large chamber. The primary aperture is large and forms an arch symmetrically above the two basal chambers in apertural view. Two supplementary apertures form on the spiral side of the test along sutures of earlier chambers.

Remarks: The relative abundances of *Gs. ruber* are major (<25%) in samples along the Mio-Pliocene contact of all three cores, increasing in abundance in the deeper cores. The tests of *Gs. ruber* are relatively small measuring 0.3 mm in diameter.

Environmental preferences: Subtropical (Kucera, 2007), warm water species (Reeder et al., 1998; Hemleben et al., 1990; Baggley, 2000). Relative abundances increase with increasing temperatures (Kucera, 2007).

Global stratigraphic range: Middle Miocene to Recent (Kennett and Srinivasan, 1983)

Regional occurrence: Middle Miocene, northern Namibian continental shelf, south of the Kunene River mouth (this study). Hay et al. (1984) listed *Gs. ruber* as being a rare to frequent species on the slope off the Walvis

Ridge during the Pliocene to Pleistocene. Wefer et al. (1998) reported the species to occur on the slope between Walvis Bay and Lüderitz during the Pliocene and along the slope of Namibia southwards to offshore Orange River during the Pleistocene.

Genus: TRILOBATUS Spezzaferri et al., 2015

Trilobatus immaturus (LeRoy, 1939)

Pl. 7, figs. 3-5

Globigerinoides sacculifer var. *immaturus* LeRoy, 1939, p. 263, pl. 3, figs. 19-21.
Globigerinoides quadrilobatus Banner and Blow, 1960, p. 17, pl. 4, figs 3a-b.
Globigerinoides trilobus immaturus Bolli et al., 1985, figs. 20.14.
Globigerinoides trilobus var. *immatura* Jenkins, 1960, p. 354, pl. 2, fig. 7a-c.
Globigerinoides immaturus Kennett and Srinivasan, 1983, p. 64, pl. 10, fig. 3; pl. 13, fig. 7-9; Kender et al., 2008, p. 520. pl. 27, fig. 3
Trilobatus immaturus Spezzaferri et al., 2015
Description: The test surface is macroperforate and cancellate. The test is trochospiral, globular and semi-circular in cross section. The chambers are rounded with three basal chambers separated by deep incised sutures overarched by a large chamber that has the width of all three lower chambers. The primary aperture forms a low arch above the three basal chambers on the apertural side. The middle basal chamber is larger than the two side chambers. Supplementary apertures form on the spiral side of the test along sutures.
Remarks: *Gs. trilobus immaturus* (revised to *Trilobatus trilobus* by Spezzaferri et al., 2015) is distinguished from *Gs. trilobus trilobus* by its smaller final chamber (Bolli, 1957). Bolli et al. (1985) identified *Gs. quadrilobatus* as being the synonym for *Gs. trilobus immaturus*.
This species was found to be highly abundant in some of the samples (<80%). The relative abundance of *T. immaturus* is higher in deeper cores (2658 and 2670). Tests are moderate in size measuring up to 0.45 mm in diameter.
Environmental preferences: Warm surface waters (Reeder et al., 1998).
Global stratigraphic range: Early Miocene to Recent (Kennett and Srinivasan, 1983)
Regional occurrence: In Miocene-aged sediments of the Congo Basin (Kender et al., 2008) to northern Namibian continental shelf, south of the Kunene River mouth (this study).

Trilobatus sacculifer (Brady, 1877)

Pl. 7, figs. 6-7

Globigerina sacculifer Brady, 1877, p. 604, pl. 80, figs. 11-17, pl. 81, fig. 2, pl. 82, fig.4.
Globigerinoides sacculifer Kennett and Srinivasan, 1983, p. 66, pl. 14, figs. 4-6; Lowry, 1987, p. 360, pl. 25, fig. 5a-b; Kender et al., 2008, p. 521, pl. 27, fig. 2.
Trilobatus sacculifer Spezzaferri et al., 2015
Description: The test surface is macroperforate. The test is trochospiral, globular and semi-circular in outline. The chambers are rounded with three basal chambers separated by deep incised sutures overarched by a chamber that is finer in texture and shaped at a rounded angle to one side. The final chamber is lobulate or sack-like in shape and is not always the largest chamber. The side chamber is often the largest. The primary aperture forms a low arch above the three basal chambers on the apertural side. The apertural arch has a thin finely punctate layer and is often not as coarsely perforated as the rest of the test. Several supplementary

apertures form on the spiral side of the test along sutures.

Remarks: The relative abundances of *T. sacculifer* form a minor component (<10%) of the planktic foraminiferal population in all three cores. The abundances are highest below the Mio-Pliocene contact. The tests are relatively small to moderate in size measuring up to 0.4 mm in diameter.

Environmental preferences: Tropical species (Kucera, 2007) preferring warm water conditions (Zachariasse et al., 1997; Reeder et al., 1998; Baggley, 2000; Hemleben et al., 1990).

Global stratigraphic range: Miocene to Recent (Kennett and Srinivasan, 1983; Jones, 1994).

Regional occurrence: In Miocene-aged sediments of the Congo Basin (Kender, 2007) to northern Namibian continental shelf, south of the Kunene River mouth (this study). Wefer et al. (1998) reported the species to occur on the slope offshore of the Orange River during the Pleistocene. Lowry (1987) gave a distribution of the species spanning the entire coastline of South Africa in surface sediments.

Genus: GLOBOQUADRINA Finlay, 1947

Globoquadrina dehiscens (Chapman, Parr and Collins, 1934)

Pl. 7, figs. 8-10

Globorotalia dehiscens Chapman et al., 1934, p. 569, pl. 11, fig. 36.

Globioquadrina dehiscens dehiscens Jenkins, 1960. P. 354, pl. 3, fig. 3a-c.

Globoquadrina dehiscens Jenkins, 1960, p. 355, pl. 3, fig. 4a-c; Kennett and Srinivasan, 1983, p. 184, pl. 45, figs. 7-9; Kender et al., 2008, p. 521, pl. 29, fig. 1.

Description: The test surface is cancellate. The test is trochospiral and roughly quadrate in outline. There are four chambers visible in the final whorl. Sutures between chambers are strongly incised. The spiral side is nearly flat. The aperture is dentate and central to the four final chambers.

Remarks: The relative abundances of *Globoquadrina dehiscens* form a minor component (<10%) of the planktic foraminiferal assemblages in core 2658. In the deeper cores (2670 and 2682) the relative abundances of *Globoquadrina dehiscens* are below 5%. The tests are relatively small to moderate in size measuring up to 0.5 mm in diameter.

Environmental preferences: Tropical to temperate surface waters (Kennett and Srinivasan, 1983; Bicchi et al., 2003).

Global stratigraphic range: Early to late Miocene (Kennett and Srinavasan, 1983)

Regional occurrence: In Miocene-aged sediments of the Congo Basin (Kender, 2007) to northern Namibian continental shelf, south of the Kunene River mouth (this study) and the southwestern shelf of South Africa (Compton et al., 2004).

Genus: ORBULINA d'Orbigny, 1839

***Orbulina universa* (**d'Orbigny, 1839)

Pl. 7, fig. 11

Orbulina universa d'Orbigny, 1839, pl. 28, fig. 2; LeRoy, 1948, p. 501, fig.1a; Kennett and Srinivasan, 1983, p. 86, pl. 20, fig. 4-6; Kender et al., 2008, p. 522, pl. 28, fig. 2

Description: The test surface is spinose and covered with many perforations of different sizes across the entire test. The test is spherical

which may enclose an earlier Globigerinid stage. There is no single large primary aperture.

Remarks: The relative abundances of *Orbulina universa* form a minor component (<10%) of the planktic foraminiferal population in core 2658. In the deeper cores (2670 and 2682) the relative abundances are mostly at <1%. The tests are relatively small to moderate in size measuring up to 0.5 mm in diameter.

Global stratigraphic range: A good stratigraphic marker with a well-defined first appearance datum in the Miocene, with the stratigraphic range extending to Recent (Kennett and Srinivasan, 1983; Jones, 1994).

Environmental preferences: Subtropical species (Kucera, 2007) preferring warmer waters (Zachariasse et al., 1997; Gallagher et al., 2001; Drinia et al., 2008; Hemleben et al., 1990).

Regional occurrence: In Miocene-aged sediments of the Congo Basin (Kender, 2007) to northern Namibian continental shelf, south of the Kunene River mouth (this study) and the southwestern shelf of South Africa (Compton et al., 2004). Wefer et al. (1998) reported the species to occur on the slope between central Namibia and offshore of the Orange River during the Pliocene and Pleistocene.

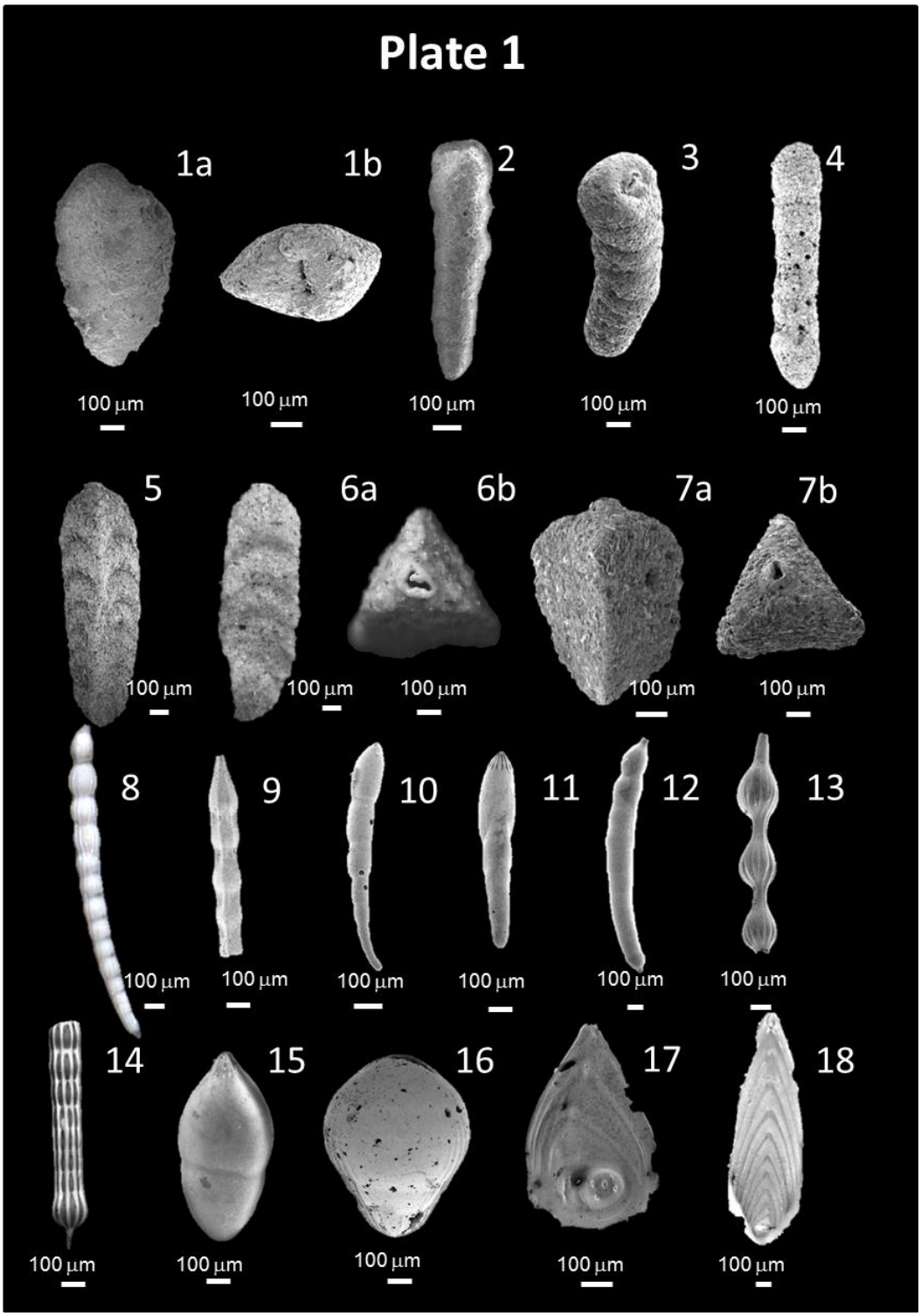

Plate 1. 1a. *Spiroplectammina* sp.; **1b.** apertural view of *Spiroplectammina* sp. (core 2670, 108 cm); **2.** *Karreriella siphonella* (core 2670, 138 cm); **3**. *Karreriella siphonella* with aperture visible at terminal chamber (core 2670, 138 cm); **4.** *Martinottiella communis* (core 2670, 168 cm); **5**. *Clavulina angularis* (core 2670, 108 cm); **6a.** *Clavulina angularis;* **6b.** apertural view of *Clavulina angularis* (core 2670, 118 cm); **7a.** *Clavulina trilatera;* **7b.** apertural view of *Clavulina trilatera* (core 2670, 148 cm)*;* **8.** *Dentalina acuta* (core 2670, 148 cm)*;* **9.** *Dentalina albatrossi* (core 2670, 178 cm)*;* **10.** *Laevidentalina inornata* (core 2670, 168 cm); **11**. *Laevidentalina* sp. A (core 2670, 108 cm); **12**. *Laevidentalina* sp. B (core 2670, 118 cm); **13.** broken test of *Grigelis semirugosa* (core 2670, 108 cm)*;* **14.** broken test of *Nodosaria latejugata* (core 2670, 158 cm); **15.** *Pseudonodosaria brevis* (core 2670, 118 cm); **16.** *Lingulina seminuda* (core 2670, 118 cm)*;* **17.** *Plectofrondicularia* sp. A (core 2670, 168 cm); **18**. *Plectofrondicularia* sp. B (core 2670, 178 cm).

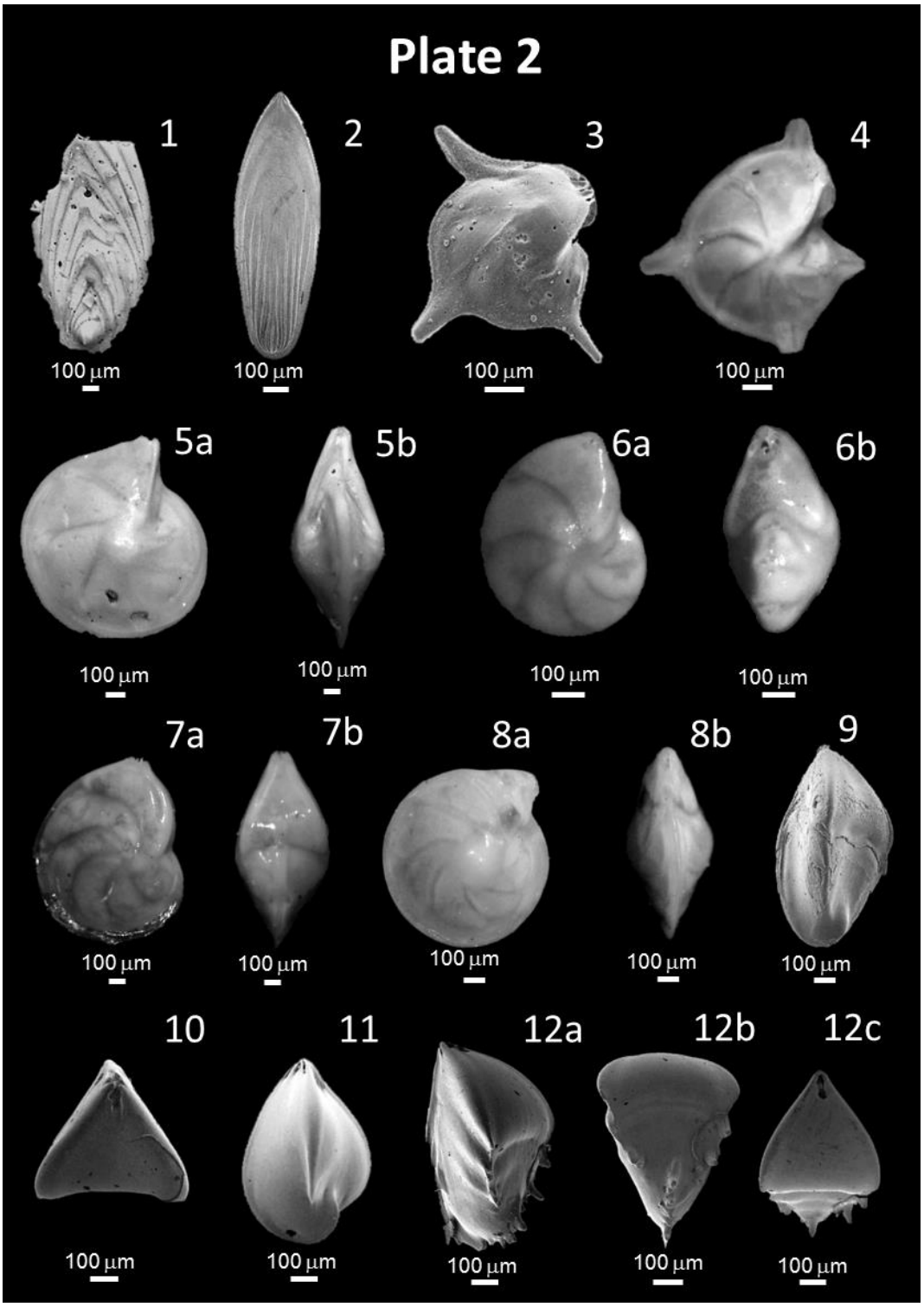

Plate 2. 1. *Plectofrondicularia* sp. B (core 2670, 168 cm); **2**. *Plectofrondicularia* sp. C (core 2670, 148 cm);; **3-4.** *Lenticulina calcar* (core 2670, 148 cm); **5a.** *Lenticulina cultrata* (spiral view); **5b.** *Lenticulina cultrata* (marginal view) (core 2670, 98 cm); **6a.** *Lenticulina gibba* (spiral view)*;* **6b.** *Lenticulina gibba* (marginal view) (core 2670, 118 cm); **7a.** *Lenticulina inornata* (spiral view); **7b.** *Lenticulina inornata* (marginal view) (core 2670, 128 cm); **8a**. *Lenticulina iota* (spiral view); **8b.** *Lenticulina iota* (marginal view) (core 2670, 158 cm); **9**. *Saracenaria italica* (core 2670, 138 cm); **10.** *Saracenaria italica* with aperture visible (core 2670, 138 cm); **11.** *Saracenaria* sp. (core 2670, 108 cm); **12a.** *Saracenaria spinosa*; **12b.** *Saracenaria spinosa* (marginal view); **12c.** *Saracenaria spinosa* with broken aperture visible (core 2670, 77 cm).

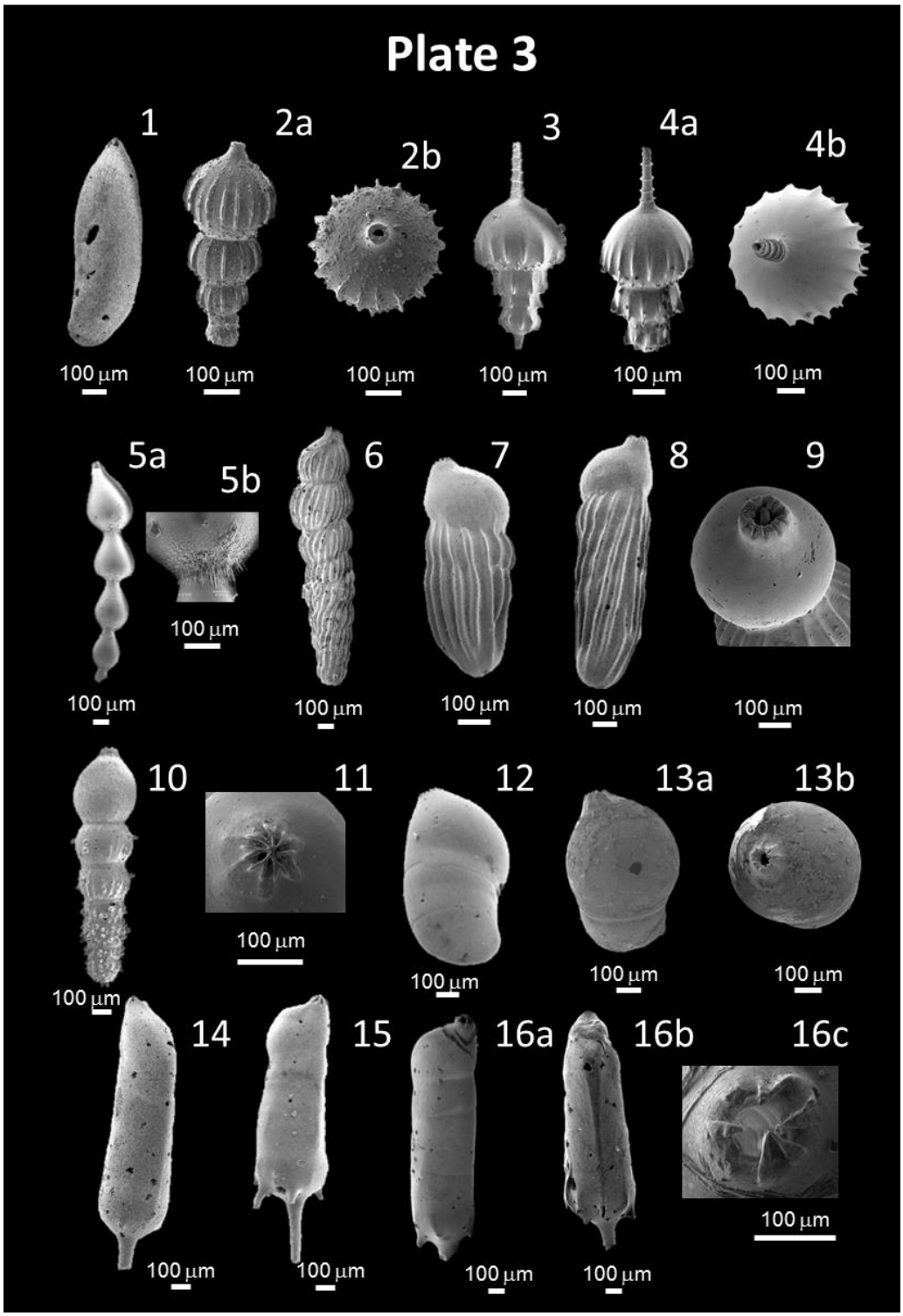

Plate 3. 1. *Astacolus crepidulus* (core 2670, 168 cm)*;* **2a**. *Amphicoryna scalaris* var. *hirsuta;* **2b**. *Amphicoryna scalaris* var. *hirsuta* (apertural view) (core 2670, 148 cm); **3.** *Amphicoryna* sp. (core 2670, 168 cm); **4a**. *Amphicoryna* sp.; **4b.** *Amphicoryna* sp. with apertural neck visible (core 2670, 148 cm); **5a.** *Amphicoryna sublineata*; **5b.** hirsute structures at base of chamber of *Amphicoryna sublineata* (core 2670, 118 cm); **6.** *Marginulina costata* (core 2670, 89 cm); **7**. *Marginulina* cf. *costata* (core 2670, 89 cm)*;* **8.** *Marginulina* cf. *costata* (core 2670, 98 cm); **9.** *Marginulina* cf. *costata* (apertural view) (core 2670, 98 cm); **10.** *Marginulina costata* var. *hirsuta* (core 2670, 148 cm); **11.** *Marginulina costata* var. *hirsuta* (apertural view) (core 2670, 148 cm); **12.** *Marginulina obesa* (core 2670, 108 cm)*;* **13a.** *Marginulina obesa* (oblique view)*;* **13b.** *Marginulina obesa* (apertural view) (core 2670, 108 cm); **14.** *Vaginulina legumen* (core 2670, 168 cm)*;* **15.** *Vaginulina* sp. (core 2670, 158 cm); **16a.** *Vaginulina* sp.; **16b.** *Vaginulina* sp. (side view); **16c.** *Vaginulina* sp. (aperture) (core 2670, 168 cm) (core 2670, 168 cm).

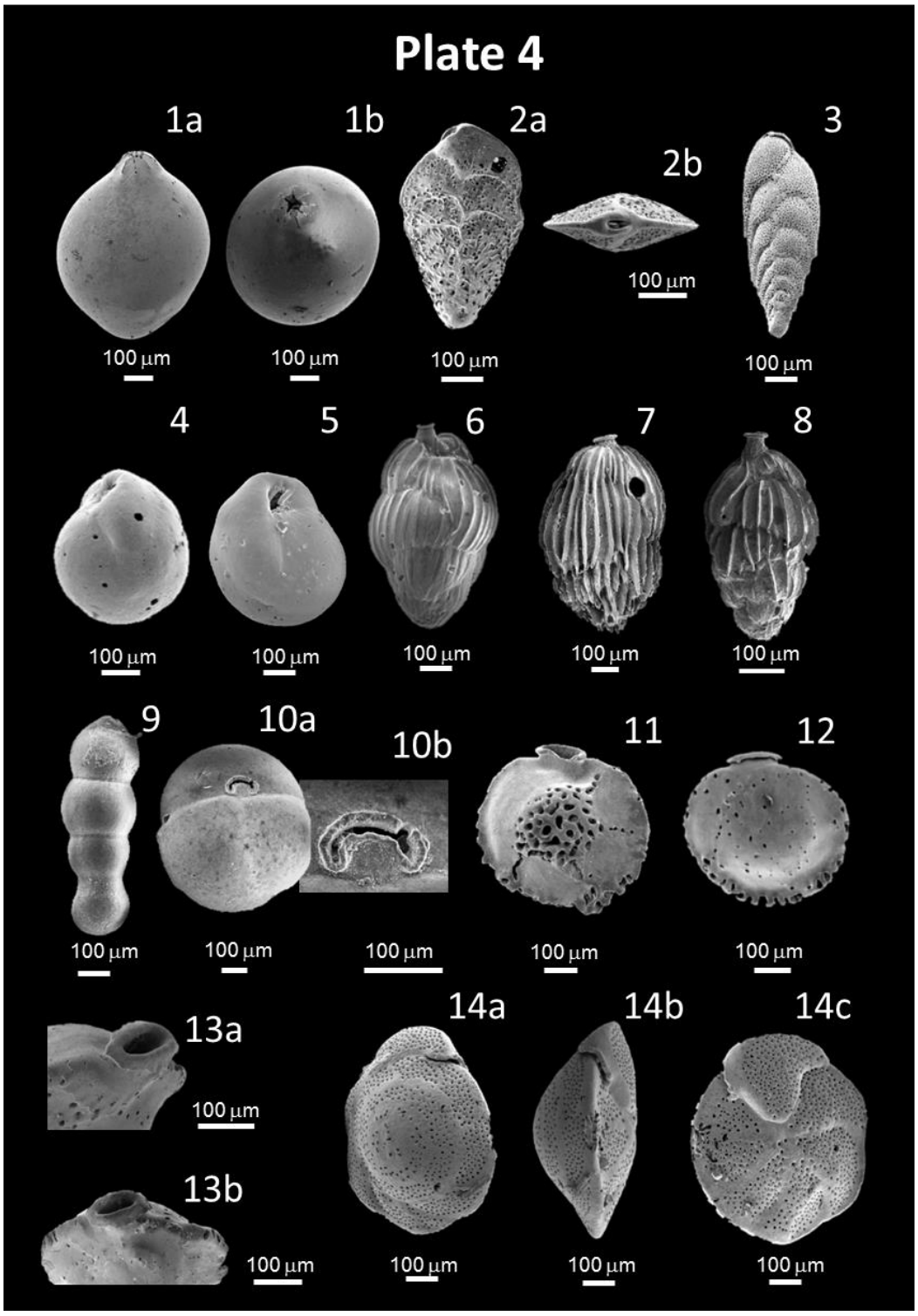

Plate 4. **1a**. *Glandulina laevigata* (core 2670, 98 cm)*;* **1b.** *Glandulina laevigata;* **2a.** *Bolivina reticulata*; **2b.** *Bolivina reticulata* (apertural view) (core 2670, 148 cm); **3.** *Brizalina alata* (core 2670, 178 cm); **4.** *Globocassidulina subglobosa* (core 2670, 178 cm); **5.** *Globocassidulina subglobosa* with aperture visible (core 2670, 108 cm); **6.** *Uvigerina peregrina* (core 2670, 178 cm); **7**. *Uvigerina pygmaea* (core 2670, 85 cm)*;* **8.** *Uvigerina spinulosa* (core 2670, 178 cm)*;* **9.** *Orthomorphina jedlitschkai* (core 2670, 118 cm)*;* **10a.** *Sphaeroidina bulloides*; **10b.** close-up of aperture of *Sphaeroidina bulloides* (core 2670, 118 cm); **11-12.** *Siphonina pulchra* (core 2670, 98 cm)*;* **13a.** aperture of *Siphonina pulchra;* **13b.** aperture of *Siphonina pulchra* (core 2670, 98 cm)*;* **14a.** *Cibicidoides crebbsi* (oblique spiral view); **14b**. *Cibicidoides crebbsi* (apertural view); **14c.** *Cibicidoides crebbsi* (umbilical view) (core 2670, 118 cm).

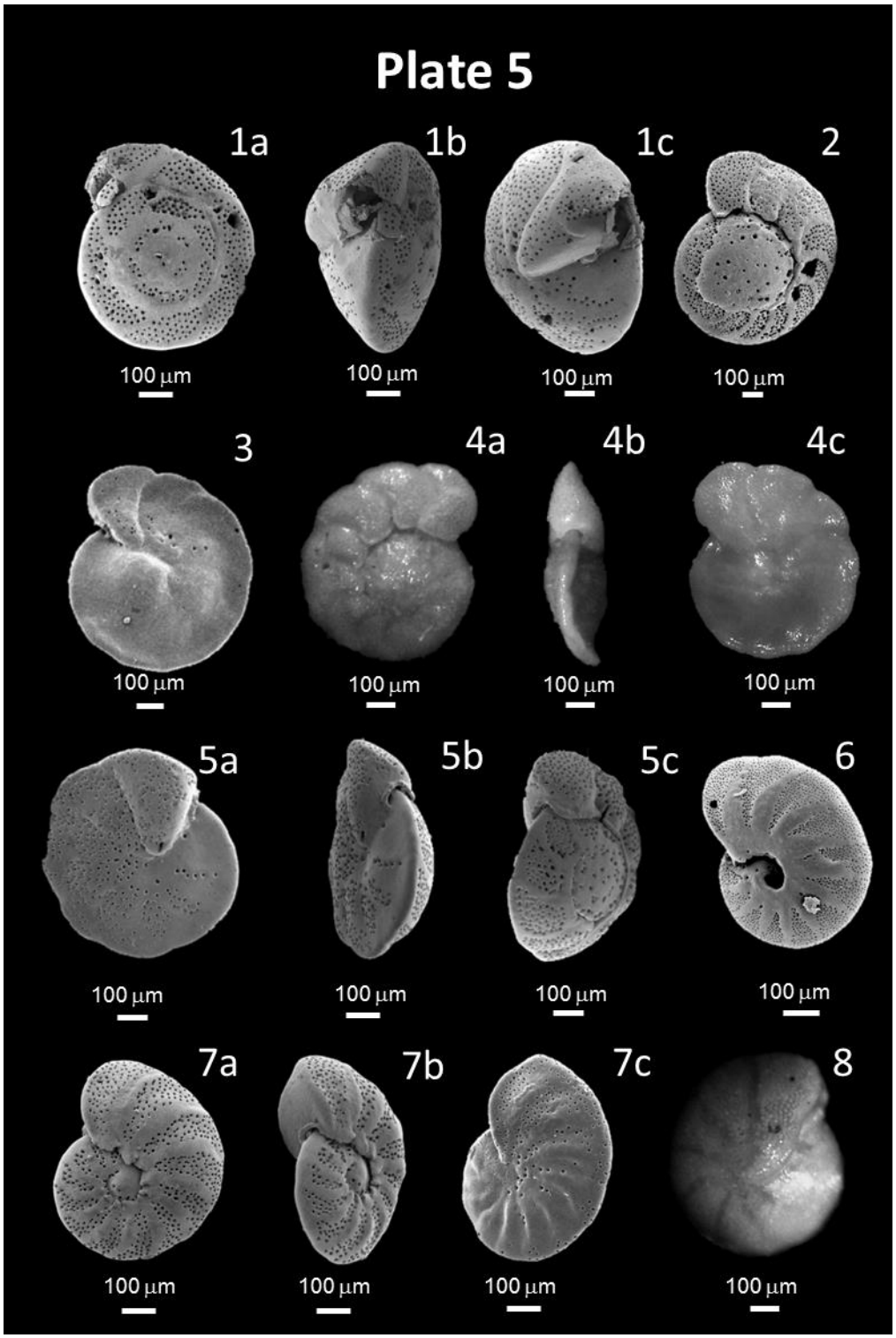

Plate 5. 1a. *Cibicidoides dutemplei* (spiral view); **1b.** *Cibicidoides dutemplei* (oblique apertural view); **1c.** *Cibicidoides dutemplei* (oblique umbilical view) (core 2670, 128 cm); **2.** *Cibicidoides pseudoungerianus* (spiral view) (core 2670, 85 cm); **3.** *Cibicidoides pseudoungerianus* (umbilical view) (core 2670, 85 cm); **4a.** *Cibicidoides pseudoungerianus* (spiral view); **4b.** *Cibicidoides pseudoungerianus* (apertural view); **4c.** *Cibicidoides pseudoungerianus* (umbilical view) (core 2670, 118 cm); **5a.** *Cibicidoides ungerianus* (umbilical view); **5b.** *Cibicidoides ungerianus* (apertural view); **5c.** *Cibicidoides ungerianus* (spiral view) (core 2670, 178 cm); **6.** *Melonis barleeanus* (core 2670, 178 cm)*;* **7a.** *Anomalinoides helicinus* (spiral view); **7b**. *Anomalinoides helicinus* (oblique apertural and spiral view); **7c**. *Anomalinoides helicinus* (oblique umbilical view) (core 2670, 178 cm); **8**. *Gyroidinoides soldanii* (umbilical view) (core 2670, 158 cm).

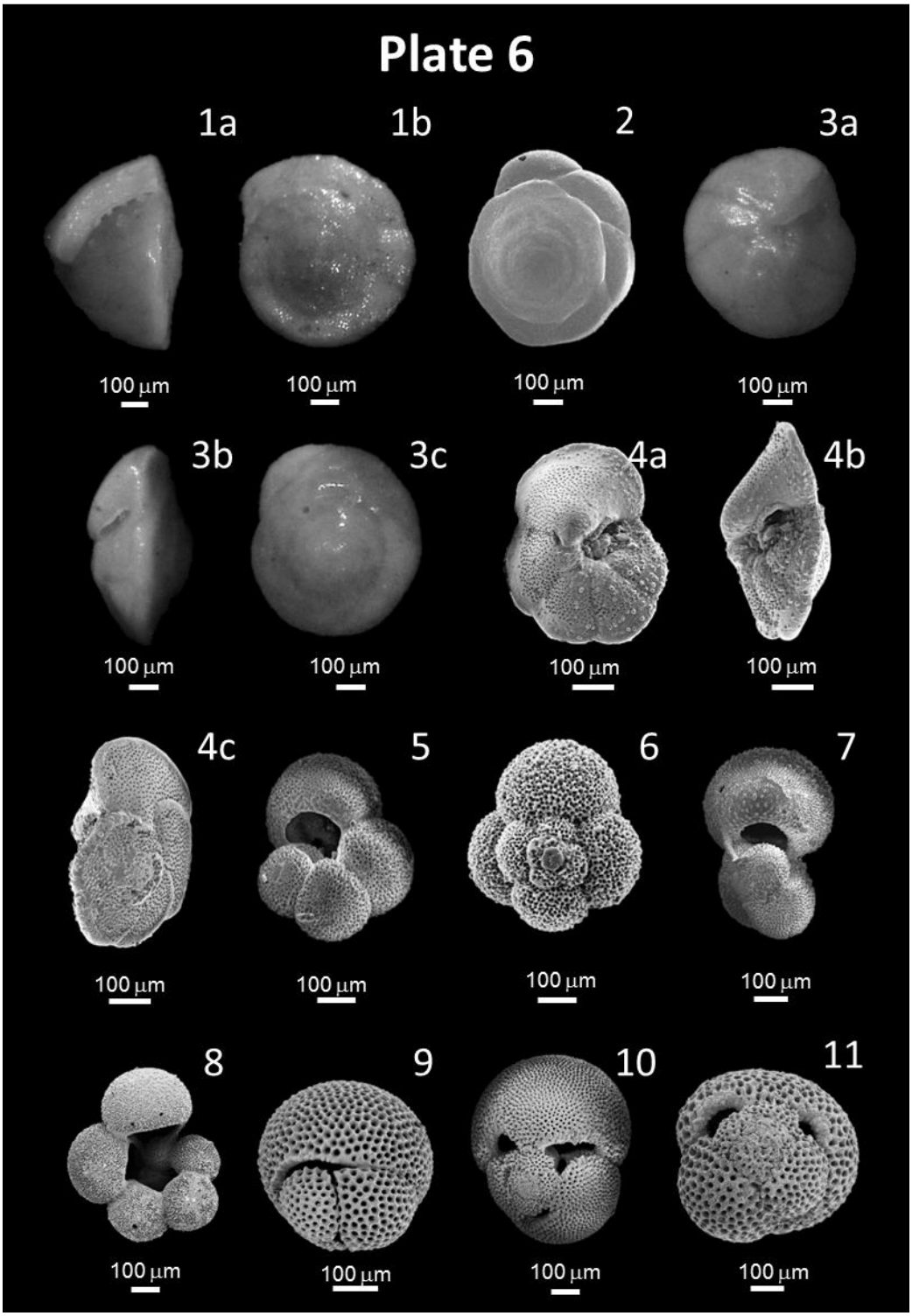

Plate 6. 1a. *Gyroidinoides soldanii* (apertural view); **1b.** *Gyroidinoides soldanii* (spiral view) (core 2670, 158 cm); **2.** *Gyroidina broeckhiana* (spiral view) (core 2670, 108 cm)**; 3a**. *Gyroidina broeckhiana* (umbilical view); **3b**. *Gyroidina broeckhiana* (apertural view)**; 3c**. *Gyroidina broeckhiana* (spiral view) (core 2670, 88 cm); **4a.** *Globorotalia praescitula* (umbilical view); **4b.** *Globorotalia praescitula* (apertural view); **4c.** *Globorotalia praescitula* (spiral view) (core 2670, 98 cm); **5.** *Globigerina bulloides* (apertural view) (core 2670, 168 cm); **6.** *Globigerina bulloides* (spiral view) (core 2670, 148 cm); **7.** *Globigerinella siphonifera* (core 2670, 148 cm)*;* **8.** *Globigerinella siphonifera* (core 2670, 148 cm)*;* **9.** *Globigerinoides bisphericus* (core 2670, 168 cm); **10.** *Globigerinoides bisphericus* (oblique spiral view showing secondary apertures) (core 2670, 168 cm); **11.** *Globigerinoides bisphericus* (lower spiral view) (core 2670, 118 cm).

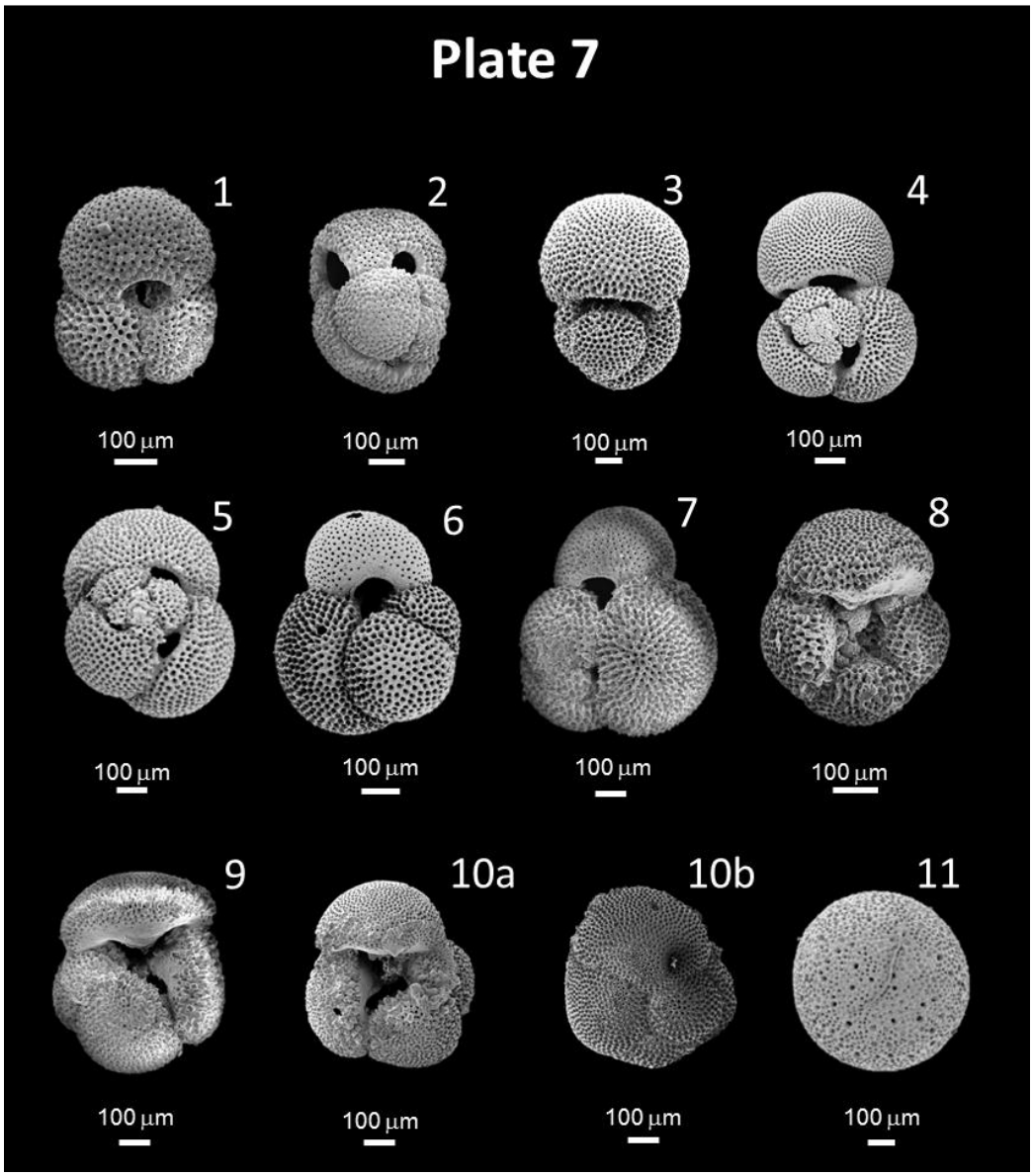

Plate 7. 1. *Globigerinoides ruber* white (primary apertural view) (core 2670, 168 cm); **2.** *Globigerinoides ruber* white (spiral view showing secondary apertures) (core 2670, 168 cm); **3.** *Trilobatus immaturus* (spiral view showing secondary apertures) (core 2670, 148 cm); **4.** *Trilobatus immaturus* (lower spiral view showing secondary apertures) (core 2670, 148 cm); **5.** *Trilobatus immaturus* (primary apertural view) (core 2670, 148 cm); **6.** *Trilobatus sacculifer* (primary apertural view) (core 2670, 89 cm); **7.** *Trilobatus sacculifer* (spiral view showing secondary apertures) (core 2670, 118 cm); **8.** *Globoquadrina dehiscens* (apertural view) (core 2670, 168 cm); **9.** *Globoquadrina dehiscens* (apertural view) (core 2670, 168 cm); **10a.** *Globoquadrina dehiscens* (apertural view); **10b.** *Globoquadrina dehiscens* (oblique spiral view) (core 2670, 138 cm); **11.** *Orbulina universa* (core 2670, 77 cm).

4.5. Distribution of middle Miocene foraminifera along the western margin of southern Africa

Some of the taxa reported from the middle Miocene in previous global studies (Table 4.1) have been described as deep-water species to occur between 1000 and 2000 m water depth on the continental slope (Miller and Katz, 1987; Katz and Miller, 1993b). The occurrence of these taxa in the Northern Hemisphere during the middle Miocene indicates their widespread distribution during the Mid-Miocene Climatic Optimum (MMCO). The MMCO refers to a warm period during the middle Miocene between 15 to 17 Ma when the global climate was at its warmest during the Neogene and since the late Eocene. Rapid cooling ended this warm period (Flower and Kennett, 1994; and references therein). During the MMCO sea-levels were higher than present day (Miller et al., 2005) which could have had an influence on the distribution of taxa coupled with additional factors that influence benthic foraminifera, e.g. organic matter delivery to the seafloor, substrate, bottom water oxygen levels, temperature and bottom water currents (Gooday, 2003).

Table 4.1. Species reported in this study and in previous studies from the Vienna Basin (Papp and Schmid, 1985), Buff Bay, Jamaica (Katz and Miller, 1993b) and the north Atlantic (Miller and Katz, 1987).

Species	This study	Vienna Basin	Buff Bay	North Atlantic
Dentalina acuta	x	x		
Globocassidulina subglobosa	x		x	x
Gyroidinoides soldanii	x	x		
Lenticulina calcar	x	x		
Lenticulina cultrata	x	x		
Lenticulina inornata	x	x		
Marginulina hirsuta	x	x		
Martinottiella communis	x	x		
Melonis barleeanus	x		x	x
Nodosaria laevigata	x	x		
Sphaeroidina bulloides	x	x		
Uvigerina pygmaea	x	x	x	
Vaginulina legumen	x	x		

Occurrences of taxa in studies based on middle Miocene deposits off the southwestern margin of Africa from Kender et al. (2008) which were at a deeper site (2000 m water depth) and Compton et al. (2004) were compared to foraminifera recorded from the northern Namibian margin to document the distribution of foraminiferal taxa along the continental margin from the Congo Basin to the southwest of South Africa. The taxa were divided into four groups (Fig. 4.3) based on Kender et al. (2008) and Compton et al. (2004). Group A (Congo-Namibia) consists of taxa reported in the Congo Basin and the northern Namibian shelf. Group B (Congo-Namibia-South Africa) consists of taxa reported throughout the western continental margin of southern Africa, including this study during the middle Miocene. Group C (Namibia)

consists of taxa only recorded in this study and group D (Namibia-South Africa) consists of taxa documented on the continental shelf from southwestern South Africa, as well as this study.

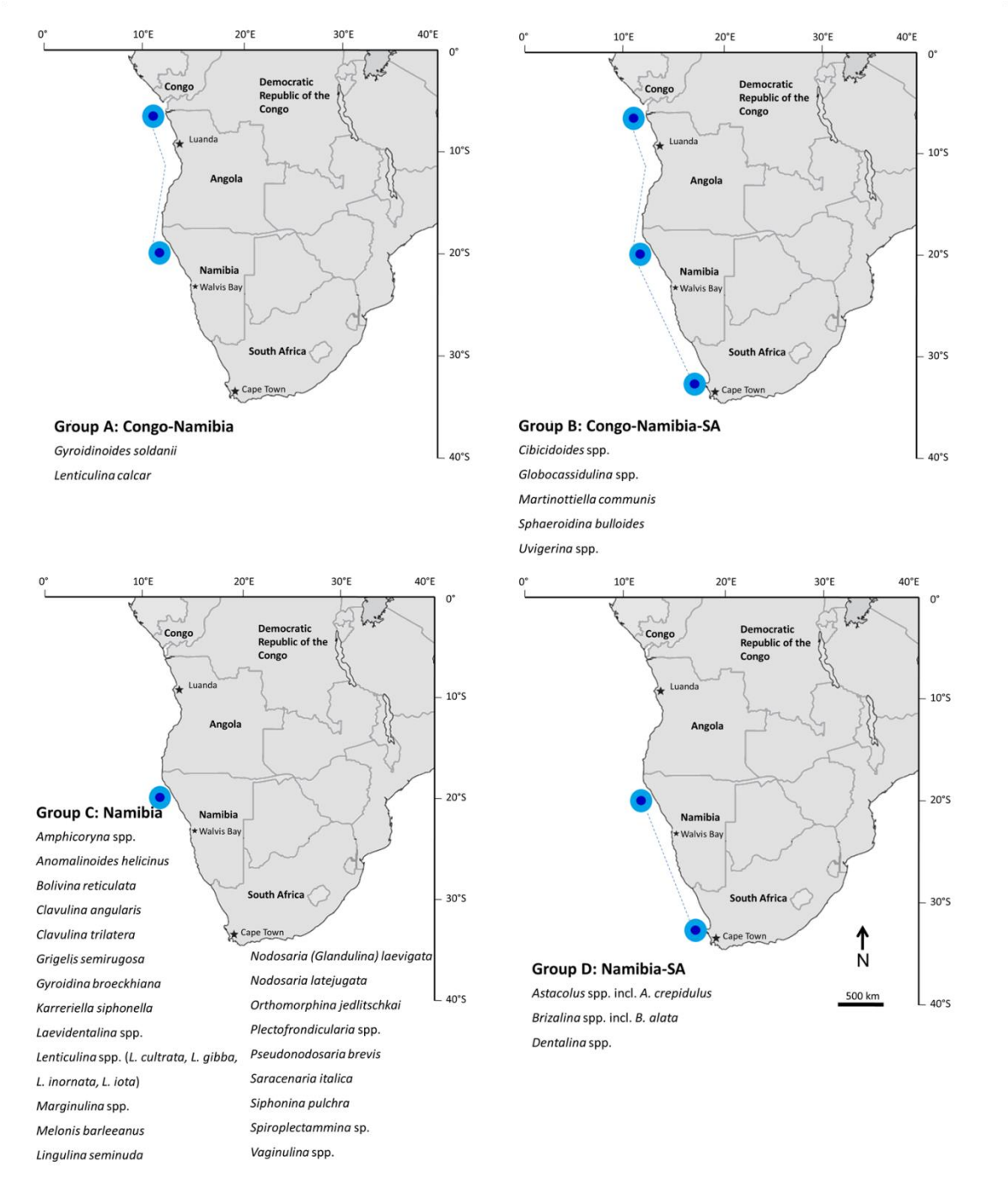

Fig. 4.3. Middle Miocene benthic foraminifera reported from the Congo Basin (Kender et al., 2008), Namibia (this study) and South Africa (Compton et al., 2004).

Nine taxa were found to be common between this study area and that of Kender et al. (2008) to the north. The study area of Kender et al. (2008) is located on the lower continental slope at depths of ~1000 m during the early-middle Miocene. Bergh et al. (2018) suggested the

assemblage discussed in this study to have lived at shallower water depths near the shelf edge (400-500 m). The continental shelf north of Cape Town is wide and one of the deepest in the world (Shepard, 1963) which may have aided in deeper water taxa (primarily reported from slope regions in other studies) occurring on the Namibian outer shelf during the middle Miocene. Common species between this study and Kender et al. (2008) have wide bathymetric distributions or were transported from shallower to deeper depths. The species *Lenticulina calcar* has a bathymetric distribution stretching to the middle slope, but Kender et al. (2008) suggested *L. calcar* tests were transported downslope. The bathymetric distribution for *L. calcar* fits the palaeodepth in this study. The species *G. soldanii* occurs on the slope and also fits the palaeodepth for the Congo Basin. Species common to both areas are epifaunal to shallow infaunal (Jorissen et al., 1998; Pezelj et al., 2013) and live under oxic to suboxic conditions (Murray, 1991; Kaiho, 1994).

Abundant taxa during the middle Miocene in the Congo Basin which were not recorded in this study include *Hanzawaia mantaensis, Uvigerina mantaensis, Bolivina tenuisstriata, Bulimina elongata, Brizalina* cf. *barbata, Uvigerina* aff. *carapitana, Brizalina alazanensis, Bulimina marginata, Glomospira* spp., *Rhabdammina* spp., *Bathysiphon* spp., *Saccammina* cf. *sphaerica, Rhizammina* spp., *Valvulinera pseudotumeeyensi, Trochammina* spp., *Tolypammina* spp., *Psammosphaera* spp. and *Nothia* spp.

Taxa such as *C. pseudoungerianus* in Group B have wide bathymetric distributions occurring at depths from the shelf to lower slope. *Sphaeroidina bulloides* and *Globocassidulina subglobosa* occur from the shelf to abyssal depths (Gallagher et al., 2001; Murgese and de Deckker, 2005; Pezelj et al., 2007; Holbourn et al., 2013). The adaptation of taxa from Group B to varying bottom water conditions allows them to occur over wide bathymetric depths. Some species have been classified as infaunal (*Globocassidulina subglobosa* and *Sphaeroidina bulloides*) and others epifaunal (*Cibicidoides* group and *Martinottiella communis*) adapted to oxic to suboxic conditions (Kaiho, 1994; Murray, 2006; Pezelj et al., 2013).

The taxa of group C have been documented for the first time for the middle Miocene along the margin. Limited middle Miocene data from the rest of the continental shelf, sample recovery and preservational bias make it difficult to determine the true extent of the distribution of group C taxa. The taxa from Group C have shelf and slope distributions and are interpreted to occur at the shelf edge of northern Namibia during the middle Miocene. The area experienced subtropical conditions during the middle Miocene when sea-levels were higher and the site was located at deeper depths on the outer shelf (Bergh et al., 2018). Sea surface temperatures were warmer than today (Pagani et al., 1999) and were influenced by the Angola Current rather than the BUS (inshore) and the Benguela Current (offshore) as the Angola-Benguela Front migrated northwards during the late Miocene (Hoetzel et al., 2015).

Taxa from group D commonly comprise less than 1% of the relative abundances in samples from this study off northern Namibia. The common species between the two areas could

represent taxa adapted to shelf conditions as both areas of Compton et al. (2004) and this study are located on the outer shelf. The taxa from this group are infaunal and adapted to oxic to dysoxic conditions (Kaiho, 1994; Kaminski et al., 2002).

Table 4.2. Planktic foraminifera reported from the continental margin of the Congo Basin (Kender, 2007), northern Namibia (this study) and southwestern South Africa (Compton et al., 2004). *reported as *Globigerinoides* spp. in Compton et al. (2004)

	Congo Basin	**Northern Namibia**	**Southwestern South Africa**
Globigerina bulloides		x	x
Globigerinella praesiphonifera	x	x	
Globigerinella obesa	x		
Globigerinoides bisphericus	x	x	*
Globigerinoides ruber		x	*
Globigerinoides subquadratus	x		
Globoquadrina dehiscens	x	x	x
Globoquadrina venezuelana	x		
Globorotalia praescitula	x	x	
Globorotalia archeomenardii	x		
Globorotalia peripheroronda	x		
Globorotalia praemenardii	x		
Globorotaloides hexagonus	x		
Globorotaloides permicus	x		
Globorotaloides suteri	x		
Orbulina bilobata	x		x
Orbulina universa	x	x	x
Paragloborotalia bella	x		
Paragloborotalia mayeri	x		
Paragloborotalia opima nana/continuosa	x		
Paragloborotalia semivera	x		
Trilobatus immaturus (previously *Gs. immaturus*)	x	x	*
Trilobatus sacculifer (previously *Gs. sacculifer*)	x	x	*
Trilobatus trilobus (previously *Gs. trilobus*)	x		*

Planktic foraminifera reported in Compton et al. (2004) are in general agreement with those from this study (Table 4.2). All species in this study area, with the exception of *Gs. ruber*, were reported in Kender (2007). More planktic species were reported from the Congo Basin. This would be expected as the higher number of planktic species can be explained by the deeper water depth in Kender (2007). It is not clear if *Gs. bisphericus*, *Gs. ruber* and *T. sacculifer* and *T. immaturus* were also present off southwestern South Africa during the middle Miocene because these taxa were only identified to genus level in Compton et al. (2004). The occurrence of the same planktic taxa in the aforementioned areas indicates similar warm surface water conditions along the entire southwestern margin of Africa. Planktic taxa that were found to occur in the middle Miocene sediments of this study and in Kender et al. (2008) can be attributed to the influence of the Angola Current on both study areas prior to the initiation of the BUS (Siesser, 1980; Bergh et al., 2018) and the northwards migration of the Angola-Benguela Current off northern Namibia (Hoetzel et al., 2015).

4.6. Conclusions

Middle Miocene foraminifera from the northern Namibian shelf have been associated with global faunal assemblages indicative of the MMCO. Although the ecological preferences of the taxa reported in previous studies are broad, taxa from the middle Miocene assemblages off northern Namibia have been classified in previous global studies as having slope distributions indicating the relatively deep palaeoenvironmental setting during the middle Miocene off northern Namibia, possibly as a result of fine-grained sediments being inhabited by species which are usually associated with slope depths.

Regionally, seventeen benthic and planktic species were found to be common between the northern Namibian and Congo Basin study areas. The planktic species common to both areas indicate the influence of the warm Angola Current in both areas during the middle Miocene. The taxa common to both areas have also been found to be the most abundant along the margin during the middle Miocene.

Thirty species have been identified in this study that were previously not reported in middle Miocene sediments of the southwestern margin of Africa and four were common between this study and in outer shelf sediments off southwestern South Africa. These species occur in trace (<1%) to minor (<10%) relative abundances in the middle Miocene northern Namibian sediments of this study.

References

Abu-Zied, R.H., Bantan, R.A., Basaham, A.S., El Mamoney, M.H., Al-Washmi, H.A., 2011. Composition, distribution, and taphonomy of nearshore benthic foraminifera of the Farasan Islands, southern Red Sea, Saudi Arabia. Journal of Foraminiferal Research 41, 349-362.

Alegret, L., Arenillas, I., Arz, J.A., Liesa, C., Melendez, A., Molina, E., Soria, A.R., Thomas, E., 2002. The Cretaceous/Tertiary boundary: sedimentology and micropalaeontology at El Mulato section, NE Mexico. Terra Nova 14, 330-336.

Alegret, L., Molina, E., Thomas, E., 2003. Benthic foraminiferal turnover across the

Cretaceous/Paleogene boundary at Agost (southeastern Spain): paleoenvironmental inferences, Marine Micropaleontology 48, 251-279.

Alegret, L., Thomas, E., 2007. Deep-Sea environments across the Cretaceous/Paleogene boundary in the eastern South Atlantic Ocean (ODP Leg 208, Walvis Ridge). Marine Micropalaeontology 64, 1-17.

Ali, M.Y., 2015. Evaluation of foraminifera and calcareous nannofossils changes across the Late Paleocene/Early Eocene transition at Nag El-Quda section, Upper Nile Valley, Egypt. Geosciences Journal 19, 641-654.

Armstrong, H.A., Brasier, M.D., 2005. Microfossils, 2nd edition. Blackwell, Oxford, 296 pp.

Asano. K., 1949. New Miocene foraminifera from Japan. Journal of Paleontology 23, 423-430.

Bagg, R.M., 1912. Pliocene and Pleistocene foraminifera from Southern California. US Government Printing Office, 513 pp.

Baggley, K.A., 2000. The Late Tortonian-Early Messinian foraminiferal record of the Abad Member (Turre Formation), Sorbas Basin, Almeria, South-east Spain. Palaeontology 43, 1069-1112.

Bandy, O.L., 1956. Ecology of foraminifera in northeastern Gulf of Mexico. United States Geological Survey Professional Paper 274, 179-204.

Banner, F.T., Blow, W.H., 1960. Some primary types of the species belonging to the superfamily Globigerinaceae.Contributions from the Cushman Foundation of Foraminiferal Research 11, 1-41.

Banner, F.T., Pereira, C.P.G., 1981. Some biserial and triserial agglutinated smaller foraminifera: their wall structure and its significance. Journal of Foraminiferal Research 11, 85-117.

Barbieri, R., Panieri, G., 2004. How are benthic foraminiferal faunas influenced by cold seeps? Evidence from the Miocene of Italy. Palaeogeography, Palaeoclimatology, Palaeoecology 204, 257-275.

Barker, R.W., 1960. Taxonomic notes on the species figured by H.B. Brady in his report on the Foraminifera dredged by H.M.S. *Challenger* during the years 1873-1876. Society of Economic Palaeontologists and Mineralogists, Special Publication 9, 1-328.

Batsch, A.I.G.C., 1791. Sechs Kupfertafeln mit Conchylien des Seesandes, gezeichnet und gestochen von A.J.G.K. Batsch, Jena, 6 pls.

Baumann, K. H., Freitag, T., 2004. Pleistocene fluctuations in the northern Benguela Current system as revealed by coccolith assemblages. Marine Micropaleontology 52, 195-215.

Bé, A.W.H., Hamlin, W.H., 1967. Ecology of Recent planktonic Foraminifera. Part 3. Distribution in the North Atlantic during the summer to 1962. Micropaleontology 13, 87-106.

Beissel, I., 1891. Die Foraminiferen der Aachener Kreide. Abhandlungen der Preußischen Geologischen Landesanstalt, Neue Folge Berlin 3, 1-76.

Belford, D.J. 1966. Miocene and Pliocene smaller foraminifera from Papua and New Guinea. Commonwealth of Australia, Department of National Development, Bureau of Mineral Resources, Geology and Geophysics, Bulletin 79, 305 pp.

Bergh, E.W., Compton, J.S., Frenzel, P., 2018. Late Neogene foraminifera from the northern Namibian continental shelf and the transition to the Benguela Upwelling System. Journal of African Earth Sciences 141, 33-48.

Bermúdez, P.J., 1949. Tertiary smaller foraminifera of the Dominican Republic. Special Publications of the Cushman Laboratory for Foraminiferal Research 25, 1-322.

Bernhard, J.M., 1986. Characteristic assemblages and morphologies from anoxic organic rich deposits: Jurassic through Holocene. Journal of Foraminiferal Research 16, 207–215.

Berthelin, G., 1880. Mémoire sur les Foraminifères fossiles de I'Etage Albien de Moncley (Doubs). Mémoires de la Société géologique de France, series 3, 1, 1-85.

Bicchi, E., Ferrero, E., Gonera, M, 2003. Palaeocimatic interpretation based on Middle Miocene planktonic Foraminifera: the Silesia Basin (Paratethys) and Monferrato (Tethys) records. Palaeogeography, Palaeoclimatology, Palaeoecology 196, 265-303.

Blow, W.H., 1959. Age, correlation and biostratigraphy of the upper Tocuto (San Lorenzo) and Pozon formations, eastern Falcon, Venezuela. Bulletins of American Paleontology 39, 67-215.

Boersma, A., 1984. Handbook of common Tertiary Uvigerina. Stony Point, New York: Microclimates Press, 207 pp.

Bolli, H.M., 1957. Planktonic foraminifera from the Oligocene-Miocene Cipero and Lengua formations of Trinidad, B.W.I. Bulletin of the US National Museum 215, 97-123.

Bolli, H.M., Beckmann, J.P., Sanders, J.B., 1994. Benthic Foraminiferal Biostratigraphy of the South Caribbean Region. Cambridge University Press, Cambridge, 408 pp.

Bolli, H.M., Saunders, J.B., Perch-Nielsen, K., 1985. Plankton Stratigraphy. Cambridge University Press, Cambridge, 1032 pp.

Boomgaart, L., 1949. Smaller Foraminifera from Bodjonegoro (Java). Smit and Dontje, Sappemeer, 175 pp.

Brady, H.B., 1877. Supplementary note on the foraminifera of the chalk (?) of the New Britain Group. Geological Magazine 4, 534-536.

Brady, H.B., 1881. Notes on some of the reticularian Rhizopoda of the Challenger Expedition, Part III. Quarterly Journal of Microscopical Science 21, 31-71.

Brady, H.B., 1884. Report of the foraminifera dredged by H.M.S. Challenger during the years 1873-1876. In: Brady, H.B. (Ed.) Report on the Scientific Results of the Voyage of the H.M.S. Challenger during the years 1873-1876. Zoology 9, 1-814.

Braga, J.M., 1960. Foraminíferos da costa de Moçambique. Etudos, Ensaios e Documentos No. 67, Junta de Investigações do Ultramar, Lisboa, 211 pp.

Brotzen, F., 1942. Die Foraminiferengattung *Gavelinella* nov. gen. und die Systematik der Rotaliformes. Årsbok Sveriges Geologiska Undersökning 36, 1-60.

Carpenter, W.B., Parker, W.K., Jones, T.R., 1862. Introduction to the study of foraminifera. Ray Society, London

Chapman, F., Parr, W.J., Collins, A.C., 1934. Tertiary foraminifera of Victoria, Australia. The Balcombian deposits of Port Phillip; Part III. Zoological Journal of

the Linnaean Society of London 38, 553-77.

Christodoulou, G., 1960. Geologische und mikropaläontologische untersuchungen auf der insel Karpathos (Dodekanes). Palaeontographica Abteilung A, 1-143.

Cicha, I., Rögl, F., Rupp, C., Ćtyroka, J., 1998. Oligocene-Miocene Foraminifera of the Central Paratethys. Abhandlungen der Seckenbergischen Naturforschenden Gesellschaft, 549, 1-325.

Cifelli, R., 1965. Planktonic foraminifera from the western North Atlantic. Smithsonian Miscellaneous Collections 148, 1-45.

Cimerman, F., Langer, M.R., 1991. Mediterranean foraminifera. Slovenska Akademija Znanosti in Umetnosti. Academia Scientiarum et Artium Slovencia 4, 30, 119 pp.

Coleman, A.R., 1980. Test structure and function of the agglutinated foraminifera *Clavulina*. Journal of Foraminiferal Research 10, 143-152.

Collinson, J., 2012. Correlation in Hydrocarbon Exploration: Proceedings of the Conference Correlation in Hydrocarbon Exploration Organized by the Norwegian Petroleum Society and Held in Bergen, Norway, 3–5 October 1988. Springer Science and Business Media.

Compton, J.S., Bergh, E.W., 2016. Phosphorite deposits on the Namibian shelf. Marine Geology 380, 290-314.

Compton, J.S., Wigley, R., McMillan, I.K., 2004. Late Cenozoic phosphogenesis on the western shelf of South Africa in the vicinity of the Cape Canyon. Marine Geology 206, 19-40.

Coryell, H.N., Rivero, F.C., 1940. A Miocene microfauna of Haiti. Journal of Palaeontology 14, 324-344.

Costa, O.G., 1855. Foraminiferi fossili della marna blu del Vaticano. Memorie della Reale Academia delle Scienze Napoli 2, 113-126.

Costa, O.G., 1856. Paleontologia del regno di Napoli, Parte II. Atti dell´Accademia Pontaniana Napoli 7, 113-378.

Cushman, J.A., 1919. Fossil foraminifera from the West Indies. Carnegie Institute. Washington Publications 291, 21-71.

Cushman, J.A., 1921. Foraminifera of the Philippine and adjacent seas. Bulletin of the United States National Museum 100, 1-608.

Cushman, J.A., 1922a. Shallow-water foraminifera of the Tortugas region. Carnegie Institute, Washington Publications 311, 1-85.

Cushman, J.A., 1922b. The foraminifera of the Byram Calcareous Marl at Byram, Mississipi, In: White, D. (ed.), Shorter Contributions to General Geology, US Geological Survey Professional Paper 129E, 82-281.

Cushman, J.A., 1923a. The foraminifera of the Atlantic Ocean: part 4 – Lagenidae. Bulletin of the United States National Museum 104, 1-228.

Cushman, J.A., 1923b. The foraminifera of the Vicksburg Group. US Geological Survey Professional Paper 133, 11-71.

Cushman, J.A., 1924. Samoan Foraminifera. Carnegie Institution, Washington. Publication 342, 75 pp.

Cushman, J.A., 1926. The foraminifera of the Velasco shale of the Tampico embayment.Bulletin of the American

Association of Petroleum Geologists 10, 581-612.

Cushman, J.A., 1927a. An outline of a re-classification of the foraminifera. Contributions from the Cushman Laboratory for Foraminiferal Research 3, 1-105.

Cushman, J.A., 1927b. Foraminifera of the genus *Siphonina* and related genera. Proceedings of the United States National Museum 72, 1-15.

Cushman, J.A., 1930. The foraminifera of the Atlantic Ocean, part 7, Nonionidae, Camerinidae, Peneroplidae and Alveolinellidae. United States National Museum Bulletin 104, 1-79.

Cushman, J.A., 1931. The foraminifera of the Atlantic Ocean. Part 8. *Rotaliidae, Amphisteginidae, Calcarinidae, Cymbaloporettidae, Globorotaliidae, Anomalinidae, Planorbulinidae, Rupertiidae,* and *Homotremidae.* United States National Museum Bulletin 104, 1-179.

Cushman, J.A., 1933. Some new foraminiferal genera. Contributions from the Cushman Laboratory of Foraminiferal Research 9, 32-38.

Cushman, J.A., 1937. A monograph of the subfamily Virgulininae of the foraminiferal family Buliminidae. Special Publications of the Cushman Laboratory for Foraminiferal Research 9, 1-228.

Cushman, J.A., 1946. Upper Cretaceous foraminifera of the gulf coastal region of the United States and adjacent areas. Geological Survey, professional paper 206, 241 pp.

Cushman, J.A., Applin, E.R., 1926. Texas Jackson Foraminifera. American Association of Petroleum Geologists Bulletin 10, 154-189.

Cushman, J.A., Jarvis, P.W., 1930. Miocene foraminifera from Buff Bay, Jamaica. Journal of Paleontology 4, 353-368.

Cushman, J.A., Renz, H.H., 1942. Eocene Midway foraminifera from Soldado Rock, Trinidad. Contributions from the Cushman Laboratory for Foraminiferal Research 18, 1-14.

Cushman, J.A., Todd, M.R., 1945. Miocene foraminifera from Buff Bay, Jamaica. Cushman Laboratory of Foraminiferal Research, Special Publication 15, 1-73.

d'Orbigny, A.D., 1826. Tableau méthodique de la classe des Céphalopodes. Annales des Sciences Naturelles 7, 245-314.

d'Orbigny, A.D., 1839. Foraminifères. In: de la Sagra, R. (Ed.). Histoire physique, politique et naturelle de l'ile de Cuba. A. Bertrand, Paris, 224 pp.

d'Orbigny, A.D., 1846. Foraminiferes Fossiles du Basin Tertiaire de Vienne (Austriche). Gide et Comp, Paris, 312pp.

Dale, D.C., McMillan, I.K., 1999. On the beach: A field guide to the Late Cainozoic micropalaeontological history, Saldanha region, South Africa. Earthyear Environmental Communications, 127 pp.

De, S., Gupta, A.K., 2010. Deep-sea faunal provinces and their inferred environments in the Indian Ocean based on distribution of Recent benthic foraminifera. Palaeogeography, Palaeoclimatology, Palaeoecology 291(3), 429-442.

De Blainville, H.M.D., 1825. Manuel de Malacologie et de Conchyliologie. F.G. Levrault, Paris, 664 pp.

De Montfort, D., 1808. Conchyliologie systématique et classification méthodique des coquilles F. Schoell, Paris 1, 409 pp.

Defrance, M.J.L., 1824. Dictionnaire des Sciences Naturelles, 32. F.G. Levrault, Paris, 567 pp.

Delage, Y., Herouard, E., 1896. Traité de Zoologie Concrète, Vol. I, La Cellule et les Protozoaires. Schleicher Freres, Paris.

Diester-Haass, L., Meyers, P.A., Bickert, T., 2004. Carbonate crash and biogenic bloom in the late Miocene: evidence from ODP sites 1085, 1086 and 1087 in the Cape Basin, southeast Atlantic Ocean. Paleoceanography 19, 1-19.

Drinia, H.A., Antonarakou, A., Kontakiotis, G., 2008. On the occurrence of Early Pliocene marine deposits in the Ierapetra Basin, Eastern Crete, Greece. Bulletin of Geosciences 83, 63-78.

Drinia, H., Antonarakou, A., Tsaparas, N., Dermitzakis, M.D., 2007. Foraminiferal stratigraphy and palaeoecological implications in turbidite-like deposits from the Early Tortonian (Late Miocene) of Greece. Journal of Micropalaeontology 26, 145-158.

Drinia, H., Tsaparas, N., Antonarakou, A., Goumas, G., 2003. Benthic foraminiferal biofacies associated with middle to early late Miocene oxygen deficient conditions in the eastern Mediterranean. In: International Conference on Environmental Science and Technology, Lemnos Island, Greece, pp. 8-10.

Ehrenberg, C.G., 1838. Über dem blossen Auge unsichtbare Kalkthierchen und Kieselthierchen als Hauptbestandtheile der Kreidegebirge. Bericht über die zu Bekanntmachung geeigneten. Verhandlungen der Königlichen Preussischen Alademie der Wissenschaften zu Berlin, 1838, 192-200.

Eichenberg, W., 1935. Die Erforschung der Mikroorganismen insbesondere der Foraminiferen der norddeutschen Erdölfelder; Teil 1-Die Foraminiferen der Unterkreide; Folge 4-Foraminiferen aus dem Apt von Wenden am Mittellandkanal. Jahresbericht des Niedersächsischen Geologischen Vereins 27, 1-40.

Ellisor, A.C., 1933. Jackson Group of formations in Texas with notes on Frio and Vicksburg. American Association of Petroleum Geologists 17, 1293-1350.

Fenero, R., Thomas, E., Alegret, L., Molina, E., 2012. Oligocene benthic foraminifera from the Fuente Caldera section (Spain, western Tethys): taxonomy and paleoenvironmental inferences. Journal of Foraminiferal Research 42, 286-304.

Fichtel, L., Moll, J.P.C., 1798. Testacea microscopica aliagua minuta ex generibus Argonauta et Nautilus ad naturam delineate et descripta. Microscopische und andere kleine Schalthiere aus den Geschlechtern Argonaute und Schiffer, nach der Natur Gezeichnet und beschrieben. Camesina, Vienna, 124 pp.

Finlay, H.J., 1947. New Zealand Foraminifera: Key species in stratigraphy—No. 5. New Zealand Journal of Science and Technology 28, 259-292.

Flint, J.M., 1899. Recent foraminifera. A descriptive catalogue of specimens dredged by the US Fish Commission Steamer Albatross. Report of the United States National Museum for 1897, 1, 249-349.

Flower, B.P., Kennett, J.P., 1994. The middle Miocene climatic transition: East Antarctic ice sheet development, deep ocean circulation and global carbon cycling. Palaeogeography, Palaeoclimatology, Palaeoecology 108, 537-555.

Fontanier, C., Jorissen, F.J., Licari, L., Alexandre, A., Anschutz, P., Carbonel, P., 2002. Live benthic foraminiferal faunas from the Bay of Biscay: faunal density, composition, and microhabitats. Deep Sea Research Part I: Oceanographic Research Papers 49(4), 751-785.

Gallagher, S.J., Smith. A.J., Jonasson, K., Wallace, M.W., Holdgate, G.R., Daniels. J., Taylor, D., 2001. The Miocene palaeoenvironmental and palaeoceanographic evolution of the Gippsland Basin, Southeast Australia: a record of Southern Ocean change. Palaeogeography, Palaeoclimatology, Palaeoecology 172, 53-80.

Gebhardt, H., 1999. Middle to Upper Miocene benthonic foraminiferal palaeoecology of the Tap Marls (Alicante Province, SE Spain) and its palaeoceanographic implications. Palaeogeography, Palaeoclimatology, Palaeoecology 145, 141-156.

Giraudeau, J., 1993. Planktonic foraminiferal assemblages in surface sediments from the southwest African continental margin. Marine Geology 110, 47-62.

Glaessner, M.F., 1937. Die Entfaltung der Foraminiferenfamilie Buliminidae. Problemy Paleontologii, Paleontologicheskaya Laboratoriya Moskovskogo Gosudarstvennogo Universiteta 2-3, 411-422.

Gooday, A.J., 2003. Benthic foraminifera (Protista) as tools in deep-water palaeoceanography: environmental influences on faunal characteristics. Advances in Marine Biology 46, 1-90.

Gümbel, C.W., 1868. Beiträge zur Foraminiferenfauna der nordalpinen Eocängebilde. Abhandlungen Bayerische Akademie der Wissenschaften 10, 670-730.

Gupta, A.K., 1993. Biostratigraphic vs. paleoceanographic importance of *Stilostomella lepidula* (Schwager) in the Indian Ocean. Micropaleontology 39, 47–51.

Hadley, W.H., 1934. Some Tertiary foraminifera from the north coast of Cuba. Bulletins of American Paleontology 20, 1-41.

Haeckel, E., 1894. Systematische Phylogenie. Entwurf eines Natürlichen Systems der Organismen auf Grund ihrer Stammesgeschichte, Theil 1, Systematische Phylogenie der Protisten und Pflanzen. Georg Reimer, Berlin, 400 pp.

Hallam, A., Wignall, P.B., 1997. Mass extinctions and their aftermath. Oxford University Press, Oxford, 328 pp.

Hanagata, S., Nobuhara, T., 2014. Illustrated guide to Pliocene foraminifera from Miyakojima, Ryukyu Island Arc, with comments on biostratigraphy. Palaeontologica Electronica, 18.1.3A, 1-140.

Hantken, M., 1875. A Clavulina szabói rétegek Faunája. I. Foraminiferák. Földtani Inézet Evkönyve 4, 1-93.

Hay, W.W., Sibuet, J.C., Barron, E.J., Brassell, S.C., Dean, W.E., Huc, A.Y., Keating, B.H., McNulty, C.L., Meyers, P.A.,

Nohara, M., Schallreuter, R.E.L., Steinmetz, J.C., Stow, D.A.V., Stradner, H., Boyce, R.E., Amidei, R., 1984, Initial Reports of the Deep Sea Drilling Project, volume 75. U.S. Government Printing Office, Washington, D.C., 1303 pp.

Hayward, B.W., Kawagata, S., Sabaa, A.T., Grenfell, H.R., van Kerckhoven, L., Johnson, K., Thomas, E., 2012. The last global extinction (Mid-Pleistocene) of deep-sea benthic foraminifera (*Chrysalogoniidae, Ellipsoidinidae, Glandulonodosariidae, Plectofrondicularriidae, Pleursostomellidae, Stilostomellidae*), their Late Cretaceous-Cenozoic history and taxonomy. Cushman Foundation for Foraminiferal Research Special publication no. 43, 408 pp.

Hedberg, H.D., 1937. Foraminifera of the Middle Tertiary Carapita Formation of northeastern Venezuela. Journal of Paleontology 8, 661-697.

Hemleben, C., Spindler, M., Anderson, O.R., 1990. Modern Planktonic Foraminifera. Springer Science and Business Media, New York, 386 pp.

Hermelin, J.O.R., 1989. Pliocene benthic foraminifera from the Ontong-Java Plateau (Western Equatorial Pacific Ocean): faunal response to changing paleoenvironment. Special Publication of the Cushman Foundation for Foraminiferal Research 26, 1-143.

Heron-Allen, E., Earland, A., 1922. Protozoa Part II – Foraminifera. British Antarctic ("Terra Nova") Expedition 1910. Zoology 6, 25-268.

Hoetzel. S., Dupont, L.M., Marret, F., Jung, G., Wefer, G., 2015. Miocene–Pliocene stepwise intensification of the Benguela upwelling over the Walvis Ridge off Namibia. Climate of the Past Discussions 11, 1913–1943.

Hofker, J., 1956. Tertiary foraminifera of coastal Ecuador: Part II, Additional notes on Eocene species. Journal of Paleontology 30, 891-958.

Holbourn, A., Henderson, A.S., MacLeod, N., 2013. Atlas of Benthic Foraminifera. Wiley-Blackwell, Oxford, 654pp.

Horváth, M., 2003. Data to revision and distribution of small Foraminifera species described by Hantken (1868, 1875) Part II. Nodosariidae and Vaginulinidae. Fragmenta Palaeontologica Hungarica 21, 5-32

Hottinger, L., Halicz, E and Reuss, Z., 1993. Recent foraminiferida from the Gulf of Aqaba, Red Sea. Slovenska Akademija Znanosti in Umetnosti, Ljubljana, 172pp.

Howarth R.J., McArthur J.M., 1997. Statistics for strontium isotope stratigraphy. A robust LOWESS fit to the marine Sr-isotope curve for 0 - 206 Ma, with look-up table for the derivation of numerical age. Journal of Geology 105, 441-456.

Jahn, B., Donner, B., Müller, P. J., Röhl, U., Schneider, R. R., Wefer, G., 2003. Pleistocene variations in dust input and marine productivity in the northern Benguela Current: evidence of evolution of global glacial–interglacial cycles. Palaeogeography, Palaeoclimatology, Palaeoecology 193, 515-533.

Jenkins, D.G., 1960. Planktonic Foraminifera from the Lakes Entrance Oil Shaft, Victoria, Australia. Micropaleontology 6, 345-371.

Jenkins, J. M., 2013. Applied micropalaeontology. Springer Science and Business Media, 270pp.

Jones, R.W., 1994. The Challenger Foraminifera. Oxford University Press, Oxford, 149 pp.

Jorissen, F.J., Wittling, I., 1999. Ecological evidence from live–dead comparisons of benthic foraminiferal faunas off Cape Blanc (Northwest Africa). Palaeogeography, Palaeoclimatology, Palaeoecology 149(1-4), 151-170.

Jorissen, F.J., Wittling, L., Peypouquet, J.P., Rabouille, C., Relexans, J.C., 1998. Live benthic foraminiferal faunas off Cape Blanc, NW Africa: community structure and microhabitats. Deep-Sea Research I 45, 2157–88.

Kaiho, K., 1994. Benthic foraminiferal dissolved-oxygen index and dissolved-oxygen levels in the modern ocean. Geology 22, 719-722.

Kaiho, K., 1999. Effect of organic carbon flux and dissolved oxygen on the benthic foraminiferal oxygen index (BFOI). Marine Micropaleontology 37, 67–76.

Kaiho, K., Hasegawa, S., 1986. Bathymetric distribution of benthic foraminifera in bottom sediments off Onahama, Fukushima Prefecture, northeast Japan. In: Matoba, Y and Kato, M. (Eds.), Studies on Cenozoic Benthic Foraminifera. Akita University, Akita, 43–52.

Kaminski, M.A., 2012. Calibration of the Benthic Foraminiferal Oxygen Index in the Marmara Sea. Geological Quarterly 56, 757-764.

Kaminski, M. A., Aksu, A., Box, M., Hiscott, R. N., Filipescu, S., Al-Salameen, M., 2002. Late Glacial to Holocene benthic foraminifera in the Marmara Sea: implications for Black Sea–Mediterranean Sea connections following the last deglaciation. Marine Geology 190, 165-202.

Karrer, F., 1878. Die Foraminiferen der Tertiären Thone von Luzon, p. 77-99. In: Drasche, R. von (Ed.), Fragmente zu einer Geologie der Insel Luzon (Philippinen). Verlag von Karl Gerold's Sohn, Wien.

Katz, M.E., Miller, K.G., 1993a. Latest Oligocene to Earliest Pliocene benthic foraminiferal biofacies of the northeastern Gulf of Mexico. Micropaleontology, 367-403.

Katz, M.E., Miller, K.G., 1993b. Miocene-Pliocene bathyal benthic foraminifera and the uplift of Buff Bay, Jamaica. Geological Society of America Memoirs 182, 219-254.

Kender, S., 2007. Foraminiferal characterisation and taxonomy of Oligocene Miocene Congo Fan deep sea sub-environments, offshore Angola. Ph.D., University College, London, 325 pp.

Kender, S., Kaminski, M.A., Jones, R.W., 2008. Early to middle Miocene foraminifera from the deep-sea Congo Fan, offshore Angola. Micropalaeontology 54, 477-568.

Kennett, J.P., Srinivasan, M.S., 1983. Neogene Planktonic Foraminifera. A Phylogenetic Atlas. Hutchinson Ross, Stroudsburg, 265 pp.

King, C., 1989. Cenozoic of the North Sea. In: Jenkins, D.G and Murray, J.W (Eds.). Stratigraphical Atlas of Fossil Foraminifera. Ellis Horwood Ltd., Chichester, 418-489.

Kohl, B., 1985. Early Pliocene benthic foraminifers from the Salina Basin,

Southeastern Mexico. Bulletins of American Palaeontology 88, 1-157.

Kucera, M., 2007. Planktonic foraminifera as tracers of past oceanic conditions. In: Hillaire-Marcel, C and de Vernal, A (Eds.). Proxies in Late Cenozoic Paleoceanography. Elsevier, Amsterdam, 213-262.

Kuhnt, W., Holbourn, A.E., Zhao, Q., 2002. The early history of the South China Sea: evolution of Oligocene-Miocene deep water environments. Revue de Micropaléontologie 45, 99-159.

Lamarck, J.B., 1804. Suite des mémoires sur les fossils des environs de Paris. Annales Muséum National d'Histoire Naturelle 5, 179-188.

Lamarck, J.B., 1812. Extrait du cours de Zoologie du Muséum d'Histoire Naturelle sur les animaux invertèbres. d'Hautel, Paris, p. 1-127.

Lankester, E.R., 1885. Protozoa, in Encyclopaedia Britannica 19, 830 – 866.

Lazarus, D., Bittniok, B., Diester-Haass, L., Billups, K., Ogawa, Y., Takahashi, K., Meyers, P., 2008. Radiolarian and sedimentologic paleoproductivity proxies in late Pleistocene sediments of the Benguela Upwelling System, ODP Site 1084. Marine Micropaleontology 68, 223-235.

Le Calvez, Y., 1977. Revision des foraminifères de la collection d'Orbigny. II. Foraminifères de I'ile de Cuba. Cahiers de Micropaleontologie 1, 1-127.

Leiter, C., Altenbach, A.V., 2010. Benthic foraminifera from the diatomaceous mud belt off Namibia: characteristic species for severe anoxia. Palaeontologica Africana 13(2), 11A, 19p.

LeRoy, D.O., Levinson, S.A., 1974. A deep-water Pleistocene microfossil assemblage from a well in the Northern Gulf of Mexico. Micropalaeontology 20, 1-37.

LeRoy, L.W., 1939. Some small foraminifera, ostracoda and otoliths from the Neogene ('Miocene') of the Rokan-Tapanoeli área, Central Sumatra. Natuurkundig Tijdschrift voor Nederlandsch Indie 99, 215-296.

LeRoy, L.W., 1948. The foraminifer *Orbulina universa* d'Orbigny, a suggested Middle Tertiary time indicator. Journal of Paleontology 22, 500-508.

Liebus, A., 1902. Ergebnisse einer mikroskopischen Untersuchung der organischen Einschlusse der oberbayerischen Molasse. Jahrbuch der Geologischen Reichsanstalt 52, 71–104.

Linnaeus, C., 1758. Systema naturae per regna Tria naturae, secundum classes, ordines genera, species, cum characteribus, differentiis, synonymis, locis. Tomus I. Editio decima, reformata. Systema Naturae, Stockholm 10, 824 pp.

Linnaeus, C., 1767. Systema naturae, sive regna tria naturae systematica propositi per dasses, ordines, genera et species. Edition 12, Stockholm, 533-1327.

Loeblich, A.R., Tappan, H., 1964. Protista 2: Sarcodina Chiefly "Thecamoebians" and Foraminiferida. Geological Society of America, 900 pp.

Loeblich, A.R., Tappan, H., 1986. Some new and revised genera and families of hyaline calcareous Foraminiferida (Protozoa). Transactions of the American Microscopical Society 105, 239-265.

Loeblich, A.R., Tappan, H., 1988. Foraminiferal Genera and their Classification. Van Nostrand Reinhold, New York, 970 pp.

Loeblich, A.R., Tappan, H., 1994. Foraminifera of the Sahul Shelf and Timor Sea. Special Publications of the Cushman Laboratory for Foraminiferal Research 31, 1-661.

Lowry, F.M.D., 1987. Foraminiferal thanatocoenoses from the continental shelf of southern Africa. Unpublished PhD. thesis, University College, 443 pp.

Macfayden, W.A., 1930. Miocene foraminifera from the clysmic area of Egypt and Sinai, with an account of the stratigraphy and a correlation of the local Miocene succession. Surveys of Egypt-Geological Survey 40, 1-149.

Marlow, J. R., Lange, C.B., Wefer, G., Rosell-Mele, A., 2000. Upwelling intensification as part of the Pliocene-Pleistocene climate transition. Science 290, 2288–2291.

Martin, R.A., 1981. Benthic foraminifera from the Orange-Lüderitz shelf southern African continental margin. Bulletin Joint Geological Survey / University of Cape Town Marine Geoscience Unit 11, 75 pp.

McMillan, I.K., 1974. Recent and relict foraminifera from the Agulhas Bank, South African Continental Margin. Unpublished M.Sc. thesis, University College of Wales, Aberystwyth, 96 pp.

McMillan, I.K., 2003. The foraminifera of the Late Valanginian to Hauterivian (Early Cretaceous) Sundays River Formation of the Algoa Basin, Eastern Cape Province, South Africa. Annals of the South African Museum 106, 1-120.

Mello, J.F., 1969. Foraminifera and stratigraphy of the upper part of the Pierre Shale and lower part of the Fox Hills Sadstone (Cretaceous), north-central South Dakota. United States Geological Survey Professional Paper 611, 121 pp.

Mikhalevich, V.I., 1981. Parallelizm I konvergentsiya v evolyutsii skeketov foraminifer. Trudy Zoologischeskogo Instituta, Akademiya Nauk SSSR 107, 19-41.

Milker, Y., Schmiedl, G., 2012. A taxonomic guide to modern benthic shelf foraminifera of the western Mediterranean Sea. Palaeontologica Electronica 15, 2:16A, 134 pp.

Milker, Y., Schmiedl, G., Betzler, C., Römer, M., Jaramillo-Vogel, D., Siccha, M. 2009. Distribution of Recent benthic foraminifera in neritic carbonate environments of the Western Mediterranean Sea. Marine Micropalaeontology 73, 207-225.

Miller, K.G., Katz, M.E., 1987. Oligocene to Miocene benthic foraminiferal and abyssal circulation changes in the north Atlantic. Micropalaeontology 33, 97-149.

Miller, K.G., Kominz, M.A., Browning, J.V., Wright, J.D., Mountain, G.S., Katz, M.E., Sugarman, P.J., Cramer, B.S., Christie-Blick,N., Pekar, S.F., 2005. The Phanerozoic record of global sea-level change. Science 310, 1293-1298.

Milne-Edwards, A., 1881. Compte rendu sommaire d'une exploration zoologique, faite dans le Méditerranée á bord du navire de l`Etat "Le Travailleur," Compte Rendu Hebdomadaire des Séances de l´Académie des Sciences, Paris, 93, 876-882.

Montanaro-Gallitelli, E., 1957. A revision of the foraminiferal family Heterohelicidae. United States National Museum, Bulletin 215, 133-154

Murgese, D.S., de Deckker, P., 2005. The distribution of deep-sea benthic foraminifera in core tops from the eastern

Indian Ocean. Marine Micropaleontology 56(1), 25-49.

Murray, J.W., 1991. Ecology and palaeoecology of benthic foraminifera. Longman, Harlow, 397pp.

Murray, J.W., 2006. Ecology and Applications of Benthic Foraminifera. Cambridge University Press, Cambridge, 426 pp.

Nuttall, W.L.F., 1928. Tertiary foraminifera from the Naparima region of Trinidad (British West Indies). Quarterly Journal of the Geological Society of London 84, 57-116.

Obaje, S.O., Okosun, E.A., 2013. Taxonomic notes on marker benthic foraminifera of Tomboy Field, offshore western Niger Delta, Nigeria. International Journal of Science and Technology 3, 357-364.

Olóriz, F., Reolid, M., Rodríguez-Tovar, F.J., 2006. Approaching trophic structure in Late Jurassic neritic shelves: A western Tethys example from southern Iberia. Earth-Science Reviews 79, 101–139.

Ovechkina, M. N., Bylinskaya, M. E., Uken, R., 2010. Planktonic foraminiferal assemblage in surface sediments from the Thukela Shelf, South Africa. African Invertebrates 51, 231-254.

Pagani, M., Arthur, M.A., Freeman, K.H., 1999. Miocene evolution of atmospheric carbon dioxide. Paleoceanography 14, 273-292.

Palmer, DBK., 1945. Notes on the foraminifera from Bowden, Jamaica, Bulletins of American Paleontology 29, 1-82.

Panieri, G., Gupta, B.K.S., 2008. Benthic foraminifera of the Blake Ridge hydrate mound, western North Atlantic Ocean. Marine Micropaleontology 66(2), 91-102.

Papp, A., Schmid, M.E., 1985. The fossil foraminifera of the Tertiary Basin of Vienna: revision of the monograph by Alcide d'Orbigny (1846). Abhandlungen der Geologischen Bundesanstalt 37, 311 pp.

Parker, F.L., 1962. Planktonic foraminiferal species in pacific sediments. Micropaleontology 8, 219-254.

Parker, W.K., Jones, T.R., 1857. Description of some foraminifera from the coast of Norway. Annals and Magazine of Natural History Series 2, 19, 273-303.

Parker, W.K., Jones, T.R., Brady, H.B., 1871. On the nomenclature of the Foraminifera.Pt. 14. The species enumerated by d'Orbigny in the Annales des Sciences Naturelles. Annals and Magazine of Natural History 8, 145-266.

Pérez-Asensio, J.N., Aguirre, J., Schmiedl, G., Civis, J., 2012. Messinian paleoenvironmental evolution in the lower Guadalquivir Basin (SW Spain) based on benthic foraminifera. Palaeogeography, Palaeoclimatology, Palaeoecology 326, 135-151.

Pezelj, Đ, Mandic, O., Coric, S., 2013. Paleoenvironmental dynamics in the southern Pannonian Basin during initial Middle Miocene marine flooding. Geologica Carpathica 64, 81-100.

Pezelj, Đ, Sremac, J., Sokač, A., 2007. Palaeoecology of the Late Badenian foraminifera and ostracoda from the SW Central Paratethys (Medvednica Mt., Croatia). Geologia Croatica 60/2, 139-150.

Phleger, F.B., Parker, F.L., 1951. Ecology of foraminifera, northwest Gulf of Mexico.Part I- Foraminifera, distribution.

Memoirs of the Geological Society of America 46, 88 pp.

Rau, A.J., 2002. A late Quaternary history of Agulhas-Benguela interactions from two sediment cores on the western continental slope of South Africa. PhD thesis. University of Cape Town, 315 pp.

Rau, A.J., Rogers, J., Lutjeharms, J.R.E., Giraudeau, J., Lee-Thorp, J.A., Chen, M.T., Waelbroeck, C., 2002. A 450-kyr record of hydrological conditions on the western Agulhas Bank Slope, south of Africa. Marine Geology 180, 183-201.

Reed, K.J., 1965. Mid-Tertiary smaller Foraminifera from a bore at Heywood, Victoria, Australia. Bulletins of American Palaeontology 49, 39-104.

Reeder, M., Rothwell, R.G., Stow, D.A.V., Kahler, G., Kenyon, N.H., 1998. Turbidite flux, architecture and chemostratigraphy of the Herodotus Basin, Levantine Sea, SE Mediterranean. In: Stoker, M.S., Evans, D and Cramp, D. (Eds.) Geological processes on Continental Margins: Sedimentation, Mass-Wasting and Stability. Geological Society Special Publications, London, 129, 19-41.

Renz, H.H., 1948. Stratigraphy and fauna of the Agua Salada Group, State of Falcon, Venezuela, Memoirs of the Geological Society of America 32, 1-219.

Reolid, M., Chakiri, S., Bejjaji, Z., 2013. Adaptive strategies of the Toarcian benthic foraminiferal assemblages from the Middle Atlas (Morocco): Palaeoecological implications. Journal of African Earth Sciences 84, 1-12.

Reuss, A.E., 1850. Neues Foraminiferen aus den Schichten des osterreichischen Tertiarbeckens. Denkschriften Akademie der Wissenschaften in Wien, Mathematisch-Naturwissenschaftliche Klasse. Cl., 1, 365- 390.

Reuss, A.E., 1851. Die fossilen Foraminiferen, Bryozoen und Anthozoen von Oberburg in Steiermark. Ein Beitrag zur fauna der oberen Nummulitenschichteh. Sitzungsberichte der Akademie der Wissenschaften 48, 49-92.

Reuss, A.E., 1860. Die Foraminiferen der Westphälischen Kreideformation. Sitzungsberichte der Kaiserlichen Akademie der Wissenschaften in Wien, Mathematisch-Naturwissenschaftliche Classe 40, 147-238.

Reuss, A.E., 1866. Über die Foraminiferen, Antozoen und Bryozoen des deutschen Septarienthones. Denkschriften der Akademie der Wissenchaften Wien 25, 117-238.

Risso, A., 1826. Historie Naturelle des Principales Productions de l'Europe Méridionale et Particulièrment de Celles des Environs de Nice et des Alpes Maritimes, vol. 5. F.G. Levrault, Paris, 470 pp.

Robertson, B.E., 1998. Systematics and paleoecology of the benthic Foraminiferida from the Buff Bay section, Miocene of Jamaica. Micropaleontology 44, 1-266.

Rögl, F., Spezzaferri, S., 2002. Foraminiferal paleoecology and biostratigraphy of the Mühlbach section (Gaindorf Formation, lower Badenian), Lower Austria. Annalen des Naturhistorischen Museums in Wien. Serie A für Mineralogie und Petrographie, Geologie und Paläontologie, Anthropologie und Prähistorie 104A, 23-75.

Russo, B., Curcio, E., Iaccarino, S., 2007. Paleoecology and paleoceanography of a Langhian succession (Tremiti Islands, southern Adriatic Sea, Italy) based on benthic foraminifera. Bolletino-Societa Paleontologica Italiana 46, 107.

Said, R., 1949. Foraminifera of the northern Red Sea. Cushman Laboratory for Foraminiferal Research, Special Publication 26, 1-44.

Saidova, K.M., 1975. Bentosnye Foraminifery Tikhogo Okeana. Institut Okeanologii P.P. Shirshova, Akademiya Nauk SSR, 875 pp.

Saidova, K.M., 1981. O sovremennom sostoyanii sistemy nadvidovykh taksonov Kaynozoyskikh bentosnykh foraminifer. Institut Okeanologii P.P. Shirshova. Akademiya Nauk SSSR, Moscow, 232 pp.

Sandidge, J.R., 1932. Foraminifera from the Ripley Formation in Alabama. The American Midland Naturalist 13, 333-377.

Schmiedl, G., Mackensen, A., 1997. Late Quaternary paleoproductivity and deep water circulation in the eastern South Atlantic Ocean: evidence from benthic foraminifera. Palaeogeography. Palaeoclimatology. Palaeoecology 130, 43-80.

Schmiedl, G., Mackensen, A., Müller, P.J., 1997. Recent benthic foraminifera from the eastern South Atlantic Ocean: dependence on food supply and water masses. Marine Micropaleontology 32, 249-287.

Schultze, M.S., 1854. Über den Organismus der Polythalamien (Foraminiferen) nebst Bemerkungen über die Rhizopoden im Allgemeinen. Engelmann, W, Leipzig.

Seguenza, G., 1862. Prime recherché intorno ai rizopodi fossili delle argille Pleistoceniche dei dintorni di Catania. Accademia Gioenia di Scienze Naturali di Catania 18, 84-126.

Sgarrella, F., Moncharmont Zei, M., 1993. Benthic foraminifera of the Gulf of Naples (Italy), systematic and autoecology. Bolletino della Societa Paleontologica Italiana 32(2), 145-264.

Shepard, F.P., 1963. Submarine Geology. Harper and Row, 557 pp.

Siesser, W.G., 1980. Late Miocene origin of the Benguela Upwelling System off Northern Namibia. Science 208(4441), 283-285.

Spezzaferri, S., Kucera, M., Pearson, P.N., Wade, B.S., Rappo, S., Poole, C.R., Morard, R., Stalder, C., 2015. Fossil and genetic evidence for the polyphyletic nature of the planktonic foraminifera" Globigerinoides", and description of the new genus Trilobatus. PLoS One 10(5), p.e0128108.

Stainforth, R.M., 1952. Classification of uniserial calcareous foraminifera. Contributions from the Cushman Foundation for Foraminiferal Research 3, 6–14.

Ten Dam, A., 1944. Die stratigraphische Gliederung des Niederländischen Paläocäns und Eozäns nach Foraminiferen (mit Ausnahme von Sud-Limburg). Mededelingen van de Geologische Stichtung 3, 5-142.

Thalmann, H. E., 1937. Mitteilungen über Foraminiferen III. Eclogae Geologicae Helvetiae 30, 337–356.

Thomas, E., 1990. Late Cretaceous through Neogene benthic foraminifers. In: Barker, P.E., Kennet, J.P et al., (Eds.). Scientific Results of the Proceedings of the Ocean Drilling Program 113, 571-594.

Thomas, F.C., 1988. Taxonomy and stratigraphy of selected Cenozoic benthic foraminifera, Canadian Atlantic margin. Micropaleontology 34, 67-82.

Tjalsma, R.C., Lohmann, G.P., 1983. Paleocene-Eocene bathyal and abyssal foraminifera from the Atlantic Ocean. Micropalaeontology, Special Publication 4, 90 pp.

Todd, R., 1942. The Foraminifera of the tropical Pacific collections of the Albatross, 1899-1900. Part 4 – Rotaliform families and planktonic families. Bulletin of the United States National Museum 161, 1-139.

Todd, R., 1954. Description of new species. In: Todd, R., Cloud, P.E., Low, D., Schmidt, R.G. Probable occurrence of Oligocene on Saipan. American Journal of Science 252/11, 673-682.

Valchev, B., Stojanova, V., Juranov, S., 2013. Paleogene hyaline benthic foraminifera (LAGENINA and ROTALIINA) from the Republic of Macedonia. Review of the Bulgarian Geological Society 74, 81-110.

Van Marle, L.J., 1991. Eastern Indonesian Late Cenozoic smaller benthic foraminifera. Verhandelingen der Koninklijke Nederlandse Akademie van Wetenschappen, Afdeeling Natuurkunde, Eerste Reeks 34, 1-328.

Van Morkhoven, F.P., Berggren, W.A., Edwards, A.S., Oertli, H.J. 1986. Cenozoic cosmopolitan deep-water benthic foraminifera. Elf Aquitaine, 421 pp.

Vilela, C.G., 1995. Ecology of Quaternary benthic foraminiferal assemblages on the Amazon shelf, northern Brazil. Geo-Marine Letters 15(3-4), 199-203.

Voloshinova, N.A., 1960. Uspekhi mikropaleontologii v dele izucheniya vnutrennego stroeniya foraminifer. In: Trudy Pervogo Seminara po Mikrofaune. Vsesoyuznyy Neftyanoy Nauchno-issledovatel'skii Geologorazvedochnyy Institut (VNIGRI). pp. 48-87.

Wefer, G., Berger, W.H., Richter, C., Adams, D.D., Anderon, L.D., Andreasen, D.J., Brüchert, V., Cambray, H., Christensen, B.A., Frost, G.M., Giraudeau., Gorgas, T.J., Hermelin, O., Lange, C.B., Laser, B., Lin, H-L., Maslin, M., Meyers, P.A., Motoyama, I., Murray, R.W., Pato, D., Perez, M.E., Pufahl, P.K., Spiess, V., Vidal. L., Wigley, R., Yamazaki, T., 1998. Proceedings of the Ocean Drilling Program volume 175, 385-428.

Weidich, K.F., 1988. On the variability of some recent fossil *Clavulina* species (Foraminifera). Abhandlungen Geologie 41, 337-357.

Weidich, K.F., 1990. Die kalkalpine Unterkreide und ihre Foraminiferenfauna. Zitteliana 17, 1-187.

Whittaker, J.E., Hodgkinson, R.L., 1979. Foraminifera of the Togopi Formation, eastern Sabah, Malaysia. British Museum (Natural History), London, 120 pp.

Williamson, W.C., 1858. On the recent Foraminifera of Great Britain. Ray Society Publications 20, 1-107.

Wilson, B., 2005. Planktonic Foraminiferal Biostratigraphy and Paleo-Ecology of the Brasso Formation (Middle Miocene) at St. Fabien Quarry, Trinidad, West Indies. Caribbean Journal of Science 41(4), 797-803.

Wilson, B., Hayek, L.A.C., 2015. Foraminifera on the Demerara Rise offshore Surinam: crustal subsidence or shallowing of an

oxygen minimum zone? Geological Magazine 152(5), 788-801.

Yassini, I., Jones, B.G., 1995. Foraminiferida and Ostracoda from estuarine and shelf environments on the southeastern coast of Australia. University of Wollongong Press, 484 pp.

Zachariasse, W. J., Jorissen, F. J., Perissoratis, C., Rohling, E. J., Tsapralis, V., 1997. Late Quaternary foraminiferal changes and the nature of sapropel S1 in Skopelos Basin. In: Proceedings of the 5th Hellenic symposium on Oceanography and Fisheries, Kavalla, Greece, pp. 15-18.

Zapata, J., Cea, C., 2002. Foraminíferos planctónicos del Archipiélago de Juan Fernández (33°41'S; 78°50'W), Chile. Boletin de la Sociedad de Biologia de Concepción 73, 53-63.

Chapter 5

Late Neogene Foraminifera from the Northern Namibian Continental Shelf and the Transition to the Benguela Upwelling System

Published article: Bergh, E.W., Compton, J.S., Frenzel, P. 2018. Late Neogene foraminifera from the northern Namibian continental shelf and the transition to the Benguela Upwelling System. Journal of African Earth Sciences 141, 33-48.

5. Late Neogene foraminifera from the northern Namibian continental shelf and the transition to the Benguela Upwelling System

Eugene W. Bergh [a, b, *], John S. Compton [b], Peter Frenzel [c]

[a] Natural History Department, Iziko South African Museum, PO Box 61, Cape Town, 8000, South Africa

[b] Marine Research Institute and Department of Geological Sciences, University of Cape Town, Private Bag X3, Rondebosch, 7701, South Africa

[c] Institut für Geowissenschaften, Friedrich-Schiller Universität Jena, D-07749, Jena, Germany

Abstract

Middle Miocene to Plio-Pleistocene foraminifera provide insights into the palaeoenvironment on the northern Namibian continental shelf located at the far northern end of the present-day Benguela Upwelling System (BUS). Biostratigraphy and Strontium Isotope Stratigraphy (SIS) of the recovered basal olive-green mud unit indicate an age of 16 to 14 Ma. A sharp, erosional contact separates the basal mud from the overlying Plio-Pleistocene gravelly pelletal phosphorite sands. Grain size data, P/B ratios and benthic diversity indices indicate a change between the middle Miocene and overlying Plio-Pleistocene palaeoenvironments linked to the timing and conditions associated with the initiation of the BUS. The different lithological units and microfossil assemblages in the olive-green mud unit and the overlying pelletal phosphorite units support the late Miocene initiation of the BUS and the northwards migration of the Angola-Benguela Front. Planktic foraminifera indicate a shift from warmer surface water conditions to cooler conditions during the initiation of the BUS. Benthic palaeobathymetric ranges and P/B ratios are consistent with outer shelf water depths suggesting a deeper palaeoenvironment during the Mid-Miocene Climatic Optimum (MMCO) than today. Benthic foraminifera in the middle Miocene are dominated by large (>1 mm) taxa and adapted to oligotrophic environments before the initiation of the BUS. The benthic assemblage composition indicates that bottom water conditions changed to eutrophic conditions during the Plio-Pleistocene under intensified upwelling conditions.

5.1. Introduction

The Benguela Upwelling System (BUS) along the west coast of South Africa and Namibia is analogous to systems off California, Peru and North Africa (Gorgas and Wilkens, 2002). Siesser (1980) proposed an onset of the northern BUS (NBUS) in the late Miocene based on nannofossil and planktic foraminiferal

assemblages which indicated high productivity levels during that time. The rate of upwelling and organic matter delivery increased during the late Miocene and middle Pliocene (Wefer et al., 1998; Robert et al., 2005) along the southwestern margin of Africa. Sea surface temperatures fluctuated since the late Miocene (Marlow et al., 2000), but saw a net decrease over time with sedimentation rates largely increasing in the middle Pliocene, early to middle Pleistocene and Holocene (Gorgas and Wilkens, 2002). Intensified upwelling in the southern BUS (SBUS) initiated in the late Oligocene and is older than upwelling conditions in the NBUS. Southern BUS upwelling has also been linked to Neogene phosphorite deposits along the South African shelf (Compton et al., 2004; Wigley and Compton, 2007) and in the NBUS to extensive Plio/Pleistocene phosphorite deposits on the Namibian shelf (Compton and Bergh, 2016). Much of the previous work related to the initiation of the BUS utilised foraminifera to infer palaeoceanographic conditions over geologic time.

Previous work on foraminifera as palaeoenvironmental indicators along the southwestern margin of Africa have largely focussed on slope records recovered by the Deep Sea Drilling Project (DSDP) and Ocean Drilling Programme (ODP). The sediment records from DSDP Leg 75 on the Walvis Ridge slope recovered foraminifera from the Cretaceous and late Miocene to Pleistocene periods (Hay et al., 1984). ODP Leg 175 sediment cores from the Namibian and South African slope contain only late Miocene to Pleistocene foraminifera (Berger et al., 1998, 2002). Despite the extensive work of previous research on upwelling of the NBUS there is still little known about Miocene foraminifera and their related palaeoenvironmental conditions from the Namibian shelf prior to the initiation of the BUS. Kender et al. (2008) documented the palaeoenvironment of a deep water setting in the Congo Basin north of the NBUS and Compton et al. (2004) documented Miocene to Pleistocene foraminifera from the southern South African continental shelf, but did not analyse the foraminifera for the palaeoenvironment.

This paper presents an analysis of Neogene foraminifera from the northern Namibian continental shelf south of the Kunene River mouth and the palaeoenvironmental transition from the middle Miocene to the onset of the NBUS during the late Miocene to Pleistocene.

5.2. Regional setting

The study area is situated offshore of Rocky Point, Namibia on the continental shelf where it intersects the Walvis Ridge (Fig. 5.1). The Walvis Ridge acts as a barrier to deep-water flow and plays a major role in deep-sea sedimentation (Berger et al., 1998). The continental shelf is divided into an inner (0-130 m water depth), middle (130-200 m water depth) and outer (extending to 400-500 m water depth) shelf (Rogers, 1977).

The rocky shoreline and inner shelf expose Precambrian basement rocks. Further offshore seaward dipping Cretaceous to early Cenozoic deposits are unconformably overlain by Neogene and Pleistocene sediments (Bremner, 1977). Sedimentation on the southwestern continental margin of Africa slowed down during the Cenozoic with the Palaeogene record

largely missing. Sediments dated to the Cenozoic on the southwestern slope are dominated by Neogene pelagic carbonate sediments while carbonate-siliciclastic authigenic sediments dominate on the shelf. The Neogene on the shelf is highly condensed, thin and erratic as a result of non-deposition, erosion, long-term eustatic sea level lowering, episodic tectonic uplift and the intensification of aridity in the continental interior (Dingle et al., 1983; Wigley and Compton, 2006). The middle and outer shelves are dominated by carbonate-rich sediments with condensed, relict phosphorite deposits exposed between 130 and 400 m water depth. The condensed Plio-Pleistocene discontinuous deposits on the shelf are contrasted by organic-rich nannofossil and diatomaceous mud deposits of 400-600m thick (Meyers et al., 1998) on the upper slope of Plio-Pleistocene age (Wefer et al., 1998; Compton and Bergh, 2016). The thick mud deposits of the slope results from the transport of finer material from the shelf onto the slope by bottom currents and internal waves (Compton and Wiltshire, 2009). The winnowing of finer grained material and transport onto the slope leaves gravel and foraminiferal-rich Pleistocene sands on the shelf (Compton and Bergh, 2016). Holocene-aged sediments are dominated by a diatomaceous mud belt that extends from south of the Kunene River mouth to Walvis Bay and is largely confined to the inner shelf (Bremner, 1977).

Sedimentation on the Namibian shelf is influenced by the BUS with upwelling of cold, nutrient-rich waters and high productivity (Lutjeharms and Stockton, 1987). The BUS is comprised of eight upwelling cells along the southwestern African coast (Lutjeharms and Meeuwis, 1987). The strongest of these cells is located off Lüderitz and upwelling decreases north and south of the Lüderitz cell (Heinrich et al., 2011). The northward flowing Benguela Current forms the eastern limb of the South Atlantic gyre and is distinct from the BUS. The Benguela Current is divided into the inner Benguela Coastal Current (BCC) and the outer Benguela Oceanic Current (BOC) (Gorgas and Wilkens, 2002) (Fig. 5.1). The cold upwelled waters of the Benguela Current meet warmer water masses of the southward flowing Angola Current between 18 and 23˚S along the Angola-Benguela Front (ABF) (Moroshkin et al., 1970) turning northwest above the Walvis Ridge (Berger et al., 1998). Poleward bottom-currents in the area transport sediment from the Kunene River southwards (Bremner and Willis, 1993; Herbert and Compton, 2007). Southeast trade winds blow alongshore and episodic katabatic winds blow aeolian dust offshore (Shannon and Nelson, 1996).

5.3. Materials and methods

A total of 38 vibracores up to 2 m in length were retrieved in 2012 by Minemakers on the outer shelf off Rocky Point, Namibia. The vibracores had an inner diameter of 9 cm. The 38 vibracores (Fig. 5.1) were assessed and three were selected (Table 5.1) based on the length of the cores and stratigraphic completeness. The cores were split and described (logged) for detailed analysis in this study. The archive half of each core was oven dried and stored. The working halves of the three split cores were sampled at 5-15 cm intervals both below and above the contact between the basal mud and the overlying gravelly pelletal phosphorite sands. To prevent the risk of contamination samples were taken at the centre of the core. Each sample was on average 10 cm^3 in volume

and left overnight in water to make processing easier. The samples were then wet sieved into <63 µm (mud), 63 µm to 2mm (sand) and >2mm (gravel) fractions. The sand fractions were placed in an ultrasonic bath for up to 1 min to clean the microfossils of finer silt and clay particles that clung to the tests. No appreciable breakage was observed among the cleaned microfossils.

The processed sand fractions of samples having large numbers of foraminifera were split using a microsplitter. Microfossils (foraminifera and ostracods) were identified, picked and foraminifera sub-samples which included planktics and benthics were counted up to a statistically significant number of at least 300 individuals per sample under a stereo-microscope. Where subsamples had less than 300 individuals all foraminifera were counted. Abundance counts for planktic foraminifera were grouped according to their associated sea surface preferences according to Bé and Tolderlund (1971), Kucera (2007) and BouDagher-Fadel (2015) to determine any differences in sea surface conditions upcore. The groups were defined as follows: *Trilobatus immaturus* + *Trilobatus sacculifer* + *Globorotalia menardii* = tropical; *Globigerinoides ruber* + *Orbulina universa* + *Globorotalia truncatulinoides* = subtropical; *Globorotalia (Globoconella) inflata* + *Globigerina bulloides* = temperate/transitional; *Neogloboquadrina pachyderma* = subpolar to polar.

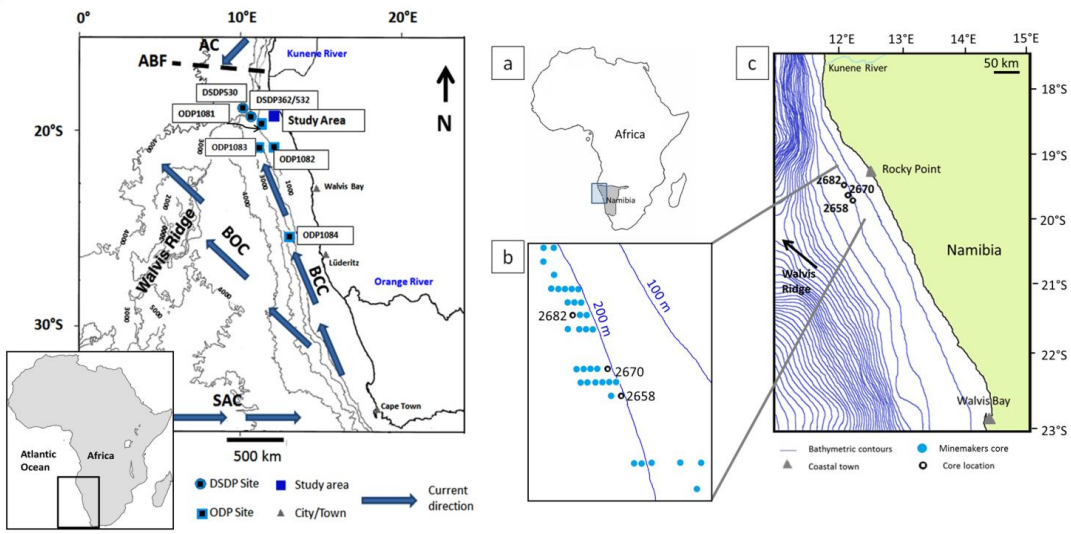

Fig. 5.1. Oceanographic setting for the southwestern margin of Africa with major ocean currents, DSDP/ODP and core sites. AC = Angola Current; BCC = Benguela Coastal Current; BOC = Benguela Ocean Current; SAC = South Atlantic Current; ABF = Angola-Benguela Front. a) Location map of Namibia with the shaded box indicating the area depicted in c; b) location of the 38 Minemakers cores and c) location of cores discussed in this study. Bathymetric contour intervals = 100m.

Table 5.1. Core depth and location coordinates of cores studied and analysed.

Core number	Type of core	Location	Core depth (mbsl)	Latitude (S)	Longitude (E)
2658	Vibracore	Namibian shelf	211	19°25'22"	12°11'44"
2670	Vibracore	Namibian shelf	219	19°21'00"	12°09'04"
2682	Vibracore	Namibian shelf	229	19°12'14"	12°03'45"

Specimens were picked for scanning electron microscope (SEM) imaging and mounted onto stubs with black adhesive carbon tabs and carbon glue. The specimens were then coated with a thin layer of Gold-Palladium using a BIO-RAD SEM coating system before SEM images were taken with a JEOL JSM 5200 and a Nova NanoSEM scanning microscope at Iziko Museums in Cape Town and the Electron Microscope Unit at the University of Cape Town, respectively.

Foraminifera, pelletal phosphorite grains, concretionary phosphorite pebbles, biogenic material (fish bone, teeth, scales), and mollusc shell fragments were picked from bulk gravel and sand size material for strontium isotope analysis (refer to Compton and Bergh (2016) for details on the SIS methodology). Planktic indicator species were identified based on Bolli et al. (1985) and Kennett and Srinivasan (1983). The indicator species were identified in core 2670 and correlated with the SIS ages and cross-correlated with cores 2658 and 2682.

Known bathymetric depths from published studies and planktic/benthic (P/B) ratios were used to determine palaeobathymetric estimates and changes in the sedimentary record. The P/B ratios are expressed in percentage (%P) (Nguyen et al., 2009) and are defined as the percentage planktics in the total foraminifer association calculated as P/(P + B) x 100 where P = number of total planktic individuals and B = number of total benthic individuals. P/B ratios are however influenced by dissolution (Kucera, 2007; Nguyen et al., 2009) transport, bottom water conditions and food availability (Pérez-Asensio et al., 2012; and references therein) which might skew results. Despite these limitations P/B ratios can indicate general changes and variations in sea level and palaeobathymetry over time (Pérez-Asensio et al., 2012).

Diversity indices (Fisher's alpha and Shannon index) were calculated using the PAlaeontologicalSTatistics (PAST) data analysis package (Hammer et al., 2001). Fisher's α-index is a measure expressing the number of species depending on the number of counted individuals following a log-series distribution (Fisher et al., 1943). The Shannon index (H) takes number of species as well as evenness of distribution between species into account and thus contains additional information compared to the α-index (Murray, 1991; Shannon, 1948).

Benthic foraminifera were grouped according to published microhabitat preferences and classified into epifaunal, epifaunal-shallow infaunal (upper 0-0.7 cm of sediment), shallow infaunal (0.7-1.5 cm), intermediate infaunal (1.5-3 cm) and deep infaunal (>3 cm) groups (Pérez-Asensio et al., 2012; and references therein) to determine any changes in assemblage compositions influenced by bottom water conditions.

5.4. Results

The stratigraphy of the cores shows an overall coarsening upward succession (Figs. 5.2 and 5.3). The base of the cores consists of clayey olive-green mud containing >80% foraminifera grading into sandy mud and muddy sand containing mollusc shell and phosphorite grains towards the top of the cores (see Compton and Bergh, 2016 for more detailed descriptions).

All foraminifera samples in the olive green mud unit have SIS ages dated to the middle Miocene from 16.1 to 14.4 Ma (Fig. 5.5). Other components (phosphorite pebbles, bone and pelletal phosphorite sand grains) from the upper part of the olive-green unit and the overlying gravelly sand units have Plio/Pleistocene SIS ages (Compton and Bergh, 2016).

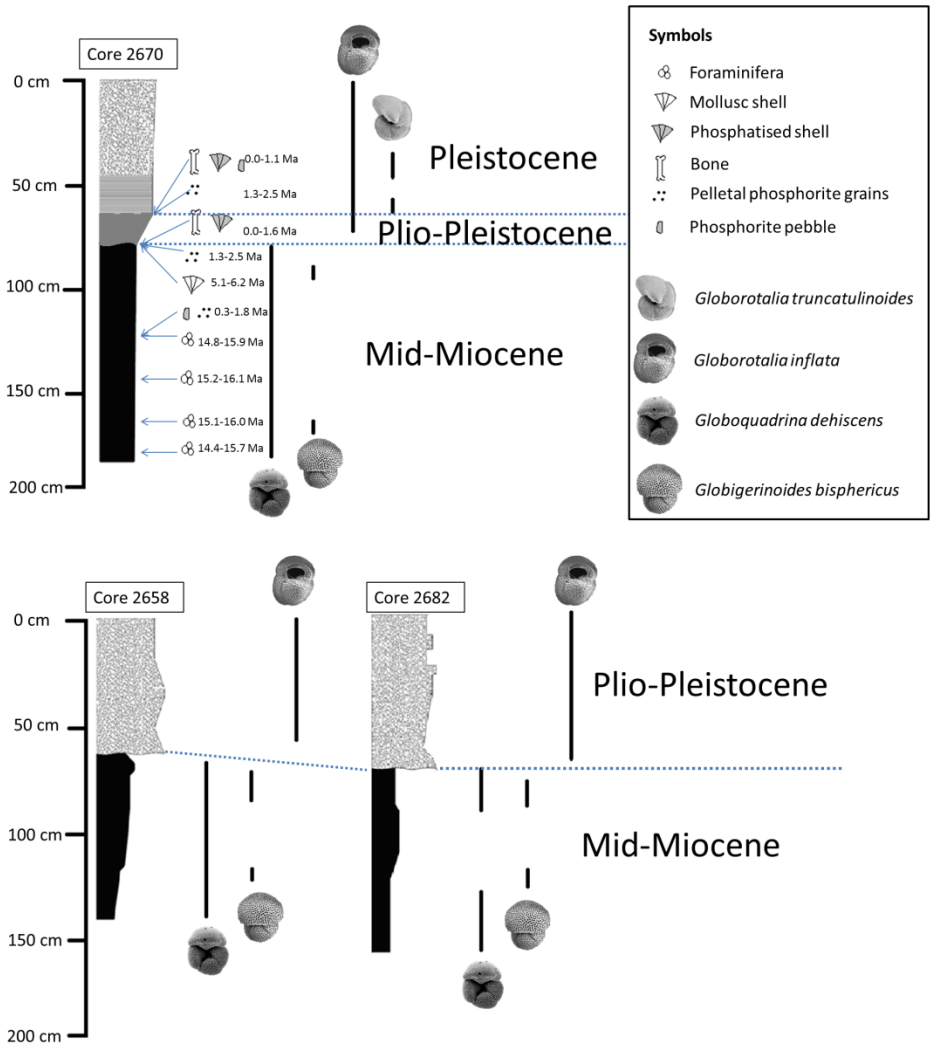

Fig. 5.2. Statigraphic model for the three cores of this study based on planktic indicators and SIS ages from core 2670 (Compton and Bergh, 2016).

The most abundant planktic foraminifera in the three cores are *T. immaturus* and *G. bulloides* (Fig. 5.4; Fig. 5.5) displaying counter-correlative trends (Fig. 5.4). The relative abundance of *G. bulloides* is lower in the middle Miocene compared to younger sediments *(G. bulloides)* in the cores and decreases in cores 2670 and 2682. *T. sacculifer* show minor peaks in the lower depths of the cores before reaching their highest abundances along the condensed contact. The relative abundances of *O. universa* also decrease in cores 2670 and 2682 with higher abundances in the upper parts of the cores. *Globigerinella praesiphonifera*, *Globoquadrina dehiscens* and *Globigerinoides bisphericus* occur in minor to

trace abundances in the cores where *Gq. dehiscens* fluctuates throughout the lower depths of the cores and has its highest relative abundances in core 2658. *Gs. ruber* occurs in trace to minor abundances in the lower half of the cores and shows similar trends to *T. sacculifer*.

Core 2658 recorded higher planktic diversity indices values. The number of planktic taxa in the mud unit of core 2658 ranged between 8 and 10. Core 2670 recorded between 4 and 9 taxa and core 2682 between 5 and 6. The Shannon H values for planktic foraminifera in core 2658 range between 1.24 and 1.56 while core 2670 recorded values of between 0.52 and 1.15 and core 2682 between 0.81 and 1.25. Fisher α values for core 2658 ranged between 1.70 and 2.42 while core 2670 recorded values between 0.72 and 1.45 and core 2682 between 1.16 and 1.86. The P/B ratios are higher in the basal mud compared to the overlying Plio-Pleistocene sandy units (Fig. 5.3) with mean P/B ratios ranging between 39 and 50%. P/B ratios however return to higher values upcore in all three cores. The mud unit of core 2658 recorded P/B ratios of between 31.0 and 45.3%. Cores 2670 (40.1-69.1%) and 2682 (37.9-53.4%) recorded higher P/B ratios than core 2658.

A large number of benthic species (Fig. 5.6) were greater than 1 mm in length. The dominant benthic taxa in the cores (Fig. 5.7) are *Uvigerina* spp. (*U. peregrina, U. spinulosa, U. pygmaea*) and *Oridorsalis* spp. *Uvigerina* spp. attain a maximum abundance in core 2658 whereas *Oridorsalis* spp. attained maximum abundance in cores 2670 and 2682. *Cibicidoides* spp. (*C. pseudoungerianus, C. ungerianus, C. dutemplei, C. crebbsi*) occur in moderate abundances (<20%) in most samples of all three cores. The relative abundances of *Lenticulina* spp. (*L. calcar, L. cultrata, L. gibba, L. inornata* and *L. iota*), *Sphaeroidina bulloides*, *Brizalina alata* and *Melonis barleeanus* all decrease in cores 2670 and 2682, and also upward towards the contact. The relative abundance of *Globocassidulina subglobosa* reaches its maximum abundance (<40%) in core 2670. The core depths at which a mixture of two assemblages characteristic of the basal mud unit and the overlying phosphorite unit occur at 69.5 to 73.5 cm in core 2658, at 88.5 to 97.8 in core 2670 and at 78.5 cm in core 2682.

Benthic foraminifera in the phosphorite units above the olive-green mud units include abundant *Ammonia beccarii, Cassidulina laevigata, Brizalina spathulata, Nonion boueanus, Elphidium advenum* and *Lobatula lobatula* (Fig. 5.8).

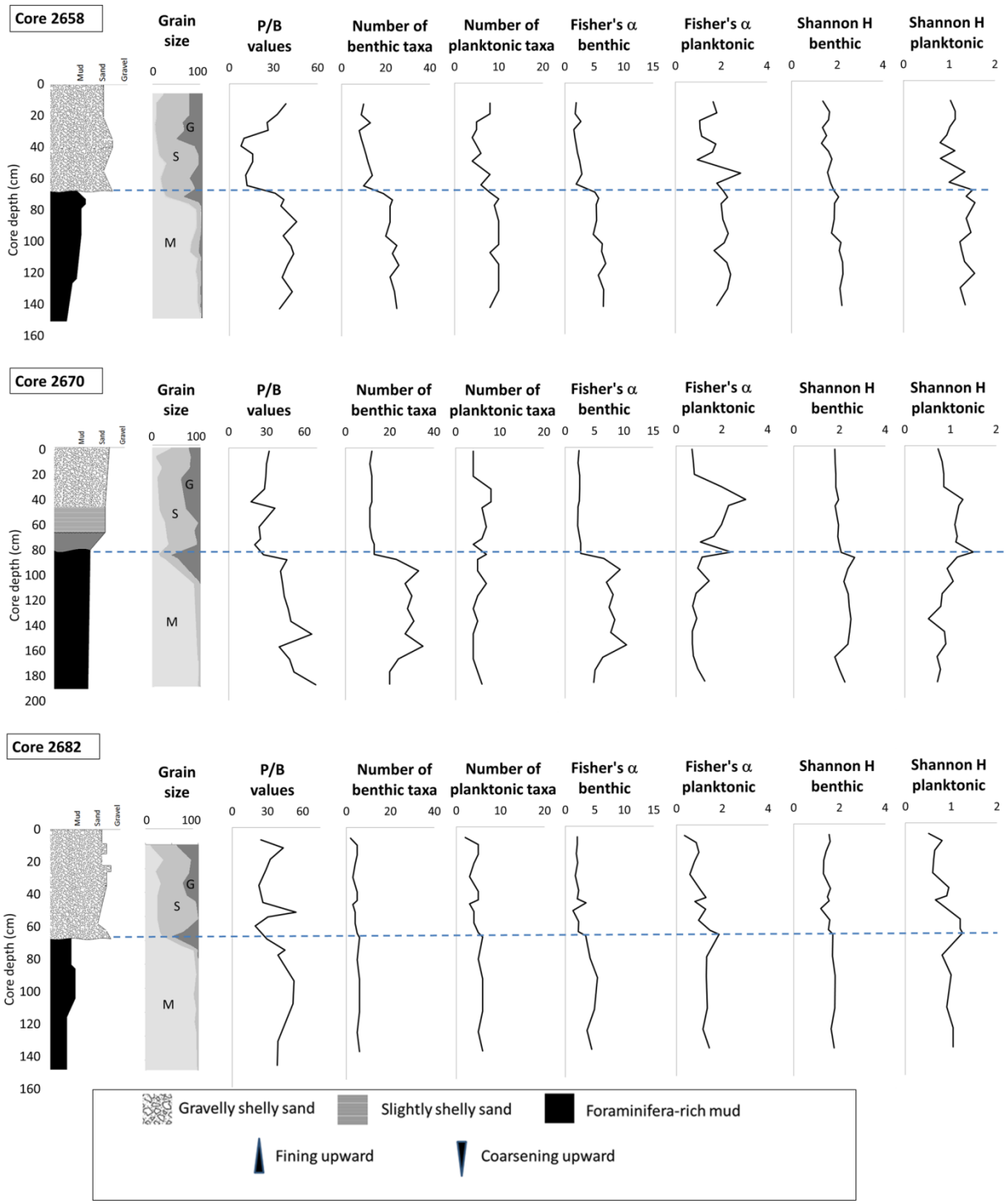

Fig. 5.3. Stratigraphy, grain size profiles (M = mud; S = sand; G = gravel), P/B ratios (%P) and diversity indices for the cores discussed in this study. The dashed line represents the contact between the middle Miocene olive green mud unit and the overlying Plio-Pleistocene sandy unit.

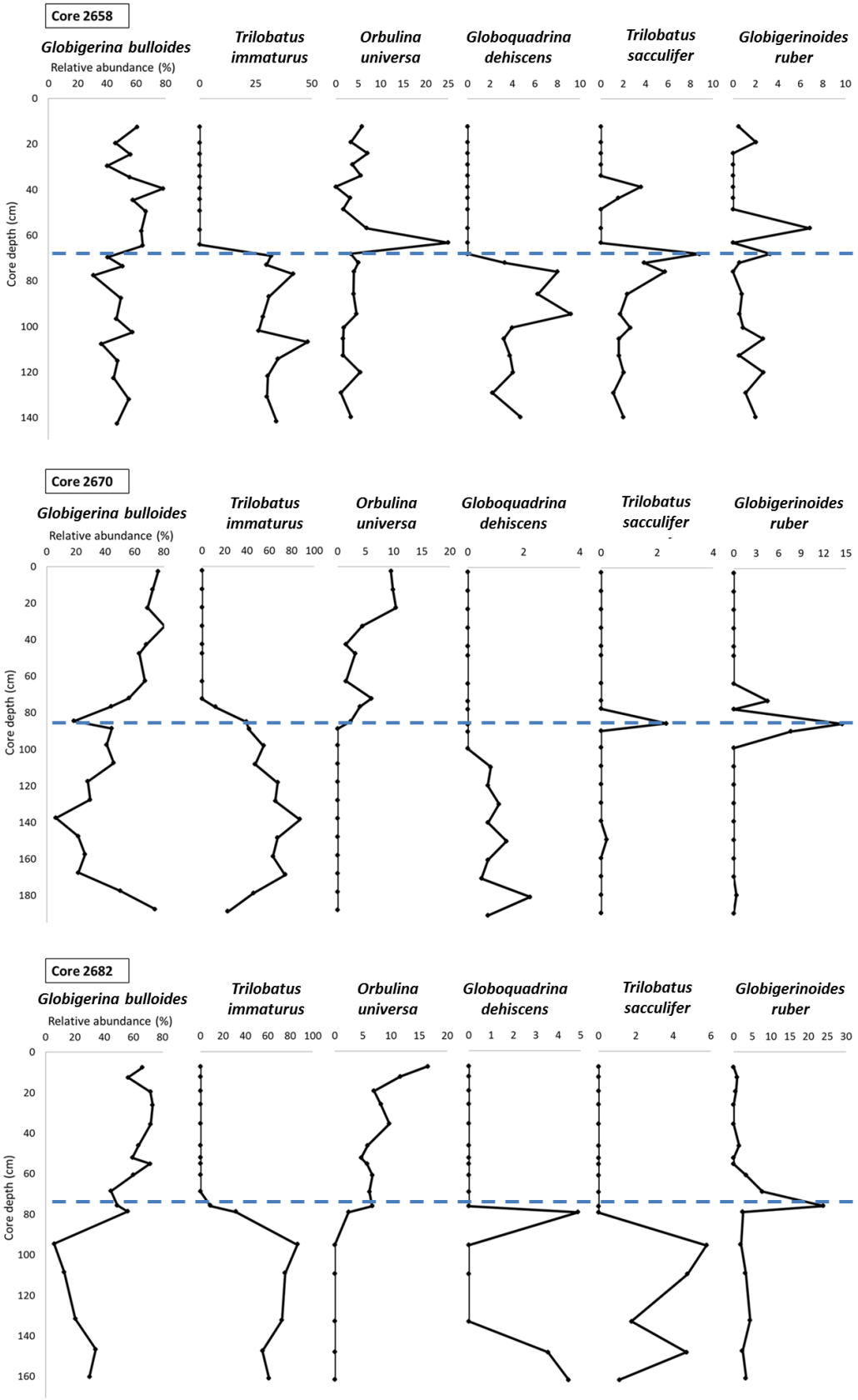

Fig. 5.4. Relative abundances of planktic foraminifera for all three cores. The dashed line represents the contact between the middle Miocene olive green mud and the overlying Plio-Pleistocene sandy unit.

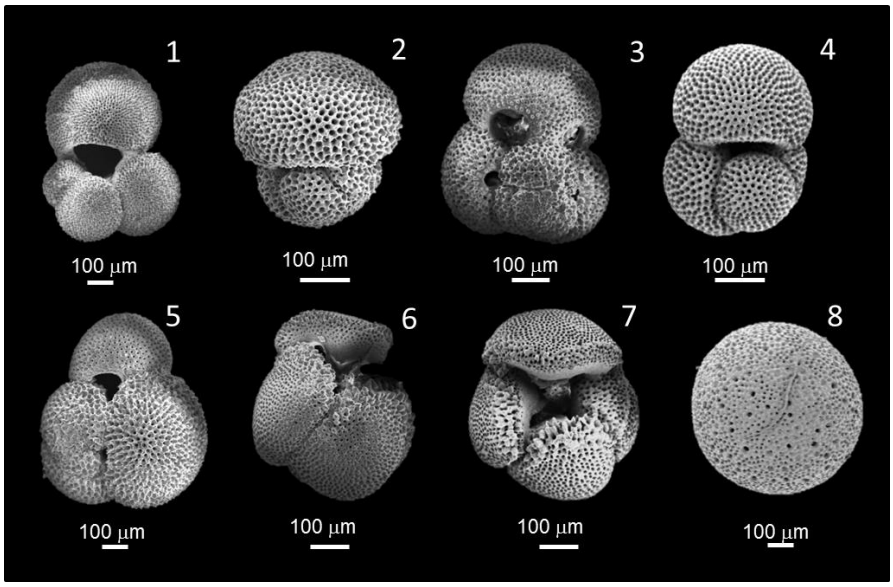

Fig. 5.5. Planktic foraminifera from this study. 1. *Globigerina bulloides* (core 2670, 105-110 cm); 2. *Globigerinoides bisphericus* (core 2670, 95-100 cm); 3. *Globigerinoides ruber* (core 2670, 145-150 cm); 4. *Trilobatus immaturus* (core 2670, 82-87 cm); 5. *Trilobatus sacculifer* (core 2670, 115-120 cm); 6. *Globoquadrina dehiscens* (core 2670, 145-150 cm); 7. *Globoquadrina dehiscens* (core 2670, 74-79 cm); 8. *Orbulina universa* (core 2670, 74-79 cm).

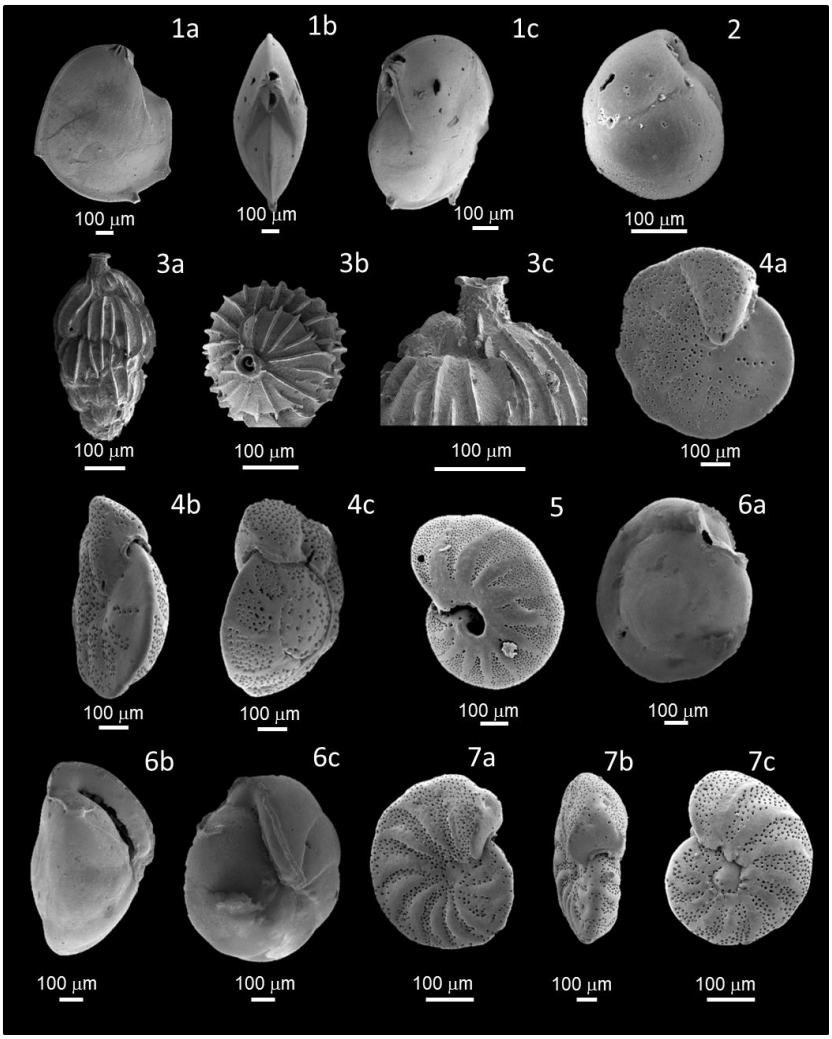

Fig. 5.6. Some of the benthic foraminifera from this study. 1a. *Lenticulina calcar* (core 2670, 175-180 cm); 1b. *Lenticulina calcar* apertural view (core 2670, 175-180); 1c. *Lenticulina calcar* (core 2670, 175-180 cm), oblique lateral view; 2. *Globocassidulina subglobosa* (core 2670, 105-110 cm); 3a-c. *Uvigerina spinulosa* (core 2670, 175-180 cm); 3b. apertural view; 3c. side view of upper test surface with protruding apertural neck; 4a-c. *Cibicidoides ungerianus* (core 2670, 175-180 cm); 4a. umbilical view; 4b. apertural view; 4c. spiral view; 5. *Melonis barleeanus* (core 2670, 145-150 cm); 6a-c. *Gyroidinoides soldanii* (core 2670, 175-180 cm); 6a. spiral view; 6b. apertural view; 6c. oblique umbilical view; 7a-c. *Anomalinoides helicinus* (core 2670, 175-180 cm); 7a. spiral view, 7b. apertural view, 7c. umbilical view.

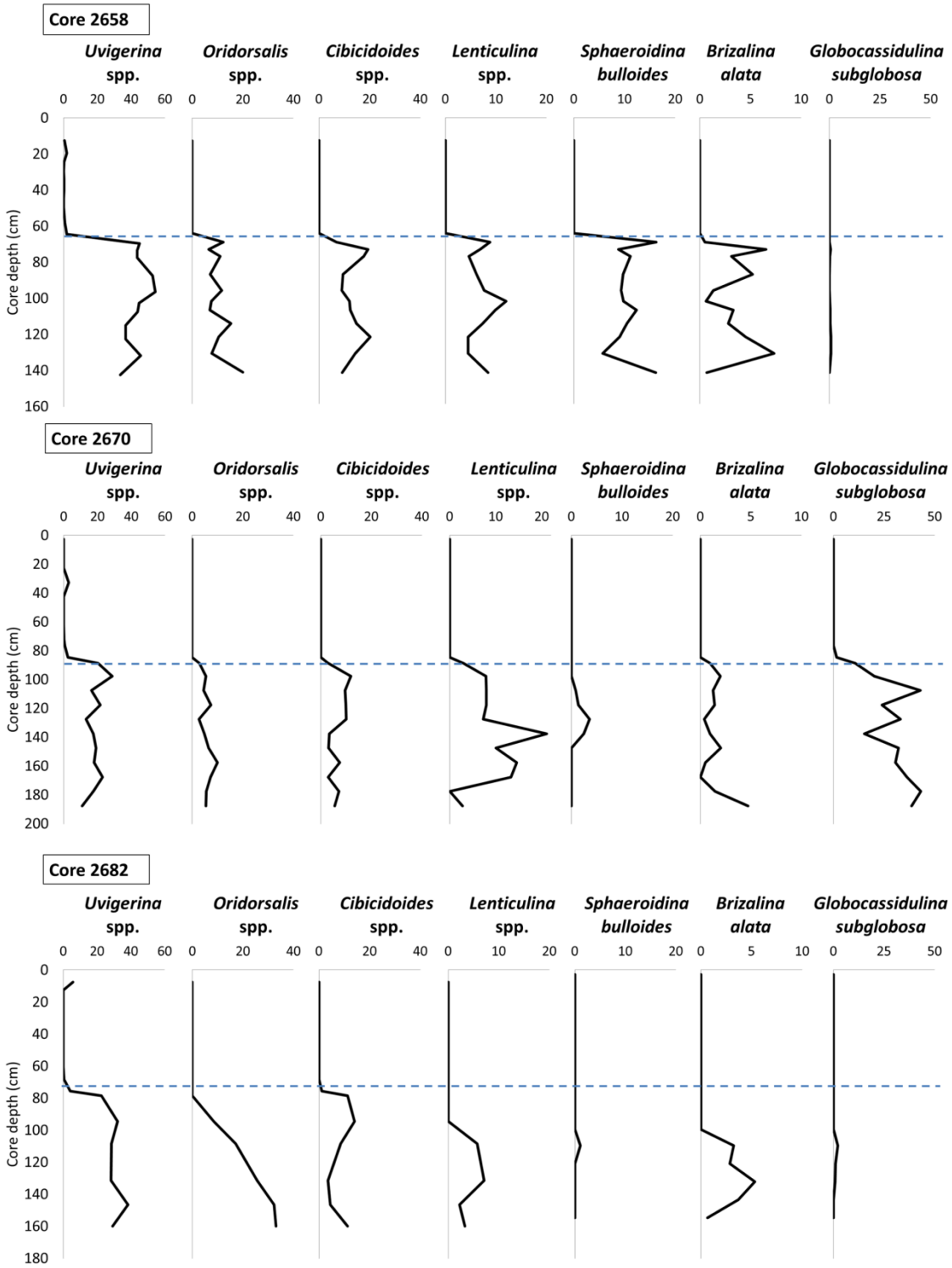

Fig. 5.7. Relative abundances (%) of middle Miocene benthic foraminifera with relatively higher proportions in all three cores of this study. The blue dashed line represents the contact between the Middle Miocene olive green mud and the overlying Plio-Pleistocene sandy unit.

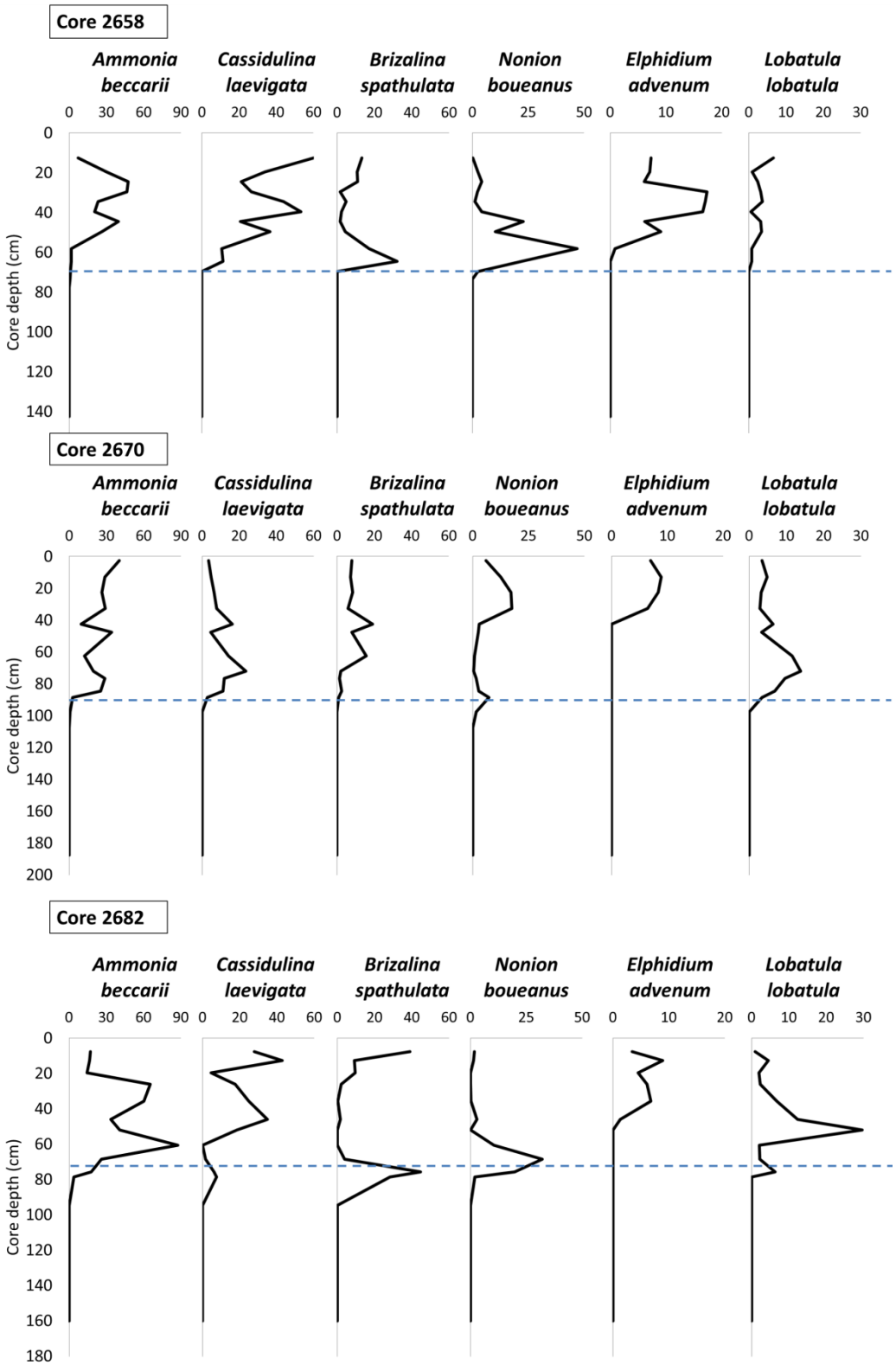

Fig. 5.8. Relative abundances (%) of Pleistocene benthic foraminifera with relatively higher proportions in all three cores of this study. The blue dashed line represents the contact between the Middle Miocene olive green mud and the overlying Plio-Pleistocene sandy unit.

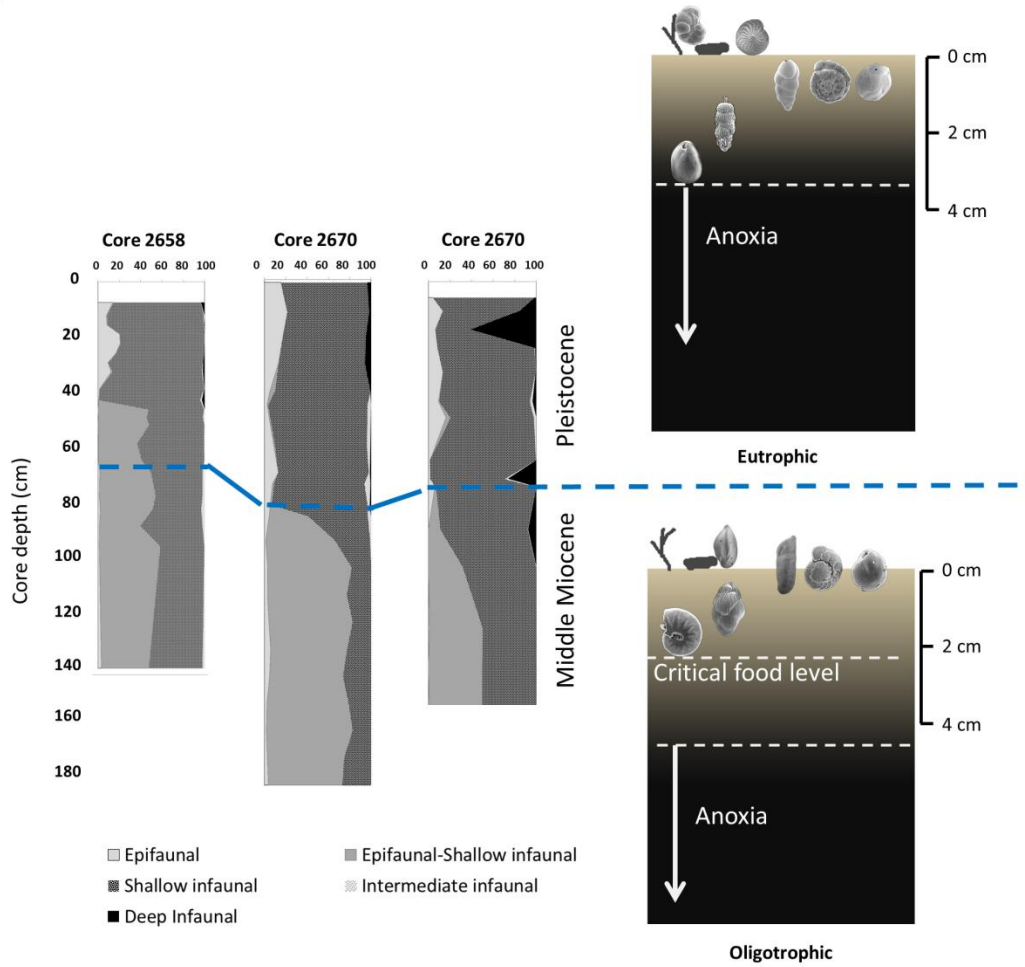

Fig. 5.9. Epifaunal-infaunal composition of the cores and microhabitats in the middle Miocene and Pleistocene.

Benthic diversity indices (numbers of benthic taxa and Fisher α) are higher compared to planktic taxa in the phosphorite units (Fig. 5.3). Core 2670 recorded higher benthic diversity indices values. The number of benthic taxa in the mud unit of core 2670 ranged between 20 and 35. Core 2658 recorded between 19 and 26 taxa and core 2682 between 12 and 20 taxa. The Shannon H values for benthic foraminifera in core 2670 range between 1.80 and 2.67 while core 2658 recorded values of between 1.75 and 2.25 and core 2682 between 1.64 and 1.82. Fisher α values for core 2670 ranged between 4.88 and 10.45 while core 2658 recorded values between 4.82 and 6.96 and core 2682 between 3.45 and 5.44.

Epifaunal-shallow infaunal foraminifera dominate the lower depths of the cores (Fig. 5.9). At 19.5 cm of core 2682 deep infaunal foraminifera reach abundances of up to 61% while shallow infaunal foraminifera become more abundant at higher depths in the three cores.

5.5. Discussion

5.5.1. Age and stratigraphic correlation to South African shelf deposits

The SIS ages of foraminiferal tests in the basal olive-green mud unit in core 2670 of between 14.4 and 16.1 Ma are consistent with the biostratigraphic ages of the indicator species *Gs. bisphericus* (early to middle Miocene; Bolli et

al., 1985) and *Gq. dehiscens* (early to late Miocene - Kennett and Srinivasan, 1983; Wade et al., 2011). Together the SIS and biostratigraphy constrain the age of the foraminiferal assemblage to the middle Miocene (Fig. 5.5; Fig. 5.10). The mud units of cores 2658 and 2682 also contain *Gs. bisphericus* and *Gq. dehiscens* indicating a middle Miocene age.

The mud unit contains reworked Pleistocene pelletal phosphorite sand (Compton and Bergh, 2016) and a phosphorite pebble in core 2670 dated by SIS (Fig. 5.5). No indicator planktic species from the Pliocene or Pleistocene were present in the olive-green mud and only occur in the overlying phosphorite-rich units.

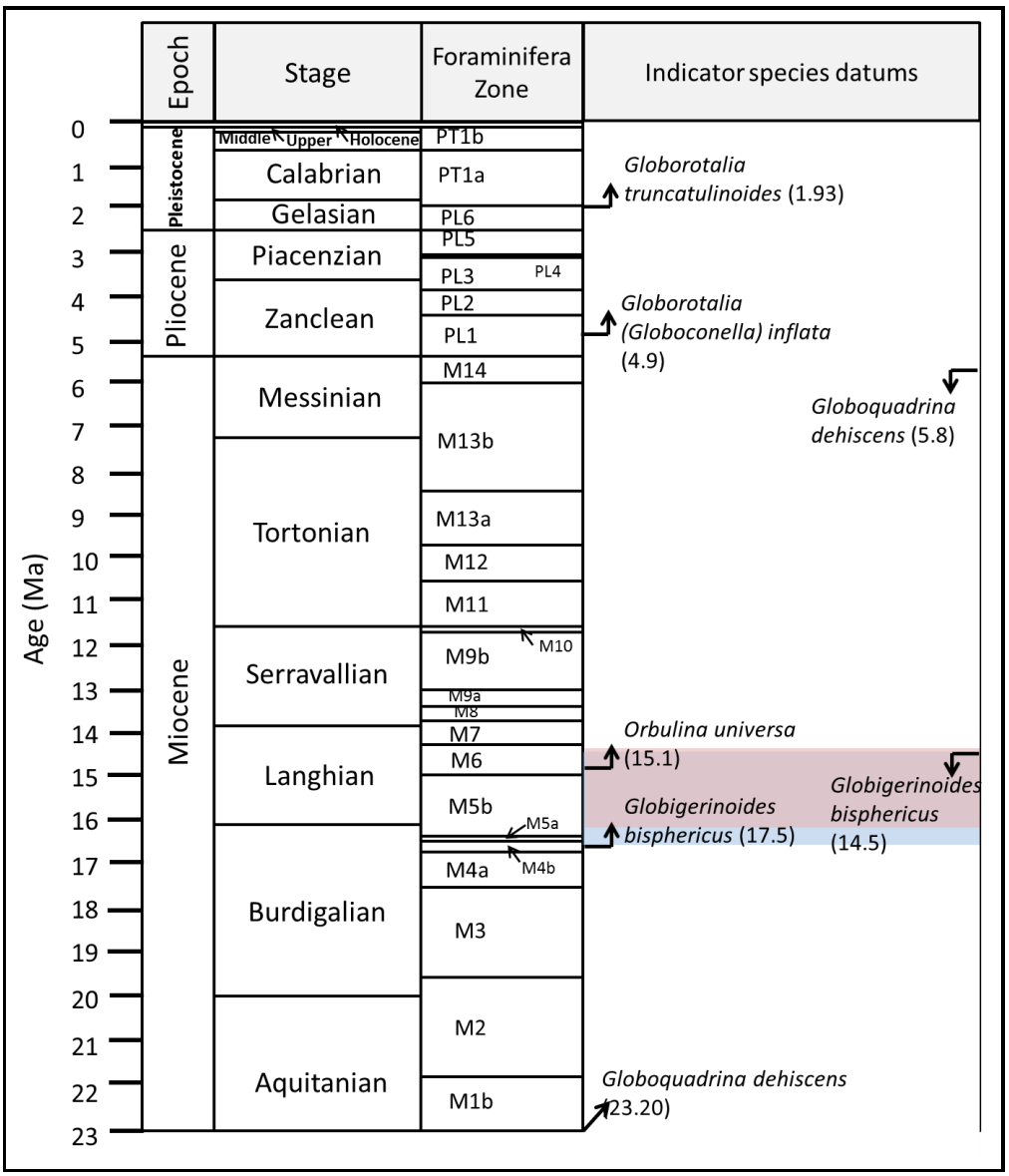

Fig. 5.10. Appearance (FAD) and disappearence (LAD) datums of planktic foraminifera taxa identified in this study based on ages from Kender et al. (2008; and references therein), Kucera and Schönfeld (2007) and Wade et al. (2011). The geologic timescale is based on the International Chronostratigraphic Chart v2017/02 with foraminifera zones from Wade et al. (2011). The pink shaded region indicates the ages from SIS and blue shaded area where the index species *Globoquadrina dehiscens* and *Globigerinoides bisphericus* correspond to each other. The age of the mud unit in the cores is indicated by the overlap of the two (blue and red) shaded areas.

Wigley and Compton (2006) recorded middle Miocene muddy sand to sandy gravel with medium to coarse quartz and glauconite sand, shell fragments and phosphorite cemented grains from the southwestern South African shelf. In contrast to the mud unit discussed in this study, which contains >80% foraminifera shells in the sand fraction, foraminifera constituted only 20% of the sand fraction in the study of Wigley and Compton (2006). The more variable sedimentary contents in middle Miocene-aged deposits between the two study areas could be a result of greater terrestrial input from rivers, such as the Berg and Olifants rivers. Onshore denudation and increased terrestrial output onto the continental shelf during the middle Miocene (Wigley and Compton, 2006) could have resulted in thicker middle Miocene mud units along the shelf margin.

The contact between the olive-green mud unit and overlying black pelletal phosphorite units in core 2670 gave SIS ages ranging from the Pliocene to Quaternary. The planktic foraminifer *Gr. (Globoconella) inflata* (FAD Pliocene) occurred above the mud unit while *Gr. truncatulinoides*, a Pleistocene indicator species appeared higher up in the cores (Fig. 5.5). The SIS ages suggest that the late Miocene to Pliocene depositional record is missing from the cores as Pleistocene foraminifera and components are present in the unit above the middle Miocene mud. The erosional contact between the olive-green mud and overlying pelletal phosphorite sandy units thus represents a hiatus. Samples from the contact between the mud unit and the overlying phosphorite units measuring of up to ~10 cm thick contain a mixture of Miocene and Plio-Pleistocene foraminifera. The mixture of the two assemblages also suggests reworked sediments along the erosional contact. The sediments of the western margin of southern Africa are commonly condensed and reworked, with onshore and offshore records incomplete (Wigley and Compton, 2006). Reworking of sediments on the western margin of Southern Africa is suggested to occur during sea level drops (Compton et al., 2004; Wigley and Compton, 2006; Compton and Bergh, 2016). The late Miocene-Pliocene hiatuses were influenced by enhanced dissolution as a result of increased CO_2 levels related to increased upwelling during cooling events (Keller and Barron, 1987), lowered sea levels, increasing amplitude of sea-level fluctuations (Compton and Bergh, 2016), uplift (Wigley and Compton, 2006; and references therein; Hoetzel et al., 2017), and increased aridification (Hoetzel et al., 2015). The increasing aridification led to lower rainfall, decreased river flow and fluvial inputs (De Wit et al., 2000). The increasing aridification during that time period in turn led to lower sedimentation rates and minor accumulation of sediments on the continental shelf (Wigley and Compton, 2006).

5.5.2. Palaeo-sea-surface conditions

The relative abundances of the planktic foraminifera and occurrence of taxa such as *T. immaturus, T. sacculifer* and *Gs. ruber* reveal warmer conditions on the Namibian continental margin during the middle Miocene consistent with previous global studies (Table 5.2). The change in planktic foraminiferal abundances records a shift in sea surface conditions between the middle Miocene and Plio-Pleistocene despite planktic diversity not changing

significantly over time (Fig. 5.3). Tropical to subtropical planktic foraminifera (Table 5.2) dominate in the middle Miocene section of the cores before the relative abundances of these taxa decrease in the Pleistocene. The dominance of the tropical to subtropical foraminifera is replaced by cooler temperate planktic foraminifera with polar to subpolar planktic foraminifera appearing in the Pleistocene record of the cores (Fig. 5.11). The high abundances of warm tropical to subtropical planktic foraminifera are supported by the occurrence of subtropic ostracods *Henryhowella* sp. and *Bairdoppilata* sp. (Fig. 5.12; Dingle et al., 2001). Data on sea surface temperatures (SST) for the middle Miocene off Namibia are not available, but global high latitude temperatures were as much as 6˚C higher (Pagani et al., 1999) than the present-day mean SST values off Namibia of less than 18˚C (Romero et al., 2015).

Table 5.2. Abundance and associated sea surface conditions of planktic foraminifera identified in this study.

Species	Age in cores	Abundance	Associated conditions	References
Trilobatus immaturus	Middle Miocene	High abundance	Tropical to subtropical	Ohta *et al.*, 2003; BouDagher-Fadel, 2015
Globigerinoides ruber	Middle Miocene-Pleistocene	Minor abundances in all cores	Tropical to subtropical (warm)	Bé and Tolderlund, 1971; Glacon, 1990; Kucera, 2007; BouDagher-Fadel, 2015
Orbulina universa	Middle Miocene-Pleistocene	Minor to major abundances in all cores	Subtropical	Tolderlund, 1971; Kucera, 2007
Trilobatus sacculifer	Middle Miocene-Pleistocene	Minor totrace abundances	Tropical (warm)	Bé and Tolderlund, 1971; Glacon, 1990; Kucera, 2007
Globorotalia menardii	Pleistocene	Minor to trace	Tropical to subtropical	Bé and Tolderlund, 1971; Kucera, 2007; BouDagher-Fadel, 2015
Globigerina bulloides	Pleistocene	Moderate to high	Temperate/transitional	Bé and Tolderlund, 1971; Kucera, 2007
Globorotalia (*Globoconella*) *inflata*	Pleistocene	Moderate to high	Temperate/transitional	Bé and Tolderlund, 1971; Kucera, 2007
Neogloboquadrina incompta / Ng. pachyderma (d)	Pleistocene	Minor	Subpolar	Bé and Tolderlund, 1971; Kucera, 2007; Lombard *et al.*, 2009
Neogloboquadrina pachyderma (s)	Pleistocene	Trace	Polar	Bé and Tolderlund, 1971; Kucera, 2007; Lombard *et al.*, 2009

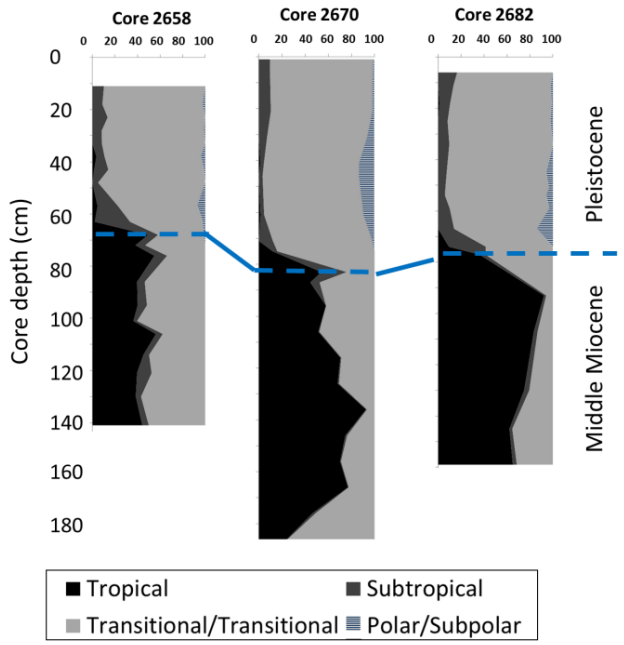

Fig. 5.11. Combined relative abundances of planktic foraminiferal groups

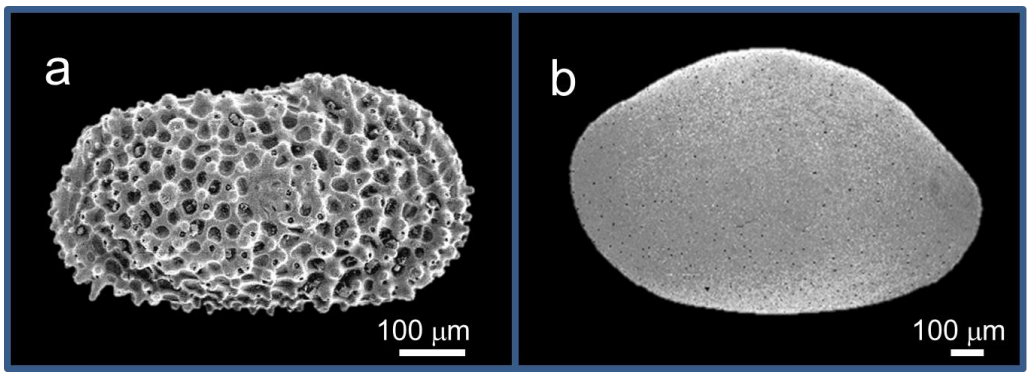

Fig. 5.12. Ostracods identified in this study. a) *Henryhowella* sp.; b) *Bairdoppilata* sp. Scalebar = 100 µm.

The high abundance of warm water planktic foraminifera reflects the influence of the warmer Angola Current flowing southwards over the Walvis Ridge prior to the onset of cooler Benguela upwelling conditions along northern Namibia in the late Miocene (Hoetzel et al., 2017). It was after the onset of the BUS that the Benguela Current shifted northwards and reached the Walvis Ridge in the late Miocene when the subtropical anticyclone strengthened as a result of Antarctic glaciation (Diester-Haass et al., 1992). Faunal changes during the middle to late Miocene have been reported elsewhere as well in which foraminiferal assemblages changed throughout the Southern Ocean. For example, in Australia, subtropical benthic foraminiferal taxa and warm water planktic foraminifera disappeared and were replaced by cool-temperate foraminifera in the neritic realm at ~14 Ma (Gallagher et al., 2001; Diester-Haass et al., 2002), which is approximately the same lower age limit of the foraminiferal assemblage of this study.

The MMCO was followed by phases of alternating cool and warm water conditions during the late Miocene when upwelling and high productivity started at ~12 Ma (Lange et al., 1999; Marlow et al., 2000; Diester-Haass et al., 2004; Heinrich et al., 2011) after which the warm water taxa were replaced by the cooler transitional species *G. bulloides and Gr. (Gc.) inflata* during the Plio-Pleistocene.

The abundance peaks in *Gs. ruber* and *T. sacculifer*, and the decrease in the relative abundance of *G. bulloides* at the contact may be related to the warming phase of the Pliocene during 4.5 to 3.2 Ma. On the slope *Gs. ruber* also showed slight abundance peaks during the early and middle Pliocene while the temperate species *Gr. (Globoconella) inflata* only appeared during the mid-Pliocene after which it increased in abundance (Hay et al., 1984). Average SST for the mid-Pliocene was 26 ˚C which is 8 ˚C warmer than the current mean SST of the area. Global cooling after 3.2 Ma resulted in a SST drop of 10 ˚C since the termination of the mid-Pliocene warming phase (Marlow et al., 2000). *G. bulloides* remained a common and abundant component within the assemblage during the late Miocene to late Pliocene (Hay et al., 1984).

5.5.3. Palaeobathymetry

Several of the Miocene benthic taxa occur over broad bathymetric ranges with most having been reported from slope depths (Fig. 5.13). The P/B ratios calculated in this study indicate outer shelf water depths during the Middle Miocene consistent with bathymetric ranges for several of these taxa. The bathymetric estimates for the middle Miocene are higher than for the Pleistocene units of the cores. Although dissolution and transport might have affected P/B ratios the presence and relatively higher abundances of smaller foraminifera such as *Globocassidulina subglobosa, Brizalina alata, Bolivina reticulata* and *Sphaeroidina bulloides*, and the occurrence of relatively high abundances of certain planktic foraminifera such as *Globigerina bulloides* and *Orbulina universa* in the Miocene units indicate that dissolution has had a low to moderate influence on P/B ratios.

The palaeobathymetric estimates which places these assemblages at deeper environments are consistent with global and local geologic events during the middle Miocene. Uplift along the southwest margin of Africa has been estimated at 100-200 m during and after the middle Miocene (Pether et al., 2000; Dale and McMillan, 2003). Global sea-level rose during the middle Miocene as a result of warming and sea-level variations during the Oligocene to Pliocene has been estimated in the order of between 30 and 60 m (Miller et al., 2005). The distribution of benthic foraminifera is influenced by food sources and availability, substrate, temperature, salinity and hydrographic conditions (Van der Zwaan et al., 1990; Jorissen et al., 2007). It is therefore possible that taxa that have been reported to occur at slope depths can also occur at deeper outer shelf depths especially along a continental shelf with a broad range such as the Namibian margin (400-500 m). Similar benthic taxa have been reported from the western continental shelf of South Africa, also dated to the middle Miocene from a water depth of 270 m (Compton et al., 2004).

Global sea level fell during the late Miocene and rose in the mid-Pliocene by 20-60 m (Dowsett and Poore, 1991; Miller et al., 2005) after which the intensification of Northern Hemisphere glaciation ended a warm period during the Pliocene (Dowsett and Poore, 1991). A fragmented Pliocene foraminiferal assemblage was described from offshore Lüderitz-Walvis Bay (Assemblage Fb in Compton and Bergh, 2016) and Compton et al. (2004) provided a list of Pliocene foraminifera from the western margin of South Africa revealing the occurrences of similar benthic foraminiferal taxa assemblages between the two areas. The sea level dropped again following the mid-Pliocene warm phase (Miller et al., 2005).

The Pleistocene to Holocene record of the Namibian shelf has yielded an entirely different assemblage compared to the Mio-Pliocene record (Fig. 5.8). Abundant calcareous Quaternary foraminifera on the Namibian shelf include *Ammonia* spp., *Elphidium* spp., *Cassidulina* spp., *Lobatula lobatula* and *Globobulimina* spp., as well as agglutinated *Rhabdammina* spp., *Hyperammina* spp. and *Trochammina* spp. (Schmiedl, 1995; Leiter and Altenbach, 2010).

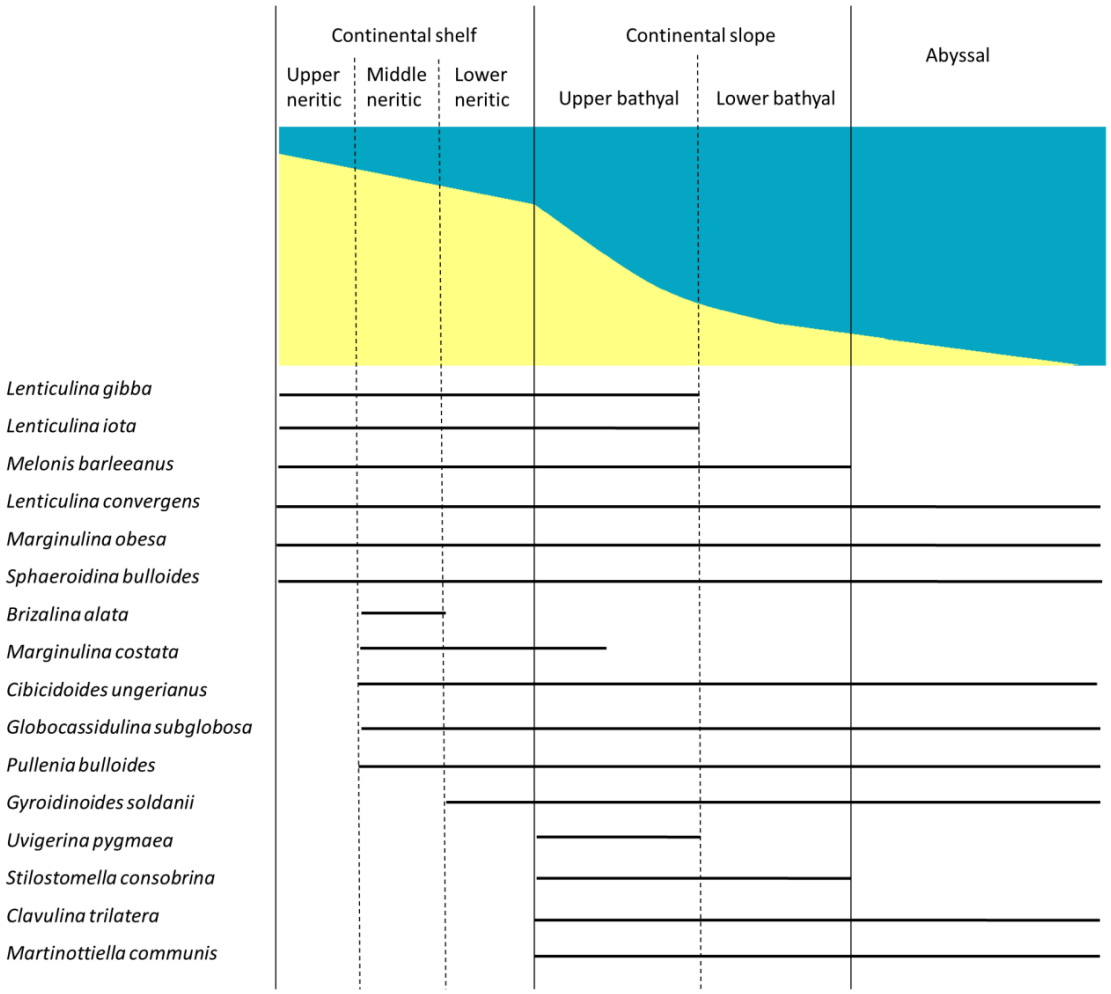

Fig. 5.13. Palaeobathymetric ranges for some of the benthic foraminifera in this study based on Pérez-Asensio et al. (2012; and references therein) and Holbourn *et al.* (2013) (black solid lines).

Taxa restricted to shelf environments such as *Ammonia* spp. and *Elphidium* spp. have also been documented in the Pleistocene units of the cores from this study (Fig. 5.8; Table 5.3). These taxa indicate the lowering of sea level from the Mio-Pliocene to Pleistocene which is associated with the initiation of the BUS along the northern Namibian margin and the northwards migration of the ABF (Hoetzel et al., 2017).

5.5.4. Sea floor conditions

Jorissen et al. (1995) proposed that the vertical distribution of epifaunal and infaunal benthic foraminifera is controlled by food and oxygen availability. The abundance of epifaunal and infaunal taxa can provide valuable clues to determining the palaeoenvironment and microhabitat of an assemblage at a given time period.

The middle Miocene benthic foraminiferal assemblage is dominated by taxa living at the epifaunal-shallow infaunal interface (Fig. 5.9). Although a relatively large number of taxa considered to be shallow infaunal have been recorded in the middle Miocene section their abundances are much lower than the epifaunal-shallow infaunal taxa (Fig. 5.9; Table 5.3). The higher epifaunal-shallow infaunal abundances and low diversity indicate oligotrophic conditions where more food is consumed at the sediment-water interface. In oligotrophic environments the vertical distribution is controlled by food availability and as the food source is almost entirely consumed by epifaunal-shallow infaunal foraminifera, small quantities of refractory organic matter are left below the sediment-water interface, which allows for fewer taxa to survive within the first few cm of the sediment (Jorissen et al., 1995). Dysoxic (0.1-0.3 ml/l O_2; Kaiho, 1994) foraminifera (*Brizalina alata, Bolivina reticulata* and *Astacolus crepidulus*) are few in number during the middle Miocene, whereas oxic (>2 ml/l O_2; Kaiho, 1994) (*Globocassidulina subglobosa, Siphonina pulchra, Cibicidoides* spp.) and suboxic (0.3-1.5 ml/l O2; Kaiho, 1994) indicator taxa (*Dentalina* spp., *Grigelis semirugosa, Nodosaria laevigata, Pseudonodosaria brevis, Plectofrondicularia* spp., *Lenticulina* spp., *Saracenaria italica, Marginulina* spp., *Uvigerina* spp. and *Oridorsalis* sp.) are abundant, indicating that oxygen levels were conducive enough for foraminifera requiring high oxygen water contents.

In certain oligotrophic environments seasonal pulsed food inputs from phytodetritus in the form of labile organic matter may reach the seafloor providing certain species indicative of high organic matter input the opportunity to flourish. The high abundances of *Uvigerina* spp. and *Globocassidulina subglobosa* (in core 2670) suggest seasonal pulses of high organic matter delivery to the seafloor (Schmiedl et al., 1997; Schmiedl and Mackensen, 1997; Berger et al., 2002) and upwelling conditions (Lutze and Coulbourn, 1984; Li and McGowran, 1994). Diester-Haass et al. (2005) used *Uvigerina* counts and accumulation rates in the South Atlantic as an indication of palaeoproductivity during the late Miocene and Pliocene, and found increased organic matter delivery during the onset of Benguela upwelling. The records in Berger et al. (1998) and Diester-Haass et al. (2005) do not extend into the middle Miocene, but the relatively high abundances of *Uvigerina* recorded for this study indicate that high

organic matter delivery to the seafloor extended back to at least the middle Miocene and prior to the initiation of the permanent BUS along the margin.

Table 5.3. Microhabitats of benthic foraminifera identified in this study as classified by Alegret et al. (2003), Perez-Asensio et al. (2012; and references therein), Murray (1976), Drinia et al. (2007) and Reolid et al. (2008).

	Life Position				
Age	**Epifaunal**	**Epifaunal-shallow infaunal**	**Shallow infaunal**	**Intermediate infaunal**	**Deep infaunal**
Pleistocene	*Elphidium advenum* *Globobulimina* spp. *Lobatula lobatula*	-	*Ammonia beccarii* *Brizalina spathulata* *Bulimina spp.* *Cancris auriculus* *Cassidulina laevigata* *Elphidium advenum* *Globobulimina spp.* *Nonion boueanus*	*Rectuvigerina nicolii*	*Globobulimina turgida*
Middle Miocene	*Karreriella siphonella* *Plectofrondicularia* spp. *Saracenaria italica* *Saracenaria spinosa*	*Anomalinoides* sp. *Cibicidoides* spp. *Globocassidulina subglobosa* *Gyroidinoides soldanii* *Lenticulina* spp. *Marginulina* spp. *Oridorsalis* sp. *Siphonina pulchra* *Sphaeroidina bulloides* *Vaginulina* spp.	*Amphicoryna* spp. *Astacolus crepidulus* *Bolivina reticulate* *Brizalina alata* *Clavulina* spp. *Dentalina* spp. *Grigelis semirugosa* *Laevidentalina* spp. *Lingulina seminuda* *Martinottiella communis* *Nodosaria laevigata* *Nodosaria latejugata* *Orthomorphina jedlitschkai* *Pullenia bulloides* *Siphonodosaria consobrina* *Spiroplectammina* sp. *Uvigerina* spp.	*Melonis barleeanus*	

In the Pleistocene section of the cores epifaunal and deeper infaunal taxa become more abundant. Environments with higher abundances of deep infaunal taxa and low diversities are characteristic of eutrophic conditions (Jorissen et al., 1995). As the vertical distribution of foraminifera in eutrophic environments is more dependent on oxygen availability, the critical oxygen level is at a shallower depth in comparison to oligotrophic environments. In eutrophic environments the degradation of organic matter consumes more oxygen where deeper infaunal taxa can survive at lower depths of the sediment profile as food availability is less critical (Jorissen et al., 1995). The shallowing of the area during the Pleistocene and intensified upwelling conditions along the margin provided more terrestrial input and organic matter (Compton and Bergh, 2016) from the coast and nearby Kunene River.

5.6. Conclusions

Index fossil planktic foraminifera *Gs. bisphericus* and *Gq. dehiscens* indicate a middle Miocene age for basal olive-green mud units from the northern Namibian shelf consistent with SIS ages of 16 to 14 Ma. The basal middle Miocene olive-green mud recovered on the shelf is dominated by the planktic taxa *G. bulloides* and *T. immaturus* and the benthic taxa *Uvigerina* spp. and *Oridorsalis* spp. The overlying pelletal phosphorites were dated to the Pleistocene with the presence of *Gr. inflata* and *Gr. truncatulinoides*, also consistent with SIS ages of <2.5 Ma. Upper Miocene to Pliocene sedimentary components are reworked and depositional units are largely missing.

There is a turnover in foraminiferal assemblages across the middle Miocene-Pleistocene depositional units. A changeover of warm water planktic species to cooler temperate water species in the area reflects the northward migration of the Angola-Benguela Front (ABF) during the late Miocene associated with the initiation of the BUS. The high abundance of tropical-subtropical planktic foraminifera are consistent with warming conditions of the Mid-Miocene Climatic Optimum (MMCO) which was followed by cooling conditions and the appearance of temperate taxa in the Plio-Pleistocene. The cooling phases were followed by a mid-Pliocene warming phase evident by increased *Gs. ruber* and *T. sacculifer* relative abundances and the subsequent decrease in abundances in the cooler upwelled Pleistocene waters of the BUS.

The benthic foraminifera indicate deeper outer shelf conditions in the middle Miocene based on bathymetric ranges and P/B ratios. These taxa are contrasted by benthic foraminifera adapted to shallower depths in the overlying units. Pleistocene foraminifera from this study and others on the Namibian shelf show that the palaeoenvironment shifted from a relatively deeper outer shelf environment during the middle Miocene to a shallower environment under cooler upwelled conditions from the late Miocene to Pleistocene.

Bottomwater conditions during the middle Miocene reflected oligotrophic conditions with high *Uvigerina* spp. and *Globocassidulina subglobosa* abundances indicating high seasonal organic matter flux to the sea floor. Oligotrophic conditions on the sea floor were replaced by eutrophic conditions in the Pleistocene during the initiation and intensification of upwelling conditions along the

margin which allowed for more infaunal taxa surviving at deeper depths within the sediment.

Acknowledgements

The cores were provided by Minemakers Pty Ltd. Melissa Oosthuizen helped with processing two of the cores. Ian McMillan and Gerhard Schmiedl helped with reviewing the identification of some of the foraminifera and provided helpful comments to the manuscript. Albe Bosman, Jody-Carynn Oliver, Pathutshedzo Mutheiwana and MirandaWaldron are also thanked for their assistance in SEM sample preparation. Funds from the National Research Foundation and Iziko Museums of South Africa were used for costs of analyses in the study.

References

Alegret, L., Molina, E., Thomas, E., 2003. Benthic foraminiferal faunal turnover across the Cretaceous/Tertiary boundary at Agost (Southeastern Spain): Paleoenvironmental Inferences. Marine Micropaleontology 48, 251-279.

Bé, A.W.H., Tolderlund, D.S., 1971. 6. Distribution and ecology of living planktonic foraminifera in surface waters of the Atlantic and Indian Oceans. In: Funnell, B.M., Riedel, W.R. (Eds.), Micropaleontology of Oceans. Cambridge University Press, London, pp. 105–149

Berger, W.H., Lange, C.B., Wefer, G., 2002. Upwelling history of the Benguela-Namibia system: a synthesis of Leg 175 results. Proceedings of the Ocean Drilling Program Scientific Results, 175, 103 pp.

Berger, W.H., Wefer, G., Richter, C., Lange, C.B., Giraudeau, J., Hermelin, O., Shipboard Scientific Party., 1998. Proceedings of the Ocean Drilling Program, Initial Reports 175, 505-531.

Bolli, H.M., Saunders, J.B., Perch-Nielsen, K., 1985. Plankton Stratigraphy. Cambridge University Press, Cambridge, 1032 pp.

BouDagher-Fadel, M.K., 2015. Biostratigraphic and geological significance of planktonic foraminifera. UCL Press, London.

Bremner, J.M., 1977. Sediments on the continental margin off Southwest Africa between Sylvia Hill and the Kunene River. Unpublished PhD thesis, University of Cape Town.

Bremner, J.M., Willis, J.P., 1993. Mineralogy and geochemistry of the clay fraction of sediments from the Namibian continental margin and the adjacent hinterland. Marine Geology 115, 85–116.

Compton, J.S., Bergh, E.W., 2016. Phosphorite deposits on the Namibian shelf. Marine Geology 380, 290-314.

Compton, J.S., Wigley, R., McMillan, I.K., 2004. Late Cenozoic phosphogenesis on the western shelf of South Africa in the vicinity of the Cape Canyon. Marine Geology 206, 19-40.

Compton, J.S., Wiltshire, J.G., 2009. Terrigenous sediment export from the western margin of South Africa on glacial to interglacial cycles. Marine Geology 266, 212-222.

Dale, D.C., McMillan, I.K., 2003. The rising and falling of the African continent, the rising and falling of global sea-level, and changing shoreline positions through time. Earthyear Journal for Sustainable Development 3, 58–59.

De Wit, M.C.J, Marshall, T.R., Partridge, T.C., 2000. Fluvial deposits and drainage

evolution. In: Partridge, T.C., Maud, R.R. (Eds.), The Cenozoic of Southern Africa. Oxford University Press, New York, pp. 3-18.

Diester-Haass, L., Billups, K., Emeis, K.C., 2005. In search of the late Miocene-early Pliocene "biogenic bloom" in the Atlantic Ocean (Ocean Drilling Program Sites 982, 925 and 1088). Paleoceanography 20, 1-13

Diester-Haass, L., Meyers, P.A., Bickert, T., 2004. Carbonate crash and biogenic bloom in the late Miocene: evidence from ODP sites 1085, 1086 and 1087 in the Cape Basin, southeast Atlantic Ocean. Paleoceanography 19, 1-19.

Diester-Haass, L., Meyers, P.A and Vidal, L. 2002. The late Miocene onset of high productivity in the Benguela Current upwelling system as part of a global pattern. Marine Geology 180, 87-103.

Diester-Haass, L., Meyers, P.A., Rothe, P., 1992. The Benguela Current and associated upwelling on the southwest African margin: a synthesis of the Neogene-Quaternary sedimentary record at DSDP sites 362 and 532. In: Summerhayes, C.P., Prell, W.L., Emeis, K.C. (Eds.), Upwelling Systems: Evolution since the Early Miocene. Geological Society of London. Special Publication 64, 331-342.

Dingle, R.V., McMillan, I.K., Majoran, S., Bisset, L. 2001., Palaeo-oceanographical implications of Early-Middle Miocene subtropical ostracod faunas from the continental shelf of the SE Atlantic Ocean. Palaeogeography, Palaeoclimatology, Palaeoecology 173, 43-60.

Dingle, R.V., Siesser, W.G., Newton, A.R., 1983. Mesozoic and Tertiary Geology of Southern Africa. A.A. Balkema, Rotterdam, 375 pp.

Dowsett, H.J., Poore, R.Z., 1991. Pliocene sea surface temperatures of the North Atlantic Ocean at 3.0 Ma. In: Cronin, T.M and Dowsett, H.J. (Eds.), Pliocene Climates. Quaternary Science Reviews 10, 189-204.

Drinia, H., Antonarakou, A., Tsaparas, N., Dermitzakis, M.D., 2007. Foraminiferal stratigraphy and palaeoecological implications in turbidite-like deposits from the Early Tortonian (Late Miocene) of Greece. Journal of Micropalaeontology 26, 145-158.

Fisher, R.A., Corbet, A.S., Williams, C.B., 1943. The relationship between the number of species and the number of individuals in a random sample of an animal population. Journal of Animal Ecology 12, 42–58.

Gallagher, S.J., Smith. A.J., Jonasson, K., Wallace, M.W., Holdgate, G.R., Daniels. J., Taylor, D. 2001., The Miocene palaeoenvironmental and palaeoceanographic evolution of the Gippsland Basin, Southeast Australia: a record of Southern Ocean change. Palaeogeography, Palaeoclimatology, Palaeoecology 172, 53-80.

Glacon, G., Grazzini, C.V., Iaccarino, S., Rehault, J.P., Randrianasolo, A., Sierro, J.F., Weaver, P., Channell, J., Torii, M., Hawthorne, T., 1990. 27. Planktonic foraminifera; events and stable isotope records in the upper Miocene, site 6541. In: Kastens, K.A., Mascle, J., et al., (Eds.) Proceedings of the Ocean Drilling Program, Scientific Results 107, 415-427.

Gorgas, T.J., Wilkens, R.H., 2002. Sedimentation rates of SW Africa since the late Miocene deciphered from spectral

analyses of borehole and GRA bulk density profiles: ODP Sites 1081-1084. Marine Geology 180, 29-47.

Hammer, Ø., Harper, D.A.T., Ryan, P.D., 2001. PAST: paleontological statistics software package for education and data analysis. Palaeontologia Electronica, 4. 9 pp. (http://palaeo-electronica.org/2001_1/past/issue1_01.htm).

Hay, W.W., Sibuet, J.C., Barron, E.J., Brassell, S.C., Dean, W.E., Huc, A.Y., Keating, B.H., McNulty, C.L., Meyers, P.A., Nohara, M., Schallreuter, R.E.L., Steinmetz, J.C., Stow, D.A.V., Stradner, H., Boyce, R.E., Amidei, R. 1984. Initial Reports of the Deep Sea Drilling Project, volume 75. U.S. Government Printing Office, Washington, D.C., 1303 pp.

Heinrich, S., Zonneveld, K.A., Bickert, T., Willems, H. 2011. The Benguela upwelling related to the Miocene cooling events and the development of the Antarctic Circumpolar Current: Evidence from calcareous dinoflagellate cysts. Paleoceanography 26, PA3209, doi:10.1029/2010PA002065.

Herbert, C., Compton, J.S., 2007. Geochronology of Holocene sediments on the western margin of South Africa. South African Journal of Geology 110, 327-338.

Hoetzel, S., Dupont, L.M., Marret, F., Jung, G., Wefer, G., 2017. Steps in the intensification of Benguela upwelling over the Walvis Ridge during Miocene and Pliocene. International Journal of Earth Sciences 106, 171-183.

Hoetzel. S., Dupont, L.M., Wefer, G., 2015. Miocene-Pliocene vegetation change in south-western Africa (ODP Site 1081, offshore Namibia). Palaeogeography, Palaeoclimatology, Palaeoecology 423, 102-108.

Holbourn, A., Henderson, A.S., MacLeod, N., 2013. Atlas of Benthic Foraminifera. Wiley-Blackwell, Oxford, 654 pp.

Jorissen, F.J., de Stigter, H.C., Widmark, J.G., 1995. A conceptual model explaining benthic foraminiferal microhabitats. Marine Micropaleontology, 26: 3-15.

Jorissen, F.J., Fontanier, C., Thomas, E., 2007. Paleoceanographical proxies based on deep-sea benthic foraminiferal assemblage characteristics. In: Hillaire-Marcel, C and De Vernal, A., (Eds.) Proxies in late Cenozoic Paleoceanography. Developments in Marine Geology. Elsevier, New York, 263-325.

Kaiho, K., 1994. Benthic foraminiferal dissolved-oxygen index and dissolved-oxygen levels in the modern ocean. Geology 22, 719-722.

Keller, G., Barron, J.A., 1987. Paleodepth distribution of Neogene deep-sea hiatuses. Paleoceanography 2, 697-713.

Kender, S., Kaminski, M.A., Jones, R.W., 2008. Early to middle Miocene foraminifera from the deep-sea Congo Fan, offshore Angola. Micropalaeontology 54, 477-568.

Kennett, J.P., Srinivasan, M.S., 1983. Neogene Planktonic Foraminifera. A Phylogenetic Atlas. Hutchinson Ross, Stroudsburg, 265 pp.

Kucera, M., 2007. Planktonic foraminifera as tracers of past oceanic conditions. In: Hillaire-Marccel, C and de Vernal, A (Eds.). Proxies in Late Cenozoic Paleoceanography. Elsevier, Amsterdam, pp. 213-262.

Kucera, M., Schönfeld, J., 2007. The origin of modern oceanic foraminiferal faunas and

Neogene climate change. Deep-Time Perspectives on Climate Change: Marrying the Signal from Computer Models and Biological Proxies. London: The Geological Society, 409-426.

Lange, C. B., Berger, W.H., Lin, H-L., Wefer, G., 1999. The early Matuyama diatom maximum off SW Africa, Benguela Current System (ODP Leg 175). Marine Geology 161, 93–114.

Leiter, C., Altenbach, A.V., 2010. Benthic foraminifera from the diatomaceous mud belt off Namibia: characteristic species for severe anoxia. Palaeontologica Africana 13(2), 11A, 19p.

Li, Q., McGowran, B., 1994. Miocene upwelling events: neritic foraminiferal evidence from southern Australia. Australian Journal of Earth Sciences 41, 593-603.

Lombard, F., Labeyrie, L., Michel, E., Spero, H.J., Lea, D. W., 2009. Modelling the temperature dependent growth rates of planktic foraminifera. Marine Micropaleontology 70, 1-7.

Lutjeharms, J. R. E., Meeuwis, J.M., 1987. The extent and variability of south-east Atlantic upwelling. South African Journal of Marine Science 5, 51–62.

Lutjeharms, J.R.E., Stockton, P.L., 1987. Kinematics of the upwelling front off Southern Africa. In: Payne, A.I.L., Gulland, J.A and Brink, K.H. (Eds.), The Benguela and Comparable Ecosystems. South African Journal of Marine Science 5 35-49.

Lutze, G.F., Coulbourn, W.T., 1984. Recent benthic foraminifera from the continental margin of northwest Africa: community structure and distribution. Marine Micropaleontology 8, 361-401.

Marlow, J. R., Lange, C.B., Wefer, G., Rosell-Mele, A., 2000. Upwelling intensification as part of the Pliocene-Pleistocene climate transition. Science 290, 2288–2291.

Meyers, P.A., Berger, W.H., Wefer, G., Adams, D., Anderson, L., Andreasen, D., Bruchert, V., Cambray, H., Christensen, B., Frost, G., Giraudeaeu, J., Gorgas, T., Hermelin, O., Jansen, F., Lange, C.B., Laser, B., Lin, H-L., Maslin, M.A., Meyers, P., Motoyama, I., Murray, R., Perez, M.E., Pufahl, P., Richter, C., Spiess, V., Vidal, L., Wigley, R., Yamazaki, T., 1998. Microbial gases in sediments from the southwest African margin. In: Wefer, G., Berger, W.H., Richter, C. et al. (Eds.), Proceedings of the Ocean Drilling Program. Initial Reports, 175. Ocean Drilling program, College Station, TX, pp. 555–560.

Miller, K.G., Kominz, M.A., Browning, J.V., Wright, J.D., Mountain, G.S., Katz, M.E., Sugarman, P.J., Cramer, B.S., Christie-Blick,N., Pekar, S.F., 2005. The Phanerozoic record of global sea-level change. Science 310, 1293-1298.

Moroshkin, K.V., Bubnov, V.A., Bulatov, R.P., 1970. Water circulation in the Eastern South Atlantic Ocean. Oceanology 10, 27-37.

Murray, J.W., 1976. A method of determining proximity of marginal seas to an ocean. Marine Geology 22, 103-119.

Murray, J.W., 1991. Ecology and palaeoecology of benthic foraminifera. Longman, Harlow, 397 pp.

Nguyen, T.M.P., Petrizzo, M.R., Speijer, R.P., 2009. Experimental dissolution of a fossil foraminiferal assemblage (Paleocene–

Eocene Thermal Maximum, Dababiya, Egypt): implications for paleoenvironmental reconstructions. Marine Micropaleontology 73, 241-258.

Ohta, S., Kaiho, K., Takei, T., 2003. Relationship between surface-water temperature and ice-sheet expansion during the Middle Miocene. Palaeogeography, Palaeoclimatology, Palaeoecology 201, 307-320.

Pagani, M., Arthur, M.A., Freeman, K.H., 1999. Miocene evolution of atmospheric carbon dioxide. Paleoceanography 14, 273-292.

Pérez-Asensio, J.N., Aguirre, J., Schmiedl, G and Civis, J. 2012. Messinian paleoenvironmental evolution in the lower Guadalquivir Basin (SW Spain) based on benthic foraminifera. Palaeogeography, Palaeoclimatology, Palaeoecology 326, 135-151.

Pether, J., Roberts, D.L and Ward, J.D., 2000. Deposits of the West Coast. In: Partridge, T.C., Maud, R.R. (Eds.), The Cenozoic of Southern Africa. Oxford University Press, New York, pp. 33-54.

Reolid, M., Rodríguez-Tovar, F.J., Nagy, J., Olóriz, F., 2008. Benthic foraminiferal morphogroups of mid to outer shelf environments of the Late Jurassic (Prebetic Zone, southern Spain): characterization of biofacies and environmental significance. Palaeogeography, Palaeoclimatology, Palaeoecology 261, 280-299.

Robert, C., Diester-Haass, L., Paturel, J., 2005. Clay mineral assemblages, siliciclastic input and paleoproductivity at ODP Site 1085 off Southwest Africa: a late Miocene-early Pliocene history of Orange river discharges and Benguela current activity, and their relation to global sea level change. Marine Geology., 216: 221-238.

Rogers, J. 1977., Sedimentation on the continental margin off the Orange River and the Namib Desert. Unpublished PhD. thesis, University of Cape Town.

Romero, O.E., Crosta, X., Kim, J-H., Pichevin, L., Crespin, J., 2015. Rapid longitudinal migrations of the filament front off Namibia (SE Atlantic) during the past 70 kyr. Global and Planetary Change 125, 1-12.

Schmiedl, G., 1995. Rekonstruktion der spätquartären Tiefenwasserzirkulation und Produktivität im östlichen Südatlantik anhand von benthischen Foraminiferenvergesellschaftungen / Late Quaternary benthic foraminiferal assemblages from the eastern South Atlantic Ocean: reconstruction of deep water circulation and productivity changes. Berichte zur Polarforschung (Reports on Polar Research) 160, 207 pp.

Schmiedl, G., Mackensen, A., 1997. Late Quaternary paleoproductivity and deep water circulation in the eastern South Atlantic Ocean: evidence from benthic foraminifera. Palaeogeography. Palaeoclimatology. Palaeoecology 130, 43-80.

Schmiedl, G., Mackensen, A., Müller, P.J., 1997. Recent benthic foraminifera from the eastern South Atlantic Ocean: dependence on food supply and water masses. Marine Micropaleontology 32, 249-287.

Shannon C.E. 1948. A mathematical theory of communication. The Bell System Technical Journal. 27, 379-423, 623-656

Shannon, L.V., Nelson, G., 1996. The Benguela: Large Scale Features and Processes and System Variability. In:Wefer, G., Berger,W.H., Siedler, G.,Webb, D.J. (Eds.), The South Atlantic: Present and Past Circulation. Springer-Verlag, Berlin Heidelberg, pp. 163–210.

Siesser, W.G., 1980. Late Miocene origin of the Benguela Upwelling System off Northern Namibia. Science 208 (4441), 283-285.

Van der Zwaan, G. J., Jorissen, F.J., de Stigter, H.C., 1990. The depth dependency of planktonic/benthic foraminiferal ratios: constraints and applications. Marine Geology 95, 1-16.

Wade, B.S., Pearson, P.N., Berggren, W.A., Pälike, H., 2011. Review and revision of Cenozoic tropical planktonic foraminiferal biostratigraphy and calibration to the geomagnetic polarity and astronomical time scale. Earth-Science Reviews 104, 111-142.

Wefer, G., Berger, W.H., Richter, C., Adams, D.D., Anderon, L.D., Andreasen, D.J., Brüchert, V., Cambray, H., Christensen, B.A., Frost, G.M., Giraudeau., Gorgas, T.J., Hermelin, O., Lange, C.B., Laser, B., Lin, H-L., Maslin, M., Meyers, P.A., Motoyama, I., Murray, R.W., Pato, D., Perez, M.E., Pufahl, P.K., Spiess, V., Vidal. L., Wigley, R., Yamazaki, T. 1998. Proceedings of the Ocean Drilling Programme, Initial Reports. Ocean Drilling Program. College Station, TX, pp. 385-428.

Wigley, R.A., Compton, J.S., 2006. Late Cenozoic evolution of the outer continental shelf at the head of the Cape Canyon, South Africa. Marine Geology 226, 1-23.

Wigley, R.A., Compton, J.S., 2007. Oligocene to Holocene glauconite–phosphorite grains from the Head of the Cape Canyon on the western margin of South Africa. Deep Sea Research Part II: Topical Studies in Oceanography 54, 1375–1395.

Chapter 6

Quaternary Foraminifera and Mollusc Assemblages from the Middle to Outer Shelf of Namibia

6. Quaternary foraminifera and mollusc assemblages from the middle to outer shelf of Namibia

Abstract

Foraminifera and mollusc fossil assemblages from the Namibian shelf are compared to assemblages from the South African shelf to determine the distribution of species during the Quaternary, a period in which the Benguela Upwelling System (BUS) intensified. The foraminiferal associations differ in each stratigraphic unit in the Walvis Bay-Lüderitz cores. On the shelf an *Uvigerina* spp.-dominated early Pleistocene association replaced deeper water Mio-Pliocene assemblages during the initiation of cold-water upwelling of the BUS. The palaeoenvironment further experienced shoaling during the middle to late Pleistocene as shallow water benthic foraminifera, dominated by *Ammonia beccarii* and *Elphidium* spp. replaced the *Uvigerina* spp.-dominated assemblage and *Carditella* spp., *Lucinoma capensis, Nassarius vinctus, Dosinia lupinus* and *Tellina analogica* became the dominant mollusc species on the shelf. These benthic foraminifera and molluscs indicate widespread inner shelf and marginal marine influences on the middle and outer shelf throughout the Pleistocene as the amplitude of sea-level fluctuations increased. The planktic foraminifera show similarities with other upwelling regions in the world with *Globigerina bulloides* being the dominant species. Warm water species such as *Globigerinoides ruber, Globorotalia menardii* and *Trilobatus sacculifer* occur as minor to trace components attributed to the inflow of warm water currents to the north and south of the region.

6.1. Introduction

The sediments underlying the Benguela Upwelling System (BUS) are enriched in organic carbon (Pedersen and Calvert, 1990; Shannon and Nelson, 1996; Mollenhauer et al., 2002, 2003), with sediment deposition on the continental margin during the Pleistocene being influenced by high-amplitude sea-level fluctuations during glacial-interglacial stages (Diester-Haass et al., 1992; Mollenhauer et al., 2002; Compton and Wiltshire, 2009).

Namibian shelf sediments are phosphorite-rich (Compton and Bergh, 2016) and the high productivity of the system has contributed to a high abundance of biogenic material (foraminifera, molluscs, ostracods, fish remains) on the continental shelf, which is important in palaeoenvironmental and geologic studies. How Pleistocene sea level fluctuations have influenced the microfossil and fossil (mainly molluscs) assemblages on the Namibian shelf have previously not been investigated. Characterising these assemblages can potentially provide a biostratigraphic reference to the different stages of the Pleistocene along the shelf. Previous studies (Table 6.1) on surface grab samples (Lowry, 1987) focussed on the occurrences of species around the Namibian and South African coast, but, because limited to surface samples, did not allow for palaeoceanographic reconstructions of the BUS. Core sediments and foraminifera of the Namibian outer shelf have also not received much attention prior to the study of Compton and Bergh (2016).

Table 6.1. Previous studies from onshore western South Africa and the western continental shelf of southern Africa documenting Neogene to Quaternary foraminifera relevant to this chapter

Study	Location of study area	Age of sediments or foraminifera	Use of foraminifera in study
Martin, 1974	Southern Namibian continental shelf	Recent (surface grab samples)	Palaeoenvironmental
Martin, 1981	Southern Namibian continental shelf	Recent (surface grab samples)	Palaeoenvironmental
Lowry, 1987	Continental margin from northern Namibia, South Africa and southern Mozambique	Recent (surface grab samples)	Taxonomic
McMillan, 1987a	Inner southernmost continental shelf of Namibia	Late Quaternary	Taxonomic
McMillan, 1987b	Southern African coast	Quaternary	Potential as stratigraphic indicators
McMillan, 1990b	Onshore sediments Cape Town, South Africa	Pleistocene	Stratigraphic indicators and palaeoenvironmental
Giraudeau, 1993	Continental margin of Namibia and western South Africa	Recent (surface grab samples)	Palaeoceanographic (planktic foraminifera)
Dale and McMillan, 1998	Inner to middle continental shelf of northwestern South Africa and Sierra Leone (West Africa)	Holocene	Environmental
Dale and McMillan, 1999	Onshore west coast of South Africa (Saldanha region)	Quaternary	Stratigraphic indicators and palaeoenvironmental classification
Compton et al., 2002	Northwestern continental shelf South Africa	Holocene	Stratigraphic indicators
Compton et al., 2004	Outer continental shelf of South Africa north of the Cape Canyon	Quaternary	Stratigraphic indicators
Diester-Haass et al., 2004	Western continental slope of South Africa	Late Miocene	Palaeoceanographic (Palaeoproductivity)
Diester-Haass et al., 2005	Northern continental slope of Namibia and western South Africa	Late Miocene	Palaeoceanographic (Palaeoproductivity)
Franceschini et al., 2005	Southwest coast of South Africa	Late Quaternary	Palaeoenvironmental
Wigley and Compton, 2006	Outer continental shelf of South Africa north of the Cape Canyon	Neogene to Quaternary	Stratigraphic indicators
Franceschini and Compton, 2007	Southwest coast of South Africa	Holocene	Taphonomic and palaeoenvironmental
Schmidt-Sinns, 2008	Continental shelf of Namibia and western South Africa	Recent (surface grab samples)	Palaeoenvironmental
Leiter and Altenbach, 2010	Central Namibian inner to middle continental shelf	Recent (surface grab samples)	Environmental
Compton and Bergh 2016 (as part of this study)	Outer continental shelf of Namibia	Neogene to Quaternary	Stratigraphic indicators
Bergh et al., 2018 (as part of this study)	Outer continental shelf of Namibia	Neogene to Quaternary	Palaeoenvironmental

Samples from Deep Sea Drilling Program (DSDP) (Hay et al., 1984) and Ocean Drilling Program (ODP) (Wefer et al., 1998) cores allowed for the interpretation of palaeoceanographic and assemblage changes over time with much of the research on the Pleistocene history of the BUS being focused on slope sediments along the southwestern margin of Africa. These slope sediments have been studied to determine sediment deposition (Diester-Haass and Rothe, 1987; Robinson et al., 2002), upwelling intensity (Baumann and Freitag, 2004) and productivity (Schmiedl and Mackensen, 1997; Marlow et al., 2000; Rau et al., 2002; Jahn et al., 2003; Baumann and Freitag, 2004; Lazarus et al., 2008).

Understanding the distributions of foraminifera on the shelf is important in biostratigraphy and in the interpretation of depositional environments, as these studies also aid in the mineral exploration industries and in understanding geological processes (Franceschini et al., 2005). South African shelf foraminifera were used to determine the stratigraphy of sediments and their associated palaeoenvironments from the Miocene to Holocene (Dale and McMillan, 1999; Compton et al., 2002, 2004; Franceschini and Compton, 2004). More recent work involving foraminifera on the Namibian shelf included the occurrence of foraminifera in anoxic environments along the Namibian margin (Leiter and Altenbach, 2010) and the biostratigraphy (Compton and Bergh, 2016; Bergh et al., 2018) of shelf sediments. Compton and Bergh (2016) provided detailed analyses on the stratigraphy, formation and geochemistry of the phosphorites on the Namibian shelf and included species lists of foraminifera and molluscs to support the strontium isotope stratigraphy and age model of the sediments.

This chapter aims to identify any potential foraminiferal assemblages in Quaternary sediments from the Namibian shelf and to document how these microfossil and mollusc assemblages were influenced during Pleistocene sea level fluctuations. In this chapter the regional distribution of foraminifera and molluscs is also discussed to elucidate whether controlling factors were widespread along the margin during the Quaternary.

6.2. Materials and Methods

Twenty vibracores less than 2 m in length from the continental shelf between the Walvis Bay-Lüderitz (16 cores) and northern Namibian shelf (4 cores) (Fig. 6.1) were retrieved by Minemakers Pty. Ltd. in 2008 and 2012, respectively. These cores were logged and split into working and archive halves. The Walvis Bay-Lüderitz cores consist of two clusters, namely the Conception and Meob Bay clusters (Fig. 6.1). The cores were sampled along depth intervals where contacts were clear and every 10 to 20 cm where units were greater than 10 cm thick. Samples selected at contacts allowed for any environmental changes to be tested for during different time intervals. The samples were washed, sieved and split into <63 μm (mud), 63 μm to 2 mm (sand) and >2 mm (gravel) fractions. The sand fractions were put in an ultrasonic cleaner for up to 1 minute to ensure all particles are disaggregated. Five cores, based on the completeness of their stratigraphy and length of record, were selected from the shallow middle (core 1307 – 199 m; core 1441 – 223 m), shallow outer (core 1401 – 244 m; core 1479 – 245 m) and deep outer shelf (core 1406 – 309 m).

Foraminifera (from the sand samples) and molluscs (from the gravel fractions) were identified in all sixteen cores. Foraminifera, other biogenic and minerogenic components in the five selected cores were counted under a stereo microscope to at least 300 individuals per sample to determine the dominant taxa (highest relative abundance) on which palaeoenvironmental interpretations rely upon. Foraminifera were counted in representative splits if individuals accounted for more than 300 in the samples. Where foraminifera were less abundant all individuals were counted in the entire sample. The mean relative abundances of the biogenic and minerogenic components, reported as %, were calculated from these counts.

Whole mollusc shells and fragments were counted. Intact bivalve shells, and where complete shells were present and matched another shell, it was counted as one individual. Complete intact bivalve shells and complete gastropod shells may give an indication of minimal transport. Fragments were identified based on a part of a shell that is broken or where multiple fragments were present. Only fragments that could be attributed to certain species were assigned to that species.

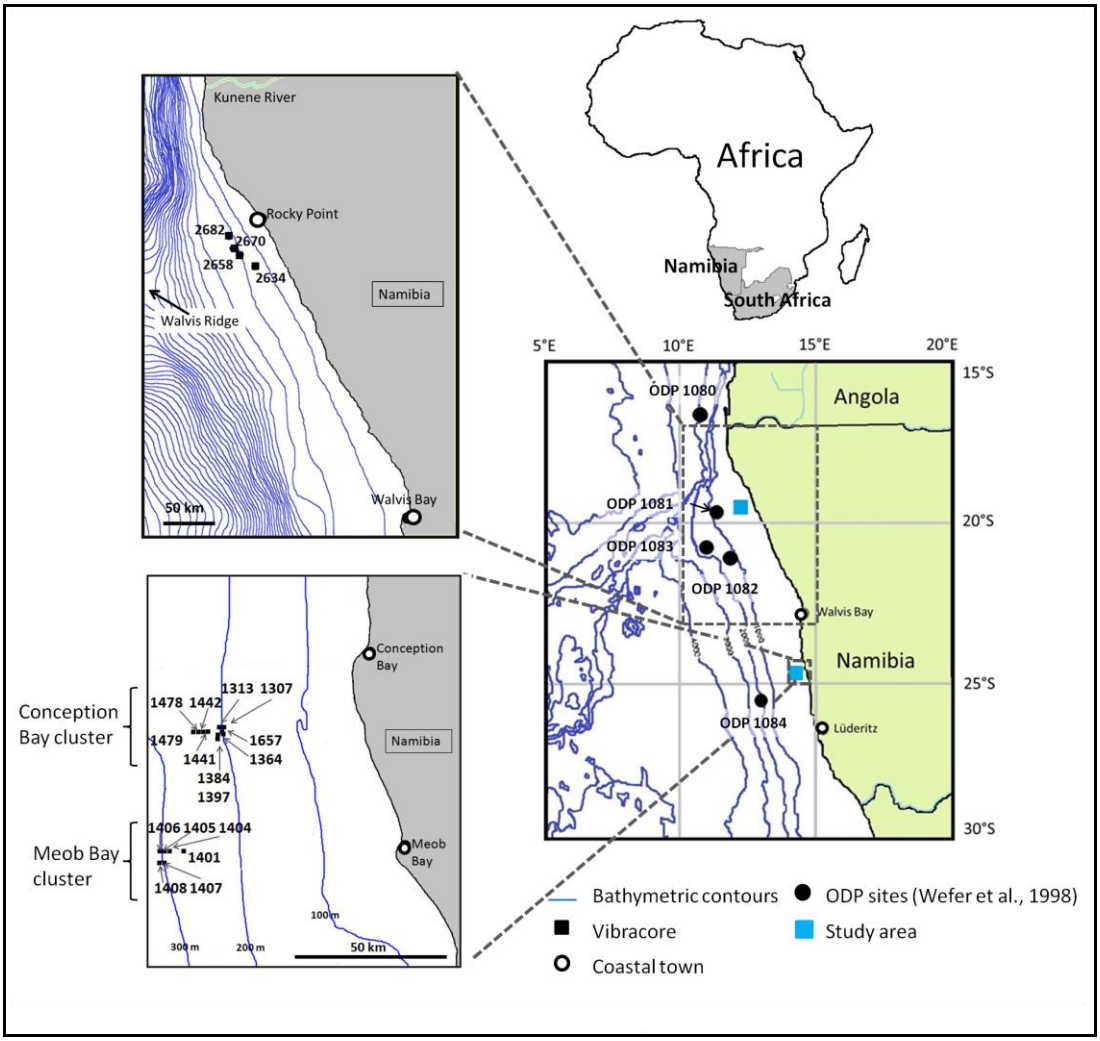

Fig. 6.1. Outline of Namibia and South Africa with the location of the cores studied. The intervals for the bathymetric lines in the upper left map are 100 m (based on maps provided by Minemakers Australia Pty. Ltd.).

The core lithology was discussed in Compton and Bergh (2016) revealing an overall coarsening upward succession (Fig. 6.2). Cores 1405, 1408 and 1406 consist of a basal olive-green mud unit grading into coarser sandy units with biogenic and authigenic grains towards the top of the cores. Six units were identified in the Walvis Bay-Lüderitz cores (Compton and Bergh, 2016). Units 6 and 5 are olive green mud units with abundant fragmented foraminifera dated to the Pliocene. Unit 4 is a black to leached brown pelletal phosphorite sandy unit (Fig. 6.3). Unit 3 is a slightly shelly sandy unit whereas unit 2 is a shelly sandy unit that contains abundant shell. Gravel components (large bone fragments, phosphorite pebbles and concretionary phosphorites) result in units 5 to 2 having coarser grain sizes in some cores. Unit 1 is a sandy gravel unit containing abundant shell fragments, whole mollusc shells and foraminifera.

Representative microfossils were picked for scanning electron microscope (SEM) imaging. The microfossils were mounted onto black adhesive carbon tabs and coated with a thin layer of Gold-Palladium using a BIO-RAD SEM coating system before SEM images were taken with a JEOL JSM-5200 scanning microscope at Iziko Museums in Cape Town.

The age model for the cores was based on a combination of strontium isotope stratigraphy (SIS) and biostragraphic planktic foraminiferal indicator species (Compton and Bergh, 2016; Bergh et al., 2018). The different sand and gravel components (foraminifera, pelletal phosphorite grains, concretionary phosphorite pebbles, fragmented fish bones, teeth, scales and mollusc shell fragments) were previously picked from bulk gravel and sand sized material and run for strontium isotope analysis (Compton and Bergh, 2016). Planktic foraminiferal indicator species were identified based on Bolli et al. (1985) and Kennett and Srinivasan (1983).

Statistical analyses were performed using the PAlaeontologicalSTatistics (PAST) data analysis package (Hammer et al., 2001). Hierarchical cluster analysis was used to estimate similarities in species composition in samples to determine sub-assemblages within the core stratigraphy with Ward's method and Euclidean distance applied.

6.3. Results

6.3.1 Stratigraphy and sedimentology

The sediment composition of the olive-green muds is composed of abundant foraminifera (55-98%) with minor amounts of echinoid spines, shell fragments, fish bone material, ostracods and pelletal phosphorite in intercalated lenses towards the top of the base unit.

With the exception of the mud unit, the pelletal phosphorite content decreases up-core (Fig. 6.3) with a maximum abundance (mean of 88.5%) in the sandy units (unit 4). Shell contents are highest (mean = 12.3%) in the shelly gravel unit (unit 1). Foraminifera are most abundant (mean = 85.4%) in the sand fractions of the olive-green mud unit (unit 5). Above unit 4 the foraminiferal abundance increases upwards and reaches a mean abundance of 12.3% in unit 1.

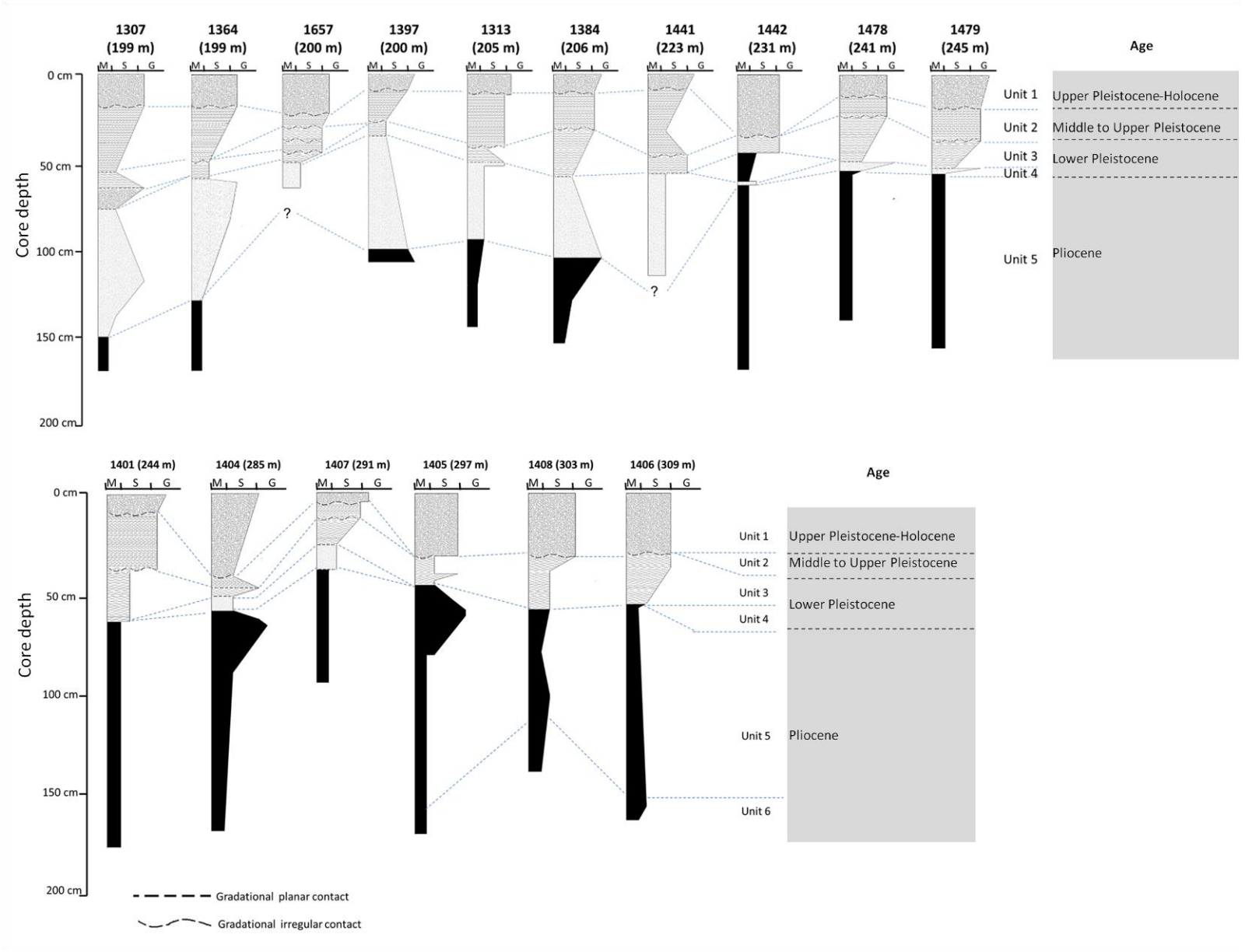

Fig. 6.2. Stratigraphy of the Conception and Meob Bay cores. The depositional ages and units are defined by Compton and Bergh (2016). Unit 6 = reworked foram layer; unit 5 = brown to olive-green mud unit; unit 4 = pelletal phosphorite sandy layer; unit 3 = slightly shelly layer; unit 2 = shelly sandy layer; unit 1 = shelly gravel layer (Compton and Bergh, 2016)

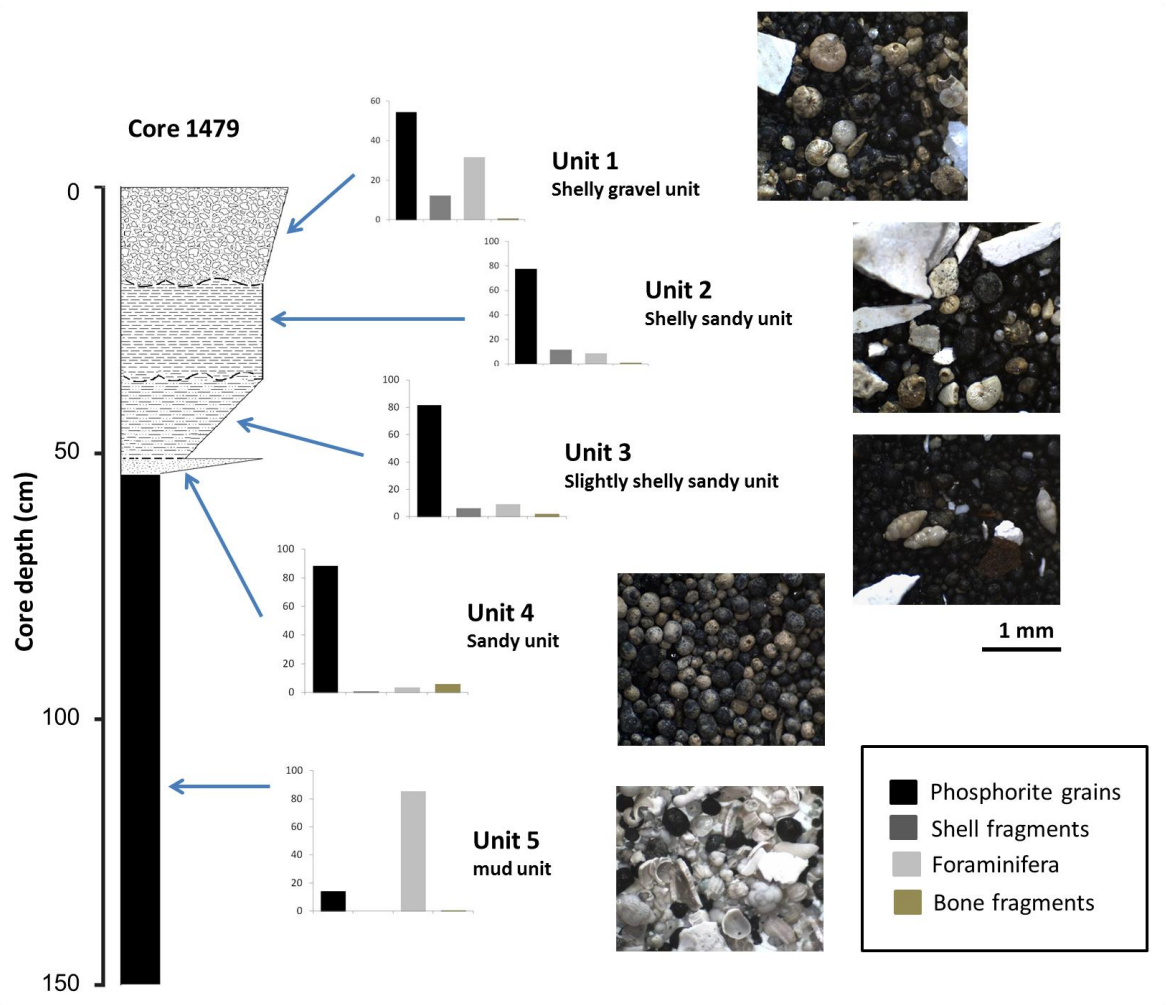

Fig. 6.3. Mean relative abundance (represented by column charts) of the major components within the complete sand fractions of core 1479 and photomicrographs of samples from each unit.

Bone material in the sand fractions comprises a small amount and only attains its highest abundance (mean = 5.8%) in the sandy units (unit 4). Other components remain negligible (<1%) throughout the successions of the cores and include echinoid spines, fish otoliths, sponge spicules, ostracods and bryozoan fragments.

6.3.2 Foraminifera

The most abundant planktic foraminiferal species preserved in all the units is *Globigerina bulloides* decreasing in abundance (Fig. 6.4; Appendix Table B.5) towards the less shelly units. Planktic species *Globorotalia (Globoconella) inflata* and *Globigerinoides ruber* (white) (<2%) have higher abundances in unit 3 relative to units 2 and 1, whereas *Neogloboquadrina incompta* recorded similar abundances across all the units with the highest abundance in unit 3. Other planktic species with low relative abundances (<1%) in both the central Namibian and northern Namibian shelf include *Neogloboquadrina dutertrei* and *Globigerinella siphonifera. Orbulina universa* recorded low numbers (<1%) on the central Namibian shelf, but higher relative abundances on the northern Namibian shelf (<47%).

The pelletal phosphorite sandy unit 4 with more than 80% pelletal phosphorite sand content

generally does not contain foraminifera (Fig. 6.3). Very few foraminifera in the sediments are agglutinated (<1% abundance) and miliolids accounted for <1% of the foraminiferal assemblages in the shelly sandy units (Appendix Tables B.14-15). The classification of biofacies on foraminiferal associations corresponds to sedimentological units of the cores.

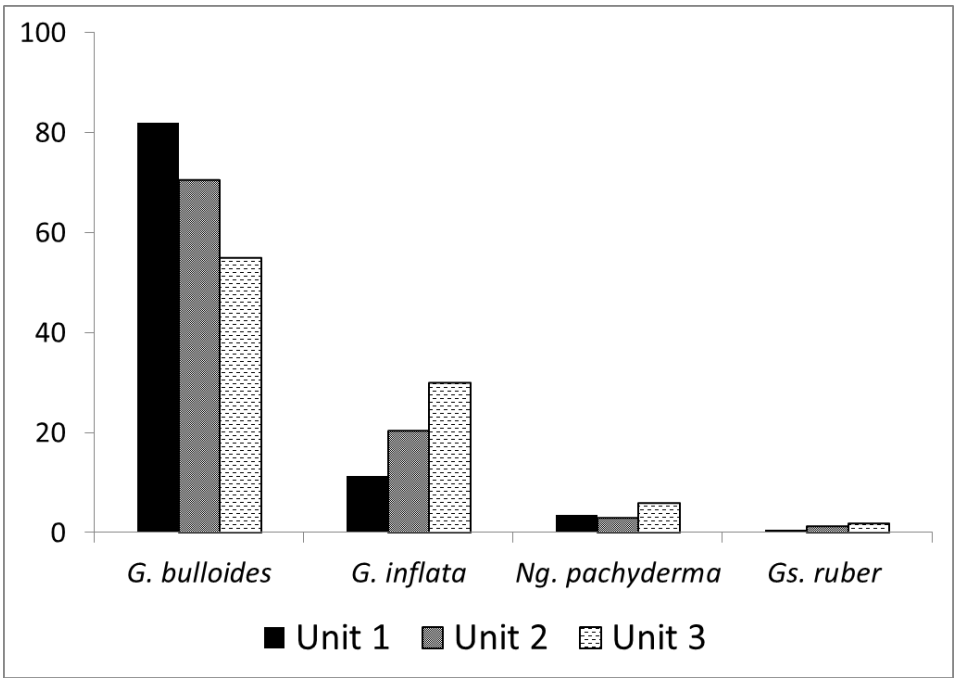

Fig. 6.4. Mean relative abundance of planktic species preserved across the three units of the Walvis Bay-Lüderitz cores. Results plotted as *Ng. pachyderma* includes the right-coiling species *Ng. incompta* as well as the left-coiling species.

Unit 3 recorded higher proportions of *Uvigerina peregrina* with *Cassidulina laevigata* and *Brizalina spathulata* increasing towards the contact between units 3 and 2. Unit 2 still had abundant *Uvigerina* spp. but their relative abundances decreased towards the contact between units 2 and 1, and *Brizalina spathulata* maintained similar abundances (Fig. 6.5). Unit 2 also recorded higher *Elphidium advenum* abundances. Unit 1 is characterised by the dominance of *Ammonia beccarii* and higher relative *Elphidium advenum* abundances.

The dominant species in the upper units of the cores (unit 1 in Walvis Bay-Lüderitz) are *Ammonia beccarii* and *Elphidium* spp. with *Cassidulina laevigata* recording similar relative abundances between the two areas (Appendix Tables B.14-15. Relative abundances for *Lobatula lobatula* are higher (>10%) in the less gravelly units of the northern Namibian cores south of the Kunene River mouth. In the less gravelly units of the northern cores, *Nonion boueanus* recorded abundances of >40%. In the deepest core south of the Kunene River mouth occurrences of *Globobulimina turgida* reach relative abundances >50% (Appendix Tables B.10-13.

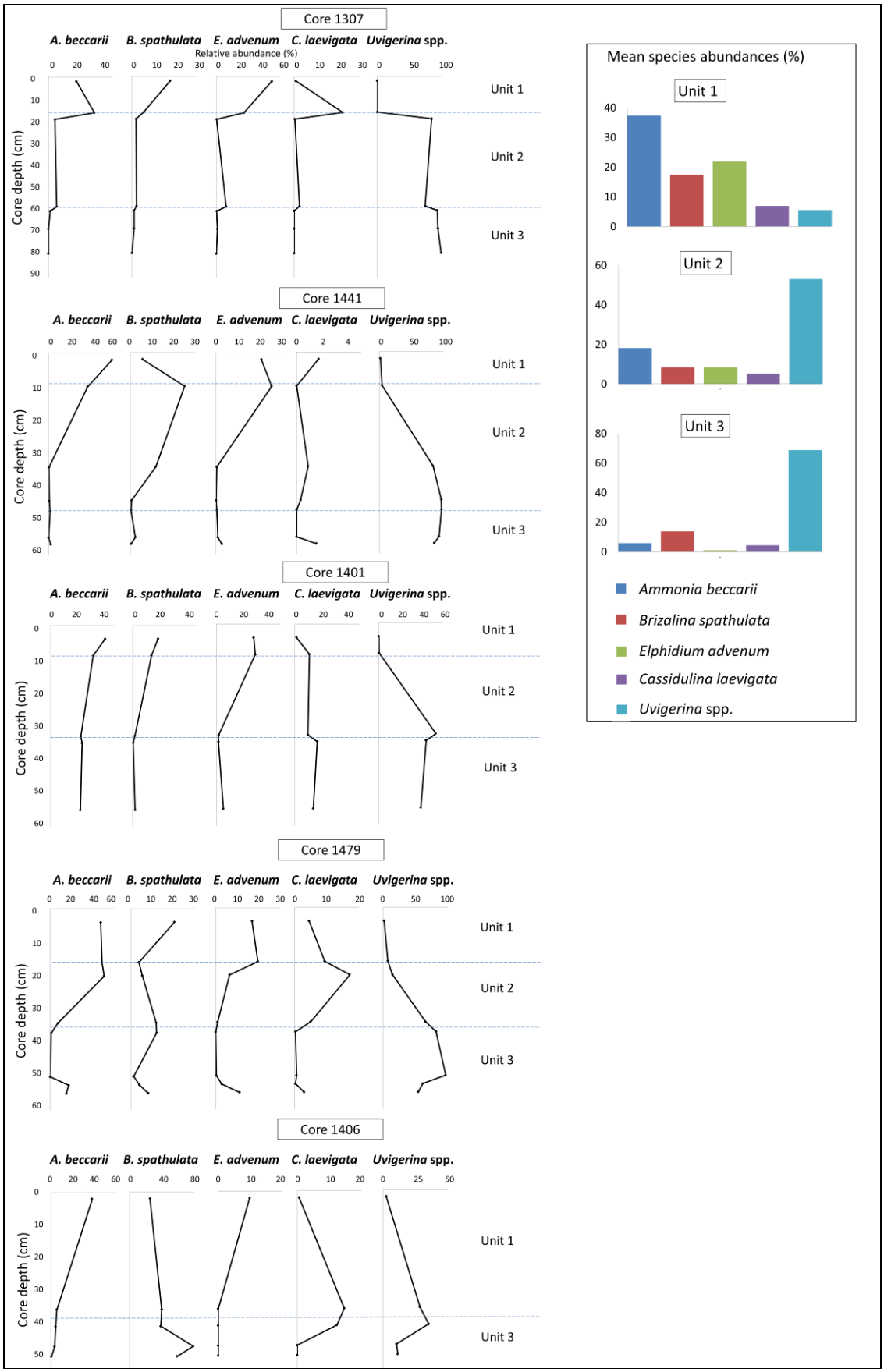

Fig. 6.5. Relative abundances (%) of benthic foraminifera in the shelly sandy units 1-3. Mean relative abundances of the major taxa in each unit over all the cores in which foraminifera was counted are indicated upper right.

Cluster analysis divided the foraminiferal assemblage containing abundant *Uvigerina* spp., *B. spathulata* and *A. beccarii* into three main fossil associations based on their relative abundances. These benthic foraminiferal associations are (1) *Uvigerina* spp., (2) *Uvigerina* spp.-*A. beccarii*-*B. spathulata* and (3) *A. beccarii* (Fig. 6.6).

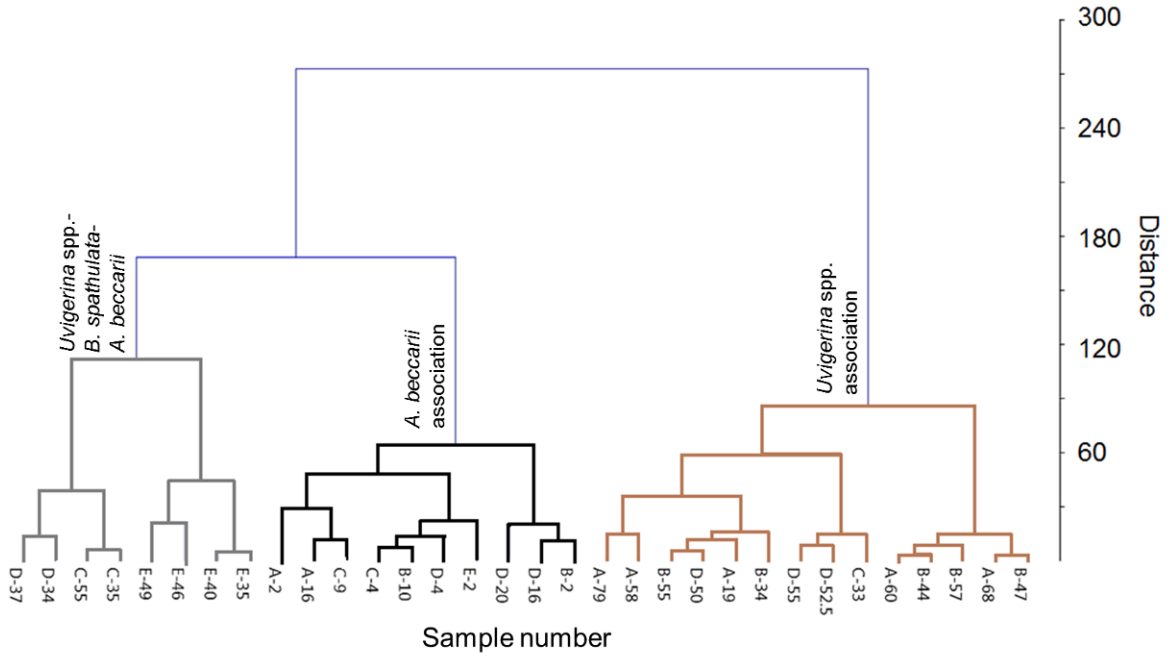

Fig. 6.6. Dendrogram from a hierarchical cluster analysis (Ward's method) based on Euclidean distance as similarity index to determine sub-assemblages. The sample number refers to the core and core depth (in cm). A = core 1307; B = core 1441; C = core 1401; D = core 1479; E = core 1406

6.3.3 Molluscs

The 25 analysed samples from the 5 selected cores yielded a total of 86 whole or near-whole bivalve shells and 110 gastropod shells (Appendix Table B.19-22), which could be assigned to 13 bivalve taxonomic groups (at the genus level at least) and 5 gastropod taxonomic groups (at the genus level at least).

The upper portions of the northern Namibian as well as the Walvis Bay-Lüderitz cores reveal similar dominant mollusc species. The most abundant whole bivalve shells are *Carditella* sp. and *Lucinoma capensis* in unit 2 of the Walvis Bay-Lüderitz cores (Fig. 6.7, 6.8; Appendix Table B.21). *Lucinoma capensis* is the most abundant fragmented shell. The dominant gastropod species throughout all the cores are *Nassarius vinctus* in whole and fragmented forms with *Turritella declivis* only observed in unit 2. *Marginella* spp. are observed in both units of the Walvis Bay-Lüderitz cores (Appendix Table B.22). In unit 2, *Dosinia lupinus* and *Tellina analogica* form a minor component (<10%) in whole and fragmented forms, but increase in relative abundance to become dominant species in unit 1. The bivalve species *Carditella* sp. and *Nucula nucleus* mostly occur as whole shells while *Lucinoma capensis* mostly occurs as fragments in unit 1.

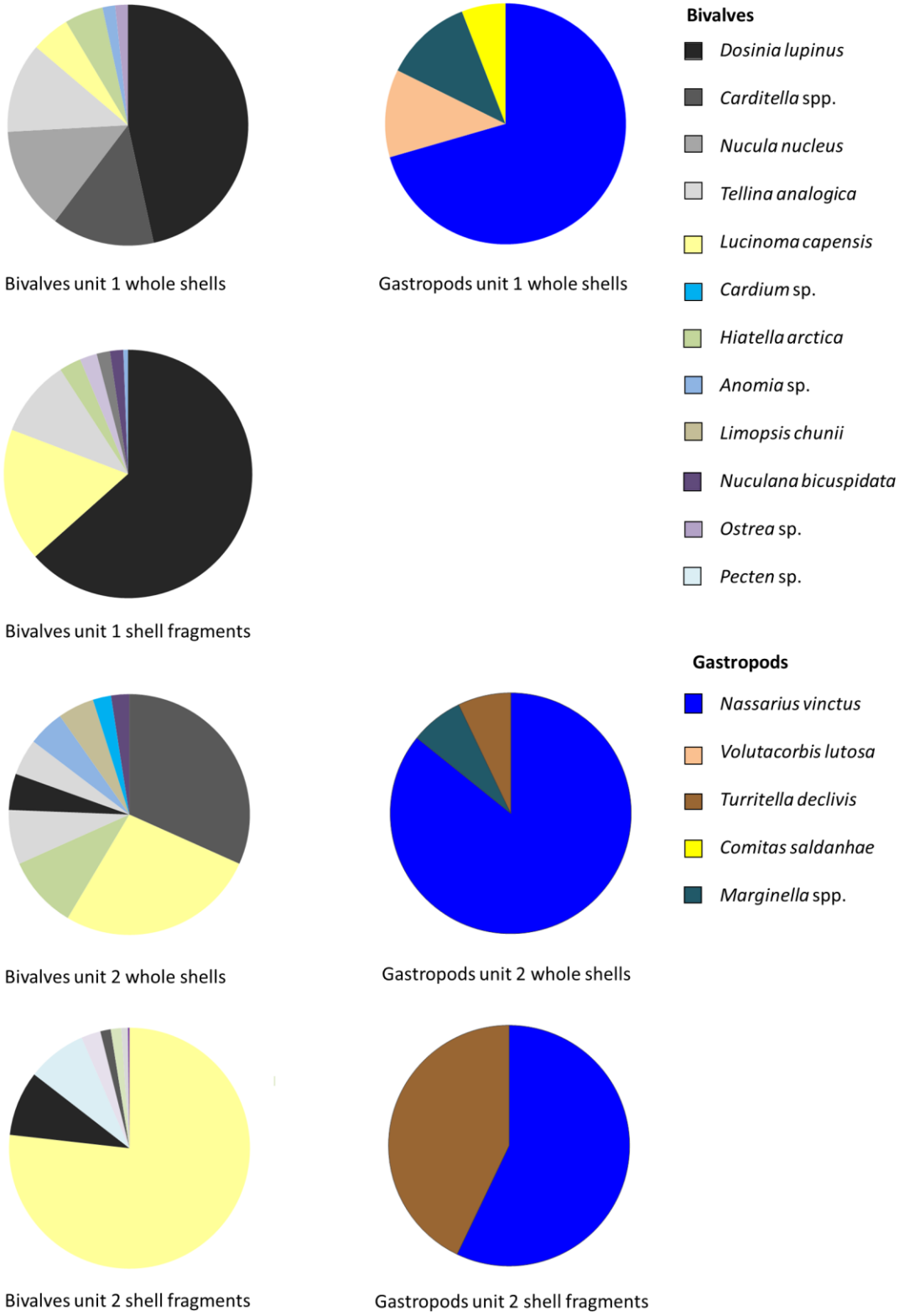

Fig. 6.7. Mean relative abundances of mollusc (bivalves on the left and gastropods on the right) shells in the Walvis Bay-Lüderitz cores

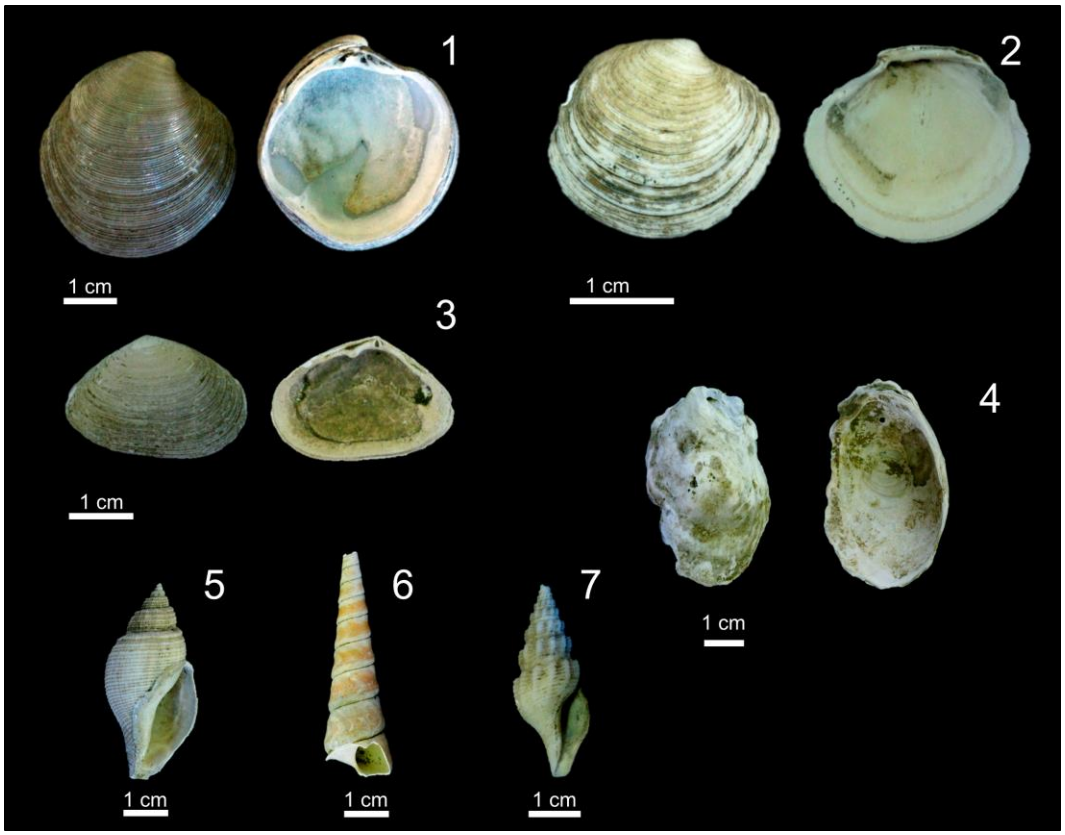

Fig. 6.8. Mollusc shells from the gravel fraction of the uppermost 2 units of the Walvis Bay-Lüderitz cores. 1. *Dosinia lupinus* (Linnaeus, 1758) (core 1407, 0-4 cm sampling interval); 2. *Lucinoma capensis* (Jaeckel and Thiele, 1931) (core 1397, 0-4 cm); 3. *Tellina (Moerella) analogica* (Sowerby III, 1904) (core 1478, 8-12 cm); 4. *Ostrea* sp. (core 1657, 0-4 cm); 5. *Nassarius vinctus* (Marrat, 1877) (core 1407, 0-4 cm); 6. *Turritella declivis* (Adams and Reeve, 1850) (core 1657, 20-24 cm); 7. *Comitas saldanhae* (Barnard, 1958) (core 1307, 0-4 cm).

The bivalve *Pecten* spp. were the only species (in fragmented form; Fig. 6.9) to have been observed in the olive-green mud unit of the northern Namibian cores. The dominant gastropod in the overlying gravelly sandy phosphorite units of the northern Namibian cores is *Nassarius vinctus* throughout, with *Volutacorbis lutosa* and *Comitas saldanhae* present, but in lower numbers (Fig. 6.10). The dominant bivalve species in the layers below the upper 10 cm of the northern Namibian cores are *Lucinoma capensis* and *Tellina analogica* (whole and fragmented). The bivalve species *Dosinia lupinus, Carditella* sp. and *Nuculana bicuspidata* are among the major bivalve components as whole shells, but decrease in the fragmented fraction. In the upper 10 cm of the cores *Dosinia lupinus* and *Tellina analogica* are the dominant bivalves in whole shell form, whereas specimens of *Lucinoma capensis* are more abundant in the fragmented fraction.

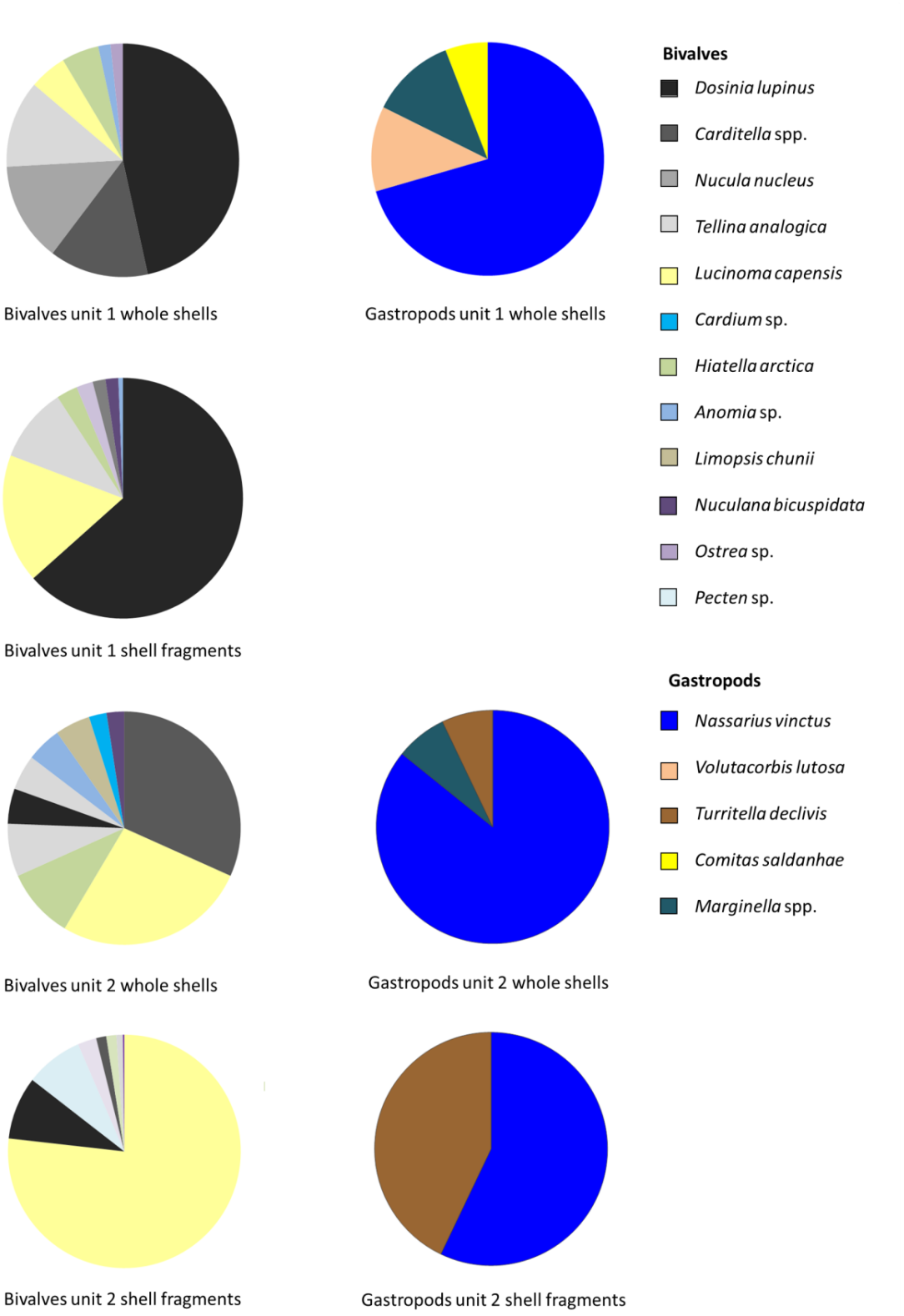

Fig. 6.9. Mean relative abundances of mollusc shells (bivalves on the left and gastropods on the right) in the northern Namibian cores.

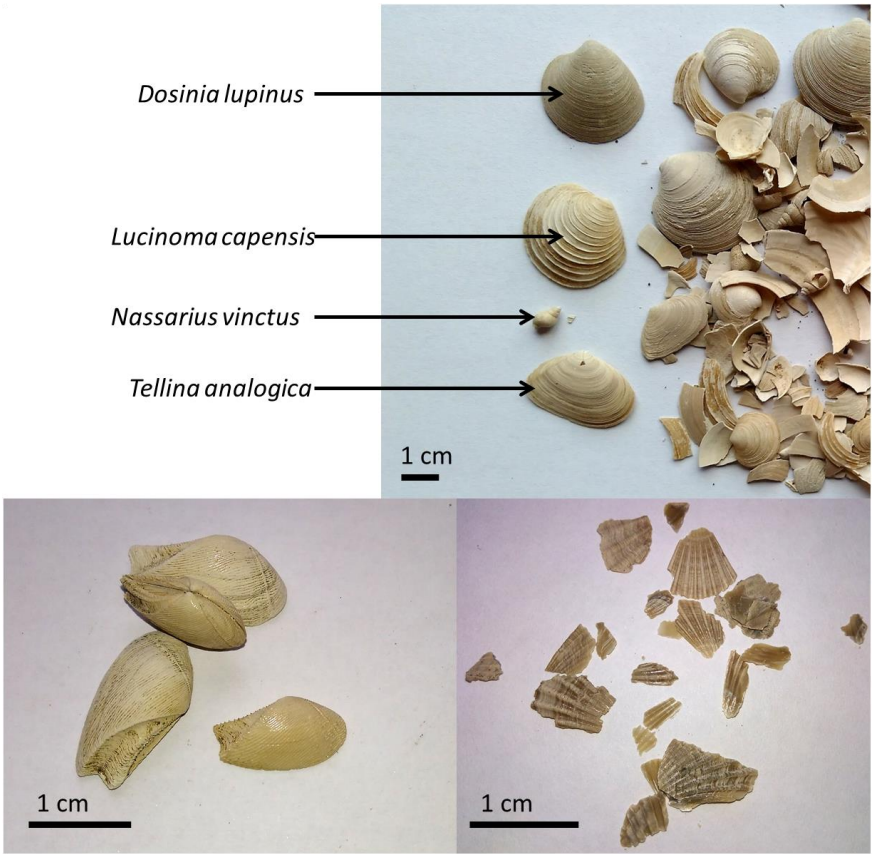

Fig. 6.10. Whole and fragmented shells (top) (core 2658, 10-15 cm sampling interval), *Nuculana bicuspidata* (bottom left) shells including articulated valves (core 2634, 78-85 cm) and *Pecten* spp. fragments (bottom right) (core 2658, 88-90 cm) from the northern Namibian cores.

6.4. Discussion

6.4.1. Biogeography

The most abundant foraminiferal planktic species preserved at the middle to outer shelf depths along the Namibian shelf during the Quaternary are *G. bulloides* and *Gr. (Gc.) inflata* (Fig. 6.11). Low abundances of *Gs. ruber* were recorded for the northern Namibian shelf and the Walvis Bay-Lüderitz region. Along the northern Namibian shelf *Ng. incompta* (previously *Ng. pachyderma* dextral) also occurs in relatively high abundances, specifically in the less shelly units. Previous studies from onshore deposits (Dale and McMillan, 1999; McMillan, 1990a, 1990b) reported few to no planktic tests where Pleistocene environments were shallower than the outer shelf deposits. This marks a progression of increased species diversity and abundances from shallow water environments preserved in onshore deposits to the outer shelf and slope.

Many of the benthic foraminiferal species recorded in this study have wide distributions stretching from the northern Namibian shelf to the south and east coasts of South Africa. These taxa are commonly associated to be cosmopolitan species (Lowry, 1987; and references therein). Two samples collected by Schmiedl (1995) at 173 m (GeoB 1021, southern Angolan shelf) and 250 m water depth (GeoB 1013, central Angolan shelf) reveal

assemblages with similar taxa. The benthic species *Bulimina marginata, Cassidulina laevigata, Lobatula lobatula, Globobulimina turgida* and *Uvigerina peregrina* were recorded at both sites by Schmiedl (1995) while *Ammonia beccarii, Bulimina gibba* and *Elphidium advenum* were found to occur only at the shallower site. Schmidt-Sinns (2008) also found the distribution of taxa on the inner shelf (up to 200 m water depth) to be widespread between Cape Town and southern Angola. The species *Quinqueloculina seminula, Rectuvigerina nicoli, Bulimina elongata, Bulimina gibba, Cancris auriculus, Cassidulina laevigata, Uvigerina peregrina* and *Elphidium advenum* recorded in this study were also found by Schmidt-Sinns (2008) to occur at inner shelf depths (Fig. 6.12 to 6.14).

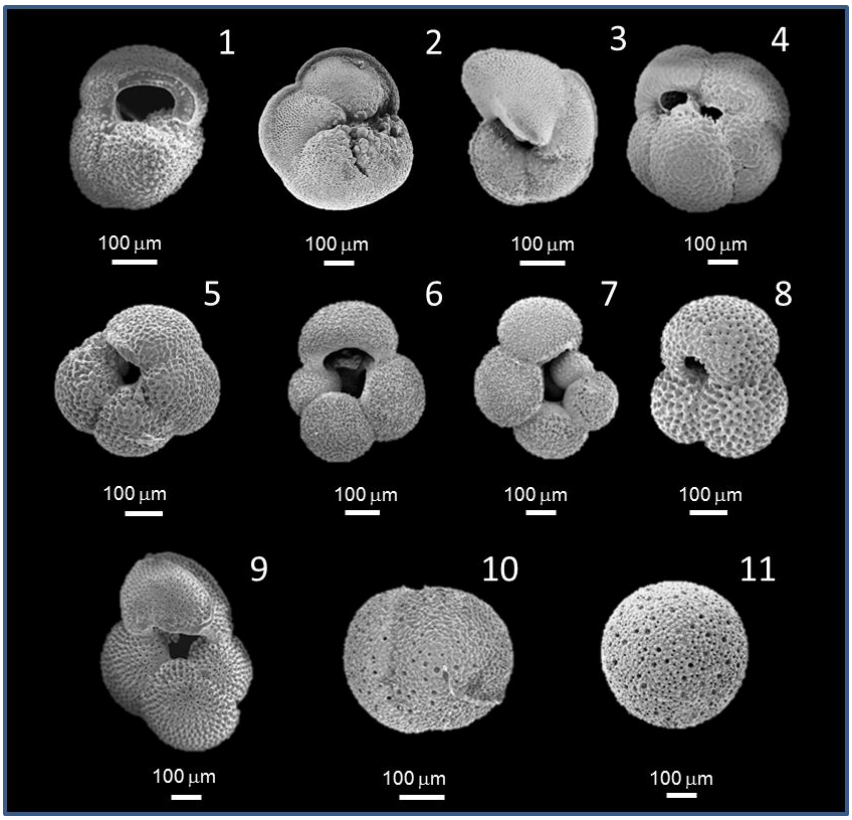

Fig. 6.11. Planktic foraminifera from the Namibian outer shelf with primary apertural views visible. 1. *Globorotalia (Globoconella) inflata* (core 2670, 98 cm); 2. *Globorotalia menardii* (core 2670, 23 cm); 3. *Globorotalia truncatulinoides* (core 2670, 23 cm); 4. *Neogloboquadrina dutertrei* (core 2670, 43 cm); 5. *Neogloboquadrina incompta* (core 2670, 85 cm); 6 *Globigerina bulloides* (core 2670, 85 cm); 7. *Globigerinella siphonifera* (core 2670, 33 cm); 8. *Globigerinoides ruber* (white) (core 2670, 13 cm); 9. *Trilobatus sacculifer* (core 2670, 63 cm); 10. *Orbulina bilobata* (core 2670, 3 cm); 11. *Orbulina universa* (core 2670, 33 cm).

Foraminifera recorded in surface grab sediments (Lowry, 1987) have also been recorded in Pleistocene sediments and outcrops (Dale and McMillan, 1999; Compton et al., 2002, 2004; Franceschini and Compton, 2004; Compton and Bergh, 2016; this study) and on the Holocene mud belt of South Africa (Dale and McMillan, 1998). McMillan (1990a) recorded similar benthic taxa from borehole and outcrop samples of the Upper Algoa Group along the south coast of South Africa which include *Ammonia* spp., *Elphidium* spp., *Nonion boueanus*, *Lobatula*

lobatula, *Quinqueloculina* cf. *seminula*, *Cancris auriculus*, *Bulimina gibba* and *Brizalina spathulata*.

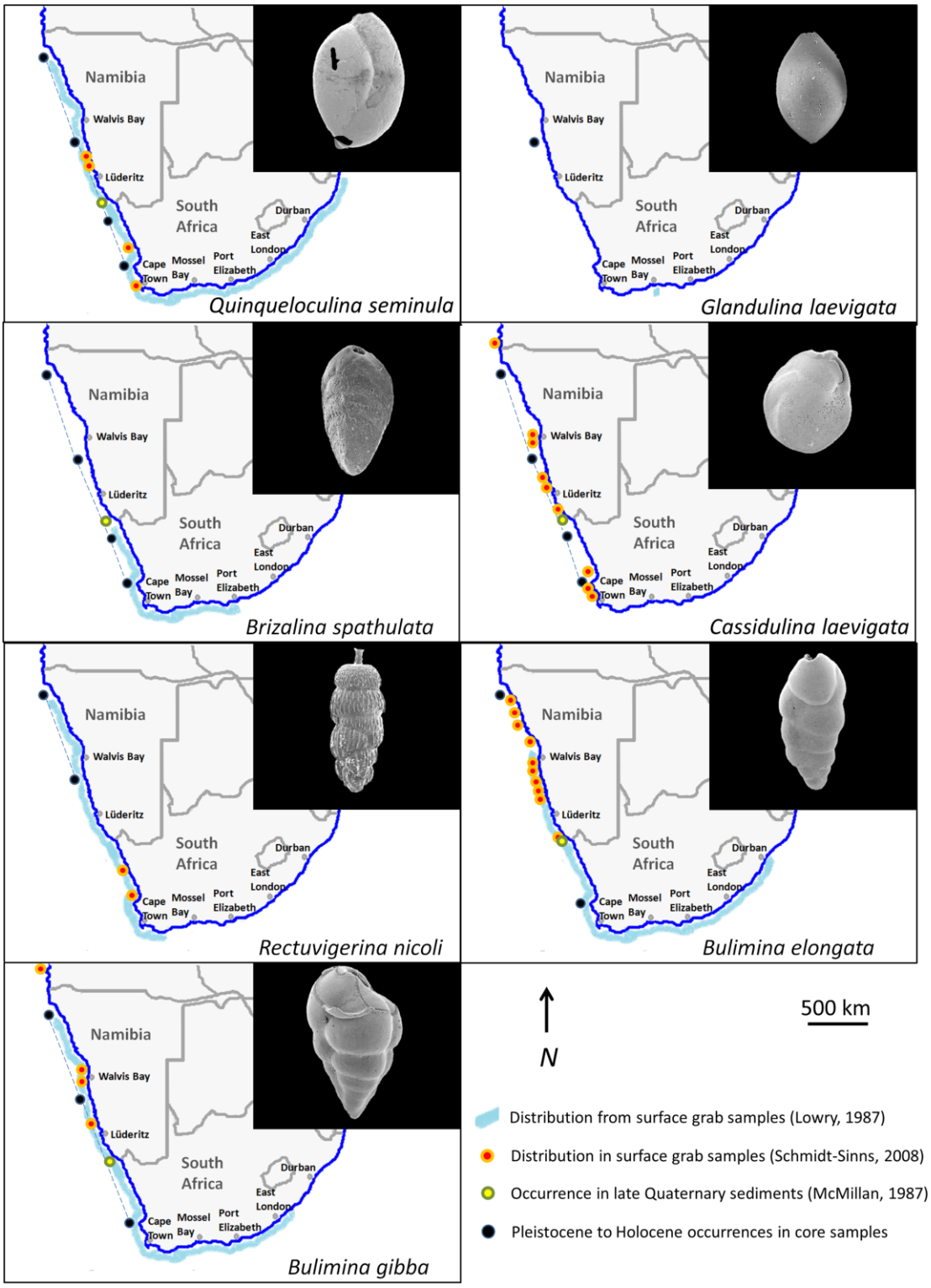

Fig. 6.12. Distribution maps of benthic foraminifera occurring in Namibian and western South African outer shelf (blue shading = Lowry, 1987; black dots = Compton et al., 2002, 2004 and this study), inner to middle late Quaternary sediments (green-yellow dots = McMillan, 1987) and inner shelf surface grab sediments (red-yellow dots = Schmidt-Sinns, 2008). Samples from McMillan (1987), Compton et al. (2002, 2004) and this study represent Pleistocene-aged foraminifera and samples from Lowry (1987) and Schmidt-Sinns (2008) are from surface grab sediments.

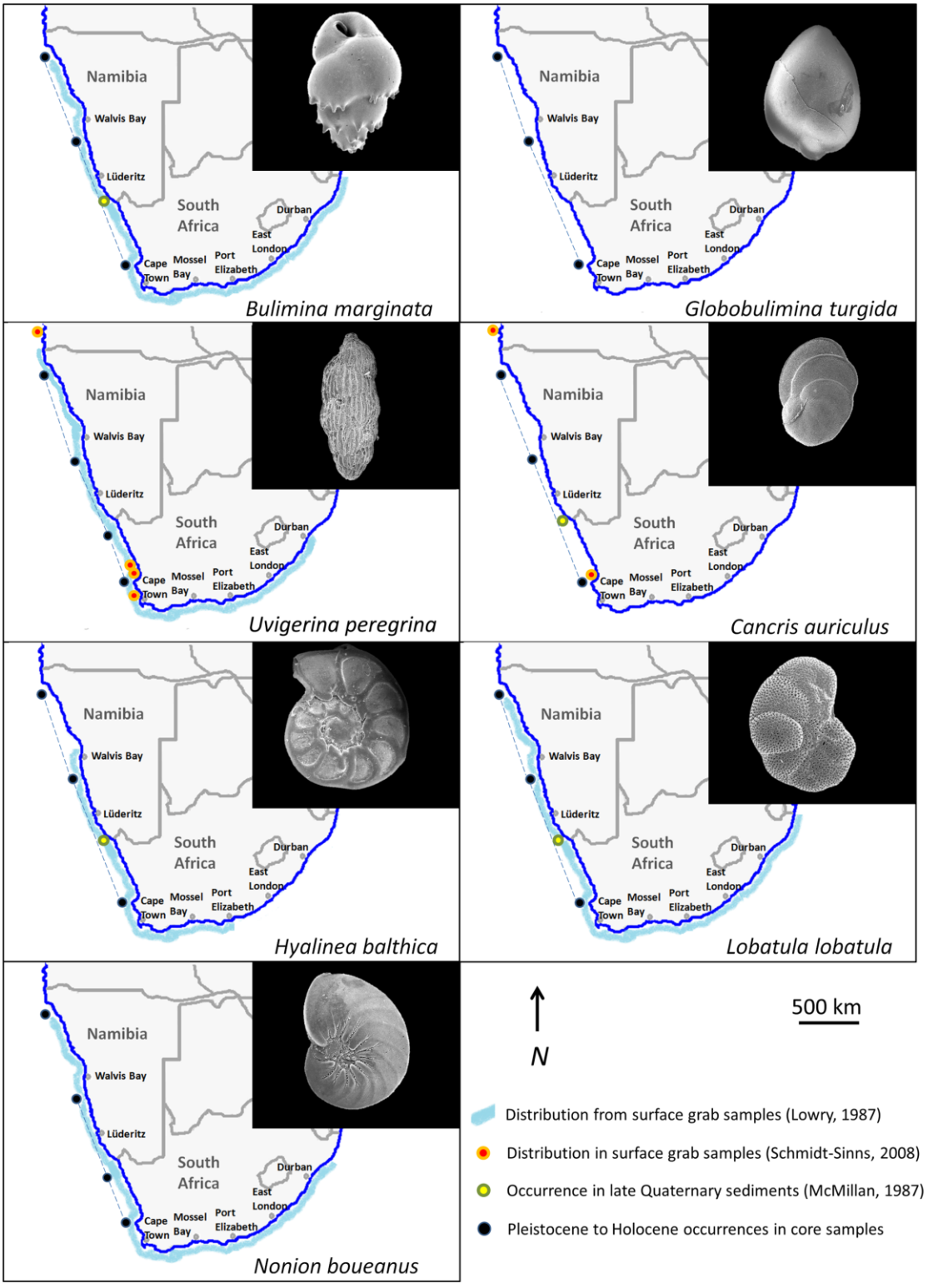

Fig. 6.13. Distribution maps of benthic foraminifera occurring in Namibian and western South African outer shelf (blue shading = Lowry, 1987; black dots = Compton et al., 2002, 2004 and this study), inner to middle late Quaternary sediments (green-yellow dots = McMillan, 1987) and inner shelf surface grab sediments (red-yellow dots = Schmidt-Sinns, 2008). Samples from McMillan (1987), Compton et al. (2002, 2004) and this study represent Pleistocene-aged foraminifera and samples from Lowry (1987) and Schmidt-Sinns (2008) are from surface grab sediments.

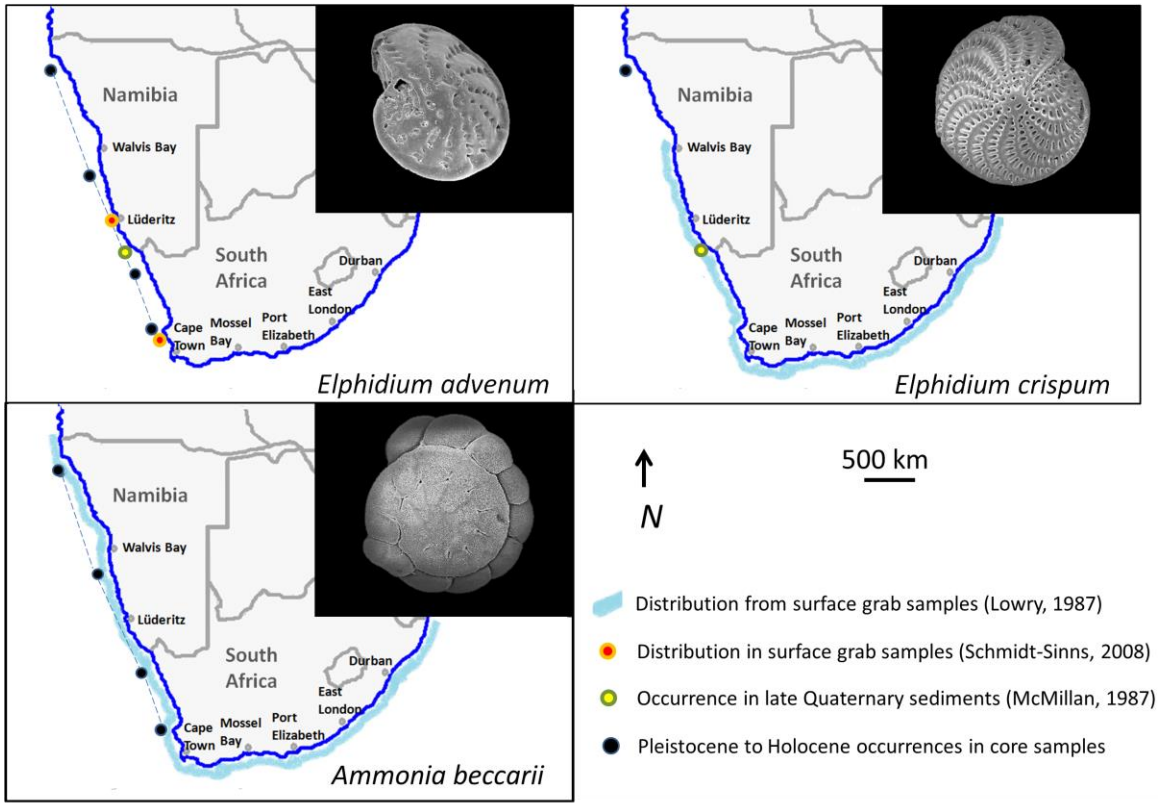

Fig. 6.14. Distribution maps of benthic foraminifera occurring in Namibian and western South African outer shelf (blue shading = Lowry, 1987; black dots = Compton et al., 2002, 2004 and this study), inner to middle late Quaternary sediments (green-yellow dots = McMillan, 1987) and inner shelf surface grab sediments (red-yellow dots = Schmidt-Sinns, 2008). Samples from McMillan (1987), Compton et al. (2002, 2004) and this study represent Pleistocene-aged foraminifera and samples from Lowry (1987) and Schmidt-Sinns (2008) are from surface grab sediments.

Most of the foraminifera species on the outer shelf occurring in Pleistocene, Holocene and surface grab samples first appeared in the sediment record at the Plio-Pleistocene as these assemblages are generally absent in older deposits, corresponding with the timing of the period in which the BUS intensified along the margin. Franceschini and Compton (2004), however, dated first occurrences of *Lobatula lobatula, Ammonia beccarii* and *Elphidium crispum* from shallow water environments to the late Miocene/Pliocene using SIS. This is in contrast to outer shelf deposits of Namibia as the Mio-Pliocene assemblages contain deeper water species (Bergh et al., 2018) and do not record similar species observed in the onshore South African marine deposits as noted by Franceschini and Compton (2004).

The major taxa between the Namibian shelf and the South African western shelf (Compton et al., 2004) are similar with minor species and diversity changes likely being attributed to small-scale ecosystem heterogeneities linked to the substrate, the seasonality and periodicity of coastal upwelling, and the relation between organic matter fluxes and dissolved oxygen contents in bottom waters (Schmiedl et al., 1997). Schmidt-Sinns (2008) found bottom water dissolved oxygen to be the major driver behind the differences between faunal compositions of the Southern Benguela and Northern Benguela regions.

6.4.2. Foraminifera on the Namibian shelf compared to slope foraminifera

The three major planktic species recorded in this study *G. bulloides, Gr. (Gc.) inflata* and *Ng. incompta* are also the dominant species recorded along the slope (Wefer et al., 1998) (Table 6.2) and continue to be the dominant species at present-day (Giraudeau, 1993). Modern distributions of *G. bulloides* show higher relative abundances along the shelf of Namibia whereas *Gr. (Gc.) inflata* increase towards the slope off northern Namibia and western South Africa. Higher relative abundances of *Ng. incompta* also occur along the Namibian margin (Giraudeau, 1993).

Table 6.2. Shelf (Compton et al., 2002, 2004; this study) and slope planktic foraminifera (Giraudeau, 1993; Wefer et al., 1998) along the western margin of Namibia and South Africa.

Planktic species	Slope	Shelf
Beella digitata	x	
Globigerina bulloides	x	x
Globigerina falconensis	x	
Globigerina quinqueloba	x	
Globigerina umbilicata	x	
Globigerinella siphonifera	x	x
Globigerinita glutinata	x	
Globigerinoides ruber	x	x
Globigerinoides truncatulinoides	x	x
Globorotalia crassaformis	x	
Globorotalia hirsuta	x	
Globorotalia inflata	x	x
Globorotalia menardii	x	x
Globorotalia scitula	x	
Globorotaloides hexagona	x	
Hastigerina siphonifera	x	
Neogloboquadrina dutertrei	x	
Neogloboquadrina pachyderma	x	x
Orbulina universa	x	x
Trilobatus sacculifer	x	x

Pleistocene foraminifera along the Namibian continental shelf are distinct from those along the slope. Present-day foraminifera on the slope are also distinct from outer shelf foraminifera below 400 m and are strongly influenced by the Oxygen Minimum Zone (OMZ) and related biogeochemical gradients (Schmiedl et al., 1997). The dominant slope species during the Pleistocene off Namibia were *Bulimina* spp. and *Uvigerina hispidocostata.* Shelf species are largely absent in slope sediments. Trace to minor abundances (<1 to 10%) of *Ammonia beccarii* and *Hyalinea balthica* were reported for the Plio-Pleistocene along the slope of Namibia and western South Africa (Wefer et al., 1998). On the northern Namibian slope very low abundances of *Quinqueloculina* spp. were reported for the Pleistocene (Berger et al., 1998). Relative abundances of *Quinqueloculina seminula* were also found to be low in this study area. The other species present in slope sediments that are also present in Pleistocene shelf sediments is *Cassidulina laevigata*, but this species has a broader bathymetric range and has been documented to also occur at bathyal depths (Schmiedl et al., 1997). *Cassidulina laevigata* formed a minor component of the slope assemblages during the early Pliocene becoming a major component during the late Pliocene and Pleistocene. Slope sediments also indicate *Bulimina marginata* to be a minor component (<10% relative abundance) of the assemblages along Namibia and South Africa during the Plio-Pleistocene.

The differences in shelf and slope assemblages as well as the differences in sediment composition imply that very few foraminiferal tests and other sand sized grains are transported from the shelf to the slope. The flow velocities

of most bottom currents observed along the margin are too weak to suspend coarser sandy material from the shelf to the slope (Shannon and Nelson, 1996) and will winnow away muddy sediment and leave sand-sized material, including foraminifera on the shelf (Fig. 6.15). Bottom currents are stronger during glacial sea-level lowstands. Compton and Wiltshire (2009) noted the transport and deposition of quartz and glauconite grains from the outermost shelf to the slope of western South Africa to occur during glacial lowstands. The fluctuating strength of the internal tides, bottom currents, turbidity flows (from rare seismic activity) and flow velocities during the Pleistocene thus account for the transport and deposition of the few shelf species documented in slope sediments in minor to trace abundances.

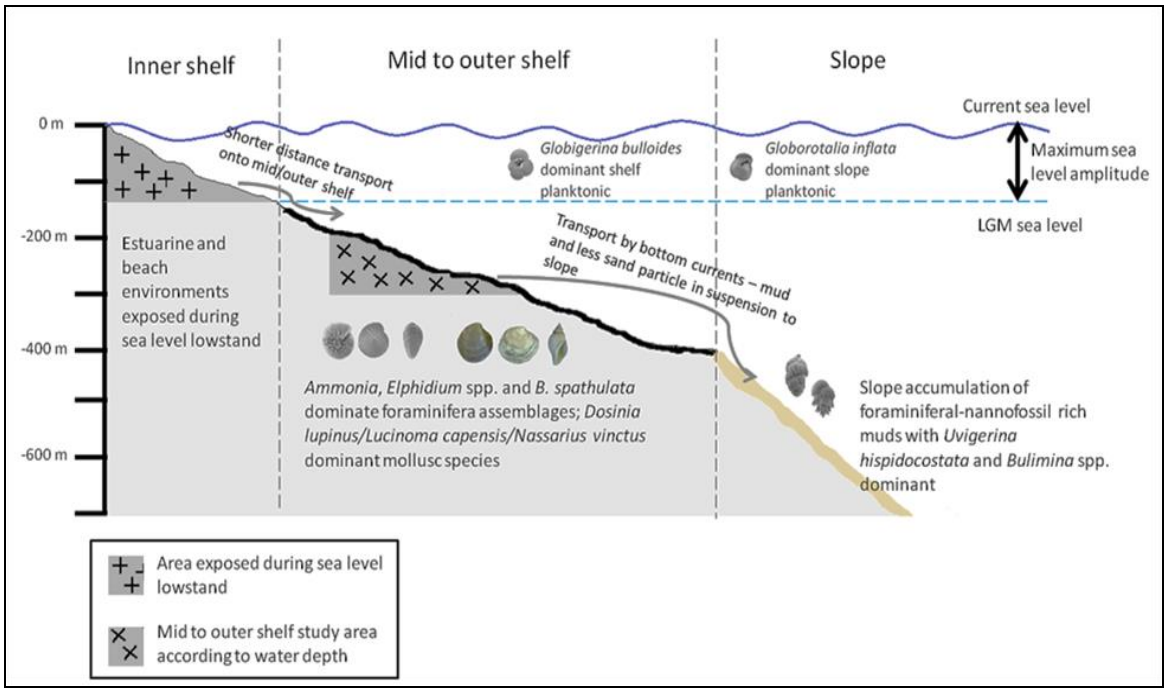

Fig. 6.15. Mid to late Pleistocene/Holocene environmental interpretation of the southwestern margin of Africa based on foraminifera and mollusc species found in outer shelf sediments. Slope data and occurrences are based on reports from ODP Leg 175 (Wefer et al., 1998) and results from cores GeoB 20601-4, 8342-6 and 8336-6 (Meteor Cruises M123 and M57/1) in Chapter 7.

6.4.3. Foraminifera and molluscs indicating cooling and shoaling conditions along the margin

Subtropical sea surface conditions indicated by warm water species *Gs. ruber, T. sacculifer* and *T. immaturus* during the middle Miocene (Bergh et al., 2018) changed to cooler conditions during the Plio-Pleistocene when *G. bulloides* and *Gr. (Gc.) inflata* became the dominant planktic taxa. Abundant *G. bulloides* has been recorded in late Pliocene sediments along the northeastern margin of South America, which has also been associated with upwelling and cooling conditions (Ibaraki, 1997). The Pliocene sediments off Walvis Bay-Lüderitz contain a mixture of deep benthic and warm subtropical planktic foraminifera. Together with *G. bulloides* and *Gr. (Gc.) inflata* the Pliocene foraminifera indicate changing conditions associated with the initiation of the BUS during the Miocene/Pliocene along the Namibian

margin (Compton and Bergh, 2016). The faunal turnover is also consistent with cooling periods between 3 and 2 Ma and 1.5 to 0.5 Ma when Namibian sea surface temperatures (SST) decreased by 3 to 5°C (Marlow et al., 2000; Lazarus et al., 2006; Etourneau et al., 2009). Marlow et al. (2000) recorded a 10°C decline in sea surface temperatures (SST) since 3.2 Ma linked to global cooling and increased upwelling associated with strengthening of southeasterly trade winds (Shi et al., 2001) along the margin.

The Angola-Benguela Front is characterised by *Gr. (Gc.) inflata-G. bulloides* (Ufkes et al., 1998) and similar assemblages, especially with regard to the presence and abundance of *G. bulloides.* Relatively high abundances of *G. bulloides* have been reported from other major upwelling regions as well, such as the Arabian Sea (Prell and Curry, 1981; Curry et al., 1992; Peeters et al., 2002), northwest Africa (Martinez et al., 1999), the eastern margin of South America (Ibaraki, 1997; Marchant et al., 1999; Mohtadi et al., 2005) and California (Sautter and Thunell, 1991). These species are regarded as transitional (Kucera, 2007) and *G. bulloides* is considered an upwelling indicator (Giraudeau, 1993). Warm subtropical to tropical *Gs. ruber* decreases (Fig. 6.4) during the Pleistocene along the Namibian shelf and *Globorotalia menardii* and *T. sacculifer* are low in numbers. These warm water species with minor abundances reach the Benguela Region through the inflow of warmer waters from the Angola Current to the north (Kemle-von Mücke and Oberhänsli, 1999) and the transport of low salinity, tropical waters into the Southern Benguela Region from the Agulhas Current (Rau et al., 2002). The higher abundances of *Orbulina universa*, identified as a subtropical species by Kucera (2007) on the northern Namibian shelf during the Pleistocene indicate the influence and proximity of the Angola Current to the north.

The Namibian outer shelf cores indicate Mio-Pliocene foraminifera (Bergh et al., 2018) being replaced by an *Uvigerina* spp.-dominated association during the Plio-Pleistocene transition (Compton and Bergh, 2016). The localised faunal turnover during the Plio-Pleistocene corresponds with the intensification of the BUS (Compton and Bergh, 2016) and the onset of major Northern Hemisphere glaciation, climate cooling and increasing glacial cycle amplitudes (Lisiecki and Raymo, 2007).

Infaunal foraminifera such as *Uvigerina* spp. became the dominant taxa in the early Pleistocene when bottom water conditions became more suitable for foraminifera adapted to more eutrophic and dysoxic conditions (Fig. 6.16) along the northern Namibian shelf, whereas suboxic indicators were more dominant during the Mio-Pliocene (Bergh et al., 2018). The benthic species *Uvigerina peregrina* has been described as a shallow infaunal species adapted to relatively high amounts of organic matter input under variable oxygenated bottom waters more adapted to dysoxic conditions (Fontanier et al., 2002; Koho et al., 2008; Table 6.3). Environments with mostly infaunal foraminifera and low diversities are characteristic of eutrophic conditions. Benthic faunal compositions are dependent upon oxygenation and organic detritus, i.e. food supply reaching the ocean floor (e.g. Altenbach and Sarnthein, 1989; Jorissen et al., 1995; Fariduddin and Loubere, 1997; Jorissen et al., 1998). The high relative abundances of

Uvigerina spp. are consistent with the occurrences of this taxon in reported eutrophic environments under high organic carbon fluxes (Fontanier et al., 2002; Licari and Mackensen, 2005).

In eutrophic environments the vertical distribution of foraminifera is more dependent on oxygen availability where oxygen concentrations fall below the lower limits of epifaunal taxa. Only deep infaunal taxa adapted to dysoxic conditions will survive below this limit as opposed to oligotrophic environments where more oxygen is consumed at the epifaunal-shallow infaunal level (Jorissen et al., 1995). The results from the Walvis Bay-Lüderitz cores are in agreement with findings by Bergh et al. (2018), which determined the benthic environment to have changed from oligotrophic conditions prior to the onset of the BUS in the late Miocene to eutrophic conditions after its initiation along the northern Namibian shelf.

Epifaunal abundances increased during the middle Pleistocene (Fig. 6.16). The early to Middle Pleistocene Transition (MPT) is marked by the change in climatic cycles where global ice volume variations shifted from being controlled by 41 kyr to 100 kyr cycles (Hays et al., 1976; Pisias and Moore, 1981; Imbrie et al., 1992; Raymo and Nisancioglu, 2003; Elderfield et al., 2012). Sea-level amplitudes increased during the middle Pleistocene dropping by as much as 120 m (Miller et al., 2005). The sea level in the study area was much closer to the modern-day coastline and shallow-water foraminifera (*Ammonia beccarii* and *Elphidium advenum*) increased in abundance (Fig. 6.17), which accounts for the observed infaunal-epifaunal ratios. These taxa indicate estuarine and littoral conditions as evidenced by previous work on foraminifera from the western shelf (McMillan, 1990b; Dale and McMillan, 1998; Dale and McMillan, 1999; Compton et al., 2002, 2004; Franceschini and Compton, 2004; Franceschini et al., 2005; Franceschini and Compton, 2007; Herbert and Compton, 2009) and south coast sediments of South Africa (McMillan, 1990a). The increasing abundance of epifaunal foraminifera along the shelf of Namibia and western South Africa is indicative of environments where a more diverse range of microhabitats are available, e.g. hard and rocky substrates for these foraminifera to attach to or the lack of softer substrate to burrow into. These shallow water foraminifera were close enough to where the outer shelf is today to be transported into the deeper area during lowered sea levels (Compton and Wiltshire, 2009).

A comparison between the onshore deposits (Dale and McMillan, 1999) and saltwater marsh foraminifera from southwestern South Africa (Franceschini and Compton, 2004; Franceschini et al., 2005; Franceschini and Compton, 2007) and the outer shelf foraminifera from western South Africa (Compton et al., 2002, 2004) indicate that taxa associated with littoral environments are preserved in onshore deposits and taxa associated with inner shelf environments are preserved in outer shelf sediments off western South Africa. This is consistent with data from this study in which inner shelf species are preserved in outer shelf sediments of Namibia.

Table 6.3. Ecological examples and taxonomic features of planktic and benthic foraminifera recorded in this study. The numbers in parentheses refer to previous studies listed at the end of this table.

Species	Ecological examples	Taxonomic features
Globigerina bulloides d'Orbigny, 1826	Temperate/ transitional (1,18); upwelling indicator (9).	Calcareous; spinose; spherical to subspherical; trochospiral; chambers globose; four chambers in final whorl; aperture umbilical and large high symmetrical arch.
Globigerinella siphonifera (d'Orbigny, 1839b)	Subtropical (18).	Calcareous; spinose; trochospiral to nearly planispiral; chambers subglobular to globular; 5 chambers visible in final whorl; aperture interiomarginal wide equatorial arch.
Globigerinoides ruber (d'Orbigny, 1839a)	Tropical to subtropical (warm) (1,5,18,30).	Calcareous; subspherical; trochospiral; three chambers visible in final whorl; deep incised sutures; primary aperture wide arched umbilical; secondary apertures on spiral side. Can occur in white and pink varieties. Pink variety extant in Atlantic ocean and extinct in the Indian Ocean since 120 ka (2).
Globorotalia (Globoconella) inflata (d'Orbigny, 1839b)	Temperate/transitional (1,18).	Calcareous; cancellate (in pre-adult stages) non-spinose; trochospiral; test subrounded to subangular; three chambers visible in final whorl; incised sutures on umbilical side; aperture umbilical to extraumbilical interiomarginal.
Globorotalia menardii (Parker, Jones and Brady, 1865)	Tropical to subtropical (1,18,30).	Calcareous; cancellate non-spinose, lobulate with thick keel around test margin and sutures on spiral side; 5 chambers visible in final whorl; deep incised sutures on umbilical side; aperture extraumbilical interiomarginal.

Table 6.3 *(continued)*

Species	Ecological examples	Taxonomic features
Globorotalia truncatulinoides (d'Orbigny, 1839b)	Transitional (1) to subtropical (1,18). Dextral (right-coiling) forms may indicate relatively warmer subsurface conditions and sinistral (left-coiling forms) cooler conditions (1,6,26).	Calcareous; non-spinose, pustulose; planoconvex; keeled; trochospiral; more than four chambers visible in final whorl; chambers subangular; deep incised sutures on umbilical side; aperture extraumbilical interiomarginal.
Neogloboquadrina dutertrei (d'Orbigny, 1839a)	Subtropical (6,19). Upwelling regions (6; and references therein).	Calcareous; rounded, subglobular with globular chambers; trochospiral; >5 chambers visible in final whorl; aperture large umbilical.
Neogloboquadrina incompta Cifelli, 1961 *Neogloboquadrina pachyderma* Ehrenberg, 1861	*Ng. pachyderma* (dextral)/*Ng. incompta* = subpolar; *Ng. pachyderma* (sinistral) = polar (1,18,21,24,30). May also indicate higher upwelling intensity (6).	Calcareous; subglobular to quadrate in shape with subquadrate chambers; trochospiral; four chambers in final whorl; aperture narrow extraumbilical to interiomarginal.
Orbulina universa (d'Orbigny, 1839a) *Orbulina bilobata* (d'Orbigny, 1846)	Transitional to subtropical (10) to tropical (1) with higher abundances in subtropical waters (1,18).	Calcareous; perforate spinose; single round spherical globular chamber; apertures cover test (areal). Tests of the form of *O. bilobata* are bilobate, i.e. two spherical chambers, one slightly smaller than the other, are externally visible.
Trilobatus sacculifer (Brady, 1877)	Tropical (1,5,18).	Calcareous; macroperforate; trochospiral; four chambers visible in final whorl; final chamber slightly elongated and lobulate; deep incised sutures; primary aperture arched umbilical; secondary apertures on spiral side.
Ammonia beccarii (Linnaeus, 1758)	Epifaunal-shallow infaunal (11,15) in muddy sand, brackish marine, hypersaline; inner shelf <50 m (16).	Calcareous; trochospiral; thick walled; test rounded; 10-12 chambers in final whorl; sutures depressed; umbilicus ornamented with tubercles and pillars; aperture interiomarginal.

Table 6.3 *(continued)*

Species	Ecological examples	Taxonomic features
Brizalina spathulata (Williamson, 1858)	Shallow infaunal (17) in suboxic to dysoxic conditions (7).	Calcareous; finely perforate; test elongate and compressed; biserial; sutures depressed; aperture a basal loop in the final chamber with toothplate.
Bulimina elongata (d'Orbigny, 1846)	Infaunal (11, 25), opportunistic in dysoxic conditions (11).	Calcareous, smooth; test elongate, broadening mid-way and becoming drawn out at apertural end; triserial; basal chambers may be tapered; chambers strongly depressed; aperture loop-shaped with bordered lip.
Bulimina gibba (Fornasini, 1902)	Infaunal (8,16) to shallow infaunal (25) in dysoxic conditions (7) preferring muddy sediments (16).	Calcareous, smooth; test elongate, broadening mid-way and becoming drawn out at apertural end; triserial; basal chambers may be tapered; chambers strongly depressed; aperture loop-shaped with bordered lip.
Bulimina marginata (d'Orbigny, 1846)	Infaunal (3,8,16) under suboxic (7) to low dysoxic conditions, muddy to fine sand sediments on inner shelf to slope depths (16,27).	Calcareous, smooth; test elongate, broadening mid-way and becoming drawn out at apertural end; basal chambers may be pointed; chambers strongly depressed; aperture loop-shaped with bordered lip.
Cancris auriculus (Fichtel and Moll, 1798)	Epiphytic (11) to shallow infaunal (25) in oxic conditions (11).	Calcareous hyaline; triserial; globular to subglobular chambers; downward extending spines around margins of chambers; elliptical arc-shaped aperture with lip.
Cassidulina laevigata (d'Orbigny, 1826)	Infaunal (3), infaunal-epifaunal (16), shallow infaunal (25), epifaunal (17) under suboxic (7), muddy and sandy sediments, from the shelf (15,16) to slope (16).	Calcareous hyaline; planispiral; test and chambers flattened; subrounded test; aperture slit extraumbilical interiomarginal.

Table 6.3 *(continued)*

Species	Ecological examples	Taxonomic features
Elphidium advenum (Cushman, 1922)	Epifaunal (25) in oxic conditions (7,24). Can occur to water depths of 500 m (4).	Calcareous; test rounded and biconvex; approximately twelve chambers separated by sutures with retral processes; primary aperture is interiomarginal.
Elphidium crispum (Linnaeus, 1758)	Epiphytic in oxic conditions (7,11,24). Shallow water depths of <50 m (11,22).	Calcareous ornamented by ponticuli between the sutures; test is subcircular in outline and lenticular in side view; approximately eighteen chambers; sutures are curved and raised, radiating from a central thickened boss; aperture is interiomarginal.
Globobulimina turgida (Bailey, 1851)	Deep infaunal (23,29) under dysoxic or temporarily anoxic conditions (7,23,24,29) found within or below denitrification zones (23).	Calcareous hyaline; globular oviform; triserial; inflated chambers overlap; sutures slightly depressed; aperture loop-shaped with toothplate.
Hyalinea balthica (Schröter, 1783)	Epifaunal (3) under suboxic conditions (7,24).	Calcareous, hyaline, smooth; test is discoidal, planispiral and flattened with a keeled margin; approximately ten chambers in the final whorl; thick limbate sutures; aperture is an interiomarginal arch.
Lobatula lobatula (Walker and Jacob, 1798)	Epiphytic (11), epifaunal (25), in oxic conditions (11).	Calcareous, microperforate to macroperforate; test is sub-circular, trochospiral; planoconvex; umbilical side is convex and the spiral side is flatter; approximately nine chambers separated by curved and flush to slightly depressed sutures; aperture is an interiomarginal slit.

Table 6.3 *(continued)*

Species	Ecological examples	Taxonomic features
Nonion boueanus (d'Orbigny, 1846)	Shallow infaunal (12) to intermediate infaunal (28) under suboxic conditions (7).	Calcareous, smooth; test is suboval, planispiral; umbilical portion is depressed with pustulose structures along inner margins of the chambers and the center of the test; pustulose structures extend one third to halfway into the suture lines from the central portion of the test; approximately sixteen chambers separated by curved sutures; aperture is an interiomarginal arch.
Quinqueloculina seminula (Linnaeus, 1758)	Epifaunal-shallow infaunal (23), epifaunal (8,17,19) under hypersaline, oxic conditions (7,24), mostly on the shelf (16).	Calcareous, porcelaneous, smooth; test is ovate in shape and subtriangular in cross-section; the outline and base of the test are rounded truncating towards the terminal end; chambers are embracing and arranged in a quinqueloculine spiral; the chambers are separated by depressed sutures; aperture is large at the terminal end of the final chamber.
Rectuvigerina nicolii (Mathews, 1945)	Infaunal in suboxic conditions across water depths ranging from the continental shelf to slope (20; and references therein).	Calcareous; test elongate, circular in cross section and triserial in early stage becoming uniserial; ornamented with longitudinal costae which cross suture lines between chambers; sutures are distinct and depressed; aperture is terminal on a short flaring neck.
Uvigerina peregrina (Cushman, 1923)	Infaunal (8,11,17), shallow infaunal (12,16) under suboxic (15) to dysoxic (11,12) and high organic carbon conditions (12,13,15,16).	Calcareous; longitudinal costae cover length of chambers and test; triserial; approximately six chambers visible externally; aperture rounded terminal on neck with lip extending outwards.

References: (1) Bé and Tolderlund, 1971; (2) Thompson et al., 1979; (3) Corliss and Chen, 1988; (4) Culver, 1988; (5) Glacon, 1990; (6) Giraudeau, 1993; (7) Kaiho, 1994; (8) Carboni and di Bella, 1996; (9) Little et al., 1997; (10) Bertini et al., 1998; (11) Goubert et al., 2001; (12) Diz et al., 2002; (13) Fontanier et al., 2002; (14) Compton et al., 2004; (15) Licari and Mackensen, 2005; (16) Murray, 2006; (17) Drinia et al., 2007; (18) Kucera, 2007; (19) Reolid et al., 2008; (20) Schmidt-Sinns, 2008; (21) Lombard et al., 2009; (22) Phipps et al., 2010; (23) Koho et al., 2011; (24) Kaminski, 2012; (25) Pérez-Asensio et al., 2012 (26) Ufkes and Kroon, 2012; (27) Holbourn et al., 2013; (28) Pérez-Asensio, 2013; (29) Kuhnt et al., 2014; (30) BouDagher-Fadel, 2015.

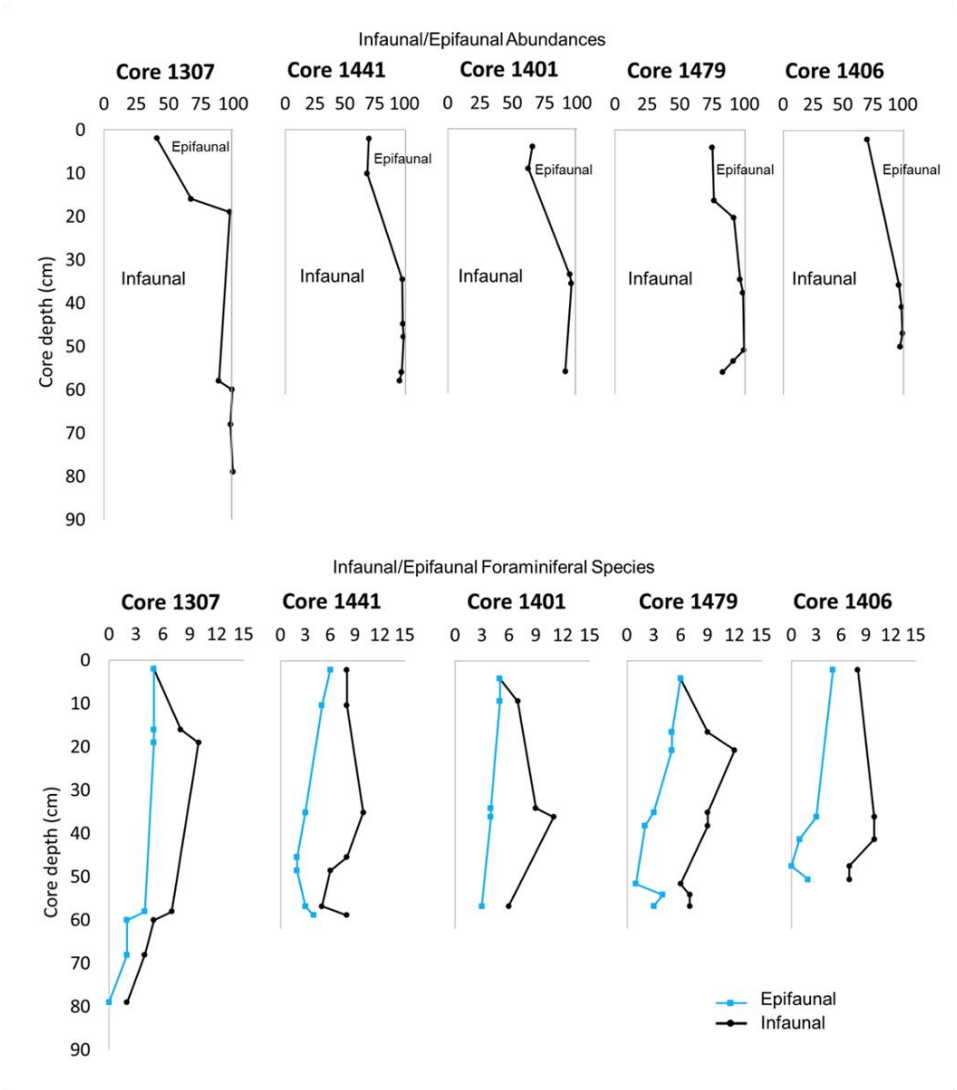

Fig. 6.16. Infaunal-epifaunal abundances expressed as relative abundances (%) and in number of species.

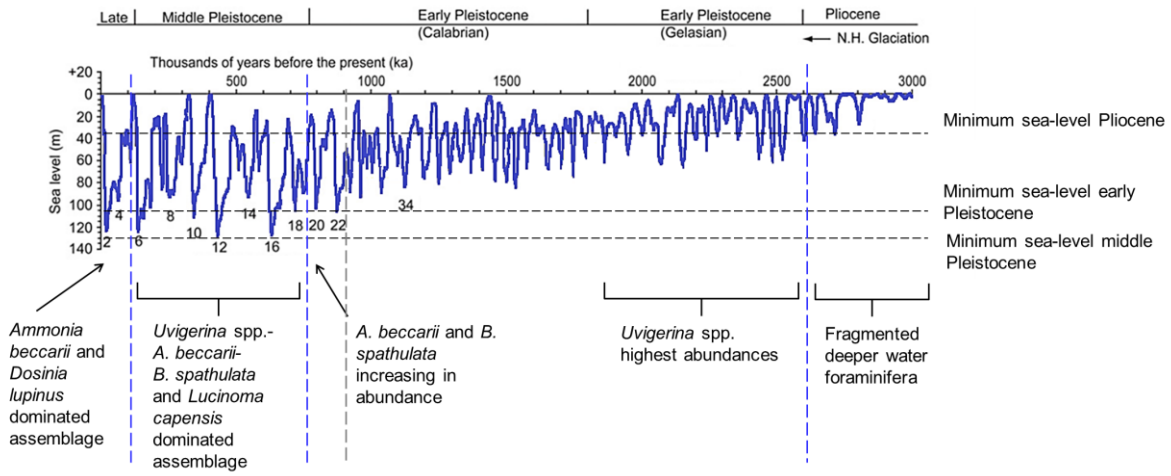

Fig. 6.17. Global range in sea level (Bintanja and van de Wal, 2008) since 3 Ma in relation to the foraminiferal and mollusc assemblages preserved in sediments of the study area. Gray dashed line = Mid-Pleistocene transition (MPT).

The mollusc assemblages across the Namibian shelf indicate similar shallow marine environments. The most abundant mollusc species in unit 2 of the Walvis Bay-Lüderitz cores, *Lucinoma capensis*, *Turritella declivis* and *Comitas saldanhae*, occur where *Brizalina spathulata* and *Uvigerina* spp. show higher abundances. The dominance of *Lucinoma capensis* in the shelly sandy units signal organic-rich conditions at the sea floor in the center of upwelling cells (Edelman-Fürstenberg, 2014) and *Turritella declivis* has been associated with upwelling conditions (Allman, 1988). The occurrence of *Turritella declivis* indicates water depths of 40 to 220 m based on present-day occurrences of the species along the south coast of South Africa. Substrate indications based on *T. declivis* are however broad, as they can occur in thick mud to coarse gravelly sands (Herbert, 2013).

The distribution of molluscs in the BUS (Fig. 6.18) is influenced by substrate, oxygen content, upwelling conditions, microhabitats and depth (Edelman-Fürstenberg, 2014; and references therein). Marine transgressions during the late Pleistocene created numerous lagoons, estuaries and embayments along the coast (Tankard and Rogers, 1978). This accounts for the variability in the mollusc assemblages accumulating in the outer shelf deposits of Namibia and South Africa. During the late Pleistocene to Holocene *Dosinia lupinus* replaced *Lucinoma capensis* as the dominant bivalve species being preserved in the sediments. During the Holocene off southwest South Africa the dominant bivalve species was also *Dosinia lupinus*, and *Nassarius vinctus* and *Volutocorbis lutosa* being the dominant gastropod species (Compton et al., 2002; Herbert and Compton, 2009). The present-day fauna on the shelf is still composed of abundant *Dosinia lupinus* (Barnard, 1964; Kilburn and Rippey, 1982). The dominance of the infaunal filter-feeding species *Lucinoma capensis* and *Dosinia lupinus* indicates fine grained sedimentation on the shelf (Barnard, 1964; Kensley, 1978; Kilburn and Rippey, 1982) and the turnover of abundant species *Dosinia lupinus* in unit 1 supports a shallowing marginal marine environment (Edelman-Fürstenberg, 2014) of up to 150 m (Walker et al., 2000), a water depth consistent with the dominance of *Ammonia beccarii.* Similar to the shallow water foraminifera, *Dosinia lupinus* has been associated with estuarine influences and environments (Branch et al., 2007). Estuarine influences on the Namibian study areas could come from the estuaries associated with the Kuiseb River entering the Atlantic south of Walvis Bay (Watson and Lemon, 1985; Bate, 1993; Meadows, 2001) and in the north near the Kunene River (Wearne and Underhill, 2005). Prodelta to delta front sandy and muddy conditions are indicated by the occurrence of the gastropod species *Nassarius vinctus* in unit 1 at water depths of less than 100 m when the sea level was up to 125 m below present day during the Last Glacial Maximum (LGM) (Miller et al., 2005). The good preservation of the shells and in places articulated valves indicate minimal disturbance, consistent with lowered sea level during the LGM and the accumulation of abundant *Dosinia* valves in the uppermost unit of the cores. Alternatively, the autochthonous deposition of articulated valves could also be explained during sea level rise, descending wave and current energy and rapid sediment burial which would cause minimal disturbance.

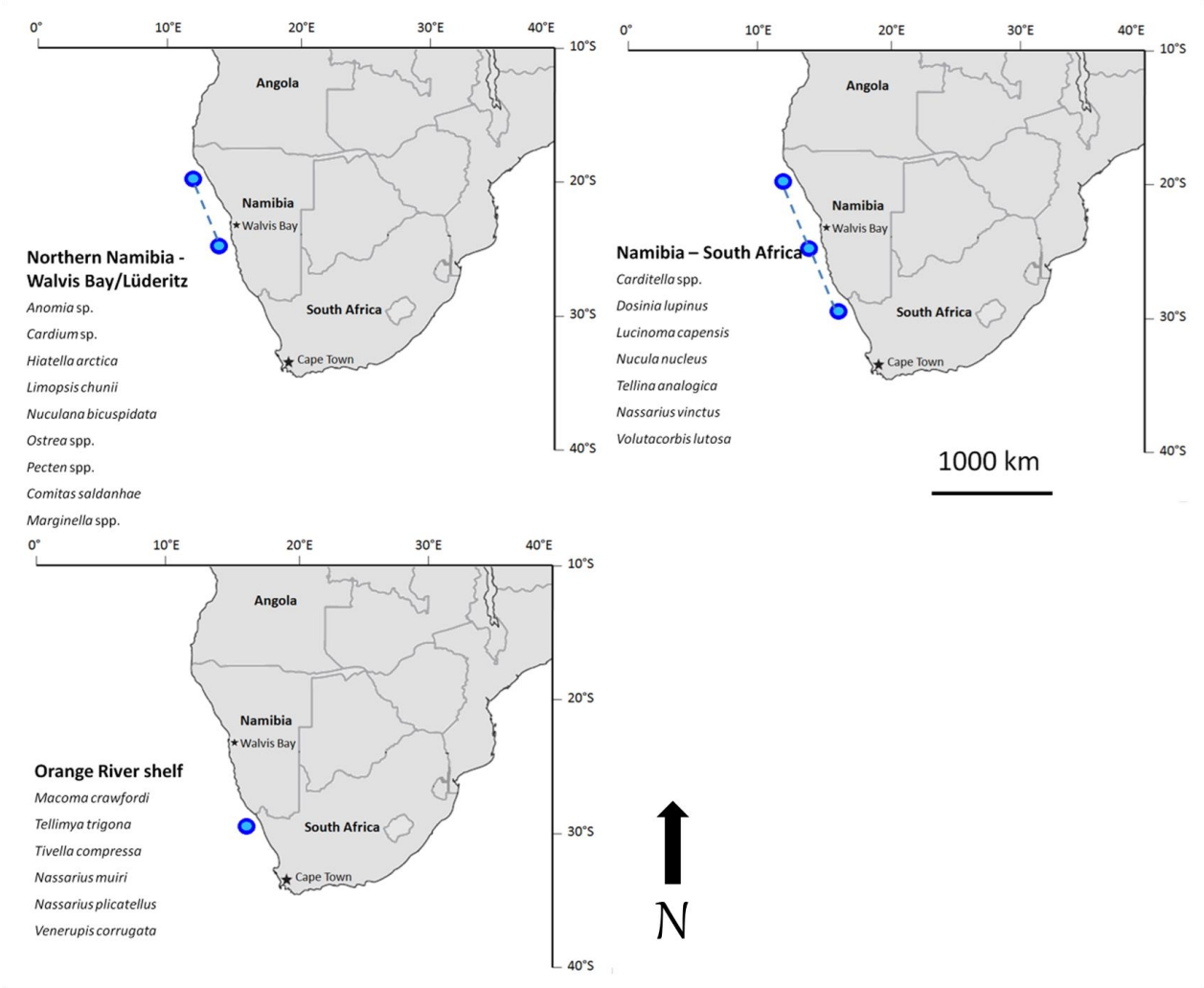

Fig. 6.18. Pleistocene to Holocene mollusc species distribution along the Namibian to Orange River outer shelf off the west coast of South Africa based on occurrences of species from Compton et al. (2002) and this study.

6.5. Conclusions

Upwelling indicator species and transitional planktic species along the Namibian margin already appeared in Plio-Pleistocene sediments, which are associated with the initiation of the BUS during the late Miocene to Pliocene. The present-day assemblages and foraminifera on the shelf in surface grab samples from previous studies can be traced back in vibracores from the shelf to the Pleistocene during a period in which the BUS intensified. The major planktic species is interpreted to be controlled by the cold upwelled waters. The planktic foraminifera are dominated by transitional to cold water species with minor occurrences of warm water species *Globigerinoides ruber*, *Globorotalia menardii*, *Trilobatus sacculifer* and *Orbulina universa*. The minor occurrences of warm water species are attributed to the inflow of warm currents from the north (Angola Current) and south (Agulhas Current) of the BUS and the high abundances of *Orbulina universa* on the northern Namibian shelf to the proximity of the Angola Current in the region.

The wide distribution of the major benthic foraminiferal taxa stretching across the BUS and into the south and east coasts of South

Africa are controlled by the microhabitat which, in turn, is influenced by substrate, organic matter fluxes and dissolved bottom water oxygen contents.

Only a few species such as *Ammonia beccarii*, *Hyalinea balthica*, *Quinqueloculina seminula*, *Cassidulina laevigata* and *Bulimina marginata* recorded from the outer shelf have also been recorded in slope sediments, but in trace to minor amounts. Apart from some taxa such as *Cassidulina* spp. and *Bulimina* spp. having broad bathymetric ranges, there is minimal transport from the shelf to slope as energy dispersion is too weak and the shelf too broad to suspend and transport sand-sized components, such as foraminifera.

A palaeoenvironmental shift from relatively deep to shallow depths has been recorded in Pleistocene sediments along the southwestern shelf of southern Africa. The Miocene-Pliocene to Plio-Pleistocene marked a period in which oceanographic and climate changes led to the turnover of foraminiferal assemblages along the southwestern margin of Africa from a warm subtropical assemblage to colder, shallow water assemblages. The shift in the palaeo-environment during the Pleistocene was most noticeable in the Walvis Bay-Lüderitz region where outer shelf sediments reveal an *Uvigerina* spp.-dominated association in the lower Pleistocene. The *Uvigerina* spp.-association indicates eutrophic conditions under high organic carbon conditions. During the middle Pleistocene *Uvigerina* spp. relative abundances decrease and epifaunal foraminifera increase indicating slightly less eutrophic conditions. This association occurs together with the mollusc species *Lucinoma capensis*, *Turritella declivis* and *Comitas saldanhae*, which indicate increased upwelling conditions. During the upper Pleistocene an *Ammonia beccarii*-association is established and the dominance of the *Lucinoma capensis* bivalve species replaced by *Dosinia lupinus* indicating mostly taxa adapted to suboxic conditions with increased epifaunal abundances in marginal marine to inner shelf environments.

The upper Pleistocene to Holocene foraminifera and molluscs have been recorded in a wide range of depositional settings along the shelf of southern Africa, which include the outer shelf, the mudbelt on the inner shelf, estuarine, lagoonal and beach environments. Their high relative abundance in the uppermost sections of the cores indicates a strong influence of estuarine, lagoonal and beach environments on the middle to outer shelf sediments.

The foraminifera and mollusc assemblages indicate that the palaeoenvironment of the area was shoaling during the Pleistocene, especially when compared to the Mio/Pliocene assemblages and is consistent with higher amplitude sea-level fluctuations, particularly sea-level lowstands of as much as 125 m below present sea level after the Mid-Pleistocene Transition. The water depth thus lowered from a deep outer shelf environment in the middle Miocene to palaeodepths fluctuating between the inner and middle shelf during the Pleistocene.

References

Adams, A., Reeve, L., 1848–50. Mollusca. In: Adams, A. (ed.), The zoology of the Voyage of HMS Samarang: Under the command of Captain Sir Edward Belcher,

C.B., F.R.A.S., F.G.S. During the Years 1843–46, pp. 1–24 (1848), 25–87 (1850). Reeve, Benham and Reeve, London.

Allman, W.D., 1988. Ecology of the Recent turritelline gastropods (Prosobranchia, Turritellidae): current knowledge and paleontological implications. Palaios 3, 259–284.

Altenbach, A.V., Sarnthein, M., 1989. Productivity record in benthic foraminifera. In: Productivity of the ocean: present and past, Wiley, New York 44, 255-269.

Bailey, J.W., 1851. Microscopical Examination of Soundings, Made by the US Coast Survey Off the Atlantic Coast of the US. Smithsonian Contributions to Knowledge 2, 1-15.

Barnard, K. H., 1958. Contributions to the knowledge of South African marine molluscs. Part I. Gastropoda: Prosobranchiata: Toxoglossa. Annals of the South African Museum 44, 73-163.

Barnard, K. H., 1964. Contributions to the knowledge of South African marine molluscs. Part V. Lamellibranchiata. Annals of the South African Museum 47, 361-593

Bate, B.H., 1993. Water relations of the vegetation along the Kuiseb River, Namibia. Madoqua 18(2), 85-91.

Baumann, K. H., Freitag, T., 2004. Pleistocene fluctuations in the northern Benguela Current system as revealed by coccolith assemblages. Marine Micropaleontology 52, 195-215.

Bè, A.W.H., Tolderlund, D.S., 1971. Distribution and ecology of planktonic foraminifera. In: Funnell, B.M., Riedel, W.R. (Eds), The micropaleontology of oceans. Cambridge University Press, London, pp. 105-149.

Berger, W.H., Wefer, G., Richter, C., Lange, C.B., Giraudeau, J., Hermelin, O., Shipboard Scientific Party. 1998. Proceedings of the Ocean Drilling Program, Initial Reports 175, 505-531.

Bergh, E.W., Compton, J.S., Frenzel, P., 2018. Late Neogene foraminifera from the northern Namibian continental shelf and the transition to the Benguela Upwelling System. Journal of African Earth Sciences 141, 33-48.

Bertini, A., Londeix, L., Maniscalco, R., Di Stefano, A., Suc, J.P., Clauzon, G., Gautier, F., Grasso, M., 1998. Paleobiological evidence of depositional conditions in the Salt Member, Gessoso-Solfifera Formation (Messinian, Upper Miocene) of Sicily. Micropaleontology, pp. 413-433.

Bintanja, R., van de Wal, R.S.W., 2008. North American ice-sheet dynamics and the onset of 100,000-year glacial cycles. Nature 454, 869-872.

Bolli, H.M., Saunders, J.B., Perch-Nielsen, K., 1985. Plankton Stratigraphy. Cambridge University Press, Cambridge, 1032 pp.

BouDagher-Fadel, M.K., 2015. Biostratigraphic and geological significance of planktonic foraminifera. UCL Press, London, 306 pp.

Brady, H.B., 1877. Supplementary note on the foraminifera of the chalk (?) of the New Britain Group. Geological Magazine 4, 534-536.

Branch, G.M., Griffiths, C.L., Branch, M.L., Beckley, L.E., 2007. Two oceans: a guide to the marine life of southern Africa. Penguin Random House, South Africa.

Carboni, M.G., Di Bella, L., 1996. The Pleistocene section of Podere Palombaro (Umbria). Geologica Romana 32, 97-108.

Cifelli, R., 1961. *Globigerina incompta*, a new species of pelagic foraminifera from the North Atlantic. Contributions from the Cushman Foundation for Foraminiferal Research 12, 83– 86.

Compton, J.S., Bergh, E.W., 2016. Phosphorite deposits on the Namibian shelf. Marine Geology 380, 290-314.

Compton, J.S., Mulabisana, J., McMillan, I.K., 2002. Origin and age of phosphorite from the Last Glacial Maximum to Holocene transgressive succession off the Orange River, South Africa. Marine Geology 186 (3-4), 243-261.

Compton, J.S., Wigley, R., McMillan, I.K., 2004. Late Cenozoic phosphogenesis on the western shelf of South Africa in the vicinity of the Cape Canyon. Marine Geology 206, 19-40.

Compton, J.S., Wiltshire, J.G., 2009. Terrigenous sediment export from the western margin of South Africa on glacial to interglacial cycles. Marine Geology 266, 212-222.

Corliss, B. H., Chen, C., 1988. Morphotype patterns of Norwegian Sea deep-sea benthic foraminifera and ecological implications. Geology 16, 716-719.

Culver, S.J., 1988. New foraminiferal depth zonation of the northwestern Gulf of Mexico. Palaios, 69-85.

Curry, W.B., Ostermann, D.R., Guptha, M.V.S., Ittekkot, V., 1992. Foraminiferal production and monsoonal upwelling in the Arabian Sea: evidence from sediment traps. Geological Society, London, Special Publications 64, 93-106.

Cushman, J.A., 1922. Shallow-water foraminifera of the Tortugas region. Carnegie Institute, Washington Publications 311, 1-85.

Cushman, J.A., 1923. The foraminifera of the Atlantic Ocean: part 4 – Lagenidae. Bulletin of the United States National Museum 104, 1-228.

d'Orbigny, A.D., 1826. Tableau méthodique de la classe des Céphalopodes. Annales des Sciences Naturelles 7, 245-314.

d'Orbigny, A.D., 1839a. Foraminifères. In: de la Sagra, R. (Ed.). Histoire physique, politique et naturelle de I'ile de Cuba. A. Bertrand, Paris, 224 pp.

d'Orbigny, A. D., 1839b. Les foraminifères des îles Canaries. In: Barker-Webb, P., Berthelot, S. (Eds.). Histoire Naturelle des Iles Canaries 2, 119-146.

d'Orbigny, A.D., 1846. *Foraminiferes Fossiles du Basin Tertiaire de Vienne (Austriche).* Gide et Comp, Paris, 312 pp.

Dale, D.C., McMillan, I. K., 1998. Mud belt and middle shelf benthonic and planktonic foraminiferal assemblages and sedimentation processes compared through the Holocene successions at two tropical African (Sierra Leone) and two temperate African (western offshore, South Africa) sites. South African Journal of Science 94, 319-340.

Dale, D.C., McMillan, I.K., 1999. On the beach: A field guide to the Late Cainozoic micropalaeontological history, Saldanha region, South Africa. Earthyear Environmental Communications, 127 pp.

Diester-Haass, L., Billups, K., Emeis, K.C., 2005. In search of the late Miocene-early Pliocene "biogenic bloom" in the Atlantic

Ocean (Ocean Drilling Program Sites 982, 925 and 1088). Paleoceanography 20, 1-13.

Diester-Haass, L., Meyers, P.A., Bickert, T., 2004. Carbonate crash and biogenic bloom in the late Miocene: evidence from ODP sites 1085, 1086 and 1087 in the Cape Basin, southeast Atlantic Ocean. Paleoceanography 19, 1-19.

Diester-Haass, L., Meyers, P.A., Rothe, P., 1992. The Benguela Current and associated upwelling on the southwest African Margin: a synthesis of the Neogene-Quaternary sedimentary record at DSDP sites 362 and 532. Geological Society, London, Special Publications 64, 331-342.

Diester-Haass, L., Rothe, P., 1987. Plio-Pleistocene sedimentation on the Walvis Ridge, southeast Atlantic (DSDP Leg 75, Site 532)—influence of surface currents, carbonate dissolution and climate. Marine Geology 77, 53-85.

Diz, P., Francés, G., Pelejero, C., Grimalt, J.O., Vilas, F., 2002. The last 3000 years in the Ría de Vigo (NW Iberian Margin): climatic and hydrographic signals. The Holocene 12, 459-468.

Drinia, H., Antonarakou, A., Tsaparas, N., Dermitzakis, M.D., 2007. Foraminiferal stratigraphy and palaeoecological implications in turbidite-like deposits from the Early Tortonian (Late Miocene) of Greece. Journal of Micropalaeontology 26, 145-158

Edelman-Furstenberg, Y., 2014. Distribution and paleoecology of molluscan skeletal remains along an upwelling tract: Benguela system, Namibian shelf. Marine Geology 353, 153-162.

Ehrenberg, C.G., 1861: Elemente des tiefen Meeresgrundes im Mexikanischen Golfstrome bei Florida: tiber die Tiefgrund-Verhaltnisse des Oceans am Eingange der Davisstrasse und bei Island. Monatsbericht der Königlichen Preussischen Akademie der Wissenschaften zu Berlin, 275 - 315.

Elderfield, H., Ferretti, P., Greaves, M., Crowhurst, S., McCave, I.N., Hodell, D., Piotrowski, A.M., 2012. Evolution of ocean temperature and ice volume through the mid-Pleistocene climate transition. Science 337, 704-709.

Etourneau, J., Martinez, P., Blanz, T., Schneider, R., 2009. Pliocene–Pleistocene variability of upwelling activity, productivity, and nutrient cycling in the Benguela region. Geology 37, 871-874.

Fariduddin, M., Loubere, P., 1997. The surface ocean productivity response of deeper water benthic foraminifera in the Atlantic Ocean. Marine Micropaleontology 32, 289–310.

Fichtel, L., Moll, J.P.C., 1798. Testacea microscopica aliagua minuta ex generibus Argonauta et Nautilus ad naturam delineate et descripta. Microscopische und andere kleine Schalthiere aus den Geschlechtern Argonaute und Schiffer, nach der Natur Gezeichnet und beschrieben. Camesina, Vienna, 124 pp.

Fontanier, C., Jorissen, F.J., Licari, L., Alexandre, A., Anschutz, P., Carbonel, P., 2002. Live benthic foraminiferal faunas from the Bay of Biscay: faunal density, composition, and microhabitats. Deep Sea Research Part I: Oceanographic Research Papers 49, 751-785.

Fornasini, C., 1902. Contributo ala conoscenza de la Bulimine Adriatiche. Memorie della Reale Accademie della Scienze dell'

lstituto di Bologna, Scienze Naturali 5, 9, 371-381.

Franceschini, G., Compton, J.S., 2004. Aeolian and marine deposits of the Tabakbaai Quarry area, Western Cape, South Africa. South African Journal of Geology 107.4, 619-632.

Franceschini, G., Compton, J.S., 2007. Abrasion of foraminifera tests along an active dune cordon, Western Cape, South Africa. Palaios 22, 686-690.

Franceschini, G., McMillan, I.K., Compton, J.S., 2005. Foraminifera of Langebaan Lagoon salt marsh and their application to the interpretation of late Pleistocene depositional environments at Monwabisi, False Bay coast, South Africa. South African Journal of Geology 108, 285-296.

Giraudeau, J., 1993. Planktonic foraminiferal assemblages in surface sediments from the southwest African continental margin. Marine Geology 110, 47-62.

Glacon, G., Grazzini, C.V., Iaccarino, S., Rehault, J.P., Randrianasolo, A., Sierro, J.F., Weaver, P., Channell, J., Torii, M., Hawthorne, T., 1990. Planktonic foraminifera; events and stable isotope records in the upper Miocene, site 6541. In: Kastens, K.A., Mascle, J., et al., (Eds.) Proceedings of the Ocean Drilling Program, Scientific Results 107, 415-427.

Goubert, E., Néraudeau, D., Rouchy, J.M., Lacour, D., 2001. Foraminiferal record of environmental changes: Messinian of the Los Yesos area (Sorbas Basin, SE Spain). Palaeogeography, Palaeoclimatology, Palaeoecology 175, 61-78.

Hammer, Ø., Harper, D.A.T., Ryan, P.D., 2001. PAST: paleontological statistics software package for education and data analysis. Palaeontologia Electronica 4, 9 pp. (http://palaeo-electronica.org/2001_1/past/issue1_01.htm).

Hay, W.W., Sibuet, J.C., Barron, E.J., Brassell, S.C., Dean, W.E., Huc, A.Y., Keating, B.H., McNulty, C.L., Meyers, P.A., Nohara, M., Schallreuter, R.E.L., Steinmetz, J.C., Stow, D.A.V., Stradner, H., Boyce, R.E., Amidei, R., 1984, Initial Reports of the Deep Sea Drilling Project, volume 75. U.S. Government Printing Office, Washington, D.C., 1303 pp.

Hays, J., Imbrie, J., Shackleton, N., 1976. Variations in the earth's orbit: pacemaker of the ice ages. Science 194, 1121–1132.

Herbert, C.T., Compton, J.S., 2007. Geochronology of Holocene sediments on the western margin of South Africa. South African Journal of Geology 110, 327-338.

Herbert, D. G., 2013. *Turritella declivis* Adams & Reeve, in Reeve, 1849 (Mollusca: Gastropoda)—a South African not an Australian Species, and a characteristic component of the Agulhas Bank benthos. African Zoology 48, 412-417.

Holbourn, A., Henderson, A.S., MacLeod, N., 2013. Atlas of Benthic Foraminifera. Wiley-Blackwell, Oxford, 654 pp.

Ibaraki, M., 1997. Closing of the Central American Seaway and Neogene coastal upwelling along the Pacific coast of South America. Tectonophysics 281, 99-104.

Imbrie, J., Boyle, E.A., Clemens, S.C., Duffy, A., Howard, W.R., Kukla, G., Kutzbach, J., Martinson, D.G., McIntyre, A., Mix, A.C., Molfino, B., Morley, J.J., Peterson, L.C., Pisias, N.G., Prell, W.L., Raymo,M.E., Shackleton, N.J., Toggweiler, J.R. 1992.

On the structure and origin of major glaciation cycles.1. Linear responses to Milankovitch. forcing. Paleoceanography 6, 205–226.

Jaeckel, S., Thiele, J., 1931. Muscheln der Deutschen Tiefsee Expedition. Wissenschaftliche Ergebnisse der Deutschen Tiefsee-Expedition auf dem Dampfer "Valdivia" 1898-1899, 21, 161-268.

Jahn, B., Donner, B., Müller, P. J., Röhl, U., Schneider, R. R., Wefer, G., 2003. Pleistocene variations in dust input and marine productivity in the northern Benguela Current: evidence of evolution of global glacial–interglacial cycles. Palaeogeography, Palaeoclimatology, Palaeoecology 193, 515-533.

Jorissen, F.J., de Stigter, H.C., Widmark, J.G., 1995. A conceptual model explaining benthic foraminiferal microhabitats. Marine micropaleontology 26, 3-15.

Jorissen, F.J., Wittling, I., Peypouquet, J.P., Rabouille, C., Relexans, J.C., 1998. Live benthic foraminiferal faunas off Cap Blanc, NW Africa: community structure and microhabitats. Deep-Sea Research I, 45, 2157–2188.

Kaiho, K., 1994. Benthic foraminiferal dissolved-oxygen index and dissolved-oxygen levels in the modern ocean. Geology 22, 719-722.

Kaminski, M.A., 2012. Calibration of the benthic foraminiferal oxygen index in the Marmara Sea. Geological Quarterly 56, 757-764.

Kemle-von Mücke, S., Oberhänsli, H., 1999. The distribution of living planktic foraminifera in relation to southeast Atlantic oceanography. In: Use of Proxies in Paleoceanography. Springer, Berlin-Heidelberg, pp. 91-115.

Kennett, J.P., Srinivasan, M.S., 1983. Neogene Planktonic Foraminifera. A Phylogenetic Atlas. Hutchinson Ross, Stroudsburg, 265 pp.

Kensley, B., 1978. Interaction between coastal processes and lagoonal fauna, between Walvis Bay and L deritzbucht, South West Africa. Madoqua 11, 55-60.

Kilburn, R., Rippey, E., 1982. Sea Shells of Southern Africa. Macmillan South Africa, Johannesburg, 249 pp.

Koho, K.A., García, R., De Stigter, H.C., Epping, E., Koning, E., Kouwenhoven, T.J., Van der Zwaan, G.J., 2008. Sedimentary labile organic carbon and pore water redox control on species distribution of benthic foraminifera: A case study from Lisbon–Setúbal Canyon (southern Portugal). Progress in Oceanography 79(1), 55-82.

Koho, K.A., Piña-Ochoa, E., Geslin, E., Risgaard-Petersen, N., 2011. Vertical migration, nitrate uptake and denitrification: survival mechanisms of foraminifers (*Globobulimina turgida*) under low oxygen conditions. FEMS Microbiology Ecology 75, 273-283.

Kucera, M., 2007. Planktonic foraminifera as tracers of past oceanic conditions. In: Hillaire-Marccel, C and de Vernal, A (Eds.). Proxies in Late Cenozoic Paleoceanography. Elsevier, Amsterdam, 213-262.

Kuhnt, T., Schiebel, R., Schmiedl, G., Milker, Y., Mackensen, A., Friedrich, O., 2014. Automated and manual analyses of the

pore density-to-oxygen relationship in *Globobulimina turgida* (Bailey). The Journal of Foraminiferal Research 44, 5-16.

Lazarus, D., Bittniok, B., Diester-Haass, L., Billups, K., Ogawa, Y., Takahashi, K., Meyers, P., 2008. Radiolarian and sedimentologic paleoproductivity proxies in late Pleistocene sediments of the Benguela Upwelling System, ODP Site 1084. Marine Micropaleontology 68, 223-235.

Lazarus, D., Bittniok, B., Diester-Haass, L., Meyers, P., Billups, K., 2006. Comparison of radiolarian and sedimentologic paleoproductivity proxies in the latest Miocene–Recent Benguela Upwelling System. Marine Micropaleontology 60, 269-294.

Leiter, C., Altenbach, A.V., 2010. Benthic foraminifera from the diatomaceous mud belt off Namibia: characteristic species for severe anoxia. Palaeontologica Africana 13(2), 11A, 19p.

Licari, L., Mackensen, A., 2005. Benthic foraminifera off west Africa (1° N to 32° S): Do live assemblages from the topmost sediment reliably record environmental variability? Marine Micropaleontology 55, 205-233.

Linnaeus, C., 1758. Systema Naturae per Regna Tria Naturae [editio decima, reformata 1 (Regnum animale)]. Salvii, Stockholm, pp. 824.

Lisiecki, L.E., Raymo, M.E., 2007. Plio–Pleistocene climate evolution: trends and transitions in glacial cycle dynamics. Quaternary Science Reviews 26, 56-69.

Little, M.G., Schneider, R.R., Kroon, D., Price, B., Bickert, T., Wefer, G., 1997. Rapid palaeoceanographic changes in the Benguela Upwelling System for the last 160,000 years as indicated by abundances of planktonic foraminifera. Palaeogeography, Palaeoclimatology, Palaeoecology 130(1), 135-161.

Lombard, F., Labeyrie, L., Michel, E., Spero, H.J., Lea, D. W., 2009. Modelling the temperature dependent growth rates of planktic foraminifera. Marine Micropaleontology 70, 1-7.

Lowry, F.M.D., 1987. Foraminiferal thanatocoenoses from the continental shelf of southern Africa. Unpublished PhD. thesis, University College London.

Marchant, M., Hebbeln, D., Wefer, G., 1999. High resolution planktic foraminiferal record of the last 13,300 years from the upwelling area off Chile. Marine Geology 161, 115-128.

Marlow, J.R., Lange, C.B., Wefer, G., Rosell-Mele, A., 2000. Upwelling intensification as part of the Pliocene-Pleistocene climate transition. Science 290, 2288–2291.

Marrat, F.P., 1877. On forty proposed new forms in the genus *Nassa*. Liverpool, 15 pp.

Martin, R.A., 1974. Benthonic foraminifera from the western coast of southern Africa. Bulletin Joint Geological Survey of South Africa/ University of Cape Town Marine Geology Programme Technical Report 6, 83-87.

Martin, R.A., 1981. Benthic foraminifera from the Orange-Lüderitz shelf southern African continental margin. Bulletin Joint Geological Survey of South Africa/ University of Cape Town Marine Geoscience Unit 11, 75 pp.

Martinez, P., Bertrand, P., Shimmield, G.B., Cochrane, K., Jorissen, F.J., Foster, J., Dignan, M., 1999. Upwelling intensity and

ocean productivity changes off Cape Blanc (northwest Africa) during the last 70,000 years: geochemical and micropalaeontological evidence. Marine Geology 158, 57-74.

Mathews, R.D., 1945. *Rectuvigerina*, a new genus of foraminifera from a restudy of *Siphogenerina*. Journal of Paleontology 19, 588-606.

McMillan, I.K. 1987a. Late Quaternary foraminifera from the southern part of offshore South West Africa/Namibia. Unpublished Ph.D. thesis, University of Wales, Aberystwyth.

McMillan, I.K. 1987b. The genus *Ammonia* Brünnich, 1772 (Foraminiferida) and its potential for elucidating the latest Cainozoic stratigraphy of South Africa. South African Journal of Science 83, 32-42.

McMillan, I.K., 1990a. A foraminiferal biostratigraphy and chronostratigraphy for the Pliocene to Pleistocene Upper Algoa Group, Eastern Cape, South Africa. South African Journal of Geology 93, 622-644.

McMillan, I.K., 1990b. Foraminifera from the Late Pleistocene (latest Eemian to earliest Weichselian) shelly sands of Cape Town city centre, South Africa. Annals of the South African Museum 99, 121-186.

Meadows, M.E., 2001. The role of Quaternary environmental change in the evolution of landscapes: case studies from southern Africa. Catena 42(1), 39-57.

Miller, K.G., Kominz, M.A., Browning, J.V., Wright, J.D., Mountain, G.S., Katz, M.E., Sugarman, P.J., Cramer, B.S., Christie-Blick, N., Pekar, S.F., 2005. The Phanerozoic record of global sea-level change. Science 310, 1293-1298.

Mohtadi, M., Hebbeln, D., Marchant, M., 2005. Upwelling and productivity along the Peru–Chile Current derived from faunal and isotopic compositions of planktic foraminifera in surface sediments. Marine Geology 216, 107-126.

Mollenhauer, G., Eglinton, T.I., Ohkouchi, N., Schneider, R.R., Müller, P.J., Grootes, P.M., Rullkötter, J., 2003. Asynchronous alkenone and foraminifera records from the Benguela Upwelling System. Geochimica et Cosmochimica Acta 67(12), 2157-2171.

Mollenhauer, G., Schneider, R.R., Müller, P.J., Spieß, V., Wefer, G., 2002. Glacial/interglacial variability in the Benguela upwelling system: Spatial distribution and budgets of organic carbon accumulation, Global Biogeochemical Cycles 16(4), 1134, doi:10.1029/2001GB001488.

Murray, J.W., 2006. Ecology and Applications of Benthic Foraminifera. Cambridge University Press, Cambridge, 426 pp.

Parker W.K., Jones T.R., Brady H. B., 1865. On the nomenclature of the Foraminifera. Part X. (continued). The species enumerated by D'Orbigny in the 'Annales des Sciences Naturelles,' 1826, vol. vii. - III. The species illustrated by models. Annals and Magazine of Natural History (3) 16 (91), 15-41.

Pedersen, T.F., Calvert, S.E., 1990. Anoxia vs. productivity: what controls the formation of organic-carbon-rich sediments and sedimentary Rocks? AAPG Bulletin 74(4), 454-466.

Peeters, F.J., Brummer, G.J.A., Ganssen, G., 2002. The effect of upwelling on the distribution and stable isotope composition of *Globigerina bulloides* and

Globigerinoides ruber (planktic foraminifera) in modern surface waters of the NW Arabian Sea. Global and Planetary Change 34, 269-291.

Pérez Asensio, J.N., 2013. Paleoecological and paleoceanographical study of messinian depostis from the lower Guadalquivir basin (SW Spain). PhD thesis, Universidad de Granada.

Pérez-Asensio, J.N., Aguirre, J., Schmiedl, G., Civis, J., 2012. Messinian paleoenvironmental evolution in the lower Guadalquivir Basin (SW Spain) based on benthic foraminifera. Palaeogeography, Palaeoclimatology, Palaeoecology 326, 135-151.

Phipps, M.D., Kaminski, M.A., Aksu, A.E., 2010. Calcareous benthic foraminiferal biofacies along a depth transect on the southwestern Marmara shelf (Turkey). Micropaleontology, 377-392.

Pisias, N.G., Moore, T.C., 1981. The evolution of Pleistocene climate: a time series approach. Earth and Planetary Science Letters 52, 450-458.

Prell, W.L., Curry, W.B., 1981. Faunal and isotopic indices of monsoonal upwelling-western arabian sea. Oceanologica Acta 4, 91-98.

Rau, A. J., Rogers, J., Lutjeharms, J. R. E., Giraudeau, J., Lee-Thorp, J. A., Chen, M. T., Waelbroeck, C., 2002. A 450-kyr record of hydrological conditions on the western Agulhas Bank Slope, south of Africa. Marine Geology 180, 183-201.

Raymo, M.E., Nisancioglu, K.H., 2003. The 41 kyr world: Milankovitch's other unsolved mystery. Paleoceanography, 18(1), doi: 10.1029/2002PA000791

Reolid, M., Rodríguez-Tovar, F.J., Nagy, J., Olóriz, F., 2008. Benthic foraminiferal morphogroups of mid to outer shelf environments of the Late Jurassic (Prebetic Zone, southern Spain): characterization of biofacies and environmental significance. Palaeogeography, Palaeoclimatology, Palaeoecology 261, 280-299.

Robinson, R. S., Meyers, P. A., Murray, R. W., 2002. Geochemical evidence for variations in delivery and deposition of sediment in Pleistocene light–dark color cycles under the Benguela Current Upwelling System. Marine Geology 180, 249-270.

Sautter, L.R., Thunell, R.C., 1991. Seasonal variability in the $\delta^{18}O$ and $\delta^{13}C$ of planktonic foraminifera from an upwelling environment: sediment trap results from the San Pedro Basin, Southern California Bight. Paleoceanography 6, 307-334.

Schmidt-Sinns, J., 2008. Rezente benthische Foraminiferen im Bereich des Benguelastroms, Südwestafrika–Verbreitungsmuster und ihre steuernden Faktoren. PhD thesis, Universitätsund Landesbibliothek, Bonn, 1-261.

Schmiedl, G., 1995. Rekonstruktion der spätquartären Tiefenwasserzirkulation und Produktivität im östlichen Südatlantik anhand von benthischen Foraminiferenvergesellschaftungen / Late Quaternary benthic foraminiferal assemblages from the eastern South Atlantic Ocean: reconstruction of deep water circulation and productivity changes. Berichte zur Polarforschung (Reports on Polar Research 160, 207 pp.

Schmiedl, G., Mackensen, A., 1997. Late Quaternary paleoproductivity and deep water circulation in the eastern South

Atlantic Ocean: evidence from benthic foraminifera. Palaeogeography. Palaeoclimatology. Palaeoecology 130, 43-80.

Schmiedl, G., Mackensen, A., Müller, P.J., 1997. Recent benthic foraminifera from the eastern South Atlantic Ocean: dependence on food supply and water masses. Marine Micropaleontology 32, 249-287.

Schröter, J.S., 1783. Einleitung in die Conchilienkenntnis nach Linné, Erster Band, 860 pp.

Shannon, L.V., Nelson, G., 1996. The Benguela: large scale features and processes and system variability. In: Wefer, G., Berger, W.H., Siedler, G., Webb, D. (Eds.). The South Atlantic: Present and Past Circulation. Springer Verlag, Heidelberg, pp. 163-210.

Shi, N., Schneider, R., Beug, H.J., Dupont, L.M., 2001. Southeast trade wind variations during the last 135 kyr: evidence from pollen spectra in eastern South Atlantic sediments. Earth and Planetary Science Letters 187, 311-321.

Sowerby, G.B. III., 1904. Mollusca of South Africa. (Pelecypoda.). Marine Investigations in South Africa, 4, 1-19.

Tankard, A.J., Rogers, J., 1978. Late Cenozoic palaeoenvironments on the west coast of southern Africa. Journal of Biogeography, 319-337.

Thompson, P.R., Bé, A.W., Duplessy, J.C., Shackleton, N.J., 1979. Disappearance of pink-pigmented Globigerinoides ruber at 120,000 yr BP in the Indian and Pacific Oceans. Nature 280(5723), 554.

Ufkes, E., Jansen, G.H.F., Brumrner, G-J. A., 1998. Living planktonic foraminifera in the eastern South Atlantic during spring: indicators of water masses, upwelling and the Congo (Zaire) River plume. Marine Micropaleontology 33, 27-53.

Ufkes, E.L.S., Kroon, D., 2012. Sensitivity of south-east Atlantic planktonic foraminifera to mid-Pleistocene climate change. Palaeontology 55(1), 183-204.

Walker, G., Jacob. E., 1798. Descriptions of *Serpula (Lagena) sulcata* and *Nautilus lobatulus*. In: Adams, G (Ed.). Essays on the microscope: containing a practical description of the most improved microscopes. Dillon and Keating, London, pp. 634-642.

Walker, S.T., Mantle, D., Bythell, J. C., Thomason, J.C., 2000. Oxidative-stress: comparison of species specific and tissue specific effects in the marine bivalves *Mytilus edulis* (L.) and *Dosinia lupinus* (L.). Comparative Biochemistry and Physiology Part B: Biochemistry and Molecular Biology 127, 347-355.

Watson, I., Lemon, R.R., 1985. Geomorphology of a Coastal Desert: The Namib, South West Africa/Namibia. Journal of Coastal Research, pp. 329-342.

Wearne, K., Underhill, L.G., 2005. Walvis Bay, Namibia: a key wetland for waders and other coastal birds in southern Africa. Bulletin-wader Study Group 107, 24.

Wefer, G., Berger, W.H., Richter, C., Adams, D.D., Anderon, L.D., Andreasen, D.J., Brüchert, V., Cambray, H., Christensen, B.A., Frost, G.M., Giraudeau., Gorgas, T.J., Hermelin, O., Lange, C.B., Laser, B., Lin, H-L., Maslin, M., Meyers, P.A., Motoyama, I., Murray, R.W., Pato, D., Perez, M.E., Pufahl, P.K., Spiess, V., Vidal. L., Wigley, R., Yamazaki, T., 1998.

Proceedings of the Ocean Drilling Program volume 175, 385-428.

Wigley, R., Compton, J.S., 2006. Late Cenozoic evolution of the outer continental shelf at the head of the Cape Canyon, South Africa. Marine Geology 226, 1-23.

Williamson, W.C., 1858. On the recent Foraminifera of Great Britain. Ray Society Publications, London, 20, 1-107

Chapter 7

Late Quaternary Foraminiferal Records from the Western Slope of South Africa

7. Late Quaternary foraminiferal records from the western slope of South Africa

Abstract

Planktic and benthic foraminifera recovered from three gravity cores on the western slope of South Africa record variations in the depositional history, palaeoceanography and palaeoecology during late Quaternary glacial-interglacial cycles spanning glacial terminations II and I. The age model was determined by oxygen isotope ($\delta^{18}O$) stratigraphy of *Globorotalia (Globoconella) inflata* and *Cibicidoides wuellerstorfi*, sediment colour reflectance and abundance of quartz and glauconite grains. Sedimentation rates are lower during glacial periods suggesting greater export of sediment beyond the margin and greater delivery of shelf quartz and glauconite to the slope during glacial lowstands. Upwelling intensity and cold surface waters during glacial periods and the inflow of warm subtropical surface waters during interglacial periods were found by principal component analysis (PCA) to play the largest roles in the planktic foraminiferal faunal composition. All three cores record a sharp decrease in *Neogloboquadrina incompta* and a sharp increase in *Globigerinoides ruber* across glacial terminations II and I. These changes are attributed to the southward shift of the Antarctic and Subantarctic polar fronts and to the increased inflow of warm surface waters in the transition from glacial to interglacial periods. Water depth variations in the most abundant benthic group *Uvigerina* spp. are attributed to the influence of bottom water nutrient and oxygen conditions. During interglacial periods the relative abundance of *U. peregrina* increase at Antarctic Intermediate Water (AAIW) depths while the relative abundance of *U. hispidocostata*, a species adapted to high-nutrient and low-oxygen bottom water conditions increases at greater water depths during glacial periods. Benthic foraminiferal PCA reveal that organic matter delivery to the seafloor, seasonality of phytodetritus input and oxygen content of bottom waters were major regulators in the faunal composition on the slope.

7.1. Introduction

The late Quaternary is characterised by high-amplitude climatic cycles since the Mid-Pleistocene Transition (MPT) (Broecker and Denton, 1990; Crundwell et al., 2008; Denton et al., 2010). The frequencies of these climatic cycles coincide with ice-sheet dynamics at high latitudes primarily in the Northern Hemisphere (Crundwell et al., 2008) and the periodicity of these cycles is controlled by the precession, obliquity and eccentricity of Earth's orbit (Berger, 1978; Imbrie et al., 1992), reflected in variability in the oceans and associated sediments over glacial-interglacial periods (e.g. Schmiedl and Mackensen, 1997). Glacial-interglacial cycles during the late Quaternary are also characterised by decreasing CO_2 in the atmosphere during ice sheet build up followed by rapid atmospheric CO_2 increase when ice sheets collapse during deglaciations (Broecker and Donk, 1970). These cycles are preserved in deep-sea marine records and for which foraminifera provide an extremely useful proxy in investigating palaeoceanographic changes during the Quaternary (e.g. Rau et al., 2002; Kucera, 2007; Crundwell et al., 2008; Denton et al., 2010; Cronin et al., 2014; Chapori et al., 2015; Petro et al., 2016; Gallagher et al., 2018).

Along the western margin of South Africa planktic foraminifera have provided useful information on sea surface conditions and oceanographic changes (Giraudeau, 1993; Rau et al., 2002). The occurrence of abundant transitional planktic foraminifera such as *Globorotalia (Globoconella) inflata* and *Globigerina bulloides* have dominated the western slope of South Africa for much of the late Quaternary (Giraudeau, 1993; Rau et al., 2002) with tropical-subtropical foraminifera forming only minor components within the assemblage compositions (Rau et al., 2002). The occurrence of minor tropical-subtropical planktic foraminifera along the western margin of South Africa has been attributed to warm water intrusions from the southern Indian Ocean as a result of 'Agulhas Leakage' (Peeters et al., 2004). The strength of these warm water intrusions is controlled by equatorward movement of the Subtropic convergence (STC) (Rau et al., 2002).

Lowry (1987) and Giraudeau (1993) found *Neogloboquadrina incompta* to be a major species in surface grab samples along the margin of South Africa and Namibia. The occurrence of polar and subpolar water taxa such as *Ng. pachyderma* and *Ng. incompta*, and the general hydrographic conditions along the margin have been attributed to the migrating STC and polar fronts related to glacial-interglacial cycles (Rau et al., 2002).

Preliminary faunal occurrence lists and records are documented in cruise reports of the DSDP, ODP and RV *Meteor*. Benthic foraminifera are useful in determining the palaeoproductivity record of the western margin of southern Africa during the Neogene. Previous studies (Diester-Haass et al., 2002, 2004) have found productivity to have increased during the Miocene, a period in which the Benguela Upwelling System (BUS) initiated in the Northern Benguela Region (NBR) (Siesser, 1980; Bergh et al., 2018). Quaternary studies along the western slope of southern Africa have shown productivity was enhanced during glacial periods (Rau, 2002) since the late Miocene (Diester-Haass et al., 1992).

Martin (1981) documented benthic foraminifera in surface sediments from the northwestern South African to southern Namibian shelf and upper slope, and found five bathymetric zones distinguishable by faunal differences. On the upper slope *Uvigerina peregrina* starts to decrease and buliminids increase in abundance (Martin, 1981). For the Benguela Region these studies have been restricted primarily to the Namibian margin. Schmiedl and Mackensen (1997) studied two late Quaternary cores from the central Namibian slope (2987 m water depth) and from the Walvis Ridge (3210 m water depth) for bottom water mass analysis, benthic foraminifera and stable carbon isotope content. Low epibenthic $\delta^{13}C$ values in the late Quaternary cores indicate enhanced organic matter fluxes with a weak North Atlantic Deep Water (NADW) influence during glacial periods on the Namibian slope (Schmiedl and Mackensen, 1997). Late Quaternary sediments and surface sediments contain low-diversity, high-productivity faunas adapted to high organic matter fluxes along the slope of Namibia (Schmiedl and Mackensen, 1997; Schmiedl et al., 1997) with high-productivity faunas such as *Cassidulina laevigata, Melonis barleeanus* and *Melonis zaandamae* replacing *Epistominella exigua* as the dominant taxa

during glacial periods (Schmiedl and Mackensen, 1997). Food supply and bottom water oxygen content were found to be the most important determining factors in the distribution of benthic foraminifera at shelf to abyssal depths on the Namibian margin of the Angola and Cape basins (Schmiedl et al., 1997).

Despite palaeoproductivity and faunal occurrence records compiled by DSDP and ODP reports and work done by Martin (1981), Lowry (1987) and Rau et al. (2002), a comprehensive study on Quaternary benthic foraminifera on the South African slope is lacking. This chapter aims to identify and analyse the planktic and benthic foraminifera from three cores along the western slope of South Africa to determine late Quaternary palaeoceanographic and palaeoenvironmental changes over the last two glacial terminations in an attempt to determine which factors are important in regulating foraminiferal distributions along the continental slope and how bottom water conditions affect benthic foraminiferal occurrences.

7.2. Materials and Methods

A core from the upper slope (874 m) and two cores from the lower slope (3522 and 3631 m) (Fig. 7.1) are investigated to determine the factors influencing foraminiferal occurrences compared to other Quaternary records. The cores were retrieved during the 2003 (M57/1) and 2016 (M123) RV *Meteor* cruises from Walvis Bay to Cape Town. Each core was spilt in half on-board and assigned as a working and archive half. The working halves were logged and sampled and the archive halves were scanned using a Smartcube© camera image scanner at 1 mm to 1 cm intervals to obtain colour reflectance data and L* values of the red/blue ratio (700 nm/400 nm) (Zabel et al., 2017). Cores GeoB8336-6 and GeoB8342-6, were retrieved during the M57/1 cruise and core GeoB 20601-4 retrieved during the M123 cruise. The samples were taken primarily at every 4 to 5 cm at the University of Bremen in Germany (GeoB 8342-6 and 8336-6) and on-board the ship (GeoB 20601-4). The sample selection allowed for an adequate resolution for this study and was also taken where contacts were visible.

The core samples were washed, sieved and split into <63 μm (mud), 63 μm to 2 mm (sand) and >2 mm (gravel) fractions. The sand fractions were placed in an ultrasonic bath for up to 1 minute to disaggregate and suspend bulk sediment particles and to remove sediment from the surfaces and interiors of foraminifera tests. No appreciable breakage of foraminiferal tests was observed. The fractions were dried in an oven at 70˚C and weighed to obtain grain size distributions. The sand fractions were further dry sieved to a >125 μm fraction to identify the foraminifera to species level under a binocular microscope. Loeblich and Tappan (1988) and Jones (1994) were consulted to confirm identifications. The foraminifera were counted to a statistically significant number (>300 individuals) to determine their relative abundances. Where certain groups (e.g. benthic foraminifera) were less than 300 individuals per sample all individuals were counted. The >125 μm size fraction was chosen for comparisons with data from previous studies and to ensure more accurate identifications (Kucera, 2007). Planktic foraminifera were identified as transitional, cold water (subpolar/polar), subtropical and tropical based on the literature (e.g. Bé and Tolderlund, 1971; Giraudeau,

1993; Kucera, 2007; BouDagher-Fadel, 2015). Non-carbonate mineral grains (primarily quartz and glauconite) were counted in the sand fractions. Where grains were too abundant a small sub-sample was taken and the results normalized to 1 gram of sediment.

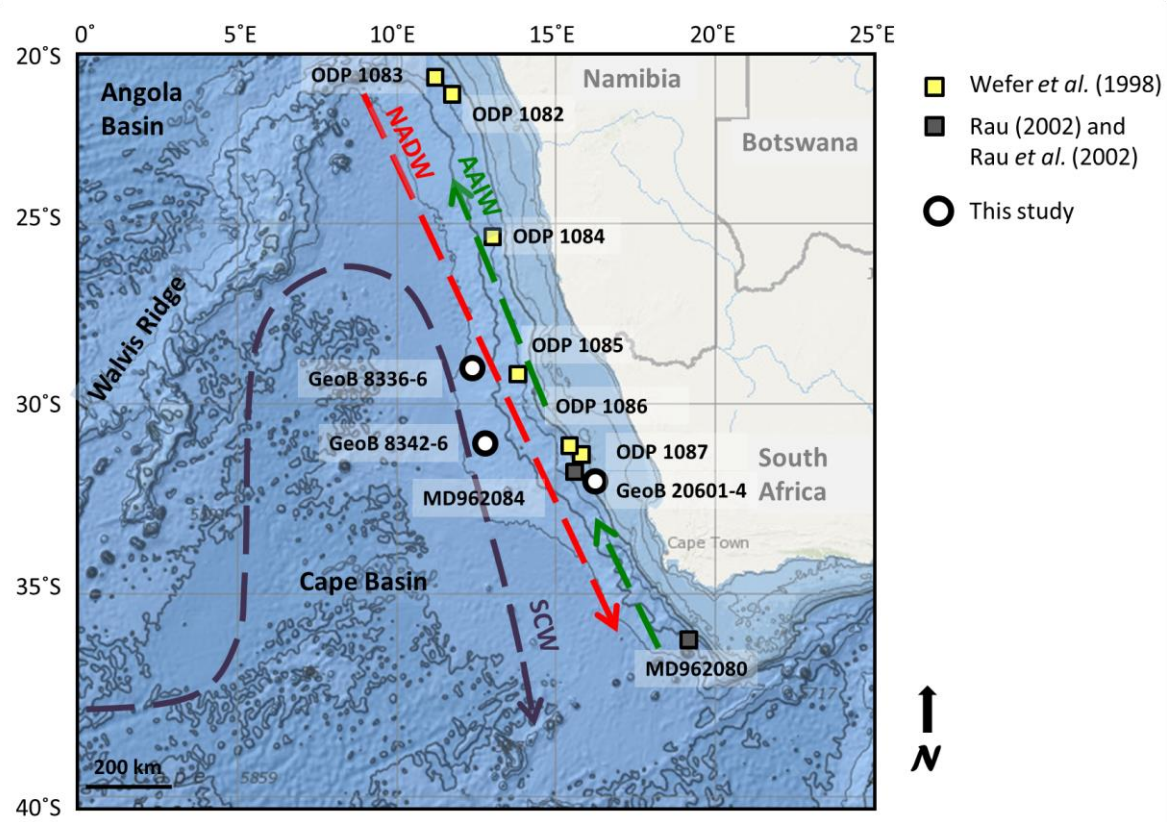

Fig. 7.1. Locations of cores discussed in this study and oceanographic features in the eastern South Atlantic. The basemap is from the National Oceanic and Atmospheric Administration (NOAA) Bathymetric Data Viewer. The flow path of deep water masses (after Lutjeharms and Stockton, 1987) are indicated by the arrowed dashed lines (purple = SCW = Southern Component Water; red = NADW = North Atlantic Deep Water; green = AAIW = Antarctic Intermediate Water). Contours are spaced at 100 m intervals up to 500 m on the shelf. Thereafter contour lines are spaced at 1000 m.

Principal component analysis (PCA) was computed using the PAlaeontologicalSTatistics (PAST) data analysis package (Hammer et al., 2001) and performed on the relative abundance data to investigate which factors influence species abundance based on the dominant taxa in the assemblages. Two matrices of planktic and benthic foraminifera per core were created for PCA. Taxa with at least three occurrences and those with at least one with >2% were included in the matrices. Benthic foraminiferal accumulation rates (BFARs) and benthic foraminiferal oxygen index (BFOI) data were added to the benthic matrix. A cross-correlation matrix was applied to the matrix used for PCA. Taxa with a high cross-correlation value (>0.9) were removed from the matrix to reduce the number of variables. Principal component analysis is a method by which the dimensionality of a multivariate data set is reduced to a few principal components (Abdi and Williams, 2010) that attempt to explain the distribution of species while retaining a large proportion of the original variability within the data (Dray, 2008).

Specimens that were identified were imaged with a scanning electron microscope (SEM). The specimens were placed onto black double-sided adhesive carbon tabs and mounted onto pin stubs before they were coated with a thin layer of Gold-Palladium using a BIO-RAD SEM coating system. Images of the specimens were then taken with a JEOL JSM-5200 and a Nova NanoSEM scanning microscope at Iziko Museums in Cape Town and the Electron Microscope Unit at the University of Cape Town, respectively.

The age model for the three cores is based on the oxygen isotope signatures of the benthic foraminifer *Cibicidoides wuellerstorfi* and as a secondary measure the planktic species *Globorotalia (Globoconella) inflata.* To obtain $\delta^{18}O$ for oxygen isotope stratigraphy and $\delta^{13}C$ for palaeoproductivity indicator plots ~3 to 10 individuals of the benthic species *C. wuellerstorfi* and 15 to 30 individuals of *Gr. (Gc.) inflata* were picked from the 350 to 425 μm size fraction for each core. The species picked were based on previous studies close to the study area (Rau, 2002; Rau et al., 2002). The number of tests picked was dependent on the amount of individuals in the samples, with more tests picked in samples where the species was more abundant. The size fraction of the specimens was based on the average shell mass needed for the detection limits of the instrumentation and to minimise the error in the analyses. The samples were analysed for $\delta^{18}O$ and $\delta^{13}C$ using a Finnigan MAT 251 gas isotope ratio mass spectrometer coupled to a Kiel I automated carbonate preparation device at the University of Bremen. The $\delta^{18}O$ and $\delta^{13}C$ results are reported relative to Vienna Pee Dee Belemnite (VPDB) with a mean error of 0.02‰.

The $\delta^{18}O$ records in the three cores were graphically correlated to the LR04 record (Lisiecki and Raymo, 2005) using the Analyseries 2.0.8 programme (Paillard et al., 1996). The $\delta^{18}O$ data were also graphically correlated with colour reflectance data and non-carbonate mineral grain counts to further support the age model.

Sedimentation rates were calculated based on the age profile obtained from the $\delta^{18}O$ plots. Benthic foraminiferal accumulation rates (BFARs) were calculated using the formula:

$$BFAR = BFN \times SR \times D$$

Where: BFN = number of benthic individuals per gram of dry bulk sediment ($bf.g^{-1}$)
SR = sedimentation rate ($cm.kyr^{-1}$)
D = dry bulk density ($g.cm^{-3}$).

Oxic (>2 ml/l O_2), suboxic (0.3 to 1.5 ml/l O_2) and dysoxic (0.1-0.3 ml/l O_2) taxa were identified based on the classification by Kaiho (1994) and their associated dissolved oxygen content preferences. Infaunal and epifaunal classification of the benthic foraminifera were based on previous studies (e.g. Murray, 1976; Alegret et al., 2003; Drinia et al., 2007; Reolid et al., 2008; Pérez-Asensio et al., 2012). Kaiho (1994) developed the benthic foraminiferal oxygen index (BFOI) to investigate bottom water oxygen conditions. The BFOI was further explored by Kaiho (1999) and used as an indicator of dissolved bottom water oxygen. In this study BFOI values were calculated for each sample based on the formula by Kaiho (1994).

$$BFOI = O / (O + D) \times 100$$

O = number of benthic oxic specimens in the sample
D = Number of benthic dysoxic specimens in the sample

7.3. Results

7.3.1 Core lithology

Core 20601-4 consists of alternating units of dark and light olive-grey nannofossil to foraminifera-rich oozes (Fig. 7.2). The sand fraction of core GeoB 20601-4 ranges between 16.8 and 75.7 wt% with a mean of 51.3 wt% (Appendix Table A.21). The deeper core GeoB 8342-6 has a lower sand content than core GeoB 20601-4 ranging between 2.4 and 34.1 wt% (Appendix Table A.22) with a mean of 16.1wt%. The deepest core GeoB 8336-6 has the lowest sand content with values ranging between 1.1 and 27.8 wt% with a mean of 9.9 wt% (Appendix Table A.23). The upper unit of core 8336-6 has a higher sand content than the rest of the core that was analysed. Foraminifera forms the largest component of the sand fractions in all the cores (>90%) with minor to trace amounts of sponge spicules, echinoid spines, radiolaria, glauconite, quartz and small rock fragments and mineral grains. Quartz grains occur mainly as translucent angular to subangular very fine sand to fine sand. Glauconite grains occur mainly as dark to pale green coloured rounded very fine sand. The mud fraction is composed primarily of nannofossils and clay minerals.

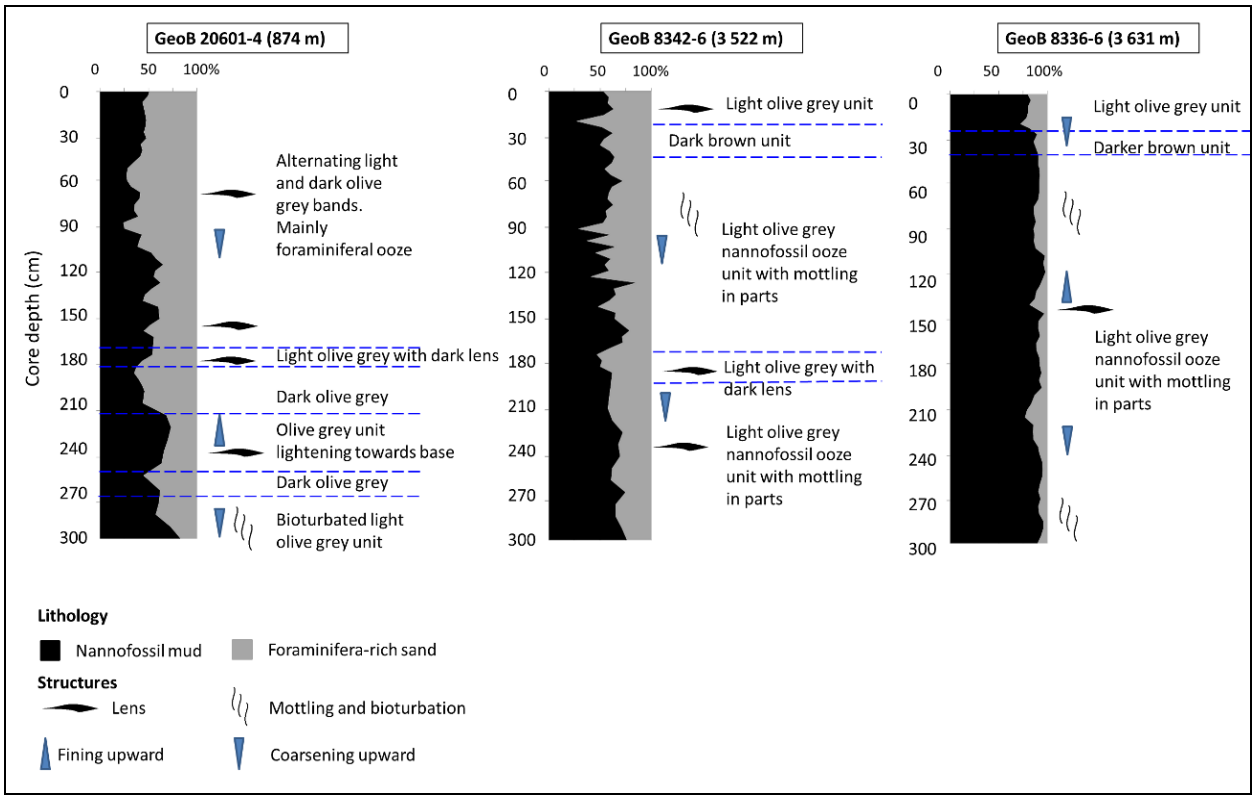

Fig. 7.2. Stratigraphy of cores GeoB 20601-4, 8342-6 and 8336-6.

7.3.2 Stable isotopes ($\delta^{18}O$ and $\delta^{13}C$) and age model

Marine isotope stages (MIS) of the three cores were identified by peak maxima and minima in the $\delta^{18}O$ record (Appendix Table C.1) correlated to the LR04 (Lisiecki and Raymo, 2005) record (Fig. 7.3) with enriched $\delta^{18}O_{C.\ wuellerstorfi}$ ($\delta^{18}O_{Cw}$) and $\delta^{18}O_{Gr.\ (Gc.)\ inflata}$ ($\delta^{18}O_{Gi}$) values indicating glacial periods (MIS 8, 6, 4, 2) and depleted $\delta^{18}O_{Cw}$ and $\delta^{18}O_{Gi}$ values indicating interglacial periods (MIS 7, 5, 3, 1). The upper 3 m of core GeoB 20601-4 extend to MIS 8 with peak

maxima of 3.63±0.01‰ and 3.70±0.01‰. The low benthic $\delta^{18}O$ value of 2.53±0.06‰ at 224 cm with a corresponding $\delta^{18}O_{Gi}$ value of 1.38±0.03‰ mark MIS 7 which is followed by an increase in $\delta^{18}O$ values between 185 and 145 cm indicating MIS 6. MIS 5e, 5c and 5a are indicated by the low $\delta^{18}O_{Cw}$ of 2.34±0.02‰, 2.33±0.02‰ and 2.59±0.04‰ at 172, 140 and 124 cm respectively. The $\delta^{18}O_{Gi}$ values are also lower at those depths. Increasing $\delta^{18}O_{Cw}$ and $\delta^{18}O_{Gi}$ following MIS 5 indicate MIS 4 where after a sharp decrease in $\delta^{18}O_{Cw}$ at 80 to 72 cm (2.97±0.03‰ to 2.71±0.03‰) values are indicative of MIS 3. MIS 2 then follows with increasing $\delta^{18}O_{Cw}$ and $\delta^{18}O_{Gi}$ values with an increasing trend until a characteristic decrease of the MIS 2/1 boundary.

The upper 3 m of GeoB 8342-6 extend to MIS 6 with the $\delta^{18}O_{Cw}$ and $\delta^{18}O_{Gi}$ generally following the trend of the LR04 curve (Fig. 7.4). The high $\delta^{18}O_{Cw}$ and $\delta^{18}O_{Gi}$ values are indicative of MIS 6. MIS 5e, 5c and 5a are indicated by the low $\delta^{18}O_{Cw}$ values of 2.72±0.04‰ (188.5 cm), 2.76±0.02‰ (164.5 cm) and 3.26±0.03‰ (140.5 cm), respectively. The $\delta^{18}O_{Cw}$ and $\delta^{18}O_{Gi}$ values thereafter show an increasing trend assigned to MIS 4 until a decrease at 84.5 cm (3.48±0.02‰) and 76.5 cm (3.64±0.01‰) correlated to MIS 3. MIS 2 then follows with an increasing trend in $\delta^{18}O_{Cw}$ and $\delta^{18}O_{Gi}$ until both decrease at the MIS 2/1 boundary and reach the lowest $\delta^{18}O_{Cw}$ value of 2.64±0.01‰ at 8.5 cm core depth.

The higher $\delta^{18}O_{Cw}$ and $\delta^{18}O_{Gi}$ values of MIS 6 in core GeoB 8336-6 are followed by lower $\delta^{18}O_{Cw}$ and $\delta^{18}O_{Gi}$ values indicative of MIS 5, with the lowest $\delta^{18}O_{Cw}$ values of 2.61±0.03‰ (223 cm) and 2.66±0.03‰ (213 cm) assigned to MIS 5e (Fig. 7.5). Low $\delta^{18}O_{Cw}$ values at 188 and 158 cm indicate MIS 5c and 5a, respectively. The $\delta^{18}O_{Cw}$ and $\delta^{18}O_{Gi}$ values thereafter show an increasing trend indicating MIS 4 until a decrease at 91 cm (3.74±0.05‰) correlated to MIS 3. MIS 2 then follows with a $\delta^{18}O_{Cw}$ and $\delta^{18}O_{Gi}$ increasing trend until a characteristic decrease of the MIS 2/1 boundary and the lowest $\delta^{18}O_{Cw}$ value of 2.61±0.04‰ (8 cm).

The $\delta^{13}C_{Globorotalia\ (Globoconella)\ inflata}$ ($\delta^{13}C_{Gi}$) values (Appendix Table C.1) in core GeoB 20601-4 range between 0.16±0.02‰ and 1.11±0.01‰ with a mean value of 0.65±0.02‰. The *C. wuellerstorfi* $\delta^{13}C$ ($\delta^{13}C_{Cw}$) values range between -0.40±0.01‰ and 1.33±0.02‰ with a mean value of 0.72±0.02‰. Between 112 cm to 172 cm the $\delta^{13}C$ record decreases for both *Gr. (Gc.) inflata* and *C. wuellerstorfi*, but increases overall to 252 cm whereas it decreases further in the *C. wullerstorfi* record to 200 cm before it increases again.

In core GeoB 8342-6 the *Gr. (Gc.) inflata* $\delta^{13}C$ values range between 0.37±0.01‰ and 1.31±0.01‰ with a mean value of 0.82±0.01‰. The *C. wuellerstorfi* $\delta^{13}C$ values in core 8342-6 range between -0.32±0.01‰ and 0.71±0.01‰ with a mean value of 0.15±0.01‰. In core GeoB 8336-6 the *Gr. (Gc.) inflata* $\delta^{13}C$ values range between 0.39±0.01‰ and 1.17±0.01‰ with a mean value of 0.87±0.01‰. The *C. wuellerstorfi* $\delta^{13}C$ values range between -0.49±0.01‰ and 0.67±0.01‰ with a mean value of 0.17±0.01‰.

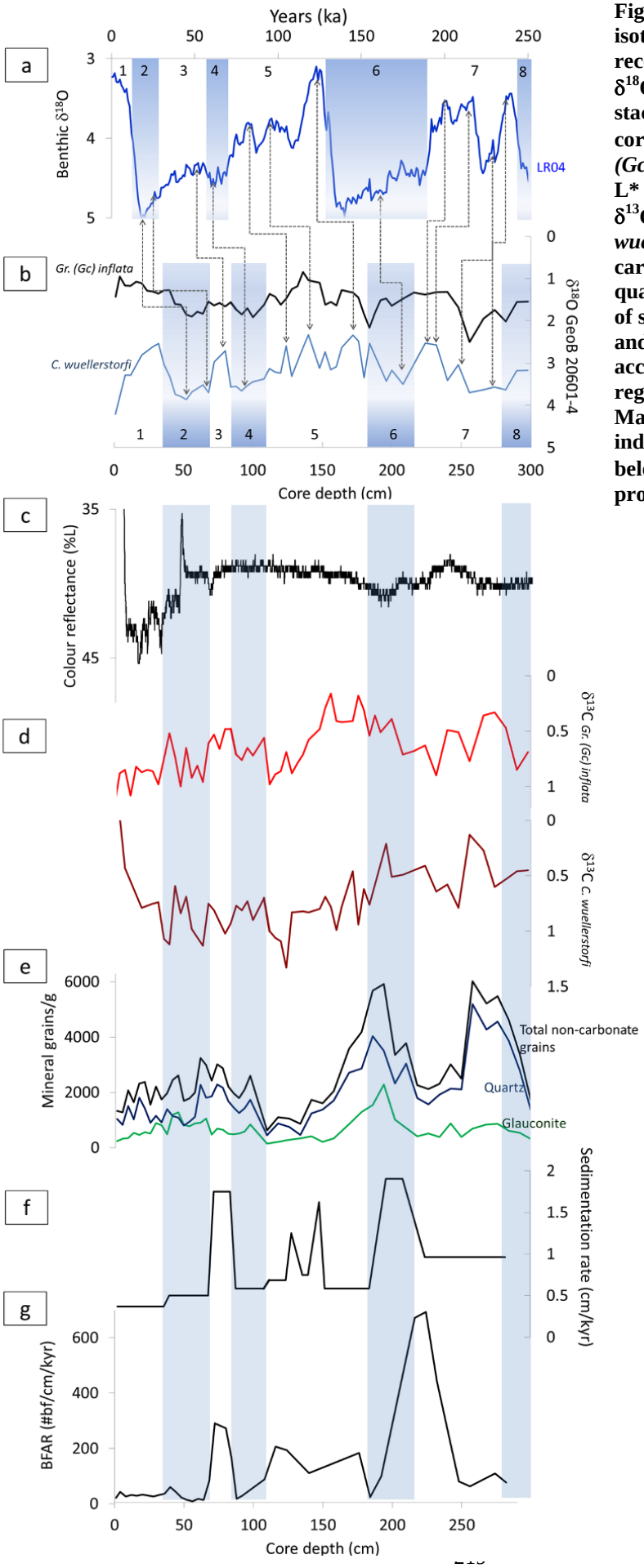

Fig. 7.3. Stable oxygen and carbon isotope profile and depositional records of core GeoB 20601-4. a) $\delta^{18}O$ record of the LR04 benthic stack (Lisiecki and Raymo, 2005) correlated to b) $\delta^{18}O$ record (*Gr. (Gc.) inflata* and *C. wuellerstorfi)*; c) L* colour reflectance record; d) $\delta^{13}C$ (*Gr. (Gc.) inflata* and *C. wuellerstorfi*) record; e) non-carbonate mineral (glauconite, quartz and total) counts per gram of sediment; f) sedimentation rate and g) benthic foraminiferal accumulation rates. The shaded regions indicate glacial periods. Marine isotope stage values are indicated above the LR04 and below the $\delta^{18}O$ (GeoB 20601-4) profiles.

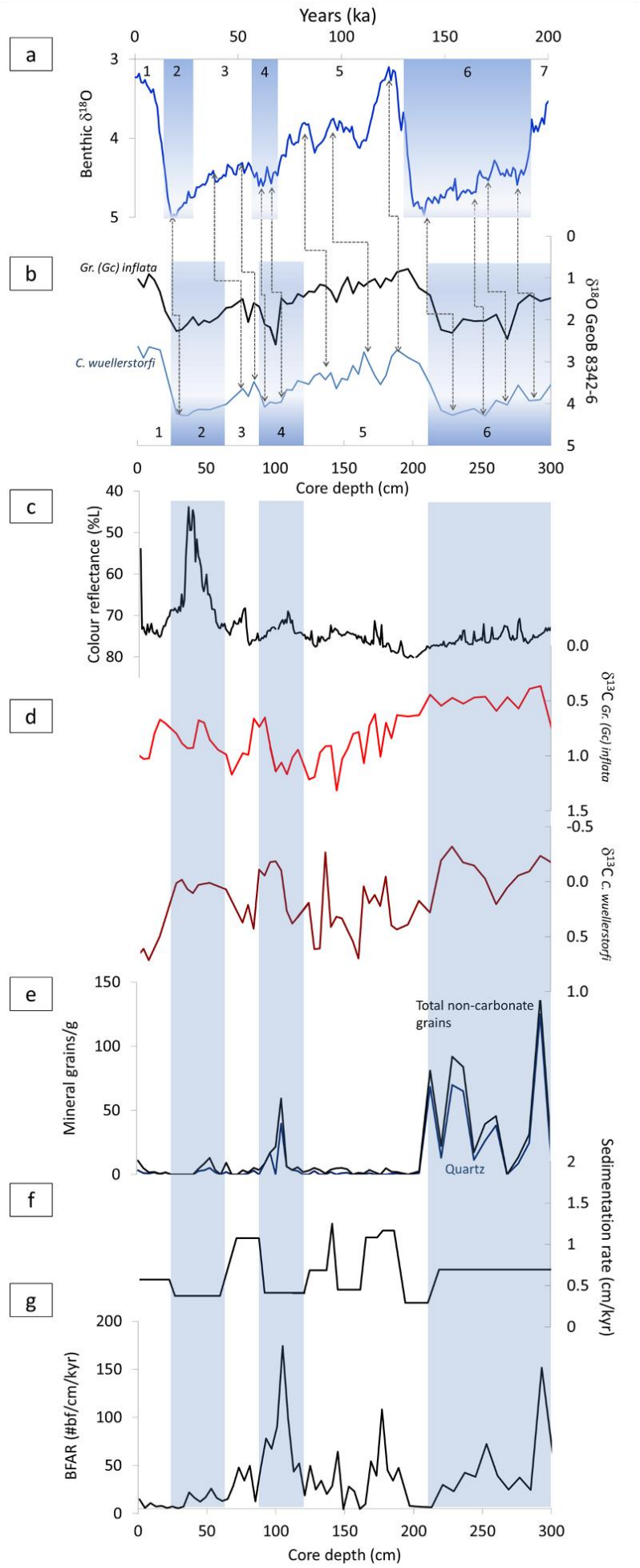

Fig. 7.4. Stable oxygen and carbon isotope profile and depositional records of core GeoB 8342-6. a) $\delta^{18}O$ record of the LR04 benthic stack (Lisiecki and Raymo, 2005) correlated to b) $\delta^{18}O$ record (*Gr. (Gc.) inflata* and *C. wuellerstorfi)*; c) L* colour reflectance record; d) $\delta^{13}C$ (*Gr. (Gc.) inflata* and *C. wuellerstorfi*) record; e) non-carbonate mineral (glauconite, quartz and total) counts per gram of sediment; f) sedimentation rate and g) benthic foraminiferal accumulation rates. The shaded regions indicate glacial periods. Marine isotope stage values are indicated above the LR04 and below the $\delta^{18}O$ (GeoB 8342-6) profiles.

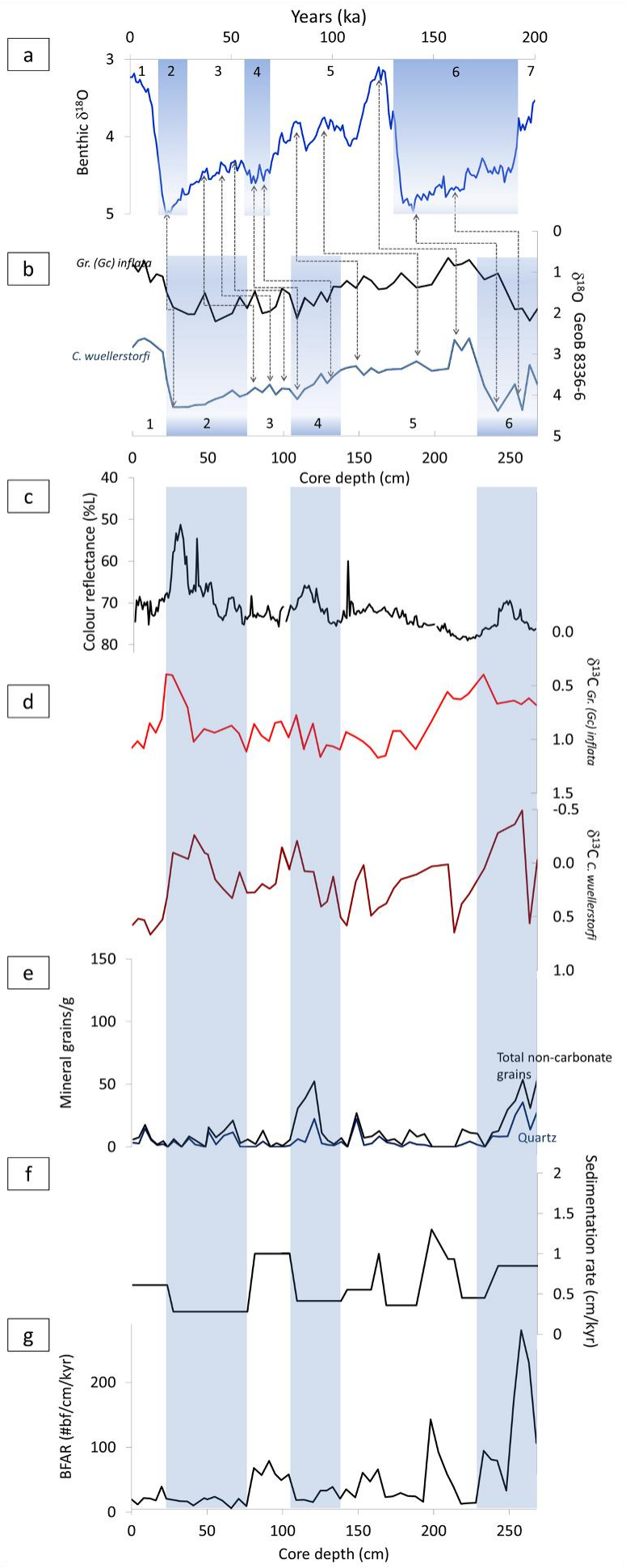

Fig. 7.5. Stable oxygen and carbon isotope profile and depositional records of core GeoB 8336-6. a) $\delta^{18}O$ record of the LR04 benthic stack (Lisiecki and Raymo, 2005) correlated to b) $\delta^{18}O$ record (*Gr. (Gc.) inflata* and *C. wuellerstorfi)*; c) L* colour reflectance record; d) $\delta^{13}C$ (*Gr. (Gc.) inflata* and *C. wuellerstorfi*) record; e) non-carbonate mineral (glauconite, quartz and total) counts per gram of sediment; f) sedimentation rate and g) benthic foraminiferal accumulation rates. The shaded regions indicate glacial periods. Marine isotope stage values are indicated above the LR04 and below the $\delta^{18}O$ (GeoB 8336-6) profiles.

7.3.3 Sedimentation and mineral content

Colour reflectance (L* values) in core GeoB 20601-4 decrease in MIS 7, 4 and 3 with the lowest L* values in MIS 2 (Fig. 7.3). Core GeoB 8342-6 exhibits a fluctuating colour reflectance pattern from MIS 6 to 3 before reaching the lowest values at MIS 2 (Fig. 7.4). In core GeoB 8336-6 L* values are lower during MIS 6, 4 and 2 (Fig. 7.5).

The highest quartz content (Appendix Tables B.23-25) in GeoB 20601-4 occurs at 264 and 184 cm. The highest glauconite content occurs at 192 cm. Quartz grains (mean = 1882 grains/g) in GeoB 20601-4 are more abundant compared to glauconite grains (mean = 678 grains/g). Non-carbonate mineral grain contents are lower in cores GeoB 8342-6 and 8336-6 compared to the shallower core 20601-4 (quartz mean in 8342-6 = 10 grains/g; 8336-6 = 6 grains/g) (Fig. 7.3, 7.4, 7.5). Glauconite content was found to be negligible in the two deeper cores. Quartz is the most abundant non-carbonate mineral in cores GeoB 8342-6 and 8336-6. Additional non-carbonate material includes phosphorite grains and lithic fragments. The highest quartz content in GeoB 8342-6 occurs at the lower end of the core between 236 and 212 cm (MIS 6) and at 104 cm (MIS 4). In core GeoB 8336-6 the highest quartz grain contents are between 254 and 268 (MIS 6), at and at 120 cm (MIS 4). The total mineral grain contents follow the same trend as quartz content in both deeper cores.

Sedimentation rates for core GeoB20601-4 range between 0.4 and 1.9 cm/kyr (Fig. 7.3) with a mean rate of 0.8 cm/kyr. Sedimentation rates for core GeoB 8342-6 are lower than core 20601-4 with values ranging between 0.3 and 1.3 cm/kyr with a mean rate of 0.6 cm/kyr. Sedimentation rates for core GeoB 8336-6 are similar to GeoB 8342-6 and also range between 0.3 and 1.3 cm/kyr with a mean rate of 0.6 cm/kyr. The sedimentation rates are particularly lower during MIS 4 and MIS 2 in all three cores.

The mean benthic foraminiferal accumulation rates (BFARs) in core GeoB 20601-4 are 125 individuals/cm^2/kyr and range between 9 and 693 individuals/cm^2/kyr. The highest BFARs in core GeoB 20601-4 are in MIS 7, 6 and 3 (Fig. 7.3). In core GeoB 8342-6 the mean BFAR is 36 individuals/cm^2/kyr ranging between 4 and 174 individuals/cm^2/kyr and are highest in MIS 6, 5 and 4 (Fig. 7.4). The mean BFAR in core GeoB 8336-6 is 57 individuals/cm^2/kyr ranging between 6 and 281 individuals/cm^2/kyr and the highest in MIS 6, 5 and 3 (Fig. 7.5).

7.3.4 Planktic foraminifera

The dominant planktic species are *Gr. (Gc.) inflata, G. bulloides, Ng. incompta, O. universa* and *Gr. truncatulinoides* in all three cores (Fig. 7.6; Appendix Tables B.6-8). The deeper cores recorded a decrease of mean abundance in *G. bulloides* whereas *Gr. (Gc.) inflata*, *Gr. truncatulinoides* and *Gs. ruber* (white) increase towards the deeper sites. Minor abundances (<5%) in the three cores were recorded for *Neogloboquadrina dutertrei, Globigerinella siphonifera, Globorotalia hirsuta, Globorotalia scitula, Globoturborotalita rubescens, Globorotalia menardii, Trilobatus sacculifer, Gs. ruber* (pink), *Orbulina bilobata, Globigerinoides conglobatus, Pulleniatina obliquiloculata, Trilobatus trilobus, Sphaeroidinella dehiscens, Globorotalia crassaformis* and *Globorotalia tumida.*

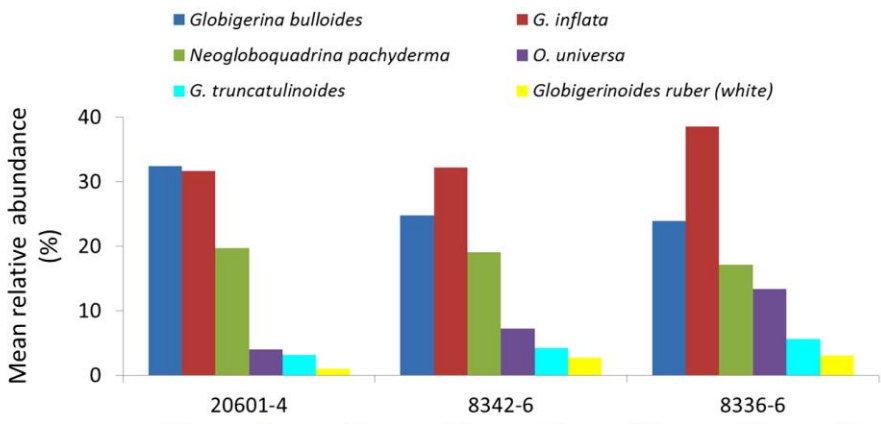

	20601-4			8342-6			8336-6		
	Min	**Max**	**Mean**	**Min**	**Max**	**Mean**	**Min**	**Max**	**Mean**
G. bulloides	5.46	50.15	32.40	6.50	40.27	24.79	2.92	43.81	22.62
Gr. inflata	4.92	52.75	31.61	15.93	48.97	32.14	8.67	72.90	33.90
Ng. incompta + Ng. pachyderma	0	55.43	19.65	0	52.27	19.1	0	58.14	15.20
O. universa	0	10.32	3.95	1.27	17.45	7.24	0.48	29.17	9.69
Gr. truncatulinoides	0.60	7.84	3.09	0.25	12.79	4.23	0.29	18.11	5.22
Gs. ruber (white)	0	3.55	1.02	0	9.82	2.67	0	9.19	3.28
Ng. dutertrei	0	3.15	0.52	0	2.64	0.41	0	1.57	0.30
Ga. siphonifera	0	1.84	0.47	0	3.31	0.66	0	7.57	1.98
Gr.hirsuta	0	3.80	0.42	0	4.36	1.78	0	4.69	1.61
Gr.scitula	0	1.30	0.28	0	3.04	0.53	0	1.19	0.33
Gt. rubescens	0	1.81	0.26	0	0.25	0.01	0	0.29	0.01
Gr. menardii	0	0.33	0.10	0	0.50	0.04	0	0.92	0.07
T. sacculifer	0	0.65	0.09	0	0.93	0.12	0	5.41	0.59
Gs .ruber (pink)	0	1.23	0.07	-	-	-	0	0.31	0.01
O. bilobata	0	0.32	0.06	0	0.74	0.08	0	1.52	0.21
Gs. conglobatus	0	0.32	0.05	0	0.31	0.02	0	0.50	0.03
P. obliquiloculata	0	0.32	0.03	0	2.38	0.26	0	6.23	0.72
T. trilobus	0	0.61	0.02	0	1.24	0.05	0	0.93	0.09
S. dehiscens	0	0.26	0.01	0	0.29	0.02	0	1.82	0.08
Gr.crassaformis	-	-	-	-	-	-	0	0.98	0.07
Gr. tumida	-	-	-	0	0.23	0	0	1.09	0.05

Fig. 7.6. Minimum, maximum and mean relative abundances (%) of planktic foraminifera in all three cores

The transitional species form a dominant proportion of the planktic foraminiferal composition in core 20601-4 (Fig. 7.7). The subtropical species are less abundant than the subpolar species *Ng. incompta*. The transitional species *Gr. (Gc.) inflata* appear to fluctuate independent of G-IG cycles from MIS 8 to 5 after which relative abundances decrease slightly in MIS 4 and 2 with increased abundances during interglacial periods MIS 3 and 1. The relative abundances of *G. bulloides* show general decreases during interglacial periods with increasing abundances during glacial periods, and display a general counter-correlative trend compared to *Ng. incompta + Ng. pachyderma*. The cold-water species *Ng. incompta* indicates varying abundances from MIS 8 to 6. At the MIS 6/5 boundary the relative abundances of *Ng. incompta + Ng. pachyderma* sharply decrease and increase at the MIS 5/4 boundary after which the relative abundances of this species decrease in MIS 3 and increase in MIS 2. Another sharp decrease in *Ng. incompta + Ng. pachyderma* relative abundances is observed at the MIS 2/1 boundary. Relative abundances of *Ng. incompta + Ng. pachyderma* then remain low in MIS 1. The relative abundances of *Gr. truncatulinoides*

and *O. universa* fluctuate independent of G-IG cycles with the highest *Gr. truncatulinoides* relative abundances occurring in MIS 7, 4 and 1. The highest *O. universa* relative abundances in GeoB 20601-4 occur in MIS 2. With the exception of MIS 4, the highest relative abundances of *Gs. ruber* are in interglacial periods and lower relative abundances occur in glacial periods. Similarly, but in lower overall relative abundances (<1%) *T. sacculifer* are higher in interglacial periods. The tropical species *Gr. menardii* also occurs in trace relative abundances (<1%) with no occurrence being recorded in MIS 8 where after this species occurs in MIS 7 to 1.

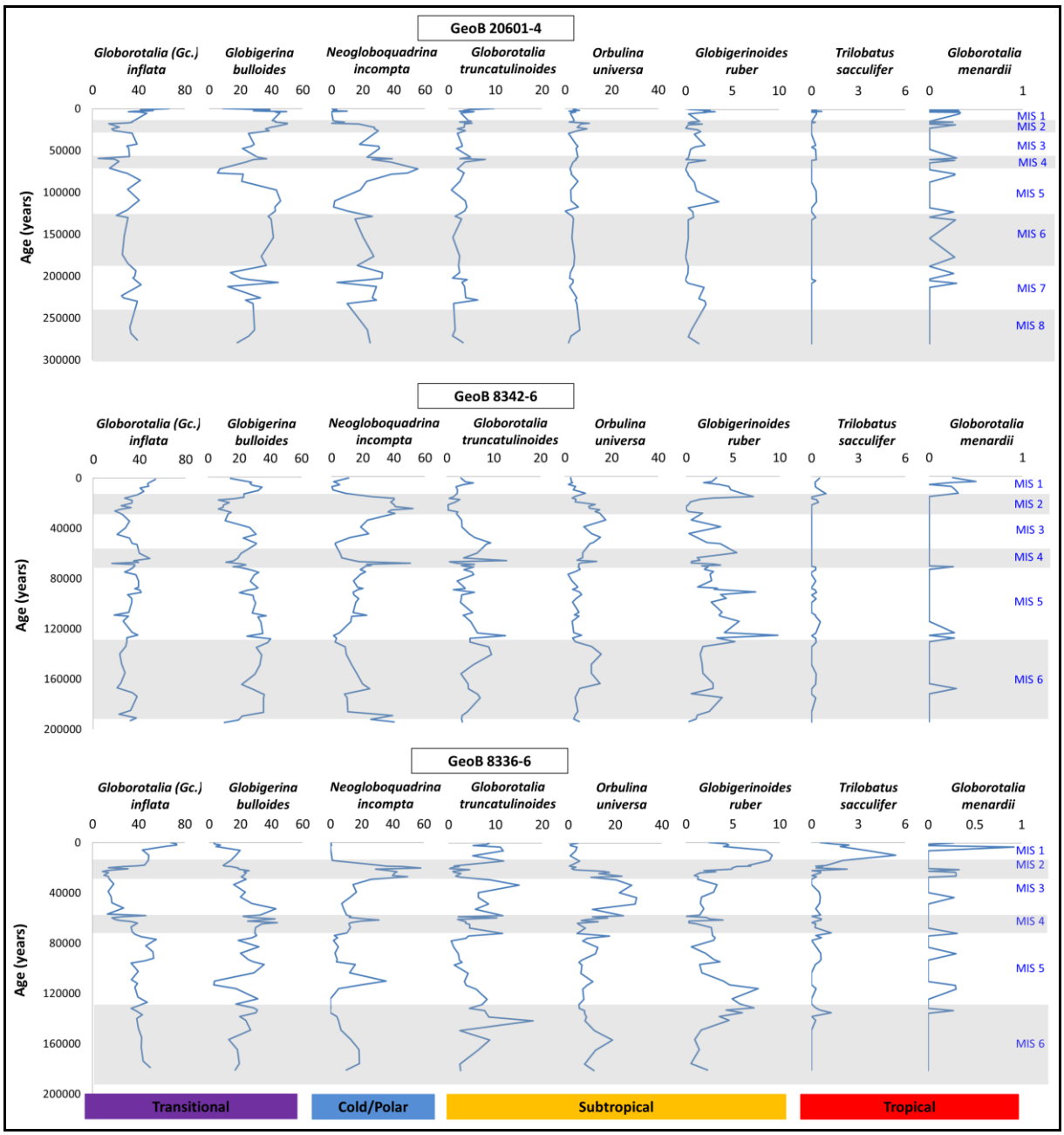

Fig. 7.7. Relative abundance plots for planktic foraminifera in cores GeoB 20601-4, 8342-6 and 8336-6.

The first principal component (PC 1, colder water) of the planktic foraminifera in core GeoB 20601-4 (Appendix D), explains 66% of the variance (Fig. 7.8) and is dominated by *Ng. incompta* + *Ng. pachyderma* and the lower negative values are dominated by *G. bulloides* and *Gr. (Gc.) inflata* (Fig. 7.9). The second principal component of the planktics (PC 2, upwelling intensity) is explained by 32% of the variance, and is positively dominated by *Gr. (Gc.) inflata* and the lower negative values are dominated by *G. bulloides*. The third principal component of the planktics (PC 3, subtropical water) is explained by 2% of the variance, and is positively dominated by *G. bulloides*, *Gr. (Gc.) inflata* and *Ng. incompta* + *Ng. pachyderma* and the lower negative values are dominated by *Gr. truncatulinoides and O. universa.*

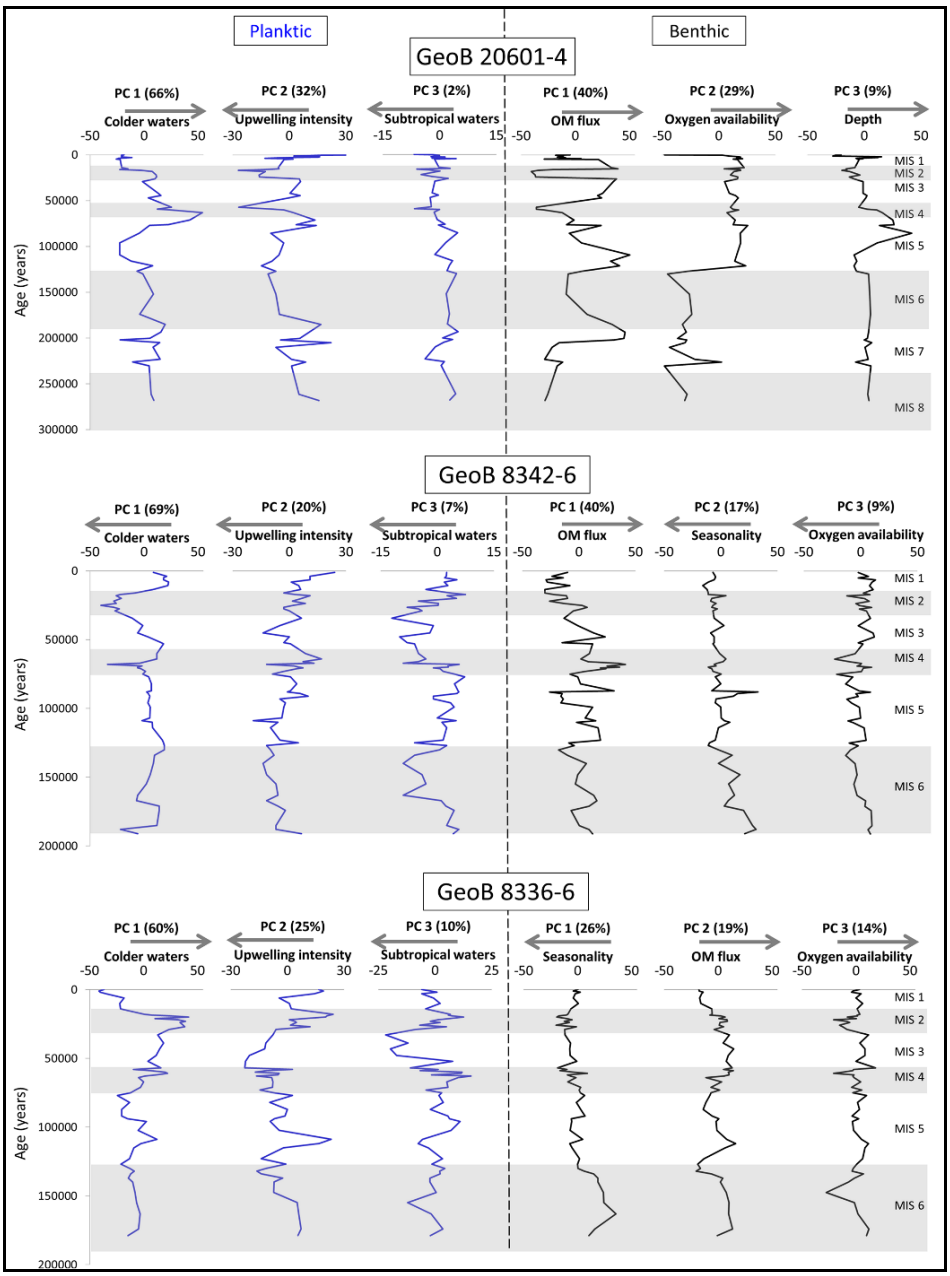

Fig. 7.8. Results of the three major principal components (PC 1 to PC 3) of the planktic and benthic taxa in cores GeoB 20601-4, 8342-6 and 8336-6. For discussion on components see sections 7.4.2 and 7.4.3.

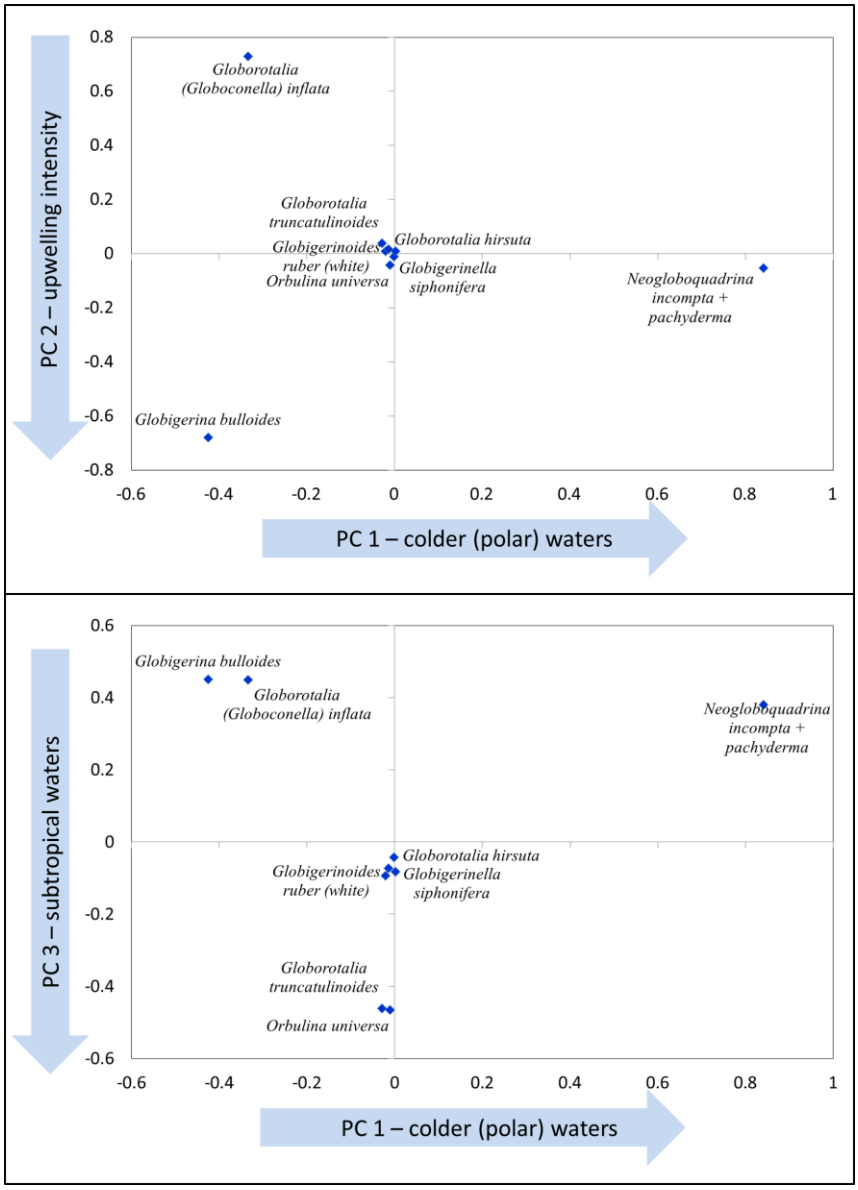

Fig. 7.9. The three principal components (PC 1 on the x-axis and PC 2 and PC 3 on the y-axes) of planktic foraminifera in core GeoB 20601-4.

In core GeoB 8342-6 *Gr. (Gc.) inflata* shows fluctuating relative abundances with little G-IG variability. More sustained lower abundances occur during MIS 3 and MIS 2. MIS 6 in GeoB 8342-6 shows *G. bulloides* to have generally higher relative abundances that gradually decrease from MIS 5 to MIS 4. The relative abundances of *G. bulloides* then increase in MIS 3 and decrease to its lowest during MIS 2 where after this species increases again in MIS 1. Similar to *G. bulloides* in core GeoB 20601-4, this species display a counter-correlative trend compared to *Ng. incompta* + *Ng. pachyderma*.

During glacial periods *Ng. incompta* + *Ng. pachyderma* are higher in relative abundances with a gradual decrease in MIS 6 towards the MIS 6/5 boundary. Sharp decreases are also recorded for this species during the end of MIS 4 and MIS 2 where the succeeding interglacials (MIS 3 and 1) recorded lower relative abundances. The relative abundances of *Gr. truncatulinoides* do not show any particular trend and are highest in the early MIS 5 and MIS 4. Higher relative abundances of *O. universa* are observed in glacial periods and towards the end of MIS 3 with the lowest

relative abundances being in MIS 5 and MIS 1. The subtropical species *Gs. ruber* displays a sharp increase in relative abundances during the early MIS 5, at the MIS 4/3 and MIS 2/1 transitions. Lower relative abundances for *Gs. ruber* in GeoB 8342-6 are during glacial periods. In this core *T. sacculifer* and *Gr. menardii* also occur in trace abundances (<1%) with *T. sacculifer* being observed more during MIS 5 and MIS 1. The tropical species *Gr. menardii* generally occurs only in interglacial periods in GeoB 8342-6 with the exception of one occurrence in MIS 6.

The first principal component (PC 1) of the planktic foraminifera in core GeoB 8342-6, explained by 69% of the variance (Fig. 7.8) is dominated by *G. bulloides* and the weaker negative values are dominated by *Ng. incompta* + *Ng. pachyderma* (Fig. 7.10). The second principal component (PC 2) of the planktic foraminifera, explained by 20% of the variance, is positively dominated by *Gr. (Gc.) inflata* and the weaker negative values dominated by *G. bulloides*. The third principal component (PC 3) of the planktic foraminifera, explained by 7% of the variance, is positively dominated by *G. bulloides* and *Ng. incompta* + *Ng. pachyderma* and the weaker negative values dominated by *O. universa*.

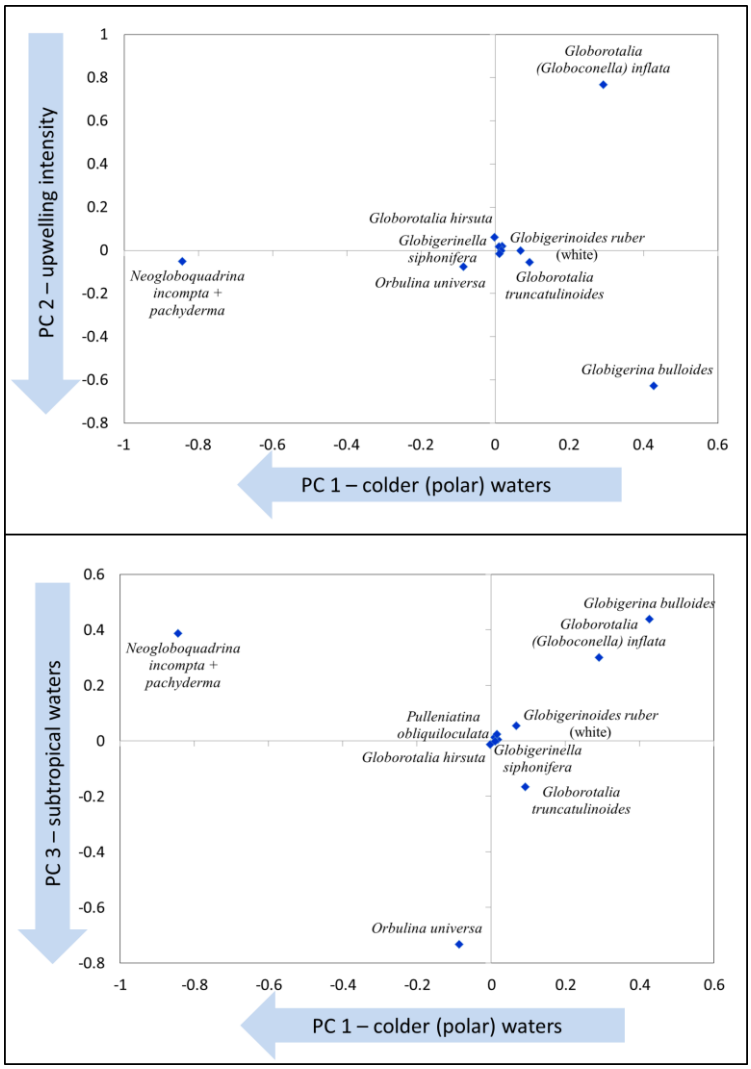

Fig. 7.10. The three principal components (PC 1 on the x-axis and PC 2 and PC 3 on the y-axes) of planktic foraminifera in core GeoB 8342-6.

In core GeoB 8336-6 the relative abundances of *Gr. (Gc.) inflata* fluctuate independent of G-IG variability with lower abundances being recorded during MIS 4 to MIS 2. The relative abundances of *G. bulloides* in GeoB 8336-6 show high values during MIS 6 with a large decrease following the MIS 6/5 transition. Thereafter *G. bulloides* does not show a particular trend, but slight increases during the glacial periods MIS 4 and MIS 2 are observed. During glacial periods and at 120 ka *Ng. incompta + Ng. pachyderma* are higher in relative abundances with the lowest values being recorded in interglacial periods. Higher abundances of *Gr. truncatulinoides* are observed towards the end of MIS 6, during the MIS 5/4 transition and during MIS 3 and MIS 1. The glacial periods MIS 4 and MIS 2 record lower relative abundances for *Gr. truncatulinoides* in GeoB 8336-6. The highest relative abundances for *O. universa* in GeoB 8336-6 are in MIS 3 and the lowest relative abundances recorded in MIS 1. Similar to core GeoB 8342-6, *Gs. ruber* displays a sharp increase in relative abundances at the MIS 6/5 and MIS 2/1 transitions with the lowest relative abundances recorded during glacial periods. In this core *T. sacculifer* occurs in trace to minor (<6%) relative abundances with the highest value recorded in MIS 1. The tropical species *Gr. menardii* occurs in trace abundances (<1%) in GeoB 8336-6 as well and mostly occurs in interglacial periods.

The first principal component (PC 1) of the planktic foraminifera in core GeoB 8336-6, explained by 60% of the variance (Fig. 7.8) is dominated by *Ng. incompta + Ng. pachyderma* and the lower negative values are dominated by *Gr. (Gc.) inflata* (Fig. 7.11). The second principal component (PC 2) of the planktic foraminifera, explained by 25% of the variance, is positively dominated by *Ng. incompta + Ng. pachyderma* and *Gr. inflata* and the weaker negative values are dominated by *G. bulloides*. The third principal component (PC 3) of the planktic foraminifera, explained by 10% of the variance, is positively dominated by *G. bulloides* and the negative values dominated by *O. universa.*

7.3.5. Benthic foraminifera

The most abundant benthic foraminifera (Appendix Tables B.16-18) in core GeoB 20601-4 are *Uvigerina* spp. (primarily *U. peregrina*), *Bulimina aculeata, Pyrgo* spp. (*P. lucernula, P. murrhina*), *Cibicidoides wuellerstorfi* and *Epistominella exigua* (Fig. 7.12). The relative abundances of *Uvigerina* spp. (primarily ribbed *U. peregrina*) in core GeoB 20601-4 display higher values during interglacial periods (MIS 7, 5, 3 and 1) and lower values during glacial periods (MIS 8, 6, 4 and 2). The highest relative abundance of *Uvigerina* spp. occurs at 127 ka. The relative abundances for *Bulimina aculeata* show increased values during glacial periods and lower values during interglacial periods. The peak relative abundance for *B. aculeata* occurs at 276 ka in MIS 8. With the exception of MIS 8 and 7, *Pyrgo* spp. (primarily *P. murrhina* and *P. lucernula*) reach maximum abundances during glacial periods and lower abundances during interglacial periods. The relative abundances for *C. wuellerstorfi* in core GeoB 20601-4 are higher during glacial periods and lower in interglacial periods with a peak relative abundance at 63 ka (18.75%). The highest relative abundance of *Epistominella exigua* occur at 223 ka in MIS 7 (14.75%) decreasing

towards the MIS 7/6 boundary where after it increases again in MIS 6 at 174 ka (8.89%). The relative abundances of *E. exigua* then decrease again and remain low until an increase at 59 ka (9.77%). Thereafter *E. exigua* relative abundances in GeoB 20601-4 decrease and remain at trace abundances (<1%) into MIS 1.

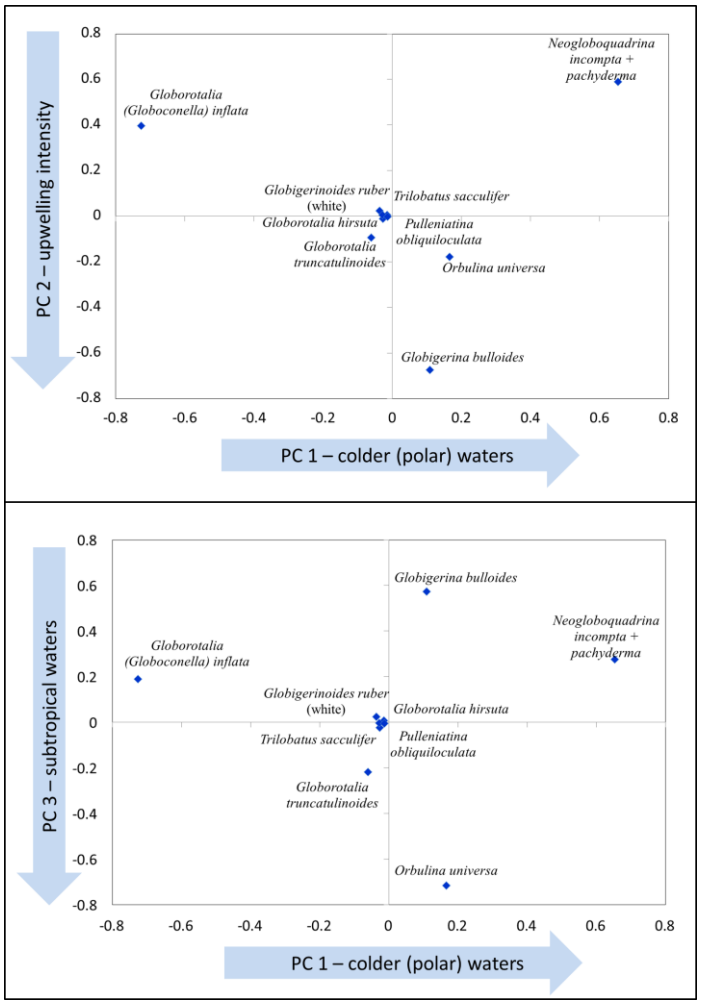

Fig. 7.11. The three principal components (PC 1 on the x-axis and PC 2 and PC 3 on the y-axes) of planktic foraminifera in core GeoB 8336-6.

The total benthic foraminifera numbers (BFN) in core 20601-4 are generally lower in glacial periods and higher in interglacial periods with a maximum BFN of 484 individuals/g and a mean BFN of 148 individuals/g (Fig. 7.12). The infaunal abundances relative to epifaunal abundances nearly mimic the benthic foraminifera numbers with a higher proportion of infaunal foraminifera occurring during interglacial periods. The majority of benthic foraminifera have a hyaline wall structure. The relative abundances of hyaline benthic foraminifera are lower during glacial periods (MIS 8, 6, 4, 2) when agglutinated and porcelaneous forms also increase. It is only during MIS 8 where agglutinated foraminifera increase above the hyaline forms.

The first principal component (PC1) (Appendix D) of the benthic foraminifera in core GeoB 20601-4, explained by 40% of the variance (Fig. 7.8) is dominated by *Uvigerina peregrina* and

Cibicioides spp. (primarily *C. crebbsi*) characterise the lowest negative value (Fig. 7.13). The second principal component (PC 2) of the benthic foraminifera, explained by 29% of the variance, is positively dominated by the BFOI and the weaker negative values are characterised by *Bulimina aculeata*. The third principal component (PC 3) of the benthics, explained by 9% of the variance, is positively dominated by *Cibicidoides pachyderma* and the weaker negative values dominated by *Cibicidoides* spp.

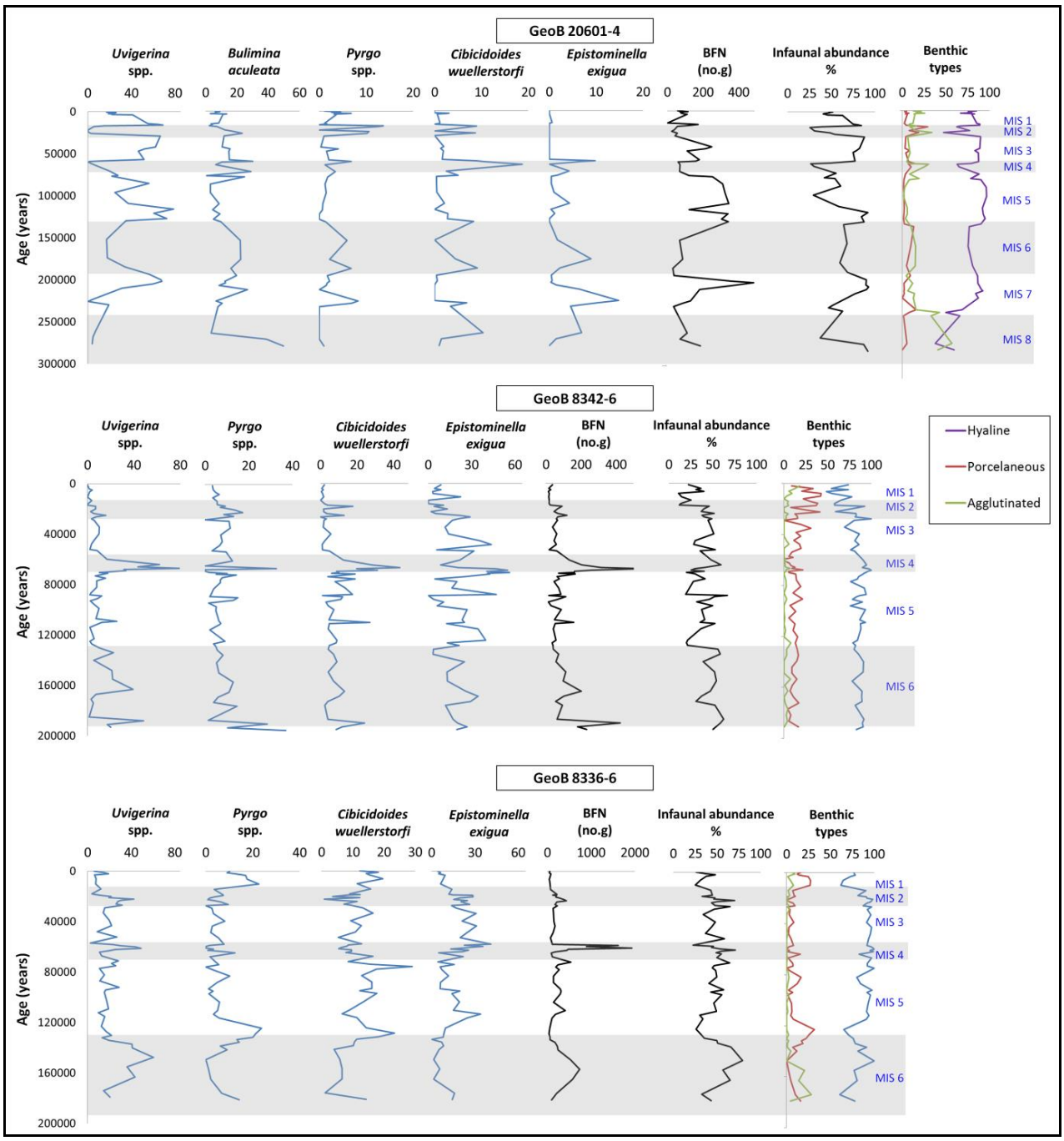

Fig. 7.12. Relative abundances (%), BFN (number of benthic foraminifera individuals), infaunal abundance relative to epifaunal abundances of benthic foraminifera and abundances of benthic foraminifera types according to wall type (hyaline, porcelaneous and agglutinated) in cores 20601-4, 8342-6 and 8336-6.

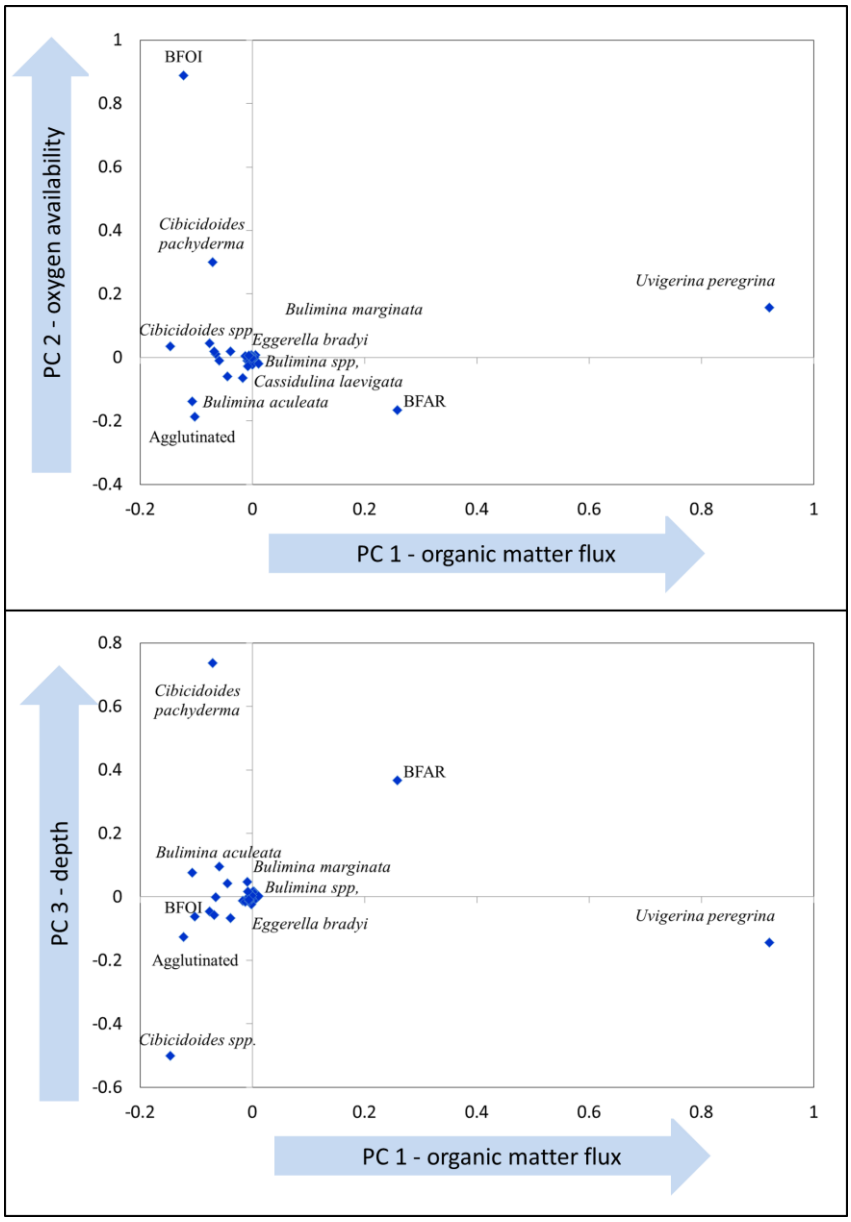

Fig. 7.13. The three principal components (PC 1 on the x-axis and PC 2 and PC 3 on the y-axes) of benthic foraminifera in core GeoB 20601-4.

In core GeoB 8342-6 *Uvigerina* spp., *Pyrgo* spp., *C. wuellerstorfi* and *E. exigua* are the dominant taxa (similar to GeoB 20601-4) while *B. aculeata* was found to be absent throughout the core (Fig. 7.12). The abundances of *Uvigerina* spp. are however lower in GeoB 8342-6 compared to GeoB 20601-4. The relative abundances of *Uvigerina* spp. (primarily *U. hispidocostata*) fluctuate independent of glacial-interglacial variability ranging between 0 (MIS 1) and 31.15% (134 ka in MIS 6). The highest relative abundances of *Pyrgo* spp. (primarily *P. murrhina* and *P. lucernula*) are in MIS 2 and 1 ranging between 0 and 37.25% (22 ka). The highest relative abundances of *C. wuellerstorfi* in core GeoB 8342-6 are at 93 ka in MIS 5 (26.32%) and at 18 ka in MIS 2 (19.23%). For *E. exigua* in GeoB 8342-6 maximum abundances occur in the early MIS 4 (at 70 ka = 56.25% and 68 ka = 54.76%) and the lowest are in MIS 1.

The highest total BFN in core GeoB 8342-6 occurs in glacial periods and low BFN at MIS 5, 3 and 1. The infaunal abundances in core 8342-6 show a decrease at glacial-interglacial boundaries (6/5, 4/3 and 2/1) where epifaunal foraminiferal abundances start to increase.

Hyaline benthic foraminifera dominate throughout core GeoB 8342-6 fluctuating independent of G-IG variability. Porcelaneous forms (miliolids and *Pyrgo* spp.) show the largest increases during MIS 2/1 when hyaline forms decrease in abundance.

The first principal component (PC 1) of the benthic foraminifera in core GeoB 8342-6, explained by 40% of the variance (Fig. 7.8) is dominated by *Epistominella exigua* and *Pyrgo* spp. characterise the lowest negative value (Fig. 7.14). The second principal component of the benthics, PC 2, explained by 17% of the variance, is positively dominated by *Globocassidulina subglobosa* and *Epistominella exigua* characterise the lowest negative value. The third principal component of the benthics, PC 3, explained by 9% of the variance, is positively dominated by *Pyrgo* spp. and the weaker negative values are dominated by *Cibicidoides wuellerstorfi.*

In core GeoB 8336-6 *Uvigerina* spp., *Pyrgo* spp., *C. wuellerstorfi* and *E. exigua* are the dominant taxa as well and *B. aculeata* was also not present in the core (Fig. 7.12). The relative abundances of *Uvigerina* spp. (primarily *U. hispidocostata*) in core GeoB 8336-6 are higher in MIS 6 with a maximum abundance at 148 ka (60.09%). Glacial periods recorded higher relative abundances of *Uvigerina* spp. whereas interglacial periods recorded lower *Uvigerina* spp. relative abundances in core GeoB 8336-6. Maximum relative abundances of *Pyrgo* spp. are reached at the peak glacial-intergalcial boundaries (MIS6/5 and MIS 2/1) with fluctuating relative abundances between MIS 5 and MIS 2. The highest relative abundance of *C. wuellerstorfi* is at 27 ka in MIS 5 (23.4%) decreasing towards MIS 1 where it increases at 14 ka (15.79%) and at 6 ka (19.61%). The relative abundances of *E. exigua* are low in MIS 6 of core GeoB 8336-6 increasing at 112 ka in MIS 5 (33.88 ka). Between MIS 5 and MIS 3 the relative abundances of *E. exigua* decrease where maximum abundances are reached where after there is a decrease in *E. exigua* from MIS 2 to MIS 1.

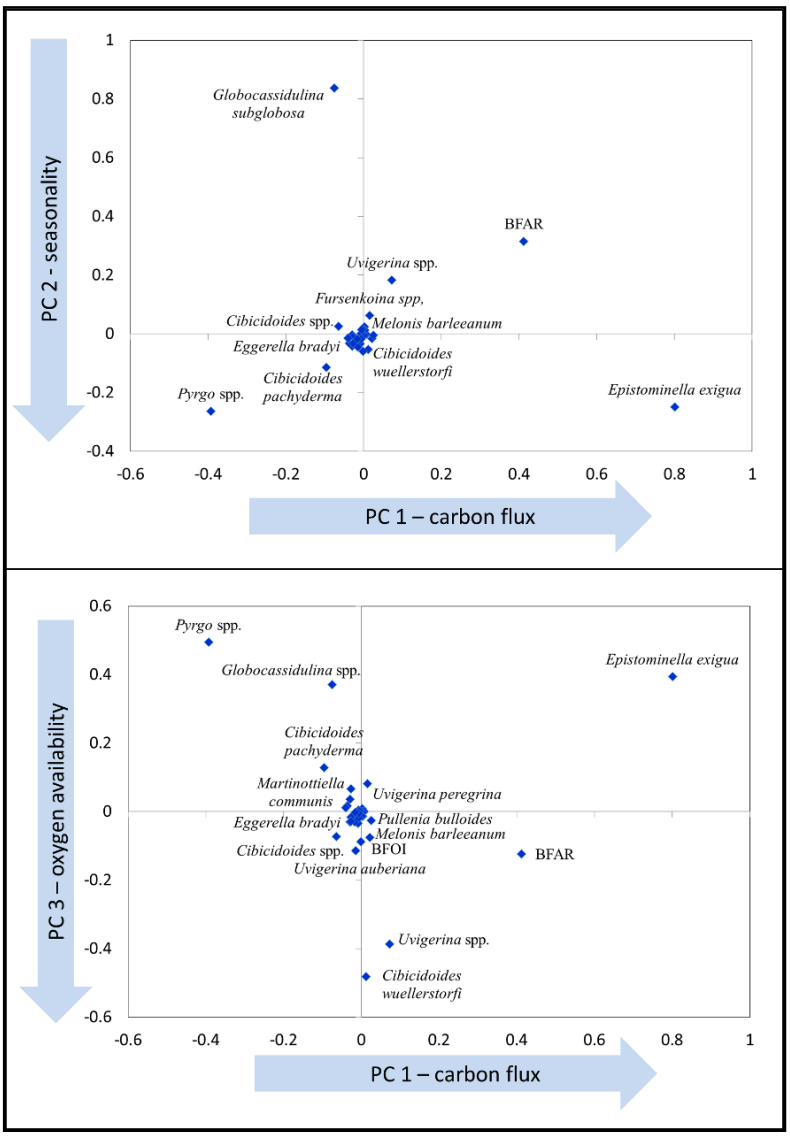

Fig. 7.14. The three principal components (PC 1 on the x-axis and PC 2 and PC 3 on the y-axes) of benthic foraminifera in core GeoB 8342-6.

Similar to core GeoB 8342-6, total BFN values in core GeoB 8336-6 are highest during glacial periods and lower BFN occur during MIS 5, 3 and 1. The infaunal abundances in core 8336-6 also show a decrease at glacial-interglacial boundaries (6/5, 4/3 and 2/1) where epifaunal foraminiferal abundances start to increase. Hyaline foraminifera remain the highest proportion throughout the core. Porcelaneous forms increase during the MIS 6/5 and MIS 2/1 transitions where hyaline forms decrease. The highest agglutinated proportions in the core are present during MIS 8.

The first principal component (PC 1) of the benthic foraminifera in core GeoB 8336-6, explained by 26% of the variance (Fig. 7.8) is dominated by *Uvigerina hispidocostata* and *Epistominella exigua* characterise the lowest negative value (Fig. 7.15). The second principal component (PC 2) of the benthic foraminifera, explained by 19% of the variance, is positively dominated by *Epistominella exigua* and *Pyrgo* spp. characterise the lowest negative value. The third principal component (PC 3), explained by 14% of the variance, is positively dominated by BFAR and BFOI and the lower negative values are dominated by *Uvigerina auberiana* and *U. hispidocostata*.

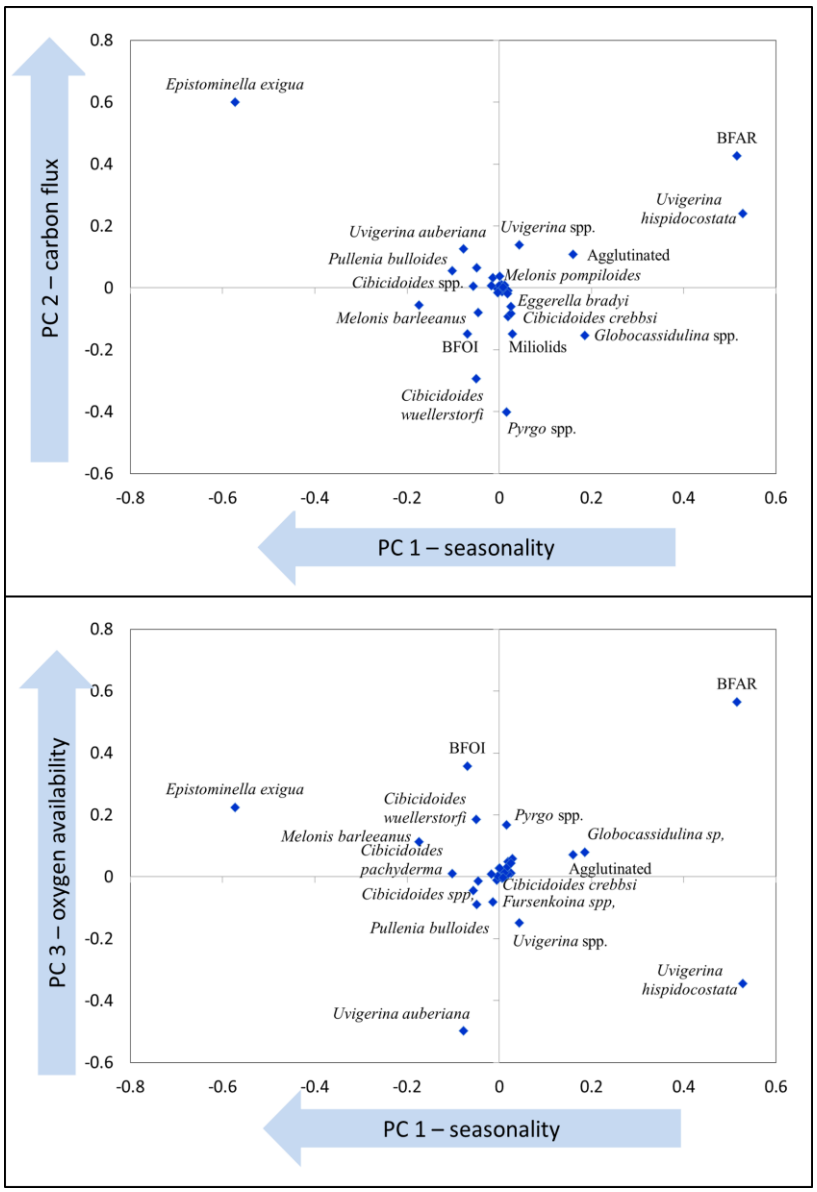

Fig. 7.15. The three principal components (PC 1 on the x-axis and PC 2 and PC 3 on the y-axes) of benthic foraminifera in core GeoB 8336-6.

The benthic foraminiferal index (BFOI) values for core 20601-4 range between 36.36 and 100 (Fig. 7.16) with a mean value of 79.83. The lowest BFOI values occur between MIS 8 and 6 before values increase substantially from MIS 5 to MIS 1. A sharp decrease in values is also observed close to the MIS 2/1 boundary and in the upper samples of GeoB 20601-4. BFOI values for core 8342-6 range between 75 and 100 with a mean value of 94.72.

The MIS 5 to MIS 4 transition shows slightly higher values before a decrease in BFOI values are observed in early MIS 2 after which values increase going into MIS 1. Core GeoB 8336-6 recorded BFOI values of between 75 and 100 with a mean value of 94.92. Glacial periods generally show lower BFOI values in GeoB 8336-6 compared to interglacial periods.

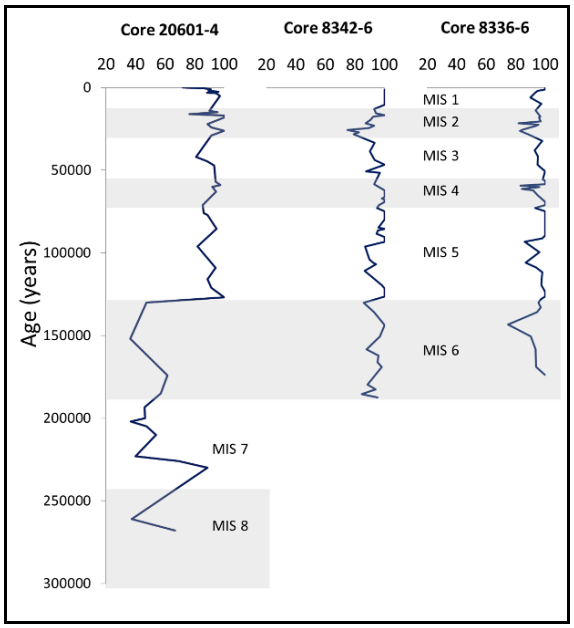

Fig. 7.16. Benthic foraminiferal oxygen index (BFOI) for the three cores of this study. The grey shaded regions indicate glacial periods

7.4. Discussion

7.4.1 Age model and depositional history

An age model for the three cores in this study was determined by combining oxygen isotope stratigraphy, colour reflectance data and non-carbonate sand mineral abundance (Fig. 7.3 to 7.5). The benthic (*C. wuellerstorfi*) $\delta^{18}O$ profile of each core was correlated with the benthic LR04 stack (Lisiecki and Raymo, 2005). Oxygen isotopic signatures in benthic foraminifera are closely tied to ice volume changes (Miller et al., 1991; Zachos et al., 2001) whereas the isotopic signatures in planktic foraminifera are additionally influenced by regional changes such as sea surface temperatures (Wefer et al., 1999). The deeper cores (GeoB 8342-6 and 8336-6) at ~3500 m display a similar $\delta^{18}O$ to the LR04 stack (Fig. 7.4 and 7.5) compared to the $\delta^{18}O$ in the shallower core (GeoB 20601-4) at 874 m water depth (Fig. 7.3) which showed less clearly defined $\delta^{18}O$ peaks. The largest shift in $\delta^{18}O$ that marks a major change in global ice volume during the MIS 6/5 (GT II) and MIS 2/1 (GT I) transitions as well as the major peaks in MIS 5a, 5c and 5e are present in the deeper cores. These shifts and transitions are also present in GeoB 20601-4 but are less pronounced. Despite this, the $\delta^{18}O$ record in GeoB 20601-4 could still be correlated to the LR04 stack through the Analyseries 2.0.8 programme (Paillard et al., 1996). The slightly deviating $\delta^{18}O$ trend of core 20601-4 could be resultant of certain samples being time averaged due to being more compact or having been displaced from their original source. It might also be possible that the shallower GeoB 20601-4 does not preserve the $\delta^{18}O$ signal as well as the deep water samples from previous stacked curves (Lisiecki and Raymo, 2005).

Colour reflectance in sediments is influenced by carbonate content, terrigenous mud inputs and settling of finer particles derived from different sources (Bozzano et al., 2002; Carter et al., 2004). Interglacial periods are generally indicated by higher colour reflectance values and glacial periods by lower values (Carter et al., 2004). In the three cores this G/IG variation was observed for part of MIS 6, for MIS 2 and MIS 1 in GeoB 20601-4, in MIS 6 to 4 and MIS 2 to 1 in GeoB 8342-6 and for much of core GeoB 8336-6.

Transport and deposition of detrital grains, particularly quartz and glauconite have been shown to increase during glacial periods along the South African margin (Compton and Wiltshire, 2009). Glauconite in GeoB 20601-4 and quartz and other non-carbonate minerals in all three cores increase during periods which were identified as glacials by the $\delta^{18}O$ record. The increases in non-carbonate minerals in the

three cores are in agreement with the glacial periods identified in the $\delta^{18}O$ record. The coincident occurences of increased mineral content during glacial periods further strengthens the age model.

Terrigenous sediment is delivered to the continental margin mainly from fluvial inputs, primarily from the Orange and Olifants rivers. Sand fed from the Orange River is transported northwards to provide a source for the Namib Desert whereas the finer mud is distributed southwards forming the mudbelt on the continental shelf (Meadows et al., 2002; Herbert and Compton, 2007). The transport of sediment from the western shelf of South Africa to the slope is influenced by high amplitude sea-level fluctuations (Compton and Wiltshire, 2009). Mineral grains such as quartz and glauconite are suspended in the water column and transported by bottom currents. The abundance of these minerals on the slope varies across glacial-interglacial stages. Glauconite was found to be more abundant in core GeoB 20601-4 and was negligible in the deeper cores. Quartz abundances also decreased from the shallow to deeper cores. The difference in abundance of quartz and glauconite between the cores can be attributed to water depth and the distance from shelf and continental sources. Compton and Wiltshire (2009) note that the abundance of quartz and glauconite decreases north of the Cape Canyon and below the upper slope base at 2000 m. Core 20601-4 is situated closer to the continental shelf (compared to cores 8342-6 and 8336-6) offshore from the Olifants River. During glacial periods more quartz, glauconite, windblown mica and lithic fragments are transported to the site because of the lowered wave base. The site was closer to a continental source during glacial periods (130 m lower water depth during the LGM) enhancing the amount reaching the site during those periods (Rau et al., 2002). Cores GeoB 8342-6 and 8336-6 are situated on the slope offshore from the Olifants and Orange Rivers respectively. The water depth is too great for substantial amounts of mineral grains to reach these sites and lesser amounts of mineral grains would reach the core sites of 8342-6 and 8336-6 compared to core 20601-4, although mineral grains, primarily quartz still show increased abundances during glacial stages compared to interglacial stages. Southeasterly trade winds and drier conditions during glacial periods (Shi et al, 2001) could potentially increase the delivery of wind blown grains. It appears that cores from deeper slope depths such as the one off the Orange River (Rau et al., 2002) and cores 8336-6 and 8342-6 from this study receive a much reduced input from continental sources from both rivers and adiabatic berg winds. In addition to windblown quartz, the sources of quartz include the erosion of Neogene outer shelf sediments and terrigenous mud derived from fluvial inputs such as the Orange and Olifants Rivers and glauconite forms as an authigenic mineral on the shelf and uppermost slope (Rau et al., 2002; Compton and Wiltshire, 2009).

Mechanisms and processes around which increased mineral content reach the slope during glacial periods along the South African margin are largely understudied, but it is accepted that similar processes extend from offshore Namibia southwards to South Africa (Monteiro et al., 2005). Submarine canyons that can facilitate widespread gravity flows such as turbidity currents are few along the western margin of

South Africa compared to other margins (Compton and Wiltshire, 2009). Therefore other mechanisms and processes of transport from the shelf to the slope need to be considered. It has been proposed that, based on studies off Namibia the vertical movement of internal tides is capable of suspending muddy sand (Compton and Wiltshire, 2009) which is then transported downslope by poleward undercurrents (Shannon and Nelson, 1996). The strength of these internal tides is stronger during glacial periods and capable of transporting coarser material during sea-level lowstands (Compton and Wiltshire, 2009). Through this process the accumulation of foraminiferal tests is also expected to increase on the slope during glacial periods. Benthic foraminiferal numbers (BFNs) and BFARs were higher primarily during glacial periods in the deeper cores but were lower during glacial periods in the shallower GeoB 20601-4 core (Fig. 7.12). This suggests that benthic tests are transported from the upper to the lower slope. Evidence for this is in the reported isolated tests of shallow shelf species *Ammonia beccarii* in glacial periods in the deeper cores. Higher BFARs could also signal higher productivity. Increased trade wind intensity during glacial periods would lead to an increase in upwelling intensity during glacial periods enhancing organic matter delivery to the seafloor. The upper core site GeoB20601-4 would, however, be under a more complex situation under the additional influences of sea-level and bottom water energy changes during those periods.

The upper 3 m of core GeoB 20601-4 extend back into MIS 8 compared to only MIS 6 in the deeper cores. This implies that the upper slope core represents a more condensed sedimentary record compared to the deeper, lower slope cores. Compton and Bergh (2016) illustrated that reworking of shelf areas can result in slope sediments up to 300 times thicker than shelf sediments off Namibia. The relative compact sedimentary record and low sedimentation rates during glacial periods in GeoB 20601-4 reflect greater sediment erosion during those periods. Sedimentation rates largely increase during interglacial periods in all three cores. It therefore follows that increased export of sediment to greater depths in the Cape Basin occurs during glacial periods as a result of enhanced shelf erosion and bottom water current strength (Compton and Wiltshire, 2009).

7.4.2. Biogeography and biostratigraphy of planktic foraminifera along the western slope of South Africa

Planktic foraminifera along the southwestern margin of Africa are indicative of the prevailing surface water hydrography of the BUS (Giraudeau, 1993). Three planktic foraminiferal zones along the margin were identified by Giraudeau (1993), namely a coastal upwelling area dominated by *Ng. incompta* and *Turborotalita quinqueloba*, an intermediate region dominated by *G. bulloides* and *Ng. incompta*, and oligotrophic offshore environments dominated by *Gr. (Gc.) inflata* and *Gr. truncatulinoides.* The dominance of *Gr. (Gc.) inflata* and *G. bulloides* in the three cores with lesser abundances of *Ng. incompta + Ng. pachyderma* and *Gr. truncatulinoides* indicates that the assemblages in the cores represent a variable mix of species associated with both oligotrophic and highly productive surface waters.

The dominance of *Ng. incompta + Ng. pachyderma* in PCA indicates a strong influence

of cold waters on the margin faunal composition. *Neogloboquadrina incompta* and *Ng. pachyderma* are subpolar to polar species (Bè and Tolderlund, 1971; Giraudeau, 1993; Kucera, 2007) and are the dominant species in waters south of the modern SAF and nearly absent in waters to the north of the STF (Barker et al., 2009). During glacial periods the Subantarctic Front Zone (SAF), the Antarctic Polar Front Zone (APF) and the Subtropical Front (STF) shift northwards (Hodell, 1993; Howard and Prell, 1992) by up to 7° latitude (Bard and Rickaby, 2009) coinciding with lower SSTs (Kasper et al., 2014). It has been proposed that the northward shift of the STF nearly shuts off Agulhas flow into the Atlantic by modulating the strength of the Agulhas Current (Rau et al., 2002; Peeters et al., 2004). A weakened Agulhas Current during glacial periods alters the contribution of heat and salt from the Indian Ocean to the Atlantic (Bard and Rickaby, 2009). The northward migration of the SAF and APF, as well as intensified southeasterly trade winds (Shi et al., 2001) supply colder surface waters over the study area and the proliferation of *Ng. incompta* + *Ng. pachyderma* in lower latitudes. This scenario would explain the high abundance of *Ng. incompta* along the southwestern margin of Africa during glacial periods. The sinistral (left-coiling) *Ng. pachyderma* also shows higher abundances during glacial periods (Fig. 7.17) in the deeper slope cores which is expected when southern polar fronts move northward and upwelling strength increases along the margin. Higher occurrences of *Ng. incompta* have also been suggested to indicate a stronger Antarctic Intermediate Water (AAIW) influence on the overlying South Atlantic Central Water (SACW) (Giraudeau, 1993).

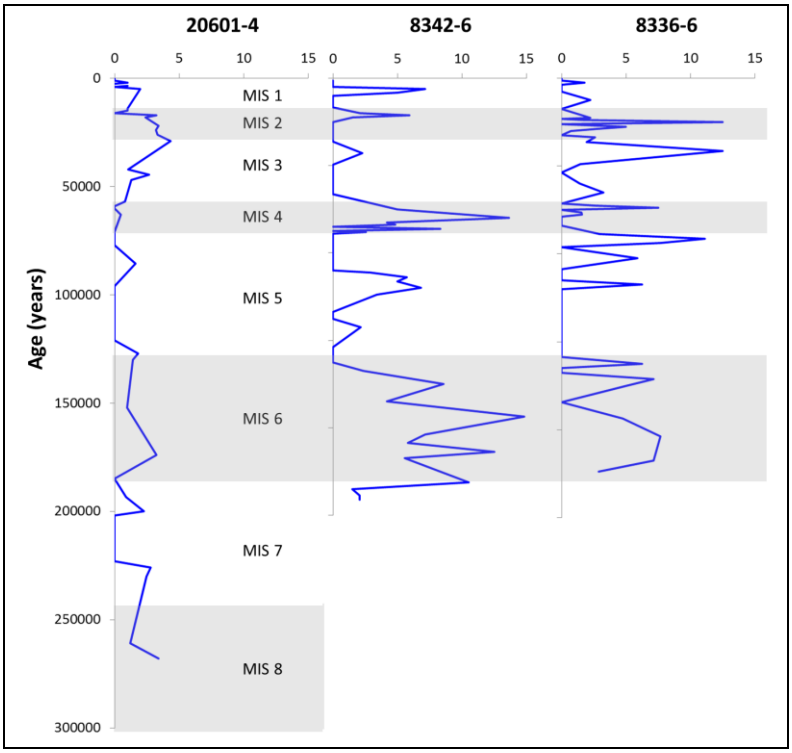

Fig. 7.17. Relative abundances (%) of *Ng. pachyderma* (sinistral) in all three cores. The shaded regions indicate glacial periods.

The relative abundance patterns of certain species such as *Ng. incompta + Ng. pachyderma* and *Gs. ruber* follow glacial-interglacial fluctuations and indicate the relation of faunal abundances to ice volume changes brought on by Milankovitch cycles. The species *G. bulloides* and *Ng. pachyderma* have been documented as being indicators of upwelling conditions (Giraudeau, 1993). Upwelling is influenced by stronger southeasterly trade winds (Shi et al., 2001). The planktic faunal occurrences in these cores indicate enhanced southeasterly trade winds and upwelling during glacial periods.

The higher mean value of *G. bulloides* in GeoB 20601-4 decreasing in relative abundances towards the deeper slope cores indicates the influence of highly productive surface waters where upwelled and oligotrophic offshore waters mix over the upper slope (Giraudeau, 1993). *G. bulloides* dominates PC2 and higher abundances of *G. bulloides* have been linked to stronger upwelling conditions (Table 7.1) and have also been reported in other upwelling regions such as the Arabian Sea (Prell and Curry, 1981; Curry et al., 1992; Peeters et al., 2002), northwest Africa (Martinez et al., 1999), the eastern margin of South America (Ibaraki, 1997; Marchant et al., 1999; Mohtadi et al., 2005) and California (Sautter and Thunell., 1991). The relative abundances of *G. bulloides* do not show any particular correlation to glacial-interglacial cycles and according to Rau et al. (2002), the abundance of this species at increasing water depths away from the shelf can be attributed to the presence of Southern Ocean and cool subpolar waters associated with the Subtropical Convergence (STC) coincident with strong upwelling conditions. The transitional species *Gr. (Gc.) inflata* is less abundant in sediments closer to the coast under upwelling centres and is ecologically adapted to deeper water depths (Groeneveld and Chiessi, 2011; and references therein). *G. bulloides* increases in relative abundance under reduced upwelling conditions and low nutrient levels (Giraudeau, 1993) which explains the higher relative abundances in the deeper cores. The higher relative abundances of *Gr. (Gc.) inflata* in interglacial periods of GeoB 20601-4 and during MIS 5 and 3 indicate lower nutrient-rich surface waters during interglacial periods.

The third principal component (PC 3) is dominated by *O. universa.* This species has been linked to a combination of nutrient-rich surface waters and warm (>18˚C) waters (Giraudeau, 1993). The increased abundances of *O. universa* in the deeper cores reflect the warmer surface conditions away from the colder coastal upwelling regions. *O. universa* indicates a strong influence of subtropical waters in the region. The subtropical (*Gs. ruber*) and tropical (*Gr. menardii*) planktic species in the cores display a generally higher occurrence during interglacial periods. A large increase in relative abundances of *Gs. ruber* is recorded during GT II and GT I in the deeper cores and generally increases during interglacials in GeoB 20601-4. The tropical species *T. sacculifer* also shows the largest increase in relative abundance following GT I in MIS 1. These occurrences are coincident with decreases in the colder water species *Ng. incompta + Ng. pachyderma.* The major differences in relative abundances of these species during the glacial terminations indicate that the shift in ocean configuration associated with major global ice volume change

have a pronounced effect on the faunal compositions along the margin.

The presence of subtropical and tropical species in the cores is related to oceanographic changes during glacial-interglacial cycles. Glacial terminations occur during a short warming phase after a long interval of cooling and when ice sheets were close to their greatest volume (Denton et al., 2010). Terminations II and I have also been linked to a decrease in the release of saline waters from the Indian to South Atlantic oceans (Kasper et al., 2004). It has also been suggested that GT II in the South Atlantic responded to interhemispheric ocean processes (Scussolini et al., 2015) with Agulhas saline leakage developing in response to cooling in the North Atlantic and peaking when the North Atlantic was warming (Marino et al., 2013). Agulhas inflow into the South Atlantic strengthens during deglaciations (Bard and Rickaby, 2009). The Agulhas Current flows along the southern margin of South Africa before it reflects back into the Indian Ocean. Rings of warm, saline Agulhas waters spin off into the South Atlantic, but with reduced strength during glacial periods (Flores et al., 1999; Goldstein et al., 1999; Rau et al., 2002; Peeters et al., 2004; Scussolini et al., 2015). The reduced Agulhas inflow into the South Atlantic during glacial periods has been attributed to shifting wind fields (Scussolini et al., 2015), weakening of the Atlantic Meridional Overturning Circulation (AMOC) (Stocker and Johnsen, 2003), the northwards migration of the subtropical front (STF) and eastward forcing of the Agulhas retroflection (Peeters et al., 2004).

During glacial terminations and interglacial periods the Antarctic and Subantarctic zones shift southward (Hodell, 1993; Howard and Prell, 1992) during times of weakened AMOC (Cheng et al., 2009; Barker et al., 2011). Therefore increased relative abundances of *Gs. ruber* during glacial terminations are in response to the Antarctic and subantarctic zones shifting further southwards during deglaciations allowing for an increase in the inflow of warmer waters into the South Atlantic.

Table 7.1. Associated conditions, Quaternary regional distribution and taxonomic features of planktic foraminifera from this study. Numbers in parentheses refer to previous studies indicated at the end of this table.

Taxon	Associated sea surface conditions	Regional distribution	Figure reference	Taxonomic features
Globigerina bulloides d'Orbigny, 1826	Temperate/ transitional (1,10); upwelling indicator (5)	One of the major species (<51%) from this study at the three sites and in Rau et al. (2002). Dominant species in Quaternary sections of ODP cores along Namibian and South African slope at intermediate depths (7) compared to deeper depths of this study. In Quaternary outer shelf sediments western South Africa (9). Major species (<30%) in surficial sediments along the entire Namibian (2,4) and South African margin (2). Abundances decrease along the South African margin (4).	Pl. 16; figs. 10a-b	Calcareous; spinose; spherical to subspherical; trochospiral; chambers globose; four chambers in final whorl; aperture umbilical; aperture large high symmetrical arch.
Globigerinella siphonifera (d'Orbigny, 1839a)	Subtropical (10)	Minor species (<8%) in Quaternary sediments along western South African slope (this study). Minor species in Quaternary sections of ODP cores along Namibian slope (7).	Pl. 16; fig. 11	Calcareous; spinose; trochospiral to nearly planispiral; chambers subglobular to globular; five chambers visible in final whorl; aperture interiomarginal wide equatorial arch.
Globigerinoides conglobatus (Brady, 1879)	Subtropical (1,10) to tropical (13)	Trace abundances along western South African slope (this study). Present in surficial sediments along the Namibian and South African margin. Abundances increase along south coast of South Africa (2).	Pl. 17; figs. 1-2	Calcareous; spinose cancellate; trochospiral; test semi-quadrate in shape; chambers subglobular; four chambers in final whorl; deep incised sutures; primary aperture umbilical low arch above three lower chambers; secondary apertures on spiral side.
Globigerinoides ruber (d'Orbigny, 1839a)	Tropical to subtropical (warm) (1,3,10,13)	Minor species (<10%) in Quaternary sediments along Namibian (7) and western South African slope (7,8, this study). In Quaternary outer shelf sediments western South Africa (9). Present in surficial sediments along the Namibian and South African margin. Abundances increase along south and east coasts of South Africa (2).	Pl. 17; figs. 3a-b	Calcareous; subspherical; trochospiral; three chambers visible in final whorl; deep incised sutures; primary aperture wide arched umbilical; secondary apertures on spiral side. Can occur in white and pink varieties. Pink variety extant in Atlantic Ocean and extinct in the Indian Ocean since 120 ka (Thompson et al., 1979).

Table 7.1 *(continued)*

Taxon	Associated sea surface conditions	Regional distribution	Figure reference	Taxonomic features
Globorotalia crassaformis (Galloway and Wissler, 1927)	Tropical (10)	Minor species in Quaternary sediments along Namibian (7) and western South African slope (8, this study)	Pl. 14; figs. 10-11	Calcareous; trochospiral; test subquadrate in shape; chambers also subquadrate to subrounded; four chambers in final whorl; deep incised sutures; aperture narrow extraumbilical to interiomarginal.
Globorotalia hirsuta (d'Orbigny, 1839a)	Subtropical (10)	Minor species (<5%) in Quaternary sediments along Namibian (7) and western South African slope (8, this study). In Quaternary outer shelf sediments western South Africa (9).	Pl. 14, fig. 12; pl. 15, figs. 1a-b	Calcareous; trochospiral; hirsute pustulose structures across test; test subrounded; four chambers in final whorl; lower chambers more inflated; incised sutures on umbilical side; aperture narrow extraumbilical to interiomarginal.
Globorotalia (Globoconella) inflata (d'Orbigny, 1839a)	Temperate/transitional (1,10)	Dominant species along Namibian (7) and western South African slope (7,8, this study). In Quaternary outer shelf sediments western South Africa (9). Dominant along slope off northern Namibia and western South Africa in surficial sediments (2,4). Also occurs along south and east coasts of South Africa (2).	Pl. 15, figs. 2a-c	Calcareous; cancellate (in pre-adult stages) non-spinose; trochospiral; test subrounded to subangular; three chambers visible in final whorl; incised sutures on umbilical side; aperture umbilical to extraumbilical interiomarginal.
Globorotalia menardii (Parker, Jones and Brady, 1865)	Tropical to subtropical (1,10,13)	Trace to minor species along Namibian (7) and western South African slope (8, this study). In Quaternary outer shelf sediments western South Africa (9). Also trace to minor in surficial sediments along Namibian and western South African margin (4). In surficial sediments on the southwestern coast (2).	Pl. 15, figs. 3a-c	Calcareous; cancellate non-spinose, lobulate with thick keel around test margin and sutures on spiral side; trochospiral; five chambers visible in final whorl; deep incised sutures on umbilical side; aperture extraumbilical interiomarginal.

Table 7.1 *(continued)*

Taxon	Associated sea surface conditions	Regional distribution	Figure reference	Taxonomic features
Globorotalia scitula (Brady, 1882)	Subpolar to transitional (1,10) to tropical (13)	Trace to minor species along Namibian (7) and western South African slope (8, this study). In Quaternary outer shelf sediments western South Africa (9). In surficial sediments along Namibian and southwestern South African margin (2,4).	Pl. 15, figs. 4a-c	Calcareous; non-spinose, lobulate; trochospiral; five chambers visible in final whorl; deep incised sutures on umbilical side; apertural chamber smoother than previous chambers; aperture extraumbilical interiomarginal with lip.
Globorotalia truncatulinoides (d'Orbigny, 1839b)	Transitional (1) to subtropical (1,10). Dextral (right-coiling) forms may indicate warmer subsurface conditions and sinistral (left-coiling forms) cooler conditions (1,4,12).	Minor species along Namibian (7) and western South African slope (7,8 this study). In Quaternary outer shelf sediments western South Africa (9). In surficial sediments from Namibian to South African margin (2).	Pl. 15, figs. 5a-6b; pl. 16, fig. 1	Calcareous; non-spinose, pustulose; planoconvex; keeled; trochospiral; more than four chambers visible in final whorl; chambers subangular; deep incised sutures on umbilical side; aperture extraumbilical interiomarginal.
Globorotalia tumida (Brady, 1877)	Tropical (10,13). Sometimes grouped with *G. menardii* as they share similar geographic distributions and little taxonomic variability (4,10).	Minor species along western South African slope (this study). In Quaternary outer shelf sediments western South Africa (8). In surficial sediments around margin of Namibia and South Africa. Abundance higher on east coast of South Africa (2).	Pl. 16, fig. 2	Calcareous; cancellate non-spinose; test elongate, lobulate with thick keel around test margin and sutures on spiral side; pustulose around margin; trochospiral; five chambers visible in final whorl; deep incised sutures on umbilical side; aperture extraumbilical interiomarginal with lip.
Globoturborotalita rubescens (Hofker, 1956)	Subtropical (1,10) to tropical (1,13)	Minor species (<5%) in Quaternary sediments along western South African slope (this study).	Pl. 16, figs. 12-13	Calcareous; cancellate spinose; small; trochospiral; four chambers in final whorl; chambers globose; aperture rounded umbilical bordered by lip.

Table 7.1 *(continued)*

Taxon	Associated sea surface conditions	Regional distribution	Figure reference	Taxonomic features
Neogloboquadrina dutertrei (d'Orbigny, 1839a)	Subtropical (4,10). Upwelling regions (4; and references therein)	Minor species along Namibian (7) and western South African slope (7,8, this study). In Quaternary outer shelf sediments western South Africa (9). In surficial sediments along Namibian and South African margin (4).	Pl. 16, figs. 3a-b	Calcareous; rounded, subglobular with globular chambers; trochospiral; >5 chambers visible in final whorl; aperture large umbilical.
Neogloboquadrina incompta (Cifelli, 1961) *Neogloboquadrina pachyderma* (Ehrenberg, 1861)	*Ng. pachyderma* (dextral)/*Ng. incompta* = subpolar; *Ng. pachyderma* (sinistral) = polar (1,10,11,13). May also indicate higher upwelling intensity (4).	Minor to abundant species along Namibian (7) and western South African slope (7,8, this study). In Quaternary outer shelf sediments western South Africa (9). In surficial sediments around Namibian and South African margin (2). Sinistral form dominant and more abundant in surficial sediments closer to coast. Dextral form dominant and more abundant in surficial sediments seaward of slope (4).	Pl. 16, figs. 4-7	Calcareous; subglobular to quadrate in shape with subquadrate chambers; trochospiral; four chambers in final whorl; aperture narrow extraumbilical to interiomarginal.
Orbulina bilobata (d'Orbigny, 1846)	Subtropical (6)	Trace to minor abundances (<2%) along the slope of western South Africa (this study). In Quaternary outer shelf sediments western South Africa (9).	Pl. 17, fig. 9	Calcareous; perforate spinose; test bilobate; one chamber partially envelops initial chamber which may be trochospiral; apertures cover entire test (areal). Two final chambered form of *O. universa*
Orbulina universa (d'Orbigny, 1839a)	Transitional to tropical (1) with higher abundances in subtropical waters (1,10)	Minor to major species (<30%) along Namibian (7) and western South African slope (7, this study). In Quaternary outer shelf sediments western South Africa (8). In surficial sediments along Namibian and South African margin (2,4). More abundant along west coast (2).	Pl. 17, fig. 10	Calcareous; perforate spinose; single round spherical globular chamber; apertures cover entire test (areal).
Pulleniatina obliquiloculata (Parker and Jones, 1865)	Tropical (1,10,13)	Minor species (<7%) along western South African margin (this study). In surficial sediments along the margin of Namibia and South Africa. Abundances increase on south and east coasts of South Africa (2).	Pl. 16, figs. 8-9	Calcareous; smooth; globular test; pustulose around aperture; initial chambers enveloped by later chambers; aperture umbilical narrow and wide, crescent-shaped stretching to both ends of test.

Table 7.1 *(continued)*

Taxon	Associated sea surface conditions	Regional distribution	Figure reference	Taxonomic features
Sphaeroidinella dehiscens (Parker and Jones, 1865)	Tropical (10,13)	Minor species (<2%) along western South African margin with occurrence and abundances increasing in deeper core (this study). In surficial sediments along the margin of South Africa. Higher abundances on northeast coast of South Africa (2).	Pl. 17, fig. 8	Calcareous; test spherical, thick, smooth in parts and pitted in parts; trochospiral; apertures may be crenulated on either side of test with flanges.
Trilobatus sacculifer (Brady, 1877)	Tropical (1,3,10)	Minor species in Quaternary sediments along Namibian (7) and western South African slope (8, this study). In Quaternary outer shelf sediments western South Africa (9). Present in surficial sediments along the Namibian and South African margin. Abundances increase along northeast coast of South Africa (2).	Pl. 17; figs. 4-5	Calcareous; macroperforate; trochospiral; four chambers visible in final whorl; final chamber slightly elongated and lobulate; deep incised sutures; primary aperture arched umbilical; secondary apertures on spiral side.
Trilobatus trilobus (Reuss, 1850)	Tropical (10,13)	Minor species (<2%) in Quaternary sediments along western South African slope (this study). In Quaternary outer shelf sediments western South Africa (8).	Pl. 17; figs. 6-7	Calcareous; spinose cancellate; trochospiral; chambers spherical or subglobular; four chambers in final whorl; middle lower chamber large projecting forwards; primary aperture umbilical low arch; secondary apertures on spiral side.

References: (1) Bé and Tolderlund, 1971; (2) Lowry, 1987; (3) Glacon, 1990; (4) Giraudeau, 1993; (5) Little et al., 1997; (6) Bertini et al., 1998; (7) Wefer et al., 1998; (8) Rau et al., 2002; (9) Compton et al., 2004; (10) Kucera, 2007; (11) Lombard et al., 2009; (12) Ufkes and Kroon, 2012; (13) BouDagher-Fadel, 2015

7.4.3. Benthic depositional environments

The benthic foraminifera from this study are primarily found on continental slopes living over a broad range of bathymetric depths. Many of the species have been reported from the east and western South Atlantic margins (Wefer et al., 1998; Schmiedl and Mackensen, 1997; Schmiedl et al., 1997; de Almeida et al., 2015; Fig. 7.18). Shelf foraminifera that occur along the margins of Namibia and western South Africa reported by Compton et al. (2004), Schmidt-Sinns (2008), Leiter and Altenbach (2010), Compton and Bergh (2016) and Bergh et al. (2018) were not abundant in the slope cores of this study. Shelf-restricted species (*Ammonia beccarii, Elphidium advenum*) occur at very low abundances, if at all in cores of this study. If glacial periods deliver more sand-sized material to the slope (Compton and Wiltshire, 2009) then there should be occurrences of at least outermost shelf foraminifera in glacial slope sediments. It would be expected that a higher proportion and more shelf species would reach the slope if transport was long-ranged between the shelf and the slope, however, only two instances of very shallow water (inner shelf) species (*Ammonia beccarii, Elphidium advenum*) were found to occur in MIS 4 sediment on the slope in this study. Trace abundances (<1%) of *Ammonia beccarii, Elphidium advenum* and *Hyalinea balthica* are reported in slope sediments (Wefer et al., 1998). Bottom water currents are therefore too weak to transport shelf-restricted foraminifera to over longer distances to the slope. The slope foraminiferal tests themselves are in good condition showing little damage suggesting minimal transport.

The cores from this study allowed for the bathymetric ranges of the species along the margin to be extended from earlier reports in the literature (Fig. 7.18). Many of the taxa documented in the ODP reports were found to occur in upper slope to lower slope sediments in cores GeoB 8342-6 and 8336-6 of this study. A few species were documented in this study (e.g. *Amphicoryna scalaris, Favulina hexagona, Nodosaria (Gladulina) laevigata, Oolina globosa, Vaginulina spinigera*) that were not reported from the ODP studies. The bathymetric extent of other taxa such as the *Lenticulina, Pyrgo* and *Quinqueloculina* genera could not be determined as these taxa were not identified to species level in the ODP reports.

The main benthic foraminifera taxa (abundances >10%) of the three cores are present in all three cores with the exception of *Bulimina aculeata* (which is absent in the deeper cores). Schmiedl et al. (1997) found buliminds and *C. laevigata* to be dominant in dead assemblages from surface sediments to the north of the South African western margin and are strongly influenced under suboxic to dysoxic conditions within the Oxygen Minimum Zone (OMZ). This is in agreement with the assemblages from the upper slope core 20601-4. Buliminids have been found to prefer muddy sediments in waters with low energy, in high food level conditions and under upwelling conditions (Murray, 1991). This suggests that the presence of *B. aculeata* at shallower depths is associated with the proximity to upwelling zones along the southwestern margin.

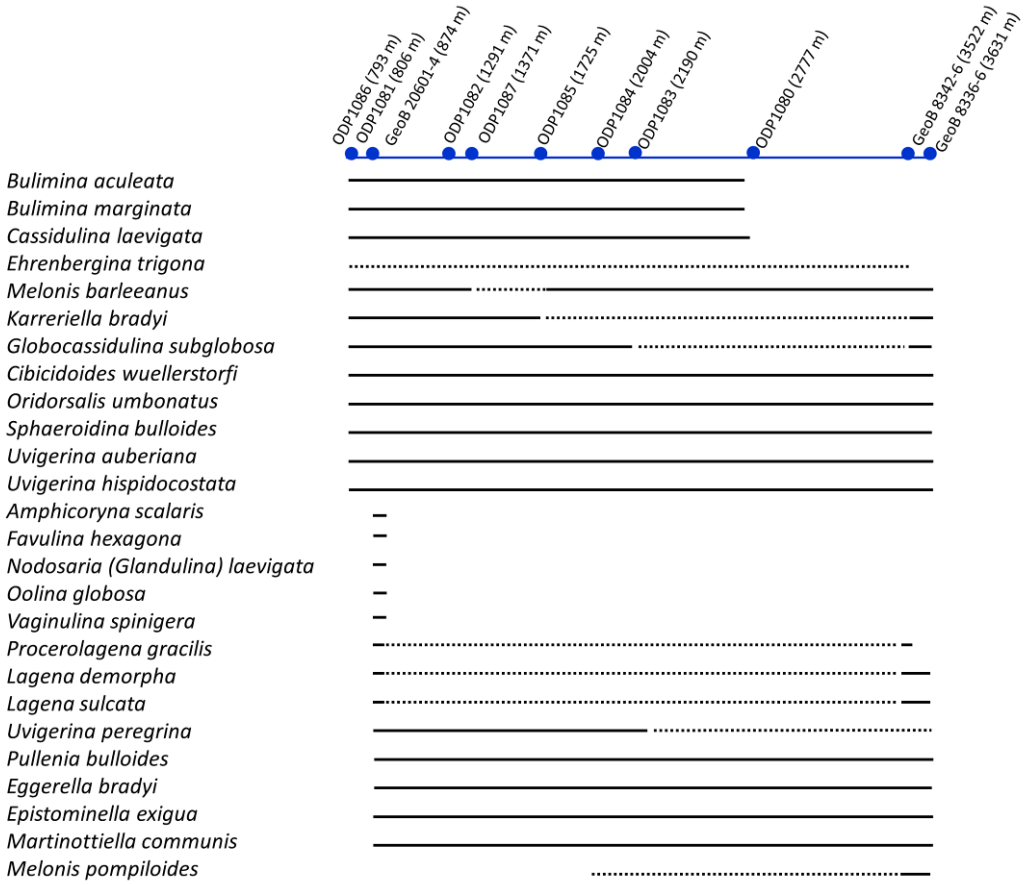

Fig. 7.18. Depth occurrences of benthic foraminifera taxa identified to species level recorded at ODP sites (Wefer et al., 1998) and in this study. The dashed lines indicate depths between two areas where species were not reported.

The most abundant benthic taxa in the cores are *Uvigerina* spp. forming a major component in the three cores (PC 1 in GeoB 206014 and 8342-6; PC 2 in GeoB 8336-6). *Uvigerina peregrina* is dominant in the upper slope core. The benthic foraminifera of the deeper cores contain abundant hispid forms (mostly *U. hispidocostata*). The observation of hispid and hispidocostate Uvigerinid forms increasing with water depth has been made in studies from the North Atlantic (van der Zwaan et al., 1986) and north Indian Ocean (Sharma and Singh, 2012). Factors affecting the distribution of Uvigerinids are not well constrained. The costate (ribbed) *U. peregrina* group occurs over wide depth distributions from the shelf to the slope, whereas hispid and hispidocostate forms are confined to lower depths. Van der Zwaan et al. (1986) suggested that oxygen may play a role in the distribution of Uvigerinids. The lower slope cores are located at a depth at which the modern NADW flows. The hispid and hispidocostate forms show increased relative abundances during glacial periods. Previous studies (Schmiedl and Mackensen, 1997; Rutberg et al., 2000; Hu et al., 2016) suggest NADW flow expands during interglacial periods along the southwestern margin of Africa. NADW is lower in nutrients and is more oxygen-rich than SCW (Bickert and Mackensen, 2003). It therefore follows that hispid and hispidocostate forms may be more adapted to depths at which the

bottom water nutrient content is higher and oxygen content lower during glacial periods of weaker NADW. This is also in agreement with the lower $\delta^{13}C$ values of GeoB8342-6 and 8336-6 (Fig. 7.4 and 7.5) during glacial periods implying the presence of an older water mass enriched in ^{12}C as a result of continued microbial decomposition of organic matter.

In contrast to the hispid and hispidocostate Uvigirinid species, the ribbed species *U. peregrina* increase in abundances during interglacial periods at the shallower GeoB 20601-4 site under the influence of Antarctic Intermediate Water (AAIW), where oxygen conditions are higher than NADW. It has been suggested that the AAIW contrastingly follow NADW fluctuations (Howe et al., 2016) as the NADW is located below southern sourced waters (Reid, 1989), suggesting that *U. peregrina* increase in relative abundances during periods in which the AAIW is weaker and, therefore, prefer conditions at shallower depths under lower bottom water oxygen conditions.

Previous studies have associated *Uvigerina peregrina* with moderate to high organic and potentially low-oxygen environments (Miller and Lohmann, 1982; Hill et al., 2003; Table 7.2) and in upwelling conditions (Lutze and Coulbourn, 1984; Li and McGowran, 1994). In addition to the presence of *Uvigerina* spp. indicating high productivity levels, $\delta^{13}C$ and BFARs can also indicate enhanced productivity (e.g. Schmiedl and Mackensen, 1997). Benthic foraminiferal $\delta^{13}C$ signatures are prone to offset as a result of high seasonal productivity through phytodetritus blooms. The degradation of phytodetritus produces a $\delta^{13}C$-depleted bottom water signature which is reflected in the benthic record (Mackensen and Bickert, 1999; Rau et al., 2002), but $\delta^{13}C$ values in planktic foraminifera can further be influenced by CO_2 inputs into the ocean, fractionation processes, the rate and depth of calcification and dissolution/vital effects (Wolf-Gladrow et al., 1999). The $\delta^{13}C_{Gi}$ values may indicate surface productivity, organic matter remineralisation and upwelling conditions (Ravelo and Hillaire-Marcel, 2007). In this study $\delta^{13}C_{Gi}$ during glacial periods are generally depleted or decrease during those periods. In cores GeoB 8342-6 and 8336-6 these values show the largest depletion followed by a rapid enrichment at glacial terminations II and I (MIS 6/5 and MIS 2/1 boundaries) indicating that global ice volume changes and the relatively rapid oceanographic changes associated with glacial terminations influence surface productivity. The $\Delta\delta^{13}C$ ($\delta^{13}C_{Gi}$- $\delta^{13}C_{Cw}$) values, similarly are high during MIS 6 and MIS 2 in the lower slope cores with a narrower degree of difference between planktic and benthic $\Delta\delta^{13}C$ during GT II and I (Fig. 7.19). The higher $\Delta\delta^{13}C$ values during glacial periods indicate surface productivity to be higher relative to benthic productivity whereas interglacial periods indicate near equal or higher benthic productivity possibly related to a higher burial rate and increase in sedimentation and retention of organic matter during those periods.

The dominance of *E. exigua* is consistent with studies to the north of the western South African slope by Schmiedl and Mackensen, (1997) and Schmiedl et al. (1997) who have found this species to occur at depths between 1700 and 4500 m in the Cape Basin off Namibia. This species forms another major component in the deeper lower slope cores (PC 2 in GeoB 8342-6

and PC 1 in GeoB 8336-6). PC 1 in which *E. exigua* dominates the assemblage in GeoB 8342-6 is interpreted as being representative of organic carbon flux as the weakest negative value was *Pyrgo* spp. Murgese and de Deckker (2005) listed *Pyrgo* spp. as low carbon flux indicators. PC 2 in core GeoB 8342-6 was interpreted as being indicative of seasonality as *G. subglobosa* is inversely related to seasonal flux of phytodetritus (Sun et al., 2006). The delivery of organic matter to the sea floor in the form of phytodetritus benefits species such as *C. wuellerstorfi* and *E. exigua* (Gooday, 1988). Although *E. exigua* has been associated with eutrophic conditions (Morigi, 2009), it has also been mentioned to be opportunistic under oligotrophic conditions benefiting from episodic sea surface phytoplankton blooms (Gooday, 1988) and a good indicator of seasonality in the palaeoproductivity record (Thomas et al., 1995; Thomas and Gooday, 1996). Although *E. exigua* exhibits highest seasonal productivity pulses at the MIS 6/5, MIS 5/4 and MIS 3/2 boundaries, its abundance fluctuates independently of glacial-interglacial cycles, which suggests seasonal productivity occurs throughout the record.

Oxygen availability forms the third major component in the three cores (PC 2 in GeoB 20601-4; PC 3 in GeoB 8342-6 and 8336-6). According to the oxygen bottom-water classification by Kaiho (1994) the bottom water environment in cores 8342-6 and 8336-6 remained under high oxic conditions while core 20601-4 showed low oxic to suboxic conditions during MIS 5. The dominance of low oxygen species in core 20601-4 is consistent with the oxygen miminum zone (OMZ) and calculated BFOI values which are generally lower compared to the deeper water cores 8342-6 and 8336-6.

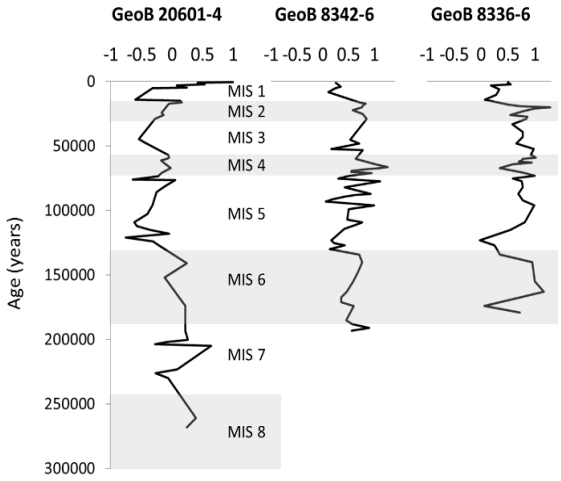

Fig. 7.19. $\Delta\delta^{13}C$ ($\delta^{13}C_{Gr.\ (Gc.)\ inflata}$ - $\delta^{13}C_{C.\ wuellerstorfi}$) in all three cores of this study

PC 3 in GeoB 20601-4 is interpreted, to a lower extent, as being indicative of water depth as *Cibicidoides crebbsi* has been identified to occur at deeper depths compared to *Cibicidoides pachyderma* (Kender et al., 2008). Depth seems to have a higher influence on the assemblage during MIS 5 and is coincident with higher BFAR and sedimentation rates during that period. PC3 shows an overall decrease towards MIS 2 but then increases again in MIS 1.

Table 7.2. Taxonomic information, ecological examples from previous studies, bathymetric and regional distribution information on the main benthic species from the three slope cores of this study incorporating data from previous studies. Numbers in parentheses refer to previous studies indicated at the end of this table. Abundances (where available): trace = <1%; low = 1-10%; moderate = 10-50%; high = >50%

Taxon	Ecological and bathymetric examples	Regional distribution	Figure reference	Taxonomic features
Bigenerina nodosaria (d'Orbigny, 1826)	Upper slope distribution (11)	Trace abundances off the Orange River slope (this study).	Pl. 8, fig. 6	Agglutinated; biserial becoming uniserial; terminal aperture.
Bolivina spp.	Infaunal (4,6) to shallow infaunal (10). Dysoxic (2), muddy sediment on the inner shelf to slope (6).	Trace abundances in cores from this study.	Pl. 11, figs. 1-2	Calcareous hyaline; biserial; loop-shaped terminal aperture.
Bulimina aculeata (d'Orbigny, 1826)	Infaunal (4,6,7), shallow infaunal (5,10) under suboxic (2) to dysoxic (5) or anoxic conditions, muddy to fine sand sediments, inner shelf to abyssal distribution (6,11).	Moderate abundances in Pliocene (17) to Quaternary sediments on the slope off South Africa (this study) and Namibia (15,17). In surficial sediments along Namibia (13,16) and South Africa (13).	Pl. 11, fig. 10; pl. 12, figs. 1a-b	Calcareous hyaline; triserial; globular to subglobular chambers; outward extending spines around test; elliptical aperture with lip.
Bulimina marginata (d'Orbigny, 1826)	Infaunal (1,4,6) under suboxic (2) to anoxic conditions, muddy to fine sand sediments, inner shelf to slope distribution (6,11).	Moderate to low abundances in Pliocene (17) to Quaternary sediments on upper slope off South Africa (this study) and Namibia (17). In southern Namibian inner to middle shelf sediments (14). In surficial shelf to upper slope sediments along Namibia and South Africa (13).	Pl. 12, figs. 2a-b	Calcareous hyaline; triserial; globular to subglobular chambers; downward extending spines around margins of chambers; elliptical arc-shaped aperture with lip.
Bulimina mexicana (Cushman, 1922)	Infaunal (4,6), shallow infaunal (10) under suboxic conditions (2), muddy to fine sand sediments, inner shelf to slope distribution (6). Primarily upper to middle slope (11)	Low abundances in Quaternary sediments on the slope off South Africa (this study) and Namibia (15,16).	Pl. 12, figs. 3-4	Calcareous hyaline; triserial; globular to subglobular chambers; downward extending spines around margins of chambers; elliptical arc-shaped aperture with lip.

Table 7.2 *(continued)*

Taxon	Ecological and bathymetric examples	Regional distribution	Figure reference	Taxonomic features
Cassidulina laevigata (d'Orbigny, 1826)	Infaunal (1), infaunal-epifaunal (6), shallow infaunal (10), epifaunal (7) under suboxic (2), muddy and sandy sediments, shelf to slope distribution (6).	Low abundances in Pliocene slope sediments. Low to moderate abundances in Quaternary slope and shelf ssediments off Namibia (14,15,16; this study) and South Africa (16; this study). Low to moderate abundances in shelf sediments along Namibia and western South Africa.	Pl. 11, figs. 4-6	Calcareous hyaline; planispiral; test and chambers flattened; subrounded test; aperture slit extraumbilical interiomarginal.
Cibicidoides crebbsi (Hedberg, 1937)	Infaunal-epifaunal (6), epifaunal (7) under oxic conditions (2)	Low to moderately abundant in Miocene to surficial shelf and slope sediments (13,15,17, this study)	Pl. 13, figs. 3a-c	Calcareous hyaline; trochospiral; test coarsely perforate; unequally biconvex; aperture interiomarginal slit.
Cibicidoides pachyderma (Rzehak, 1886)	Epifaunal-shallow infaunal (6,10) under oxic conditions (2) primarily on the upper slope (11).	Low to moderate abundances in Quaternary slope sediments off western South Africa (17, this study) and Namibia.	Pl. 13, figs. 4a-c	Calcareous hyaline; trochospiral; test unequally biconvex; approximately ten chambers in final whorl; sutures curve towards central boss; aperture interiomarginal slit.
Cibicidoides wuellerstorfi (Schwager, 1866)	Epifaunal (1,7,10), infaunal-epifaunal (2). Primarily slope species (11) under oxic conditions (2).	Low to moderate abundances in Miocene sediments off western South Africa. Moderate abundances in Plio-Pleistocene sediments off western South Africa and Namibia (15,17, this study). Low to moderate abundances in surficial shelf to slope sediments from Namibia (13,16) to southern Mozambique (13).	Pl. 13, figs. 5a-c	Calcareous; test trochospiral planoconvex; approximately ten chambers in final whorl; sutures curve towards umbilicus; aperture interiomarginal slit.
Dentalina sp.	Infaunal (6), shallow infaunal (10), epifaunal (7) under suboxic to dysoxic conditions (2).	Low abundances in Miocene to Recent shelf and slope sediments off Namibia and South Africa (13,17, this study).	Pl. 9, fig. 7	Calcareous hyaline; test elongate; uniserial; chamber size increase towards aperture; aperture terminal.

Table 7.2 *(continued)*

Taxon	Ecological and bathymetric examples	Regional distribution	Figure reference	Taxonomic features
Eggerella bradyi (Cushman, 1911)	Infaunal (4,6), shallow infaunal (10). Slope to abyssal distribution (11).	Low to trace abundances in Pliocene to Quaternary sediments along the western margin of Southern Africa (17, this study).	Pl. 8, figs. 1-2	Agglutinated; initially trochospiral becoming triserial; chambers subglobular; aperture terminal slit.
Ehrenbergina trigona (Goës, 1896)	Epifaunal (6) under suboxic (2), muddy conditions in cold water from the outer shelf to slope (6)	Trace abundances in Quaternary (this study) to surficial (13) slope sediments off Namibia (15) and western South Africa (this study).	Pl. 11, fig. 9	Calcareous; test semi-triangular; serrated periphery; sutures slightly depressed; aperture oval terminal.
Epistominella exigua (Brady, 1884)	Epifaunal (1), epifaunal-shallow infaunal (6) in muddy sediments on slope (6) and at abyssal depths (11).	Minor to high abundances in Pliocene to Quaternary sediments off Namibia (15,16) and South Africa (17, this study). More abundant along lower slope (this study).	Pl. 13, figs. 6a-d	Calcareous; test flattened unequally biconvex; trochospiral; five chambers in last whorl; aperture interiomarginal slit.
Favulina hexagona (Williamson, 1848)	Infaunal (12)	Trace abundances in upper slope Quaternary sediments off western South Africa (this study).	Pl. 10, figs. 8a-b	Calcareous; test globular; unilocular; elevated hexagonal ridges forming reticulate ornamentation across test; aperture circular terminal on neck.
Fissurina spp.	Infaunal (1, 4), epifaunal-shallow infaunal (10) under suboxic conditions (2).	Trace to low abundances in Pliocene to Quaternary shelf and slope sediments off South Africa (13,17, this study) and Namibia (15).	Pl. 10, figs. 9-10	Calcareous hyaline; unilocular; ridges along margin of test; aperture terminal on long neck.
Globobulimina turgida (Bailey, 1851)	Infaunal (4,7), deep infaunal (6,10) under dysoxic conditions (2) in muddy sediments; shelf and slope distribution (6).	Low abundances on upper slope off South Africa (this study) and Namibia (16). In surficial Namibian slope sediments (17).	Pl. 12, figs. 5a-b	Calcareous hyaline; globular oviform; triserial; inflated chambers overlap; sutures slightly depressed; aperture loop-shaped with toothplate.

Table 7.2 *(continued)*

Taxon	Ecological and bathymetric examples	Regional distribution	Figure reference	Taxonomic features
Globocassidulina crassa (d'Orbigny, 1839a)	Infaunal (1, 6) in muddy sediments, shelf to slope distribution (6).	Low to moderate abundances in Quaternary slope sediments off western South Africa (this study). In surficial shelf sediments between Cape Town and Port Elizabeth (13).	Pl. 11, figs. 7a-b	Calcareous; test slightly elongate inflated and globular; trochospiral; sutures depressed; aperture slit in extended terminal chamber.
Globocassidulina subglobosa (Brady, 1881)	Infaunal (1,4,6,7), epifaunal-shallow infaunal (10) at slope to abyssal depths (11) in oxic conditions (2).	Moderate to high abundances in Miocene to Quaternary and surficial slope sediments off Namibia (15,16, this study) and western South Africa (17, this study).	Pl. 11, figs. 8a-b	Calcareous; test small, inflated and globular; trochospiral; sutures slightly depressed; aperture slit along terminal chamber.
Gyroidinoides orbicularis (d'Orbigny, 1826)	Epifaunal (4,5,6,7), epifaunal-shallow infaunal (10) under suboxic conditions in muddy sediment; shelf to slope distribution (6,11).	Low to moderate abundances in Miocene (this study) to Quaternary shelf to slope sediments off Namibia and South Africa (13,15, this study). In surficial sediments in shelf to upper slope sediments between Cape Town and Port Elizabeth (13).	Pl. 14, figs. 7-9	Calcareous; trochospiral; planoconvex; sutures flush and radial on spiral side; aperture interiomarginal slit.
Lagena demorpha (Rymer Jones, 1872)	Epifaunal-shallow infaunal (10), epifaunal (7) in suboxic conditions (2).	Trace abundances in Quaternary lower slope sediments (this study).	Pl. 10, figs. 3-4	Calcareous; test globular to flask shaped; unilocular; costate; large pores along lower edges of ridges; round aperture on long neck.
Lagena sulcata (Walker and Jacob, 1798)	Epifaunal-shallow infaunal (10), epifaunal (7) in suboxic conditions (2).	Trace abundances in Quaternary lower slope sediments (this study) and inner to middle shelf of southern Namibia (14).	Pl. 10, figs. 6a-b	Calcareous hyaline; test globular with long neck; unilocular; ridges along length of test; round aperture on neck.
Lenticulina gibba (d'Orbigny, 1839a)	Epifaunal (1,4,6,7), epifaunal-shallow infaunal (10) under suboxic (2), muddy sediments, outer shelf to slope distribution (6).	Low to moderately abundant genus from Miocene to Quaternary in shelf and slope sediments off Namibia and South Africa (13,17, this study).	Pl. 9, figs. 10-11	Calcareous; planispiral; biconvex; ~6 to 9 chambers in final whorl; sutures are flush; aperture radiate and terminal.

Table 7.2 *(continued)*

Taxon	Ecological and bathymetric examples	Regional distribution	Figure reference	Taxonomic features
Martinottiella communis (d'Orbigny, 1826)	Epifaunal (6), shallow infaunal (4,5,10). Mostly abundant in oxic conditions, muddy sediments, shelf to slope distribution (6,11).	Trace to low abundances in Miocene to Quaternary slope sediments off Namibia (13; this study) and western South Africa (16; this study).	Pl. 8, figs. 5a-b	Agglutinated; mostly uniserial; sutures depressed; aperture round terminal on short neck.
Melonis barleeanus (Williamson, 1858)	Infaunal (4,6,7), shallow infaunal (10) under suboxic conditions (2); muddy sediments from outer shelf to slope (6,11).	Low to moderate abundances in Miocene to Quaternary outer shelf to slope sediments off Namibia (15,16, this study) and western South Africa (this study).	Pl. 14, figs. 1a-b	Calcareous; test near symmetrical biconvex; planispiral; sutures and apertural face imperforate; aperture interiomarginal slit.
Melonis pompilioides (Fichtel and Moll, 1798)	Infaunal (4,5,6,7), shallow infaunal (3, 11) under suboxic conditions (2); muddy sediments, outer shelf to slope (6,11). Morphologically similar to *M. sphaeroides*, but bathymetrically separated with *M. sphaeroides* being the deeper form occurring at mid-slope to abyssal depths (11).	Trace abundances in Quaternary lower slope sediments off western South Africa (this study) and Namibia (15). In surficial Namibian slope sediments (16).	Pl. 14, figs. 2-3	Calcareous; test near symmetrical biconvex; planispiral; sutures and apertural face imperforate; deep and open umbilici; aperture interiomarginal slit. Slightly more inflated compared to *M. barleeanus.*
Nodosaria (Glandulina) laevigata (d'Orbigny, 1826)	Infaunal (6), shallow infaunal (10)	Trace abundances in Miocene to Quaternary shelf and slope sediments off Namibia and South Africa (13, this study)	Pl. 9, figs. 8-9	Calcareous; test ovate and globular; final chamber largest and inflated; sutures flush, aperture terminal radiate.
Oolina globosa (Montagu, 1803)	Epifaunal-shallow infaunal (5) under oxic to dysoxic conditions.	Trace abundances in Quaternary lower slope sediments off western South Africa (this study).	Pl. 9, fig. 12	Calcareous; globular with spines at bottom of test; unilocular; aperture terminal radiate.

Table 7.2 *(continued)*

Taxon	Ecological and bathymetric examples	Regional distribution	Figure reference	Taxonomic features
Oridorsalis umbonatus (Reuss, 1851)	Epifaunal (1,4,6,7), epifaunal-shallow infaunal (10) under suboxic conditions (2); muddy sediments from shelf to abyssal depths (6,11).	Moderate abundances in Miocene to Quaternary slope sediments off Namibia (15,16, this study) and western South Africa (17, this study). In southern Namibian inner to middle shelf sediments (14).	Pl. 14, figs. 6a-c	Calcareous; trochospiral; biconvex; slightly depressed sutures; aperture interiomarginal.
Procerolagena gracilis (Williamson, 1848)	Cosmopolitan (9)	Trace abundances in Quaternary lower slope sediments off western South Africa (this study).	Pl. 10, fig. 7	Calcareous, elongate and extended at both ends; unilocular; aperture rounded terminal.
Pullenia bulloides (d'Orbigny, 1846)	Infaunal (1,4,6,7), shallow infaunal (10) in suboxic conditions (2); muddy sediments from outer shelf to abyssal depths (6,11).	Low to moderate abundances in Miocene to Quaternary outer shelf to slope sediments off Namibia (15, this study) and western South Africa (17, this study). In surficial sediments along the Namibian (16) and South African margin (13).	Pl. 14, figs. 4-5	Calcareous; subglobular; planispiral; sutures slightly depressed; aperture narrow crescentic slit interiomarginal extending along the test periphery to both umbilical regions.
Pyrgo lucernula (Schwager, 1866)	Epifaunal (1,4,6) at middle slope to abyssal depths (11).	Trace to low abundances in Quaternary lower slope sediments off western South Africa (this study) and Namibia (15). In southern Namibian inner to middle shelf sediments (14). Trace abundances in surficial upper slope sediments off the Orange River mouth and southern Mozambique (13).	Pl. 9, figs. 1-3	Calcareous porcelaneous, imperforate; ovate; biconvex; keeled periphery; chambers inflated; aperture circular terminal on short neck with tooth.
Pyrgo murrhina (Schwager, 1866)	Epifaunal (1,4,6) at slope to abyssal depths (11).	Trace to low abundances in Quaternary lower slope sediments off western South Africa (this study) and Namibia (15). Trace abundances in surficial shelf and slope sediments off the Orange River mouth and Port Elizabeth (13).	Pl. 9, figs. 4a-b	Calcareous porcelaneous, imperforate; test slightly compressed compared to *P. lucernula*; ovate; biconvex; keeled periphery; chambers slightly inflated; aperture circular terminal on short neck with tooth.

Table 7.2 *(continued)*

Taxon	Ecological and bathymetric examples	Regional distribution	Figure reference	Taxonomic features
Pyrgo serrata (Bailey, 1861)	Epifaunal (1,4,6) at shelf to abyssal depths (11)	Trace abundances in lower slope sediments off western South Africa (this study). Trace abundances in surficial upper slope sediments north of the Orange River mouth (13).	Pl. 9, figs. 5-6	Calcareous porcelaneous, tests from this study relatively large; imperforate; serrated margin; biconvex; keeled periphery; chambers slightly inflated; aperture rounded, terminal.
Quinqueloculina laevigata (d'Orbigny, 1839b)	Epifaunal-shallow infaunal (10), epifaunal (4,7,8) under oxic conditions (2) in hypersaline conditions mostly on the shelf (6).	Trace abundances in slope sediments off western South Africa (this study). Trace abundances in surficial shelf sediments off Cape Town (13).	Pl. 8, fig. 12	Calcareous porcelaneous; imperforate; chambers slightly inflated and one half length of coil; sutures depressed; aperture rounded terminal with tooth.
Siphotextularia concava (Karrer, 1868)	Infaunal (4) on the shelf and slope (11).	Trace to moderate abundances in Miocene to Quaternary slope sediments off Namibia and western South Africa (17, this study). Trace abundances on shelf of eastern South Africa (13).	Pl. 8, fig. 7	Agglutinated; flattened; biserial; approximately eleven chambers visible externally; chambers increase in size and become inflated towards terminal end; aperture terminal slit.
Sphaeroidina bulloides (d'Orbigny, 1826)	Epifaunal-shallow infaunal, infaunal (4) under suboxic conditions (2) at shelf to abyssal depths (11).	Trace to high abundances in Miocene to Quaternary slope sediments off Namibia (15, this study) and western South Africa (17, this study).	Pl. 13, fig. 2	Calcareous; imperforate; test subglobular with globular chambers; trochospiral; slightly depressed sutures; three chambers in final whorl; aperture near junction of three chambers; aperture crescentic.
Uvigerina auberiana (d'Orbigny, 1839a)	Infaunal (4,6) under suboxic conditions (2) at shelf to abyssal depths (11).	Low to high abundances in Miocene to Quaternary slope sediments off western South Africa (17, this study). In surficial Namibian slope sediments (16).	Pl. 12, figs. 6-7	Calcareous; hispid; triserial; globular chambers; approximately six chambers visible externally; aperture rounded terminal on neck with lip extending outwards.

Table 7.2 *(continued)*

Taxon	Ecological and bathymetric examples	Regional distribution	Figure reference	Taxonomic features
Uvigerina hispidocostata (Cushman and Todd, 1945)	Infaunal (6)	Low to high abundances in Quaternary slope sediments off Namibia and western South Africa (17, this study).	Pl. 12, figs. 8a-b	Calcareous; hispid with longitudinal costae covering a portion of chambers; triserial; globular shaped chambers; approximately eight to ten chambers visible externally; aperture rounded terminal on neck with lip extending outwards.
Uvigerina peregrina (Cushman, 1923)	Infaunal (4,5,7), shallow infaunal (6) under suboxic (2) to dysoxic (5) and high organic carbon conditions (6).	Low to high abundances in Quaternary upper slope sediments off western South Africa (this study) and Namibia (15). Common in surficial shelf to slope sediments along Namibia (13,16) and South Africa (13).	Pl. 12, figs. 9a-b	Calcareous; longitudinal costae cover length of chambers and test; triserial; approximately six chambers visible externally; aperture rounded terminal on neck with lip extending outwards.
Uvigerina proboscidea (Schwager, 1866)	Infaunal (4,6) under suboxic conditions (2) primarily at slope depths (11).	Low abundances in Quaternary lower slope sediments off western South Africa (this study) and Namibia (15).	Pl. 13, figs. 1a-b	Calcareous; test mostly hispid; triserial; aperture rounded terminal on neck
Vaginulina spinigera (Linnaeus, 1758)	Epifaunal-shallow infaunal (10), epifaunal (4)	Trace abundances in Quaternary upper slope sediments off western South Africa (this study).	Pl. 10, fig. 2	Calcareous; test large and elongate; flattened; test broadens as chambers are added; sutures slightly depressed; two long extended basal spines project outward in opposite directions; aperture terminal radiate.

Ecology and bathymetry references: (1) Corliss and Chen, 1988; (2) Kaiho, 1994; (3) Kaminski et al., 1995; (4) Carboni and di Bella, 1996; (5) Goubert et al., 2001; (6) Murray, 2006; (7) Drinia et al., 2007; (8) Reolid et al., 2008; (9) Majewski, 2010; (10) Pérez-Asensio et al., 2012; (11) Holbourn et al., 2013; (12) Stojanova and Petrov, 2018.

Regional distribution references: (13) Lowry, 1987; (14) McMillan, 1987; (15) Schmiedl and Mackensen, 1997; (16) Schmiedl et al., 1997; (17) Wefer et al., 1998.

This study = results from entire thesis including data from Namibian outer shelf and South African slope cores.

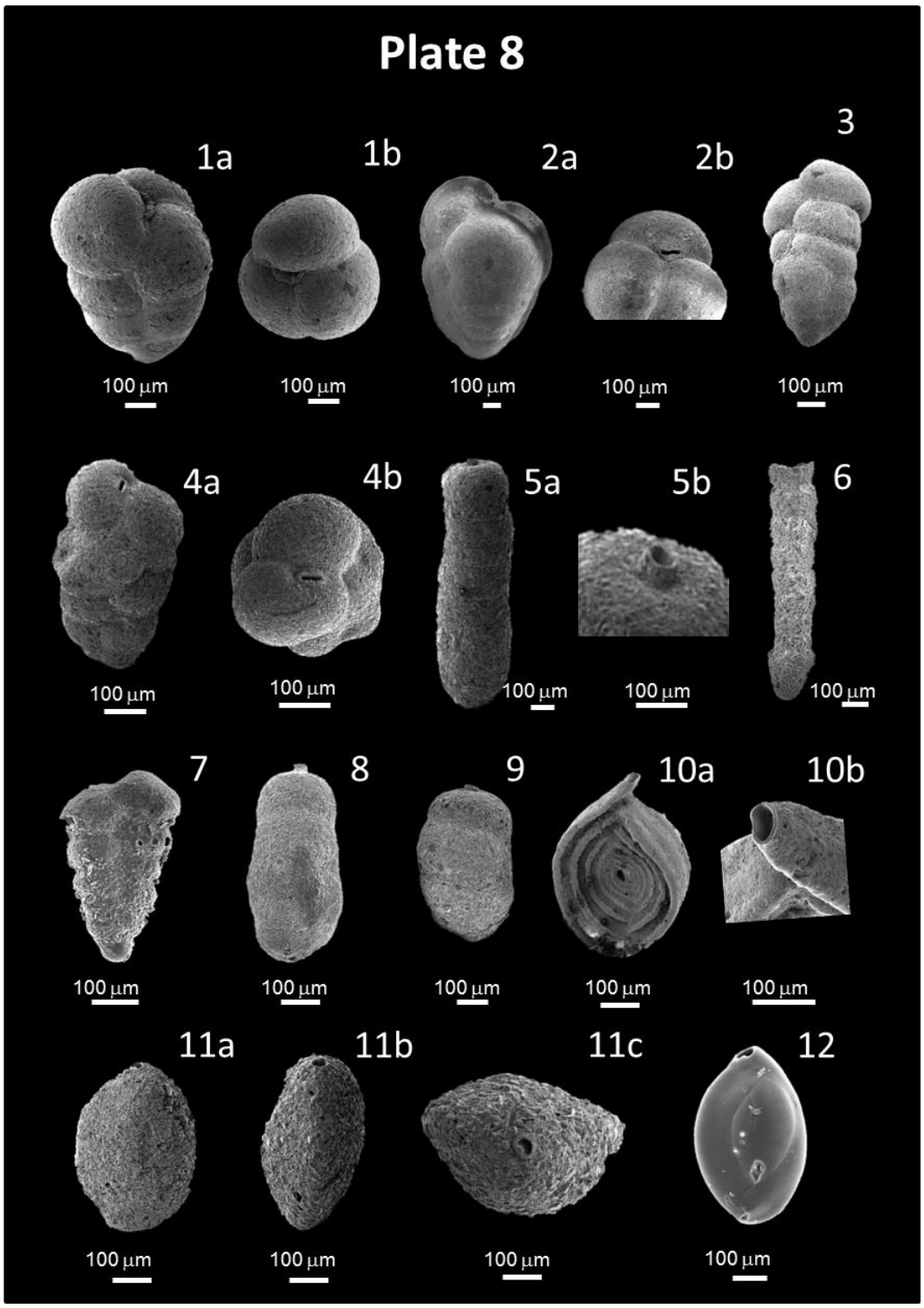

Plate 8. 1a. *Eggerella bradyi;* **1b.** *Eggerella bradyi* (apertural view) (GeoB 8336, 199 cm); **2a.** *Eggerella bradyi;* **2b.** three upper chambers of *Eggerella bradyi* with aperture visible (GeoB 8336, 189 cm); **3.** *Karreriella bradyi* (GeoB 8336, 189 cm); **4a.** *Karreriella bradyi* with aperture visible; **4b.** *Karreriella bradyi* (apertural view) (GeoB 8336, 229 cm); **5a.** *Martinottiella communis;* **5b.** aperture of *Martinottiella communis* (GeoB 8336, 254 cm); **6.** *Bigenerina nodosaria* (GeoB 8336, 254 cm)*;* **7**. *Siphotextularia concava* (GeoB 8336, 399 cm); **8-9.** *Cylindroclavulina bradyi* (GeoB 8336, 254 cm); **10a.** *Spiroloculina communis*; **10b.** aperture on neck of *Spiroloculina communis* (GeoB 8336, 210 cm)*;* **11a.** *Siphonaperta* sp.; **11b**. side view of *Siphonaperta* sp.; **11c.** *Siphonaperta* sp (apertural view) (GeoB 8336, 254 cm); **12.** *Quinqueloculina laevigata* (GeoB 8336, 210 cm).

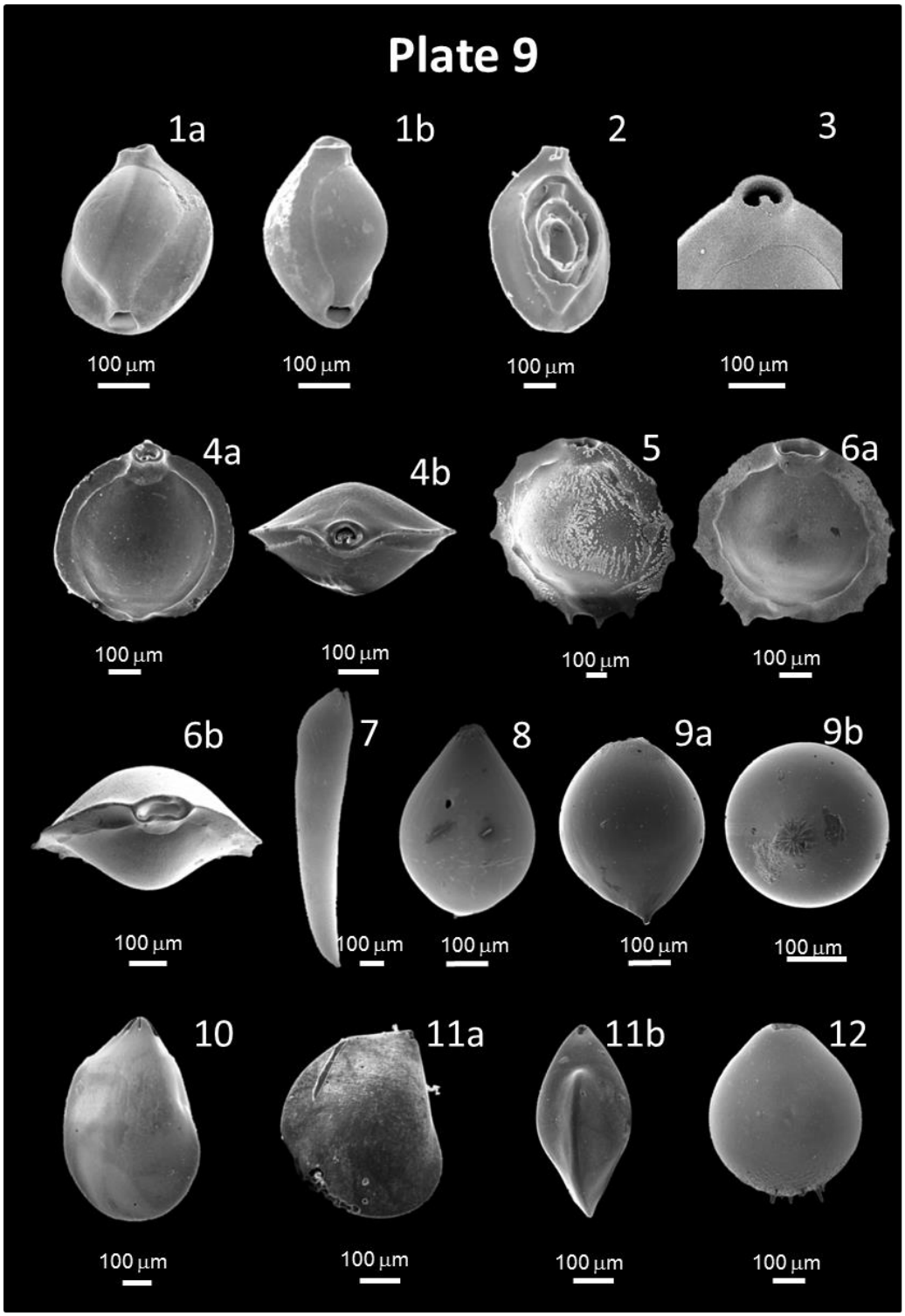

Plate 9. 1a. *Pyrgo lucernula;* **1b.** *Pyrgo lucernula* (side view) (GeoB 8336, 289 cm); **2.** internal chambers of *P. lucernula* (GeoB 8336, 404 cm); **3.** Aperture of *P. lucernula* (GeoB 8336, 289 cm); **4a.** *Pyrgo murrhina;* **4b.** *Pyrgo murrhina* (apertural view) (GeoB 8336, 204 cm); **5-6.** *Pyrgo serrata* (GeoB 8336, 204 cm)*;* **6b.** *Pyrgo serrata* (apertural view) (GeoB 8336, 204 cm); **7.** *Dentalina* sp. (GeoB 8336, 199 cm); **8-9.** *Nodosaria laevigata* (GeoB 8336, 339 cm); **9b.** *Nodosaria (Glandulina) laevigata* (apertural view) (GeoB 8336, 339 cm); **10-11.** *Lenticulina gibba* (GeoB 8336, 254 cm; 264 cm); **11b.** *Lenticulina gibba* (marginal view) (GeoB 8336, 264 cm); **12.** *Oolina globosa* (GeoB 8336, 299 cm).

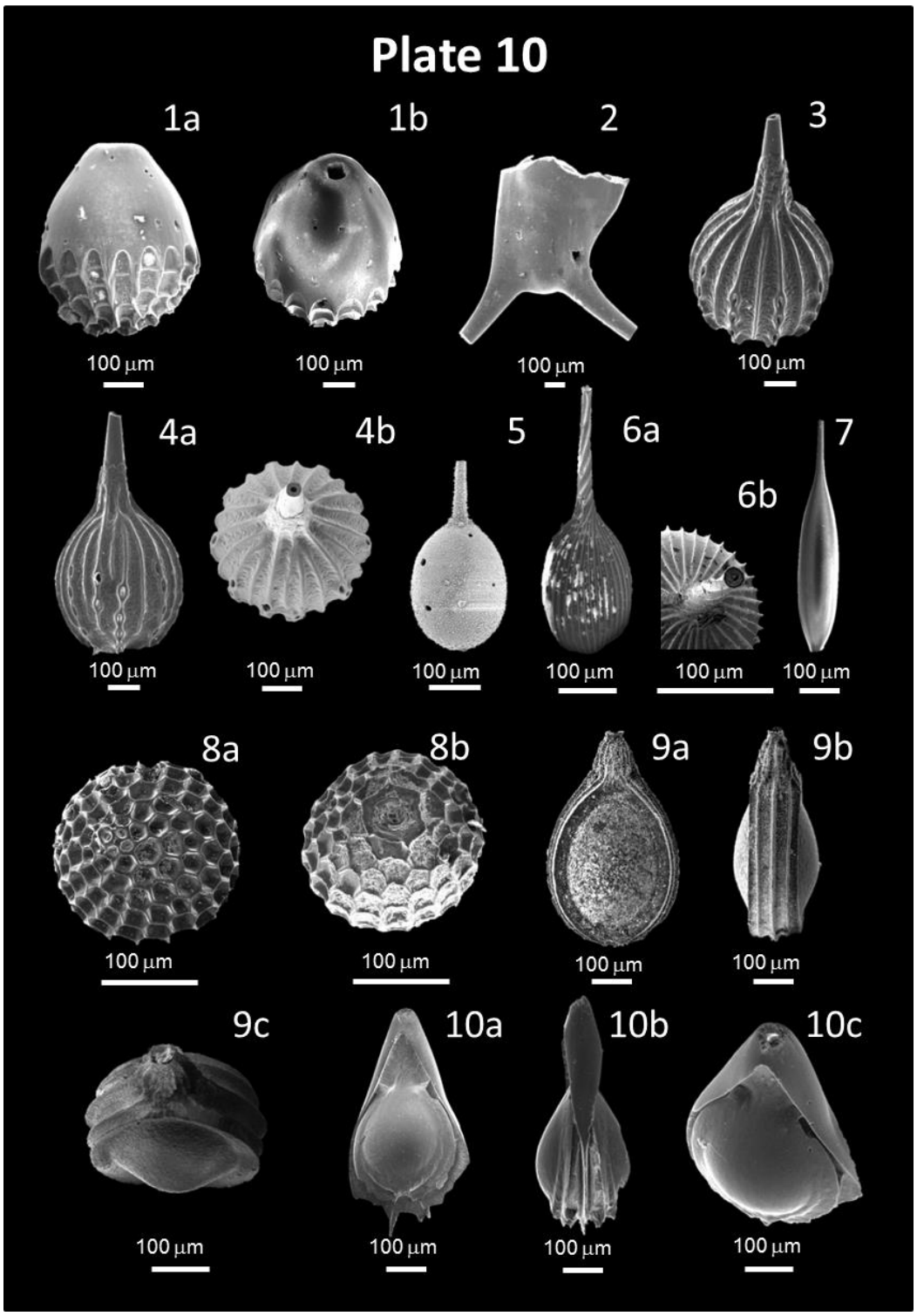

Plate 10. 1a. *Oolina seminuda;* **1b.** *Oolina seminuda* with aperture visible (GeoB 8336, 299 cm); **2.** Lower portion of *Vaginulina spinigera* with basal spines (GeoB 8336, 289 cm); **3-4**. *Lagena demorpha* (GeoB 8336, 279 cm; 254 cm)*;* **4b.** *Lagena demorpha* (apertural view) (GeoB 8336, 254 cm); **5.** hirsute *Lagena* sp. with borings (GeoB 8336, 259 cm); **6a.** *Lagena sulcata;* **6b.** aperture on neck of *L. sulcata* (GeoB 8336, 279 cm); **7.** broken *Procerolagena gracilis* (GeoB 8336, 199 cm); **8.** *Favulina hexagona;* **8b.** *Favulina hexagona* (apertural view) (GeoB 20601, 73 cm); **9-10.** *Fissurina* spp. (GeoB 8336, 299 cm; 274 cm).

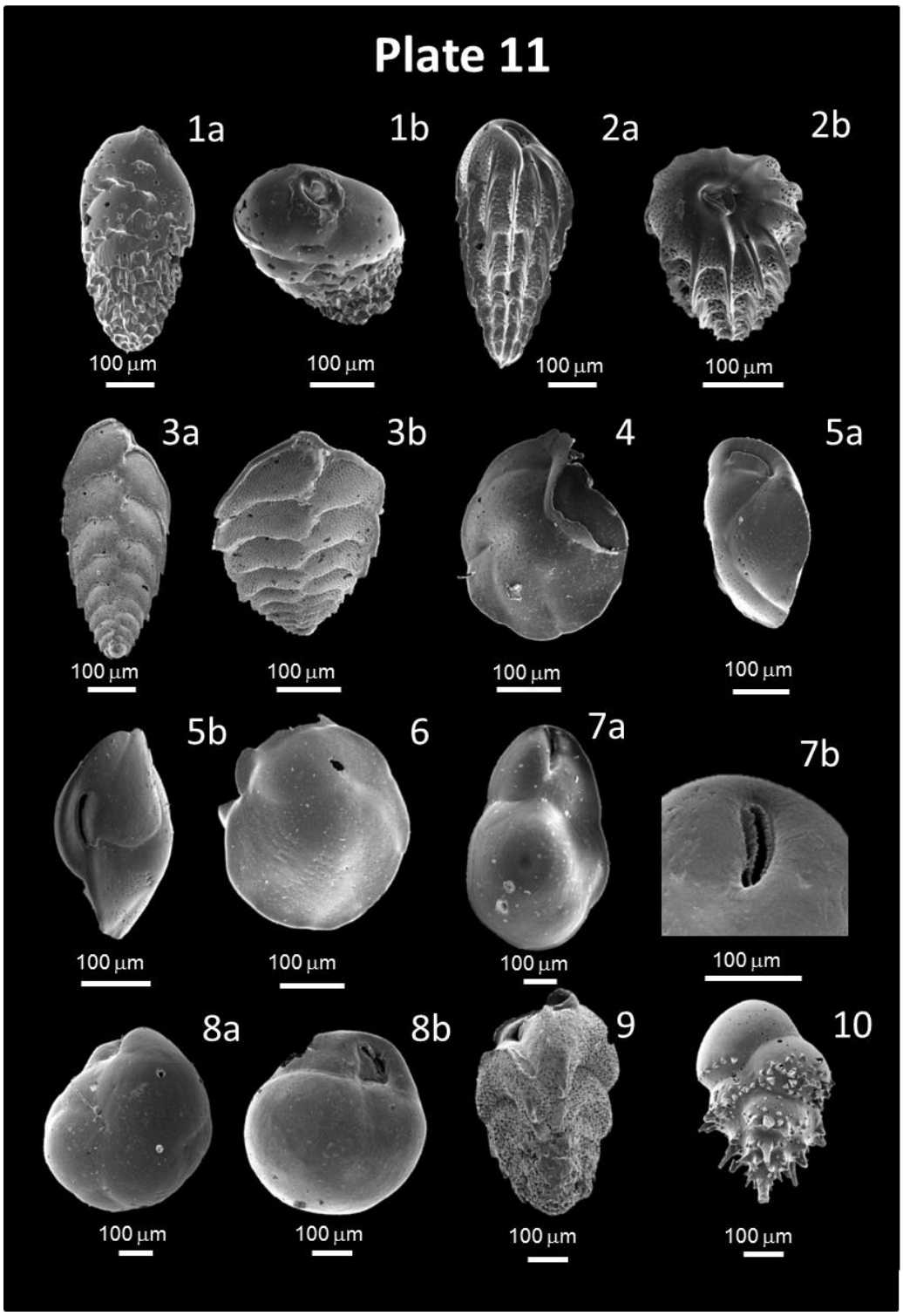

Plate 11. 1-2. *Bolivina* spp. (GeoB 20601, 249 cm) ; **3.** *Brizalina alata* (GeoB 20601, 73 cm); **4.** *Cassidulina laevigata* (spiral view) (GeoB 20601, 73 cm); **5a**. *Cassidulina laevigata* (oblique marginal view); **5b.** *Cassidulina laevigata* (apertural view) (GeoB 20601, 73 cm); **6.** *Cassidulina laevigata* (umbilical view) (GeoB 20601, 73 cm); **7a.** *Globocassidulina crassa*; **7b.** aperture of *Globocassidulina crassa* (GeoB 20601, 69 cm); **8.** *Globocassidulina subglobosa* (GeoB 20601, 233 cm); **9**. *Ehrenbergina trigona* (GeoB 8336, 329 cm)*;* **10.** *Bulimina aculeata* (GeoB 20601, 73 cm).

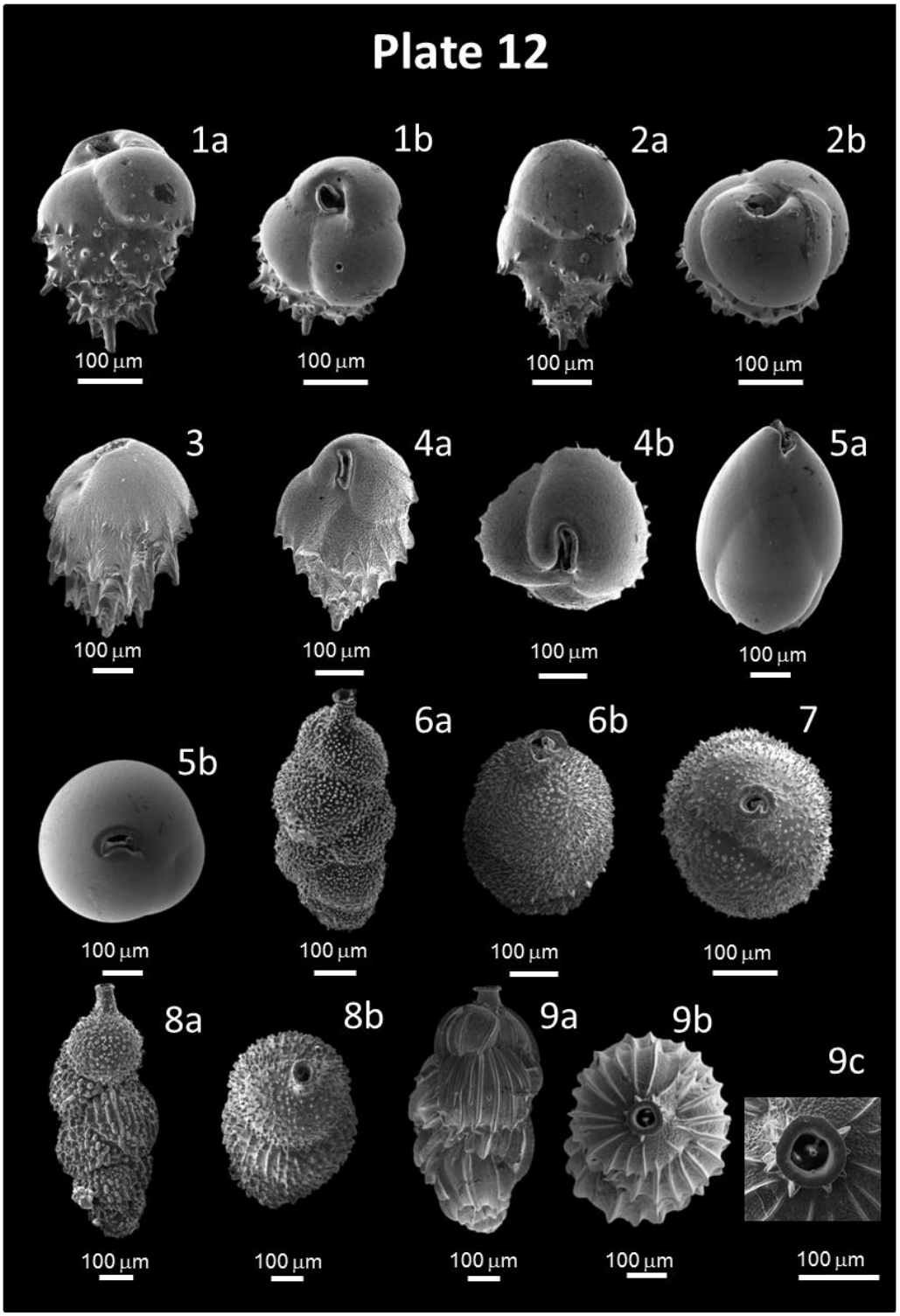

Plate 12. 1a. *Bulimina aculeata*; **1b.** *Bulimina aculeata* (apertural view) (GeoB 20601, 73 cm); **2a.** *Bulimina marginata;* **2b.** *Bulimina marginata* (apertural view) (GeoB 20601, 73 cm); **3-4.** *Bulimina mexicana*; **4b.** *Bulimina mexicana* (apertural view) (GeoB 20601, 73 cm); **5a.** *Globobulimina turgida;* **5b**. *Globobulimina turgida* (apertural view) (GeoB 20601, 73 cm); **6a**. *Uvigerina auberiana;* **6b.** *Uvigerina auberiana* with aperture visible; **7.** *Uvigerina auberiana* (apertural view) (GeoB 8336, 301 cm); **8a**. *Uvigerina hispidocostata*; **8b**. *Uvigerina hispidocostata* (apertural view) (GeoB 8336, 301 cm); **9a.** *Uvigerina peregrina;* **9b.** *Uvigerina peregrina* (apertural view); **9c**. aperture of *Uvigerina peregrina* (GeoB 20601, 73 cm).

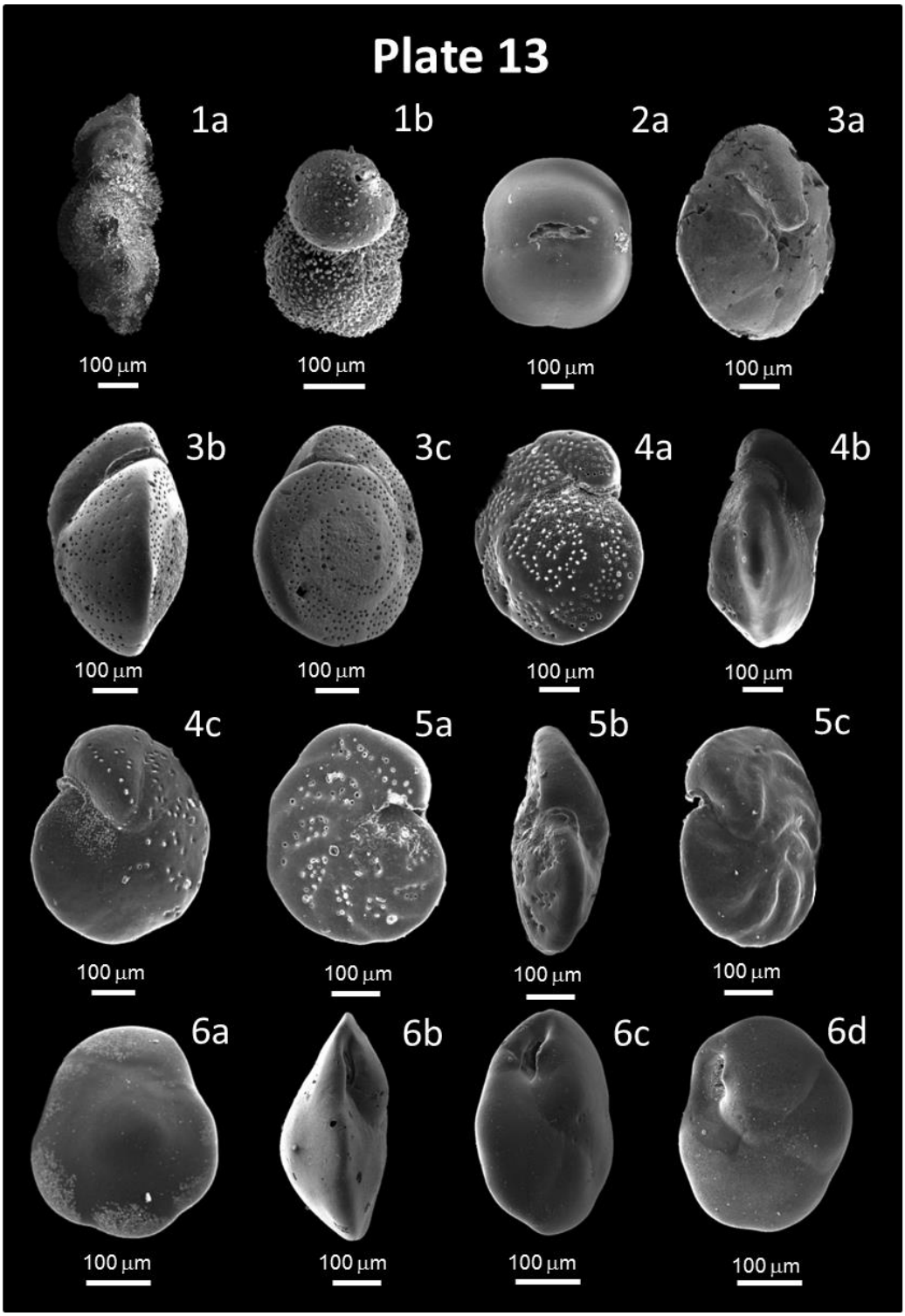

Plate 13. 1a. *Uvigerina proboscidea;* **1b.** *Uvigerina proboscidea* (oblique apertural view) (GeoB 8336, 110 cm); **2.** *Sphaeroidina bulloides* with slightly broken aperture. (GeoB 8336, 414 cm)*;* **3a.** *Cibicidoides crebbsi* (oblique umbilical view)*;* **3b.** *Cibicidoides crebbsi* (apertural view); **3c.** *Cibicidoides crebbsi* (oblique spiral view) (GeoB 8336, 234 cm); **4a**. *Cibicidoides pachyderma* (oblique spiral view)*;* **4b.** *Cibicidoides pachyderma* (apertural view); **4c.** *Cibicidoides pachyderma* (oblique umbilical view) (GeoB 8336, 299 cm); **5a.** *Cibicidoides wuellerstorfi* (spiral view); **5b.** *Cibicidoides wuellerstorfi* (apertural view); **5c.** *Cibicidoides wuellerstorfi* (oblique umbilical view) (GeoB 8336, 299cm); **6a.** *Epistominella exigua* (spiral view); **6b**. *Epistominella exigua* (marginal view); **6c**. *Epistominella exigua* (oblique umbilical view); **6d.** *Epistominella exigua* (umbilical view) (GeoB 8336, 299 cm).

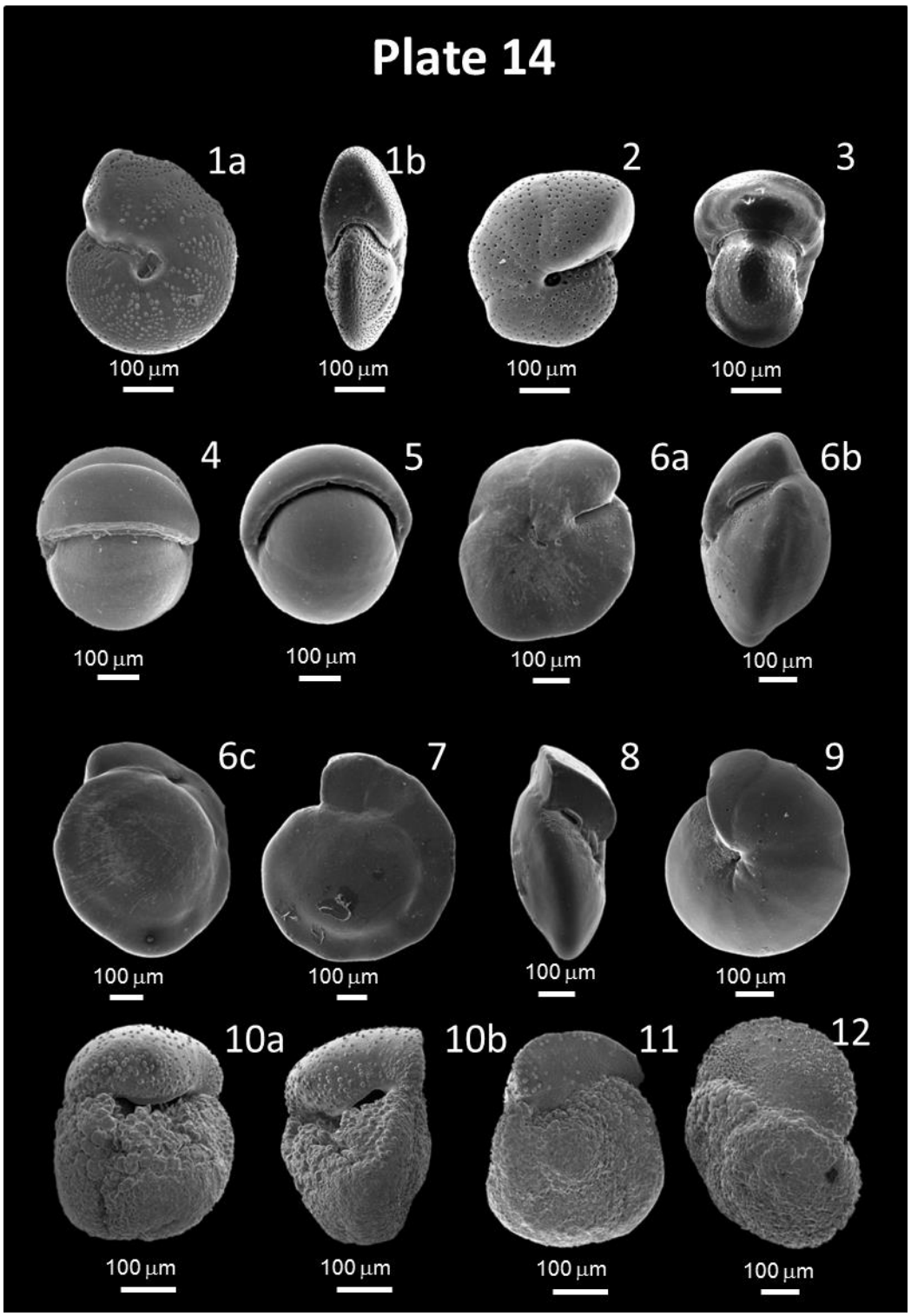

Plate 14. 1a. *Melonis barleeanus* (umbilical view); **1b.** *Melonis barleeanus* (apertural view) (GeoB 8336, 299 cm); **2.** *Melonis pompilioides* (umbilical view) (GeoB 8336, 379 cm); **3.** *Melonis pompilioides* (apertural view) (GeoB 8336, 299 cm); **4-5.** *Pullenia bulloides* (GeoB 8336, 284 cm); **6a.** *Oridorsalis umbonatus* (umbilical view); **6b.** *Oridorsalis umbonatus* (apertural view); **6c**. *Oridorsalis umbonatus* (oblique spiral view) (GeoB 8336, 284 cm); **7.** *Gyroidinoides orbicularis* (spiral view); **8.** *Gyroidinoides orbicularis* (apertural view); **9.** *Gyroidinoides orbicularis* (umbilical view) (GeoB 8336, 299 cm); **10a.** *Globorotalia crassaformis* (umbilical view); **10b.** *Globorotalia crassaformis* (marginal apertural view); **11.** *Globorotalia crassaformis* (spiral view) (GeoB 8336, 259 cm); **12.** *Globorotalia hirsuta* (spiral view) (GeoB 8336, 299 cm).

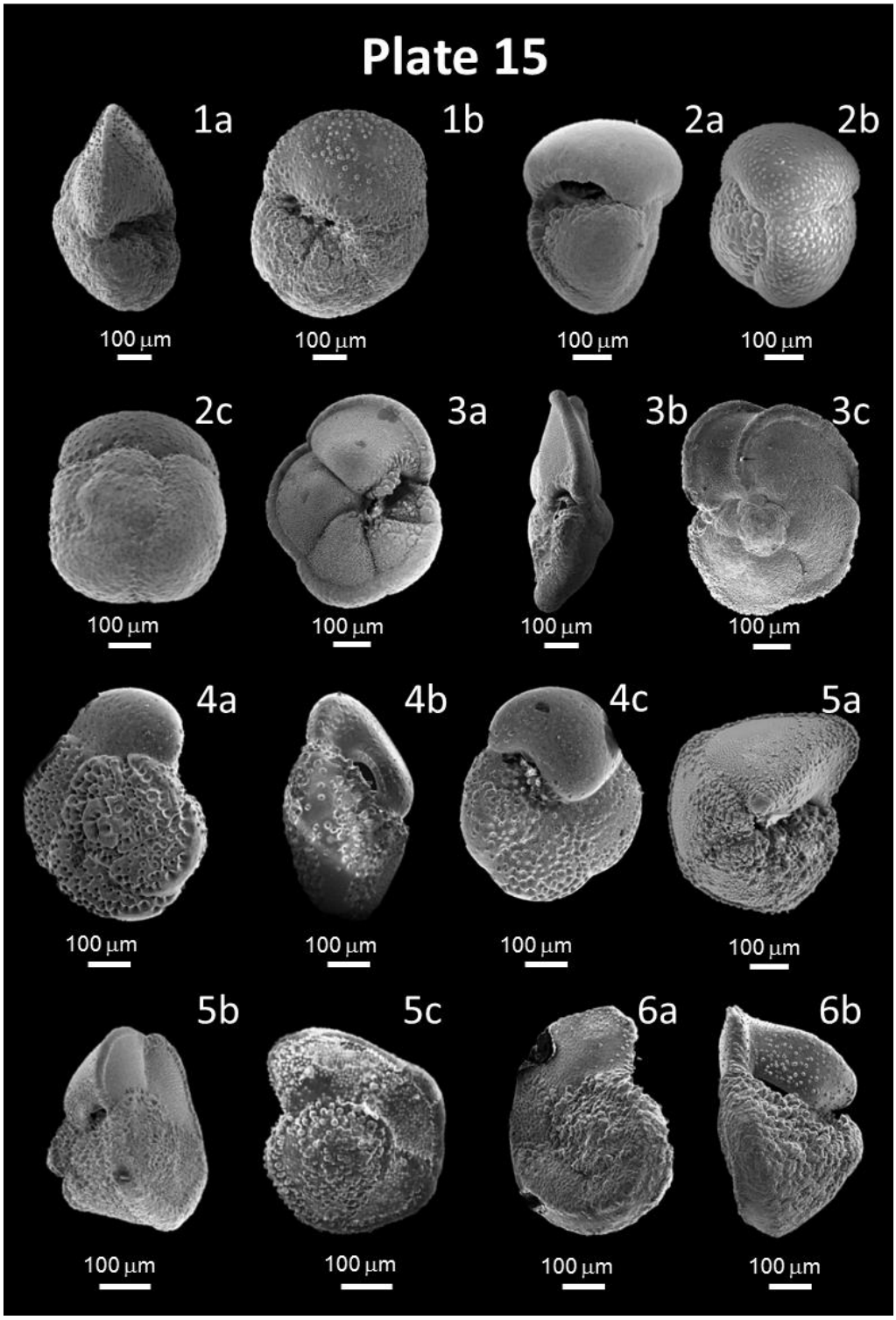

Plate 15. 1a. *Globorotalia hirsuta* (marginal view) (GeoB 8336, 299 cm); **1b.** *Globorotalia hirsuta* (umbilical view) (GeoB 8336, 299 cm); **2a.** *Globorotalia (Globoconella) inflata* (apertural view); **2b.** *Globorotalia (Globoconella) inflata* (oblique side and spiral view); **2c.** *Globorotalia (Globoconella) inflata* (spiral view) (GeoB 8336, 299 cm); **3a**. *Globorotalia menardii (*umbilical view); **3b.** *Globorotalia menardii* (apertural marginal view); **3c.** *Globorotalia menardii* (spiral view) (GeoB 8336, 229 cm); **4a.** *Globorotalia scitula* (spiral view); **4b.** *Globorotalia scitula* (marginal view); **4c.** *Globorotalia scitula* (umbilical view) (GeoB 8336, 299 cm); **5a**. *Globorotalia truncatulinoides* sinistral (umbilical view); **5b.** *Globorotalia truncatulinoides* sinistral (oblique spiral and apertural view), **5c.** *Globorotalia truncatulinoides* sinistral (spiral view) (GeoB 8336, 130 cm); **6a.** *Globorotalia truncatulinoides* dextral (spiral view) **6b.** *Globorotalia truncatulinoides* dextral (apertural view) (GeoB 8336, 130 cm).

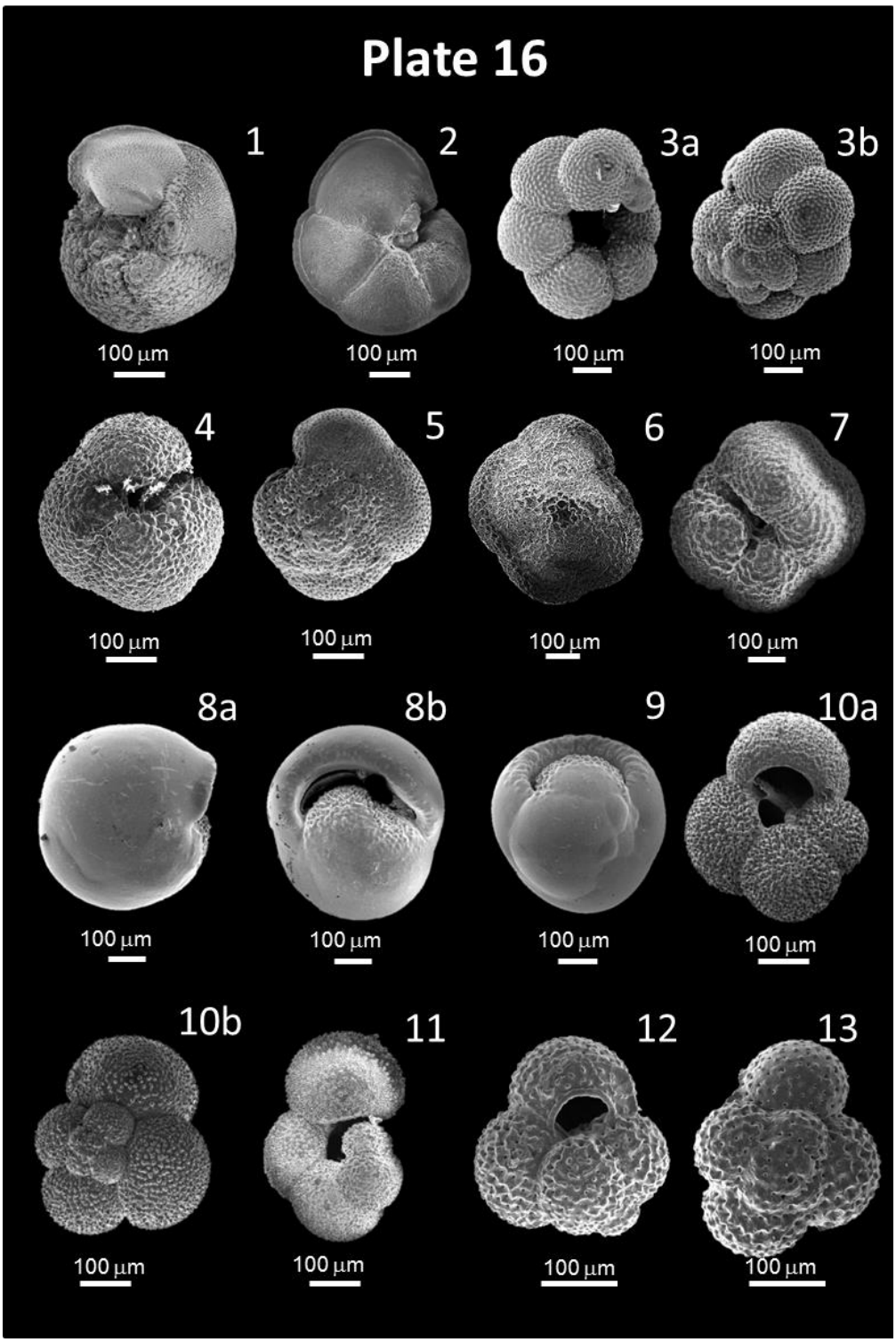

Plate 16. 1. *Globorotalia truncatulinoides* dextral (umbilical view) (GeoB 8336, 130 cm); **2.** *Globorotalia tumida* (GeoB 8336, 414 cm); **3a.** *Neogloboquadrina dutertrei* (umbilical view); **3b**. *Neogloboquadrina dutertrei* (spiral view) (GeoB 8336, 299 cm); **4.** *Neogloboquadrina pachyderma* sinistral (umbilical view) (GeoB 8336, 279 cm); **5.** *Neogloboquadrina pachyderma* sinistral (spiral view) (GeoB 8336, 279 cm); **6.** *Neogloboquadrina incompta/Neogloboquadrina pachyderma* dextral (spiral view) (GeoB 8336, 279 cm); **7.** *Neogloboquadrina incompta/Neogloboquadrina pachyderma* dextral (umbilical view) (GeoB 8336, 279 cm); **8-9.** different views of *Pulleniatina obliquiloculata* (GeoB 8336, 279 cm; 284 cm); **10a**. *Globigerina bulloides* (umbilical apertural view); **10b.** *Globigerina bulloides* (spiral view) (GeoB 8336, 279 cm); **11.** *Globigerinella siphonifera* (GeoB 8336, 229 cm); **12.** *Globoturborotalita rubescens* (umbilical apertural view) (GeoB 20601, 177 cm); **13.** *Globoturborotalita rubescens* (spiral view) (GeoB 20601, 177 cm).

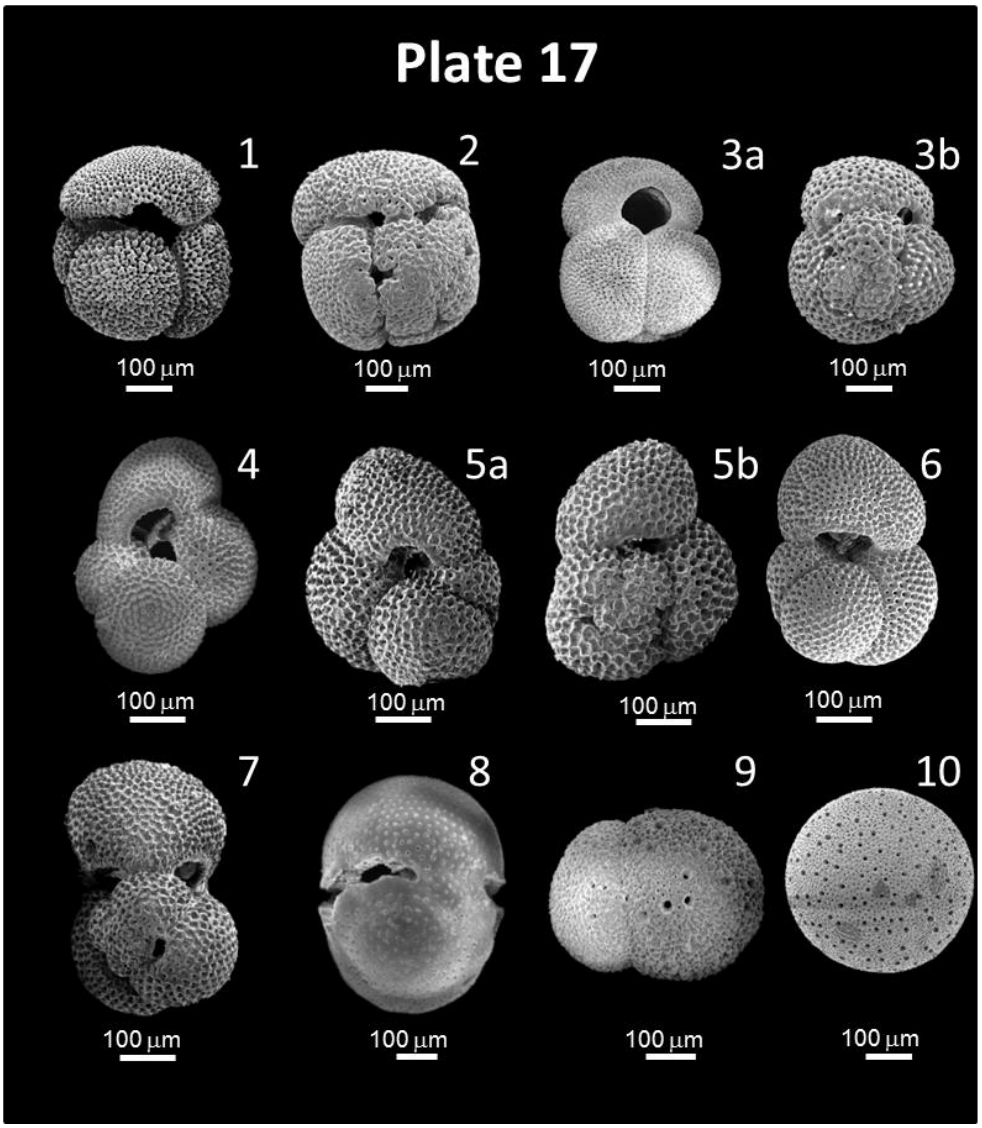

Plate 17. 1. *Globigerinoides conglobatus* (umbilical primary apertural view) (GeoB 8336, 168 cm); **2.** *Globigerinoides conglobatus* (spiral view with secondary apertures visible) (GeoB 8336, 149 cm); **3a**. *Globigerinoides ruber* (umbilical view); **3b.** *Globigerinoides ruber* (spiral view with secondary apertures visible) (GeoB 8336, 299 cm); **4-5a.** *Trilobatus sacculifer* (umbilical primary apertural view) (GeoB 8336, 233; 149 cm); **5b.** *Trilobatus sacculifer* (spiral view with secondary apertures visible) (GeoB 8336, 149 cm); **6.** *Trilobatus trilobus* (umbilical primary apertural view) (GeoB 8336, 81 cm); **7.** *Trilobatus trilobus* (spiral view with secondary apertures visible) (GeoB 8336, 69 cm); **8.** *Sphaeroidinella dehiscens* (GeoB 8336, 168 cm); **9.** *Orbulina bilobata* (GeoB 8336, 168 cm); **10.** *Orbulina universa* (GeoB 8336, 299 cm).

7.5. Conclusions

The planktic and benthic foraminifera provide records between MIS 8 and MIS 1 in the upper 3 m section of the upper slope core GeoB 20601-4 and between MIS 6 and MIS 1 in the lower slope cores GeoB 8342-6 and 8336-6. Glacial periods indicated by the oxygen isotopes correspond to increased non-carbonate mineral abundances when lower sea level enhances delivery of shelf sediment to the slope, supported by less sediment reflectance, indicating more terrigenous input. Sedimentation rates and benthic foraminiferal accumulation rates (BFARs) are higher during interglacial periods suggesting a reduced export of sediment to beyond the slope.

Although *Gr. (Gc.) inflata* is the most abundant planktic foraminiferal species in the cores, *G. bulloides*, *Ng. incompta* + *Ng. pachyderma* and *O. universa* reveal the major factors important in determining the distribution and abundance of planktic taxa along the margin. Upwelling intensity is shown to be a major influence in regulating planktic abundances along the margin. The increased relative abundances of *Ng. incompta* + *Ng. pachyderma* indicate greater influence of subpolar and polar waters in the Southern Ocean during glacial periods.

The transitional species *Gr. (Gc.) inflata* increase in overall abundance in the lower slope cores and *G. bulloides* and *Ng. incompta* + *Ng. pachyderma* decrease towards the upper core, indicating that these taxa respond to coastal upwelling processes along the margin. The subtropical species *O. universa*, *Gr. truncatulinoides* and *Gs. ruber* also increase in lower slope cores owing to warmer surface waters offshore.

Subtropical species *O. universa* and *Gr. truncatulinoides* indicate the influence of inflow of warmer South Indian Ocean waters into the South Atlantic through Agulhas leakage. These two species, along with the subtropical-tropical species *Gs. ruber, T. sacculifer* and *Gr. menardii* are higher in abundances primarily during interglacial periods. *Gs. ruber* shows the highest increases during glacial terminations II and I, suggesting increased inflow of warm subtropical waters into the study area in the transition to interglacial periods.

The benthic foraminifera are composed of taxa known from slope depths with few occurrences of shelf species suggesting bottom water currents are not strong enough to transport sand-sized material over long distances from the shelf to the slope. There are, however, certain taxa displaying depth variations. Buliminids and, in particular, *B. aculeata* are present in relatively high abundances at the upper slope core site whereas *B. aculeata* is absent in the lower slope cores. This distribution is attributed to the adaptation of *B. aculeata* to coastal upwelling conditions on the margin.

The most abundant benthic group in all three cores is *Uvigerina* spp. Results from this study suggest that the *Uvigerina* spp. abundances are influenced by depth, organic matter delivery to the seafloor, oxygen content and deep and intermediate water mass circulation. Benthic fauna from the upper slope core is composed of mostly ribbed *U. peregrina* while lower slope cores are dominated by *U. hispidocostata.* Glacial periods show *U. hispidocostata* increasing in relative abundances at the deeper core sites and *U. peregrina* decreasing in

relative abundances at the upper slope site, indicative of high-nutrient, low-oxygen bottom water conditions under the influence of southern component water and a strengthened intermediate water component, respectively.

The dominance of *Uvigerina* spp., *E. exigua* and *C. wuellerstorfi* indicates that organic matter delivery to the seafloor and seasonality of phytodetritus are major regulators in the faunal composition. The abundance of *Uvigerina* spp. and *C. wuellerstorfi* in the faunal composition indicates that the bottom water conditions are high in oxygen and nutrients.The increase in abundance of *C. wuellerstorfi* during glacial periods at the deeper core site indicates a higher inflow of more oxygenated water associated with the NADW.

References

Abdi, H., Williams, L.J., 2010. Principal component analysis. Wiley interdisciplinary reviews: computational statistics 2, 433-459.

Alegret, L., Molina, E., Thomas, E., 2003. Benthic Foraminiferal Faunal Turnover Across the Cretaceous/Tertiary Boundary at Agost (Southeastern Spain): Paleoenvironmental Inferences. Marine Micropaleontology 48, 251-279.

Bailey, J.W., 1851. Microscopical examination of soundings made by the U.S. Coast Survey off Atlantic coast of the U.S. Smithsonian Contributions to Knowledge 2, 1-15.

Bailey, L.W., 1861. Notes on new species of microscopical organisms, chiefly from the Para River, South America. Boston Journal of Natural History 7(3), 329-351.

Bard, E., Rickaby, R.E., 2009. Migration of the subtropical front as a modulator of glacial climate. Nature 460, 380-384.

Barker, S., Diz, P., Vautravers, M.J., Pike, J., Knorr, G., Hall, I.R., Broecker, W.S., 2009. Interhemispheric Atlantic seesaw response during the last deglaciation. Nature 457, 1097.

Barker, S., Knorr, G., Edwards, R.L., Parrenin, F., Putnam, A.E., Skinner, L.C., Wolff, E., Ziegler, M., 2011. 800 000 years of abrupt climate variability. Science, 334, 347-351.

Bè, A.W.H., Tolderlund, D.S., 1971. Distribution and ecology of planktonic foraminifera. In: Funnell, B.M., Riedel, W.R. (Eds), The micropaleontology of oceans. Cambridge University Press, London, pp. 105-149.

Berger, A.L., 1978. Long-term variations of daily insolation and Quaternary climatic changes. Journal of the Atmospheric Sciences 35, 2362-2367.

Bergh, E.W., Compton, J.S., Frenzel, P., 2018. Late Neogene foraminifera from the northern Namibian continental shelf and the transition to the Benguela Upwelling System. Journal of African Earth Sciences 141, 33-48.

Bertini, A., Londeix, L., Maniscalco, R., Di Stefano, A., Suc, J.P., Clauzon, G., Gautier, F., Grasso, M., 1998. Paleobiological evidence of depositional conditions in the Salt Member, Gessoso-Solfifera Formation (Messinian, Upper Miocene) of Sicily. Micropaleontology, pp. 413-433.

Bickert, T., Mackensen, A., 2003. Last Glacial to Holocene changes in South Atlantic deep water circulation. In: The South Atlantic in the Late Quaternary. Springer, Berlin, Heidelberg, 671-693.

BouDagher-Fadel, M.K., 2015. Biostratigraphic and geological significance of planktonic foraminifera. UCL Press, London, 306 pp.

Bozzano, G., Kuhlmann, H., Alonso, B., 2002. Storminess control over African dust input to the Moroccan Atlantic margin (NW Africa) at the time of maxima boreal summer insolation: a record of the last 220 kyr. Palaeogeography, Palaeoclimatology, Palaeoecology 183, 155-168.

Brady, H.B., 1877. Supplementary note on the foraminifera of the chalk (?) of the New Britain Group. Geological Magazine 4, 534-536.

Brady, H.B., 1879. Notes on some of the reticularian Rhizopoda of the "Challenger" Expedition. Part I. On new or little known arenaceous types. Quaterly Journal of Microscopical Sciences 19, 20-67.

Brady, H.B., 1881. Notes on some of the reticularian Rhizopoda of the Challenger Expedition, Part III. Quarterly Journal of Microscopical Science 21, 31-71.

Brady, H.B., 1882. Report on the foraminifera. P. 716 in: Tizard, A; Murray, J., Exploration of the Faroe Channel during the summer of 1880, in Her Majesty's hired ship 'Knight Errant'. Proceedingsof the Royal Society of Edinburgh 11.

Brady, H.B., 1884. Report of the foraminifera dredged by H.M.S. Challenger during the years 1873-1876. In Brady, H.B. (Ed.) Report on the Scientific Results of the Voyage of the H.M.S. Challenger during the years 1873-1876. Zoology 9, 814 pp.

Broecker, W.S., Denton, G.H., 1990. What drives glacial cycles? Scientific American 262, 43-50.

Broecker, W.S., Donk, J., 1970. Insolation changes, ice volumes, and the O^{18} record in deep-sea cores. Reviews of Geophysics 8, 169-198.

Carboni, M.G., Di Bella, L., 1996. The Pleistocene section of Podere Palombaro (Umbria). Geologica Romana 32, 97-108.

Carter, R.M., Gammon, P.R., Millwood, L., 2004. Glacial–interglacial (MIS 1–10) migrations of the subtropical front across ODP Site 1119, Canterbury Bight, Southwest Pacific Ocean. Marine Geology 205, 29-58.

Chapori, N.G., Chiessi, C.M., Bickert, T., Laprida, C., 2015. Sea-surface temperature reconstruction of the Quaternary western South Atlantic: New planktonic foraminiferal correlation function. Palaeogeography, Palaeoclimatology, Palaeoecology 425, 67-75.

Cheng, H., Edwards, R.L., Broecker, W.S., Denton, G.H., Kong, X., Wang, Y., Zhang, R., Wang, X. 2009., Ice age terminations. Science 326(5950), 248-252.

Cifelli, R., 1961. *Globigerina incompta*, a new species of pelagic foraminifera from the North Atlantic. Contributions from the Cushman Foundation for Foraminiferal Research 12, 83– 86.

Compton, J.S., Bergh, E.W., 2016. Phosphorite deposits on the Namibian shelf. Marine Geology 380, 290-314.

Compton, J.S., Wigley, R., McMillan, I.K., 2004. Late Cenozoic phosphogenesis on the western shelf of South Africa in the vicinity of the Cape Canyon. Marine Geology 206, 19-40.

Compton, J.S., Wiltshire, J.G., 2009. Terrigenous sediment export from the western margin of South Africa on glacial

to interglacial cycles. Marine Geology 266, 212-222.

Corliss, B.H., Chen, C., 1988. Morphotype patterns of Norwegian Sea deep-sea benthic foraminifera and ecological implications. Geology 16, 716-719.

Cronin, T.M., DeNinno, L.H., Polyak, L., Caverly, E.K., Poore, R.Z., Brenner, A., Rodriguez-Lazaro, J., Marzen, R.E., 2014. Quaternary ostracode and foraminiferal biostratigraphy and paleoceanography in the western Arctic Ocean. Marine Micropaleontology 111, 118-133.

Crundwell, M., Scott, G., Naish, T., Carter, L., 2008. Glacial-interglacial ocean climate variability from planktonic foraminifera during the Mid-Pleistocene transition in the temperate Southwest Pacific, ODP Site 1123. Palaeogeography, Palaeoclimatology, Palaeoecology 260, 202-229.

Curry, W.B., Ostermann, D.R., Guptha, M.V.S., Ittekkot, V., 1992. Foraminiferal production and monsoonal upwelling in the Arabian Sea: evidence from sediment traps. Geological Society, London, Special Publications 64, 93-106.

Cushman, J.A., 1911. A monograph of the Foraminifera of the North Pacific Ocean. Part II. Textulariidae. Bulletin of the United States National Museum 71(2), 1-108.

Cushman, J.A., 1922. Foraminifera of the Atlantic Ocean, Part 3. Textulariidae. United States National Museum Bulletin 104, 1–143.

Cushman, J.A., 1923. The foraminifera of the Atlantic Ocean: part 4 – Lagenidae. Bulletin of the United States National Museum 104, 1-228.

Cushman, J.A., Todd, M.R., 1945. Miocene foraminifera from Buff Bay, Jamaica. Cushman Laboratory of Foraminiferal Research, Special Publication 15, 1-73.

d'Orbigny, A.D., 1826. Tableau méthodique de la classe des Céphalopodes. Annales des Sciences Naturelles 7, 245-314.

d'Orbigny, A.D., 1839a. Foraminifères. In: de la Sagra, R. (ed.). Histoire physique, politique et naturelle de I'ile de Cuba. A. Bertrand, Paris, 224 pp.

d'Orbigny, A. D., 1839b. Les foraminifères des îles Canaries. In: Barker-Webb, P., Berthelot, S. (eds.). Histoire Naturelle des Iles Canaries 2, 119-146.

d' Orbigny, A.D., 1846. Die fossilen Foraminiferen des tertiären Beckens von Wien. Foraminifères fossiles du bassin tertiaire de Vienne. 312 pp.

De Almeida, F.K., De Mello, R.M., Costa, K.B., Toledo, F.A., 2015. The response of deep-water benthic foraminiferal assemblages to changes in paleoproductivity during the Pleistocene (last 769.2 kyr), western South Atlantic Ocean. Palaeogeography, Palaeoclimatology, Palaeoecology 440, 201-212.

Denton, G.H., Anderson, R.F., Toggweiler, J.R., Edwards, R.L., Schaefer, J.M., Putnam., A.E., 2010. The Last Glacial Termination. Science 328, 1652-1656.

Diester-Haass, L., Meyers, P.A., Bickert, T., 2004. Carbonate crash and biogenic bloom in the late Miocene: evidence from ODP sites 1085, 1086 and 1087 in the Cape Basin, southeast Atlantic Ocean. Paleoceanography 19, 1-19.

Diester-Haass, L., Meyers, P.A., Rothe, P., 1992. The Benguela Current and associated upwelling on the southwest African Margin: a synthesis of the Neogene-Quaternary sedimentary record at DSDP

sites 362 and 532. Geological Society, London, Special Publications 64, 331-342.

Diester-Haass, L., Meyers, P.A., Vidal, L. 2002. The late Miocene onset of high productivity in the Benguela Current upwelling system as part of a global pattern. Marine Geology 180, 87-103.

Dray, S. 2008., On the number of principal components: A test of dimensionality based on measurements of similarity between matrices. Computational Statistics and Data Analysis 52, 2228-2237.

Drinia, H., Antonarakou, A., Tsaparas, N., Dermitzakis, M.D., 2007. Foraminiferal stratigraphy and palaeoecological implications in turbidite-like deposits from the Early Tortonian (Late Miocene) of Greece. Journal of Micropalaeontology 26, 145-158.

Ehrenberg, C.G., 1861. Elemente des tiefen Meeresgrundes im Mexikanischen Golfstrome bei Florida: tiber die Tiefgrund-Verhaltnisse des Oceans am Eingange der Davisstrasse und bei Island. Monatsbericht der Königlichen Preussischen Akademie der Wissenschaften zu Berlin, 275 - 315.

Fichtel, L., Moll, J.P.C., 1798. Testacea microscopica aliagua minuta ex generibus Argonauta et Nautilus ad naturam delineate et descripta. Microscopische und andere kleine Schalthiere aus den Geschlechtern Argonaute und Schiffer, nach der Natur Gezeichnet und beschrieben. Camesina, Vienna, 124 pp.

Flores, J.A., Gersonde, R., Sierro, F.J., 1999. Pleistocene fluctuations in the Agulhas Current Retroflection based on the calcareous plankton record. Marine Micropaleontology 37, 1-22.

Gallagher, S.J., Sagawa, T., Henderson, A., Saavedra-Pellitero, M., de Vleeschouwer, D., Black, H., Itaki, T., Toucanne, S., Bassetti, M.A., Clemens, S., Anderson, W., 2018. East Asian monsoon history and paleoceanography of the Japan Sea over the last 460,000 years. Paleoceanography and Paleoclimatology, doi: 10.1029/2018PA003331

Galloway, J.J., Wissler, S.G., 1927. Pleistocene foraminifera from the Lomita Quarry, Palos Verdes Hills, California. Journal of Paleontology 1(1), 35-87.

Giraudeau, J., 1993. Planktonic foraminiferal assemblages in surface sediments from the southwest African continental margin. Marine Geology 110, 47-62.

Glacon, G., Grazzini, C.V., Iaccarino, S., Rehault, J.P., Randrianasolo, A., Sierro, J.F., Weaver, P., Channell, J., Torii, M., Hawthorne, T., 1990. 27. Planktonic foraminifera; events and stable isotope records in the upper Miocene, site 6541. In: Kastens, K.A., Mascle, J., et al., (Eds.) Proceedings of the Ocean Drilling Program, Scientific Results 107, 415-427.

Goës, A., 1896. Reports on the dredging operations off the West Coast of Central America to the Galapagos, to the West Coast of Mexico, and in the Gulf of California, in charge of Alexander Agassiz, carried on by U.S. Fish Commission Steamer “Albatros”, during 1891, Lieut. Commander Z. L. Tanner, U.S.N., commanding. Bulletin of the Museum of Comparative Zoology at Harvard College 29 (1), 1-103.

Goldstein, S.L., Hemming, S.R., Kish, S., Rutberg, R., 1999. Strontium isotopes in South Atlantic detritus: A surface current

proxy and tracer of Agulhas leakage. In: Ninth Annual VM Goldschmidt Conference.

Gooday, A.J., 1988. A response by benthic foraminifera to the deposition of phytodetritus in the deep sea. Nature 332, 70-73.

Goubert, E., Néraudeau, D., Rouchy, J.M., Lacour, D., 2001. Foraminiferal record of environmental changes: Messinian of the Los Yesos area (Sorbas Basin, SE Spain). Palaeogeography, Palaeoclimatology, Palaeoecology 175, 61-78.

Groeneveld, J., Chiessi, C.M., 2011. Mg/Ca of Globorotalia inflata as a recorder of permanent thermocline temperatures in the South Atlantic. Paleoceanography and Paleoclimatology, 26(2), PA2203, doi:10.1029/2010PA001940

Hammer, Ø., Harper, D.A.T., Ryan, P.D., 2001. PAST: paleontological statistics software package for education and data analysis. Palaeontologia Electronica, 4. 9 pp. (http://palaeo-electronica.org/2001_1/past/issue1_01.htm).

Hedberg, H.D., 1937. Foraminifera of the middle Tertiary Carapita Formation of northeastern Venezuela. Journal of Paleontology, 661-697.

Herbert, C., Compton, J.S., 2007. Geochronology of Holocene sediments on the western margin of South Africa. South African Journal of Geology 110, 327-338.

Hill, T.M., Kennett, J.P., Spero, H.J., 2003. Foraminifera as indicators of methane-rich environments: a study of modern methane seeps in Santa Barbara Channel, California. Marine Micropaleontology 49, 123-138.

Hodell, D.A., 1993. Late Pleistocene paleoceanography of the South Atlantic sector of the Southern Ocean: Ocean Drilling Program Hole 704A. Paleoceanography 8, 47-67.

Hofker, J., 1956. Tertiary foraminifera of coastal Ecuador: Part II, Additional notes on the Eocene species. Journal of Paleontology, pp. 891-958.

Holbourn, A., Henderson, A.S., MacLeod, N., 2013. Atlas of Benthic Foraminifera. Wiley-Blackwell, Oxford, 654 pp.

Howard, W.R., Prell,W.L., 1992. Late Quaternary surface circulation of the southern Indian Ocean and its relationship to orbital variations. Paleoceanography 7, 79-117.

Howe, J.N., Piotrowski, A.M., Oppo, D.W., Huang, K.F., Mulitza, S., Chiessi, C.M., Blusztajn, J., 2016. Antarctic intermediate water circulation in the South Atlantic over the past 25,000 years. Paleoceanography 31, 1302-1314.

Hu, R., Noble, T.L., Piotrowski, A.M., McCave, I.N., Bostock, H.C., Neil, H.L., 2016. Neodymium isotopic evidence for linked changes in Southeast Atlantic and Southwest Pacific circulation over the last 200 kyr. Earth and Planetary Science Letters 455, 106-114.

Ibaraki, M., 1997. Closing of the Central American Seaway and Neogene coastal upwelling along the Pacific coast of South America. Tectonophysics 281, 99-104.

Imbrie, J., Boyle, E.A., Clemens, S.C., Duffy, A., Howard, W.R., Kukla, G., Kutzbach, J., Martinson, D.G., McIntyre, A., Mix, A.C., Molfino, B., 1992. On the structure and origin of major glaciation cycles 1. Linear

responses to Milankovich forcing. Paleoceanography 7, 701-738.

Jones, R.W., 1994. The Challenger Foraminifera. Oxford University Press, Oxford, 149 pp.

Kaiho, K., 1994. Benthic foraminiferal dissolved-oxygen index and dissolved-oxygen levels in the modern ocean. Geology 22, 719-722.

Kaiho, K., 1999. Effect of organic carbon flux and dissolved oxygen on the benthic foraminiferal oxygen index (BFOI). Marine Micropalaeontology 37, 67–76.

Kaminski, M.A., Boersma, E., Tyszka, J., Holbourn, A.E.L., 1995. Response of deep-water agglutinated foraminifera to dysoxic conditions in the California Borderland basins. Grzybowski Foundation Special Publication 3, 131-140.

Karrer, F., 1868. Die Miocene Foraminiferen fauna von Kostej im Banat. Sitzungberichte der Kaiserlichen Akademie der Wissenschaften in Wein. Mathematisch-Naturwissenschaftliche Classe 74(7), 272-284.

Kasper, S., Van Der Meer, M.T J., Mets, A., Zahn, R., Sinninghe Damsté, J.S., Schouten, S. 2014. Salinity changes in the Agulhas leakage area recorded by stable hydrogen isotopes of C 37 alkenones during Termination I and II. Climate of the Past 10, 251-260.

Kender, S., Kaminski, M.A., Jones, R.W., 2008. Early to middle Miocene foraminifera from the deep-sea Congo Fan, offshore Angola. Micropalaeontology 54, 477-568.

Kucera, M., 2007. Planktonic foraminifera as tracers of past oceanic conditions. In: Hillaire-Marccel, C and de Vernal, A (Eds.). Proxies in Late Cenozoic Paleoceanography. Elsevier, Amsterdam, 213-262.

Leiter, C., Altenbach, A.V., 2010. Benthic foraminifera from the diatomaceous mud belt off Namibia: characteristic species for severe anoxia. Palaeontologica Africana 13(2), 11A, 19p.

Li, Q., McGowran, B., 1994. Miocene upwelling events: neritic foraminiferal evidence from southern Australia. Australian Journal of Earth Sciences 41, 593-603.

Linnaeus, C., 1758. Systema naturae per regna Tria naturae, secundum classes, ordines genera, species, cum characteribus, differentiis, synonymis, locis. Tomus I. Editio decima, reformata. Systema Naturae, Stockholm 10, 824 pp.

Lisiecki, L.E., Raymo, M.E., 2005. A Pliocene-Pleistocene stack of 57 globally distributed benthic $\delta^{18}O$ records. Paleoceanography 20, PA1003, doi:10.1029/2004PA001071.

Little, M.G., Schneider, R.R., Kroon, D., Price, B., Bickert, T., Wefer, G., 1997. Rapid palaeoceanographic changes in the Benguela Upwelling System for the last 160,000 years as indicated by abundances of planktonic foraminifera. Palaeogeography, Palaeoclimatology, Palaeoecology 130(1), 135-161.

Loeblich, A.R., Tappan, H., 1988. Foraminiferal Genera and their Classification. Van Nostrand Reinhold, New York, 970 pp.

Lombard, F., Labeyrie, L., Michel, E., Spero, H.J., Lea, D. W., 2009. Modelling the temperature dependent growth rates of planktic foraminifera. Marine Micropaleontology 70, 1-7.

Lowry, F. M. D., 1987. Foraminiferal thanatocoenoses from the continental shelf of southern Africa. Unpublished Ph.D. thesis, University College, London, 443 pp.

Lutjeharms, J.R.E., Stockton, P.L., 1987, Kinematics of the upwelling front off southern Africa. South African Journal of Marine Science 5, 35–49.

Lutze, G.F., Coulbourn, W. T., 1984. Recent benthic foraminifera from the continental margin of northwest Africa: community structure and distribution. Marine Micropaleontology 8, 361-401.

Mackensen, A., Bickert, T., 1999. Stable carbon isotopes in benthic foraminifera: Proxies for deep and bottom water circulation and new production. In: Fischer, G., Wefer, G. (Eds.), Use of Proxies in Paleoceanography: Examples from the South Atlantic. Springer-Verlag, Berlin, pp. 229-254.

Majewski, W., 2010. Benthic foraminifera from West Antarctic fiord environments: An overview. Polish Polar Research 31(1), 61-82.

Marchant, M., Hebbeln, D., Wefer, G., 1999. High resolution planktic foraminiferal record of the last 13,300 years from the upwelling area off Chile. Marine Geology 161, 115-128.

Marino, G., Zahn, R., Ziegler, M., Purcell, C., Knorr, G., Hall, I.R., Ziveri, P., Elderfield, H. 2013. Agulhas salt - leakage oscillations during abrupt climate changes of the Late Pleistocene. Paleoceanography 28, 599-606.

Martin, R.A., 1981. Benthic foraminifera from the Orange-Lüderitz shelf southern African continental margin. Bulletin Joint Geological Survey / University of Cape Town Marine Geoscience Unit 11, 75 pp.

Martinez, P., Bertrand, P., Shimmield, G.B., Cochrane, K., Jorissen, F.J., Foster, J., Dignan, M., 1999. Upwelling intensity and ocean productivity changes off Cape Blanc (northwest Africa) during the last 70,000 years: geochemical and micropalaeontological evidence. Marine Geology 158, 57-74.

McMillan, I.K., 1987. Late Quaternary foraminifera from the southern part of offshore southwest Africa/Namibia. Unpublished PhD thesis. University College of Wales, Aberystwyth. 565 pp.

Meadows, M.E., Rogers, J., Lee-Thorp, J.A., Bateman, M.D., Dingle, R.V., 2002. Holocene geochronology of a continental-shelf mudbelt off southwestern Africa. Holocene 12, 59–67.

Miller, K.G., Lohmann, G.P., 1982. Environmental distribution of Recent benthic foraminifera on the northeast United States continental slope. Geological Society of America Bulletin 93, 200-206.

Miller, K.G., Wright, J.D., Fairbanks, R.G., 1991. Unlocking the ice house: Oligocene-Miocene oxygen isotopes, eustasy, and margin erosion. Journal of Geophysical Research: Solid Earth 96, 6829-6848.

Mohtadi, M., Hebbeln, D., Marchant, M., 2005. Upwelling and productivity along the Peru–Chile Current derived from faunal and isotopic compositions of planktic foraminifera in surface sediments. Marine Geology 216, 107-126.

Montagu, G., 1803. Testacea Britannica, or natural history of British shells, marine, land and fresh-water, including the most minute. J.S. Hollis, Romsey, England, 1–606.

Monteiro, P.M.S., Nelson, G., van der Plas, A., Mabille, E., Bailey, G.W., Klingelhoeffer, E., 2005. Internal tide–shelf topography interactions as a forcing factor governing the large-scale distribution and burial fluxes of particulate organic matter (POM) in the Benguela upwelling system. Continental Shelf Research 25, 1864–1876.

Morigi, C., 2009. Benthic environmental changes in the Eastern Mediterranean Sea during sapropel S5 deposition. Palaeogeography, Palaeoclimatology, Palaeoecology 273, 258-271.

Murgese, D.S., de Deckker, P., 2005. The distribution of deep-sea benthic foraminifera in core tops from the eastern Indian Ocean. Marine Micropaleontology 56, 25-49.

Murray, J.W., 1976. A method of determining proximity of marginal seas to an ocean. Marine Geology 22, 103-119.

Murray, J.W., 1991. Ecology and distribution of benthic foraminifera. In: Lee, J.J., Anderson, O.R. (Eds.), Biology of Foraminifera. Academic Press, New York, pp. 221–254.

Murray, J.W., 2006. Ecology and applications of benthic foraminifera. Cambridge University Press, 426 pp.

Paillard, D., Labeyrie, L., Yiou, P., 1996. Macintosh program performs time-series analysis. Eos, Transactions American Geophysical Union 77, 379-379.

Parker, W.K., Jones, T.R., 1865. On some foraminifera from the North Atlantic and Arctic Oceans, including Davis Straits and Baffin's Bay. Philosophical transactions of the Royal Society of London 155, 325-441.

Parker W.K., Jones T.R., Brady H. B., 1865. On the nomenclature of the Foraminifera. Part X. (continued). The species enumerated by D'Orbigny in the 'Annales des Sciences Naturelles,' 1826, vol. vii. - III. The species illustrated by models. Annals and Magazine of Natural History (3) 16 (91), 15-41.

Peeters, F.J.C., Acheson, R., Brummer, G.J.A., de Ruijter, W.P.M., Schneider, R.R., Ganssen, G.M., Ufkes, E., Kroon, D., 2004. Vigorous exchange between the Indian and Atlantic oceans at the end of the past five glacial periods. Nature 430, 661–665.

Peeters, F.J.C., Brummer, G.J.A., Ganssen, G., 2002. The effect of upwelling on the distribution and stable isotope composition of *Globigerina bulloides* and *Globigerinoides ruber* (planktic foraminifera) in modern surface waters of the NW Arabian Sea. Global and Planetary Change 34, 269-291.

Pérez-Asensio, J.N., Aguirre, J., Schmiedl, G., Civis, J., 2012. Messinian paleoenvironmental evolution in the lower Guadalquivir Basin (SW Spain) based on benthic foraminifera. Palaeogeography, Palaeoclimatology, Palaeoecology 326, 135-151.

Petro, S.M., Pivel, M.A. G., Coimbra, J.C., Mizusaki, A.M.P., 2016. Paleoceanographic changes through the last 130 ka in the Western South Atlantic based on planktonic foraminifera. Revista Brasileira de Paleontologia 19, 3-14.

Prell, W.L., Curry, W.B., 1981. Faunal and isotopic indices of monsoonal upwelling-western arabian sea. Oceanologica Acta 4, 91-98.

Rau, A.J., 2002. A late Quaternary history of Agulhas-Benguela interactions from two

sediment cores on the western continental slope of South Africa. PhD thesis. University of Cape Town, 315 pp.

Rau, A. J., Rogers, J., Lutjeharms, J. R. E., Giraudeau, J., Lee-Thorp, J. A., Chen, M. T., Waelbroeck, C., 2002. A 450-kyr record of hydrological conditions on the western Agulhas Bank Slope, south of Africa. Marine Geology 180, 183-201.

Ravelo, A. C., Hillaire-Marcel, C., 2007. Chapter Eighteen the use of oxygen and carbon isotopes of foraminifera in Paleoceanography. Developments in Marine Geology p1, 735-764.

Reid, J.L., 1989. On the total geostrophic circulation of the South Atlantic Ocean: Flow patterns, tracers, and transports. Progress in Oceanography 23, 149-244.

Reolid, M., Rodríguez-Tovar, F.J., Nagy, J., Olóriz, F., 2008. Benthic foraminiferal morphogroups of mid to outer shelf environments of the Late Jurassic (Prebetic Zone, southern Spain): characterization of biofacies and environmental significance. Palaeogeography, Palaeoclimatology, Palaeoecology 261, 280-299.

Reuss, A.E., 1850. Neues Foraminiferen aus den Schichten des österreichischen Tertiärbeckens. Denkschriften Akademie der Wissenschaften in Wien, Mathematisch-Naturwissenschaftliche Klasse. Cl. 1, 365- 390.

Reuss, A.E., 1851. Die fossilen Foraminiferen, Bryozoen und Anthozoen von Oberburg in Steiermark. Ein Beitrag zur fauna der oberen Nummulitenschichteh. Sitzungsberichte der Akademie der Wissenschaften 48, 49-92.

Rutberg, R.L., Hemming, S.R., Goldstein, S.L., 2000. Reduced North Atlantic Deep Water flux to the glacial Southern Ocean inferred from neodymium isotope ratios. Nature 405, 935.

Rymer Jones ,F. W., 1872. On some recent forms of Lagenae from deep-sea soundings in the Java seas. Transactions Linnaean Society, London XXX, 45-69.

Rzehak, A., 1886. Die Foraminiferen Fauna der Neogenformation der Umgebung von Mähr-Ostrau. Verhandlungen des naturforschenden Vereines in Brünn 24, 77-126

Sautter, L.R., Thunell, R.C., 1991. Seasonal variability in the $\delta^{18}O$ and $\delta^{13}C$ of planktonic foraminifera from an upwelling environment: sediment trap results from the San Pedro Basin, Southern California Bight. Paleoceanography 6, 307-334.

Schmidt-Sinns, J., 2008. Rezente benthische Foraminiferen im Bereich des Benguelastroms, Südwestafrika– Verbreitungsmuster und ihre steuernden Faktoren. PhD thesis, Universitäts und Landesbibliothek, Bonn, 1-261.

Schmiedl, G., Mackensen, A., 1997. Late Quaternary paleoproductivity and deep water circulation in the eastern South Atlantic Ocean: Evidence from benthic foraminifera. Palaeogeography, Palaeoclimatology, Palaeoecology 130, 43-80.

Schmiedl, G., Mackensen, A., Müller, P.J., 1997. Recent benthic foraminifera from the eastern South Atlantic Ocean: dependence on food supply and water masses. Marine Micropaleontology 32, 249-287.

Schwager, C., 1866. Fossile Foraminiferen von Kar Nikobar, Reise der Oesterreichischen

Fregatte Novara um Erde in den Jahren 1857, 1858, 1859 unten den Befehlen des Commodore B. Von WuellerstorfUrbair. Geologischer Theil, Geologische Beobachtung no. 2, Palaeontologische Mittheilung 2, 187–268.

Scussolini, P., Marino, G., Brummer, G.J.A., Peeters, F.J., 2015. Saline Indian Ocean waters invaded the South Atlantic thermocline during glacial termination II. Geology 43, 139-142.

Shannon, L.V., Nelson, G., 1996. The Benguela: Large Scale Features and Processes and System Variability. In: Wefer, G., Berger,W.H., Siedler, G.,Webb, D.J. (Eds.), The South Atlantic: Present and Past Circulation. Springer-Verlag, Berlin, Heidelberg, pp. 163–210.

Sharma, V., Singh, A.D., 2012. The Genus Uvigerina from the Neogene of Andaman Nicobar: Paleoenvironmental Implications. ONGC Bulletin 47, 88-104.

Shi, N., Schneider, R., Beug, H.J., Dupont, L.M., 2001. Southeast trade wind variations during the last 135 kyr: evidence from pollen spectra in eastern South Atlantic sediments. Earth and Planetary Science Letters 187, 311-321.

Siesser, W.G., 1980. Late Miocene origin of the Benguela Upwelling System off Northern Namibia. Science 208 (4441), 283-285.

Stocker, T.F., Johnsen, S.J., 2003. A minimum thermodynamic model for the bipolar seesaw. Paleoceanography, 18(4), doi: 10.1029/2003PA000920

Stojanova, V., Petrov, G., 2018. Paleoecological significance of benthic foraminiferal fauna from the Ovče Pole basin, Republic of Macedonia. Geologica Macedonica 32(1), 45-57.

Sun, X., Corliss, B.H., Brown, C.W., Showers, W.J., 2006. The effect of primary productivity and seasonality on the distribution of deep-sea benthic foraminifera in the North Atlantic. Deep Sea Research Part I: Oceanographic Research Papers 53(1), 28-47.

Thomas, E., Booth, L., Maslin, M., Shackleton, N.J., 1995. Northeastern Atlantic benthic foraminifera during the last 45,000 years: changes in productivity seen from the bottom up. Paleoceanography 10, 545-562.

Thomas, E., Gooday, A.J., 1996. Cenozoic deep-sea benthic foraminifers: Tracers for changes in oceanic productivity? Geology 24, 355-358.

Thompson, P.R., Bé, A.W., Duplessy, J.C., Shackleton, N.J., 1979. Disappearance of pink-pigmented Globigerinoides ruber at 120,000 yr BP in the Indian and Pacific Oceans. Nature 280(5723), 554.

Ufkes, E.L.S., Kroon, D., 2012. Sensitivity of south-east Atlantic planktonic foraminifera to mid-Pleistocene climate change. Palaeontology 55(1), 183-204.

Van der Zwaan, G.J., Jorissen, F.J., Verhallen, P.J.J.M., Von Daniels, C.H., 1986. Atlantic-European Oligocene to recent Uvigerina: taxonomy, paleoecology and paleobiogeography (Vol. 35). Utrecht University.

Walker, G., Jacob. E., 1798. Descriptions of *Serpula (Lagena) sulcata* and *Nautilus lobatulus*. In: Adams, G (Ed.). Essays on the microscope: containing a practical description of the most improved microscopes. Dillon and Keating, London, 634-642.

Wefer, G., Berger, W.H., Bijma, J., Fischer, G., 1999. Clues to ocean history: a brief

overview of proxies. In: Fischer, G and Wefer, G., (Eds.) Use of Proxies in Palaeoceanography: Examples from the South Atlantic. Springer-Verlag, Berlin, pp 1-68.

Wefer, G., Berger, W.H., Richter, C., Adams, D.D., Anderon, L.D., Andreasen, D.J., Brüchert, V., Cambray, H., Christensen, B.A., Frost, G.M., Giraudeau., Gorgas, T.J., Hermelin, O., Lange, C.B., Laser, B., Lin, H-L., Maslin, M., Meyers, P.A., Motoyama, I., Murray, R.W., Pato, D., Perez, M.E., Pufahl, P.K., Spiess, V., Vidal. L., Wigley, R., Yamazaki, T. 1998. Proceedings of the Ocean Drilling Program volume 175, 385-428.

Williamson, W.C., 1848. On the Recent British species of the genus Lagena. Annals and Magazine of Natural History. 1, 1-20.

Williamson, W.C., 1858. On the Recent Foraminifera of Great Britain. Ray Society, London, 107 pp.

Wolf-Gladrow, D.A., Riebesell, U.L.F., Burkhardt, S., Buma, J. 1999., Direct effects of CO_2 concentration on growth and isotopic composition of marine plankton. Tellus B: Chemical and Physical Meteorology 51, 461-476.

Zabel, M., and cruise participants. 2017. Climate Archives in Coastal Waters of Southern Africa–Cruise No. M123.

Zachos, J., Pagani, M., Sloan, L., Thomas, E., Billups, K., 2001. Trends, rhythms, and aberrations in global climate 65 Ma to present. Science 292 (5517), 686-693.

Chapter 8

Late Quaternary Variations in Deep and Intermediate Water Masses along the Western Slope of South Africa

8. Late Quaternary variations in deep and intermediate water masses along the western slope of South Africa

Abstract

The neodymium isotopic composition (εNd) of planktic foraminifera from three cores on the western margin of South Africa provides a late Quaternary record of variations in North Atlantic Deep Water (NADW), Lower Circumpolar Deep Water (LCDW), Antarctic Bottom Water (AABW) and Antarctic Intermediate Water (AAIW) masses. A comparison of εNd records from a core at 874 m water depth and from two cores at 3522 and 3631 m water depth reveals a stronger influence of Southern Component Water (SCW) masses (LCDW and AABW) along the margin during the MIS 6 and MIS 2 peak glacial periods. The strength of the SCW decreases and NADW increases during glacial terminations (GT) II and I. The benthic $\delta^{13}C_{C.\ wuellerstorfi}$ record from these cores is largely consistent with the εNd interpretation of changes in distinct water masses along the margin. The Nd isotopic compositions and *Cibicidoides wuellerstorfi* relative abundances also show a negative correlation suggesting that *C. wuellerstorfi* can be a useful indicator of deep water masses when combined with εNd and $\delta^{13}C$ records. The variation in AAIW influence along the margin is lower across glacial to interglacial cycles and is stronger during the glacial periods and weakest during mid-interglacial periods. Glacial Termination I corresponds to a weakened AAIW while NADW strengthens at deeper depths along the margin.

8.1. Introduction

The ocean's conveyer belt, the Meridional Overturning Circulation (MOC) plays an important role in regulating Earth's climate (Howe et al., 2017). The MOC is composed of various ocean currents and transports relatively warm South Atlantic surface waters to the North Atlantic (Berger and Wefer, 1996; Rutberg et al., 2000) where it cools before sinking and flowing to the South Atlantic as North Atlantic Deep Water (NADW). The South Atlantic Ocean, as part of the Atlantic Meridional Overturning Component (AMOC) (Lynch-Stieglitz et al., 2007; Delworth et al., 2008) plays a crucial role in thermohaline circulation and the distribution of water masses (Berger and Wefer, 1996; Kuhn and Diekmann, 2002). A proportion of the waters of the AMOC originate in the Indian Ocean and is transported by the Agulhas Current around the South African margin with leakage into the South Atlantic contributing to the heat and salinity of the Atlantic (Gordon et al., 1992; Lutjeharms, 1996; Piotrowski et al., 2012). Transfer of water masses between ocean basins also affects regional carbon storage, nutrient contents, temperature, evaporation and precipitation balances (Piotrowski et al., 2012; Howe et al., 2016).

The modern eastern South Atlantic is strongly stratified as a result of these different water masses from the North Atlantic, western South Atlantic, the Antarctic Circumpolar Current and the South Indian Ocean (Reid, 1989; Sarnthein et al., 1994; Talley, 1996). The South Atlantic provides a good opportunity to determine depth distributions of deep water masses during glacial-interglacial transitions because it reveals

the interactions between the southward-flowing North Atlantic Deep Water (NADW) and the northward-flowing Southern Component Water (SCW) (Reid, 1989). The configuration and depths at which these deep-water masses flow, change in relation to glacial-interglacial climate cycles (Clark et al., 2002; Hu et al., 2016a). Proxies of glacial-interglacial water mass variations in the South Atlantic Ocean are needed to understand late Quaternary palaeoceanographic changes.

Bulk sediment and foraminiferal $\delta^{13}C$ can provide a useful proxy to trace deep water masses in the South Atlantic (Schmiedl and Mackensen, 1997; Bickert and Wefer, 1999; Bickert and Mackensen, 2003). Northern-sourced waters, such as the NADW can be traced based on their higher $\delta^{13}C$ values compared to lower $\delta^{13}C$ values of southern-sourced waters (Bickert and Mackensen, 2003).

The neodymium isotope content in seawater provides an additional useful tracer of water masses (e.g. Palmer and Elderfield, 1985; Piotrowski et al., 2005; Franzese et al., 2006) owing to the short residence time of Nd which gives rise to varying Nd isotopic values among the different water masses (Piotrowski et al., 2012). For example, the Nd isotopic composition ($^{143}Nd/^{144}Nd$), expressed as εNd (epsilon neodymium), of waters sourced from the Pacific Ocean ranges between -4 and 0, whereas waters sourced from the North Atlantic Ocean (e.g. NADW) have εNd values less than -14 (Piepgrass and Wasserburg, 1987; Pahnke et al., 2008). Antarctic Intermediate Water (AAIW) has an εNd value of approximately -8 (Hu et al., 2016a) while deep waters in the South Atlantic Ocean have an εNd value that ranges between -9 and -6 (Rutberg et al., 2000) depending upon the changes in water masses over time (Piepgrass and Wasserburg, 1982, 1987; Goldstein and Hemming, 2003; Pahnke et al., 2008). The Nd composition of seawater is influenced by the age and chemical composition of inputs into ocean basins and by the source area of the water masses (Vance and Burton, 1999; Rutberg et al., 2000; Goldstein and Hemming, 2003; Pahnke et al., 2008; Piotrowski et al., 2012). However, the influence of Nd input from local sources along the flow path of the water masses is still largely not understood (Piotrowski et al., 2012).

εNd has been measured from various marine components, including foraminifera tests (e.g. Vance and Burton, 1999; Burton and Vance 2000; Klevenz et al., 2008; Roberts et al., 2012; Tachikawa et al., 2014; Hu et al., 2016a, 2016b; von Koslowski, 2017), bulk sediment Fe-Mn leachates (Piotrowski et al., 2012) and ferro-manganese nodules (Piotrowski et al., 2005; Franzese et al., 2006). εNd has been measured from Neogene (~8 Ma) benthic foraminifera (Klevenz et al., 2008), but planktic foraminifera also preserve bottom water εNd values (Roberts et al., 2012; Tachikawa et al., 2014) being in agreement with seawater εNd values (Palmer and Elderfield, 1985; Hu et al., 2016a). As the tests of planktic foraminifera sink to the ocean floor, the εNd value of the tests changes (Vance and Burton, 1999; Burton and Vance 2000). When these tests are buried in sediments they acquire a diagenetic Fe-Mn oxyhydroxide coating which may have a higher Nd concentration than the original foraminiferal calcite test. Palmer and Elderfield (1985) and Tachikawa et al. (2014) have, however, found that there is not much variation between the εNd

of the tests and their Fe-Mn oxyhydroxide coatings. The tests of planktic foraminifera lose their outer organic layers after death and the inner layers are exposed to sea water after which Fe-Mn oxides, Fe oxides and hydroxides precipitate on the tests. During taphonomic processes, authigenic minerals and the organic and calcitic layers of the test acquire the Nd isotopic signature of the bottom and pore waters (Tachikawa et al., 2014).

Foraminifera εNd values can provide a high-resolution record on a submillennial scale of water mass changes (Vance and Burton, 1999; Burton and Vance, 2000; Tachikawa et al., 2014), which can be directly matched with biostratigraphic, palaeomagnetic, isotopic and palaeoenvironmental records (Burton and Vance, 2000). εNd is largely unaffected by biological inputs (Arsouze et al., 2008; Pahnke et al., 2008; Tachikawa et al., 2014; Howe et al., 2017), chemical processes (Klevenz et al., 2008; Pahnke et al., 2008), and the preservation state of foraminiferal tests, remaining the same across all species in a sample (Tachikawa et al., 2014).

Along the western margin of South Africa Hu et al. (2016a) measured Nd from samples in core ODP1087 and von Koslowski (2017) measured the Nd isotopic composition in bulk foraminifera in a few selected samples from MIS 3 to MIS 1 in cores GeoB 8342-6 and 8336-6 to indicate bottom water mass changes during the Last Glacial Maximum (LGM). Von Koslowski (2017) also found no difference in neodymium isotope content between bulk samples and picked tests from the same sample. The sample ages in von Koslowski (2017) relied upon planktic foraminiferal occurrences and colour reflectance (L*) data as the $\delta^{18}O$ age model for the cores was not developed at the time. The $\delta^{18}O$ age model for the cores has now been determined (Chapter 7) and in this chapter it is used to build upon and extend the record measured by von Koslowski (2017) by focusing on the εNd of planktic foraminifera in cores GeoB 8342-6 (3522 m water depth), 8336-6 (3631 m water depth) and 20601-4 (874 m water depth).

Determining and assessing the changes in oceanographic configuration along the southwestern margin of Africa during the Quaternary is important in understanding the role of the southeastern Atlantic in modulating global climate-ocean interactions over time. The objective in measuring εNd in these cores is to assess the variation in deep water mass changes during glacial-interglacial cycles along the western slope of South Africa and allows us to determine if glacial terminations have a pronounced influence on deep water masses during the late Quaternary. The εNd records are also compared to the $\delta^{13}C$ and *C. wuellerstorfi* abundance records to determine if these records correspond in providing a similar record of deep and intermediate water masses during the late Quaternary.

8.2. Study Area

The three cores GeoB 8342-6, 8336-6 and 20601-4 are located adjacent to the Cape Basin on the western continental slope of South Africa (Fig. 8.1). The South Atlantic Ocean has been opening since the early Cretaceous (~125 to 130 Ma) rifting of the western margin of Africa from the eastern margin of South America (Larson and Ladd, 1973; Noël and Melguen, 1978; Nürnberg and Müller, 1991). The Walvis

Ridge stretches from the northern Namibian margin to the Mid-Atlantic Oceanic Ridge in a southwesterly direction and separates the abyssal Cape Basin to the south from the Angola Basin to the north. The Walvis Ridge also acts as a barrier for inflow of deep Southern Component Water (SCW) into the Angola Basin. To the south, the Cape Basin is separated from the Agulhas Basin by the Agulhas Ridge (Nelson and Hutchings, 1983).

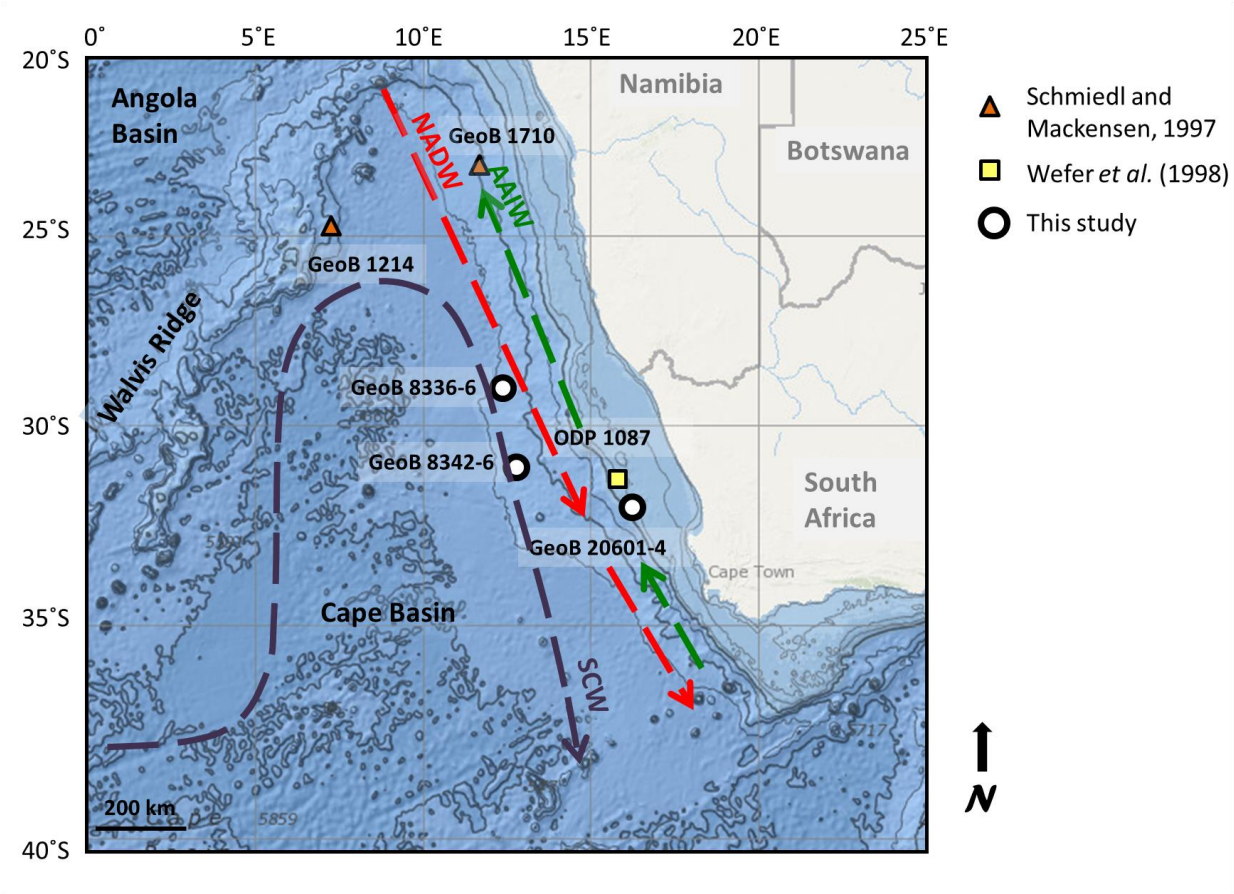

Fig. 8.1. Location of cores along the western margin of southern Africa which have been studied for deep water masses in the late Quaternary. The basemap is from the National Oceanic and Atmospheric Administration (NOAA) Bathymetric Data Viewer. The flow path of deep water masses (after Lutjeharms and Stockton, 1987) are indicated by the arrowed dashed lines (purple = SCW = Southern Component Water; red = NADW = North Atlantic Deep Water; green = AAIW = Antarctic Intermediate Water). Contours are spaced at 100 m intervals up to 500 m on the shelf. Thereafter contour lines are spaced at 1000 m.

Cores GeoB 8342-6 and 8336-6 are situated at 3522 m and 3631 m, respectively, close to the NADW/SCW interface (Fig. 8.2). Core GeoB 20601-4 is situated at 874 m water depth within the modern-day flow of the Antarctic Intermediate Water (AAIW) mass. All three cores are composed of a mix of muddy nannofossil ooze and foraminiferal ooze whose sand fraction is dominated by (>99%) planktic foraminifera.

Southern Component Water (SCW) forms the deepest ocean masses in the South Atlantic consisting of the densest (Adkins et al., 2002)

and coldest (<0˚C) (Whitworth et al., 1998; Waelbroeck et al., 2002; Kawano et al., 2006) water masses that include Antarctic Bottom Water (AABW), which forms in the Ross and Weddell Sea (Piepgras and Wasserburg, 1982; Rahmstorf, 2002; Delworth et al., 2008) at depths >4500 m water depth, and Lower Circumpolar Deep Water (LCDW) to 4000 m water depth (Reid et al., 1989) (Fig. 8.2). These water masses flow northwards, transferring heat along its way and play an important role in the storage of carbon dioxide in the deep ocean (Kuhlbrodt et al., 2007). North Atlantic Deep Water (NADW) which forms in the North Atlantic (Gordon, 2009; Deaney et al., 2017) flows southwards above the LCDW between 1600 and 4000 m water depth at temperatures between 1.5˚C and 4˚C (Emery and Meincke, 1986; Broecker, 1991; Waelbroeck et al., 2002). The saline NADW is enriched in dissolved oxygen and has low silicate concentrations. Above the NADW, the Upper Circumpolar Deep Water (UCDW) mass flows between 1000 and 1600 m at temperatures in excess of 1.7˚C (Martinson and McKee, 2012) and the oxygen-rich, nutrient-poor (Arz et al., 1999; Stramma and England, 1999) Antarctic Intermediate Water (AAIW) mass flows northward between 500 and 1000 m water depth (Emery and Meincke, 1986; Reid et al., 1989) at temperatures between 2˚C and 6˚C (Emery and Meincke, 1986). The South Atlantic Central Water (SACW) at 200 to 500 m water depth and the South Atlantic Subtropical Surface Water (SASSW) at <200 m form the uppermost water masses of the Cape Basin (Emery and Meincke, 1986; Reid, 1989; Stramma and Peterson, 1989) at temperatures between 5˚C and 18˚C (Emery and Meincke, 1986).

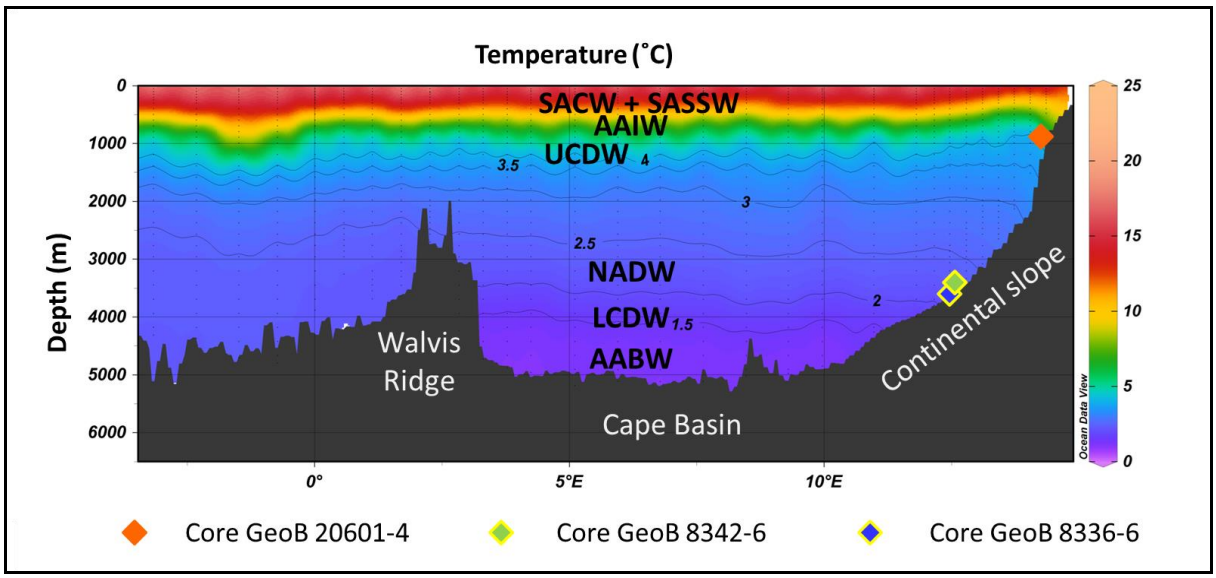

Fig. 8.2.The major deep water masses of the southeast Atlantic according to temperature (from references cited within text) and core locations of the three cores measured for εNd in this study. AABW = Antarctic Bottom Water; LCDW = Lower Circumpolar Deep Water; NADW = North Atlantic Deep Water; UCDW = Upper Circumpolar Deep Water; AAIW = Antarctic Intermediate Water; SACW = South Atlantic Central Water; SASSW = South Atlantic Subtropical Surface Water. Section at 30˚S latitude created in Ocean Data View (Schlitzer, 2018) from references cited within text and data from the CARINA (CARbon IN the Atlantic) project (Key et al., 2009).

8.3. Materials and Methods

8.3.1 Age model and stable carbon isotopes

The age model for the three cores is based on the $\delta^{18}O$ records of *Cibicidoides wuellerstorfi* and *Globorotalia (Globoconella) inflata* and the graphic correlation of these to the non-carbonate mineral grain abundance (primarily quartz and glauconite) and colour (L*) variations downcore. Oxygen and carbon stable isotope stratigraphy was constructed from the analysis of between 3 to 10 individual tests of the benthic species *C. wuellerstorfi* and between 15 to 30 individual tests of *Gr. (Gc.) inflata* picked from the 350 to 425 μm size fraction. The species picked were based on previous studies close to the study area (Rau, 2002; Rau et al., 2002). The number of tests picked was dependent on the amount of individuals in the samples, with more tests picked in samples where the species was more abundant. The size fraction of the specimens was based on the average shell mass needed for the detection limits of the instrumentation and to minimise the error in the analyses. The picked samples were cleaned in an ultrasonic bath under ultrapure water and then analysed for $\delta^{18}O$ and $\delta^{13}C$ using a Finnigan MAT 251 gas isotope ratio mass spectrometer coupled to a Kiel I automated carbonate preparation device at the University of Bremen. The $\delta^{18}O$ and $\delta^{13}C$ results are reported relative to Vienna Pee Dee Belemnite (VPDB) with a mean error of 0.02‰. The $\delta^{18}O$ records in the three cores were graphically correlated to the stacked LR04 composite record (Lisiecki and Raymo, 2005) using the Analyseries 2.0.8 programme (Paillard et al., 1996).

$\Delta\delta^{13}C$ (difference between $\delta^{13}C_{C.\ wuellerstorfi}$ and $\delta^{13}C_{Gr.\ (Gc.)\ inflata}$) values were calculated to evaluate if there were any productivity variations associated with the deep and intermediate water masses.

Colour reflectance data (L*) were obtained from scanning the red/blue ratio (700 nm/400 nm) of the archive halves of each core using a smartcube© camera image scanner at 1 mm to 1 cm intervals (Zabel et al., 2017). Sediment colour reflectance is influenced by carbonate content, dust input and settling of finer particles derived from different sources and may correspond to glacial and interglacial cycles (Bozzano et al., 2002; Carter et al., 2004). For example, changes in sediment inputs may indicate interglacial periods by a higher colour reflectance than glacial periods (Carter et al., 2004).

Compton and Wiltshire (2009) found that glauconite and quartz minerals increased during glacial periods along the southwestern margin of South Africa and decreased during interglacial periods. They showed that the variations in the quartz and glauconite mineral content could be used to differentiate glacial-interglacial (G-IG) cycles in the cores. The abundance of the non-carbonate mineral grains was determined by counting the number of glauconite and quartz grains in the sand fraction under a stereo microscope. The total glauconite and quartz grain content was normalized to 1 g of dry bulk sediment.

Faunal abundance records of cold water species indicating glacial periods (*Ng. incompta* + *Ng. pachyderma*) and warmer tropical to subtropical species indicating interglacial periods (*Globorotalia menardii* and *Globigerinoides ruber*) also matched the MIS periods identified

by the $\delta^{18}O$ records, colour reflectance and non-carbonate mineral variation (Chapter 7).

8.3.2 Neodymium Analysis

Processed, sieved and dried samples from the >63 μm fractions of the working halves of the three cores were selected for Nd isotope analysis at core depths corresponding to G/IG periods and MIS boundaries (glacial to interglacial transitions) recovered in the three cores (MIS 6/5, 4/3 and 2/1). Between 9 and 69 mg of mixed species of planktic foraminifera were handpicked. The amount picked depended on the available sample and nature of fragmentation of the tests. Fragmented or discoloured foraminifera that looked different from the rest of the sample were not picked to reduce the risk of including redeposited or reworked material in the analysis. One sample in core GeoB 8336-6 at 109.5 cm was large enough to split and run as a duplicate. Two samples were analysed to test if there is a difference in the Nd isotope composition of samples exclusively handpicked and bulk samples that included a mixture of mostly fragmented foraminifera.

Two methods of preparation of tests prior to Nd isotope analysis have been carried out in previous studies. In the first, foraminifera were chemically cleaned in an oxidative-reductive process to remove authigenic phases (termed 'cleaned') (Vance and Burton, 1999; Burton and Vance, 2000; Piotrowski et al., 2012; Tachikawa et al., 2014). In the other method tests were only mechanically cleaned (termed 'uncleaned') (Piotrowski et al., 2012; Tachikawa et al., 2014; Howe et al., 2016; Hu et al., 2016a, 2016b; Howe et al., 2017). The Nd content in the tests decreases with increased cleaning, but Tachikawa et al. (2014) concluded that both cleaned and uncleaned samples provided the same εNd results. In this study, tests were only mechanically cleaned before Nd analysis was carried out.

The mechanical cleaning procedure used followed that of established steps in previous studies (e.g. Piotrowski et al., 2012). Foraminifera tests were crushed between two clean glass slides and placed in cleaned small glass beakers with 5 ml de-ionised water. The tests appeared to be clean externally (Fig. 8.3a), but the crushed samples revealed brown mud stuck to the internal surface of the tests (Fig. 8.3b). The samples were then placed in an ultrasonic bath for 3 minutes for cleaning. The water was pipetted off and the sample was examined to see if any silt or clay particles were still stuck to the crushed foraminifera. Samples that still had mud stuck to the crushed tests were placed back in the ultrasonic bath for another minute in 5 ml de-ionised water. The process was repeated until the samples appeared to be as clean as possible (Fig. 8.3c). The excess water was pipetted off and the samples were then oven dried at 70°C, weighed and placed in vials. The crushed and cleaned samples were reduced in mass from the original picked sample by between 22 and 67% (Table 8.1).

Samples were analysed following the steps of von Koslowski (2017) in a clean laboratory at the Radiogenic Isotope Facility at the University of Cape Town (UCT). The samples were placed in 500 μl ultrapure water and up to 1 ml 1 M acetic acid and centrifuged for 10 minutes at 4500 rpm in an attempt to further separate any undissolved mud material from the crushed tests. The supernatant was then transferred into 1.5 ml acid-cleaned centrifuge tubes and

centrifuged for 10 minutes at 10 000 rpm. The supernatant was transferred to an acid-cleaned Teflon vial and dried overnight at 60°C and re-dissolved in nitric acid for 1 hour. The dried samples were dissolved again in the acid and the Nd was separated by stepwise rinsing the sample in resin bead columns with 2M HNO_3, 0.05M HNO_3 and 0.25M HCl. The Nd separate was dried and analysed with a NuPlasma HR multi-collector ICP-MS at the Department of Geological Sciences at UCT. The samples were analysed with 50 ppb 2% HNO_3 solutions using a Nu-Instrument DSN-100 Desolvating Nebulizer. The εNd value for each sample was calculated using the equation:

$$\varepsilon_{Nd} = \left[\frac{(^{143}\mathrm{Nd}/^{144}\mathrm{Nd})_{sample}}{(^{143}\mathrm{Nd}/^{144}\mathrm{Nd})_{CHUR}} - 1\right] x\ 10^4$$

Where ε_{Nd} = deviation of $^{143}Nd/^{144}Nd$ of a sample from the bulk Earth $^{143}Nd/^{144}Nd$ chondritic uniform reservoir (CHUR) ratio measured in chondrites (0.512638) (Jacobsen and Wasserburg, 1980).

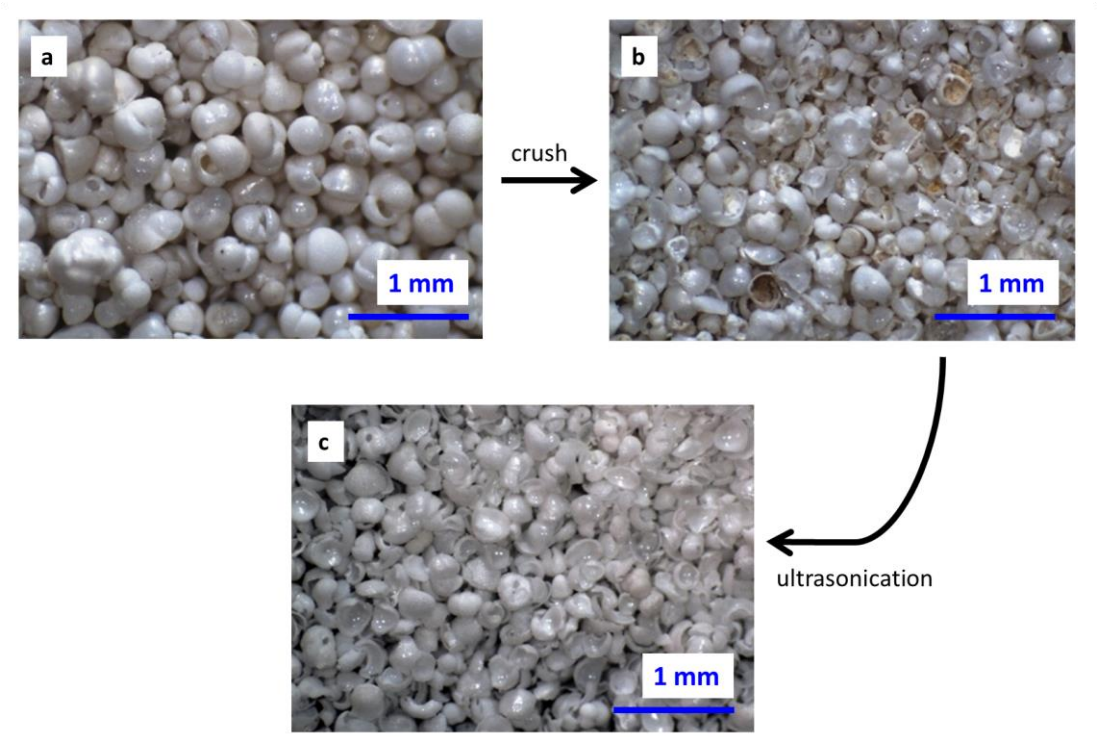

Fig. 8.3. Sample from GeoB 8336-6 at 8.5 cm chosen for Nd-isotope analysis. a) picked mostly whole planktic foraminifera; b) crushed sample showing brown mud on inside of tests; c) crushed sample cleaned in ultrasonic bath before chemical processing for Nd analysis.

One sample (core 8336-6; 109.5 cm) measured for reproducibility were within range of error (-8.49±0.47 and -8.30±0.26). The εNd value of samples taken from the same core depths from von Koslowski are also the same within error, deviating by between 0.1 and 0.48 epsilon units.

The εNd records were matched and correlated with the benthic $\delta^{13}C$ and *C. wuellerstorfi* relative abundance records to determine if these three methods indicate similar results for water mass changes. The relative abundances of *C. wuellerstorfi* were obtained by counting the

benthic foraminifera in a statistically significant number of foraminifera (>300 individuals) in the >125 μm size fraction. All benthic foraminifera were counted in samples containing less than 300 individual foraminifera tests and the relative abundances were determined as percentage. The relative abundances of *C. wuellerstorfi* were graphically compared to εNd values of the measured samples.

Pearson r correlation values were calculated and linear regression correlation coefficient (r^2) graphs constructed to determine if a correlative relationship exists between εNd values and *C. wuellerstorfi* relative abundances. Statistical significance was assessed by the p-value and discussed for relationships significant at the 95% confidence interval, i.e. p-value <0.05.

8.4. Results

Marine isotope stages (MIS) of the three cores were identified by peak maxima and minima in the $\delta^{18}O$ record of all three cores (Appendix Table C.1) correlated to the LR04 record (Lisiecki and Raymo, 2005) (Fig. 8.4 to 8.6). Enriched $\delta^{18}O_{C.\ wuellerstorfi}$ ($\delta^{18}O_{Cw}$) and $\delta^{18}O_{Gr.\ (Gc.)\ inflata}$ ($\delta^{18}O_{Gi}$) values indicate glacial periods (MIS 8, 6, 4, 2) and depleted $\delta^{18}O_{Cw}$ and $\delta^{18}O_{Gi}$ values indicate interglacial periods (MIS 7, 5, 3, 1). The identification of MIS periods from the $\delta^{18}O$ records largely matches the colour reflectance and non-carbonate mineral content of the cores.

Lower values of colour reflectance indicate glacial periods and higher values indicate interglacial periods. Higher abundances of non-carbonate minerals (quartz in GeoB 8342-6 and 8336-6, and glauconite and quartz in GeoB 20601-4) correspond with glacial periods and lower abundances with interglacial periods. The exception to this is in core GeoB 20601-4 where relatively high abundances of non-carbonate minerals occur in MIS 3 and early MIS 7.

The Nd isotope results from von Koslowski (2017) and this study are shown in Table 8.1 and εNd values are plotted in Fig. 8.7. The εNd in samples taken from the same core depths from von Koslowski and in this study deviates by 0.10 (0.9%) to 0.48 (4.6%) from measured values in this study. The εNd value of the duplicate sample (core 8336-6; 109.5 cm) deviated by 0.19 (2.2%) from the original samples. Samples that included fragmented foraminifera (core 8336-6; 41.5 and 27.5 cm) deviated by 0.65 (8.3%) and 0.77 (10.6%) from εNd values measured in samples with whole, non-fragmented tests from the same core depths.

Pearson r correlation values between εNd and *C. wuellerstorfi* relative abundances range from -0.22 (r^2=0.049; p-value = 0.947) in core GeoB 8342-6, -0.81 (r^2=0.65; p-value = 0.018) in core GeoB 8336-6 and 0.80 (r^2=0.65; p-value = 0.012) in core GeoB 20601-4 (Fig. 8.8). Removing the youngest four samples (MIS 2 and 1) from core GeoB 8342-6 changes the correlation value to -0.78 (r^2=0.61; p-value = 0.117). Correlation coefficients for cores GeoB 8336-6 and GeoB 20601-4 are statistically significant at the 95% (i.e. <0.05) confidence level.

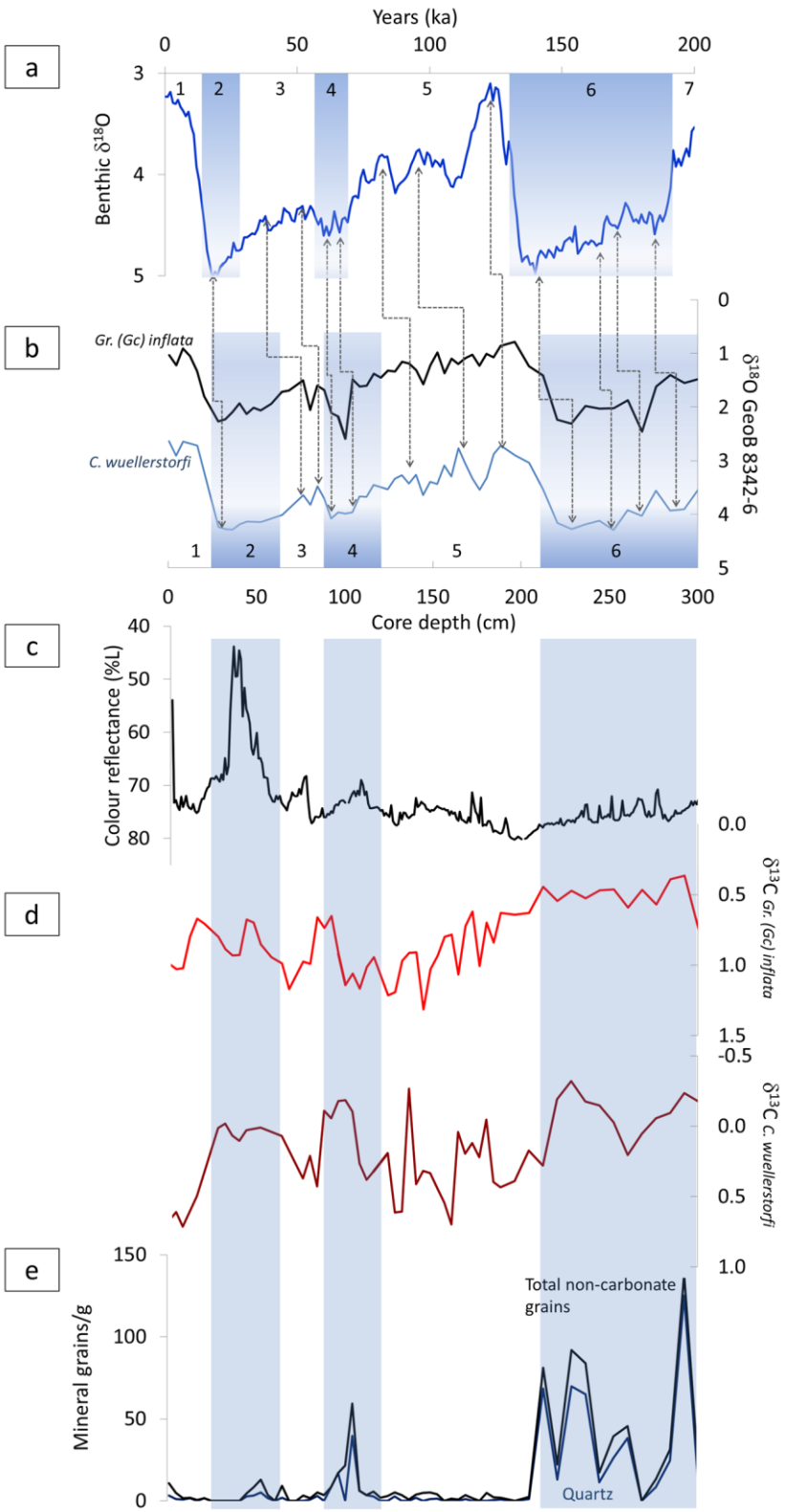

Fig. 8.4. Age model of core GeoB 8342-6 derived from stable oxygen isotopes, colour reflectance and non-carbonate mineral grain counts. a) $\delta^{18}O$ record of the LR04 benthic stack (Lisiecki and Raymo, 2005) correlated to b) $\delta^{18}O$ record (*Gr. (Gc.) inflata* and *C. wuellerstorfi)*; c) L* colour reflectance record d) $\delta^{13}C$ (*Gr. (Gc.) inflata* and *C. wuellerstorfi*) record; e) non-carbonate mineral (glauconite, quartz and total) counts per g of sand fraction. Marine isotope stage values are indicated above the LR04 plot and below the $\delta^{18}O$ (GeoB 8342-6) profile.

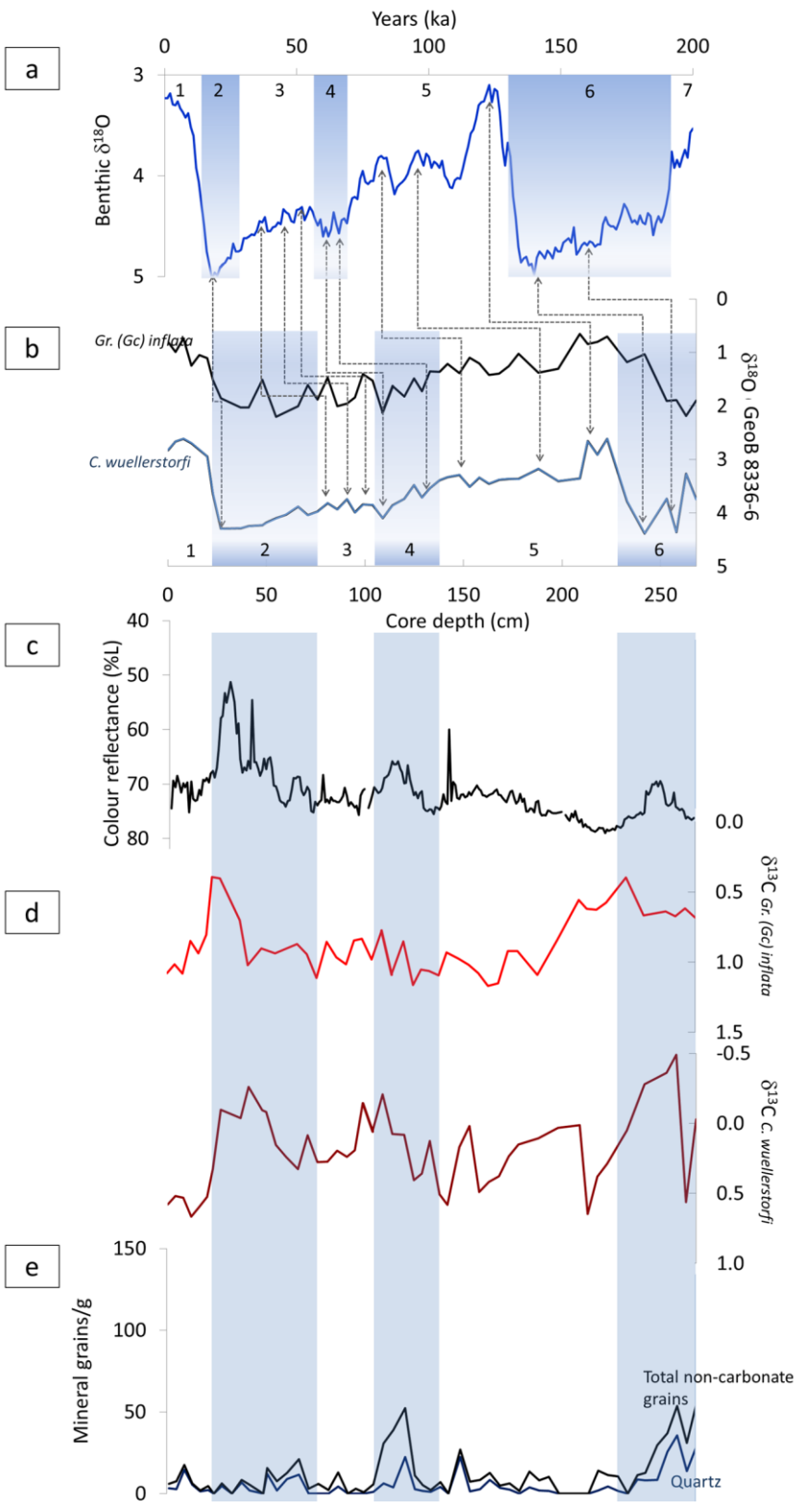

Fig. 8.5. Age model of core GeoB 8336-6 derived from stable oxygen isotopes, colour reflectance and non-carbonate mineral grain counts. a) $\delta^{18}O$ record of the LR04 benthic stack (Lisiecki and Raymo, 2005) correlated to b) $\delta^{18}O$ record (*Gr. (Gc.) inflata* and *C. wuellerstorfi)*; c) L* colour reflectance record; d) $\delta^{13}C$ (*Gr. (Gc.) inflata* and *C. wuellerstorfi*) record; e) non-carbonate mineral (glauconite, quartz and total) counts per g of sand fraction. Marine isotope stage values are indicated above the LR04 plot and below the $\delta^{18}O$ (GeoB 8336-6) profile.

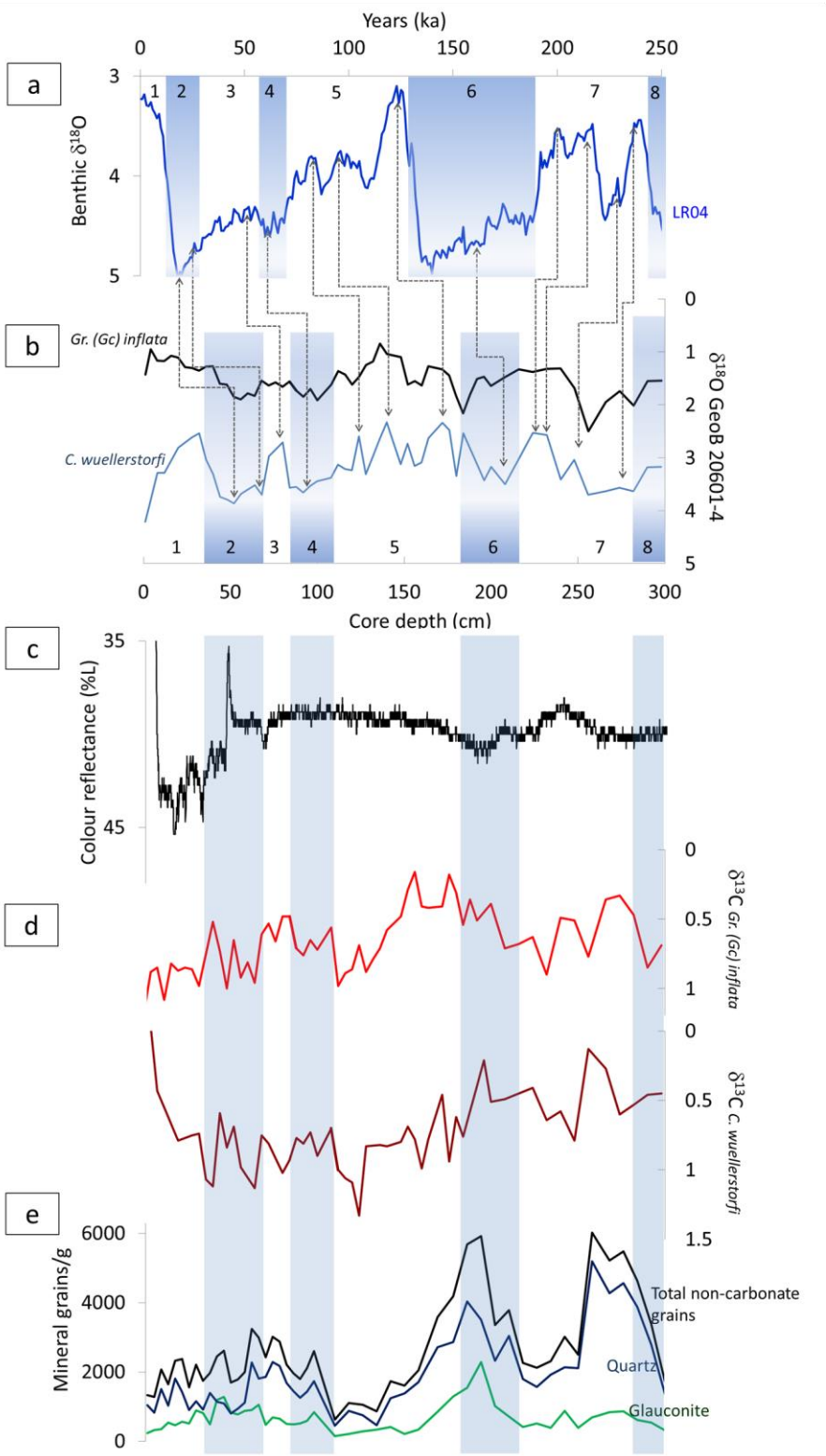

Fig. 8.6. Age model of core GeoB 20601-4 derived from stable oxygen isotopes, colour reflectance and non-carbonate mineral grain counts. a) $\delta^{18}O$ record of the LR04 benthic stack (Lisiecki and Raymo, 2005) correlated to b) $\delta^{18}O$ record (*Gr. (Gc.) inflata* and *C. wuellerstorfi)*; c) L* colour reflectance record; d) $\delta^{13}C$ (*Gr. (Gc.) inflata* and *C. wuellerstorfi*) record; e) non-carbonate mineral (glauconite, quartz and total) counts per g of sand fraction. Marine isotope stage values are indicated above the LR04 plot and below the $\delta^{18}O$ (GeoB 20601-4) profile.

Table 8.1. Mass of picked and mechanically cleaned foraminifera, Nd ratios and calculated Nd-isotope measurements with 2σ errors for cleaned samples analysed in von Koslowski (2017) and in this study. The suffix –D following the core depth value refers to duplicate samples. The suffix –B following the core depth in values from von Koslowski (2017) refers to bulk sand samples. Cleaned masses not indicated in von Koslowski (2017).

Core	Core depth (cm)	Picked mass (g)	Cleaned mass (g)	$^{143}Nd/^{144}Nd$	±2σ internal	εNd	Calculated ±2σ	Age	Study
8342-6	16.5	0.061	0.023	0.512099	0.000015	-10.51	0.30	MIS 1	This study
8342-6	16.5	0.022	-	0.512124	0.000019	-10.03	0.37	MIS 1	v/Koslowski, 2017
8342-6	16.5	0.021	-	0.512107	0.000019	-10.36	0.37	MIS 2	v/Koslowski, 2017
8342-6	28.5	0.040	0.019	0.512214	0.000015	-8.28	0.29	MIS 2	This study
8342-6	36.5	0.037	0.019	0.512221	0.000013	-8.14	0.25	MIS 2	This study
8342-6	40.5	0.021	-	0.512241	0.000014	-7.74	0.27	MIS 2	v/Koslowski, 2017
8342-6	52.5	0.043	0.016	0.512227	0.000013	-8.01	0.25	MIS 2	This study
8342-6	68.5	0.020	-	0.512196	0.000018	-8.62	0.35	MIS 3	v/Koslowski, 2017
8342-6	68.5B	0.029	-	0.512185	0.000014	-8.84	0.27	MIS 3	v/Koslowski, 2017
8342-6	88.5	0.069	0.047	0.512163	0.000010	-9.27	0.20	MIS 3	This study
8342-6	108.5	0.032	0.015	0.512160	0.000016	-9.32	0.31	MIS 4	This study
8342-6	196.5	0.056	0.031	0.512126	0.000013	-9.99	0.25	MIS 5	This study
8342-6	236.5	0.052	0.017	0.512261	0.000013	-7.35	0.26	MIS 6	This study
8342-6	260.5	0.048	0.020	0.512212	0.000014	-8.32	0.28	MIS 6	This study
8342-6	292.5	0.048	0.021	0.512190	0.000017	-8.75	0.33	MIS 6	This study
8336-6	8.5	0.044	0.027	0.512092	0.000015	-10.65	0.30	MIS 1	This study
8336-6	8.5	0.030	-	0.512087	0.000017	-10.75	0.33	MIS 1	v/Koslowski, 2017
8336-6	20.5	0.037	0.019	0.512142	0.000018	-9.67	0.34	MIS 1	This study
8336-6	27.5	0.013	0.009	0.512239	0.000024	-7.79	0.46	MIS 2	This study
8336-6	27.5D	0.030	0.014	0.512206	0.000015	-8.44	0.30	MIS 2	This study
8336-6	27.5	0.023	-	0.512224	0.000015	-8.08	0.29	MIS 2	v/Koslowski, 2017
8336-6	41.5	0.017	0.008	0.512265	0.000016	-7.27	0.31	MIS 2	This study
8336-6	41.5D	0.032	0.019	0.512226	0.000015	-8.04	0.29	MIS 2	This study
8336-6	60.5	0.025	-	0.512188	0.000013	-8.78	0.25	MIS 3	v/Koslowski, 2017
8336-6	60.5B	0.029	-	0.512193	0.000016	-8.99	0.31	MIS 3	v/Koslowski, 2017
8336-6	95.5	0.029	0.021	0.512168	0.000013	-9.17	0.26	MIS 3	This study
8336-6	109.5	0.009	0.007	0.512203	0.000024	-8.49	0.47	MIS 4	This study
8336-6	109.5D	0.024	0.017	0.512213	0.000013	-8.30	0.26	MIS 4	This study
8336-6	125.5	0.019	0.010	0.512164	0.000013	-9.25	0.25	MIS 4	This study
8336-6	218.5	0.032	0.022	0.512094	0.000014	-10.61	0.28	MIS 5	This study
8336-6	242.5	0.030	0.021	0.512199	0.000019	-8.56	0.37	MIS 6	This study
8336-6	263.5	0.026	0.015	0.512239	0.000016	-7.79	0.32	MIS 6	This study
20601-4	20.5	0.019	0.010	0.512188	0.000030	-8.77	0.58	MIS 1	This study
20601-4	28.5	0.021	0.013	0.512209	0.000023	-8.37	0.45	MIS 1	This study
20601-4	76.5	0.020	0.015	0.512193	0.000023	-8.67	0.45	MIS 3	This study
20601-4	108.5	0.014	0.010	0.512227	0.000030	-8.02	0.59	MIS 4	This study
20601-4	156.5	0.025	0.019	0.512186	0.000017	-8.81	0.33	MIS 5	This study
20601-4	200.5	0.024	0.018	0.512250	0.000019	-7.58	0.36	MIS 6	This study
20601-4	240.5	0.030	0.021	0.512165	0.000017	-9.22	0.33	MIS 7	This study
20601-4	266.5	0.031	0.021	0.512244	0.000023	-7.68	0.45	MIS 7	This study

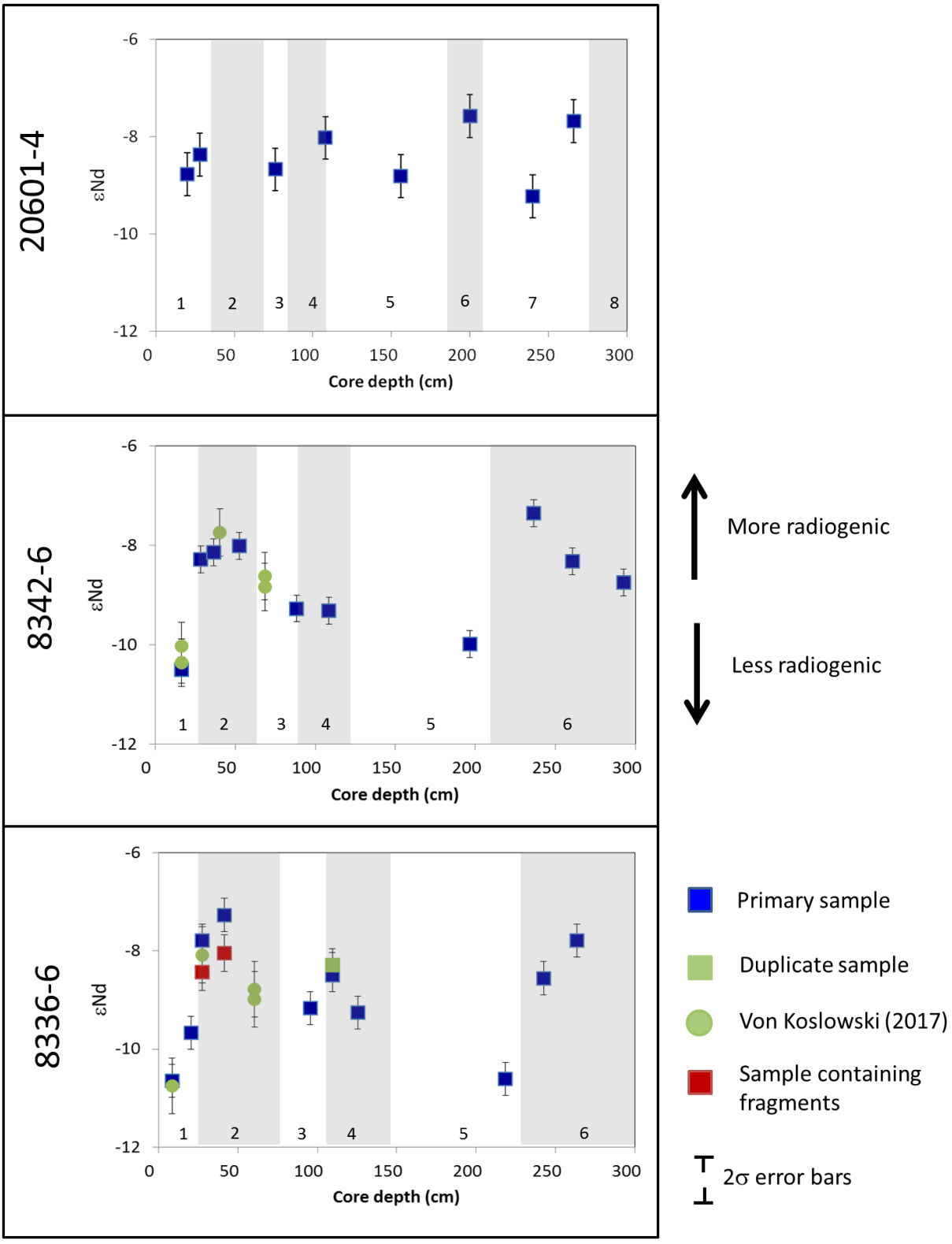

Fig. 8.7. εNd values with 2σ standard error bars of samples in the three cores (GeoB 20601-4 at 874 m water depth; GeoB 8342-6 at 3522 m water depth and GeoB 8336-6 at 3631 m water depth) of this study and from von Koslowski (2017). The MIS periods are indicated by the numbers above the x-axis.

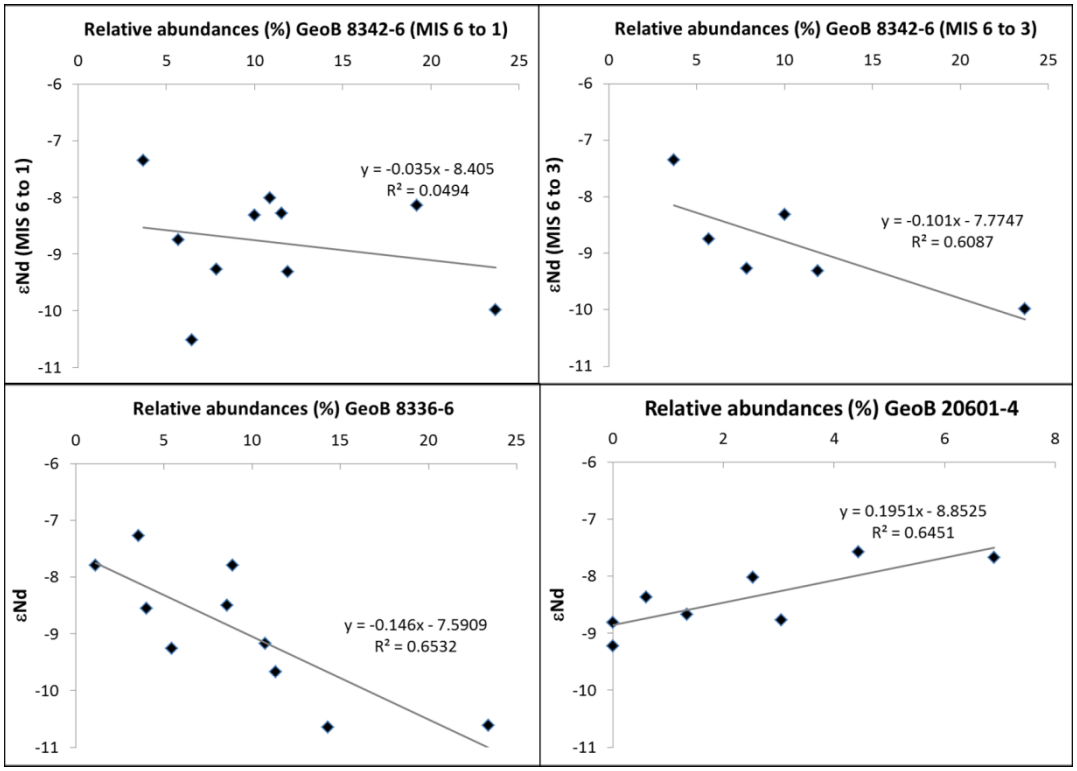

Fig. 8.8. Correlation between *C. wuellerstorfi* relative abundances and εNd in the three cores of this study. All samples of GeoB 8342-6 in the plot on the upper left image, samples of GeoB 8342-6 with the upper four samples removed in the plot on the upper right image, core GeoB 8336-6 samples in the plot on the lower left image and core GeoB 20601-4 samples in the plot on the lower right image.

8.5. Discussion

8.5.1. Deep water masses along the western South African margin

AABW is a major part of the SCW and its formation is driven by brine rejection associated with sea ice growth (Boyle and Keigwin, 1982; Curry and Lohmann, 1982). When sea ice forms in greater abundance during glacial periods, the amount of SCW is expected to increase and can be identified by a mean εNd value of -8 (Rutberg et al., 2000). In contrast, the formation of NADW may decrease during glacial periods when North Atlantic sea ice becomes extensive enough to shut off the supply of sinking salty surface waters (Boyle and Keigwin, 1982; Curry and Lohmann, 1982; Aiken and England, 2008). When the sea ice melts during IG periods, freshwater release benefits the formation of the slightly warmer and less dense NADW (Emery, 2001; Aiken and England, 2008; Gordon, 2009) resulting in increased northern-sourced water production in the Northern Hemisphere and its penetration into the South Atlantic Ocean. NADW can be identified by a mean εNd value of -10.5 (Piepgrass and Wasserburg, 1987; Pahnke et al., 2008).

The anticipated trends outlined above are supported by the εNd results of this study. Core GeoB 8342-6 (3522 m) records increasingly radiogenic εNd values during MIS 6 followed by a sharp decrease during GT II (MIS 6/5 boundary) (Fig. 8.7, 8.10, 8.11 and 8.13). Core GeoB 8336-6 (3631 m) displays εNd values and trends similar to core GeoB 8342-6, becoming

increasingly radiogenic during MIS 6 and then decreasing sharply during GT II. These radiogenic εNd values indicate a strengthened SCW and a weakened NADW during MIS 6 (Fig. 8.9) in the deeper core sites (GeoB 8342-6 and 8336-6) of the study area. During the onset of MIS 5 (GT II) the SCW weakens and NADW strengthens. Off Namibia (GeoB 1214 and 1710; Fig. 8.1), Schmiedl and Mackensen (1997), based on benthic foraminiferal faunal distributions and $\delta^{13}C_{Cw}$ found the influx of NADW into the eastern South Atlantic is also strongest during interglacial periods MIS 7, 5 and 1, with NADW not being traceable or very weak during glacial periods MIS 4 and MIS 2. The observed higher εNd values before GT II occur when the sea-ice edge expanded by 3-5° latitude northwards, sea-ice seasonality decreased and SSTs reached ~0°C in the central and eastern Atlantic (Bianchi and Gersonde, 2002). Deep water formation occurs close to areas of polar ice formation and is sensitive to changes in ice surface area and volume (Gordon, 1974). The decreasing εNd values during the late MIS 6 and abrupt change during the transition into MIS 5 recorded in this study can be associated with a decline in SCW production which affects the strength and flow speed of the SCW (Krueger et al., 2012). This decline in SCW occurred during a time (132-125 ka) when ice coverage rapidly retreated and global temperatures and sea levels rose (Bianchi and Gersonde, 2002; Cortese and Abelmann, 2002), which strengthened NADW production (Böhm et al., 2015).

The $\delta^{13}C$ record of *C. wuellerstorfi* is useful because this species appears to secrete calcite close to ambient bottom water carbon isotopic values (Woodruff et al., 1980; Zahn et al., 1986; Bickert and Wefer, 1996). Nutrient-depleted NADW has high $\delta^{13}C$ values (>1‰) in the North Atlantic (Kroopnick, 1985) that decrease as NADW flows southward from the oxidation of organic material, whereas SCW has lower $\delta^{13}C$ values (Krueger et al., 2012; and references therein).

The occurrence and strength of bottom water currents can influence the benthic foraminiferal assemblages. For example, the abundance of *C. wuellerstorfi* has been found to be a good tracer of NADW (Lohmann, 1978a; Schmiedl and Mackensen, 1997). During MIS 6 the records from this study indicate relatively low *C. wuellerstorfi* abundances compared to GT II when the NADW strengthened. This species is favoured by well ventilated and oxygenated environments (Kaiho, 1994) such as the NADW, as well as higher inputs of phytodetritus (Gooday, 1988). The $\delta^{13}C$ records of this study (Fig. 8.10 and 8.11) also indicate a shift from SCW-dominated waters to a strengthened NADW during the MIS 6/5 transition (GT II).

From MIS 6 to 3 in core GeoB 8342-6 the relative abundance of *C. wuellerstorfi* increases with less radiogenic εNd values and decreases with more radiogenic εNd values (Fig. 8.10), and is reflected by the negative correlation between the two records (Fig. 8.8). A similar trend is observed throughout core GeoB 8336-6. The combination of more radiogenic εNd values and lower *C. wuellerstorfi* abundances indicates southern-sourced waters (SCW) while the combination of less radiogenic εNd values with higher *C. wuellerstorfi* abundances indicates an increase in the influence of northern-sourced waters, i.e. NADW. These results suggest that *C. wuellerstorfi* can provide a useful proxy for

changes in the relative influence of NADW and SCW, consistent with previous studies in which it has been documented that certain taxa can indicate the presence of particular water masses (Streeter, 1973; Schnitker, 1974; Lohmann, 1978a, 1978b; Schnitker, 1979, 1980).

From MIS 5 to MIS 3 the εNd record shows a northern-sourced component that gradually weakens. Previous studies (Fig. 8.13) have found glacial-interglacial variations in bottom water masses and found a return to a stronger NADW during interglacial periods (Boyle and Keigwin, 1982; Rutberg et al., 2010; Hu et al., 2016a). Hu et al. (2016a) found the NADW to weaken and shoal during glacial periods along the South African western continental margin consistent with other studies where benthic foraminiferal assemblages and the $\delta^{13}C$ values of South Atlantic benthic foraminifera suggest less NADW flow during glacial periods (Curry and Lohmann, 1982; Kuhn and Diekmann, 2002; and references therein). The shallow water equivalent of NADW that occurs during glacial periods has been referred to as Glacial North Atlantic Intermediate Water (GNAIW) (Böhm et al., 2015).

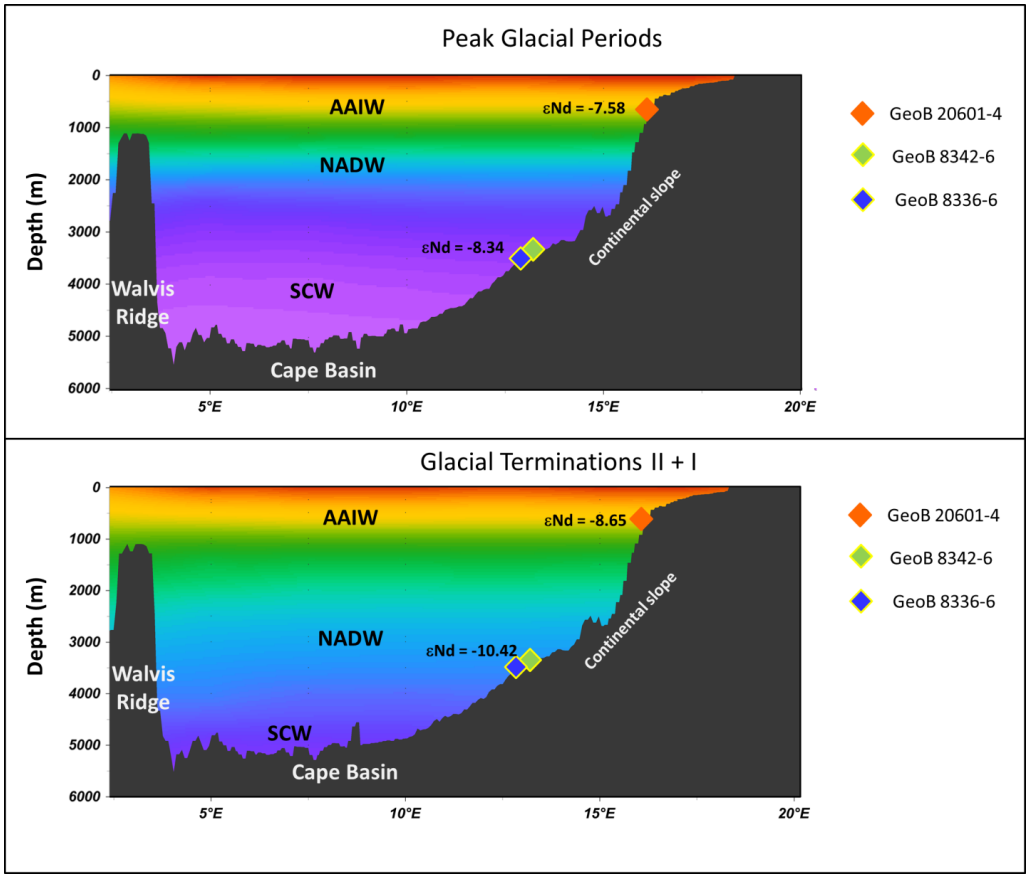

Fig. 8.9. Major bottom water mass configurations during peak glacial periods (MIS 6 and 2) and glacial terminations II and I in the southeast Atlantic with mean εNd values. SCW = Southern Component Waters (AABW + LCDW); NADW = North Atlantic Deep Waters; AAIW = Antarctic Intermediate Waters. Sections were created in Ocean Data View (Schlitzer, 2018) at 30°S latitude. The colour schemes are reflected to represent the different water masses and not measured physical properties.

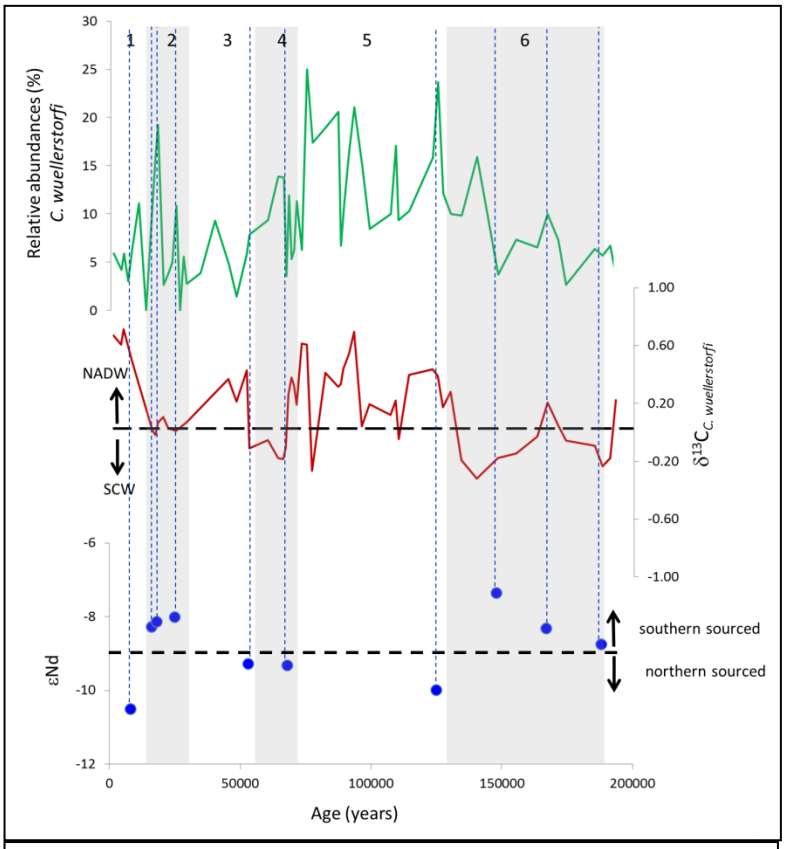

Fig. 8.10. Graphic correlation (dashed lines) of *C. wuellerstorfi* relative abundances, $\delta^{13}C$ and εNd values in core GeoB 8342-6. The MIS intervals (1-6) are indicated as numbers at the top of the plots. The black horizontal dashed line indicates average values at which the water masses can be distinguished based on references cited within the text.

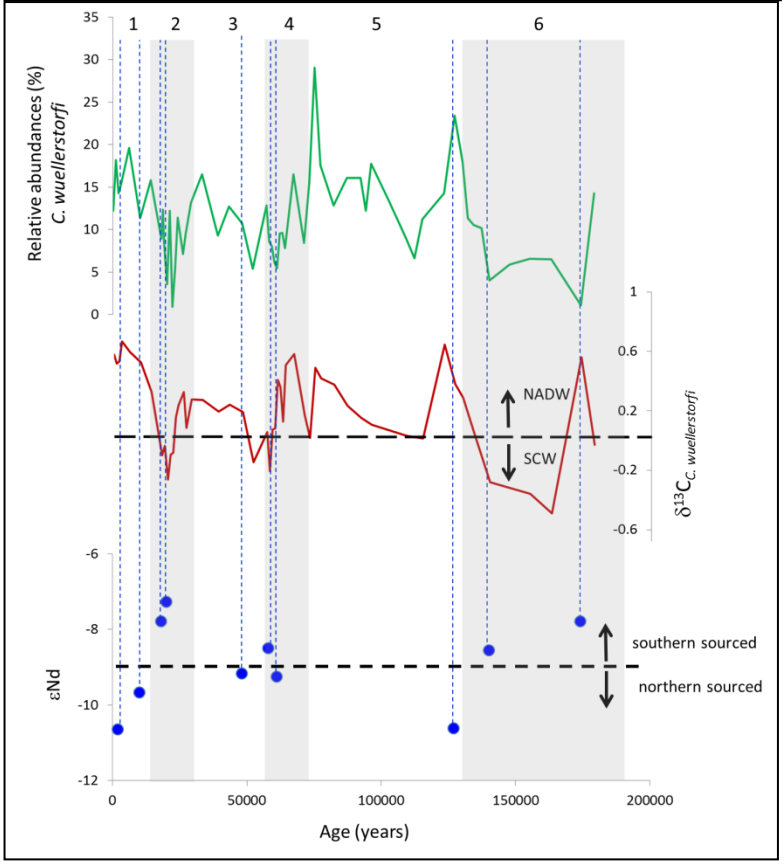

Fig. 8.11. Graphic correlation (dashed lines) of *C. wuellerstorfi* relative abundances, $\delta^{13}C$ and εNd values in core GeoB 8336-6. The MIS intervals (1-6) are indicated as numbers at the top of the plots. The black horizontal dashed lines indicate average values at which the water masses can be distinguished based on references cited within the text.

In this study only, a slight shift to a stronger northern source is observed at the MIS 4/3 transition in core GeoB 8336-6, a shift not nearly as large as observed during GT II. The

high εNd values documented in Rutberg et al. (2000) during glacial stages MIS 4 and MIS 2 signify a strong influence of southern-sourced waters in the subpolar region. The cores to the south of the study area analysed by Rutberg et al., (2000) recorded more radiogenic (less negative) εNd values compared to cores in this study owing to its more southern location (Fig. 8.13). The radiogenic εNd values recorded in samples associated with deglaciations in this study are lower than found in previous studies and show that the influence of NADW strength is greater in this study area compared to shallower areas (Hu et al., 2016a) and areas to the south (Rutberg et al., 2000; Hu et al., 2016a) owing to the deeper water depths of cores in this study and penetration of NADW flow from the north.

The LGM (MIS 2, 18 and 26 ka) is reflected in records from the southwestern margin of Africa (Franzese et al., 2006; Clark et al., 2012; Piotrowski et al., 2012). The LGM resulted from lower northern summer insolation, reduced CO_2 concentrations in the atmosphere and lower sea surface temperatures which affected global ocean-climate systems and contributed to the formation of increased sea ice (Clark et al., 1999, 2009). Gebbie (2014) documented that the NADW shoaled by ~1000 m to form the GNAIW during the LGM, in agreement with previous studies that document a reduced presence of northern-sourced water in the western North Atlantic Ocean (Howe et al., 2017). In contrast, the amount of NADW relative to SCW increased during the last deglaciation in the Atlantic Ocean (Pahnke et al., 2008; Roberts et al., 2012; Piotrowski et al., 2012; Wei et al., 2016; von Koslowski, 2017).

During MIS 2 the εNd record returns to similar radiogenic values as seen in MIS 6 and indicates a strengthened SCW source. The MIS 2 samples containing fragments have εNd values of between 8.3 and 10.6%. These values fall outside the standard error of 2.3% associated with samples containing exclusively whole tests and the split duplicate sample in core 8336-6 at 109.5 cm. This implies that fragmented foraminifera are a potential source of increased uncertainty and should be avoided. The fragmented foraminifera may represent older or shallower water tests that were redeposited or reworked. Material from shallower depths has been reported to be reworked along the southwestern margin of South Africa during glacial periods (Compton et al., 2002; Compton and Wiltshire, 2009). Reworked tests transported downslope during MIS 2 may explain the greater uncertainty in the εNd values.

The transition from MIS 2 to MIS 1, GT I is associated with a progressive sharp decrease in εNd values indicating a strengthened NADW, a similar trend to that of the MIS 6 to MIS 5 transition. The $\delta^{13}C$ record across GT I in cores GeoB 8342-6 and 8336-6 shows an enrichment of ~0.8‰ similar to GT II. The shift in the $\delta^{13}C_{Cw}$ record is in agreement with a previous study by Bickert and Mackensen (2003), which recorded a $\delta^{13}C_{Cw}$ shift in the order of 1.4 to 2.1‰ during the late Pleistocene to Holocene transition in the South Atlantic indicating a strengthening of NADW penetration into the South Atlantic. These records are also supported by the $\Delta\delta^{13}C$ record which shows increased palaeoproductivity during glacial periods and a sharp decrease in the productivity record during the MIS6/5 and the MIS 2/1 transitions (Fig.

8.12). The northern core GeoB 8336-6 also shows higher $\delta^{13}C$ and $\Delta\delta^{13}C$ values for most of the MIS 6 to MIS 1 record compared to core GeoB 8342-6 (Fig. 8.10 to 8.12) which could reflect decreasing nutrient inputs as the SCW flow path curves south of the Walvis Ridge flowing back southwards along the South African margin (Lutjeharms and Stockton, 1987; Fig. 8.1).

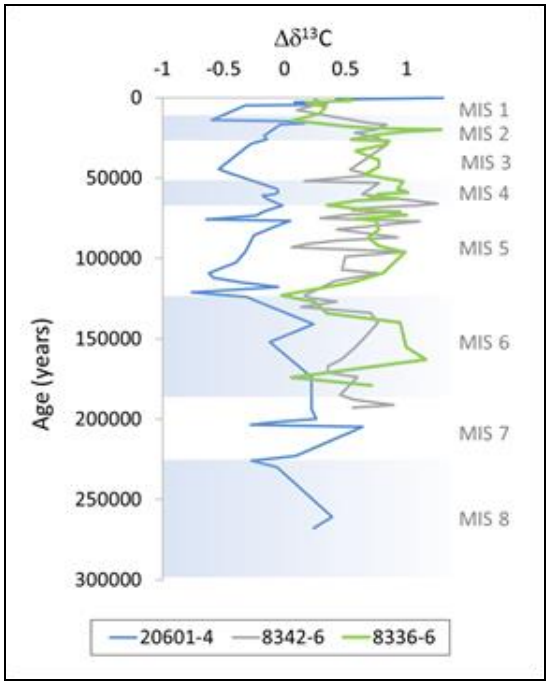

Fig. 8.12. $\Delta\delta^{13}C$ ($\delta^{13}C_{Gr.\ (Gc.)\ inflata}$ - $\delta^{13}C_{C.\ wuellerstorfi}$) in all three cores of this study

C. wuellerstorfi relative abundance increased during GT I and MIS 1 in core GeoB 8336-6, reflecting NADW strengthening. This trend from GT I to MIS 1, however, is not clearly observed in core 8342-6 and show that *C. wuellerstorfi* relative abundances alone cannot conclusively indicate NADW influence. It is possible that the abundances of *C. wuellerstorfi* were additionally influenced by changes in the organic matter inputs, seasonality of food pulses and factors which would influence the abundances of other taxa as well.

Von Koslowski (2017) recorded similar Holocene εNd values for cores GeoB 8342-6 and 8336-6 compared to modern eastern NADW (ENADW) εNd values of ~-10.9 ± 1.2 (Jeandel, 1993; Stichel et al., 2012; Garcia-Solsona et al., 2014) suggesting that deep water configurations did not change significantly during the Holocene. The early MIS 5 and MIS 1 εNd values (-10.51 and -9.99 for MIS 5; -10.65 and -10.61 for MIS1) from this study are also in agreement with modern ENADW εNd values. This suggests that bottom water mass configurations during GT II and I were similar to modern conditions where NADW gradually displaces SCW.

8.5.2. Glacial-interglacial intermediate water mass variations along the western South African margin

Core GeoB20601-4 is located at a water depth (874 m) within the range of the present-day AAIW and provides a record back to MIS 7. AAIW circulation is an important contributor to the ocean-climate system, yet the behavior of this water mass over glacial-interglacial cycles is not fully understood (Pahnke et al., 2008), with much of AAIW research focused on the past 25 kyr (Howe et al., 2016). The εNd record for core GeoB 20601-4 largely shows variation within the modern AAIW range (Fig. 8.14).

The εNd values measured in interglacial periods (MIS 7, 5, 3, 1) indicate a weak AAIW influence at the core site, whereas during glacial periods (MIS 6, 4 and 2) and early stages of interglacial periods of MIS 7 and MIS 1 (GT I) the AAIW strengthens. The strength of the AAIW along the margin seems to mimic the reported increased SCW production during

glacial periods (Rutberg et al., 2000; Hu et al., 2016a) and a weakened AAIW occurs during periods of stronger NADW influence. The NADW has previously been suggested to accompany variations in AAIW fluxes (Howe et al., 2016).

Productivity seems to increase during glacial periods at the upper slope site (Fig. 8.12) when AAIW strengthens suggested by the εNd record (Fig. 8.7, 8.13, 8.14). These glacial-interglacial variations in the AAIW input reflect the influence of the shifting polar fronts consistent with indications from polar planktic foraminifera species which suggest the northward movement of the polar fronts (Rau et al., 2002). This northward shift may be explained by the melting of Antarctic sea ice during GT II. Aiken and England (2008) mention AAIW production decreases during the melting of Antarctic ice. The behaviour of SCW in the deeper cores and AAIW in core GeoB 20601-4 in the study area suggests that both southern-sourced waters strengthen during glacial periods with AAIW recording more radiogenic values across glacial and interglacial periods (Fig. 8.13) while NADW are stronger in the Atlantic during interglacial periods.

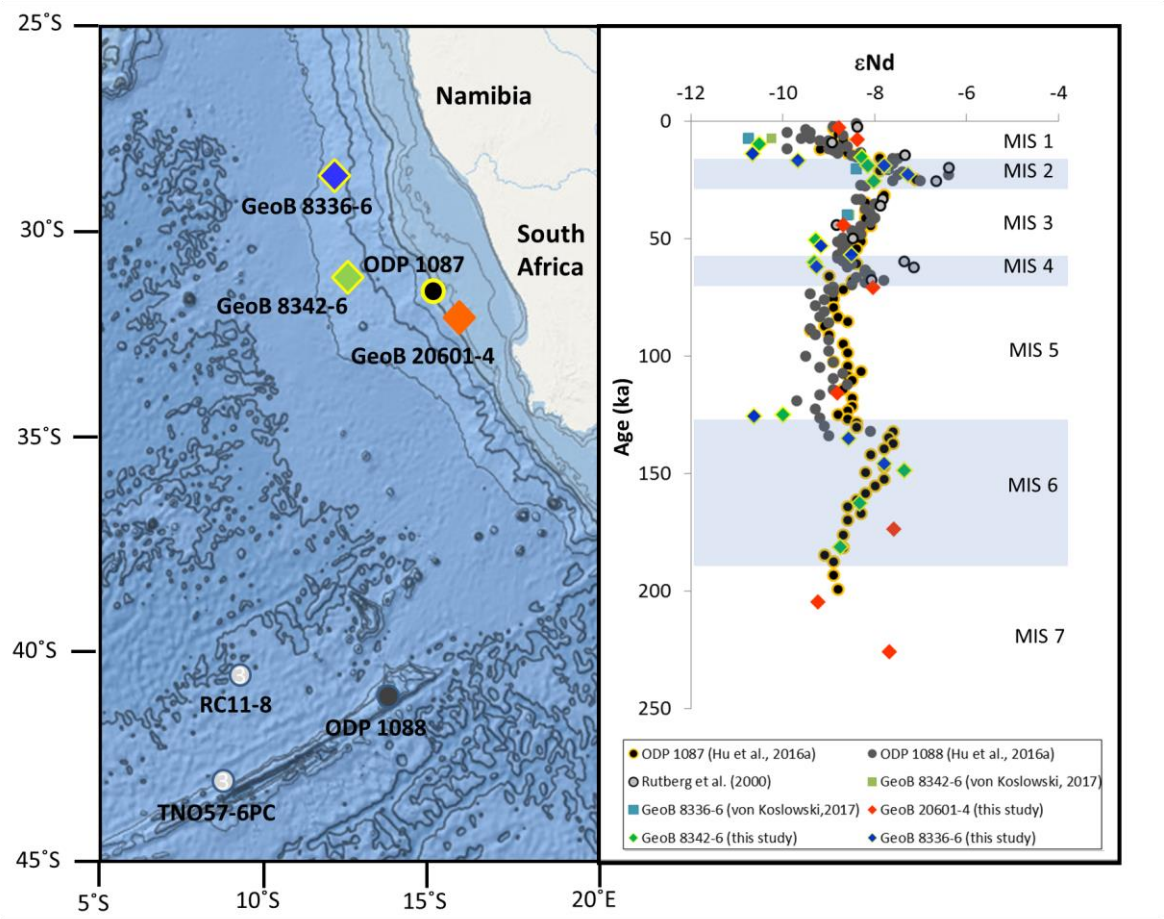

Fig. 8.13. Core locations and εNd of foraminifera in previous studies and for this study. Glacial periods are shown in the light blue shaded areas of the plot. The ocean basemap is from the National Oceanic and Atmospheric Administration (NOAA) Bathymetric Data Viewer.

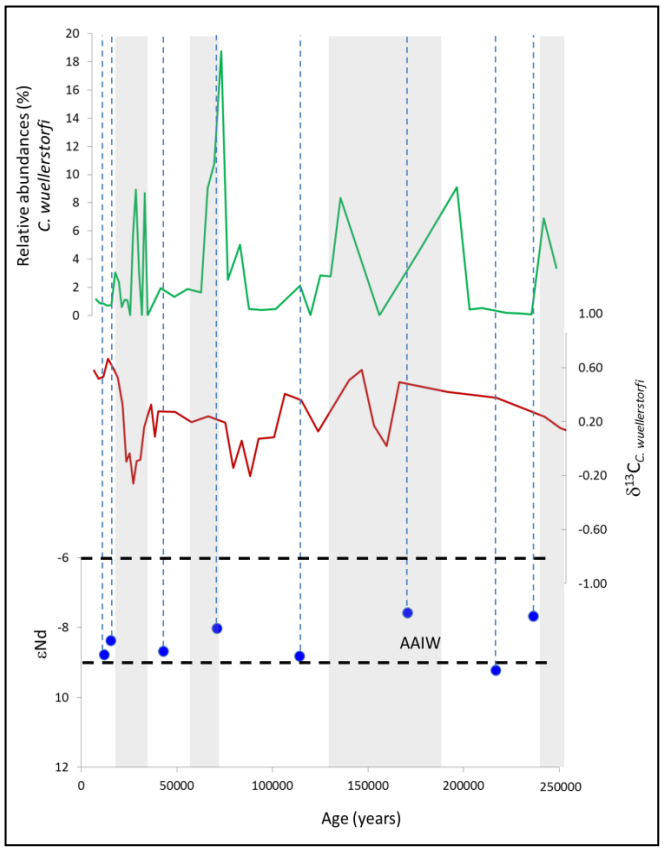

Fig. 8.14. Comparison (indicated by dashed lines) between *C. wuellerstorfi* relative abundances, $\delta^{13}C$ and εNd values in core GeoB 20601-4. Glacial periods are indicated by the shaded regions. The black horisontal dashed lines indicate the range of AAIW εNd values based on references cited within the

During MIS 1 εNd values in the AAIW decrease as in the two deep water cores. The increasing $\delta^{13}C$ values and *C. wuellertsorfi* abundances at these two sites support a weaker southern sourced water mass during MIS 1 when NADW strengthened. Although these three records are consistent with each other, the overall weak and positive correlation between the εNd values and the $\delta^{13}C$ and *C. wuellertsorfi* in core GeoB 20601-4 can possibly be explained by the shallower water depth and closer proximity to the continental shelf and upwelling processes. The $\delta^{13}C$ record may include coastal upwelling productivity and organic matter inputs rather than the presence or influence of the NADW, as the deep water mass would not reach the core site. The intensified circulation of AAIW during glacial periods, which is rich in oxygen content (Arz et al., 1999; Stramma and England, 1999) also favours *C. wuellerstorfi*, which is more adapted to high oxygen bottom waters (Gooday, 1988).

8.6. Conclusions

Late Quaternary neodymium isotopic (εNd) records from foraminifera recovered from 3.5 km water depth indicate a strong SCW influence during glacial maxima (MIS 6 and 2). The largest decreases in εNd occur during glacial terminations (GT II and I) indicating the switch from SCW to NADW over the study area. NADW influence then gradually decreases from MIS 5 to 2 where SCW influence peaks again before decreasing in the Holocene.

There is a strong inverse correlation between εNd and *Cibicidoides wuellerstorfi* relative abundances for most part of the deeper cores' records where decreasing εNd values are matched with increasing *C. wuellerstorfi* relative abundances during times of enhanced NADW flow along the margin and the opposite for increased SCW flow. The *C. wuellerstorfi* (favoured by high oxygen contents) relative abundance increases during times when NADW influence increases are attributed to the well ventilated nature of the NADW compared to the southern sourced water masses of the AABW and LCDW. Relative abundances of *C. wuellerstorfi* are however influenced by seasonal inputs of phytodetritus and productivity and may possibly account for discrepancies in the MIS 2 and MIS 1 record of core GeoB 8342-6. Basing deep water mass reconstructions on *C. wuellerstorfi* abundances should therefore be confirmed by other methods as well, such as εNd and benthic $\delta^{13}C$ analyses. The $\delta^{13}C$ record for core GeoB 8336-6 does show increased SCW influence in the study area during glacial periods, but the rapid decline in εNd values indicating decreased SCW influence during glacial terminations is consistent with the largest increase in $\delta^{13}C$ values to the order of ~1‰. The εNd and $\delta^{13}C$ records indicate similar NADW/SCW configurations during the early MIS 5 and MIS 1. The $\Delta\delta^{13}C$ record indicates similar shifts in productivity associated with the high nutrient SCW changing to lower nutrient NADW during glacial terminations. The $\Delta\delta^{13}C$ trend also indicates that AAIW is relatively lower in nutrient content compared to the deeper cores.

AAIW in the study area shows a different overall trend compared to the deeper water sites, but still reflects slight glacial-interglacial variations. The strength of AAIW is greater during glacial periods and weakens during interglacial periods. An overall weak and positive correlation exist between the εNd values, $\delta^{13}C$ and *C. wuellertsorfi* relative abundances in core GeoB 20601-4 which is explained by the proximity of coastal upwelling productivity to the upper slope and intensified AAIW circulation during glacial periods which would increase oxygen content, favouring higher *C. wuellerstorfi* abundances.

References

Adkins, J.F., McIntyre, K., Schrag, D.P., 2002. The salinity, temperature, and δ18O of the glacial deep ocean. Science 298(5599), 1769-1773.

Aiken, C.M., England, M.H., 2008. Sensitivity of the present-day climate to freshwater forcing associated with Antarctic sea ice loss. Journal of Climate 21, 3936-3946.

Arsouze, T., Dutay, J-C., Kageyama, M., Lacan, F., Alkama, R., Marti, O., Jeandel, C., 2008. Influence of the Atlantic thermohaline circulation on neodymium isotopic composition at the Last Glacial Maximum – a modelling sensitivity study. Climate of the Past Discussions 4, 309-334.

Arz, H.W., Pätzold, J., Wefer, G., 1999. The deglacial history of the western tropical Atlantic as inferred from high resolution stable isotope records off northeastern Brazil. Earth and Planetary Science Letters 167(1), 105-117.

Berger, W.H., Wefer, G., 1996. Expeditions into the past: Paleoceanographic studies in the South Atlantic. In: Wefer, G and Berger, W.H., Siedler, G., Webb, D.J. (Eds.), The South Atlantic: Present and Past

Circulation. Springer-Verlag, Berlin, 363-410.

Bianchi, C., Gersonde, R., 2002. The Southern Ocean surface between Marine Isotope Stages 6 and 5d: Shape and timing of climate changes. Palaeogeography, Palaeoclimatology, Palaeoecology 187, 151-177.

Bickert, T., Mackensen, A., 2003. Last Glacial to Holocene changes in South Atlantic deep water circulation. In: The South Atlantic in the Late Quaternary. Springer, Berlin, Heidelberg, 671-693.

Bickert, T., Wefer, G., 1999. South Atlantic and benthic foraminifer $\delta^{13}C$ deviations: implications for reconstructing the Late Quaternary deep-water circulation. Deep Sea Research Part II: Topical Studies in Oceanography 46, 437-452.

Böhm, E., Lippold, J., Gutjahr, M., Frank, M., Blaser, P., Antz, B., Fohlmeister, J., Frank, N., Andersen, M.B., Deininger. M., 2015. Strong and deep Atlantic meridional overturning circulation during the last glacial cycle. Nature 517, 73.

Boyle, E.A., Keigwin, L.D., 1982. Deep circulation of the North Atlantic over the last 200,000 years: Geochemical evidence. Science 218(4574), 784-787.

Bozzano, G., Kuhlmann, H., Alonso, B., 2002. Storminess control over African dust input to the Moroccan Atlantic margin (NW Africa) at the time of maxima boreal summer insolation: a record of the last 220 kyr. Palaeogeography, Palaeoclimatology, Palaeoecology 183, 155-168.

Broecker, W.S., 1991. The great ocean conveyor. Oceanography 4(2), 79-89.

Burton, K.W., Vance, D., 2000. Glacial–interglacial variations in the neodymium isotope composition of seawater in the Bay of Bengal recorded by planktonic foraminifera. Earth and Planetary Science Letters 176, 425-441.

Carter, R.M., Gammon, P.R., Millwood, L., 2004. Glacial–interglacial (MIS 1–10) migrations of the subtropical front across ODP Site 1119, Canterbury Bight, Southwest Pacific Ocean. Marine Geology 205, 29-58.

Clark, P.U., Alley, R.B., Pollard, D., 1999. Northern Hemisphere ice-sheet influences on global climate change. Science 286, 1104-1111.

Clark, P.U., Dyke, A.S., Shakun, J.D., Carlson, A.E., Clark, J., Wohlfarth, B., Mitrovica, J.X., Hostetler, S.W., McCabe, A.M., 2009. The last glacial maximum. Science 325, 710-714.

Clark, P.U., Pisias, N.G., Stocker, T.F., Weaver, A.J., 2002. The role of the thermohaline circulation in abrupt climate change. Nature, 415, 863-869.

Clark, P.U., Shakun, J.D., Baker, P.A., Bartlein, P.J., Brewer, S., Brook, E., Carlson, A.E., H., Kaufman, D.S., Liu, Z., Marchitto, T.M. 2012. Global climate evolution during the last deglaciation. Proceedings of the National Academy of Sciences 109, E1134-E1142.

Compton, J.S., Malubisana, J., McMillan, I.K., 2002. Origin and age of phosphorite from the Last Glacial Maximum to Holocene transgressive succession off the Orange River, South Africa. Marine Geology 186, 243-261.

Compton, J.S., Wiltshire, J.G., 2009. Terrigenous sediment export from the western margin of South Africa on glacial

to interglacial cycles. Marine Geology 266, 212-222.

Cortese, G.., Abelmann, A., 2002. Radiolarian-based paleotemperatures during the last 160 kyr at ODP Site 1089 (Southern Ocean, Atlantic Sector). Palaeogeography, Palaeoclimatology, Palaeoecology 182, 259-286.

Curry, W.B., Lohmann, G.P., 1982. Carbon isotopic changes in benthic foraminifera from the western South Atlantic: Reconstruction of glacial abyssal circulation patterns. Quaternary Research 18(2), 218-235.

Deaney, E.L., Barker, S., van de Flierdt, T., 2017. Timing and nature of AMOC recovery across Termination 2 and magnitude of deglacial CO_2 change. Nature communications 8, 14595.

Delworth, T.L., Clark, P.U., Holland, M., Johns, T., Kuhlbrodt, T., Lynch-Stieglitz, C., Seager, R., Weaver, A.J., R. Zhang., 2008. The potential for abrupt change in the Atlantic Meridional Overturning Circulation. In: Abrupt Climate Change. A report by the U.S. Climate Change Science Program and the Subcommittee on Global Change Research. U. S. Geological Survey, Reston, 258-359.

Emery, W.J., 2001. Water types and water masses. Encyclopedia of Ocean Sciences 6, 3179-3187.

Emery, W.J., Meincke, J., 1986. Global water masses-summary and review. Oceanologica Acta 9, 383-391.

Franzese, A.M., Hemming, S.R., Goldstein, S.L., Anderson, R.F., 2006. Reduced Agulhas Leakage during the Last Glacial Maximum inferred from an integrated provenance and flux study. Earth and Planetary Science Letters 250, 72-88.

Garcia-Solsona, E., Jeandel, C., Labatut, M., Lacan, F., Vance, D., Chavagnac, V., Pradoux, C. 2014., Rare earth elements and Nd isotopes tracing water mass mixing and particle–seawater interactions in the SE Atlantic. Geochimica et Cosmochimica Acta 125, 351–372.

Gebbie, G., 2014. How much did glacial North Atlantic water shoal? Paleoceanography 29, 190-209.

Goldstein, S.L., Hemming, S.R., 2003. Long-lived isotopic tracers in oceanography, paleoceanography, and ice-sheet dynamics. Treatise on Geochemistry 6, 625.

Gooday, A.J., 1988. A response by benthic foraminifera to the deposition of phytodetritus in the deep sea. Nature 332, 70-73.

Gordon, A.L., 1974. Varieties and variability of Antarctic bottom water. In: Processus de Formation des Eaux Oceaniques Profondes (en particulier en Mediterranee Occidentale). Editions du Centre National de la Recherche Scientifique, Paris, 215, 33–47.

Gordon, A. L., 2009. Bottom water formation. Ocean Currents, 263-269.

Gordon, A.L., Weiss, R.F., Smethie, W.M., Warner, M.J., 1992. Thermocline and intermediate water communication between the South Atlantic and Indian Oceans. Journal of Geophysical Research: Oceans 97, 7223-7240.

Howe, J.N., Piotrowski, A.M., Hu, R., Bory, A., 2017. Reconstruction of east–west deep water exchange in the low latitude Atlantic

Ocean over the past 25,000 years. Earth and Planetary Science Letters 458, 327-336.

Howe, J.N., Piotrowski, A.M., Oppo, D.W., Huang, K.F., Mulitza, S., Chiessi, C.M., Blusztajn, J., 2016. Antarctic intermediate water circulation in the South Atlantic over the past 25,000 years. Paleoceanography 31, 1302-1314.

Hu, R., Noble, T.L., Piotrowski, A.M., McCave, I.N., Bostock, H.C., Neil, H.L., 2016a. Neodymium isotopic evidence for linked changes in Southeast Atlantic and Southwest Pacific circulation over the last 200 kyr. Earth and Planetary Science Letters 455, 106-114.

Hu, R., Piotrowski, A.M., Bostock, H.C., Crowhurst, S., Rennie, V., 2016b. Variability of neodymium isotopes associated with planktonic foraminifera in the Pacific Ocean during the Holocene and Last Glacial Maximum. Earth and Planetary Science Letters 447, 130-138.

Jacobsen, S.B., Wasserburg, G.J., 1980. Sm-Nd isotopic evolution of chondrites. Earth and Planetary Science Letters 50, 139-155.

Jeandel, C., 1993. Concentration and isotopic composition of Nd in the South Atlantic Ocean. Earth and Planetary Science Letters 117, 581–591.

Kaiho, K., 1994. Benthic foraminiferal dissolved-oxygen index and dissolved-oxygen levels in the modern ocean. Geology 22, 719-722.

Kawano, T., Fukasawa, M., Kouketsu, S., Uchida, H., Doi, T., Kaneko, I., Aoyama, M., Schneider, W., 2006. Bottom water warming along the pathway of lower circumpolar deep water in the Pacific Ocean. Geophysical Research Letters 33(23), doi: 10.1029/2006GL027933

Key, R.M., Tanhua, T., Olsen, A., Hoppema, M., Jutterström, S., Schirnick, C., Van Heuven, S., Lin, X., Wallace, D.W., Mintrop, L., 2009. The CARINA data synthesis project: introduction and overview. Earth System Science Data 2, 105-121.

Klevenz, V., Vance, D., Schmidt, D.N., Mezger, K., 2008. Neodymium isotopes in benthic foraminifera: core-top systematics and a down-core record from the Neogene south Atlantic. Earth and Planetary Science Letters 265, 571-587.

Kroopnick, P.M., 1985. The distribution of ^{13}C of ΣCO_2 in the world oceans. Deep Sea Research Part A. Oceanographic Research Papers 32, 57-84.

Krueger, S., Leuschner, D.C., Ehrmann, W., Schmiedl, G., Mackensen, A., 2012. North Atlantic Deep Water and Antarctic Bottom Water variability during the last 200ka recorded in an abyssal sediment core off South Africa. Global and Planetary Change 80, 180-189.

Kuhlbrodt, T., Griesel, A., Montoya, M., Levermann, A., Hofmann, M., Rahmstorf, S., 2007. On the driving processes of the Atlantic meridional overturning circulation. Reviews of Geophysics 45(2), doi:10.1029/2004RG000166

Kuhn, G., Diekmann, B., 2002. Late Quaternary variability of ocean circulation in the southeastern South Atlantic inferred from the terrigenous sediment record of a drift deposit in the southern Cape Basin (ODP Site 1089). Palaeogeography, Palaeoclimatology, Palaeoecology 182, 287-303.

Larson, R.L., Ladd, J.W., 1973. Evidence for the opening of the South Atlantic in the Early Cretaceous. Nature 246, 209.

Lisiecki, L.E., Raymo, M.E., 2005. A Pliocene-Pleistocene stack of 57 globally distributed benthic $\delta^{18}O$ records. Paleoceanography 20, PA1003, doi:10.1029/2004PA001071.

Lohmann, G.P., 1978a. Abyssal benthonic foraminifera as hydrographic indicators in the western South Atlantic Ocean. The Journal of Foraminiferal Research 8(1), 6-34.

Lohmann, G.P., 1978b. Response of the Deep Sea to Ice Ages. Oceanus 21(4), 58-64.

Lutjeharms, J.R.E., 1996. The exchange of water between the South Indian and South Atlantic Oceans. In: The South Atlantic. Springer, Berlin, Heidelberg, 125-162.

Lutjeharms, J.R.E., Stockton, P.L., 1987, Kinematics of the upwelling front off southern Africa. South African Journal of Marine Science 5, 35–49.

Lynch-Stieglitz, J., Adkins, J.F., Curry, W.B., Dokken, T., Hall, I.R., Herguera, J.C., Hirshci, J.J-M., Ivanova, E.V., Kissel, C., Marchal, O., Marchitto, T.M., McCave, I.N., McManus, J.F., Mulitza, S., Ninnemann, U., Peeters, F., Yu, E-F., Zahn, R., 2007. Atlantic meridional overturning circulation during the Last Glacial Maximum. Science 316, 66-69.

Martinson, D.G., McKee, D.C., 2012. Transport of warm Upper Circumpolar Deep Water onto the western Antarctic Peninsula continental shelf. Ocean Science, 8(4), 433-442.

Nelson, G., Hutchings, L., 1983. The Benguela upwelling area. Progress in Oceanography 12, 333-356.

Noël, D., Melguen, M., 1978. Nannofacies of cape basin and walvis ridge sediments, lower Cretaceous to Pliocene (leg 40). Initial Reports of the Deep Sea Drilling Project 60, 473-510.

Nürnberg, D., Müller, R.D., 1991. The tectonic evolution of the South Atlantic from Late Jurassic to present. Tectonophysics 191, 27-53.

Pahnke, K., Goldstein, S.L., Hemming, S.R., 2008. Abrupt changes in Antarctic Intermediate Water circulation over the past 25,000 years. Nature Geoscience 1, 870.

Paillard, D., Labeyrie, L., Yiou, P., 1996. Macintosh program performs time-series analysis. Eos, Transactions American Geophysical Union 77, 379-379.

Palmer, M.R., Elderfield, H., 1985. Variations in the Nd isotopic composition of foraminifera from Atlantic Ocean sediments. Earth and Planetary Science Letters 73, 299-305.

Piepgras, D.J., Wasserburg, G.J., 1982. Isotopic composition of neodymium in waters from the Drake Passage. Science 217, 207–217.

Piepgras, D.J., Wasserburg, G.J., 1987. Rare earth element transport in the western North Atlantic inferred from Nd isotopic observations. Geochimica et Cosmochimica Acta 51, 1257-1271.

Piotrowski, A.M., Galy, A., Nicholl, J.A. L., Roberts, N., Wilson, D.J., Clegg, J.A., Yu, J., 2012. Reconstructing deglacial North and South Atlantic deep water sourcing using foraminiferal Nd isotopes. Earth and Planetary Science Letters 357, 289-297.

Piotrowski, A.M., Goldstein, S.L., Hemming, S.R., Fairbanks, R.G., 2005. Temporal relationships of carbon cycling and ocean

circulation at glacial boundaries. Science 307, 1933-1938.

Rahmstorf, S., 2002. Ocean circulation and climate during the past 120,000 years. Nature, 419, 207.

Rau, A.J., 2002. A late Quaternary history of Agulhas-Benguela interactions from two sediment cores on the western continental slope of South Africa. PhD thesis. University of Cape Town, 315 pp.

Rau, A. J., Rogers, J., Lutjeharms, J. R. E., Giraudeau, J., Lee-Thorp, J. A., Chen, M. T., Waelbroeck, C., 2002. A 450-kyr record of hydrological conditions on the western Agulhas Bank Slope, south of Africa. Marine Geology 180, 183-201.

Reid, J.L., 1989. On the total geostrophic circulation of the South Atlantic Ocean: Flow patterns, tracers, and transports. Progress in Oceanography 23, 149-244.

Roberts, N.L., Piotrowski, A.M., Elderfield, H., Eglinton, T.I., Lomas, M.W., 2012. Rare earth element association with foraminifera. Geochimica et Cosmochimica Acta 94, 57-71.

Rutberg, R.L., Hemming, S.R., Goldstein, S.L., 2000. Reduced North Atlantic Deep Water flux to the glacial Southern Ocean inferred from neodymium isotope ratios. Nature 405, 935.

Sarnthein, M., Winn, K., Jung, S. J., Duplessy, J. C., Labeyrie, L., Erlenkeuser, H., Ganssen, G., 1994. Changes in east Atlantic deepwater circulation over the last 30,000 years: Eight time slice reconstructions. Paleoceanography 9, 209-267.

Schlitzer, R., 2018. Ocean Data View, odv.awi.de

Schmiedl, G., Mackensen, A., 1997. Late Quaternary paleoproductivity and deep water circulation in the eastern South Atlantic Ocean: Evidence from benthic foraminifera. Palaeogeography, Palaeoclimatology, Palaeoecology 130, 43-80.

Schnitker, D., 1974. West Atlantic abyssal circulation during the past 120,000 years. Nature 248(5447), 385.

Schnitker, D., 1979. The deep waters of the western North Atlantic during the past 24,000 years, and the re-initiation of the western boundary undercurrent. Marine Micropaleontology 4, 265-280.

Schnitker, D., 1980. Quaternary deep-sea benthic foraminifers and bottom water masses. Annual Review of Earth and Planetary Sciences 8(1), 343-370.

Stichel, T., Frank, M., Rickli, J., Haley, B.A., 2012. The hafnium and neodymium isotope composition of seawater in the Atlantic sector of the Southern Ocean. *Earth and Planetary Science Letters* 317–318, 282–294.

Stramma, L., England, M., 1999. On the water masses and mean circulation of the South Atlantic Ocean. Journal of Geophysical Research: Oceans 104(C9), 20863-20883.

Stramma, L., Peterson, R.G., 1989. Geostrophic transport in the Benguela Current Region. Journal of Physical Oceanography 19, 1440-1448.

Streeter, S.S., 1973. Bottom Water and Benthonic Foraminifera in the North Atlantic—Glacial-Interglacial Contrasts 1. Quaternary Research 3(1), 131-141.

Tachikawa, K., Piotrowski, A.M., Bayon, G., 2014. Neodymium associated with foraminiferal carbonate as a recorder of seawater isotopic signatures. Quaternary Science Reviews 88, 1-13.

Talley, L.D., 1996. Antarctic intermediate water in the South Atlantic. In :The South Atlantic. Springer, Berlin, Heidelberg, 219-238.

Vance, D., Burton, K., 1999. Neodymium isotopes in planktonic foraminifera: a record of the response of continental weathering and ocean circulation rates to climate change. Earth and Planetary Science Letters 173, 365-379.

Von Koslowski, R., 2017. Glacial-interglacial variations of the water masses in the southeast Atlantic Ocean derived from foraminiferal neodymium isotope ratios. Unpublished M.Sc., University of Cape Town, 75 pp.

Waelbroeck, C., Labeyrie, L., Michel, E., Duplessy, J.C., McManus, J.F., Lambeck, K., Balbon, E., Labracherie, M., 2002. Sea-level and deep water temperature changes derived from benthic foraminifera isotopic records. Quaternary Science Reviews 21(1-3), 295-305.

Wefer, G.A., Berger, W.H., Bickert, T., Donner, B., Fischer, G., von Mücke, S.K., Meinecke, G., Müller, P.J., Mulitza, S., Niebler, H.S., Pätzold, J. 1996. Late Quaternary surface circulation of the South Atlantic: The stable isotope record and implications for heat transport and productivity. In: The South Atlantic. Springer, Berlin, Heidelberg, 461-502.

Wei, R., Abouchami, W., Zahn, R., Masque, P., 2016. Deep circulation changes in the South Atlantic since the Last Glacial Maximum from Nd isotope and multi-proxy records. Earth and Planetary Science Letters 434, 18-29.

Whitworth III, T., Orsi, A.H., Kim, S.-J., Nowlin Jr., W.D., 1998. Water masses and mixing near the Antarctic Slope Front. Antarctic Research Series 75, 1–27.

Woodruff, F., Savin, S.M., Douglas, R.G., 1980. Biological fractionation of oxygen and carbon isotopes by recent benthic foraminifera. Marine Micropaleontology 5, 3–11.

Zabel, M., and cruise participants., 2017. Climate Archives in Coastal Waters of Southern Africa–Cruise No. *M123*.

Zahn, R., Winn, K., Sarnthein, M., 1986. Benthic foraminiferal $\delta^{13}C$ and accumulation rates of organic carbon: *Uvigerina peregrina* group and *Cibicidoides wuellerstorfi*. Paleoceanography 1, 27–42.

Chapter 9

Synthesis and Conclusions

9. Synthesis and Conclusions

9.1. Introduction

The use of fossil foraminifera is crucial in understanding the stratigraphy and the environmental and oceanographic changes along the southwestern margin of Africa. In this study fossil foraminifera have aided in the dating of Namibian shelf and western South African slope sediments, the determination of palaeo-environmental changes associated with the Benguela Upwelling System (BUS) and the environmental and oceanographic changes during the Neogene and Quaternary.

This chapter provides a synthesis of this thesis and discusses the results in addressing the main objectives, which include the determination of the stratigraphy, the biogeography and the environmental significance of planktic and benthic foraminifera recovered in Namibian shelf and western South African slope sediments. This chapter furthermore outlines the limitations, future endeavours and recommendations of this project and for further foraminiferal research along the western margin of South Africa.

9.2.1. Stratigraphy of shelf sediments along the southwestern margin of Africa

The upper units of shelf sediments of western South Africa and Namibia are rich in phosphorite deposits owing to the highly productive BUS (Compton et al., 2004; Compton and Bergh, 2016). Phosphorite is an important mineral resource to the agricultural sector and Compton and Bergh (2016) provided an assessment into the size, geochemistry, distribution and origin of phosphorite deposits along the shelf of Namibia. The marine sedimentary record of the southwestern shelf of Africa records the timing of the initiation and the intensification of the BUS. Sediments from the South African shelf have been dated using strontium isotope stratigraphy (SIS) (Compton et al., 2002, 2004; Wigley and Compton, 2006, 2007) and found that phosphogenesis started in the latest Oligocene along the western margin of South Africa with major phosphorite formation throughout the early Miocene with Miocene phosphorites being reworked in Pleistocene sediments. Along the Namibian shelf phosphorite formation was found to start in the latest Miocene, but was most intense in the Plio/Pleistocene, significantly younger than in areas of the southern BUS (Compton and Bergh, 2016).

The middle Miocene shelf sediments south of the Kunene River are composed of a calcareous olive-green mud rich in foraminifera and nannofossils. The olive-green mud unit was dated to 16 to 14 Ma using SIS (Compton and Bergh, 2016) and planktic indicator foraminifera *Globigerinoides bisphericus* and *Globoquadrina dehiscens* (Bergh et al., 2018). Phosphorite in the middle Miocene unit is restricted to a few grains and is interpreted to be reworked material (Compton and Bergh, 2016).

The sand fractions of the Pliocene unit from the Walvis Bay-Lüderitz shelf were found to be a mixture of foraminifera and pelletal phosphorites. The foraminifera from this unit were largely fragmented, but species identification determined the assemblage to have been reworked and is composed of Mio-Pliocene foraminifera. The planktic index species (*Globorotalia (Globoconella) inflata*) in the unit together with

SIS provided a date of the unit underlying the sandy pelletal phosphorite units off central Namibia to be Plio-Pleistocene (Compton and Bergh, 2016).

The shelf record along the margin of western South Africa and Namibia is highly condensed with several erosional contacts having been recorded throughout the shelf (Compton et al., 2004; Wigley and Compton, 2006, 2007; Compton and Bergh, 2016). This is no different along the northern Namibian shelf as the middle-Miocene olive-green mud unit is overlain by a black pelletal phosphorite-rich layer dated to the Pleistocene. The age determined by SIS was confirmed by the planktic indicator *Globorotalia truncatulinoides* (Fig. 9.1). These phosphorite units are composed of abundant pelletal phosphorite, phosphorite pebbles, glauconite, minor quartz, foraminifera, bryozoan fragments, fish material (teeth, scales, otoliths, vertebrae, bone fragments), whale bone fragments, ostracods, and fragmented and whole mollusc shells (gastropods and bivalves). The Walvis Bay-Lüderitz cores, which coarsen upwards allowed for the determination of three age periods in which the phosphorite units formed. A slightly shelly muddy unit was found to be early Pleistocene to middle Pleistocene in age. The moderately shelly phosphorite sand unit was dated to the middle to late Pleistocene and the upper gravelly shelly phosphorite sand units were found to be late Pleistocene to Holocene in age (Compton and Bergh, 2016).

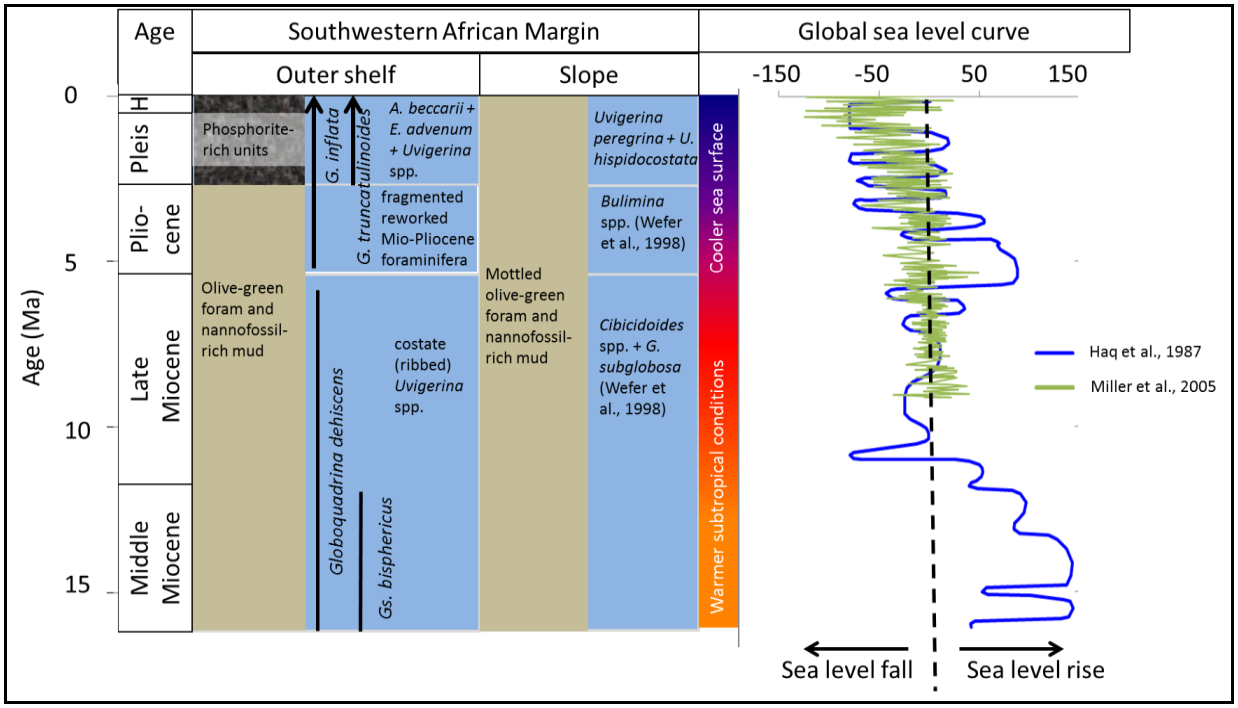

Fig. 9.1. Synthesis of results from this study including indicator species for the Miocene, Pliocene, Pleistocene and Holocene (H) shelf sediments and benthic foraminifera with high relative abundances related to sea level curves (Haq et al., 1987; Miller et al., 2005). Taxa indicated for the Miocene and Pliocene slope are from Wefer et al. (1998).

The Namibian slope sediments are ~300 times thicker than the shelf sediments (Wefer et al., 1998; Compton and Bergh, 2016). The sediments along the slope of western South Africa and Namibia are brown to olive-green in colour with abundant foraminifera, nannofossils and minor to trace abundances of quartz and glauconite (Compton and Wiltshire, 2009; this study). The ages of the slope sediments are determined by nannofossil and planktic foraminiferal indicator species (Wefer et al., 1998) and carbonate $\delta^{18}O$, primarily benthic *Cibicidoides wuellerstorfi* and planktic *Globorotalia (Globoconella) inflata* foraminifera (Rau et al., 2002; this study).

The sedimentation rate along the margin was determined to be between 0.3 and 1.3 cm/kyr in this study with higher sedimentation rates primarily during interglacial periods and lower during glacial periods owing to an increased export of sediment to greater depths in the Cape Basin during glacial periods as a result of an increase in the energy levels at the shelf-slope break, such as the strength of bottom water currents (Compton and Wiltshire, 2009). Consequently, benthic foraminiferal accumulation rates (BFARs) are also higher during interglacial periods compared to glacial periods. The enhanced glacial bottom water current strength allows for the entrainment and transport of sand-sized particles (Compton and Wiltshire, 2009) including foraminiferal tests to lower depths of the basin which could influence the observed BFARs.

9.2.2. Late Cenozoic distribution and influences on planktic foraminifera along the southwestern margin of Africa

Abundant planktic taxa dated to the middle-Miocene in northern Namibian outer shelf sediments include *Trilobatus immaturus* and *Globigerina bulloides* (Bergh et al., 2018). The relative abundances of *T. immaturus* decrease at the middle-Miocene/Pleistocene contact where this species completely disappears in the Pleistocene section of the cores. The relative abundances of *G. bulloides* increases in the phosphorite units to become the dominant species in the Pleistocene sections of the northern Namibian as well as the Walvis Bay-Lüderitz cores. Indicator planktic species *Globoquadrina dehiscens* and *Globigerinoides bisphericus* only occur in the middle Miocene units. These species (*T. immaturus, G. bulloides, Gq. dehiscens* and *Gs. bisphericus*) were also recorded in middle Miocene deposits of the Congo Basin (Kender et al., 2008).

The high relative abundance of planktic species *T. immaturus* with lesser abundances of *Gs. ruber* and *T. sacculifer* indicate warmer sea surface conditions during a period in which global sea surface temperatures were higher during the Mid Miocene Climatic Optimum (You et al., 2009) and the southward extent of the Angola-Benguela Front relative to the modern-day position (Hoetzel et al., 2017) which allowed for warmer conditions along the northern Namibian margin.

The minor relative abundances of *Globigerinoides ruber* (white) increases at the middle Miocene/Pleistocene boundary of the northern Namibian cores while *Trilobatus sacculifer* decrease in the Pleistocene section of the cores. In the Plio-Pleistocene units of the northern Namibian and Walvis Bay-Lüderitz cores *Gr. (Gc.) inflata* and *Gr. truncatulinoides* appear to form minor to trace abundances in the Pleistocene sections of the cores. Other minor planktic species in the Pleistocene sections of the cores along the Namibian shelf include *Gs ruber*

(white), *Globorotalia menardii, T. sacculifer* and *Orbulina universa*.

The shelf of Namibia and western South Africa in Recent (surface grab) sediments are dominated by *G. bulloides.* These shelf assemblages from surface grab samples (Lowry, 1987; Giraudeau, 1993) containing abundant *G. bulloides, Gr. (Gc.) inflata, Neogloboquadrina pachyderma* and minor abundances of *Gs ruber* (white), *Gr. menardii, T. sacculifer* and *O. universa* have therefore been present along the margin since the early Pleistocene owing to their occurrence in the early Pleistocene sections of the cores of this study. The occurrences of these taxa in noticeable and high abundances indicate cooler sea surface conditions along the margin relative to the warmer conditions of the middle Miocene.

In contrast to the shelf sediments from this study recording abundant *G. bulloides,* the South African slope sediments recorded *Gr. (Gc.) inflata* as the dominant planktic species followed by *G. bulloides* with decreasing relative abundances at lower depths. The relative abundances of the subtropical species *O.universa* and *Gs. ruber* (white) increase towards the lower depths of the three cores of this study. The transitional species *Gr. (Gc.) inflata* and *G. bulloides* do not display a particular glacial-interglacial cyclicity whereas the colder water species *Ng. pachyderma* displays general higher relative abundances during glacial periods and lower relative abundances during interglacial periods. The subtropical and tropical species *Gs. ruber* (white) and *Gr. menardii* are generally higher in relative abundance during interglacial periods. The tropical species *T. sacculifer* display higher relative abundances during MIS 1, particularly in the deeper GeoB 8336-6 core.

Results from this study indicate upwelling intensity, the northwards migration of the polar fronts during glacial periods and the intrusion of warm South Indian Ocean waters allowing for increased Agulhas Leakage (Rau et al., 2002) during interglacial periods are the major drivers of the observed planktic faunal compositions on the slope. Previous studies have highlighted *Gr. (Gc.) inflata* to be indicative of oligotrophic waters (Giraudeau, 1993), *G. bulloides* of upwelling conditions (Giraudeau, 1993), *Ng. pachyderma* of colder polar and subpolar waters (Bé and Tolderlund, 1971; Kucera, 2007; BouDagher-Fadel, 2015) and subtropical species *O. universa* and *Gs. ruber* of intrusion of warmer waters from the southern Indian Ocean through Agulhas Leakage in the late Quaternary (Rau et al., 2002).

9.2.3. Late Cenozoic distribution and palaeoenvironments of benthic foraminifera along the southwestern margin of Africa

The benthic foraminifera dated to the middle Miocene were relatively large with many taxa >1 mm compared to the smaller foraminifera dated to the Quaternary along the shelf and slope. The middle Miocene assemblage is dominated by costate *Uvigerina* spp. from the *U. peregrina* group. Taxa from the middle Miocene unit on the northern Namibian outer shelf have been recorded as slope foraminifera and in deeper settings (e.g. Kender et al., 2008) indicating that during the MMCO sea level was also higher along the Namibian margin. Ocean floor conditions also changed from oligotrophic environments during the middle Miocene where few infaunal taxa can survive to eutrophic conditions in the Pleistocene where an increase in infaunal taxa was recorded.

The Namibian Pleistocene benthic assemblage is dominated by abundant *Uvigerina peregina, Elphidium advenum* and *Ammonia beccarii.* The taxa associated with this assemblage were found to have wide distributions across the BUS and into the south and east coasts of South Africa in marine surficial sediments when compared to data from previous studies (Martin, 1981; Lowry, 1987; Schmidt-Sinns, 2008). Three associations in the Pleistocene sections of the Walvis Bay-Lüderitz cores were identified corresponding to the three phosphorite units identified in Compton and Bergh (2016). In unit 3, the slightly shelly muddy unit (early to middle Pleistocene) *Uvigerina* spp. dominated the association. In unit 2, the moderately shelly phosphorite sand unit (middle to late Pleistocene) *Elphidium advenum* dominated the association and *Ammonia beccarii* increased in relative abundance. In unit 1, the gravelly shelly phosphorite sand unit (late Pleistocene to Holocene) *Ammonia beccarii* dominates the association. Units 2 and 1 also corresponded to mollusc assemblages with *Lucinoma capensis* (bivalve), *Turritella declivis* and *Comitas saldanhae* (gastropods) dominating unit 2 and *Dosinia lupinus* (bivalve) and *Nassarius vinctus* (gastropod) dominating unit 1. These assemblages are also indicative of gradual shoaling conditions on the shelf during the Pleistocene consistent with increasingly lower sea-levels and greater sea-level amplitudes (Miller et al., 2005; Fig. 9.1). The shelf assemblages dated to the middle Pleistocene to Holocene also reflect inner shelf and marginal marine influences.

The benthic assemblages along the shelf are different from slope assemblages. The few species of benthic taxa occurring in very low relative abundances (<1%) in this study and in previous studies include *Ammonia beccarii, Hyalinea balthica, Quinqueloculina seminula, Cassidulina laevigata* and *Bulimina marginata*. Transport from the shelf to the slope was therefore found to be minimal as energy dispersion is too weak (Compton and Wiltshire, 2009) and the shelf too broad to suspend and transport large amounts of sand-sized components which include foraminifera. Taxa such as *Cassidulina* spp. (e.g. *C. laevigata*) and *Bulimina* spp. (*B. gibba, B. marginata, B. mexicana*) have broad bathymetric ranges and occur on the shelf and slope in higher abundances compared to the exclusively shelf species.

The predominant benthic foraminifera on the slope during the Pleistocene are *Uvigerina* spp. In the upper slope core GeoB 20601-4 *Uvigerina peregrina* is the dominant benthic species. In the deeper cores GeoB 8342-6 and 8336-6 *Uvigerina hispidocostata* is the dominant species. Wefer et al. (1998) also found *U. hispidocostata* to be a major species in ODP cores. The differences in *Uvigerina* spp. in the three cores are attributed to the depth preferences of these taxa in which costate *Uvigerina* spp. (e.g. *U. peregrina*) prefer shallower conditions compared to hispid and hispidocostate species (e.g. *U. hispidocostata, U. auberiana, U. proboscidea*). The hispid and hispidocostate forms show increased relative abundances during glacial periods when the influence of the nutrient-poor and oxygen-rich North Atlantic Deep Water (NADW) is weaker along the margin and $\delta^{13}C$ content is lower. The costate *U. peregrina* is more abundant during interglacial periods when the nutrient-poor and oxygen-rich AAIW is weaker and $\delta^{13}C$ content is higher. It therefore follows that costate, hispid and hispidocostate *Uvigerina* forms increase in abundance during periods of high nutrients and lower oxygen when the NADW and AAIW are weaker along the margin.

The benthic abundances were too low to extract neodymium isotopic compositions (εNd). Planktic foraminifera were sampled to determine bottom water mass variations along the western slope of South Africa. Planktic foraminifera preserve the bottom water εNd in their tests upon burial on the seafloor (Roberts et al., 2012; Tachikawa et al., 2014) and provide reliable results on changing deep water masses in the South Atlantic (Tachikawa et al., 2014; von Koslowski, 2017). Results from this study indicated by εNd, $\delta^{13}C_{C.\ wuellerstorfi}$ and *C. wuellerstorfi* relative abundances show that Southern Component Water (SCW) weakens and North Atlantic Deep Water (NADW) strengthens during Glacial Termination II (GT II). From MIS 5 to MIS 2 NADW gradually weakens again and SCW strengthens when there is a shift to a stronger influence of NADW along the margin during GT I. At the upper slope core site (874 m) AAIW showed glacial-interglacial fluctuations mirroring SACW/NADW variations illustrated by previous studies (Rutberg et al., 2001; Hu et al., 2016).

9.3. Limitations and future prospects

The resolution of data from foraminifera can still be improved upon spatially and on temporal scale. The complications in attaining a good temporal and spatial foraminiferal record, particularly from the shelf along southwestern Africa, are the substrates and erosional features along the margin not allowing for continuous records to be retrieved. Vibracores from the shelf and gravity cores in transects across different depths could be retrieved in future projects to determine the extent of oceanographic changes along the margin. The lack of data from Miocene sediments across the margin makes it difficult to identify periodicity or changes in the palaeoenvironments during this time period. This project indicates the occurrence of a completely different assemblage during the Pleistocene compared to the middle Miocene. The fragmented foraminifera recovered in Pliocene sediments from the Walvis Bay-Lüderitz cores show a mixture of Miocene and Pliocene foraminifera. Whether this assemblage is indicative of a transitional phase into colder conditions or whether the foraminifera are completely reworked would require more material to be studied. Either additional material should be recovered from the continental shelf, or marine sediments from slope cores could potentially be analysed to determine how gradual or abrupt the changes in depositional environments and assemblages were during the initiation of the BUS.

Although the age models were based on the cross-correlation between $\delta^{18}O$, mineral counts and faunal abundances, some of the specific MIS periods are not clearly identified by these methods. The identification of these MIS periods hinges upon the assumption or observations that no hiatuses are present in the record. The ages of the slope cores could be refined further, particularly GeoB 20601-4. Additional sampling for $\delta^{18}O$ on a higher resolution could be undertaken and the upper portion of the cores dated by ^{14}C obtained from accelerator mass spectrometry (AMS). Obtaining ^{14}C dates would allow for the presence of at least the MIS 3 to MIS 1. We should aim for a higher resolution and accurate assignment of the MIS periods to link the results of palaeoceanographic studies to particular time frames.

This study determined sea surface conditions based on planktic foraminiferal faunal compositions. It could be determined that certain

periods were warmer or cooler than others based on the faunal analyses, but how warm was warm? How cool was cool? We need to be more accurate and Mg/Ca palaeothermometry (Barker et al., 2005; van Raden et al., 2011) can address this question. Data from extant modern foraminifera in seawater could also be determined and compared to the fossil record. Future research in oceanographic and climate change studies could add to these data by sampling on decadal and multi-decadal timescales.

The study area and timeframe can be expanded to determine the interaction between ocean masses within the BUS as well as north and south of the system over a longer time period. This would potentially determine if the influence of SCW and NADW along the margin strengthened or weakened over time. Results from this study on whether the AAIW responds to glacial-interglacial cycles or glacial terminations remain promising and further εNd data are needed to verify this, possibly from additional cores at similar depths along the margin. Cores retrieved at varying depths over wider areas at the boundaries between NADW, UCDP and AAIW can aid in understanding this water mass along the margin. Additional methods such as foraminiferal Ca/Cd (Lynch-Styglietz, 2006; and references therein) can also further be employed to investigate the behaviour of deep and intermediate water masses. Analysing these isotopes and trace elements holds potential for understanding how the water masses from the southeast Atlantic influence the heat budget, nutrients and carbon storage of the oceans over time.

9.4. Summary and conclusions

This study provides the following main findings:

1. Planktic indicator foraminifera *Globoquadrina dehsicens* and *Globigerinoides bisphericus* support strontium isotope stratigraphy (SIS) results for the olive-green mud unit of the northern Namibian shelf dating the unit to 16 to 14 Ma.
2. Foraminifera preserved in the olive-green mud unit in cores from the northern Namibian shelf are indicative of the globally recorded Mid-Miocene Climatic Optimum (MMCO) indicating a deeper water depth and warmer sea surface conditions prior to the initiation of the BUS.
3. The middle Miocene benthic foraminifera indicate oligotrophic ocean floor conditions along the Namibian shelf while the Pleistocene benthic foraminifera indicate eutrophic ocean floor conditions.
4. The pelletal phosphorite units unconformably overlying the middle Miocene olive-green mud units yield a Plio-Pleistocene age supported by the planktic indicator foraminifera *Globorotalia (Globoconella) inflata* and *Globorotalia truncatulinoides.*
5. Foraminifera preserved in the pelletal phosphorite units are indicative of cooler conditions dated to a period in which the BUS had initiated and intensified. The palaeoenvironment was progressively shoaling during the Pleistocene as sea-level amplitudes increased.
6. Apart from the high productivity and upwelling conditions along the Namibian margin during the Pleistocene, benthic foraminifera distributions were also influenced by changing sea level amplitudes with the *Uvigerina* spp.-

dominated association occurring in deeper shelf deposits and the *Ammonia beccarii* association occurring in the shallower shelf deposits.

7. Pleistocene planktic foraminifera distributions are influenced by glacial-interglacial cycles, upwelling, which, in turn is influenced by strong southeasterly trade winds and polar/subtropical sea surface water penetration into the South Atlantic Ocean.
8. Quaternary benthic foraminifera distributions along the western South African slope are primarily influenced by organic matter fluxes, seasonality of phytoplankton blooms and oxygenation.
9. The dominant *Uvigerina* spp. on the slope show a relation to deep and intermediate water strength. The hispid and hispidocostate forms at deeper slope depths, under the influence of NADW/SCW variations increase during glacial periods whereas the costate *U. peregrina* increase during interglacial periods under the influence of varying AAIW. All Uvigerinid forms show increased relative abundances during periods of higher nutrient water mass dominance and lower oxygen conditions.
10. Glacial terminations (GT II and I) influence deep water masses along the western slope of South Africa in which a major shift from predominantly Southern Component Water (SCW) to a predominantly North Atlantic Deep Water (NADW) signal was recorded through neodymium isotopic compositions (εNd) in the tests of planktic foraminifera.
11. Neodymium isotopic compositions (εNd) in planktic foraminifera indicate glacial-interglacial variability in the strength of the Antarctic Intermediate Water (AAIW). During glacial periods the AAIW is stronger along the margin whereas during interglacial periods the AAIW weakens.
12. The variation of water masses during the late Quaternary displayed by εNd agrees with the measured $\delta^{13}C_{C.\ wuellerstorfi}$ in slope samples. Radiogenic εNd values are in agreement with lower $\delta^{13}C_{Cw}$ values which are indicative of the nutrient-rich SCW whereas less radiogenic (lower) values agree with lower $\delta^{13}C_{Cw}$ indicative of the nutrient-depleted and oxygen-rich NADW.
13. The relative abundances of *Cibicidoides wuellerstorfi* generally correlate well with the εNd in planktic foraminifera, but the abundances of benthic foraminifera may be influenced by upwelling conditions, seasonality of phytoplankton blooms and inter-species competition.

References

Barker, S., Cacho, I., Benway, H., Tachikawa, K., 2005. Planktonic foraminiferal Mg/Ca as a proxy for past oceanic temperatures: a methodological overview and data compilation for the Last Glacial Maximum. Quaternary Science Reviews 24, 821-834.

Bè, A.W.H., Tolderlund, D.S., 1971. Distribution and ecology of planktonic foraminifera. In: Funnell, B.M., Riedel, W.R. (Eds), The micropaleontology of oceans. Cambridge University Press, London, pp. 105-149.

Bergh, E.W., Compton, J.S., Frenzel, P., 2018. Late Neogene foraminifera from the northern Namibian continental shelf and the transition to the Benguela Upwelling

System. Journal of African Earth Sciences 141, 33-48.

BouDagher-Fadel, M.K., 2015. Biostratigraphic and geological significance of planktonic foraminifera. UCL Press, London, pp 306.

Compton, J.S., Bergh, E.W., 2016. Phosphorite deposits on the Namibian shelf. Marine Geology 380, 290-314.

Compton, J.S., Mulabisana, J., McMillan, I.K., 2002. Origin and age of phosphorite from the Last Glacial Maximum to Holocene transgressive succession off the Orange River, South Africa. Marine Geology 186(3-4), 243-261.

Compton, J.S., Wigley, R., McMillan, I.K., 2004. Late Cenozoic phosphogenesis on the western shelf of South Africa in the vicinity of the Cape Canyon. Marine Geology 206(1-4), 19-40.

Compton, J.S., Wiltshire, J.G., 2009. Terrigenous sediment export from the western margin of South Africa on glacial to interglacial cycles. Marine Geology 266, 212-222.

Giraudeau, J., 1993. Planktonic foraminiferal assemblages in surface sediments from the southwest African continental margin. Marine Geology 110, 47-62.

Haq, B.U., Hardenbol, J.A.N., Vail, P.R., 1987. Chronology of fluctuating sea levels since the Triassic. Science 235(4793), 1156-1167.

Hoetzel, S., Dupont, L.M., Marret, F., Jung, G., Wefer, G., 2017. Steps in the intensification of Benguela upwelling over the Walvis Ridge during Miocene and Pliocene. International Journal of Earth Sciences 106, 171-183.

Hu, R., Noble, T.L., Piotrowski, A.M., McCave, I.N., Bostock, H.C., Neil, H.L., 2016. Neodymium isotopic evidence for linked changes in Southeast Atlantic and Southwest Pacific circulation over the last 200 kyr. Earth and Planetary Science Letters 455, 106-114.

Kender, S., Kaminski, M.A., Jones, R.W., 2008. Early to middle Miocene foraminifera from the deep-sea Congo Fan, offshore Angola. Micropalaeontology 54, 477-568.

Kucera, M., 2007. Planktonic foraminifera as tracers of past oceanic conditions. In: Hillaire-Marccel, C., de Vernal, A (Eds.). Proxies in Late Cenozoic Paleoceanography. Elsevier, Amsterdam, 213-262.

Lowry, F.M.D., 1987. Foraminiferal thanatocoenoses from the continental shelf of southern Africa. Unpublished PhD thesis, University College London.

Lynch-Stieglitz, J., 2006. Tracers of past ocean circulation. Treatise on Geochemistry 6, 433-451.

Martin, R.A., 1981. Benthic foraminifera from the Orange-Lüderitz shelf southern African continental margin. Bulletin Joint Geological Survey/University of Cape Town Marine Geoscience Unit 11, 75 pp.

Miller, K.G., Kominz, M.A., Browning, J.V., Wright, J.D., Mountain, G.S., Katz, M.E., Sugarman, P.J., Cramer, B.S., Christie-Blick, N., Pekar, S.F., 2005. The Phanerozoic record of global sea-level change. Science 310, 1293–1298.

Rau, A. J., Rogers, J., Lutjeharms, J.R.E., Giraudeau, J., Lee-Thorp, J.A., Chen, M.T and Waelbroeck, C., 2002. A 450-kyr record of hydrological conditions on the western Agulhas Bank Slope, south of Africa. Marine Geology 180, 183-201.

Roberts, N.L., Piotrowski, A.M., Elderfield, H., Eglinton, T.I., Lomas, M.W., 2012. Rare earth element association with

foraminifera. Geochimica et Cosmochimica Acta 94, 57-71.

Rutberg, R.L., Hemming, S.R., Goldstein, S.L., 2000. Reduced North Atlantic Deep Water flux to the glacial Southern Ocean inferred from neodymium isotope ratios. Nature 405, 935.

Schmidt-Sinns, J., 2008. Rezente benthische Foraminiferen im Bereich des Benguelastroms, Südwestafrika– Verbreitungsmuster und ihre steuernden Faktoren. PhD thesis, Universitätsund Landesbibliothek, Bonn, 1-261.

Tachikawa, K., Piotrowski, A.M., Bayon, G., 2014. Neodymium associated with foraminiferal carbonate as a recorder of seawater isotopic signatures. Quaternary Science Reviews 88, 1-13.

Van Raden, U.J., Groeneveld, J., Raitzsch, M., Kucera, M., 2011. Mg/Ca in the planktonic foraminifera *Globorotalia inflata* and *Globigerinoides bulloides* from Western Mediterranean plankton tow and core top samples. Marine Micropalaeontology 78, 101-112.

Von Koslowski, R., 2017. Glacial-interglacial variations of the water masses in the southeast Atlantic Ocean derived from foraminiferal neodymium isotope ratios. Unpublished Master's thesis, University of Cape Town, 75 pp.

You, Y., Huber, M., Müller, R.D., Poulsen, C.J., Ribbe, J., 2009. Simulation of the middle Miocene climate optimum. Geophysical Research Letters, 36(4).

Wefer, G., Berger, W.H., Richter, C., Adams, D.D., Anderon, L.D., Andreasen, D.J., Brüchert, V., Cambray, H., Christensen, B.A., Frost, G.M., Giraudeau., Gorgas, T.J., Hermelin, O., Lange, C.B., Laser, B., Lin, H-L., Maslin, M., Meyers, P.A., Motoyama, I., Murray, R.W., Pato, D., Perez, M.E., Pufahl, P.K., Spiess, V., Vidal. L., Wigley, R., Yamazaki, T., 1998. Proceedings of the Ocean Drilling Program volume 175, 385-428.

Wigley, R.A., Compton, J.S., 2006. Late Cenozoic evolution of the outer continental shelf at the head of the Cape Canyon, South Africa. Marine Geology 226(1-2), 1-23.

Wigley, R.A., Compton, J.S., 2007. Oligocene to Holocene glauconite–phosphorite grains from the Head of the Cape Canyon on the western margin of South Africa. Deep Sea Research Part II: Topical Studies in Oceanography 54(11-13), 1375-1395.

Appendix A

Grain Size

Table A.1. Masses (in gram) and percentages of grain sizes (G = gravel; S = sand; M = mud) in core 2634.

Core depth (cm)	G (g)	S (g)	M (g)	Sum	%G	%S	%M
17.5	0.04	14.41	1.71	16.16	0.25	89.17	10.58
22.5	0.01	18.05	2.47	20.53	0.05	87.92	12.03
27.5	0.12	21.21	2.22	23.54	0.51	90.10	9.43
32.5	0.40	29.37	2.93	32.70	1.22	89.82	8.96
37.5	0.75	39.15	3.36	43.25	1.73	90.52	7.77
42.5	0.38	32.48	3.16	36.02	1.05	90.17	8.77
47.5	0.28	38.17	2.65	41.10	0.68	92.87	6.45
52.5	0.44	39.43	2.78	42.65	1.03	92.45	6.52
57.5	0.87	49.97	3.24	54.09	1.61	92.38	5.99
62.5	1.27	40.13	2.71	44.11	2.88	90.98	6.14
67.5	1.03	45.42	2.81	49.26	2.09	92.20	5.70
72.5	1.23	40.91	2.48	44.62	2.76	91.69	5.56
77.5	1.43	27.29	1.85	30.57	4.68	89.27	6.05
81.5	18.00	41.58	3.34	62.92	28.61	66.08	5.31
91.5	10.84	34.67	2.06	47.57	22.79	72.88	4.33
96.0	17.56	19.70	2.91	40.16	43.73	49.05	7.25
97.5	11.74	4.87	1.99	18.59	63.15	26.20	10.70
101.0	9.59	3.60	8.79	21.98	43.63	16.38	39.99
102.5	72.99	5.27	12.25	90.51	80.64	5.82	13.53
108.5	0.24	26.4	16.23	42.86	0.56	61.60	37.87
114.0	0.46	32.12	17.64	50.22	0.92	63.96	35.13

Table A.2. Masses (in gram) and percentages of grain sizes (G = gravel; S = sand; M = mud) in core 2658 (provided by Melissa Oosthuizen)

Core depth (cm)	G (g)	S (g)	M (g)	Sum	%G	%S	%M
7.5	5.62	10.02	5.16	20.80	27.05	48.26	24.69
12.5	11.59	28.25	5.07	44.91	25.81	62.89	11.30
19.5	16.55	41.52	7.79	65.86	25.12	63.04	11.83
24.5	30.47	40.70	6.51	77.68	39.22	52.40	8.38
29.5	15.39	22.92	3.69	42.00	36.64	54.58	8.78
34.5	20.18	14.93	4.31	39.42	51.19	37.88	10.93
39.5	6.14	30.56	5.90	42.60	14.42	71.74	13.84
44.5	4.43	36.14	8.18	48.75	9.08	74.14	16.78
49.5	3.12	24.59	11.43	39.14	7.96	62.84	29.20
57.5	12.51	26.46	9.15	48.12	26.00	55.00	19.01
64.5	5.13	20.44	7.34	32.91	15.59	62.11	22.30
69.5	23.04	17.82	16.83	57.69	39.94	30.89	29.17
74.5	1.47	4.12	12.70	18.29	8.04	22.52	69.44
77.5	0.04	2.85	23.23	26.12	0.15	10.90	88.95
87.5	0.54	3.66	36.23	40.43	1.33	9.05	89.62
96.5	1.07	3.57	18.04	22.68	4.72	15.72	79.55
102.5	1.99	6.57	28.17	36.73	5.40	17.89	76.70
107.5	0.09	3.48	35.98	39.55	0.22	8.80	90.98
115.0	0.28	2.88	23.32	26.48	1.05	10.88	88.07
122.5	0.36	2.82	34.73	37.91	0.95	7.45	91.61
131.0	0.56	2.32	25.60	28.48	1.98	8.14	89.88
142.5	0.07	1.11	41.29	42.47	0.17	2.61	97.22
159.5	0.15	3.97	72.21	76.33	0.19	5.20	94.61

Table A.3. Masses (in gram) and percentages of grain sizes (G = gravel; S = sand; M = mud) in core 2670

Core depth (cm)	G (g)	S (g)	M (g)	Sum	%G	%S	%M
2.5	79.63	101.86	23.96	205.45	38.76	49.58	11.66
12.5	8.58	27.64	17.39	53.61	16.00	51.56	32.44
22.5	12.69	45.03	12.92	70.64	17.96	63.75	18.29
32.5	15.64	20.25	13.83	49.72	31.46	40.73	27.82
42.5	11.09	29.22	11.66	51.97	21.34	56.22	22.44
47.5	2.33	27.20	8.73	38.26	6.09	71.09	22.82
62.5	0.94	32.83	9.94	43.71	2.15	75.11	22.74
72.0	9.26	15.44	9.03	33.73	27.45	45.78	26.77
76.5	32.82	11.61	19.72	64.15	51.16	18.10	30.74
84.5	5.39	7.06	24.95	37.40	14.41	18.88	66.71
88.5	0.38	2.15	25.64	28.17	1.35	7.63	91.02
97.5	0.00	2.38	29.35	31.73	0.00	7.50	92.50
107.5	0.01	1.40	27.42	28.83	0.03	4.86	95.11
117.5	0.31	2.48	34.91	37.70	0.82	6.58	92.60
127.5	0.58	2.55	33.05	36.18	1.60	7.05	91.35
137.5	0.00	2.12	40.45	42.57	0.00	4.98	95.02
147.5	0.00	3.11	36.29	39.40	0.00	7.89	92.11
157.5	0.00	1.54	36.01	37.55	0.00	4.10	95.90
167.5	0.00	1.68	46.13	47.81	0.00	3.51	96.49
177.5	0.00	1.58	38.98	40.56	0.00	3.90	96.10
187.5	0.00	0.90	29.93	30.83	0.00	2.92	97.08

Table A.4. Masses (in gram) and percentages of grain sizes (G = gravel; S = sand; M = mud) in core 2682 (provided by Melissa Oosthuizen)

Core depth (cm)	G (g)	S (g)	M (g)	Sum	%G	%S	%M
7.5	6.32	10.24	9.85	26.41	23.93	38.77	37.30
12.5	12.26	42.57	2.85	57.68	21.26	73.80	4.94
19.5	11.12	27.64	8.28	47.04	23.64	58.76	17.60
27.0	43.12	51.10	10.00	104.22	41.37	49.03	9.60
34.5	16.01	23.55	5.16	44.72	35.80	52.66	11.54
46.0	26.19	47.27	11.68	85.14	30.76	55.52	13.72
52.0	4.99	23.91	7.06	35.96	13.88	66.49	19.63
56.0	2.03	21.98	8.18	32.19	6.31	68.28	25.41
60.5	6.93	30.27	13.63	50.83	13.63	59.55	26.81
68.5	5.08	39.15	21.25	65.48	7.76	59.79	32.45
75.5	48.6	16.33	6.35	71.28	68.18	22.91	8.91
78.5	23.14	12.35	12.65	48.14	48.07	25.65	26.28
94.5	0.01	4.55	27.31	31.87	0.03	14.28	85.69
108.5	0.06	3.33	25.78	29.17	0.21	11.42	88.38
131.5	0.00	2.15	24.57	26.72	0.00	8.05	91.95
146.5	0.00	0.93	32.86	33.79	0.00	2.75	97.25
160.0	0.00	2.01	36.17	38.18	0.00	5.26	94.74

Table A.5. Masses (in gram) and percentages of grain sizes (G = gravel; S = sand; M = mud) in core 1307 (199 m water depth)

Core depth (cm)	G (g)	S (g)	M (g)	Sum	%G	%S	%M
2	8.98	7.38	0.49	16.85	53.29	43.80	2.91
16	7.25	19.03	1.19	27.47	26.39	69.28	4.33
19	3.25	17.44	1.44	22.13	14.69	78.81	6.51
58	3.28	15.03	0.79	19.10	17.17	78.69	4.14
60	0.93	14.56	0.72	16.21	5.74	89.82	4.44
68	0.55	8.61	0.48	9.64	5.71	89.32	4.98
72	24.2	10.84	1.84	36.88	65.62	29.39	4.99
79	11.51	16.73	1.73	29.97	38.41	55.82	5.77
83	0.06	4.78	0.81	5.65	1.06	84.60	14.34
105	0.10	8.78	1.90	10.78	0.93	81.45	17.63
127	0.67	8.53	1.79	10.99	6.10	77.62	16.29
149	5.12	8.73	1.05	14.90	34.36	58.59	7.05
160	0.35	2.45	5.32	8.12	4.31	30.17	65.52
178	0.00	0.13	4.57	4.70	0.00	2.77	97.23

Table A.6. Masses (in gram) and percentages of grain sizes (G = gravel; S = sand; M = mud) in core 1364 (199 m water depth)

Core depth (cm)	G (g)	S (g)	M (g)	Sum	%G	%S	%M
2	6.61	5.29	0.78	12.68	52.13	41.72	6.15
17	3.80	9.31	0.81	13.92	27.30	66.88	5.82
21	5.76	13.69	0.91	20.36	28.29	67.24	4.47
35	4.93	8.48	0.86	14.27	34.55	59.43	6.03
50	2.44	11.06	0.72	14.22	17.16	77.78	5.06
61	0.95	15.67	0.89	17.51	5.43	89.49	5.08
63	5.51	11.23	1.36	18.10	30.44	62.04	7.51
85	1.29	11.04	1.87	14.20	9.08	77.75	13.17
107	0.08	10.02	2.59	12.69	0.63	78.96	20.41
133	0.25	8.12	2.19	10.56	2.37	76.89	20.74
135	0.00	1.77	7.46	9.23	0.00	19.18	80.82
157	0.00	0.02	9.73	9.75	0.00	0.21	99.79
175	0.00	0.05	6.99	7.04	0.00	0.71	99.29

Table A.7. Masses (in gram) and percentages of grain sizes (G = gravel; S = sand; M = mud) in core 1657 (200 m water depth).

Core depth (cm)	G (g)	S (g)	M (g)	Sum	%G	%S	%M
2	11.32	5.48	0.86	17.66	64.1	31.03	4.87
18	5.82	10.04	1.06	16.92	34.4	59.34	6.26
22	6.18	10.16	1.1	17.44	35.44	58.26	6.31
29	4.84	23.13	1.63	29.6	16.35	78.14	5.51
35	4.09	20.76	2.29	27.14	15.07	76.49	8.44
42	3.32	17.49	1.69	22.5	14.76	77.73	7.51
46	0.36	15.73	1.89	17.98	2	87.49	10.51
57	0.08	6.78	1.58	8.44	0.95	80.33	18.72

Table A.8. Masses (in gram) and percentages of grain sizes (G = gravel; S = sand; M = mud) in core 1397 (200 m water depth).

Core depth (cm)	G (g)	S (g)	M (g)	Sum	%G	%S	%M
2	9.67	11.08	0.83	21.58	44.81	51.34	3.85
11	4.37	12.51	1.14	18.02	24.25	69.42	6.33
24	4.70	13.54	0.70	18.94	24.82	71.49	3.70
27	0.63	11.40	1.03	13.06	4.82	87.29	7.89
34	0.54	13.97	0.99	15.50	3.48	90.13	6.39
36	1.12	15.49	2.90	19.51	5.74	79.40	14.86
58	0.07	7.55	2.33	9.95	0.70	75.88	23.42
80	0.65	9.56	2.46	12.67	5.13	75.45	19.42
97	1.09	8.09	1.31	10.49	10.39	77.12	12.49
101	7.17	9.86	3.04	20.07	35.72	49.13	15.15

Table A.9. Masses (in gram) and percentages of grain sizes (G = gravel; S = sand; M = mud) in core 1313 (205 m water depth)

Core depth (cm)	G (g)	S (g)	M (g)	Sum	%G	%S	%M
2	15.94	15.25	1.42	32.61	48.88	46.76	4.35
9	4.02	7.82	0.70	12.54	32.06	62.36	5.58
12	2.29	9.69	1.06	13.04	17.56	74.31	8.13
34	1.58	11.62	0.64	13.84	11.42	83.96	4.62
41	0.98	8.50	0.73	10.21	9.60	83.25	7.15
44	0.31	11.07	0.96	12.34	2.51	89.71	7.78
51	1.62	9.49	2.89	14.00	11.57	67.79	20.64
53	0.10	7.54	2.53	10.17	0.98	74.14	24.88
75	0.08	7.11	1.69	8.88	0.90	80.07	19.03
97	0.31	9.06	2.60	11.97	2.59	75.69	21.72
99	0.08	3.89	4.08	8.05	0.99	48.32	50.68
121	0.00	0.02	5.24	5.26	0.00	0.38	99.62
144	0.00	0.01	5.75	5.76	0.00	0.17	99.83

Table A.10. Masses (in gram) and percentages of grain sizes (G = gravel; S = sand; M = mud) in core 1384 (206 m water depth)

Core depth (cm)	G (g)	S (g)	M (g)	Sum	%G	%S	%M
2	13.27	18.93	2.09	34.29	38.70	55.21	6.10
8	5.23	13.84	1.03	20.10	26.02	68.86	5.12
12	2.39	8.21	1.00	11.60	20.60	70.78	8.62
29	2.58	19.61	1.76	23.95	10.77	81.88	7.35
32	1.05	8.30	0.73	10.08	10.42	82.34	7.24
38	3.37	10.64	0.63	14.64	23.02	72.68	4.30
40	1.46	9.07	0.65	11.18	13.06	81.13	5.81
56	0.72	14.25	1.63	16.60	4.34	85.84	9.82
58	0.15	18.04	5.29	23.48	0.64	76.83	22.53
80	0.07	8.59	2.61	11.27	0.62	76.22	23.16
101	6.36	5.62	1.86	13.84	45.95	40.61	13.44
103	0.66	4.57	5.50	10.73	6.15	42.59	51.26
125	0.08	1.10	6.45	7.63	1.05	14.42	84.53
149	0.00	0.83	5.31	6.14	0.00	13.52	86.48

Table A.11. Masses (in gram) and percentages of grain sizes (G = gravel; S = sand; M = mud) in core 1441 (223 m water depth)

Core depth (cm)	G (g)	S (g)	M (g)	Sum	%G	%S	%M
2	13.27	18.93	2.09	34.29	38.70	55.21	6.10
8	5.23	13.84	1.03	20.10	26.02	68.86	5.12
12	2.39	8.21	1.00	11.60	20.60	70.78	8.62
29	2.58	19.61	1.76	23.95	10.77	81.88	7.35
32	1.05	8.30	0.73	10.08	10.42	82.34	7.24
38	3.37	10.64	0.63	14.64	23.02	72.68	4.30
40	1.46	9.07	0.65	11.18	13.06	81.13	5.81
56	0.72	14.25	1.63	16.60	4.34	85.84	9.82
58	0.15	18.04	5.29	23.48	0.64	76.83	22.53
80	0.07	8.59	2.61	11.27	0.62	76.22	23.16
101	6.36	5.62	1.86	13.84	45.95	40.61	13.44
103	0.66	4.57	5.50	10.73	6.15	42.59	51.26
125	0.08	1.10	6.45	7.63	1.05	14.42	84.53
149	0.00	0.83	5.31	6.14	0.00	13.52	86.48

Table A.12. Masses (in gram) and percentages of grain sizes (G = gravel; S = sand; M = mud) in core 1442 (231 m water depth)

Core depth (cm)	G (g)	S (g)	M (g)	Sum	%G	%S	%M
7	4.86	17.00	1.59	23.45	20.72	72.49	6.78
31	4.28	28.86	3.08	36.22	11.82	79.68	8.50
39	3.56	19.56	1.93	25.05	14.21	78.08	7.70
42	0.20	3.67	2.47	6.34	3.15	57.89	38.96
55	0.00	0.50	3.80	4.30	0.00	11.63	88.37
57	0.02	4.85	1.07	5.94	0.34	81.65	18.01
59	0.00	1.25	4.44	5.69	0.00	21.97	78.03
81	0.00	1.73	2.66	4.39	0.00	39.41	60.59
103	0.00	0.16	3.34	3.50	0.00	4.57	95.43
125	0.00	1.67	4.74	6.41	0.00	26.05	73.95
147	0.00	2.88	3.12	6.00	0.00	48.00	52.00
155	0.00	6.52	4.87	11.39	0.00	57.24	42.76

Table A.13. Masses (in gram) and percentages of grain sizes (G = gravel; S = sand; M = mud) in core 1478 (241 m water depth)

Core depth (cm)	G (g)	S (g)	M (g)	Sum	%G	%S	%M
2	16.09	25.02	2.45	43.56	36.94	57.44	5.62
10	6.84	22.69	1.79	31.32	21.84	72.45	5.72
14	4.43	22.07	1.51	28.01	15.82	78.79	5.39
22	2.72	18.57	2.48	23.77	11.44	78.12	10.43
25	2.15	11.33	1.63	15.11	14.23	74.98	10.79
50	0.26	18.43	1.95	20.64	1.26	89.29	9.45
54	10.38	18.00	2.03	30.41	34.13	59.19	6.68
57	0.64	6.12	3.35	10.11	6.33	60.53	33.14
79	0.00	0.48	4.16	4.64	0.00	10.34	89.66
101	0.00	0.03	3.80	3.83	0.00	0.78	99.22
123	0.00	0.45	3.58	4.03	0.00	11.17	88.83
143	0.00	2.30	3.46	5.76	0.00	39.93	60.07

Table A.14. Masses (in gram) and percentages of grain sizes (G = gravel; S = sand; M = mud) in core 1401 (244 m water depth).

Core depth (cm)	G (g)	S (g)	M (g)	Sum	%G	%S	%M
4	11.44	20.93	2.29	34.66	33.01	60.39	6.61
9	3.03	13.58	0.77	17.38	17.43	78.14	4.43
33	3.52	15.61	2.17	21.3	16.53	73.29	10.19
35	0.23	1.90	4.84	6.97	3.30	27.26	69.44
55	0.07	0.87	6.02	6.96	1.01	12.5	86.49
57	0.00	0.42	5.70	6.12	0.00	6.86	93.14
79	0.00	0.22	6.71	6.93	0.00	3.17	96.83
101	0.00	0.27	5.24	5.51	0.00	4.90	95.10
123	0.00	0.11	4.79	4.90	0.00	2.24	97.76
145	0.00	0.13	5.58	5.71	0.00	2.28	97.72
155	0.01	0.22	5.58	5.81	0.17	3.79	96.04

Table A.15. Masses (in gram) and percentages of grain sizes (G = gravel; S = sand; M = mud) in core 1479 (245 m water depth).

Core depth (cm)	G (g)	S (g)	M (g)	Sum	%G	%S	%M
2	7.06	11.42	0.63	19.11	36.94	59.76	3.3
16	3.92	13.90	1.15	18.97	20.66	73.27	6.06
20	3.67	17.86	1.25	22.78	16.11	78.40	5.49
34	2.98	17.77	2.18	22.93	13.00	77.50	9.51
37	2.60	16.06	2.06	20.72	12.55	77.51	9.94
50	1.47	17.25	1.35	20.07	7.32	85.95	6.73
53	3.49	11.68	2.65	17.82	19.58	65.54	14.87
55	0.00	3.23	2.84	6.07	0.00	53.21	46.79
77	0.00	0.04	3.21	3.25	0.00	1.23	98.77
99	0.00	0.03	3.11	3.14	0.00	0.96	99.04
121	0.00	2.24	3.02	5.26	0.00	42.59	57.41
149	0.00	0.19	2.55	2.74	0.00	6.93	93.07

Table A.16. Masses (in gram) and percentages of grain sizes (G = gravel; S = sand; M = mud) in core 1404 (285 m water depth)

Core depth (cm)	G (g)	S (g)	M (g)	Sum	%G	%S	%M
2	7.06	11.42	0.63	19.11	36.94	59.76	3.3
16	3.92	13.90	1.15	18.97	20.66	73.27	6.06
20	3.67	17.86	1.25	22.78	16.11	78.40	5.49
34	2.98	17.77	2.18	22.93	13.00	77.50	9.51
37	2.60	16.06	2.06	20.72	12.55	77.51	9.94
50	1.47	17.25	1.35	20.07	7.32	85.95	6.73
53	3.49	11.68	2.65	17.82	19.58	65.54	14.87
55	0.00	3.23	2.84	6.07	0.00	53.21	46.79
77	0.00	0.04	3.21	3.25	0.00	1.23	98.77
99	0.00	0.03	3.11	3.14	0.00	0.96	99.04
121	0.00	2.24	3.02	5.26	0.00	42.59	57.41
149	0.00	0.19	2.55	2.74	0.00	6.93	93.07

Table A.17. Masses (in gram) and percentages of grain sizes (G = gravel; S = sand; M = mud) in core 1404 (285 m water depth).

Core depth (cm)	G (g)	S (g)	M (g)	Sum	%G	%S	%M
2	17.08	17.46	1.32	35.86	47.63	48.69	3.68
5	2.09	6.44	0.39	8.92	23.43	72.20	4.37
11	1.71	5.81	0.83	8.35	20.48	69.58	9.94
13	0.90	11.14	1.33	13.37	6.73	83.32	9.95
25	0.98	12.68	1.65	15.31	6.40	82.82	10.78
27	0.43	14.57	1.82	16.82	2.56	86.62	10.82
49	0.00	7.75	1.62	9.37	0.00	82.71	17.29
71	0.05	7.38	2.52	9.95	1.01	74.17	25.33
94	0.10	5.58	2.45	8.13	0.00	68.63	30.14

Table A.18. Masses (in gram) and percentages of grain sizes (G = gravel; S = sand; M = mud) in core 1405 (297 m water depth).

Core depth (cm)	G (g)	S (g)	M (g)	Sum	%G	%S	%M
2	6.52	19.26	1.03	26.81	24.32	71.84	3.84
30	4.81	23.52	4.07	32.40	14.85	72.59	12.56
33	0.98	16.97	2.42	20.37	4.81	83.31	11.88
45	1.13	13.63	1.61	16.37	6.90	83.26	9.84
48	7.09	10.65	1.12	18.86	37.59	56.47	5.94
70	0.00	8.80	2.06	10.86	0.00	81.03	18.97
92	0.00	5.74	2.69	8.43	0.00	68.09	31.91
114	0.00	6.47	3.00	9.47	0.00	68.32	31.68
136	0.00	6.38	2.68	9.06	0.77	70.42	29.58
158	0.07	4.97	3.55	8.59	0.00	57.86	41.33
160	0.00	3.23	5.12	8.35	0.00	38.68	61.32
169	0.00	0.65	5.73	6.38	0.00	10.19	89.81

Table A.19. Masses (in gram) and percentages of grain sizes (G = gravel; S = sand; M = mud) in core 1408 (303 m water depth).

Core depth (cm)	G (g)	S (g)	M (g)	Sum	%G	%S	%M
2	2.47	10.46	0.47	13.40	18.43	78.06	3.51
28	1.89	14.59	2.09	18.57	10.18	78.57	11.25
31	2.16	11.02	1.23	14.41	14.99	76.47	8.54
36	0.81	10.17	1.36	12.34	6.56	82.41	11.02
38	0.32	6.28	0.70	7.30	4.38	86.03	9.59
54	0.26	7.07	2.80	10.13	2.57	69.79	27.64
56	0.12	12.03	4.01	16.16	0.74	74.44	24.81
78	0.00	11.2	2.48	13.68	0.22	81.87	18.13
100	0.03	5.37	3.22	8.62	0.00	62.30	37.35
120	0.00	2.31	4.14	6.45	0.00	35.81	64.19
122	0.00	2.03	3.87	5.90	0.00	34.41	65.59
135	0.00	0.40	3.93	4.33	0.00	9.24	90.76

Table A.20. Masses (in gram) and percentages of grain sizes (G = gravel; S = sand; M = mud) in core 1406 (309 m water depth).

Core depth (cm)	G (g)	S (g)	M (g)	Sum	%G	%S	%M
2	5.47	13.23	1.24	19.94	27.43	66.35	6.22
36	1.69	15.03	2.18	18.9	8.94	79.52	11.53
40	2.09	10.36	1.13	13.58	15.39	76.29	8.32
46	0.94	10.27	1.32	12.53	7.50	81.96	10.53
49	0.02	4.80	1.02	5.84	0.34	82.19	17.47
71	0.00	5.79	2.31	8.10	0.00	71.48	28.52
93	0.00	5.01	1.52	6.53	0.00	76.72	23.28
115	0.00	4.63	1.51	6.14	0.00	75.41	24.59
137	0.00	4.31	2.71	7.02	0.43	61.40	38.60
157	0.03	4.17	2.07	6.27	0.00	66.51	33.01
159	0.00	3.03	2.17	5.20	0.00	58.27	41.73
164	0.00	0.27	3.77	4.04	0.00	6.68	93.32

Table A.21. Masses (in gram) and percentages of grain sizes (S = sand; M = mud) in core GeoB 20601-4 (874 m water depth) (provided by Teboho Mosito).

Core depth (cm)	>63 S (g)	<63 M (g)	Sum	%S	%M
1	2.79	2.90	5.68	49.00	51.00
4	2.15	2.11	4.26	50.54	49.46
8	3.17	2.47	5.65	56.17	43.83
12	3.28	2.73	6.02	54.59	45.41
16	3.46	3.03	6.49	53.33	46.67
20	2.90	2.66	5.55	52.16	47.84
24	2.79	2.48	5.26	52.95	47.05
28	3.05	2.53	5.57	54.66	45.34
32	2.98	2.75	5.73	52.02	47.98
36	3.68	2.68	6.36	57.89	42.11
40	2.19	1.72	3.91	56.10	43.90
44	3.03	2.17	5.20	58.33	41.67
48	3.45	1.86	5.30	65.01	34.99
52	4.00	1.60	5.60	71.49	28.51
56	3.84	1.47	5.31	72.28	27.72
60	4.42	1.72	6.14	71.93	28.07
64	4.13	1.95	6.08	67.94	32.06
68	3.15	2.25	5.40	58.29	41.71
72	3.01	2.09	5.11	59.00	41.00
76	2.89	1.61	4.49	64.23	35.77
80	3.77	2.06	5.83	64.70	35.30
84	3.26	2.14	5.40	60.40	39.60
88	4.22	1.35	5.57	75.70	24.30
92	4.49	1.51	5.99	74.84	25.16
96	3.34	2.54	5.87	56.83	43.17
100	3.31	2.27	5.58	59.33	40.67
104	3.61	2.29	5.91	61.16	38.84
108	2.38	2.68	5.06	47.01	52.99
112	2.73	3.75	6.48	42.07	57.93
116	2.07	3.89	5.96	34.72	65.28
120	3.26	4.35	7.61	42.83	57.17
124	2.74	3.43	6.17	44.42	55.58
128	2.55	4.27	6.82	37.37	62.63
132	2.49	2.86	5.35	46.56	53.44
136	3.05	2.63	5.68	53.63	46.37
140	3.26	2.61	5.87	55.49	44.51
144	3.07	4.67	7.74	39.68	60.32

Table A.21. *(continued)*

Core depth (cm)	>63 S (g)	<63 M (g)	Sum	%S	%M
148	2.92	4.55	7.47	39.11	60.89
152	2.31	3.70	6.01	38.40	61.60
156	3.55	3.85	7.40	47.92	52.08
160	3.89	3.22	7.12	54.70	45.30
164	2.92	3.65	6.57	44.48	55.52
172	3.93	4.74	8.67	45.34	54.66
176	2.95	3.45	6.39	46.11	53.89
180	3.17	2.44	5.61	56.56	43.44
184	3.74	2.27	6.01	62.27	37.73
188	3.95	2.16	6.12	64.61	35.39
192	4.07	2.70	6.76	60.15	39.85
196	3.70	2.84	6.54	56.56	43.44
200	3.50	2.98	6.47	54.01	45.99
208	3.72	2.95	6.68	55.75	44.25
216	2.20	4.79	6.99	31.46	68.54
224	1.45	3.99	5.45	26.67	73.33
232	2.18	5.14	7.31	29.76	70.24
240	2.56	4.98	7.54	33.96	66.04
248	2.72	4.75	7.47	36.37	63.63
256	3.03	2.46	5.49	55.20	44.80
266	2.38	3.90	6.28	37.86	62.14
274	2.72	4.23	6.95	39.10	60.90
282	2.74	3.72	6.47	42.42	57.58
290	1.73	4.59	6.32	27.33	72.67
298	1.22	6.03	7.25	16.77	83.23

Table A.22. Masses (in gram) and percentages of grain sizes (S = sand; M = mud) in core GeoB 8342-6 (3522 m water depth).

Core depth (cm)	>63 S (g)	<63 M (g)	Sum	%S	%M
0.5	1.21	4.03	5.24	23.09	76.91
4.5	1.90	5.98	7.88	24.11	75.89
8.5	1.58	4.29	5.87	26.92	73.08
12.5	2.81	5.43	8.24	34.10	65.90
16.5	2.01	6.10	8.11	24.78	75.22
20.5	0.79	6.98	7.77	10.17	89.83
24.5	1.43	5.87	7.30	19.59	80.41
28.5	1.60	7.43	9.03	17.72	82.28
32.5	1.08	5.41	6.49	16.64	83.36
36.5	0.42	3.30	3.72	11.29	88.71
40.5	0.91	5.81	6.72	13.54	86.46
44.5	1.43	7.11	8.54	16.74	83.26
48.5	0.81	5.35	6.16	13.15	86.85
52.5	0.56	5.35	5.91	9.48	90.52
56.5	0.86	5.78	6.64	12.95	87.05
60.5	1.22	4.39	5.61	21.75	78.25
64.5	0.76	4.23	4.99	15.23	84.77
68.5	0.96	3.86	4.82	19.92	80.08
72.5	0.93	4.10	5.03	18.49	81.51
76.5	1.20	4.73	5.93	20.24	79.76
80.5	1.55	7.13	8.68	17.86	82.14
84.5	1.24	5.93	7.17	17.29	82.71
88.5	1.11	5.96	7.07	15.70	84.30
92.5	0.36	7.03	7.39	4.87	95.13
96.5	0.30	7.45	7.75	3.87	96.13
100.5	0.15	6.04	6.19	2.42	97.58
104.5	0.20	4.90	5.10	3.92	96.08
108.5	0.23	5.20	5.43	4.24	95.76
112.5	0.80	5.90	6.70	11.94	88.06
116.5	0.94	5.93	6.87	13.68	86.32
120.5	1.26	5.60	6.86	18.37	81.63
124.5	0.85	5.86	6.71	12.67	87.33
128.5	0.97	4.3	5.27	18.41	81.59
132.5	0.80	4.23	5.03	15.90	84.10
136.5	1.27	5.87	7.14	17.79	82.21
140.5	0.75	6.05	6.80	11.03	88.97

Table A.22. *(continued)*

Core depth (cm)	>63 S (g)	<63 M (g)	Sum	%S	%M
144.5	0.60	5.08	5.68	10.56	89.44
148.5	1.32	5.04	6.36	20.75	79.25
152.5	1.04	5.97	7.01	14.84	85.16
156.5	1.55	6.36	7.91	19.60	80.40
160.5	1.74	5.90	7.64	22.77	77.23
164.5	1.57	5.69	7.26	21.63	78.37
168.5	1.18	6.64	7.82	15.09	84.91
172.5	1.63	7.01	8.64	18.87	81.13
176.5	0.76	4.38	5.14	14.79	85.21
180.5	1.60	5.45	7.05	22.70	77.30
184.5	1.77	5.88	7.65	23.14	76.86
188.5	1.40	4.58	5.98	23.41	76.59
196.5	1.36	4.60	5.96	22.82	77.18
204.5	1.10	4.29	5.39	20.41	79.59
212.5	0.97	6.54	7.51	12.92	87.08
220.5	1.12	7.00	8.12	13.79	86.21
228.5	1.04	6.35	7.39	14.07	85.93
236.5	0.65	5.49	6.14	10.59	89.41
244.5	0.97	6.95	7.92	12.25	87.75
252.5	0.65	4.59	5.24	12.40	87.60
260.5	0.93	5.52	6.45	14.42	85.58
268.5	1.39	5.16	6.55	21.22	78.78
276.5	1.10	5.15	6.25	17.60	82.40
284.5	1.01	5.34	6.35	15.91	84.09
292.5	0.71	5.99	6.70	10.60	89.40
300.5	0.86	5.36	6.22	13.83	86.17

Table A.23. Masses (in gram) and percentages of grain sizes (S = sand; M = mud) in core GeoB 8336-6 (3631 m water depth).

Core depth (cm)	>63 S (g)	<63 M (g)	Sum	%S	%M
0.5	1.17	4.58	5.75	20.35	79.65
4.5	1.07	5.20	6.27	17.07	82.93
8.5	1.03	4.15	5.18	19.88	80.12
12.5	1.26	5.11	6.37	19.78	80.22
16.5	1.56	5.68	7.24	21.55	78.45
20.5	1.91	4.95	6.86	27.84	72.16
23.5	1.13	5.06	6.19	18.26	81.74
27.5	0.65	5.45	6.10	10.66	89.34
32.5	0.90	5.44	6.34	14.20	85.80
37.5	0.59	4.57	5.16	11.43	88.57
41.5	0.54	5.29	5.83	9.26	90.74
48.5	0.64	6.15	6.79	9.43	90.57
50.5	0.57	6.35	6.92	8.24	91.76
55.5	0.54	6.18	6.72	8.04	91.96
60.5	0.55	6.05	6.60	8.33	91.67
66.5	0.43	4.67	5.10	8.43	91.57
71.5	0.67	6.38	7.05	9.50	90.50
76.5	0.82	5.01	5.83	14.07	85.93
81.5	0.92	5.76	6.68	13.77	86.23
86.5	0.93	6.84	7.77	11.97	88.03
91.5	1.01	6.07	7.08	14.27	85.73
95.5	0.98	6.44	7.42	13.21	86.79
99.5	1.05	6.43	7.48	14.04	85.96
104.5	0.89	6.49	7.38	12.06	87.94
109.5	0.16	6.16	6.32	2.53	97.47
114.5	0.26	5.81	6.07	4.28	95.72
120.5	0.13	6.25	6.38	2.04	97.96
125.5	0.36	6.59	6.95	5.18	94.82
129.5	0.57	6.76	7.33	7.78	92.22
133.5	0.91	7.10	8.01	11.36	88.64
138.5	0.97	6.54	7.51	12.92	87.08
142.5	1.33	5.90	7.23	18.4	81.6
148.5	0.22	6.68	6.90	3.19	96.81
153.5	0.69	6.88	7.57	9.11	90.89
158.5	0.71	6.87	7.58	9.37	90.63
163.5	0.47	5.64	6.11	7.69	92.31

Table A.23. *(continued)*

Core depth (cm)	>63 S (g)	<63 M (g)	Sum	%S	%M
168.5	0.82	6.35	7.17	11.44	88.56
173.5	0.80	6.43	7.23	11.07	88.93
178.5	0.63	7.05	7.68	8.20	91.80
183.5	0.51	6.01	6.52	7.82	92.18
188.5	0.49	7.49	7.98	6.14	93.86
193.5	0.58	6.18	6.76	8.58	91.42
198.5	0.40	6.40	6.80	5.88	94.12
203.5	0.94	6.21	7.15	13.15	86.85
209.5	1.17	5.80	6.97	16.79	83.21
213.5	1.54	5.82	7.36	20.92	79.08
218.5	1.64	5.48	7.12	23.03	76.97
223.5	1.13	6.66	7.79	14.51	85.49
228.5	1.14	6.56	7.70	14.81	85.19
233.5	1.00	6.01	7.01	14.27	85.73
238.5	0.70	6.68	7.38	9.49	90.51
242.5	0.62	6.76	7.38	8.40	91.60
248.5	0.24	4.10	4.34	5.53	94.47
253.5	0.35	6.66	7.01	4.99	95.01
258.5	0.34	5.91	6.25	5.44	94.56
263.5	0.58	6.97	7.55	7.68	92.32
268.5	0.67	6.57	7.24	9.25	90.75
273.5	0.43	5.58	6.01	7.15	92.85
278.5	0.64	6.19	6.83	9.37	90.63
283.5	0.51	5.41	5.92	8.61	91.39
288.5	0.24	5.28	5.52	4.35	95.65
293.5	0.23	5.05	5.28	4.36	95.64
298.5	0.49	6.85	7.34	6.68	93.32

Appendix B

Foraminifera, Mollusc and Non-carbonate Mineral Counts

Table B.1. Planktic foraminifera counts for core 2634

Core depth (cm)	*Globigerina bulloides*	*Globigerinella siphonifera*	*Globigerinoides ruber* (w)	*Globigerinoides truncatulinoides*	*Globorotalia inflata*	*Globorotalia menardii*	*Neogloboquadrina dutertrei*	*Neogloboquadrina pachyderma* (d) \ *Ng. incompta*	*Neogloboquadrina pachyderma (s)*	*Orbulina bilobata*	*Orbulina universa*	Sum
17.5	35	2	3		2		5	1			17	65
22.5	38		4		3		1			1	32	79
27.5	24		1		4		3	2	1	1	24	60
32.5	27	1	1		2		3	1			31	66
37.5	42		1		7			4	1	2	39	96
42.5	67	3	4	1	7		1	2		2	59	146
47.5	62	4	2		19		5	2			54	148
52.5	72	1	2		30		2	2			58	167
57.5	83	3	2		32		2	2			73	197
62.5	112	2	4		30		2	2	1	1	12	166
67.5	135		7		36		2	1	1		18	200
72.5	130	3	6		59		5	4	1		54	262
76.5	105	1	2		33		3	8	1		5	158
81.5	90	1	1		4			2			1	99
91.5	153	4	2	1	16	1	1	5			1	184
99	68	1	2		7			1			1	80
101	72	1	1		23			1				98
102.5	97	5	3		23			4			1	133
108.5	12	0	0	0	6	0	0	1	0	0	0	19

Table B.2. Planktic foraminifera counts for core 2658.

Sample depth (cm)	*Globigerina bulloides*	*Globigerinella siphonifera*	*Globigerinoides bispherícus*	*Trilobatus immaturus*	*Globigerinoides ruber*	*Trilobatus sacculifer*	*Globoquadrina dehiscens*	*Globorotalia inflata*	*Globorotalia* spp.	*Neogloboquadrina dutertrei*	*Ng. pachyderma* (d)/ *Ng. incompta*	*Neogloboquadrina pachyderma* (s)	*Orbulina bilobata*	*Orbulina universa*	Sum
12.5	125	3			1			60		3			1	13	206
19.5	68	4			3			64			2	1		6	148
24.5	64	7						32	3					8	114
29.5	44	5						55				1		4	109
34.5	20							13		1				2	36
39.5	22	2				1		2			1				28
44.5	37	6				1		17				1		2	64
49.5	40	2						17						1	60
58	28	2			3			3	2		1	2		3	44
64.5	31	2							1		1			13	48
69.5	37	2		29	3	8			8		1			3	91
73.5	92	4		54	1	7	6	1	6					10	181
77.5	54	8	1	73	0	10	14		5					7	172
87.5	127	4	2	79	2	6	17		9					10	256
96.5	81	3		49	1	3	16		11					9	173
103	131	1		60	2	6	10		14					4	228
108	68	3		90	5	3	6		9					3	187
115	88	4		65	1	3	9		12					4	186
123	66	5	3	45	4	3	6		7					9	148
132	99	3		54	2	2	4		13					3	180
143	70			51	3	3	7		10					5	149

Table B.3. Planktic foraminifera counts for core 2670

Sample depth (cm)	*Globigerina bulloides*	*Globigerinella siphonifera*	*Globigerinoides bisphericus*	*Trilobatus immaturus*	*Globigerinoides ruber*	*Trilobatus sacculifer*	*Globoquadrina dehiscens*	*Globorotalia inflata*	*Globorotalia* spp.	*Neogloboquadrina dutertrei*	*Ng. pachyderma* (d) / *Ng. incompta*	*Neogloboquadrina pachyderma* (s)	*Orbulina bilobata*	*Orbulina universa*	Sum
2.5	125	3			1			60		3			1	13	206
12.5	68	4			3			64			2	1		6	148
22.5	64	7						32	32					8	143
32.5	44	5						55				1		4	109
42.5	20							13		1				2	36
47.5	22	2				1		2			1				28
62.5	37	6				1		17				1		2	64
72	40	2						17						1	60
76.5	28	2			3			3	3		1	2		3	45
84.5	31	2							0		1			13	47
88.5	37	2		29	3	8			0		1			3	83
97.5	92	4		54	1	7		1	7					10	176
108	54	8	1	73		10	14		14					7	181
118	127	4	2	79	2	6	16		16					10	262
128	81	3		49	1	3	16		16					9	178
138	131	1		60	2	6	9		9					4	222
148	68	3		90	5	3	6		6					3	184
158	88	4		65	1	3	7		7					4	179
168	66	5	3	45	4	3	7		6					9	148
178	99	3		54	2	2	13		4					3	180
188	70			51					7					5	133

Table B.4. Planktic foraminifera counts for core 2682

Sampling depth (cm)	*Globigerina bulloides*	*Globigerinella siphonifera*	*Globigerinoides biscphericus*	*Trilobatus immaturus*	*Globigerinoides ruber*	*Trilobatus sacculifer*	*Globoquadrina dehiscens*	*Globorotalia inflata*	*Globorotalia* spp.	*Neogloboquadrina dutertrei*	*Ng. pachyderma* (d) / *Ng. incompta*	*Neogloboquadrina pachyderma* (s)	*Orbulina bilobata*	*Orbulina universa*	sum
7.5	125	3			1			60		3			1	13	206
12.5	68	4			3			64			2	1		6	148
19.5	64	7						32						8	111
26	44	5						55				1		4	109
35.5	20							13		1				2	36
46	22	2				1		2			1				28
52	37	6				1		17				1		2	64
60.5	40	2						17						1	60
68.5	28	2			3			3	2		1	2		3	44
75.5	31	2							1		1			13	48
78.5	37	2		29	3	8			8		1			3	91
94.5	92	4		54	1	7	6	1	6					10	181
109	54	8	1	73		10	14		5					7	172
132	127	4	2	79	2	6	17		9					10	256
147	81	3		49	1	3	17		11					9	174
160	131	1		60	2	6	10		14					4	228

Table B.5. Planktic foraminifera counts for Walvis Bay-Lüderitz cores 1406, 1441, 1307

Core	Core depth (cm)	*Globigerina bulloides*	*Globigerinella siphonifera*	*Globigerinoides ruber*	*Globorotalia (Globoconella) inflata*	*Globorotalia menardii*	*Globorotalia truncatulinoides*	*Neogloboquadrina dutertrei*	*Ng. incompta + Ng. pachyderma*	*Orbulina universa*	Sum
1406	**2**	50	1		13				10	1	75
1406	**35**	41			23			1	4		69
1406	**40**	22			15				2		39
1406	**46**	30	2		30				2		64
1406	**49**	44	4	2	32	1			4	1	88
1441	**2**	268		1	21			3	8	3	304
1441	**10**	237	1	3	50		2	1	8	3	305
1441	**34**	34			6				2		42
1441	**44**	18		2	7				1		28
1441	**47**	2			1						3
1441	**55**	1									1
1307	**2**	98		1	1				2		102
1307	**16**	276		5	10		2		5	2	300
1307	**19**	34			4				1		39
1307	**58**	6			3						9
1307	**60**	2							2		4
1307	**68**				1						1
1401	**4**	285			17			1			303
1401	**9**	21			7	3					28
1401	**33**	22			8		1				31
1401	**35**	16		5	5		2				28
1401	**55**	5			3						8
1479	**4**	110		2	13		1		1		127
1479	**16**	170			28				5	4	208
1479	**20**	173			67				1	1	242
1479	**34**	23		1	5				4	1	34
1479	**37**	24									24
1479	**50**	3			1						4

Table B.6. Planktic foraminifera counts for core GeoB 20601-4

Core sample depth (cm)	*Globigerina bulloides*	*Globigerinella siphonifera*	*Globigerinoides conglobatus*	*Globigerinoides ruber* (pink)	*Globigerinoides ruber* (white)	*Globigerinoides sacculifer*	*Globorotalia (Globoconella) inflata*	*Globorotalia hirsuta*	*Globorotalia menardii*	*Globorotalia scitula*	*Globorotalia truncatulinoides*	*Globoturborotalita rubescens*	*Neogloboquadrina dutertrei*	*Neogloboquadrina pachyderma*	*Orbulina bilobata*	*Orbulina universa*	*Pulleniatina obliquiloculata*	*Sphaeroidinella dehiscens*	*Trilobatus trilobus*	Not identified	Sum
1	28	1			1	1	212	6	1	1	31		8			15				15	320
4.5	94	1			6	1	164	1			21	1	2	4		12				24	331
8.5	133	1			9		142	2	1	1	15		2	12		12				12	342
13	95	2			6	2	163	5	1	1	10	1		3		19				1	309
17	90	4	1		10		153	2		2	14		10	6		10				14	316
21	127	1		1	8		126	7		1	8	1	6	35		6			1	25	353
25	157	2	1		7	1	98	1	1	4	17	1				14				12	316
29	130				5	1	125	5	1	4	16	1	3	1		14				1	307
33	140	2			1	1	145	1	1	1	8	1	1			7					309
37	135	2			5		120	2		1	14	4	7	3		13				28	334
41	168	1			2	1	135	3	1	1	19	1	4	12		14				32	394
45	143	5	1		1		117	4		1	8	1	5	28		6				18	338
49	170	3			6		102	4			17	1			1	35					339
53	176	6			1		50	2	1	1	12	2	1	62	1	24				14	353
57	120			2			71	1			10			84		16					304
61	115	5		1	4		53	1		1	6	3		88		30				12	319
65	120	5			5		57			1	11	1	1	94	1	16					312
69	82	3	1		3		112	4		1	6	1	2	90		5			2	14	326
73	112	2			8	1	149			1	11	7	6	69	1	18				2	387
77	83	4			3		92	1		1	9	1	4	94	1	17					310
81	78	2			2	1	115	3		1	6	1	3	112	1	17			1	22	365
85	106	1	1	2	1	1	110		1		16	1	5	78		19					342
89	120	2		4		1	16	2		3	8	1	3	127	1	15				22	325
93	106				8		72	1	1	2	29	1	1	96		18				35	370
97	82	1			1		80				12	2		132		12				26	348
109	25	3					54	14		1	7			204		8				52	368
117	20	1			1		98		1		12	1	1	178		10	1			42	366
125	82				1		112		1	1	12		1	145		10				12	377
133	68	3			3		136			1	8	1		74		18				15	327
141	145		1		4	1	102			3	2			62		8				8	336
149	142	1	1		11	1	126			1	11	1		6		8	1				310
157	142	1			1		116				13	2	7	4		19				33	338
168	161	7	1	1	3		115		1	1	13	1	2	40	1			1		33	381
177	133	1			3	1	72				5	2		92		11				31	351
185	144	1			1		112		1	2	10		1	55		13	1			22	363
193	142				1		94				3		2	70		10	1			21	344
201	126						98		1		9			102		15	1			25	377
209	137				1		115			1	8	1		62		14				36	375
217	52	1			1		144		1		9		3	128		9				36	384
225	73						131				3		1	115		7				27	357
233	98					1	131	1			15			88		13				28	375
241	155				1		131		1		10			12		12				27	349
249	42	1			7		150				12		1	102		7				33	355
257	118				5		90	1		2	13			94		18				17	358
267	78				7		90				21			97		15				29	337
275	102				8		141			2	4			36		18				52	363
283	102				2		114				5		1	81	1	22				23	351
291	90	1			1		118			1	3			84		9				47	354
299	64				5		139				11			88		5				45	357

Table B.7. Planktic foraminifera counts for core GeoB 8342-6

Core sample depth (cm)	*Globigerina bulloides*	*Globigerinella siphonifera*	*Globigerinoides conglobatus*	*Globigerinoides ruber* (white)	*Globigerinoides sacculifer*	*Globorotalia (Globoconella) inflata*	*Globorotalia crasaformis*	*Globorotalia hirsuta*	*Globorotalia menardii*	*Globorotalia scitula*	*Globorotalia truncatulinoides*	*Globorotalia tumida*	*Globoturborotalita rubescens*	*Neogloboquadrina dutertrei*	*Neogloboquadrina pachyderma*	*Orbulina bilobata*	*Orbulina universa*	*Pulleniatina obliquiloculata*	*Sphaeroidinella dehiscens*	*Trilobatus trilobus*	Not identified	Sum
0.5	58	2		13	2	217		9	1	5	12				44		10			1	28	402
4.5	112	9		11	1	192		9	2	10	16			1	5		11			5	18	402
8.5	115	8		8	1	201		6	1	13	24	1		7	15		14			1	12	427
12.5	112	3	1	14	1	190	1	10		1	13			3	20		6	1	1	1	18	396
16.5	144	6		19	1	169		7	1	1	8			11			19	6		2	22	416
20.5	115	9		17	2	156		7	1	4	8			7	4		13	1			13	357
24.5	74	10	1	19	3	124		8	1	7	7			5	30		28			1	5	323
28.5	83	6		26		98		2		4	5			4	95		15			1	22	361
32.5	62	2		11		116		15		6	2				152		12			1		379
36.5	21	2		5	1	109		10		2	9			1	130		15				18	323
40.5	62	2		2	2	151		10		6	8			2	173		20			1	15	454
44.5	39	4		1		98		8		2	1				162	3	52				33	403
48.5	38	2				128		11		1	1				160	1	40				8	390
52.5	22					76		6			1				174	2	35				15	331
56.5	43					75		6		1	1				156		60				63	405
60.5	63	1		1		96		4		1	10			1	155	2	55	1			38	428
64.5	44			6		86		1		2	7				139	1	51				5	342
68.5	42	2		2		120		6		2	12				88		67				43	384
72.5	108	1		15		113		14		4	13		1	1	77	1	33			1	24	406
76.5	104	2		1		70		6		1	16			1	80		38	1			17	337
80.5	83	1		4		115		13		1	22			1	44	1	56				27	368
84.5	112	12		8		122		9		4	34				10	2	44		1		4	362
88.5	101	3		12		125		12		6	28			1	7		35					330
92.5	78	4		20		148		13		1	24				20		28			1	33	370
96.5	64	2		4		166		4		1	12				22		26				38	339
101	55	1		5		120		15			44				48		18				38	344
105	40			2		138		15			2				62		48				45	352
109	75			2		58		10			8				184		25				2	364
113	90			11		133		10			22				84		22					372
117	74	3		13		128		14			11				90		21	1				355
121	58	4		6		128		9		3	14			8	79		22				34	365
125	80			9	1	135		13	1	1	22				82		22	1			18	385
129	101	4		7	1	113		8		3	13			1	66		23	1			18	359
133	133	3		12		112		8		6	22			6	90		19					411
137	93	5		8		116		8		3	18				58		4	1				314
141	101			10	1	145		6			8			3	52		11				34	371
145	104			4		128		4			12			1	54		18					325
149	108			12		130		4		3	14				72		17					360
153	110	4		13	1	174	3	6		1	6			3	74		14				25	434
157	65	6		24	1	135		8		1	19				45		20					324
161	118	1		15		122		7		5	13		1	1	58		29				38	408
165	96	1		14	1	109		7		1	10			1	57		16	1			14	328
169	114	4		10		125		7			11				58		12				33	374
173	104	2		14		112		7		2	20				51		22	1			31	366
177	138			13	1	67		5		1	13			3	83		15				31	370
181	123	5		14	1	118		9		1	15			1	50		23	1			25	386
185	120	3		20	2	92	1	5			18			1	44		11	6			31	354
189	129	4	1	15	1	124		10	1	5	24			4	18	1	14	8	1		8	368
197	84	1		33		130		6			42			3	4		24	8		1		336
205	147	2	1	12	1	106		1	1	2	18			6	12		12	5	1		38	365
213	132			18	1	101		5		3	17			5	8		15	2	1		38	346
221	138	1		8		126				1	40				39		51	3			39	446
229	138			6		92				1	38				38		62	2			23	400
237	118	1		6		87		1		1	20				46		40	1			35	356
245	100	1		6	1	92		3		1	10				54	1	38	2			25	334
253	76	1		10	1	84				1	16				70	1	53				38	351
261	100	1		10		72			1		16			1	85		22	1			38	347
269	139	1		2		131				1	25			1	32		20				32	384
277	130	3		14	1	139				1	26				36		16					366
285	130			9		118					16				38	2	20				33	366
293	75	3		4		77				1	11				135	1	15	2			20	344
301	75			4		142					12				96		14				38	381
309	38			1		116				1	12				145		22	1			25	361

Table B.8. Planktic foraminifera counts for core GeoB 8336-6

Core sample depth (cm)	*Globigerina bulloides*	*Globigerinella siphonifera*	*Globigerinoides conglobatus*	*Globigerinoides hirsuta*	*Globigerinoides ruber* (pink)	*Globigerinoides ruber* (white)	*Globigerinoides sacculifer*	*Globorotalia (Globoconella) inflata*	*Globorotalia crassaformis*	*Globorotalia menardii*	*Globorotalia scitula*	*Globorotalia truncatulinoides*	*Globoturborotalita rubescens*	*Neogloboquadrina dutertrei*	*Neogloboquadrina pachyderma*	*Orbulina bilobata*	*Orbulina universa*	*Pulleniatina obliquiloculata*	*Sphaeroidinella dehiscens*	*Trilobatus trilobus*	Not identified	Sum
0.5	12	18		18		9	2	253		1	1	33		5	2		16	1		1		372
4.5	13	10		12		16	5	268			1	30		3	1		3			2		364
8.5	30	6		12		19	10	304			1	22		3	3		4			3		417
12.5	14	14		10		13	6	210		3	2	36		4			12					324
16.5	63	24		4		27	11	137			1	37		1	1		10			1		317
20.5	64	26		12		34	20	180			2	19		3	3		3	3		1		370
23.5	48	16		6		31	7	168			1	41	1	3	4		17	1		2		346
27.5	38	8		4		28	4	190				5			137		2	1				417
32.5	40	6		5		27	1	153			1	9			140		7			2		391
37.5	56	3		7		22	3	106				5		2	188		13		1	1		407
41.5	64	6		1		17	1	47			2	1			200		5					344
48.5	58	7		5		15	7	94	3	1		14		3	89	1	8					305
50.5	81	3		6		6		42	2		1	3			120	1	48					313
55.5	77	4		1		11	2	30		1	4	4			149	1	61			1		346
60.5	80	4		2		5	2	46	1	1	1	9			141		44		1	1		338
66.5	72	6		2		3		32		1		5			131	1	75					328
71.5	64	3		2		4	1	42			1	8			154	1	30					310
76.5	94	9		3		5		57			1	35			103	6	81					394
81.5	52	10		5		11		61				50			48	5	90					332
86.5	94	10		9		12	2	54			1	26			69	4	88	1			35	405
91.5	72	6		7		6	2	58		1	1	23		1	46	4	105				27	359
95.5	106	10		3		6	2	64			2	33		1	28	4	110	1			15	385
99.5	157	6		1		7	1	98			2	21			32	1	38	2				366
105	112	6		4		5	2	44			1	40			36	1	81				10	342
110	63	6		11				134				6			38	1	30					289
115	86	6		10		7	1	83				34			41	1	55				3	327
121	133	5		7		8	2	52				6		1	70	1	25				3	313
126	111	4		3		13	2	64			2	9			103	1	18					330
130	79	15		11		1	1	76			1	12		2	63		41			3	16	321
134	145	4		1		1		111			1	12			43		13					331
139	120	9		6		4	1	138			2	16		1	42		16					355
143	132	15		7		12	1	148			1	20	1		57		32			1	15	442
149	94	5		12		9	4	110		1	1	37			36		12					321
154	107	11		2		10	1	130			2	15		1	9	2	62					352
159	88	12		6		10	2	135			2	12		1	15		26				10	319
164	64	11		16		10		188			1	2			7		21			1	20	341
169	109			6		2	1	157			1	4			17		43					340
174	68	8		5		7	2	176		1	1	7		1	10		39	1		1	10	337
179	85	9		6		10	2	178	1		1	8		1	15		19	1				336
184	117	15		16		15	2	185			1	12			16	1	19	2			10	411
189	145	5		8		6	1	136			2	5			65	1	24	1			10	409
194	102	2		7		6		140	1			15			44	1	19	12			5	354
199	12	3		5		14		118				12			126		37	15			10	352
204	10	4		16		16		133		1	1	13			68		27	18	1		35	343
210	58	7	1	10		26	1	123		1	4	20		4	19		21	21	1		20	337
214	95	6		8		15		120			2	25					20	14				305
219	60	2		8		20		165			2	25		2			16	15	2		30	347
224	110	5	1	10		28	1	150	2		4	17		3	3		18	16	7		10	385
229	116	6	1	5		16	2	125	1	1	1	29		2			26	7	2		33	373
234	120	5	2	1	1	24	5	151			2	32		3			28	5	1		18	398
239	66	2	1	1		12		145			1	29		3	14	1	26				35	336
243	92	1				18	1	150			1	71		5	21		28	3		1		392
249	98	1				6		145				9		2	25	1	41				40	368
254	40	3			1	3		135			1	28		5	42		60					318
259	64	1				5		148	2		1	22		1	65		41					350
264	72	2				2		163			1	9			70		26				28	373
269	58	6				8		173			1	9			35	1	38	1			15	345
274	82					4		145		1		3		1	52	1	23				21	333
279	98	1				3		173			1	5			69	2	70	1			60	483
284	97	2		1		6		118				8			51	1	72	1			27	384
289	80	4			1	8		101				20			54	1	61				3	333
294	81	1				3		104				15			66		33				35	338
299	93			1		2		69			1	6		1	115		23				25	336

Table B.9. Right coiling (d = dextral) *Neogloboquadrina incompta* and left coiling (s = sinistral) *Neogloboquadrina pachyderma* counts in cores GeoB 20601-4, 8342-6 and 8336-6

GeoB 20601-4			GeoB 8342-6			GeoB 8336-6		
Core depth (cm)	Right coiling (d)	Left coiling (s)	Core depth (cm)	Right coiling (d)	Left coiling (s)	Core depth (cm)	Right coiling (d)	Left coiling (s)
0.5			0.5	44		0.5	2	
4.5	4		4.5	5		4.5	1	
8.5	12		8.5	13	1	8.5	55	1
12.5	3		12.5	19	1	12.5		
16.5	99	1	16.5			16.5	1	
20.5	35		20.5	4		20.5	44	1
24.5			24.5	30		23.5	4	
28.5	99	1	28.5	93	2	27.5	132	3
32.5			32.5	143	9	32.5	140	
36.5	99	2	36.5	128	2	37.5	179	3
40.5	100	1	40.5	173		41.5	175	25
44.5	100	1	44.5	162		48.5	89	
48.5			48.5	160		50.5	114	6
52.5	60	2	52.5	173		55.5	144	4
56.5	82	2	56.5	155		60.5	139	1
60.5	85	3	60.5	155		66.5	131	
64.5	91	3	64.5	139		71.5	150	4
68.5	87	3	68.5	86	2	76.5	101	2
72.5	66	3	72.5	76		81.5	42	6
76.5	93	1	76.5	80		86.5	67	1
80.5	109	3	80.5	44		91.5	46	
84.5	77	1	84.5	10		95.5	70	1
88.5	126	1	88.5	7		99.5	30	1
92.5	96		92.5	19	1	104.5	36	
96.5	132		96.5	19	3	109.5	37	1
100.5	203	1	100.5	46	2	114.5	37	3
108.5	178		104.5	59	3	120.5	70	
116.5	145		108.5	184		125.5	128	2
124.5	74		112.5	77	7	129.5	62	1
132.5	61	1	116.5	90		133.5	43	
140.5	6		120.5	77	2	138.5	42	
148.5	4		124.5	82		142.5	57	
156.5	40		128.5	66		148.5	33	1
167.5	92		132.5	90		153.5	8	1
176.5	54	1	136.5	58		158.5	12	1
184.5	69	1	140.5	52		163.5	7	
192.5	101	1	144.5	54		168.5	16	1
200.5	60	2	148.5	72		173.5	10	
208.5	126		152.5	68	2	178.5	15	
216.5	114	1	156.5	33	2	183.5	15	1
224.5	86	2	160.5	38	2	188.5	65	
232.5	12		164.5	41	3	193.5	44	
240.5	102		168.5	57	2	198.5	126	
248.5	94		172.5	51		203.5	68	
256.5	97		176.5	83		209.5	18	
266.5	35	1	180.5	50		213.5		
274.5	79	2	184.5	46	1	218.5		

Table B.9. *(continued)*

GeoB 20601-4			GeoB 8342-6			GeoB 8336-6		
Core depth (cm)	Right coiling (d)	Left coiling (s)	Core depth (cm)	Right coiling (d)	Left coiling (s)	Core depth (cm)	Right coiling (d)	Left coiling (s)
282.5	83	1	188.5	18		223.5	15	1
290.5	85	3	196.5	4		228.5		
			204.5	6		233.5		
			212.5	33		238.5	13	1
			220.5	42	1	242.5	19	1
			228.5	64	6	248.5	25	
			236.5	69	3	253.5	40	2
			244.5	46	8	258.5	60	5
			252.5	65	5	263.5	65	5
			260.5	81	5	268.5	34	1
			268.5	28	4	273.5	35	17
			276.5	34	2	278.5	59	7
			284.5	34	4	283.5	47	4
			292.5	133	2	288.5	54	
			300.5	94	2	293.5	66	
			308.5	142	3	298.5	114	

Table B.10. Benthic foraminifera counts for core 2634

Core depth (cm)	*Ammonia beccarii*	*Brizalina spathulata*	*Bulimina* spp.	*Cancris auriculus*	*Cassidulina laevigata*	*Elphidium advenum*	*Elphidium crispum*	*Globobulimina turgida*	*Lobatula lobatula*	*Nonion boueanus*	*Oolina* spp.	*Quinqueloculina* spp.	*Uvigerina* spp.	Sum
17.5	149	53	36		13	31	4		2	14			4	306
22.5	169	36	29		12	41	3		3	18			4	315
27.5	137	38	16		9	45	9		1	24			8	287
32.5	120	65	13		13	36	20		3	10			4	284
37.5	122	32	28		10	35	9		1	13		1	7	258
42.5	170	55	35		15	33	17		2	25			6	358
47.5	140	43	33		19	22	26		2	22			3	310
52.5	144	17	16		16	30	19		1	28			10	281
57.5	146	4	20		19	30	42		5	36			15	317
62.5	134	7	30		43	40	20		3	21			13	311
67.5	142	11	28		17	37	31		10	37			10	323
72.5	177	1	10		13	31	29		6	40			13	320
76.5	56	4	21	2	19	70	25		40	11	1	2	2	253
81.5	58	1	23	8	7	62	45		46	11		10	1	272
91.5	62	1	17	4	15	50	43		32	21		4	5	254
99	53	6	23	7	12	84	48		58	15	2	15	1	324
101	51	5	28	4	32	29	27		29	23		8	6	242
102.5	51	5	20	4	38	33	6		16	19		7	5	204
108.5	6	2	4		1	7	2	1	1	4			1	29

Table B.11. Benthic foraminifera counts for core 2658

Sample depth (cm)	*Ammonia beccarii*	*Amphicoryna* spp.	*Anomalinoides* sp.	*Brizalina alata*	*Brizalina spathulata*	*Bulimina gibba*	*Bulimina marginata*	*Cancris auriculus*	*Cassidulina laevigata*	*Cibicidoides* cf.*bradyi*	*Cibicidoides* spp.	*Cibicidoides ungerianus*	*Dentalina* spp.	*Elphidium advenum*	*Globobulimina turgida*	*Globocassidulina subglobosa*	*Karreriella* spp.	*Lenticulina calcar*	*Lenticulina cultrata*	*Lenticulina gibba*
12.5	24				44	3			198					24	11					
19.5	93				33	34			105					22						
24.5	156				36	15	2	2	70					20	2					
29.5	143				5	4	1		82					53						
34.5	75				16	14	4		142					55						
39.5	67				8	4	1		174					54	1					
44.5	134				6	12		1	70					21	5					
49.5	84				14	17	3	1	117					29	5					
58	6				60	61		9	38					3	1					
64.5	6				115	80		7	41						9					
69.5	2		2	1		1		3		1		13	2					16	1	
73.5	2	1	7	20		2				33		26				2	2	13	6	1
77.5		1	1	10						53		4	4			1		9	2	
87.5		1	4	16						18	1	10	8					11	6	
96.5		3	2	4						15		12	3				3	13	4	3
102.5		3	4	2						14	3	21	5			1	5	23	8	3
207.5		5	1	8						13	1	16	4			1	3	11	10	2
115		2	7	8						15	5	22	6			1	3	11	6	2
122.5		3	5	12						27	4	23	5			2	3	8	2	2
131.75		4	7	18						7	2	26	2			2	2	3	4	
142.5		7	4	2						6		20	6				9	10	8	4

Table B.11. *(continued)*

Sample depth (cm)	*Lenticulina inornata*	*Lobatula lobatula*	*Marginulina* spp.	*Martinottiella* sp.	*Melonis barleeanum*	Miliolids	*Nodosaria laevigata*	*Nodosaria spp.*	*Nonion boueanus*	*Oridorsalis* sp. + *Gyroidina. broeckhiana*	*Plectofrondicularia* spp.	*Pullenia bulloides*	*Rectuvigerina nicoli*	*Saracenaria italica*	*Siphonina* sp.	*Siphonodosaria consobrina*	*Sphaeroidina bulloides*	*Uvigerina* spp.	Sum
12.5		22				2			1									2	331
19.5		3							8				3					6	307
24.5		8							14				2					1	328
29.5		10							7										305
34.5		12							4									1	323
39.5		2							14									1	326
44.5		11				2			77				1						340
49.5		11							33				3						317
58		3					1		165				1					3	351
64.5		3							79				6					7	353
69.5	1		3		1				5	25					1		33	91	202
73.5	1		0	1	5					20		1		1	3	1	27	133	308
77.5	4		4	1	1			7		36	1	2		1		1	36	140	319
87.5	2		1	1	2	1				22	2			1	6		30	162	305
96.5	3		2	1	1					35				1	3	1	28	163	300
102.5	4		8	1	6					24				3	6		31	141	316
207.5	1			1	5					17				3	4		30	106	242
115	2		5	1	6					44	1			1			30	105	283
122.5			2	2	8					28	1			3	2		24	98	264
131.75	4		1	1	5					19				1	4	3	14	112	241
142.5	2		4	1	1	2				57	1			2		1	46	95	288

Table B.12. Benthic foraminifera counts for core 2670

Sample depth (cm)	*Ammonia beccarii*	*Amphicoryna* spp.	*Anomalinoides* sp.	*Astacolus crepidulus*	*Bolivina reticulata*	*Brizalina alata*	*Brizalina* sp.	*Brizalina spathulata*	*Bulimina marginata*	*Bulimina* spp.	*Cassidulina laevigata*	*Cibicidoides* spp.	*Clavulina* spp.	*Dentalina* + *Laevidentalina* spp.	*Elphidium advenum*	*Globobulimina turgida*	*Globocassidulina subglobosa*	*Gyroidinoides soldanii*	*Karrierella* spp.	*Lenticulina calcar*	*Lenticulina inornata*	*Lenticulina iota*	*Lenticulina* spp.
2.5	116							23			10				20	7							
13	71							18			12				22	3							
22.5	82							26			20				26	10							
32.5	113							23		1	30				25	16							
42.5	23							45	1	4	38					2							
47.5	82							19	3	3	11												
62.5	29							37			33					2							
72	48							5	6	6	58					3							
76.5	75							4	0	2	31					2							
84.5	66							7	18	18	29					4	4						
88.5	6					2		2	2	2	6	6					22		2				6
97.5	2	1	1			5				1		30					51		2	4	3	2	11
108			3		1	3				8		23	1	1			102		6	2	2	4	11
118		3	4		1	3				1		21	3	2			51		3	2	3	3	9
128			7		2	1						25	4	4			82		8	2	5	3	8
138		2	7	1		2				1		7	3	3			31		11	8	9	17	9
148		2	5	1	3	4						6	1	1			64		7	2	7	3	8
158		1	3	1	5	1	1			1		15	2	2			61	1	3	6	4	5	14
168		1	1	1	1							4	2	1			49		3	2	4		12
178		2	6		13	3	2					15	1	1			90		6				
188			5		9	12	16					14	4	2			98		9	2			5

Table B.12. *(continued)*

Sample depth (cm)	*Lobatula lobatula*	*Marginulina* spp.	*Martinotiniella* sp.	Miliolid	*Nodosaria laevigata*	*Nodosaria latejugata*	*Nonion boueanus*	*Oridorsalis* sp. + *Gyroidina. broeckhiana*	*Plectofrondicularia* spp.	*Rectuvigerina nicoli*	*Saracenaria* spp.	*Siphonina* sp.	*Siphonodosaria consobrina*	*Sphaeroidina*	*Spiroplectammina* sp.	*Uvigerina* spp.	*Vaginulina* spp.	Sum
2.5	10						17											203
13	12						31											169
22.5	10						53											227
32.5	11			1			68									12		300
42.5	15			14			7											149
47.5	8			3			6			11								146
62.5	27			4			2			10								144
72	34						1			3						1		165
76.5	25			5			4			18						2		168
84.5	18						7			7						7		185
88.5	7	2		15			15	21		6		2			2	42		168
97.5		1		14	2		4	80	1	3	1	1	1		4	73	2	300
108		2		5				88	1		2	4	1	2	3	39	2	316
118		2		13	1			112	3		3	5	1	3	5	46	3	306
128		2		22	1			68	2		2	5	2	9	5	33		302
138		2		11	3			123	1		7	1	1	5	6	36	1	308
148		5		4	1			62	1		3	1	4		2	38		235
158		3			4	3		105	2		2	1			1	36	2	285
168		1	1					135	2						2	31	2	255
178		1			1			61	1			4				37		244
188		2			2			68				5				28		281

Table B.13. Benthic foraminifera counts for core 2682

Sampling depth (cm)	*Ammonia beccarii*	*Amphicoryna* spp.	*Anomalinoides* sp.	*Bolivinia reticulata*	*Brizalina alata*	*Brizalina spathulata*	*Bulimina marginata*	*Bulimina* spp.	*Cancris auriculus*	*Cassidulina laevigata*	*Cibicidoides* spp.	*Dentalina* + *Laevidentalina* spp.	*Elphidium advenum*	*Globobulimina turgida*	*Globocassidulina subglobosa*	*Lenticulina calcar*	*Lenticulina iota*	*Lenticulina* sp.	*Lobatula lobatula*	*Marginulina* spp.	Miliolids
7.5	56					126		6		90			11	6					3		
12.5	56					31		1	1	145			30	53					15		1
19.5	45					30	4	10		14			14	187					6		
26	193					6	3	9	3	52			18	3					7		
35.5	186					1				77			21	2					21		
46	79					4		9		82			3	12					29		3
52	11									5									8		2
60.5	42																		1		
68.5	47					7				3				55					4		
75.5	17					43				6	1								6		
78.5	2			7		15				4	6	2		4							
94.5			3	24	3						13	4			2					1	
109		1	9	16	3						9	2			1	1	4	1		2	
132		2	9	7	6						4	5			1	1		7			
147		3	7	5	5						6	2						3			
160		1	3	11	1						17	4					1	4			

Table B.13. *(continued)*

Sampling depth (cm)	*Nodosaria latejugata*	*Nonion boueanus*	*Oridorsalis* sp. + *Gyroidina. broeckhiana*	Plectofrondicularia spp.	*Rectuvigerina nicoli*	Siphonina sp.	*Siphonodosaria consobrina*	*Sphaeroidina bulloides*	Uvigerina spp.	*Vaginulina legumen*	sum
7.5		6							19		323
12.5		5									338
19.5											310
26					1						295
35.5		1									309
46		7			7						235
52					1						27
60.5		5									48
68.5		58			5				1		180
75.5		19							4		96
78.5		1							12		53
94.5			8			1	1	1	30		91
109			18	1		5		1	30	1	105
132	4		29			1		3	32	1	112
147			44	1		4			52	2	134
160			50	1		3		3	44	4	147

Table B.14. Benthic foraminifera counts for Walvis Bay-Lüderitz cores 1406, 1441, 1307, 1401

Core	Core depth (cm)	*Ammonia beccarii*	*Amphicoryna scalaris*	*Brizalina spathulata*	*Bulimina* spp.	*Bulimina marginata*	*Cancris auriculus*	*Cassidulina laevigata*	*Elphidium advenum*	*Elphidium crispum*	*Globobulimina turgida*	*Hyalinea balthica*	*Lagena* sp.	*Lobatula lobatula*	*Nodosaria (Glandulina) laevigata*	*Nonion boueanus*	*Oolina hexagona*	*Quinqueloculina* spp.	*Rectuvigerina nicoli*	*Uvigerina* spp.	Sum
1406	**2**	119		79			5	2	30		9	49		7		1		1		1	305
1406	**35**	17		124		5	5	45			9			4	1	8		1	3	84	341
1406	**40**	14		126		9		40			3			3		12			1	94	342
1406	**46**	10		240	16	2					2					2				33	351
1406	**49**	1		168			3	32						3		43			2	50	351
1441	**2**	210		20	1		1	6	75		4	11		5		2		12		2	351
1441	**10**	131		91	5	1	1		93		4	8		5			1	4	1	1	356
1441	**34**	1		46		1	1	3	1		1			5	1	1		0	2	272	369
1441	**44**	2		2				1	0		1			3		1		1	1	307	363
1441	**47**	4		1			1		1		1					2				292	349
1441	**55**	0		7					2		1	1		4		6				231	307
1307	**2**	82		67				3	195			7		12			1	6		1	376
1307	**16**	130		20	3	1	4	82	94		7			14		1		5		1	378
1307	**19**	22		8		1	2	1	1		2	1		5	1	15		1	1	289	369
1307	**58**	28		9				11	40		1	3		4		11				217	382
1307	**60**	4		3			1		1						10					283	362
1307	**68**	0		1					1					1		2				94	167
1401	**4**	134		62			1	4	92		6	10		4		1		2		1	321
1401	**9**	116		50	1			39	106		9	11		11				2	1		355
1401	**33**	89		6			6	38	7		3	2		7		16			1	158	366
1401	**35**	150	3	2	5	3	8	106	10		2			5		33		3		37	402
1401	**55**	19		1	4		1	12	4							6		1		6	109

Table B.15. Benthic foraminifera counts for core 1479

Core	Core depth (cm)	*Ammonia beccarii*	*Amphicoryna scalaris*	*Brizalina spathulata*	*Bulimina* spp.	*Bulimina marginata*	*Cancris auriculus*	*Cassidulina laevigata*	*Elphidium advenum*	*Elphidium crispum*	*Globobulimina turgida*	*Hyalinea balthica*	*Lagena* sp.	*Lobatula lobatula*	*Nodosaria (Glandulina) laevigata*	*Nonion boueanus*	*Oolina hexagona*	*Quinqueloculina* spp.	*Rectuvigerina nicoli*	*Uvigerina* spp.	Sum
1479	**4**	169		73			1	16	61		3	18		5		3		1		3	357
1479	**16**	162	1	13	2	1	2	31	66		12	6		2		10		1		10	335
1479	**20**	193		20	3	1	1	66	25		1	1	1	2	1	8	1	1	1	9	355
1479	**34**	45		76		8	8	32	6		8			8		28			2	117	372
1479	**37**	9		116		6	6	3			6	3				15			6	144	351
1479	**50**			5				2	1		1					1				300	360
1479	**52.5**	63		15			1	1	10		10	18		2		20				185	377
1479	**55**	57		31				11	42		1	19		1		9				160	386

Table B.16. Benthic foraminifera counts for core GeoB 20601-4

Core sample depth (cm)	*Bolivina* spp.	*Bulimina aculeata*	*Bulimina marginata*	*Bulimina mexicana*	*Bulimina* spp.	*Cassidulina laevigata*	*Chilostomella oolina*	*Cibicidoides pachyderma*	*Cibicidoides* spp.	*Cibicidoides wuellerstorfi*	*Dentalina* spp.	*Eggerella bradyi*	*Epistominella exigua*	*Favulina hexagona*	*Fissurina* spp.	*Fursenkoina* spp.	*Globobulimina* spp.	*Globocassidulina spp.*	*Gyroidinoides orbicularis*	*Karerriella bradyi*	*Lagena demorpha*	*Lagena* spp.	*Lenticulina* spp.	*Martinottiella communis*	*Melonis barleeanus*	Agglutinated	Miliolids	*Nodosaria laevigata*	*Nodosaria spp.*	*Oolina globosa*	*Oridorsalis umbonatus*	*Procerolagena gracilis*	*Pullenia bulloides*	*Pyrgo* spp.	*Siphonaperta* sp.	*Sphaeroidina bulloides*	*Spiroloculina communis*	*Ehrenbergina trigona*	*Uvigerina auberiana*	*Uvigerina hispidocostata*	*Uvigerina peregrina*	*Uvigerina spp.*	*Vaginulina legumen*	*Vaginulina spinigera*	*Vaginulina sp.*	Not identified	Sum
1		5	1	6	2				29								1		1	1			1	1		8	1		1					1							20					5	85
4.5	1	10	2			1			39														1	1	3	15		1	2		1		5							19					8	111
8.5	1	7				1			38								1	1	1	2				1		20		1			1		3	1	1					30					7	117
13		9	2					47	7								1	2		4			2	3	2	11	1	4					5	3						30					7	140
17		9	2					36	8									2		1				3	1	26							9	2						25					9	133
21		4	5					40	5	4							1					1		4	4	15	1	1					7	2						32					5	131
25	1	17	1					19	24	3	1									1		1		2		13							4					1		27		1			10	127
29		18					1	28	6	1								1		3				5		11	3		1				6	3				2		65					10	164
37		15						21	4	2		1	1								1		1	4	3	10	2	1					2	6						98		1			6	179
41	2	6	1					16	6	2		1											1	1	2	9	2						3	3						116					10	181
45	1	7						1	11												1		1	2	3	5	7							4						116					10	169
49		2						5	13	5		2												1	3	9	2	2	6				12	1						13				4	8	88
53		4						2	11	5		2			1										1		6						7	2					1	2				1	11	56
57		4						5	9	1		4									1						2																		7	33
61		15	1					8	8			12			1									3			5	1	1				9	10											11	85
65		16			1			3	10	6		11															2		1		1		7	6						2						69
69		24						7	2									1		4				1		4							2	3		6				136					14	205
73		32	2		1			19	10	6				3			1			6						5							1	13		8				191				1	10	310
77		23	3					6	3	2							1			3						1							6	8		6				77		1	1		8	149
81		47	4		3			30	11	6				1						6			3			2	1						5	18		6				148					29	320
85		37	2					25	2	4							1			2						2	1						5	8		10				126					19	245
89		40	1			6		6	6	12		2	13											1		1	7		1				9	4			1			2					20	133
93		20						29	23	21		13	13											1			1	1	1				11	38				1							22	195
97		5						19	4	15		11							2					1			7		2				1	8						4			1			80
109		34				1		29	3	3		2	5						2					4							3		4	8						24						118
117		1	5		1			60	1	9		2	3				1		4									1			1	1	4	31				1		48					6	179
125	1	55						74		1		1	1		1				10									1					4	16			1			49				1	7	223
133		7						72	6	1			1						9									1					3	6				1		134					1	242
141		6	1					124		1			2				2		4				4				1				2		3	3						51				1	3	208
149		12	1					32	3	3		5	6				6						7	1				2					1	2		2		2		50					6	141
157		14				1		8	3			1	1				1						4	2	2	1	1						2	12		2				250					12	317
168	1	32	3			21		12	9	10		3	4						1				3	4	2	2	4							3		1				213					18	352
177		16	2			5		7	5	9		4											6	3		3	3		1					15		4		1		234					4	325
185		7				5		1	3	6															2	4	6				3		1	3		2				25					3	72
193		26	1			5			2				2			1	2		3					3		9	1	1	2		6		7	5		3				20					5	118
201		10			1				1	2			4						4							5	1	1	1		1		1	1					1	7					4	45
209		7	1			1		1	1	4			1			1	1							1		1		2			1	1	3			1				15						44
217	4	46	1		3			3	5	1		1	1				1							3		17					3		4	6						130					4	233
225	4	22	3					3		1			1										1	2		8					5		4	3						122					3	182
233	3	36	8					5	5	1		2	1		1	2	2	1						1		9					2		5	5						190	4				4	287
241	4	12	3			4		1	1				2				5							4		11					1		2	4		1				83					2	140
249	3	29	2			1		6	2			1	7			3	2						5	1		9								3				1		13	20			1		109
257		4				12	2		3				9			2	1				1					6	1	1					5	3		3				2	1				4	61
267		3				2	1			2			3				1		1							6							2	5											3	29
275	1	7	1			4			5	3		4	4										2		1	15	1	2			7			8						17					7	89
283		2				3			1	6		1	4				1							6		16		1					10		3				4						58
291	1	26	3						1	1			1						1					1		22						1	3						3					3	67
299		51	1							1													1			40					1	1	1		1				3	1					103

Table B.17. Benthic foraminifera counts for core GeoB 8342-6

Core depth (cm)	Agglutinated	*Ammonia beccarii*	*Bulimina aculeata*	*Cibicidoides pachyderma*	*Cibicidoides* spp.	*Cibicidoides wuellerstorfi*	*Eggerella bradyi*	*Ehrenbergina trigona*	*Epistominella exigua*	*Fissurina* spp.	*Fursenkoina* spp.	*Globobulimina* spp.	*Globocassidulina* spp.	*Gyroidinoides orbicularis*	*Lagena demorpha*	*Lagena hispida*	*Lagena sulcata*	*Lenticulina* sp.	*Martinottiella communis*	*Melonis barkeanum*	*Melonis pompiloides*	Miliolids	*Oolina globosa*	*Oridorsalis umbonatus*	*Pocerolagena gracilis*	*Pullenia bulloides*	*Pyrgo* spp.	*Sphaeroidina bulloides*	*Uvigerina auberiana*	*Uvigerina hispidocostata*	*Uvigerina peregrina*	*Uvigerina proboscidea*	*Uvigerina* spp.	Not identified	Sum
0.5	5			5		2	1		3	3				1				2			2		1				3						6	34
4.5	1			2	1	1	2		1				2							2	0	2					6		2				2	24
8.5	1			2	1	2			3				1						1	1	2	2		3			5		4			1	5	34
12.5				1		1	2		1	2			3						1	1	0	2					12		1	3			3	33
16.5				4	1	2			1				1		1				1		0	2		1			11		1		1		3	30
20.5				1		1			2	1											0						2						2	9
24.5				4	2						1			1					1		0			1			6			2	2			20
28.5				1	3	3				1	1								1	1	0	2		1			8						4	26
32.5					1	3			2				1	1					1	1	0						7						2	19
36.5				1	1	5			1			1	2	1						2	3			2		1	2			1			1	2	26
40.5				1	4	1			5	1		2								1	5	1		1		1	8		3				1	3	38
44.5				1	4	2			1	2	3	1								4	3	2					19	1	1				2	5	51
48.5					3	2	2		2	1	1		1					1		1	4			1		2	5		3				11	40
52.5				1	4	5	1		10	3	3			1						3	0	2				1	5		5		1		1	46
56.5							1		11		5			1	2			1		1	3	2					4		4				3	38
60.5				4	5	3			11	1	5		1							3	1			1				9	2		1		7	54
64.5				1	1	1			6	2	3	1								2	2	1					6		2			1	7	36
68.5					1	1			3		1		1							2	0					1	8		4		3		1	26
72.5						4			6	1	1	1	3		1					7	1	1		3			5		5		2		2	43
76.5			1	1	2	2			15		1	1	1							3	0	1					7		3	1	1		2	42
80.5				1	4	1	1		31	5			4		1				1	3	0			1		1	8	1		2	1	1	4	71
84.5					1	1			1	1	1			1					1	3	1						3	1	2					17
88.5					1	4			16	4	1									5	0	2					8		3			4	3	51
92.5						3			7	1	1				1					2	3					2	3		2			2	5	32
96.5					1	5			3	2										2	1	2							5			6	9	36
101					2	4			6	2			1		1					2	0					2	3		1			3	2	29
105					3	2			26						1				1	5	0	1		1	1	2			5			3	5	56
109						5			23	1						1		1		2	1					1						5	2	42
113					5	5	1		38		1				1				1	10	0	1			1	3	1		5			14	6	93
117					5	7			63	1							1			8	1						7		9			2	8	112
121					3	6			29	1				1		1			1	4	1						5		5			5	9	71
125					1	12			45				1						1	14	2		2				9	1	5			6	7	106
129					4	3			12	1	1				1				1	7	1						6		4			1	6	48
133					1	11	2		2		1			1	2				1	3	1						4		4			5	5	43
137		1			1	8			9				1						1	2	1	3		1			7		3			5	3	46
141					5	7			6				1					1	1	1	1			1			2		1			3	7	37
145						7			16	2	1									1	0	1				1	1		1				3	34
149					2	1							7							1	0						2		1			1		15
153					5	9		1	1	4	1	1	16	1	2				2	6	0	1	2	1			11		5			4	10	83
157					4	13			3	1	2	1	14		1				2	6	0		1	1			15		4	2		4	5	79
161					5	4			2				1							2	0						2		2			1		19
165						5	1		2	2			1							1	2	1	1				6		5			2	4	33
169					2	6			19		5		2	1						5	1	1		2			4		6			2	15	71
173					4	6			14		4		3							2	3					1	8		4			5	6	60
177					6	15	1		22	1	4		2		1					4	0	1		2		2	4		2	2		10	9	88
181					4	6		1	8	3	2		6							5	0			1			8		5			10	5	64
185						6	1		20	1	4	1	3							4	2	3		1			3		1			2	6	58
189						10		1	25	2	1		3	1						1	0		1	1			10		1	1		4	1	63
197					1	9	2		5	1				2				1		1	0	1		1			4		1	1			7	37
205					2	4	1		7	2				3				1			0	1					4		2			1	5	33
213						3	1		1	1			1	1						3	0	1		1			4	1		3		4	5	30
221					4	6			2	5	4		5	1	1			1		1	0	2					7		3	2		14	3	61
229					2	7			11	3	2		2							4	1			1			4					4	3	44
237					5	2		1	7	1			10				2			3	0	2					3		2	1		7	8	54
245					2	5	5		9	3	1		6	1			1			1	2	1	1				9		1	1	1	12	6	68
253					5	6	1		24	3	6	1	11		1	1		1		1	1	4					5		1			17	3	92
261					2	7	2	1	24	1	2		10		1			1	1	3	1	1				1	4		1			4	3	70
269					9	4			16	2	2		6							2	0	2		1		1	4		1			2	3	55
277					4	2	1		9	1	1		21		1			1		3	3	1	2	1	1		12		1			3	8	76
285						3		1	8	1	4		17		1				2	3	2	1	1				1		1				1	47
293					8	11	1	1	39	3	9		66		1				4	8	3	2				1	13		7			15	1	193
301					2	7	2	1	28	1	13		27				1		2		1			1		2	6		2	1		7	1	105
309					4	6	1	2	32	5	6		49					3		3	0	1		3			26		3			11	8	163

Table B.18. Benthic foraminifera counts for core GeoB 8336-6.

Core sample depth	Agglutinated	*Cibicidoides crebbsi*	*Cibicidoides pachyderma*	*Cibicidoides* spp.	*Cibicidoides wuellerstorfi*	*Eggerella bradyi*	*Ehrenbergina trigona*	*Epistominella exigua*	*Fissurina* spp.	*Fursenkoina* spp.	*Globobulimina* spp.	*Globocassidulina* spp.	*Gyroidinoides orbicularis*	*Karreriella bradyi*	*Lagena demorpha*	*Lagena sulcata*	*Lenticulina* spp.	*Melonis barleeanum*	*Melonis pompiloides*	Miliolids	*Oolina globosa*	*Oridorsalis umbonatus*	*Pullenia bulloides*	*Pyrgo* spp.	*Siphotextularia concava*	*Sphaeroidina bulloides*	*Uvigerina auberiana*	*Uvigerina hispidocostata*	*Uvigerina peregrina*	*Uvigerina proboscidea*	*Uvigerina* spp.	Not identified	Sum
0.5		6	9		6	3		2				1					2	4	0	3	1	1		5		1	1	2				2	49
4.5		1	5		6	3		2										3	0	1	1	1		3			3	2				2	33
8.5		2	3	1	9	3		3	2	1	1	4					1	3	0	1	2			8			8	4				7	63
12.5		4	1	1	10	1		6	1	3		1						12	0	5	1			11		1		4				3	65
16.5		1		1	10	2		4	2	3								3	0	5		1		9			4					6	51
20.5		3	5	9	11	7		6		2		1					1	5	0	4		4		22			7					10	97
23.5		1	2	1	9	1		8	3	2								6	2	2	1	4	1	2			3	2		2		5	57
27.5			1	1	9	2		12		1		1						12	6	2	1			7			1	2			1	8	67
32.5		3	4	6	10	2		12	3	2								11	0	2		3	4	6			5				1	7	81
37.5			6	5	7			23		2							1	9	4	1		2		6			7	1			2	5	81
41.5			1	1	2	1		16		1						1		4	0	1		1	5	2			9	2			1	3	51
48.5		8	3	9	15			24	4	2								14	4			1	6	2			10	5		6	3	7	123
50.5		1	2	7	1	2		17	2	6								7	0			2	9	1			28	8		1	10	6	110
55.5			6	10	7			32	1	3								4	0				13	5			29	4			7	9	130
60.5			4	3	9			16		3							2	5	1	1		1	1	5			9	6			7	6	79
66.5			2	1	3	1		11	1	4								2	0					4			8				3	2	42
71.5			1	1	9	1		13	1	3	2							4	2	1			3				9	11			10	11	82
76.5			2	3	10	2	1	13	2	2	2							8	2	1	1	2		2			7	3			2	8	73
81.5			1	1	15			28			1				1		1	9	4			2		3			8	1			4	9	88
86.5		1	2	1	8			18	1	3								13	4		1	4		7			12	2			3	5	85
91.5			1	1	14			34	2	1	2							7	3		2	1	3	3			8	6	1	1	8	11	109
95.5			4	1	10	1		23		2							1	3	9		2	2	2	2			3	4			1	8	78
99.5				1	3			11									1	3	10			1		3			8	6			1	8	56
104.5			3	1	10		1	32	1	1								8	3		1	2	1	6						2		1	73
109.5			2	5	11			29							1		1	12	3	2	1	3	3	2			12	12		1	5	12	117
114.5			3	6	11			48							1			10	0	2	1	1	5				20	12			9	7	136
120.5			5	7	7			26							1		2	3	3			3	3				18	23			9	2	112
125.5			1	2	5	1		12		4	1							1	2		1	2	7	3			21	23			1	3	90
129.5				1	12			32		1	1		5					17	2				9	1			18	11			3	7	120
133.5			2	6	10			22		6	3	1						11	3		1	1	3	9			13	4			4	4	103
138.5			2	1	5		1	3		2			2				1	10	10	2		1	3	8			4	2			1	5	63
142.5		2	1	1	19	1		25	1	2	1							12	17			1	2	2			11	2			2	13	115
148.5		1		1	6			3				1						7	10	2	1	6	1	3		1	6	6			8	5	68
153.5		1		7	17			17	1			1				1		9	10	2	1	2	2	6			9	10			5	8	109
158.5		3		3	25			5		2	1	1					1	5	4			6					17	4			1	8	86
163.5		5		5	13	1		5	1			8					1	12	1	1	4	4	2	2		1	2	5			1		74
168.5		1	2		10	2		9	3			13						1	4	5	1	2	1	8		1	10	1			1	3	78
173.5		2	2	2	13			5				14	1	1				2	2	6	1	5	1	4			5	2			2	11	81
178.5		1		3	14		1	5	1			6	1					3	4	1	2	3	1	1		1	9	11			5	13	86
183.5		1		6	12		1	19		1		3	1					6	9	4	1	1	1	3			4	6			6	10	95
188.5			1	1	14	2		11	3	4	1							5	8			5	4	1		2	6	1			5	5	79
193.5				1	7			10		1								4	4			2		3		2	4	5				9	52
198.5		1		1	9	1		15	2	5								11	1	1		9	1	5			9	6			4	14	95
203.5		4	3		8			41	2	4			1					6	5	2		6		4		1	5	6			1	22	121
209.5		1	1	2	10			22	2		1							6	3	2		8		5			6	5			3	12	89
213.5					9			6	2	1			4					3	0	5		4	1	15			5	3				5	63
218.5				1	11	1		4										3	2	2		2		10			2	6				3	47
223.5		1	1		9			4	1			1	1					1	2	1	1	2		10			5	5			1	4	50
228.5		1	1	1	6	1					1	10					1	1	0	2		3	2	7			4	3				9	53
233.5			1	2	14	1		9	1	1	3	23	2					5	1	6		6		19			6	16			4	9	129
238.5			3		10	1	1	8		1		3						2	11	1	3	1		6			4	26			10	4	95
242.5		1	3		4	4		5	1	2		4						3	5	3		1		9			14	24			3	14	100
248.5			1	1	4		1	1	2	3		1	1				1	1	2			3					11	25			5	5	68
253.5	34	3		2	12			10	7	4		10			1	2	1	3	1	2		3	3	2			21	36			9	16	182
258.5	17	4	2	1	9	1		2	2	2		10						6	2	4	1	3		3			3	46			11	8	137
263.5	23	1	1	1	1			14	2	2		2				1	1	4	1	3	1	2	2	6			3	10				8	89
268.5			1	1	7	2		7	1			3				1		1	1	1	1		1	7			2	7			1	4	49
273.5			2	1	2	4		5	2	1					1	1		1	4	1	1	1		2			3	5			4	7	48
278.5		1	1		9	1		7		4		1			2	2		2	3	1		7	3	7			3	4			2	8	68
283.5		2	4		11	8	2	13	2	2		3	2			1	1	3	2	1	2	1	6	4			4	9			1	15	99
288.5		1		1	7		1	4				5	1					4	1			2		2			6	9			1	10	55
293.5		1	2	2	4	2		8		3		4	3				1		2	2	1		1	2			4	8			3	2	55
298.5			1	4	15	1		17	1	3		5	1		1			5	7	1	2			5			6	17			6	7	105

Table B.19. Bivalve counts for northern Namibian shelf cores

Core	Core depth (cm)	Condition	*Anomia* sp.	*Carditella* sp.	*Cardium* sp.	*Dosinia lupinus*	*Hiatella arctica*	*Limopsis chunii*	*Lucinoma capensis*	*Mytilus* sp.	*Nucula nucleus*	*Nuculana bicuspidata*	*Ostrea*	*Pecten* sp.	*Tellina analogica*
2658	8	Whole							1						5
		Chipped							1						1
		Fragments							16						6
2658	13	Whole			2	4			3						5
		Chipped													1
		Fragments				8			8						5
2658	20	Whole				2									1
		Chipped													1
		Fragments				4			27				1		5
2658	25	Whole			1										
		Chipped													
		Fragments				4			8				1		6
2658	40	Whole			1										
		Chipped													
		Fragments							25						12
2658	30	Whole													
		Chipped													
		Fragments							6		1				10
2658	35	Whole													
		Chipped													1
		Fragments							10						8
2658	50	Whole													
		Chipped													
		Fragments							3						5
2658	70	Whole													
		Chipped													
		Fragments												10	
2658	88	Fragments												20	
2658	97	Fragments												35	
2658	103	Fragments												55	
2658	108	Fragments												10	
2658	115	Fragments												22	
2658	123	Fragments												25	
2658	143	Fragments												9	
2658	160	Fragments												2	
2670	3	Whole				4			1		2				
		Chipped													1
		Fragments				4			18						18
2670	13	Whole							1						
		Chipped							1						
		Fragments							4						24

Table B.19. *(continued)*

Core	Core depth (cm)	Condition	*Anomia* sp.	*Carditella* sp.	*Cardium* sp.	*Dosinia lupinus*	*Hiatella arctica*	*Limopsis chunii*	*Lucinoma capensis*	*Mytilus* sp.	*Nucula nucleus*	*Nuculana bicuspidata*	*Ostrea*	*Pecten* sp.	*Tellina analogica*
2670	23	Whole				2			4						
		Chipped													
		Fragments				2			30						
2670	33	Whole							12						
		Chipped													1
		Fragments							16						
2670	43	Whole							1		1				
		Chipped													
		Fragments							16		1				8
2634	81	Whole			3	4			2			5			
		Chipped										2			2
		Fragments				4			10						5
2634	92	Whole			2										
		Chipped			2				1						1
		Fragments							10						
2634	96	Whole			1										
		Chipped													
		Fragments							4	8		2			

Table B.20. Gastropod counts for northern Namibian shelf cores

Core	Core depth (cm)	Condition	*Comitas saldanhae*	*Marginella* spp.	*Nassarius vinctus*	*Turritella declivis*	*Volutacorbis lutosa*	Unidentified
2658	8	Whole			5			
		Chipped						
		Fragments			1			
2658	13	Whole						
		Chipped						
		Fragments						10
2658	20	Whole						
		Chipped						
		Fragments						
2658	25	Whole	1		20			
		Chipped			5			
		Fragments						
2658	40	Whole			14			
		Chipped	1					
		Fragments						
2658	30	Whole			2			
		Chipped			1			
		Fragments			1			
2658	35	Whole			5			
		Chipped						
		Fragments			1			
2658	50	Whole						
		Chipped						
		Fragments						10
2658	70	Whole						
		Chipped						
		Fragments						
2658	88	Fragments	1		20			
2658	97	Fragments			5			
2658	103	Fragments						
2658	108	Fragments			14			
2658	115	Fragments	1					
2658	123	Fragments						
2658	143	Fragments			2			
2658	160	Fragments			1			
2670	3	Whole			1			
		Chipped			5			
		Fragments						
2670	13	Whole			1			
		Chipped						
		Fragments						

Table B.20. *(continued)*

Core	Core depth (cm)	Condition	*Comitas saldanhae*	*Marginella* spp.	*Nassarius vinctus*	*Turritella declivis*	*Volutacorbis lutosa*	Unidentified
2670	23	Whole			5			
		Chipped						
		Fragments			1			
2670	33	Whole						
		Chipped						
		Fragments						10
2670	43	Whole						
		Chipped						
		Fragments						
2634	81	Whole	1		20			
		Chipped			5			
		Fragments						
2634	92	Whole			14			
		Chipped	1					
		Fragments						
2634	96	Whole			2			
		Chipped			1			
		Fragments			1			

Table B.21. Bivalve counts for the Walvis Bay-Lüderitz cores

Core	Sample depth (cm)	Condition	*Anomia sp.*	*Carditella sp.*	*Cardium sp.*	*Dosinia lupinus*	*Hiatella arctica*	*Lucinoma capensis*	*Nucula nucleus*	*Ostrea*	*Pecten sp.*	*Tellina analogica*
1441	2	whole				2						
		chipped				2						
		fragments			16		4				2	
1397	2	whole			1	3	1		1			
		fragments			8	1	2					
		chipped	1									
1384	2	whole			1	1						2
		chipped				3						
		fragments			24	1		1			4	
1407	2	whole				2						
		chipped						1				
		fragments			3		6					
1307	2	whole			1	3						
		chipped							1			1
		fragments	1			4		1	1			5
1364	2	whole			2	1			2			
		chipped				1						
		fragments		1	16		3				3	
1406	2	whole						1				
		chipped										
		fragments			4		10					
1475	2	whole			1	4			1			1
		chipped							3			
		fragments		2	12	3	5	1			2	
1479	2	whole			1	2	1	1				3
		chipped					1					
		fragments			14						1	
1657	2	whole				3						
		chipped			1					1		
		fragments			12				4		1	
1441	10	whole										
		chipped						2				
		fragments				4		88				
1384	12	whole										1
		chipped										
		fragments				1	20					

Table B.21. *(continued)*

Core	Sample depth (cm)	Condition	*Anomia sp.*	*Carditella sp.*	*Cardium sp.*	*Dosinia lupinus*	*Hiatella arctica*	*Lucinoma capensis*	*Nucula nucleus*	*Ostrea*	*Pecten sp.*	*Tellina analogica*
1384	8	whole	1	1								
		chipped										
		fragments			1	1	45					
1364	17	whole					1					
		chipped				1						
		fragments			4		12		1			
1406	36	whole										
		fragments					3		10			
1307	16	whole			2	1						
		chipped										
		fragments			10		30					
1479	37	whole										
		fragments					6			6		
1479	34	whole										
		chipped										
		fragments					8			16		
1479	20	whole					2					
		chipped										
		fragments				2	20					
1479	16	whole			1			1				
		chipped										
		fragments			4		18				2	
1307	19	whole										
		chipped										
		fragments		5		1	12			12	1	
1307	58	whole			1							
		chipped	1									
		fragments					20					
1478	10	fragments	1	2	1	16						
1442	7	whole		2		1		1				
		fragments		4		24						
1657	22	whole										1
		chipped							2			
		fragments			8		3					
1657	29	whole			7							
		chipped						8				
		fragments									1	

Table B.22. Gastropod counts for Walvis Bay-Lüderitz cores

Core	Sample depth (cm)	Condition	*Comitas saldanhae*	*Marginella*	*Nassarius vinctus*	*Turritella declivis*	*Volutacorbis lutosa*
1441	2	Whole					
		Chipped					
		Fragments					
1397	2	whole			1		
		fragments					
		Chipped					
1384	2	whole			1		
		chipped					
		fragments					
1407	2	whole			1		1
		chipped					
		fragments					
1307	2	whole	1		5		
		chipped					
		fragments					
1364	2	whole		1			
		chipped			1		
		fragments					
1406	2	whole					
		chipped			1		1
		fragments					
1475	2	whole					
		chipped		1			
		fragments			4		
1479	2	whole			1		
		chipped					
		fragments					
1657	2	whole			1		
		chipped					
		fragments			1		
1441	10	whole					
		chipped					
		fragments				1	

Table B.22. *(continued)*

Core	Sample depth (cm)	Condition	*Comitas saldanhae*	*Marginella*	*Nassarius vinctus*	*Turritella declivis*	*Volutacorbis lutosa*
1384	12	whole					
		chipped					
		fragments			1		
1384	8	whole			1		
		chipped					
		fragments					
1364	17	whole			2		
		chipped					
		fragments					
1406	36	whole					
		chipped					
		fragments					
1307	16	whole			4		
		chipped					
		fragments					
1479	37	whole					
		chipped					
		fragments					
1479	34	whole					
		chipped					
		fragments					
1479	20	whole					
		chipped				1	
		fragments					
1479	16	whole					
		chipped					
		fragments				2	
1307	19	whole					
		chipped					
		fragments					
1307	58	whole					
		chipped					
		fragments					

Table B.22. *(continued)*

Core	Sample depth (cm)	Condition	*Comitas saldanhae*	*Marginella*	*Nassarius vinctus*	*Turritella declivis*	*Volutacorbis lutosa*
1478	10	whole			1		
1657	22	whole			8		
		chipped				1	
		fragments					
1657	29	whole		2	8		
		chipped					
		fragments			3		

Table B.23. Masses of subsample and counts of non-carbonate minerals in core GeoB 20601-4 (874 m water depth)

Core depth (cm)	Mass of subsample (g)	Quartz	Glauconite	Phosphorite	Other lithic
0.5	0.021	22	5		1
4.5	0.024	20	8		3
8.5	0.039	59	14		8
12.5	0.031	32	17	1	1
16.5	0.043	78	20		2
20.5	0.021	30	12		8
24.5	0.023	21	12	3	
28.5	0.038	44	34	3	3
32.5	0.040	37	33		
36.5	0.043	60	21		4
40.5	0.035	40	42	2	2
44.5	0.039	43	50		9
48.5	0.036	29	30	1	1
52.5	0.037	35	29		2
56.5	0.049	55	43		
60.5	0.032	73	29		2
64.5	0.033	60	35		4
68.5	0.058	108	28	1	4
72.5	0.042	96	29	1	1
76.5	0.044	96	29	1	1
80.5	0.042	71	21	1	
84.5	0.049	71	24		1
88.5	0.039	49	20		1
92.5	0.052	75	31		4
96.5	0.038	66	32	1	
108.5	0.044	20	7		1
116.5	0.018	16	4		
124.5	0.062	47	18		1
132.5	0.038	18	13		2
140.5	0.053	66	22	1	3
148.5	0.036	50	8		
156.5	0.052	89	18		
167.5	0.049	133	42	1	
176.5	0.047	135	61	1	
184.5	0.054	218	84	2	3
192.5	0.041	144	94	2	3

Table B.23. *(continued)*

Core depth (cm)	Mass of subsample (g)	Quartz	Glauconite	Phosphorite	Other lithic
200.5	0.039	91	40		
208.5	0.046	140	33		1
216.5	0.045	81	19		2
224.5	0.054	85	28		2
232.5	0.038	73	15		
240.5	0.044	94	39		
248.5	0.053	112	21		
256.5	0.045	234	31	2	4
266.5	0.050	214	42		5
274.5	0.060	274	52		3
282.5	0.070	271	43	3	7
290.5	0.044	123	24		2
298.5	0.034	46	11		1

Table B.24. Masses of subsample and counts of non-carbonate minerals in core GeoB 8342-6 (3522 m water depth)

Core depth (cm)	Mass of subsample (g)	Quartz	Glauconite	Phosphorite	Other lithic
0.5	0.919	3		2	5
4.5	1.627	2	1		5
8.5	1.245	1			1
12.5	2.453	4			1
16.5	1.709				1
20.5	0.584	1			
24.5	1.115				
28.5	1.418				
32.5	0.758				
36.5	0.284				
40.5	0.591				
44.5	1.102	3			2
48.5	0.586	2		1	2
52.5	0.384	2			3
56.5	0.557	1			1
60.5	0.931				
64.5	0.546	1			4
68.5	0.697				
72.5	0.704				
76.5	0.896				3
80.5	1.196	1			1
84.5	0.950	3			2
88.5	0.840				3
92.5	0.241	2			
96.5	0.177	3			
100.5	0.092				2
104.5	0.101	4			2
108.5	0.160	1			
112.5	0.575	2			
116.5	0.692	2			2
120.5	0.990			1	1
124.5	0.636				2
128.5	0.759	2			2
132.5	0.581				2
136.5	1.005				1
140.5	0.514	1			1

Table B.24. *(continued)*

Core depth (cm)	Mass of subsample (g)	Quartz	Glauconite	Phosphorite	Other lithic
144.5	0.399				2
148.5	0.958	1			4
152.5	0.739	1			2
156.5	1.171				
160.5	1.308				2
164.5	1.190				1
168.5	0.824	1			2
172.5	1.271				2
176.5	0.554				
180.5	1.222				6
184.5	1.407	1			2
188.5	1.101	1			1
196.5	1.055				
204.5	0.832	1			1
212.5	0.714	49			9
220.5	0.854	11			8
228.5	0.772	54			17
236.5	0.477	31			9
244.5	0.697	8			4
252.5	0.458	12			6
260.5	0.680	26			5
268.5	1.027				
276.5	0.821	7			4
284.5	0.734	18			5
292.5	0.456	57			6
300.5	0.585	6			5

Table B.25 Masses of subsample and counts of non-carbonate minerals in core GeoB 8336-6 (3631 m water depth)

Core depth (cm)	Mass of subsample (g)	Quartz	Glauconite	Phosphorite	Other lithic
0.5	1.170	4			3
4.5	1.068	3		4	1
8.5	1.027	15		2	1
12.5	1.264	7		1	
16.5	1.562	2		1	
20.5	1.906	4		1	4
23.5	1.128				
27.5	0.647	3			1
32.5	0.900				
37.5	0.587	4			1
41.5	0.537	1		1	1
48.5	0.636	0	0	0	0
50.5	0.569	7			2
55.5	0.535	1			3
60.5	0.554	5		1	1
66.5	0.427	5			4
71.5	0.669				2
76.5	0.819				5
81.5	0.916			2	
86.5	0.928	4		2	6
91.5	1.012				
95.5	0.978				3
99.5	1.045				1
104.5	0.888	1		2	2
109.5	0.162	1			4
114.5	0.257	1	1		8
120.5	0.134	3	1		3
125.5	0.358	1		1	2
129.5	0.573	1			2
133.5	0.912	1			1
138.5	0.972	4		1	2
142.5	1.332	5		2	4
148.5	0.223	2			4
153.5	0.688	1		1	3
158.5	0.710	2			4
163.5	0.469	4			2

Table B.25. *(continued)*

Core depth (cm)	Mass of subsample (g)	Quartz	Glauconite	Phosphorite	Other lithic
168.5	0.818	3		1	
173.5	0.801	2			3
178.5	0.632				1
183.5	0.514	2			5
188.5	0.491	1		1	2
193.5	0.582	1			5
198.5	0.395				
203.5	0.944				
209.5	1.170				
213.5	1.542				
218.5	1.641	3			20
223.5	1.131	5			8
228.5	1.144	2	1		9
233.5	1.001				
238.5	0.701	6		2	
242.5	0.623	5		1	2
248.5	0.235	2			5
253.5	0.351	9	1	1	2
258.5	0.336	12			6
263.5	0.578	8		2	8
268.5	0.673	20		5	13
273.5	0.428	5		1	6
278.5	0.640	3		1	4
283.5	0.505	2.5	2		4
168.5	0.818	3		1	
173.5	0.801	2			3

Appendix C

Carbon ($\delta^{13}C$) and Oxygen ($\delta^{18}O$) Isotope Data

Table C.1. $\delta^{13}C$ and $\delta^{18}O$ (‰) with errors in *Gr. (Gc.) inflata* and *C. wuellerstorfi* tests of GeoB cores 20601-4, 8342-6 and 8336-6.

GeoB core	Sample depth (cm)	*Globorotalia (Globoconella) inflata*				*Cibicidoides wuellerstorfi*			
		$\delta^{13}C$ VPDB	SD $\delta^{13}C$	$\delta^{18}O$ VPDB	SD $\delta^{18}O$	$\delta^{13}C$ VPDB	SD $\delta^{13}C$	$\delta^{18}O$ VPDB	SD $\delta^{18}O$
20601-4	0.5	1.11	0.01	1.43	0.05	-0.40	0.01	4.21	0.04
20601-4	4.5	0.88	0.01	0.95	0.02				
20601-4	8.5	0.85	0.02	1.16	0.04	0.43	0.01	3.29	0.01
20601-4	12.5	1.08	0.02	1.17	0.02	0.55	0.01	3.29	0.01
20601-4	16.5	0.82	0.01	1.07	0.03				
20601-4	20.5	0.87	0.01	1.11	0.02	0.79	0.02	2.81	0.04
20601-4	24.5	0.85	0.02	1.29	0.03				
20601-4	28.5	0.86	0.02	1.30	0.03	0.75	0.01	2.61	0.02
20601-4	32.5	0.98	0.01	1.35	0.02	0.74	0.02	2.54	0.03
20601-4	36.5	0.75	0.01	1.28	0.05	1.07	0.01	3.04	0.02
20601-4	40.5	0.52	0.01	1.27	0.02	1.12	0.00	3.31	0.04
20601-4	44.5	0.73	0.02	1.60	0.03	0.59	0.03	3.74	0.03
20601-4	48.5	1.00	0.01	1.62	0.06	0.84	0.01	3.79	0.03
20601-4	52.5	0.65	0.01	1.85	0.02	0.69	0.03	3.86	0.05
20601-4	56.5	0.92	0.01	1.90	0.04	0.98	0.02	3.68	0.02
20601-4	60.5	0.81	0.01	1.78	0.02				
20601-4	64.5	0.96	0.01	1.83	0.02	1.13	0.03	3.52	0.05
20601-4	68.5	0.61	0.01	1.54	0.01	0.75	0.01	3.70	0.01
20601-4	72.5	0.53	0.01	1.63	0.02	0.81	0.01	2.97	0.03
20601-4	76.5	0.66	0.03	1.58	0.03				
20601-4	80.5	0.48	0.01	1.66	0.01	1.02	0.02	2.71	0.03
20601-4	84.5	0.48	0.02	1.56	0.03	0.93	0.01	3.57	0.02
20601-4	88.5	0.71	0.01	1.73	0.01	0.77	0.01	3.55	0.04
20601-4	92.5	0.76	0.01	1.85	0.02	0.81	0.01	3.66	0.01
20601-4	96.5	0.65	0.01	1.70	0.03	0.73	0.00	3.53	0.03
20601-4	100.5	0.72	0.01	1.91	0.01	0.90	0.01	3.44	0.06
20601-4	108.5	0.56	0.01	1.62	0.02	0.70	0.02	3.38	0.02
20601-4	112.5	0.98	0.01	1.36	0.02	1.00	0.01	3.13	0.04
20601-4	116.5	0.89	0.02	1.43	0.03	1.06	0.01	3.21	0.01
20601-4	120.5	0.86	0.01	1.62	0.01	1.09	0.02	3.24	0.05
20601-4	124.5	0.69	0.01	1.47	0.02	1.33	0.02	2.59	0.04
20601-4	128.5	0.88	0.01	1.25	0.03	0.83	0.02	3.31	0.03
20601-4	132.5	0.79	0.01	1.18	0.02				
20601-4	136.5	0.71	0.01	0.84	0.03	0.82	0.01	2.64	0.05
20601-4	140.5	0.58	0.01	1.04	0.02	0.83	0.02	2.33	0.02
20601-4	148.5	0.48	0.01	1.10	0.05	0.80	0.03	3.12	0.04
20601-4	152.5	0.29	0.02	1.62	0.02	0.69	0.01	2.73	0.02
20601-4	156.5	0.16	0.02	1.55	0.03	0.78	0.02	3.15	0.04
20601-4	160.5	0.41	0.02	1.63	0.04	0.99	0.02	3.09	0.07
20601-4	164.5	0.42	0.02	1.27	0.02	0.78	0.01	2.63	0.03
20601-4	172.5	0.41	0.02	1.33	0.02	0.46	0.01	2.34	0.02
20601-4	176.5	0.18	0.02	1.44	0.02	0.94	0.01	2.48	0.02
20601-4	180.5	0.31	0.02	1.83	0.02	0.62	0.01	3.34	0.05

Table C.1. *(continued)*

GeoB core	Sample depth (cm)	*Globorotalia (Globoconella) inflata*				*Cibicidoides wuellerstorfi*			
		$\delta^{13}C$ VPDB	SD $\delta^{13}C$	$\delta^{18}O$ VPDB	SD $\delta^{18}O$	$\delta^{13}C$ VPDB	SD $\delta^{13}C$	$\delta^{18}O$ VPDB	SD $\delta^{18}O$
20601-4	184.5	0.54	0.02	2.16	0.04	0.76	0.02	2.54	0.01
20601-4	188.5	0.36	0.02	1.81	0.03				
20601-4	192.5	0.51	0.01	1.51	0.01	0.21	0.02	3.43	0.01
20601-4	196.5	0.45	0.04	1.47	0.05	0.51	0.02	3.17	0.02
20601-4	200.5	0.39	0.02	1.64	0.03	0.49	0.00	3.50	0.03
20601-4	208.5	0.71	0.03	1.48	0.05				
20601-4	216.5	0.68	0.01	1.33	0.02				
20601-4	224.5	0.63	0.03	1.38	0.03	0.41	0.05	2.53	0.06
20601-4	232.5	0.90	0.03	1.32	0.04	0.64	0.01	2.57	0.03
20601-4	240.5	0.49	0.02	1.31	0.03	0.58	0.01	3.41	0.05
20601-4	248.5	0.51	0.01	1.68	0.01	0.79	0.01	3.04	0.03
20601-4	256.5	0.77	0.03	2.50	0.04	0.13	0.01	3.70	0.01
20601-4	266.5	0.36	0.02	1.95	0.03	0.27	0.01	3.63	0.03
20601-4	274.5	0.33	0.01	1.74	0.04	0.60	0.02	3.57	0.02
20601-4	282.5	0.47	0.02	2.01	0.03	0.53	0.01	3.63	0.04
20601-4	290.5	0.85	0.00	1.55	0.01	0.46	0.01	3.18	0.02
20601-4	298.5	0.69	0.02	1.54	0.02	0.45	0.01	3.17	0.01
8342-6	0.5	0.99	0.01	1.04	0.01	0.67	0.00	2.64	0.02
8342-6	4.5	1.03	0.01	1.22	0.01	0.61	0.01	2.91	0.02
8342-6	8.5	1.02	0.01	0.91	0.01	0.71	0.01	2.64	0.03
8342-6	12.5	0.80	0.01	1.05	0.01				
8342-6	16.5	0.67	0.01	1.33	0.02	0.50	0.00	2.72	0.02
8342-6	20.5	0.70	0.01	1.80	0.01				
8342-6	28.5	0.80	0.01	2.27	0.01	0.01	0.01	4.23	0.02
8342-6	32.5	0.89	0.01	2.22	0.03	-0.02	0.01	4.27	0.02
8342-6	36.5	0.93	0.01	2.10	0.01	0.07	0.01	4.28	0.02
8342-6	40.5	0.93	0.01	1.93	0.02	0.11	0.01	4.18	0.03
8342-6	44.5	0.68	0.01	2.13	0.01	0.03	0.01	4.13	0.02
8342-6	48.5	0.70	0.00	2.01	0.01		0.32		0.37
8342-6	52.5	0.85	0.01	2.07	0.01	0.01	0.00	4.14	0.02
8342-6	58.5	0.94	0.00	1.94	0.03				
8342-6	64.5	0.99	0.01	1.71	0.01	0.07	0.01	4.01	0.04
8342-6	68.5	1.17	0.01	1.69	0.01				
8342-6	76.5	0.98	0.00	1.50	0.03	0.37	0.00	3.64	0.01
8342-6	80.5	0.99	0.01	2.06	0.02	0.21	0.01	3.82	0.03
8342-6	84.5	0.66	0.01	1.60	0.01	0.43	0.01	3.48	0.02
8342-6	88.5	0.74	0.01	1.69	0.00	-0.11	0.01	3.70	0.04
8342-6	92.5	0.65	0.01	2.12	0.02	-0.06	0.00	4.08	0.01
8342-6	96.5	0.92	0.01	2.18	0.03	-0.18	0.00	3.96	0.02
8342-6	100.5	1.14	0.00	2.58	0.02	-0.18	0.00	3.99	0.02
8342-6	104.5	1.06	0.00	1.49	0.01	-0.10	0.00	3.97	0.00
8342-6	108.5	1.17	0.01	1.62	0.01	0.26	0.00	3.67	0.03
8342-6	112.5	1.01	0.01	1.60	0.02	0.38	0.01	3.68	0.02

Table C.1. *(continued)*

GeoB core	Sample depth (cm)	*Globorotalia (Globoconella) inflata*				*Cibicidoides wuellerstorfi*			
		$\delta^{13}C$ VPDB	SD $\delta^{13}C$	$\delta^{18}O$ VPDB	SD $\delta^{18}O$	$\delta^{13}C$ VPDB	SD $\delta^{13}C$	$\delta^{18}O$ VPDB	SD $\delta^{18}O$
8342-6	116.5	0.94	0.00	1.38	0.02	0.32	0.01	3.45	0.02
8342-6	120.5	1.08	0.00	1.46	0.01				
8342-6	124.5	1.21	0.00	1.32	0.03	0.19	0.01	3.53	0.02
8342-6	128.5	1.19	0.00	1.33	0.02	0.61	0.01	3.33	0.03
8342-6	132.5	0.97	0.01	1.15	0.02	0.61	0.00	3.27	0.03
8342-6	136.5	0.91	0.01	1.19	0.01	-0.27	0.00	3.42	0.02
8342-6	140.5	0.91	0.01	1.31	0.01	0.41	0.01	3.26	0.03
8342-6	144.5	1.31	0.01	1.58	0.02	0.32	0.01	3.64	0.02
8342-6	148.5	1.03	0.01	1.22	0.02	0.33	0.01	3.39	0.02
8342-6	152.5	0.93	0.00	0.98	0.01	0.44	0.00	3.44	0.02
8342-6	156.5	0.80	0.01	1.37	0.01	0.54	0.00	3.09	0.03
8342-6	160.5	0.78	0.00	1.10	0.02	0.70	0.01	3.29	0.02
8342-6	164.5	1.07	0.00	1.20	0.02	0.04	0.00	2.76	0.02
8342-6	168.5	0.72	0.01	1.09	0.02	0.20	0.01	3.06	0.01
8342-6	172.5	0.62	0.01	1.03	0.02	0.12	0.01	3.34	0.02
8342-6	176.5	1.01	0.01	1.23	0.01	0.22	0.01	3.54	0.02
8342-6	180.5	0.70	0.01	1.01	0.01	-0.05	0.01	3.32	0.02
8342-6	184.5	0.84	0.00	1.08	0.02	0.40	0.01	2.88	0.01
8342-6	188.5	0.63	0.01	0.86	0.02	0.44	0.01	2.72	0.04
8342-6	196.5	0.64	0.00	0.79	0.02	0.39	0.01	2.90	0.02
8342-6	204.5	0.63	0.02	1.24	0.01	0.17	0.01	3.04	0.02
8342-6	212.5	0.44	0.01	1.41	0.01	0.28	0.01	3.54	0.03
8342-6	220.5	0.54	0.01	2.23	0.02	-0.19	0.00	4.16	0.01
8342-6	228.5	0.47	0.00	2.31	0.03	-0.32	0.01	4.27	0.01
8342-6	236.5	0.53	0.01	1.98	0.02	-0.18	0.01	4.19	0.02
8342-6	244.5	0.47	0.00	2.03	0.02	-0.15	0.01	4.12	0.02
8342-6	252.5	0.46	0.04	2.02	0.05	-0.03	0.01	4.29	0.03
8342-6	260.5	0.59	0.01	1.87	0.02	0.20	0.01	3.92	0.03
8342-6	268.5	0.47	0.01	2.46	0.02	0.05	0.01	4.03	0.03
8342-6	276.5	0.57	0.00	1.62	0.01	-0.06	0.00	3.56	0.03
8342-6	284.5	0.39	0.01	1.40	0.02	-0.09	0.01	3.93	0.01
8342-6	292.5	0.37	0.01	1.55	0.02	-0.24	0.01	3.91	0.02
8342-6	300.5	0.75	0.01	1.48	0.02	-0.18	0.01	3.54	0.02
8342-6	308.5	0.81	0.00	1.17	0.01	0.22	0.01	3.42	0.02
8342-6	316.5	0.66	0.00	0.82	0.01	0.27	0.01	3.01	0.01
8336-6	0.5	1.08	0.01	0.81	0.03	0.58	0.01	2.83	0.06
8336-6	4.5	1.02	0.01	0.99	0.01	0.52	0.01	2.66	0.02
8336-6	8.5	1.08	0.01	0.73	0.02	0.53	0.02	2.61	0.04
8336-6	12.5	0.85	0.01	1.24	0.02	0.67	0.01	2.69	0.01
8336-6	16.5	0.94	0.00	1.05	0.01	0.60	0.01	2.82	0.03
8336-6	20.5	0.81	0.01	1.11	0.02	0.52	0.01	2.94	0.04
8336-6	23.5	0.39	0.01	1.52	0.02	0.33	0.01	3.65	0.02
8336-6	27.5	0.40	0.01	1.86	0.04	-0.10	0.01	4.30	0.05

Table C.1. *(continued)*

GeoB core	Sample depth (cm)	*Globorotalia (Globoconella) inflata*				*Cibicidoides wuellerstorfi*			
		$\delta^{13}C$ VPDB	SD $\delta^{13}C$	$\delta^{18}O$ VPDB	SD $\delta^{18}O$	$\delta^{13}C$ VPDB	SD $\delta^{13}C$	$\delta^{18}O$ VPDB	SD $\delta^{18}O$
8336-6	37.5	0.70	0.01	2.03	0.01	-0.04	0.01	4.28	0.04
8336-6	41.5	1.02	0.02	2.03	0.03	-0.26	0.02	4.25	0.02
8336-6	48.5	0.90	0.02	1.51	0.03	-0.09	0.00	4.23	0.04
8336-6	55.5	0.94	0.02	2.20	0.04	0.16	0.02	4.10	0.04
8336-6	66.5	0.87	0.02	2.00	0.02	0.33	0.03	3.88	0.05
8336-6	71.5	0.94	0.01	1.61	0.02	0.09	0.02	4.04	0.02
8336-6	76.5	1.11	0.00	1.88	0.04	0.28	0.02	3.98	0.02
8336-6	81.5	0.85	0.01	1.47	0.02	0.27	0.01	3.81	0.05
8336-6	86.5	0.97	0.01	2.01	0.03	0.19	0.01	3.94	0.01
8336-6	91.5	1.01	0.02	1.96	0.00	0.24	0.01	3.74	0.05
8336-6	95.5	0.85	0.00	1.84	0.01	0.19	0.01	3.99	0.03
8336-6	99.5	0.83	0.01	1.40	0.01				
8336-6	104.5	0.98	0.01	1.52	0.02	0.06	0.01	3.85	0.05
8336-6	109.5	0.77	0.01	2.13	0.03	-0.21	0.01	4.09	0.03
8336-6	114.5	1.09	0.01	1.63	0.02	0.07	0.01	3.86	0.02
8336-6	120.5	0.85	0.02	1.83	0.02	0.08	0.03	3.73	0.02
8336-6	125.5	1.16	0.02	1.49	0.04	0.41	0.01	3.48	0.05
8336-6	129.5	1.05	0.01	1.72	0.01	0.36	0.02	3.71	0.01
8336-6	133.5	1.06	0.02	1.36	0.03	0.13	0.01	3.54	0.01
8336-6	138.5	1.10	0.01	1.36	0.01	0.51	0.02	3.39	0.04
8336-6	142.5	0.93	0.02	1.21	0.03	0.58	0.01	3.33	0.03
8336-6	148.5	0.97	0.01	1.38	0.02	0.17	0.01	3.29	0.03
8336-6	153.5	1.02	0.01	1.10	0.01	0.02	0.01	3.52	0.02
8336-6	158.5	1.08	0.01	1.21	0.04	0.49	0.01	3.34	0.06
8336-6	163.5	1.17	0.01	1.42	0.03	0.42	0.01	3.45	0.01
8336-6	168.5	1.15	0.02	1.39	0.03	0.38	0.01	3.38	0.03
8336-6	173.5	0.92	0.02	1.25	0.01	0.23	0.01	3.36	0.03
8336-6	178.5	0.92	0.01	1.03	0.03	0.15	0.02	3.37	0.01
8336-6	188.5	1.09	0.01	1.38	0.02	0.11	0.01	3.17	0.03
8336-6	198.5	0.84	0.01	1.30	0.03	0.03	0.01	3.40	0.03
8336-6	209.5	0.56	0.02	0.66	0.04	0.01	0.00	3.36	0.01
8336-6	213.5	0.62	0.01	0.84	0.02	0.65	0.01	2.66	0.03
8336-6	218.5	0.63	0.00	0.80	0.03	0.38	0.01	2.91	0.01
8336-6	223.5	0.57	0.01	0.70	0.02	0.29	0.01	2.61	0.03
8336-6	233.5	0.40	0.01	1.18	0.02	0.05	0.01	3.78	0.01
8336-6	242.5	0.67	0.01	1.04	0.03	-0.28	0.01	4.38	0.03
8336-6	253.5	0.64	0.01	1.91	0.01	-0.36	0.01	3.73	0.04
8336-6	258.5	0.67	0.01	1.89	0.02	-0.49	0.01	4.36	0.02
8336-6	263.5	0.62	0.01	2.19	0.01	0.56	0.02	3.27	0.04
8336-6	268.5	0.68	0.02	1.90	0.02	-0.03	0.01	3.75	0.01

Appendix D

Principal Component Analysis (PCA) Data

Table D.1. Planktic PCA results for core GeoB 20601-4.

Component	PC 1	PC 2	PC 3
Globigerina bulloides	-0.425	-0.680	0.450
Globigerinella siphonifera	-0.001	-0.010	-0.043
Globigerinoides ruber (white)	-0.021	0.010	-0.093
Globorotalia (Globoconella) inflata	-0.334	0.729	0.449
Globorotalia hirsuta	0.003	0.009	-0.082
Globorotalia truncatulinoides	-0.028	0.039	-0.461
Neogloboquadrina dutertrei	-0.014	0.017	-0.073
Ng. incompta + Ng. pachyderma	0.841	-0.053	0.381
Orbulina universa	-0.011	-0.042	-0.465
Variance	65.80	31.57	1.63

Table D.2. Planktic PCA results for core GeoB 8342-6

Component	PC 1	PC 2	PC 3
Globigerina bulloides	0.427	-0.628	0.438
Globigerinella siphonifera	0.018	0.020	0.005
Globigerinoides ruber (white)	0.068	-0.001	0.054
Globorotalia (Globoconella) inflata	0.291	0.768	0.301
Globorotalia hirsuta	-0.002	0.061	-0.014
Globorotalia scitula	0.010	0.017	0.013
Globorotalia truncatulinoides	0.092	-0.054	-0.166
Neogloboquadrina dutertrei	0.016	-0.001	0.024
Ng. incompta + Ng. pachyderma	-0.844	-0.05	0.387
Orbulina universa	-0.086	-0.075	-0.732
Pulleniatina obliquiloculata	0.011	-0.015	-0.002
Variance	69.44	19.95	6.84

Table D.3. Planktic PCA results for core GeoB 8336-6

Component	PC 1	PC 2	PC 3
Globigerina bulloides	0.109	-0.674	0.573
Globigerinella siphonifera	-0.027	-0.01	-0.024
Globigerinoides ruber (white)	-0.036	0.023	0.025
Globorotalia (Globoconella) inflata	-0.725	0.396	0.189
Globorotalia hirsuta	-0.028	0.005	-0.003
Globorotalia truncatulinoides	-0.061	-0.094	-0.218
Ng. incompta + Ng. pachyderma	0.654	0.590	0.275
Orbulina universa	0.166	-0.178	-0.716
Pulleniatina obliquiloculata	-0.013	-0.002	-0.006
Trilobatus sacculifer	-0.015	0.005	0.007
Variance	59.93	24.89	9.70

Table D.4. Benthic PCA results for core GeoB 20601-4. Taxa specified as genus spp. include species that could not definitively be identified.

Component	PC 1	PC 2	PC 3
Agglutinated	-0.103	-0.187	-0.063
Bolivina spp.	0.007	-0.012	-0.004
Bulimina aculeata	-0.107	-0.138	0.075
Bulimina marginata	0.003	-0.010	0.017
Bulimina spp.	0.000	-0.007	-0.004
Cassidulina laevigata	-0.018	-0.065	-0.012
Cibicidoides pachyderma	-0.071	0.300	0.737
Cibicidoides spp.	-0.146	0.036	-0.501
Cibicidoides wuellerstorfi	-0.065	0.011	-0.001
Eggerella bradyi	-0.076	0.045	-0.045
Epistominella exigua	-0.045	-0.059	0.043
Fissurina spp.	-0.003	0.002	-0.004
Fursenkoina spp,	-0.002	-0.014	0.005
Globobulimina turgida	0.001	-0.018	0.016
Gyroidinoides orbicularis	-0.009	-0.010	0.048
Karerriella bradyi	0.005	0.007	-0.006
Lagena demorpha	-0.004	0.000	-0.008
Lenticulina spp.	0.004	0.002	0.010
Martinottiella communis	-0.004	-0.019	0.003
Melonis barleeanus	-0.002	0.009	-0.024
Miliolids	-0.039	0.019	-0.066
Nodosaria laevigata	-0.007	-0.008	-0.001
Nodosaria spp.	-0.012	0.005	-0.015
Oridorsalis umbonatus	0.000	-0.022	0.003
Pyrgo spp.	-0.068	0.019	-0.057
Rectobolivina	-0.005	0.004	-0.014
Siphonaperta	-0.059	-0.009	0.096
Spiroloculina communis	0.011	-0.019	0.002
Uvigerina auberiana	-0.002	0.004	-0.004
Uvigerina hispidocostata	-0.001	-0.001	0.004
Uvigerina peregrina	0.921	0.158	-0.143
Uvigerina spp.	-0.008	-0.027	0.016
Vaginulina spinigera	-0.006	0.007	-0.009
BFAR	0.258	-0.165	0.367
BFOI	-0.122	0.888	-0.126
Variance	39.94	29.36	9.20

Table D.5. Benthic PCA results for core GeoB 8342-6. Taxa specified as genus spp. include species that could not definitively be identified.

Component	PC 1	PC 2	PC 3
Agglutinated	-0.016	-0.017	-0.003
Cibicidoides pachyderma	-0.095	-0.115	0.128
Cibicidoides spp.	-0.064	0.025	-0.073
Cibicidoides wuellerstorfi	0.012	-0.054	-0.481
Eggerella bradyi	-0.026	-0.011	-0.016
Ehrenbergina trigona	0.003	0.025	0.009
Epistominella exigua	0.801	-0.249	0.394
Fissurina spp.	-0.008	-0.034	-0.034
Fursenkoina spp.	0.016	0.062	0.081
Globobulimina turgida	-0.007	-0.004	0.004
Globocassidulina spp.	-0.075	0.838	0.371
Gyroidinoides orbicularis	-0.029	-0.042	-0.030
Lagena demorpha	0.004	0.013	-0.013
Lagena hispida	0.008	-0.002	0.000
Lagena sulcata	0.002	0.011	-0.001
Lenticulina sp.	0.001	-0.004	-0.014
Martinottiella communis	-0.029	-0.004	0.037
Melonis barleeanus	0.023	-0.016	-0.075
Melonis pompiloides	-0.017	-0.021	-0.029
Miliolids	-0.036	-0.032	0.017
Oolina globosa	-0.005	0.015	0.002
Oridorsalis umbonatus	-0.026	-0.011	-0.029
Pullenia bulloides	0.026	-0.006	-0.026
Pyrgo spp.	-0.393	-0.263	0.494
Sphaeroidina bulloides	-0.006	-0.017	-0.006
Uvigerina auberiana	-0.014	-0.045	-0.114
Uvigerina hispidocostata	-0.039	-0.015	0.012
Uvigerina peregrina	-0.026	-0.033	0.066
Uvigerina spp.	0.073	0.183	-0.386
BFAR	0.413	0.315	-0.124
BFOI	-0.002	-0.060	-0.088
Variance	40.40	17.20	9.02

Table D.6. Benthic PCA results for core GeoB 8336-6. Taxa specified as genus spp. include species that could not definitively be identified.

Component	PC 1	PC 2	PC 3
Agglutinated	0.160	0.108	0.071
Cibicidoides crebbsi	0.019	-0.092	0.050
Cibicidoides pachyderma	-0.046	-0.080	-0.014
Cibicidoides spp.	-0.057	0.006	-0.044
Cibicidoides wuellerstorfi	-0.051	-0.293	0.186
Eggerella bradyi	0.026	-0.082	0.013
Epistominella exigua	-0.573	0.600	0.225
Fissurina spp.	0.012	-0.009	0.001
Fursenkoina spp.	-0.014	0.033	-0.081
Globobulimina turgida	-0.006	0.000	-0.011
Globocassidulina spp.	0.185	-0.154	0.08
Gyroidinoides orbicularis	0.019	-0.009	0.009
Lagena demorpha	0.005	0.010	0.008
Lagena sulcata	0.012	0.010	0.014
Lenticulina spp.	0.006	-0.012	-0.005
Melonis barleeanus	-0.174	-0.055	0.113
Melonis pompiloides	-0.001	0.007	0.028
Miliolids	0.029	-0.149	0.059
Oolina globosa	0.018	-0.019	0.032
Oridorsalis umbonatus	0.025	-0.060	0.043
Pullenia bulloides	-0.049	0.066	-0.090
Pyrgo spp.	0.015	-0.401	0.168
Sphaeroidina bulloides	-0.004	-0.016	0.003
Ehrenbergina trigona	0.008	0.003	-0.002
Uvigerina auberiana	-0.078	0.126	-0.497
Uvigerina hispidocostata	0.528	0.240	-0.345
Uvigerina proboscidea	-0.017	0.007	0.009
Uvigerina spp.	0.043	0.139	-0.148
BFAR	0.516	0.426	0.565
BFOI	-0.069	-0.149	0.357
Variance	25.69	19.34	13.53